

PHASE EQUILIBRIA & THERMODYNAMIC MODELLING OF THE TERNARY SYSTEM $\text{CO}_2 + 1\text{-DECANOL} + N\text{-TETRADECANE}$

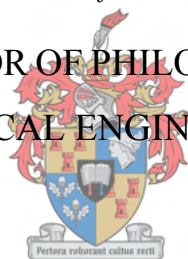
by

Machelle Ferreira

Dissertation presented for the Degree

of

DOCTOR OF PHILOSOPHY
(CHEMICAL ENGINEERING)



in the Faculty of Engineering
at Stellenbosch University

100

The financial assistance of the National Research Foundation (NRF) towards this research is hereby acknowledged. Opinions expressed, and conclusions arrived at, are those of the author and are not necessarily to be attributed to the NRF.

Supervisor

Prof. C.E. Schwarz

December 2018

DECLARATION

By submitting this thesis electronically, I declare that the entirety of the work contained therein is my own, original work, that I am the sole author thereof (save to the extent explicitly otherwise stated), that reproduction and publication thereof by Stellenbosch University will not infringe any third-party rights and that I have not previously in its entirety or in part submitted it for obtaining any qualification.

Please note: In the case of dissertations in format stipulated in 2018 Policies and Rules par. 6.9.5.2 to 6.9.5.4, the following general declaration should be added as a second paragraph, in addition to the above declaration: refer to the (par 6.11.5.4, page 215). Also refer to additional declarations in par. 6.9.15.

This dissertation includes 1 original paper published in peer-reviewed journals or books and 3 unpublished publications. The development and writing of the papers (published and unpublished) were the principal responsibility of myself and, for each of the cases where this is not the case, a declaration is included in the dissertation indicating the nature and extent of the contributions of co-authors.

Date: December 2018

ABSTRACT

Experimental data and predictive process models, tested at various operating conditions, have shown that supercritical fluid fractionation is a feasible process when aimed at the separation of detergent range 1-alcohols and *n*-alkanes with similar boiling points. Although this process shows good separation performance, it was previously found that distinct solute + solute interactions occur that influence the predictive capability of thermodynamic models. *The aim of this study was to obtain a fundamental understanding of the solute + solute interactions in the CO₂ + 1-decanol + n-tetradecane ternary system; firstly, through the generation of phase equilibria data and secondly, through the evaluation of thermodynamic models, with solute + solute binary interaction parameters (BIPs) incorporated into their algorithm, to correlate the new VLE data.* The aim was achieved through the following objectives:

- (1) Studying the high-pressure phase equilibria of the CO₂ + 1-decanol + *n*-tetradecane ternary system;
- (2) Studying the low-pressure phase equilibria of the 1-decanol + *n*-tetradecane binary system;
- (3) Selecting 4 suitable thermodynamic models available within a commercial process simulator and studying the modelling of the ternary and binary phase equilibria data with new solute + solute BIPs obtained from the experimental data.

The first objective was met in two parts namely, the measurement of new high-pressure bubble- and dew-point data (HPBDP) and the measurement of new high-pressure vapour-liquid equilibria data (HPVLE). The HPBDP experiments were conducted between $T = 308$ K and $T = 358$ K using a visual static synthetic method. CO₂ free *n*-tetradecane mass fractions (w_c^{red}) of 0.2405, 0.5000, 0.6399, 0.7698, 0.8162 and 0.9200 g/g were investigated, and the total solute mass fractions were varied between 0.015 g/g and 0.65 g/g. An increase in the solute + solute interactions were observed when increasing the *n*-tetradecane composition and decreasing the temperature. The distinct solute + solute interactions lead to the formation of a liquid-gas hole in the three-phase surface, cosolvency effects and miscibility windows.

For the HPVLE data, a state of the art high-pressure analytical view cell was used to study four ternary mixtures at $T = 308$ K, 328 K and 348 K and pressures between $P = 8.0$ and 16.4 MPa. The equipment allowed for equilibrium to be achieved after which samples of the co-existing phases were taken simultaneously. Phase composition data for four tie lines were obtained and ternary phase diagrams constructed. A similar outcome to the HPBDP experimental results were observed. In general, for $w_c^{red} \geq 0.9004$ g/g, 1-decanol will be the more soluble compound and for $w_c^{red} \leq 0.2403$ g/g, *n*-tetradecane will be the more soluble compound. Furthermore, within the complex phase behaviour region ($w_c^{red} = \pm 0.6245$ g/g), separation of residual *n*-tetradecane from 1-decanol in the mixtures are postulated to be impossible. However, separation experiments are required on a pilot plant setup to verify this assumption.

To achieve the second objective, the phase behaviour complexities brought on by the 1-decanol + *n*-tetradecane interactions were further evaluated through the measurement of new low-pressure vapour-liquid equilibria data (LPVLE). The experiments were conducted at sub-atmospheric pressure ($P = 40$ kPa) using an all glass dynamic recirculating still. The binary system displayed positive azeotropy, inferring Type I-A fluid phase behaviour. The presence of the azeotrope and the non-unity activity coefficients confirmed that the binary system exhibits non-ideal phase behaviour.

Four thermodynamic models, available within Aspen Plus[®], were evaluated for their ability to correlate (RK-Aspen, SR-Polar and PC-SAFT) and to predict (PSRK) all three sets of experimental data. PSRK made use of previously determined low-pressure activity coefficient group-group parameters and thus served as a purely predictive model. For the remaining three models, the HPVLE and LPVLE data were used with the built-in data regression function in Aspen Plus[®] to regress solute + solute BIPs. For the HPBDP BIPs a plug-and-play method was applied to manually regress representative values instead of exact values.

Objective 3 was achieved by evaluating the performance of the models with varying solute + solute BIPs in their specific model algorithm, i.e. BIPs regressed using low-pressure data were used to represent high-pressure data and vice versa as summarised in *Table i*.

TABLE I: SUMMARY OF RK-ASPEN, SR-POLAR AND PC-SAFT SOLUTE + SOLUTE BIPs THAT CAN BE USED TO CORRELATE LPVLE, HPVLE AND HPBDP DATA

New Experimental data	Solute + solute BIPs								
	RK-Aspen			SR-Polar			PC-SAFT		
	LPVLE	HPVLE	HPBDP	LPVLE	HPVLE	HPBDP	LPVLE	HPVLE	HPBDP
LPVLE	✓	✓*	✓*	✓	✗	✗	✓	✗	✗
HPVLE	✗	✓	✓	✗	✓	✓	✓*	✓*	✓*
HPBDP	✓†	✓	✓	✓†	✓	✓	✗	✗	✗

† Dew-point region for $w_c^{red} \leq 0.6399$ g/g only.

‡ Liquid phase composition at $T = 348$ K only.

*With $k_{b,ij} = 0$.

RK-Aspen was the only model to produce an accurate representation of each set of experimental data, which included the complex phase behaviour regions. SR-Polar was a close second, lagging in the representation of the LPVLE data. On a purely predictive front, PSRK can be used to represent accurate HPBDP and LPVLE data but should not be used to predict HPVLE data. Lastly, PC-SAFT can produce reasonable LPVLE and HPVLE data but failed to correlate the HPBDP data accurately. The models, presented in order of decreasing performance, were RK-Aspen > SR-Polar > PSRK > PC-SAFT. Lastly, the RK-Aspen model with HPBDP solute + solute BIPs provided the most accurate model fit (quantitatively and qualitatively) within the complex phase behaviour region of the HPBDP, HPVLE and LPVLE data. Overall, this thesis provided valuable insight into the role that solute + solute interactions play in generating complex phase behaviour and fractionation difficulties. In future studies, solute + solute interactions should not be ignored as they will help improve not only the design of pilot plant experiments, but also process models.

OPSOMMING

Eksperimentele data en voorspellende prosesmodelle, wat by verskeie bedryfstoeistande getoets is, het getoon dat superkritiese vloeier fraksionering 'n lewensvatbare proses is wanneer dit gemik is op die skeiding van 1-alkohole en n -alkane met soortgelyke kookpunte. Alhoewel hierdie proses goeie skeiding toon, is daar voorheen bevind dat opgeloste stof interaksies die voorspellingsvermoë van termodinamiese modelle beïnvloed. *Die doel van hierdie ondersoek was om 'n fundamentele begrip van die opgeloste stof interaksies in die CO_2 + 1-dekanol + n -tetradekaane ternêre sisteem te verkry: eerstens, deur fase-ewewigdata te genereer, en tweedens, deur die evaluering van termodinamiese modelle, wat van binêre interaksie parameters (BIPs) gebruik maak, om die nuwe fase-ewewigdata te korreleer.* Hierdie doel is deur die volgende doelwitte bereik: (1) Bestudeer die hoë druk fase ewewig van die CO_2 + 1-dekanol + n -tetradekaane ternêre sisteem; (2) Bestudeer die lae druk fase ewewig van die 1-dekanol + n -tetradekaane binêre sisteem; (3) Kies 4 gepaste termodinamiese modelle wat in 'n kommersiële proses simulator beskikbaar is en bestudeer die termodinamiese modellering van die ternêre en binêre fase-ewewigdata met nuwe opgeloste stof-BIPs bepaal deur die eksperimentele data.

Die eerste doelwit is in twee dele bereik: nuwe hoë druk borrel- en doupunt data (HPBDP) en nuwe hoë druk damp-vloeistof ewewigdata (HPVLE) is gemeet. Die HPBDP eksperimente is tussen $T = 308 \text{ K}$ en $T = 358 \text{ K}$ met 'n visuele staties-sintetiese metode uitgevoer. CO_2 -vry n -tetradekaane massafraksies (w_c^{red}) van 0.2405, 0.5000, 0.6399, 0.7698, 0.8162 en 0.9200 g/g is bestudeer en die totale opgeloste stof massafraksies is tussen 0.015 g/g en 0.65 g/g varieer. 'n Toename in opgeloste stof interaksies is met 'n toename in n -tetradekaane samestelling en 'n afname in temperatuur waargeneem. Die opgeloste stof interaksies het gelei tot die vorming van 'n vloeistof-gas gaping in die drie-fase gebied, saam-oplosbaarheid, en mengbaarheidsgebiede.

Om die HPVLE data te meet is 'n moderne hoë druk visuele analitiese sel gebruik. Vier mengsels is by $T = 308 \text{ K}$, 328 K en 348 K , en by drukke tussen $P = 8.0$ en 16.4 MPa bestudeer. In hierdie toerusting kan monsters van die ewilibrum fases gelyktydig geneem word. Die fase-samestellingsdata van vier bindlyne is verkry en ternêre fase-diagramme is gekonstrueer. Die HPVLE data het soortgelyke gevolgtrekkings as die HPBDP data na vore gebring. Oor die algemeen was 1-dekanol meer oplosbaar vir die $w_c^{\text{red}} \geq 0.9004 \text{ g/g}$ mengsel en n -tetradekaane meer oplosbaar vir die $w_c^{\text{red}} \leq 0.2403 \text{ g/g}$ mengsel. In die komplekse fasegedragsgebied ($w_c^{\text{red}} = \pm 0.6245 \text{ g/g}$) word daar postuleer dat skeiding van residuele n -tetradekaane van 1-dekanol onmoontlik is. Skeidingseksperimente op 'n loodsaanleg word egter benodig om hierdie aanname te bevestig.

Om die tweede doelwit te bereik, is die komplekse fasegedrag wat deur 1-dekanol + n -tetradekaane interaksies veroorsaak word, verder evalueer. Nuwe lae druk damp-vloeistof ewewigdata (LPVLE) is vir hierdie binêre stelsel by sub-atmosferiese druk ($P = 40 \text{ kPa}$) in 'n dinamiese hersirkulerende distilleerder gemeet. Hierdie binêre sisteem toon 'n positiewe aseptroop, wat moontlik Tipe I-A vloeier

fasegedrag aandui. Die teenwoordigheid van 'n aseptroop en die aktiwiteitskoëffisiënt waardes het bevestig dat die sisteem nie-ideale fasegedrag uitoefen.

Vier termodinamiese modelle, almal beskikbaar in Aspen Plus[®], is evalueer op grond van hul vermoë om die drie stelle eksperimentele data te korreleer (RK-Aspen, SR-Polar, en PC-SAFT) en te voorspel (PSRK). PSRK gebruik voorheen bepaalde lae druk aktiwiteitskoëffisiënt groep-groep parameters en dien dus as 'n suiwer voorspellende model. Vir die ander drie modelle is die HPVLE en LPVLE data saam met die ingeboude regressiefunksie in Aspen Plus[®] gebruik om opgeloste stof BIPs te bepaal. Verteenwoordigende waardes van die HPBDP BIPs is met die hand bepaal.

Die derde doelwit is bereik deur die werksverrigting van die modelle met wisselende opgeloste stof BIPs te evalueer, met ander woorde om die LPVLE BIPs te gebruik om hoë druk data te voorspel, en anders om, soos opgesom in *Tabel i*.

TABEL II: OPSOMMING VAN RK-ASPEN, SR-POLAR EN PC-SAFT OPGELOSTE STOF BIPs WAT GEBRUIK KAN WORD OM LPVLE, HPVLE EN HPBDP DATA TE KORRELEER

Nuwe Eksperimentele data	Opgeloste stof BIPs								
	RK-Aspen			SR-Polar			PC-SAFT		
	LPVLE	HPVLE	HPBDP	LPVLE	HPVLE	HPBDP	LPVLE	HPVLE	HPBDP
LPVLE	✓	✓*	✓*	✓	✗	✗	✓	✗	✗
HPVLE	✗	✓	✓	✗	✓	✓	✓ [‡]	✓ [‡]	✓ [‡]
HPBDP	✓ [†]	✓	✓	✓ [†]	✓	✓	✗	✗	✗

[†] Douppunt gebied slegs vir $w_c^{red} \leq 0.6399$ g/g.

[‡] Vloeistof samestelling slegs by $T = 348$ K.

*Met $k_{b,ij} = 0$.

RK-Aspen was die enigste model wat 'n akkurate voorstelling van elke datastel kon lewer, ook in die komplekse fasegedragsgebiede. SR-Polar se werksverrigting was amper so goed soos dié van RK-Aspen, maar kon nie die LPVLE data so goed voorstel nie. PSRK kan gebruik word om HPBDP en LPVLE data akkuraat voor te stel, maar word nie vir HPVLE data aangeraai nie. PC-SAFT kan LPVLE en HPVLE data redelik voorstel, maar kan nie HPBDP data akkuraat korreleer nie. Die modelle word in volgorde van afname in werksverrigting voorgestel as: RK-Aspen > SR-Polar > PSRK > PC-SAFT. RK-Aspen, in kombinasie met die HPBDP opgeloste stof BIPs, bied die mees akkurate model passing (kwantitatief en kwalitatief) in die komplekse fasegedragsgebied van die HPBDP, HPVLE, en LPVLE data. Oor die algemeen het hierdie proefskrif waardevolle insig gegee tot die rol wat opgeloste stof BIPs speel. Die opgeloste stof interaksies veroorsaak komplekse fase-gedrag en fraksionele probleme. In toekomstige studies moet opgeloste stof interaksies nie geïgnoreer word nie, aangesien dit nie net die ontwerp van proefnemingsaanlegte sal verbeter nie, maar ook prosesse modelle sal verbeter.

ACKNOWLEDGEMENTS

This work is based on the research supported in part by the National Research Foundation of South Africa (Grant specific unique reference number (UID) 103214) and Sasol Technology (Pty) Ltd. The author acknowledges that opinions, findings and conclusions or recommendations expressed in this thesis are that of the author, and that of the sponsors accepts no liability whatsoever in this regard.

Aspen Plus® is a registered trademark of aspen Technology Inc.

The author would like to express her personal gratitude to the following people who have contributed to the completion of this work:

- My supervisor, Prof. C. E. Schwarz, not only for all your valuable guidance and great amount of help to the successful completion of this work, but for allowing me the honour of learning from you and always leaving your door open to me for any issues. Thank you for all your time and help, it truly is appreciated.
- To Sonja Smith, a close friend and honoured colleague for helping me with my Afrikaans abstract.
- To the workshop staff, for always helping to fix an issue when things did not always go according to plan.
- To Mrs. H Botha, for your guidance and expertise with the gas chromatography work.
- To my fellow colleagues and friends without whom the days would have felt unbearably long. Thank you for the sun sessions and motivational talks over coffee when needed.
- To my brothers, Alex and Jason, thank you for being there to cheer me up at times of need and for always understanding when I was unable to attend special moments with you.
- To my parents, Belindie and Johan, who supported me through this time not only emotionally but at times, financially too. Without you this work would not have been possible and for that I will be forever grateful.
- To my husband, Janti Kriel for your unwavering patience, love and support throughout this time. Thank you for not allowing me to give up during times of struggle and always remaining by my side.

NOMENCLATURE & ABBREVIATIONS

List of Symbols

Symbol	Description	Symbol	Description
A	Solvent/CO ₂	M	Molar value
A	Helmholtz energy	M_w	Molecular weight
A	Association site	m	Equation of state parameter
A_1	1 st order Van der Waals interactions	m	Number of carbon atoms in 1-alcohol chain
A_2	2 nd order Van der Waals interactions	m	Mean segment number in the fluid
A_3	3 rd order Van der Waals interactions	N	Number of chemical species
a	Equation of state energy parameter	n	Total moles
B	Solute/1-decanol	n	Number of carbon atoms in n -alkane chain
B	Association site	ΔP	Change in pressure
B_{ii}	Virial coefficient	P	Pressure
b	Equation of state co-volume parameter	$p_{1,i}$	Pure component polar parameter
C	Solute/ n -tetradecane	$p_{2,i}$	Pure component polar parameter
C_i	Carbon chain of length i	$p_{3,i}$	Pure component polar parameter
$C1$	Compressibility of the hard chain fluid	Q	Original Van der Waals surface area
c	Equation of state parameter	Q_i	Quadrupolar moment
$c_{1,i}$	Mathias and Copeman parameter	q	Group area
$c_{2,i}$	Mathias and Copeman parameter	R	Universal gas constant
$c_{3,i}$	Mathias and Copeman parameter	R	Original Van der Waals volume
C_{1-9}	Extended Antoine equation constant	r	Response factor
D	Parameter in L/W consistency test	r	Group volume
d	Equation of state parameter	ΔS^{sat}	Entropy of vaporisation
d	Segment diameter parameter	ΔS	Parameter in L/W consistency test
F	The degrees of freedom	S	Entropy
f	Fugacity of a pure component	T	Temperature
\hat{f}	Fugacity of a component in solution	T_B	Boiling point temperature
G	Gibbs free energy	T_M	Melting point temperature
\bar{G}	Partial molar Gibbs energy	u	Packing fraction
$g_{ii}^{hs}(d_{ii})$	Radial pair distribution function	V	Volume
ΔH^{sat}	Heat of vaporisation	v	Specific molar volume
H	Enthalpy	v	Number of groups (UNIFAC)
I_2	Pure fluid integral of A_2	W	Parameter in L/W consistency test
I_3	Pure fluid integral of A_3	w	Parameter in L/W consistency test
K_i	K-value of solute i	w	Mass fraction/composition

Symbol	Description	Symbol	Description
K_j	K-value of solute j	w_c^{red}	Reduced/CO ₂ free <i>n</i> -tetradecane mass fraction
k_{ij}	Binary interaction parameter	X	Group mole fraction in the liquid
$k_{a,ij}$	Energy binary interaction parameter	X^{Ai}	Mole fraction of molecule i not bonded to site A
$k_{b,ij}$	Co-volume binary interaction parameter	x	Liquid mass/mole fraction
k	Number of critical points for phase rule	x_p	Fraction of dipolar/quadrupolar segment
k	Boltzmann constant	y	Vapour mass/mole fraction
L	Parameter in L/W consistency test	Z_m	Compressibility factor
l_{ij}	Binary interaction parameter	z	Co-ordination number
\bar{M}	Partial molar property		

List of Greek Symbols

Symbol	Description	Symbol	Description
$\alpha(T)$	Equation of state parameter	\emptyset	Critical points for phase rule
α_{ij}	Relative solubility	φ	Fugacity coefficient
γ	Activity coefficient	$\hat{\varphi}$	Fugacity coefficient (species in solution)
Γ	Activity coefficient of a group	Φ	Group molecular volume
$\Gamma(T)$	Integration constant	θ	Group surface fraction
η	Polar parameter	ω	Acentric factor
η	Packing fraction	ρ	Density
μ	Chemical potential	δ	Virial coefficient
μ_i	Dipole moment	τ	Generated function
π	Number of phases	σ	Segment diameter parameter
ψ	Generated function	κ^{AiBj}	Effective association volume
ζ	Reduced segment density	ε/k	Segment energy parameter
Δ^{AB}	Association strength	ε^{AiBj}/k	Association energy parameter

Subscripts

Symbol	Description	Symbol	Description
<i>A</i>	1-decanol/more volatile component	<i>k</i>	Type of group (UNIFAC)
<i>Approx.</i>	Approximate	<i>comp</i>	Component
<i>B</i>	<i>n</i> -tetradecane/less volatile component	<i>min</i>	Minimum
<i>C</i>	Critical point	<i>max</i>	Maximum
<i>A + B</i>	High pressure binary mixture	<i>m</i>	Less soluble component
<i>A + C</i>	High pressure binary mixture	<i>m</i>	Molar
<i>A + B + C</i>	High pressure ternary system	<i>mn/nm</i>	Interaction between group m and n
<i>a</i>	Parameter a	<i>n</i>	More soluble component
<i>b</i>	Parameter b	<i>n</i>	number
<i>c</i>	Component C/ <i>n</i> -alkane	<i>P</i>	Pressure
<i>c</i>	Critical	<i>r</i>	Reduced
<i>c</i>	Combinatorial part	<i>r</i>	Residual part
<i>i</i>	Species/component i	<i>ref</i>	Reference
<i>j</i>	Species/component j	<i>s</i>	Solutes
<i>ij</i>	Interaction between species i and j	<i>std</i>	Standard
<i>k</i>	Number of equilibrium pairs measured		

Superscripts

Symbol	Description	Symbol	Description
<i>assoc</i>	Association contribution	<i>polar</i>	Polar/Quadrupolar contribution
0	Interaction parameter index	<i>R</i>	Residual
1	Interaction parameter index	<i>red</i>	Reduced
2	2 nd order Interaction parameter index	<i>res</i>	Molar residual
<i>Bub</i>	Bubble point / boiling point	<i>sat</i>	Saturation characteristic
<i>chain</i>	Chain contribution	<i>seg</i>	Segment reference system
<i>disp</i>	Dispersive contribution	<i>v</i>	Vapour phase
<i>E</i>	Excess	<i>α</i>	Phase α
<i>hc</i>	Hard-chain reference system	<i>β</i>	Phase β
<i>hs</i>	Hard-sphere fluid system contribution	<i>π</i>	Total number of phases
<i>ig</i>	Ideal gas	*	Effectiveness
<i>l</i>	Liquid phase		

Abbreviations

Symbol	Description	Symbol	Description
$n\text{-C}_{14}$	n -tetradecane	DIPPR	Design Institute for Physical Properties
1-C ₁₀ OH	1-decanol	NIST	National Institute of Standards & Technology
AAD	Average Absolute Deviation	NRF	National Research Foundation
BIPs	Binary Interaction Parameters	TDE	Thermodynamic Data Engine
CEPs	Critical End-points	MSDS	Material Safety Data Sheets
DCEP	Double Critical End-point	PPE	Personal Protective Equipment
LCEP	Lower critical End-point	SANAS	South African National Accreditation System
UCEP	Upper critical End-point	HPBDP	High-pressure bubble- and dew-point
TCP	Tricritical point	HPVLE	High-pressure vapour-liquid equilibria
UID	Unique Reference Number	LPVLE	Low-pressure vapour-liquid equilibria
NDP	Number of Data Points	DDB	Dortmund Databank
DRS	Data Regression System	OF	Objective Function
$l + g$	Liquid-gas hole/phase	SFF	Supercritical fluid fractionation
$l - l$	Liquid-liquid	lg_A	Critical point of component A
l_1	Liquid component 1	lg_B	Critical point of component B
l_2	Liquid component 2	$l = g$	Continuous critical line
EoS	Equations of State	$l_1 = l_2$	Critical line
FID	Flame Ionisation Detector	$l_1 = g$	Critical line
MS	Mass Spectrometry	$l_2 = g$	Critical line
GC	Gas Chromatography	$l_1 = l_2 = g$	Critical endpoints of three-phase equilibria
IS	Internal Standard	$l_1 = g + l_2$	Three-phase critical endpoint locus
PS	Pressurised Solvent	$l_1 = l_2 + g$	Closed loop critical endpoint locus
PT	Pressure transmitter	$l - g$	Liquid-gas
TT	Temperature transmitter	$l_1 l_2 g$	Liquid-liquid-gas three-phase critical surface
Pt-100	Platinum resistance element	llg	Smaller three-phase equilibrium locus
Pv	Vacuum gauge	LLV	Liquid-liquid-vapour
VP	Vacuum pump	VLLE	Vapour-liquid-liquid equilibria
R	ROLSI™ sampler	VLE	Vapour-liquid-equilibria
V	Vapour component	PVT	Pressure-Volume-Temperature
S	Solid component	CSSRL	Constant solute + solute ratio lines

Thermodynamic Model Abbreviations

Symbol	Description
CPA	Cubic Plus Association
LCVM	Linear Combinations of Vidal and Michelsen mixing rules
MHV1	Modified Huron-Vidal mixing rules
MHV2	Modified Huron-Vidal 2 nd order approximation mixing rules
NRTL	Non-Random Two-Liquids
PC-SAFT	Perturbed-Chain Statistical Association Fluid Theory
PC-PSAFT	Perturbed-Chain Polar Statistical Association Fluid Theory
PR	Peng-Robinson
PR-BM	Peng-Robinson-Boston-Mathias
PSRK	Predictive Soave-Redlich-Kwong
RK	Redlich-Kwong
RK-Aspen	Redlich-Kwong-Soave with Mathias mixing rules
RKS-BM	Redlich-Kwong-Soave-Boston-Mathias
SAFT	Statistical Association Fluid Theory
SRK	Soave-Redlich-Kwong
SR-POLAR	Redlich-Kwong-Soave with Schwarzenegger-Renon mixing rules
UNIFAC	Universal Quasi Chemical Functional-group Activity Coefficient
UNIQUAC	Universal Quasi Chemical
vdW	Van der Waals
W-S	Wong-Sandler mixing rules

CONTENTS

DECLARATION	I
ABSTRACT	III
OPSOMMING	V
ACKNOWLEDGEMENTS	VII
NOMENCLATURE & ABBREVIATIONS.....	IX
CHAPTER 1.....	1
INTRODUCTION	1
1.1. PROJECT MOTIVATION	1
1.2. STUDY AIM AND OBJECTIVES	5
1.3. PROJECT SCOPE.....	6
1.4. THESIS OVERVIEW	8
1.5. SIGNIFICANT CONTRIBUTIONS	9
1.6. SCIENTIFIC CONTRIBUTIONS.....	9
CHAPTER 2.....	11
BINARY AND TERNARY PHASE EQUILIBRIA.....	11
2.1. PHASE BEHAVIOUR OF BINARY SUB-SYSTEMS.....	11
2.1.1. <i>Fluid-Modifier Mixtures.....</i>	12
2.1.2. <i>Fluid-Solute Mixtures</i>	14
2.1.3. <i>Phase behaviour Transitions and Trends in Homologous Series of n-alkanes and n-alkanols.....</i>	15
2.1.4. <i>Literature Data for the CO₂ Binary Sub-systems</i>	19
2.1.5. <i>Classification of the CO₂ Binary Sub-systems</i>	23
2.1.6. <i>Literature Data for the 1-alcohol + n-alkane Sub-systems.....</i>	25
2.2. PHASE BEHAVIOUR OF TERNARY SYSTEMS	25
2.2.1. <i>Ternary Phase Diagrams.....</i>	25
2.2.2. <i>Literature Data for CO₂ + 1-decanol + n-tetradecane</i>	31
2.2.3. <i>Closed Liquid-gas Hole in the Three-phase Surface.....</i>	32
2.2.4. <i>Cosolvency Effects.....</i>	34
2.2.5. <i>Closed Isobaric Miscibility Windows</i>	36
2.2.6. <i>Classification of the CO₂ + 1-decanol + n-tetradecane System and Third Binary Sub-system.....</i>	38
2.3. CHAPTER OUTCOMES	41
CHAPTER 3.....	43
HOLISTIC THERMODYNAMIC MODEL SELECTION.....	43
3.1. INDUSTRIAL RELEVANCE OF ASPEN PLUS®	43
3.2. PHASE EQUILIBRIA FUNDAMENTALS	44
3.3. CUBIC EoS PROPERTY METHODS.....	45
3.4. PREDICTIVE PROPERTY METHODS IN ASPEN PLUS®	46
3.4.1. <i>UNIFAC Group Contribution Method</i>	46

3.4.2. EoS- G^E Mixing Rules	48
3.4.3. PSRK and RKSMHV2 Model Predictions of the CO ₂ Binary Sub-Systems	50
3.4.4. Li-Correction for Size-Asymmetric Gas-Alkane Systems	51
3.4.5. PSRK Model	53
3.5. FLEXIBLE PROPERTY METHODS IN ASPEN PLUS®	54
3.5.1. RK-Aspen Model	56
3.5.2. SR-Polar Model	57
3.6. ASSOCIATION EoS PROPERTY METHODS IN ASPEN PLUS®	58
3.6.1. SAFT EoS Framework	58
3.6.2. SAFT Family Developments	59
3.6.3. PC-SAFT Model	61
3.6.3.1. Hard-chain Fluids and Chain Connectivity	62
3.6.3.2. Association Term – 2B Model	63
3.6.3.3. Dispersion Term	64
3.6.3.4. Polar/Quadrupolar Terms	65
3.7. SIMULATION APPROACH	67
3.7.1. Pure Component Parameter Regressions	68
3.7.2. Alpha(T) Parameter Regressions	69
3.7.3. Binary Interaction Parameter Regressions	69
3.8. CHAPTER OUTCOMES	70
CHAPTER 4.....	73
EXPERIMENTAL MATERIALS AND METHODS.....	73
4.1. MEASUREMENT TECHNIQUES.....	73
4.1.1. High-Pressure Phase Equilibria	73
4.1.2. Low-Pressure Phase Equilibria	74
4.2. HPBDP PHASE EQUILIBRIA MEASUREMENTS.....	76
4.2.1. Experimental Setup and Apparatus	76
4.2.2. Experimental Procedure	77
4.3. HPVLE PHASE EQUILIBRIA MEASUREMENTS	77
4.3.1. Experimental Setup and Apparatus	77
4.3.2. Experimental Procedure	78
4.4. LPVLE PHASE EQUILIBRIA MEASUREMENTS	79
4.4.1. Experimental Setup and Apparatus	79
4.4.2. Experimental Procedure	81
4.4.3. Experimental Error Analysis	81
4.5. ACCURACY OF DATA.....	83
4.5.1. Calibration Curves for GC Analysis	83
4.5.2. High-Pressure Experimental Measurements	84

4.5.3. Low-Pressure Experimental Measurements	85
4.6. MATERIALS	85
4.7. CHAPTER OUTCOMES	87
CHAPTER 5.....	89
SUPER- AND NEAR-CRITICAL PHASE EQUILIBRIA OF THE TERNARY SYSTEM CO₂ + 1- DECANOL + N-TETRADECANE	89
5.1. HPBDP RESULTS AND DISCUSSION	89
5.1.1. Verification of Experimental Setup	89
5.1.2. Experimental Results	90
5.1.3. Comparison to CO ₂ Binary Sub-systems	96
5.1.4. Temperature Inversions and Effects	98
5.1.5. Section Outcomes	102
5.2. COMPLEX PHASE BEHAVIOUR	103
5.2.1. Azeotrope and Cosolvency Effects	103
5.2.2. Near-Critical Liquid-gas Hole	107
5.2.3. Closed Isobaric Miscibility Windows	109
5.2.4. Section Outcomes	110
5.3. HPVLE RESULTS AND DISCUSSION	111
5.3.1. Verification of Experimental Setup	111
5.3.2. Experimental Results	113
5.3.3. Relative Solubility of the Ternary System	117
5.3.4. Section Outcomes	119
5.4. CLASSIFICATION OF THE TERNARY SYSTEM	120
5.4.1. Transition Sequence of Fluid Phase Behaviour	120
5.4.2. Binary Sub-systems and the Ternary System	120
5.4.3. Section Outcomes	121
5.5. CHAPTER OUTCOMES	122
CHAPTER 6.....	123
LOW PRESSURE PHASE EQUILIBRIA OF 1-ALCOHOL + N-ALKANE BINARY SYSTEMS	123
6.1. VERIFICATION OF EXPERIMENTAL SETUP	124
6.1.1. Pure Component Vapour Pressure Data	124
6.1.2. Thermodynamic Consistency Tests	125
6.1.3. Reproducibility Tests	126
6.2. LPVLE RESULTS AND DISCUSSION	129
6.2.1. Experimental Difficulties	129
6.2.2. Positive Azeotropy	135
6.2.3. Phase Behaviour Classification	136
6.3. CHAPTER OUTCOMES	136

CHAPTER 7.....	139
PURE COMPONENT & BINARY INTERACTION PARAMETER ESTIMATION	139
7.1. PURE COMPONENT PARAMETERS	139
7.1.1. <i>Critical Properties and Acentric Factors</i>	139
7.1.2. <i>Saturated Vapour Pressure Data</i>	140
7.1.3. <i>PSRK</i>	142
7.1.4. <i>RK-Aspen and SR-Polar</i>	143
7.1.5. <i>Alpha(T) Parameter</i>	144
7.1.6. <i>PC-SAFT</i>	145
7.2. BINARY INTERACTION PARAMETERS	146
7.2.1. <i>Group + Group Parameters</i>	146
7.2.2. <i>Solute + Solvent</i>	150
7.2.3. <i>Solute + Solute</i>	151
7.2.3.1. <i>Regressions with Bubble- and Dew-point Data</i>	152
7.2.3.2. <i>Regressions with VLE Data</i>	156
7.3. CHAPTER OUTCOMES	157
CHAPTER 8.....	159
THERMODYNAMIC MODELLING USING ASPEN PLUS®	159
8.1. HIGH-PRESSURE PHASE BEHAVIOUR RESULTS	159
8.1.1. <i>RK-Aspen</i>	160
8.1.2. <i>SR-Polar</i>	169
8.1.3. <i>PC-SAFT</i>	177
8.1.4. <i>PSRK</i>	185
8.2. LOW-PRESSURE PHASE BEHAVIOUR RESULTS.....	190
8.2.1. <i>RK-Aspen</i>	190
8.2.2. <i>SR-Polar</i>	192
8.2.3. <i>PC-SAFT</i>	193
8.2.4. <i>PSRK</i>	195
8.3. OPTIMUM THERMODYNAMIC MODEL & SOLUTE + SOLUTE BIPs	196
8.4. CHAPTER OUTCOMES	205
CHAPTER 9.....	209
CONCLUSIONS AND RECOMMENDATIONS.....	209
9.1. PART 1: ACHIEVEMENT OF KEY OBJECTIVES 1 AND 2	210
9.2. PART 2: ACHIEVEMENT OF KEY OBJECTIVE 3	213
9.3. RECOMMENDATIONS FOR FUTURE WORK	214
CHAPTER 10.....	217
REFERENCES	217
CHAPTER 11.....	235
APPENDICES.....	235

A. SUPPLEMENTARY LITERATURE DATA	II
<i>A1. High-pressure Measurement Techniques</i>	II
<i>A2. Low-pressure Measurement Techniques</i>	V
<i>A3. Thermodynamic Consistency Tests</i>	VII
B. DETAILED EXPERIMENTAL PROCEDURES	XII
<i>B1. HPBDP Experimental Procedure</i>	XII
<i>B2. HPVLE Experimental Procedure</i>	XVII
<i>B3. LPVLE Experimental Procedure</i>	XL
C. CALIBRATION DATA AND CERTIFICATES	XLII
<i>C1. High-pressure Calibrations</i>	XLIII
<i>C2. Barnett Pressure Calibration</i>	XLVII
<i>C3. HPBDP Large Cell Pt-100 Calibration</i>	XLIX
<i>C4. LPVLE Pt-100 Calibrations</i>	L
<i>C5. Low-Pressure Calibration</i>	LIII
D. PRECAUTIONARY MEASURES	LIV
E. RAW EXPERIMENTAL RESULTS	LVI
<i>E1. HPBDP experimental data</i>	LVI
<i>E2. HPVLE experimental data</i>	LIX
<i>E3. LPVLE experimental data</i>	LXI
F. TERNARY PHASE DIAGRAMS (HPBDP)	LXX
G. GAS CHROMATOGRAPHY CALIBRATION CURVES	LXXVI
H. SUPPLEMENTARY MODELLING RESULTS	LXXXII

Chapter 1

INTRODUCTION

The design of separation processes usually requires thermodynamic data, more specifically, phase equilibria. As more than 40% of the cost in industrial processes are related to their specific separation units, the need for accurate thermodynamics is imperative [1]. When commencing with the design of a separation unit it is often questioned whether sufficient data and/or suitable models are available for the specific process. The answer to this question varies with respect to the availability of suitable models in process simulators. Fortunately, several commercial simulators, e.g. Aspen Plus®, have a wide spectrum of thermodynamic models to choose from [2]. In CO₂ systems containing a 1-alcohol with $m \leq 10$ and a n -alkane with $n \leq 16$, where m and n represent the number of carbon atoms in the *alky*-chains of the 1-alcohol and n -alkane, respectively, complex phase behaviour regions occur near the critical point of the solvent [3]. These complexities often cause predictive and thermodynamic models to fail for such systems. Experimental phase equilibria data can contribute to bridging this gap and aid in the fundamental understanding of the distinct solute + solute binary interactions that occur between these large, complex molecules when mixed with a third supercritical species.

The aim of this chapter is to introduce the topic of this thesis, define the binary sub-systems and ternary system to be measured, formulate the aim and key objectives and provide an outline for the project.

1.1. PROJECT MOTIVATION

Alcohols in the range $C_8 - C_{20}$ are commonly referred to as detergent range alcohols due to their use in the manufacturing of detergents [4]. These detergent alcohols are further used in the chemical industry for the manufacturing of surfactants and for the preparation of plasticizers [5], [6]. The Oxo process is generally applied as a downstream process in the petroleum industry to synthesize alcohols in the range $C_3 - C_{20}$. At times, the feedstock will be obtained directly from a synthetic fuel manufacturing plant. The feedstock is predominantly made up of olefins but also n -alkanes and small amounts of oxygenates [7]. On an industrial scale, the n -alkanes present in the feedstock do not take part in the alcohol production process. Therefore, the process is often incomplete, resulting in a mixture of unconverted $C_{10} - C_{15}$ n -alkanes and isomeric alcohols [6], [8]. In order for the 1-alcohol to be effective in other

processes, e.g. for the production of alcohol ethoxylate surfactants, the residual *n*-alkanes will need to be removed from the alcohol using a suitable post-production separation process [9].

The process of separating the C_{10} - C_{15} detergent range 1-alcohols and *n*-alkanes is complicated by crossover boiling (T_B) and melting points (T_M) as shown in *Table 1-1*. Experimental data and predictive process models, tested at various operating conditions, have shown that supercritical fluid fractionation (SFF) is a feasible process for the separation of these similar boiling point and melting point components [4], [10]–[19]. SFF applications involve the separation of components exhibiting different phase behaviour after a supercritical solvent is added [13]. The solvent is at conditions exceeding its critical point and will preferentially dissolve the *n*-alkane, above the 1-alcohol.

TABLE 1- 1: BOILING AND MELTING POINTS OF 1-ALCOHOLS AND N-ALKANES WITHIN THE RANGE C_{10} – C_{15} [20]–[23].

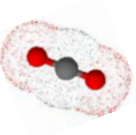
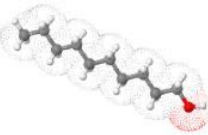
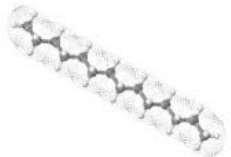
Carbon number	<i>1-alcohol</i>		<i>n-alkane</i>	
	T_B (K)	T_M (K)	T_B (K)	T_M (K)
C_{10}	504	280	447	243
C_{11}	516	292	469	247
C_{12}	532	297	489	264
C_{13}	554	305	509	267
C_{14}	562	313	526	279
C_{15}	583	317	543	289

The unique solvent characteristics of supercritical fluids were discovered over 100 years ago, after common gases such as CO_2 and ethylene were pressurised and found to dissolve complex organic compounds [24]. Today, the most well-known example is the commercial use of supercritical fluids in the coffee industry [24], [25]. Here, supercritical CO_2 is used in the decaffeination process of coffee, successfully replacing the organic solvent, dichloromethane, and avoiding the release of volatile organic compounds. Increased research efforts from both academic and industrial sectors have shown that supercritical CO_2 can further be applied in old and new applications, like extraction, dying, cleaning, polymer processing and waste water treatment, to name only a few [26]–[28]. The use of CO_2 in other industrial processes such as polymerization and organic synthesis has not yet been fully developed but shows potential. Thus, improvements on existing separation processes will continue for years to come. The critical properties of CO_2 , $T_c = 304.2$ K and $P_c = 7.38$ MPa, make it ideal for separating detergent range alkanes and alcohols [20]. Furthermore, CO_2 is non-toxic, non-flammable, inert and easy to acquire. It is for these reasons that CO_2 is the selected solvent for use in this study.

Supercritical CO_2 has shown success in separating detergent range alcohols and *n*-alkanes, amongst others 1-decanol and *n*-dodecane [13], [16], [19]. The phase behaviour of the ternary CO_2 + 1-decanol + *n*-dodecane system revealed significant interactions between the detergent range 1-alcohol and *n*-alkane in the presence of supercritical CO_2 . Another study conducted on the separation of 1-dodecanol and *n*-tetradecane in the presence of supercritical CO_2 shows similar interactions between the 1-alcohol and

n-alkane [11], [17]. In both studies, components with close boiling points were investigated with the *n*-alkane having a slightly lower normal boiling point than the 1-alcohol. To maintain the close boiling point perspective this project studies the binary interactions between 1-decanol and *n*-tetradecane in the presence of supercritical CO₂. Here, in this system, the 1-alcohol is more volatile than the *n*-alkane but at the same time, the 1-alcohol is less soluble in CO₂ than the *n*-alkane [17], [18]. The physical properties of the components used in this work are presented in *Table 1-2*.

TABLE 1- 2: PHYSICAL PROPERTIES OF CO₂, 1-DECANOL AND *N*-TETRADECANE [20]–[23]. THE 3D STRUCTURES WERE DRAWN USING CHEMSKETCH [29].

<i>Compound</i>	<i>CO₂</i>	<i>1-decanol</i>	<i>n-tetradecane</i>
3D Structure			
Carbon number	C	C ₁₀	C ₁₄
Molecular Weight (g/mol)	44.01	158.28	193.39
Normal T_B (K)	194.7 [‡]	504	526
Normal T_M (K)	194.7 [†]	280	279
Polarity	Quadrupolar	Slightly Polar	Non-polar
Density (kg/m ³)	1.98	829.7	762.8
Critical Temperature (K)	304.2	688	693
Critical Pressure (bar)	7.38	23.1	15.7

[†] At 1 atm, gas deposits directly to a solid at $T < 194.7$ K

[‡] At 1 atm, the solid sublimates directly to a gas at $T > 194.7$ K

The proposed SFF process for separating the close-boiling detergent range 1-alcohol from its corresponding *n*-alkane is shown in *Figure 1-1* [12]. The approach involves a feed and solvent stream to be sent to a fractionation column, S-101. Two phases will then exit S-101, one a liquid product stream at the bottom (with residual 1-alcohol) and the second the loaded supercritical fluid at the top of S-101. The supercritical fluid is sent to a pressure reducer, PR-101, before separating the solvent from the accompanying extract (mainly *n*-alkanes) in a separator, S-102. Before recycling the solvent back to S-101 it will first be condensed in E-101, compressed in C-101 and heated in E-102. A history on the development of supercritical fluid technology and fundamental studies on the application of supercritical fluids can be found in various publications [1], [24], [26]–[28], [30], [31].

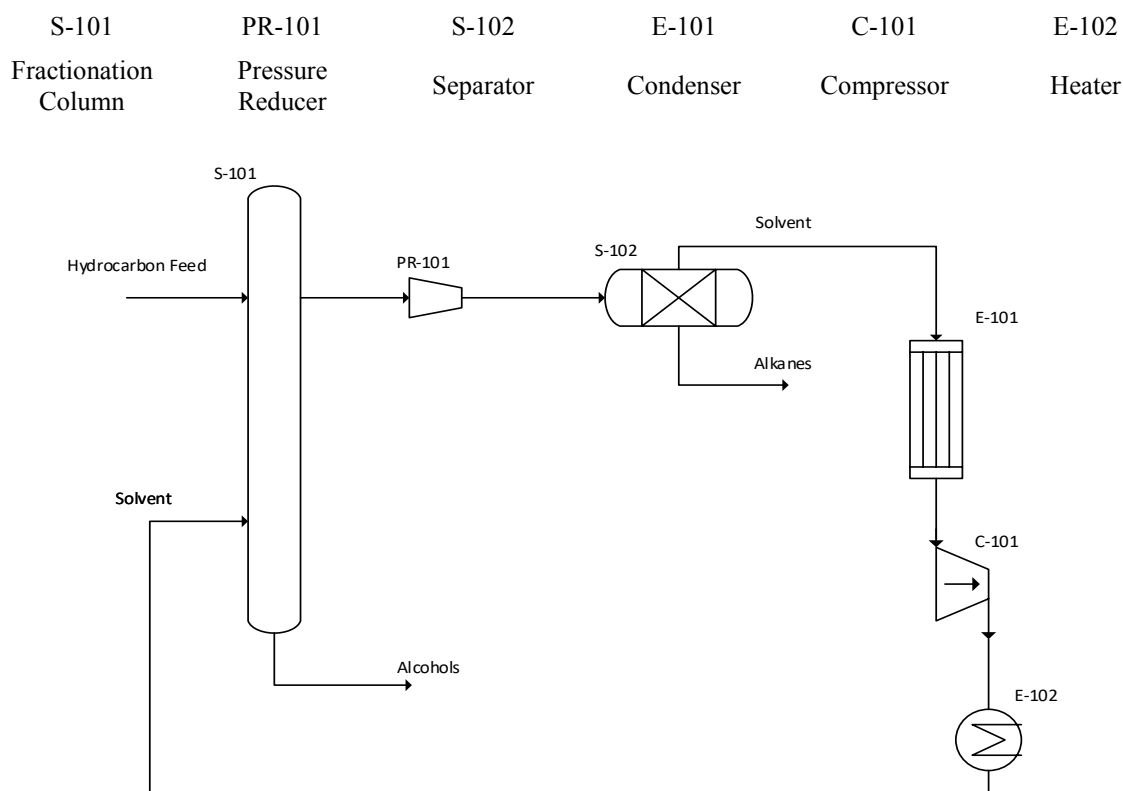


FIGURE 1- 1: SCHEMATIC OF PROPOSED SFF PROCESS. ADAPTED AND REDRAWN USING ZAMUDIO [12], [18].

In SFF applications, the solutes usually consist of larger, more complex molecules than the solvent. Complex multiphase equilibria can occur in these asymmetric mixtures, especially close to the critical point of the solvent [3], [32]–[39]. These complexities occur due to distinct solute + solute interactions in the multicomponent mixtures which result in, amongst others, cosolvency effects and liquid-liquid-gas (l_1l_2g) three-phase regions. Patton et al. [40] first observed unexpected fluid multiphase behaviour for the ternary system CO_2 + 1-decanol + n -tetradecane when they found a two-phase liquid-gas (l - g) hole in the l_1l_2g three-phase surface. This phenomenon was later confirmed by extensive experimental investigations on related ternary systems comprising of CO_2 as the near-critical solvent and 1-alcohols + n -alkanes as the two heavier solutes [32], [38]. The systems were investigated to formulate a mechanism to distinguish what type of three-phase fluid behaviour can be expected. In the past, the complex phase behaviour regions have been avoided due to difficulties in process control. Thus, there remains a lack of fundamental understanding of the global phase behaviour of the systems. With the correct insight into the phase behaviour of these multicomponent systems the phenomena can be better understood, applied and controlled in the design of separation processes.

Thermodynamic property models describe the relationship between thermodynamic properties and thus enable mathematical representations of phase diagrams. To use the knowledge of phase behaviour in this manner, it is important to correlate the phase information in the most accurate thermodynamic models available. Chemical engineers regularly use equations of state (EoS) to predict the pressure, volume and temperature data for real fluid systems [41]–[45]. The application of the van der Waals

(vdW) mixing rules to define the interaction parameters are only applicable to mildly non-ideal systems, which is not the case for the current study [46]. Several *EoS* have been developed as an expansion on the vdW *EoS* to take into consideration mixture complexities. The most popular *EoS*s, especially in the petrochemical industry, include (i) Peng-Robinson (PR) [47] and (ii) Redlich-Kwong (RK) [48] which forms the basis of (iii) the Soave-Redlich-Kwong (SRK) *EoS* [49]. Although both the SRK and PR equations provide highly accurate phase equilibria data for hydrocarbons, the vdW one-fluid mixing rules restrict their use for correlating the interested system. However, these *EoS* form the basis of various flexible and predictive mixing rules as well as statistical thermodynamic models that have become the focus point in recent years for holistic modelling of complex multiphase equilibria [50]. Several of these thermodynamic models are found in commercial simulators, e.g. Aspen Plus®. They provide a way for fast and simple calculations of complex multiphase systems and are becoming increasingly popular compared to in-house developed programs [51]. The reason for selecting models available within Aspen Plus® is to ultimately allow for the development of a process model within a process simulator, like the work done by Zamudio et al.[12].

1.2. STUDY AIM AND OBJECTIVES

The CO₂ + 1-decanol + *n*-tetradecane system is an important model system for the separation of detergent range *n*-alkanes and 1-alcohols; however, obtaining new equilibria data for the complex ternary system can be time consuming and costly.

*The aim of this study is to obtain a fundamental understanding of the solute + solute interactions in the CO₂ + 1-decanol + *n*-tetradecane ternary system firstly, through the generation of phase equilibria data and secondly, through the evaluation of thermodynamic models, with solute + solute BIPs incorporated into their algorithm.* To achieve this aim, the following key objectives need to be met:

1. Study the high-pressure phase equilibria of the CO₂ + 1-decanol + *n*-tetradecane ternary system:
 - 1.1. Measure bubble- and dew-point data for six (1-decanol + *n*-tetradecane) mixtures in supercritical CO₂.
 - 1.2. Measure vapour-liquid equilibria (VLE) data for four (1-decanol + *n*-tetradecane) mixtures in supercritical CO₂.
 - 1.3. Characterise the complex phase behaviour of the ternary system.
 - 1.4. Assess the ability of CO₂ to separate the solutes, 1-decanol and *n*-tetradecane.
2. Study the low-pressure phase equilibria of the 1-decanol + *n*-tetradecane binary system:
 - 2.1. Measure isobaric VLE data of the 1-decanol + *n*-tetradecane binary system.
 - 2.2. Measure isobaric VLE data of four pertinent binary systems with the same 4 carbon number difference as the 1-decanol + *n*-tetradecane system.
 - 2.3. Characterise the phase behaviour of the 1-decanol + *n*-tetradecane binary system.

3. Study the thermodynamic modelling of the $\text{CO}_2 + 1\text{-decanol} + n\text{-tetradecane}$ ternary system and the $1\text{-decanol} + n\text{-tetradecane}$ binary system:
 - 3.1. Select at least 4 suitable thermodynamic models within a commercial process simulator that can be used to correlate the ternary and binary systems.
 - 3.2. Generate new solute + solute BIPs using the new HPBDP, HPVLE and LPVLE experimental data.
 - 3.3. Identify whether high-pressure solute + solute BIPs can be used to improve the modelling of low-pressure data and vice versa.
 - 3.4. Establish the solute + solute parameter set to be used by each of the thermodynamic models that will result in the overall best representation of the measured equilibrium data.
 - 3.5. Identify the best suited thermodynamic model for representing the experimental HPBDP, HPVLE and LPVLE data.

1.3. PROJECT SCOPE

The predominant outcome of this research project is to define and understand the interactions between 1-decanol and n -tetradecane and inevitably improve the thermodynamic modelling of the complex $\text{CO}_2 + 1\text{-decanol} + n\text{-tetradecane}$ ternary system. In Chapter 5, the present study provides *new high-pressure bubble- and dew-point (HPBDP) ternary data and inferred critical end-point data* to characterise the complex l_1l_2g three-phase behaviour. To date, no classification on the type of phase behaviour of the $\text{CO}_2 + 1\text{-decanol} + n\text{-tetradecane}$ ternary system, has been made. Therefore, in Chapter 2, the binary classifications of Van Konynenburg and Scott [52], [53] were adapted to ternary systems to describe the observed fluid phase behaviour. The VLE data of the $\text{CO}_2 + 1\text{-decanol} + n\text{-tetradecane}$ system can be used to describe and solve problems regarding the design analysis and control of supercritical fluid processes. Thus, *new high-pressure vapour-liquid-equilibrium (HPVLE) data of the ternary system* are provided on ternary phase diagrams, alongside the HPBDP data (see Chapter 5). The slope of the HPVLE tie lines are used to assess the ability of supercritical CO_2 to separate the two solutes, 1-decanol and n -tetradecane. The HPBDP and HPVLE experiments were conducted within the temperature range (308 K – 358 K), pressure range (6 MPa – 27 MPa) and solute composition range (0.015 g/g – 0.7 g/g) at which SFF applications take place.

In addition, non-ideal phase behaviour might be illustrated by systems containing both a polar and non-polar component. Based on this and the complex phase behaviour phenomena in the ternary system, a systematic and extensive experimental study of binary 1-alcohol + n -alkane VLE data has been carried out in Chapter 6. The *low-pressure vapour-liquid-equilibrium (LPVLE) phase behaviour of the (i) 1-pentanol + n -nonane, (ii) 1-hexanol + n -decane, (iii) 1-heptanol + n -undecane, (iv) 1-octanol + n -dodecane and (v) 1-decanol + n -tetradecane binary systems were measured* at a sub-atmospheric pressure of 40 kPa.

Obtaining binary and ternary phase equilibrium data demands time and resources that are not always readily available. The development of computerised simulation software aided in this requirement, making robust and industrial relevant thermodynamic models valuable. In Chapter 3, the property methods available within the commercial software program, Aspen Plus®, are investigated to select a minimum of 4 suitable models. The approach for generating high- and low-pressure solute + solute BIPs are discussed in Chapter 7, followed by *an assessment of the ability of BIPs to improve the model correlations of the new HPBDP, HPVLE and LPVLE data* in Chapter 8. Finally, the aim of this study is addressed in Chapter 9, i.e., what the influence of the solute + solute interactions are on the separation of 1-decanol and *n*-tetradecane and how this understanding can be used to improve pilot plant experiments. Lastly, the conclusions of this research project are summarised and the model system that resulted in the most accurate representation of the thermodynamic properties of the CO₂ + 1-decanol + *n*-tetradecane system are discussed that will inevitably be used to improve future process models.

1.4. THESIS OVERVIEW

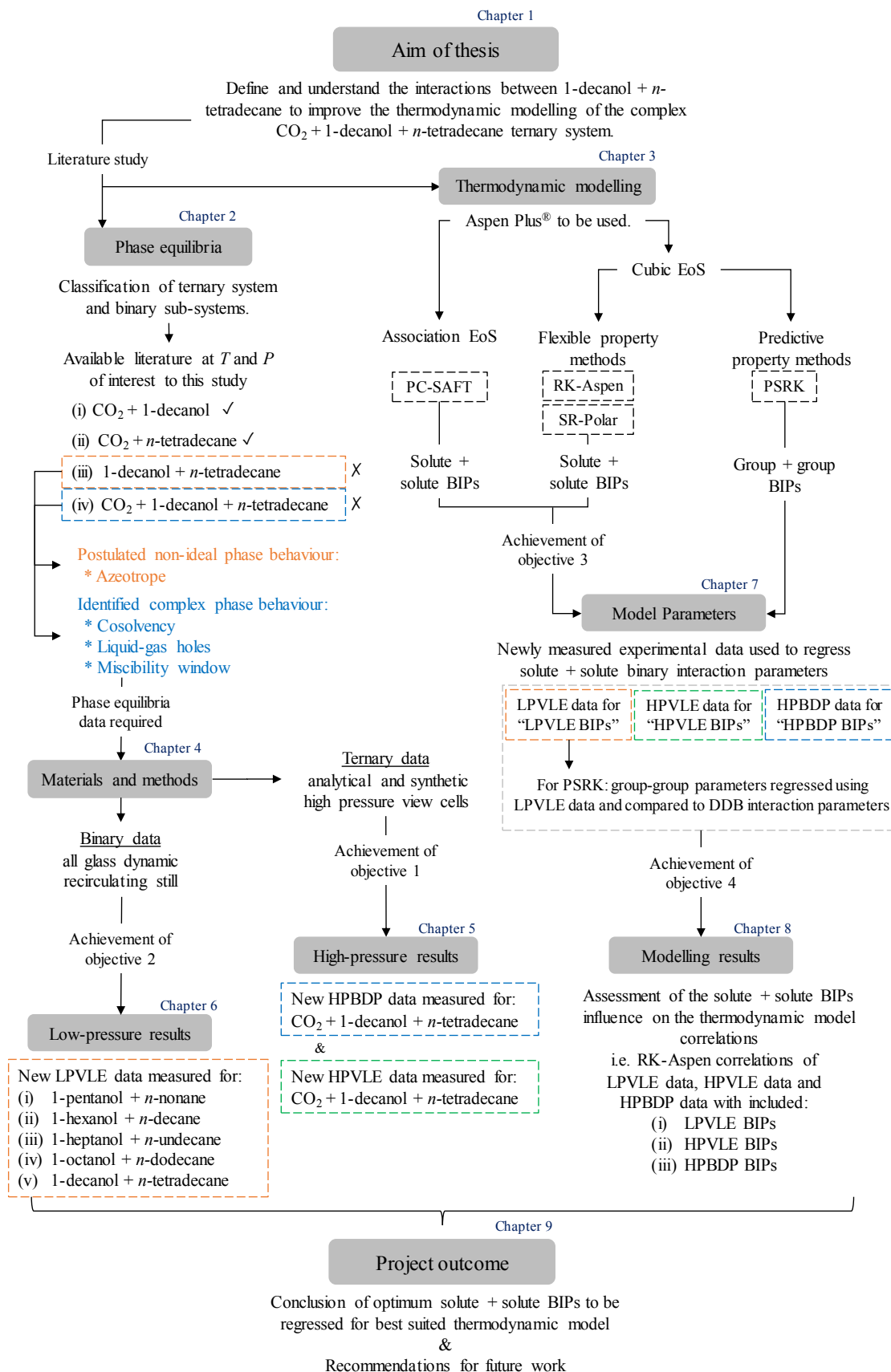


FIGURE 1- 2: FLOW DIAGRAM PRESENTING AN OVERVIEW OF THIS THESIS AND THE ACHIEVEMENT OF EACH KEY OBJECTIVE.

1.5. SIGNIFICANT CONTRIBUTIONS

This research leads to the following significant scientific contributions:

- (i) HPBDP data of six (1-decanol + *n*-tetradecane) mixtures in supercritical CO₂ that are used to classify the ternary system and link the *l-g* hole and miscibility window to cosolvency effects.
- (ii) HPVLE data of four CO₂ + 1-decanol + *n*-tetradecane mixtures that were used to construct tie lines on ternary phase diagrams and assess the ability of supercritical CO₂ to separate the two solutes, 1-decanol and *n*-tetradecane.
- (iii) LPVLE data of five (1-alcohol + *n*-alkane) binary systems at sub-atmospheric conditions.
- (iv) Solute + solute BIPs obtained for three thermodynamic models using the three different experimental data sets (HPBDP, HPVLE and LPVLE). The thermodynamic models provide an outcome for the best approach to quantifying solute + solute interactions.
- (v) Assessing the capabilities of one purely predictive thermodynamic model to capture the phase behaviour of the CO₂ + 1-decanol + *n*-tetradecane mixtures.

1.6. SCIENTIFIC CONTRIBUTIONS

The work presented in this thesis contributed to the following **publication**:

M. Ferreira and C.E. Schwarz, Super- and near-critical fluid phase behaviour and phenomena of the ternary system CO₂ + 1-decanol + *n*-tetradecane, *The Journal of Chemical Thermodynamics*. 111 (2017) 88-99.

The work presented in this thesis contributed to the following papers **submitted for publication**:

- (i) M. Ferreira and C.E. Schwarz, Low-pressure VLE measurements and thermodynamic modelling, with PSRK and NRTL, of binary 1-alcohol + *n*-alkane systems, *The Journal of Chemical & Engineering Data*, submitted 1 August 2018, manuscript reference number: je-2018-006802.
- (ii) M. Ferreira and C.E. Schwarz, High-pressure VLE measurements and PSRK modelling of the complex CO₂ + 1-decanol + *n*-tetradecane ternary system, *The Journal of Supercritical Fluids*, to be submitted 7 September 2018, manuscript reference number: SUPFLU_2018_502.

The work presented in this thesis contributed to the following paper in **preparation for publication**:

M. Ferreira and C.E. Schwarz, Thermodynamic modelling of the CO₂ + 1-decanol + *n*-tetradecane system with RK-Aspen, SR-Polar and PC-SAFT in Aspen Plus[®], *Fluid Phase Equilibria*, to be submitted November 2018

The work presented in this thesis contributed to the following conferences:

- (i) M. Ferreira and C.E. Schwarz, Process modelling of the phase behaviour of the CO₂ + 1-decanol + *n*-tetradecane systems, *Poster presentation* at the 15th European Meeting on Supercritical Fluids, Essen, Germany (May 2016).
- (ii) C.E. Schwarz, S.A.M. Smith, M. Ferreira, S.P. Nortjé, High pressure bubble- and dew-point measurements for ternary solute + supercritical solvent mixtures, *Oral presentation* at the 24th IUPAC International Conference on Chemical Thermodynamics, Guilin, China (August 2016).
- (iii) M. Ferreira and C.E. Schwarz, High-pressure phase equilibria of the ternary system CO₂ + 1-decanol + *n*-tetradecane, *Oral presentation* at the 16th European Meeting on Supercritical Fluids, Lisbon, Portugal (April 2017).
- (iv) M. Ferreira and C.E. Schwarz, Obtaining solute + solute binary interaction parameters from different sources for the ternary system CO₂ + 1-decanol + *n*-tetradecane, *Oral presentation* at the 29th European Symposium on Applied Thermodynamics, Bucharest, Romania (May 2017).
- (v) M. Ferreira and C. E. Schwarz, Phase Equilibria and Thermodynamic Modelling of the Ternary System CO₂ + 1-decanol + *n*-tetradecane, *Oral presentation* at the 10th World Congress of Chemical Engineering, Spain, Barcelona (October 2017).

Chapter 2

BINARY AND TERNARY PHASE EQUILIBRIA

This chapter introduces the first part of this thesis, which is devoted to the phase behaviour characteristics of the ternary system and its three binary sub-systems. The solubility behaviour of a solute in supercritical CO₂ is strongly affected when a second low-volatile component is added [54]. Therefore, investigations of the binary and ternary phase behaviour are of considerable interest to understand the thermodynamic properties of processing with supercritical CO₂.

The aim of this chapter is not to review all aspects of binary and ternary phase behaviour, but to provide a critical analysis of the phase behaviour types, trends, transitions and classes relevant to the work done in this study.

First, a systematic study on the phase behaviour of the three binary sub-systems: CO₂ + 1-decanol, CO₂ + *n*-tetradecane and 1-decanol + *n*-tetradecane is conducted in this chapter (which includes a full literature review of available binary data). The study will aid in the understanding of the solute + solvent and solute + solute interactions taking place within the ternary system. The unexpected phenomena of the CO₂ + 1-decanol + *n*-tetradecane system cannot directly be predicted considering only the binary sub-systems. Therefore, in addition, an extensive literature study is also conducted for the ternary system. From this knowledge, the thermodynamic phenomena expected in this ternary system at near- and supercritical conditions are characterised. In so doing, the correct thermodynamic models can be developed and used to calculate the fluid phase equilibria of the interested system. The chapter will close with a discussion of the research gaps in open literature for the ternary system CO₂ + 1-decanol + *n*-tetradecane and how each will be addressed throughout this work.

2.1. PHASE BEHAVIOUR OF BINARY SUB-SYSTEMS

The phase behaviour of pure component and binary mixtures are characterized by the generation of points and lines. These include:

- (i) The location of the three-phase l_1l_2g equilibria.
- (ii) The number and kind of critical endpoints (CEPs).
- (iii) The critical lines occurring.

Furthermore, binary data is generally studied as it is less complex to measure than ternary data. This is why binary systems have been widely studied over the last several decades to identify possible means of separation [55]. Van Konynenburg and Scott [52] classified binary mixtures throughout the entire pressure-temperature-composition (P - T - w_s) range. It is therefore convenient to use their classification to describe the fluid phase behaviour of the binary sub-systems of importance to this study.

The classification can be summarised into six main types of phase behaviour, each dependent on the components in the mixture (see *Figure 2-1*). Here, ‘main types’ simply refers to those that have been proven with experimental evidence. In fluid-modifier mixtures a solute is added to slightly modify the solvents solvation characteristics [56]. In fluid-solute mixtures the solvent is used to dissolve the solute in the mixture (supercritical separation processes). Based on this, the 1-decanol + n -tetradecane system will exhibit phase behaviour of a fluid-modifier mixture and the CO_2 binary sub-systems that of a fluid-solute mixture.

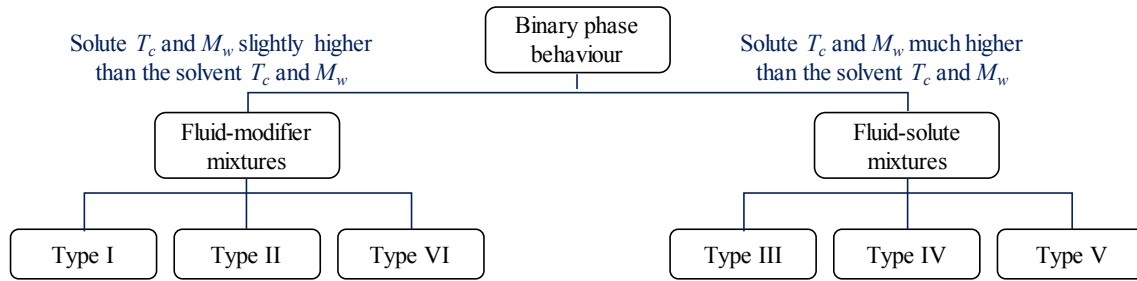


FIGURE 2- 1: VAN KONYNENBURG AND SCOTT [52] CLASSIFICATION SYSTEM OF BINARY PHASE BEHAVIOUR. ADAPTED AND REDRAWN USING ZAMUDIO [18].

2.1.1. FLUID-MODIFIER MIXTURES

Figure 2-2 shows the pressure-temperature (P - T) projections containing all the topological information required for (a) Type I, (b) Type II and (c) Type VI fluid phase behaviour, respectively.

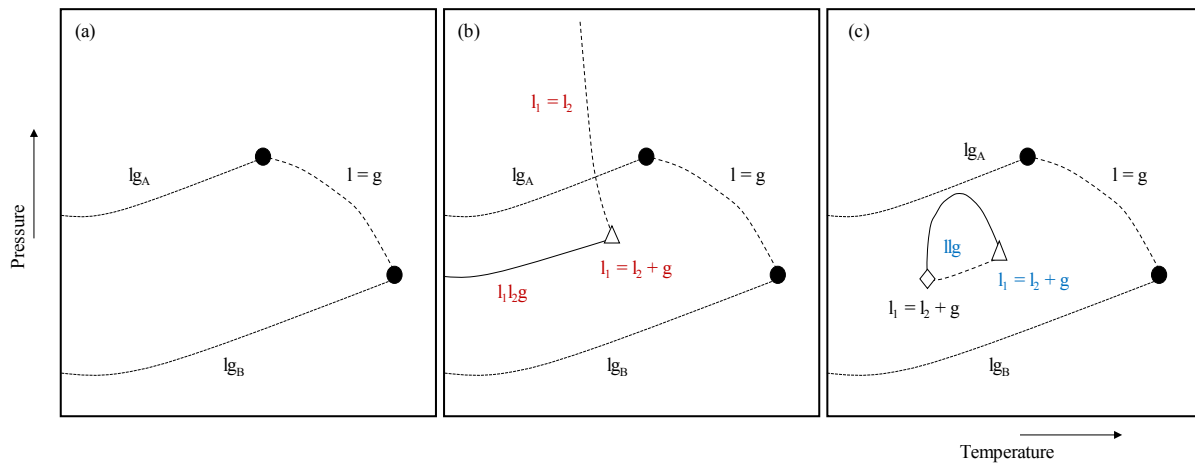


FIGURE 2- 2: (A) TYPE I; (B) TYPE II; AND (C) TYPE VI FLUID PHASE BEHAVIOUR FOR BINARY SYSTEMS PER THE VAN KONYNENBURG AND SCOTT CLASSIFICATION [52], [53]. ● PURE COMPONENT CRITICAL POINT; ◇ LCEP; Δ UCEPS. ADAPTED AND REDRAWN USING PETERS AND GAUTER [34].

The characteristics of each Type are discussed briefly per the classification by Van Konynenburg and Scott [52], [53]. Detailed discussions are available in literature elsewhere [34], [36], [37], [57], [58].

Type I fluid phase behaviour is identified in systems exhibiting:

- (i) Similar molecular size or diameters
- (ii) Similar interaction strengths
- (iii) Critical properties of comparable magnitude

$l = g$	Continuous critical line connecting the critical points of the pure components (lg_A and lg_B)
---------	--

Type II fluid phase behaviour is identified in systems exhibiting:

- (i) Partial miscibility at subcritical temperatures
- (ii) Non-ideal mixtures
- (iii) Components with similar sized molecules (solutes)

$l_1 l_2 g$	Three-phase equilibrium locus (at lower temperatures)
$l = g$	Continuous critical line connecting the critical points of the pure components (lg_A and lg_B)
$l_1 = l_2 + g$	Upper critical endpoint (UCEP) of the $l_1 l_2 g$ locus (the two liquid phases are critical in the presence of a gaseous phase) – two liquid phases are formed from one liquid phase
$l_1 = l_2$	Critical line at lower temperatures and pressures, which merges with the UCEP of the $l_1 l_2 g$ locus

Type VI fluid phase behaviour is identified in systems exhibiting:

- (i) The so-called closed-loop $l_1 = l_2$ immiscibility region
- (ii) Non-ideal mixtures
- (iii) Three-phase region bounded by two CEPs of the same nature

$l_1 = l_2 + g$	Lower critical endpoint (LCEP) of the llg locus at lower temperatures (the two liquid phases are critical in the presence of a gaseous phase)
$l_1 = l_2 + g$	UCEP of the llg locus at higher temperatures
llg	Smaller three-phase equilibrium locus connecting LCEP and DCEP to form three-phase region
$l = g$	Continuous critical line connecting the critical points of the pure components (lg_A and lg_B)

2.1.2. FLUID-SOLUTE MIXTURES

Figure 2-3 shows the P - T projections containing all the topological information required for (a) Type III, (b) Type IV and (c) Type V fluid phase behaviour, respectively.

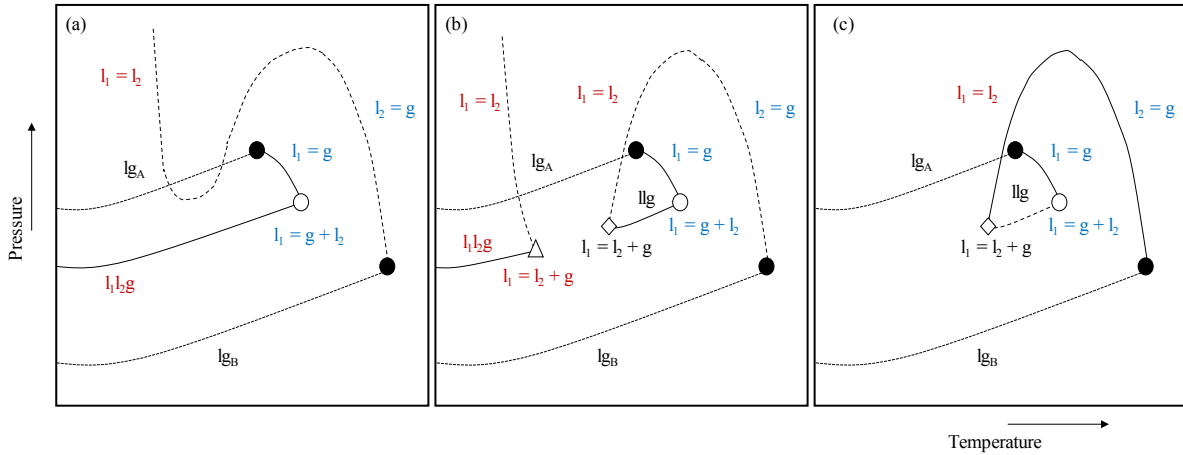


FIGURE 2- 3: (A) TYPE III; (B) TYPE IV; AND (C) TYPE V FLUID PHASE BEHAVIOUR FOR BINARY SYSTEMS PER THE VAN KONYNENBURG AND SCOTT CLASSIFICATION [52], [53]. • PURE COMPONENT CRITICAL POINT; Δ UCEP OF L_1L_2G ; \diamond LCEP OF LLG ; \circ UCEP OF LLG . ADAPTED AND REDRAWN USING PETERS AND GAUTER [34].

The characteristics of each Type are discussed briefly per the classification by Van Konynenburg and Scott [52], [53]. Detailed discussions are available in literature elsewhere [34], [36], [37], [57], [58].

Type III fluid phase behaviour is identified in systems exhibiting:

- (i) Liquid-liquid immiscibility near T_C of more volatile solute (a decrease in the components mutual solubility)
- (ii) Non-ideal liquid mixtures at high temperatures and pressures
- (iii) Components with different sized molecules

l_1l_2g	Three-phase equilibrium locus (at lower temperatures)
$l_1 = l_2$	Critical line shifts to higher temperatures and pressures
$l_2 = g$	Critical line changed in nature from $l_1 = l_2$ when moving from high pressure to low pressure (merges with the critical point of the pure component (lg_B) with the highest temperature)
$l_1 = g + l_2$	UCEP terminating the l_1l_2g locus (the liquid phase l_1 and the gaseous phase g are critical in the presence of the liquid phase l_2) – a vapour and a liquid phase are formed from a gas phase
$l_1 = g$	UCEP (merges with the critical point of the pure component with the lowest temperature)

Type IV fluid phase behaviour is identified in systems exhibiting:

- (i) Discontinued liquid-liquid immiscibility at intermediate temperatures
- (ii) Non-ideal mixtures
- (iii) Components with different sized molecules (but less obvious than Type III)

l_1l_2g	Three-phase equilibrium locus (at lower temperatures)
llg	Smaller three-phase equilibrium locus (additional at higher temperatures and pressures) – interrupts the $l = g$ critical line previously seen in Type II systems.
$l_1 = g + l_2$	UCEP terminating the llg locus at higher temperatures and pressures.
$l_1 = l_2 + g$	LCEP terminating the llg locus at lower temperatures and pressures; and the UCEP terminating the l_1l_2g locus at lower temperatures and pressures (see Type II).

UCEP and LCEP refer to the location of these points relative to the corresponding three-phase locus (l_1l_2g or llg).

Type V fluid phase behaviour is identified in systems exhibiting:

- (i) Difference in molecular size of components become significant
- (ii) Almost ideal system
- (iii) Complete miscibility at lower temperatures

llg	Smaller three-phase equilibrium locus (additional at higher temperatures and pressures) – interrupts the $l = g$ critical line previously seen in Type II systems.
$l_1 = g + l_2$	UCEP terminating the llg locus at higher temperatures and pressures.
$l_1 = l_2 + g$	LCEP terminating the llg locus at lower temperatures (at a temperature below T_C of component)

2.1.3. PHASE BEHAVIOUR TRANSITIONS AND TRENDS IN HOMOLOGOUS SERIES OF N-ALKANES AND N-ALKANOLS

Critical curves will at times form a sequence, i.e. the CEP on a three-phase curve, merges with another CEP on a different curve. Generally, this is a transition in both homologous series from Type IV to Type II and Type IV to Type III fluid phase behaviour occurring due to an increase and decrease in the miscibility of the components, respectively.

Type IV \rightarrow Type II:

When the components in a Type IV mixture start to experience an increase in miscibility (due to a decrease in the carbon number of the solute), the LCEP (terminating the llg locus) will start tending towards the UCEP (at higher temperatures and pressures) [54]. Regarding Figure 2-3 (b), one can imagine the llg three-phase locus to begin shrinking. Once the UCEP and LCEPs merge, the llg locus would have disappeared, and a tricritical point, (TCP) will form (see Figure 2-4 (a)). Therefore, the phase transition results in a point where all three phases have become critical simultaneously ($l_1 = l_2 = g$).

Type IV \rightarrow Type III:

On the other hand, when the components in a Type IV mixture start to experience a decrease in miscibility (due to an increase in the carbon number of the solute), the LCEP (terminating the llg locus) will start to tend towards the UCEP of the l_1l_2g locus (at lower temperatures and pressures) [54]. Regarding Figure 2-3 (b), one can imagine the llg three-phase locus to begin expanding. Once the upper and lower CEPs merge a double critical endpoint, (DCEP) will form (see Figure 2-4 (b)).

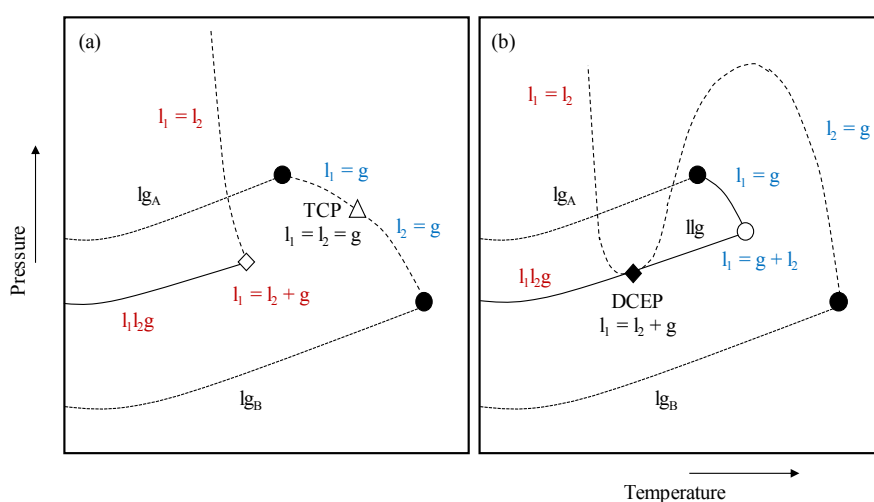


FIGURE 2- 4: FLUID PHASE BEHAVIOUR OF BINARY SYSTEMS TRANSITIONING FROM (A) TYPE II AND IV, TRICRITICAL POINT, AND (B) TYPE III AND IV, DOUBLE CRITICAL POINT. ADAPTED AND REDRAWN USING GAUTER ET AL. [54].

The sequence of the three-phase characteristics (between Type II, III and IV phase behaviour) links back to the transition sequence derived by Luks and co-workers [59]–[62] who used only the l_1l_2g three-phase behaviour in binary systems of CO₂ and 1-alcohols or n -alkanes to formulate a mechanism to distinguish what type of fluid phase behaviour can be expected. The trends established are shown in Figure 2-5 and indicate that with an increasing carbon number the following transformation sequence of the types of fluid phase behaviour will be encountered:

$$\text{Type II} \rightarrow \text{Type IV} \rightarrow \text{Type III}$$

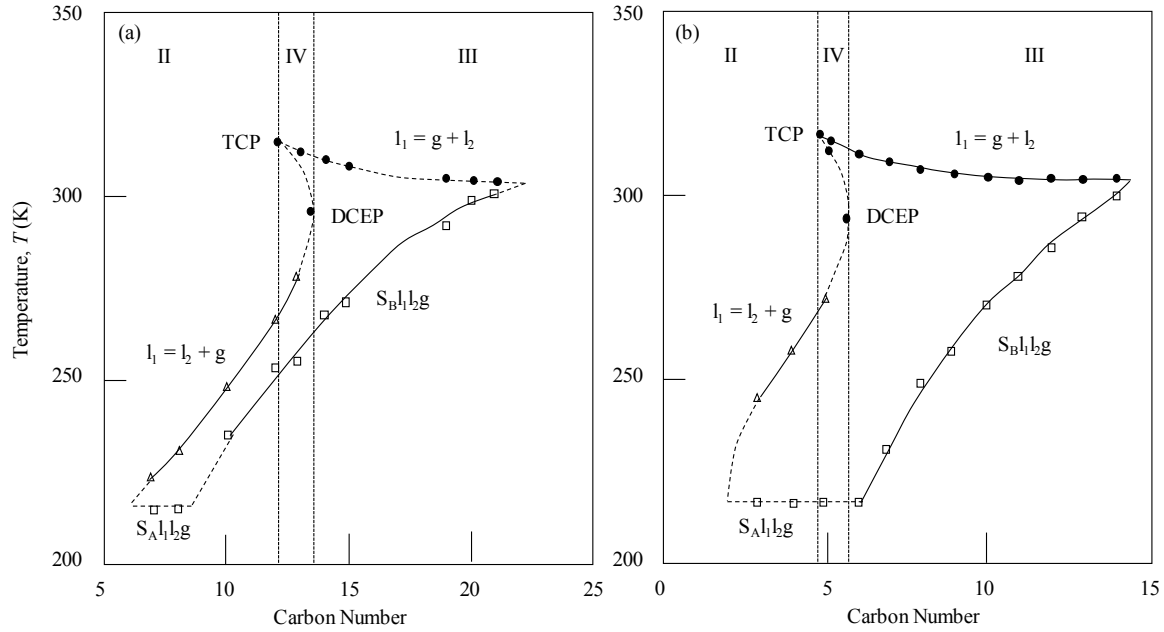


FIGURE 2- 5: THREE-PHASE BEHAVIOUR, INCLUDING THE CRITICAL ENDPOINTS, OF THE HOMOGENOUS SERIES OF BINARY MIXTURES OF (A) CO_2 AND n -ALKANES, (B) CO_2 AND n -ALKANOLS. ADAPTED AND REDRAWN USING PETERS ET AL. [36].

Furthermore, *Figure 2-5* was constructed to aid in determining whether a three-phase region will occur for certain CO_2 + 1-alcohol and CO_2 + n -alkane mixtures. **From *Figure 2-5*, Type III fluid phase behaviour is inferred for both CO_2 binary sub-systems of interest to this study.** However, a phase diagram classification can only be made for the mixtures after they have been investigated with the minimum number of variables needed to fully define each system. The Gibbs phase rule can be used to ensure that the system of interest is fully defined [63]:

$$F = N - \pi + 2 \quad (2.1)$$

To understand what is anticipated from the high-pressure experimental data, the inferred Type III phase behaviour of the binary mixtures can be used qualitatively. Type III behaviour assumes that two liquid phases exist throughout the phase diagram, $\pi = 2$ and limiting the system to two chemical species, $N = 2$ the phase rule is simplified to $F = 2$. The degrees of freedom necessary to fix the system is therefore two, consisting of temperature and pressure.

Figure 2-6 illustrates the transition of a homologous series of binary systems when decreasing the solute carbon number. However, the phase rule by van Pelt [64], Peters [37] and Stamoulis [65] indicates that tricriticality is not possible in a binary system. Their phase rule has an additional term \emptyset , which takes into consideration the number of extra conditions, i.e. critical points, and is defined by:

$$\emptyset = k - 1 \quad (2.2)$$

Here, the number of extra conditions is dependent on a critical point of order k . Therefore, $k = 2$ for a normal critical point, $k = 3$ for a tricritical point, and $k = 4$ for a tetra-critical point and so forth. The phase rule is now written as follows:

$$F = N - \pi + 2 - \phi \quad (2.1)$$

The minimum number of chemical species for a critical point of order k can be defined by taking into consideration the following two constraints: $F \geq 0$ and $\pi \geq k$. Therefore:

$$N \geq 2k - 3 \quad (2.4)$$

Consequently, for a TCP to occur at least three components must be present in the system (ternary mixtures).

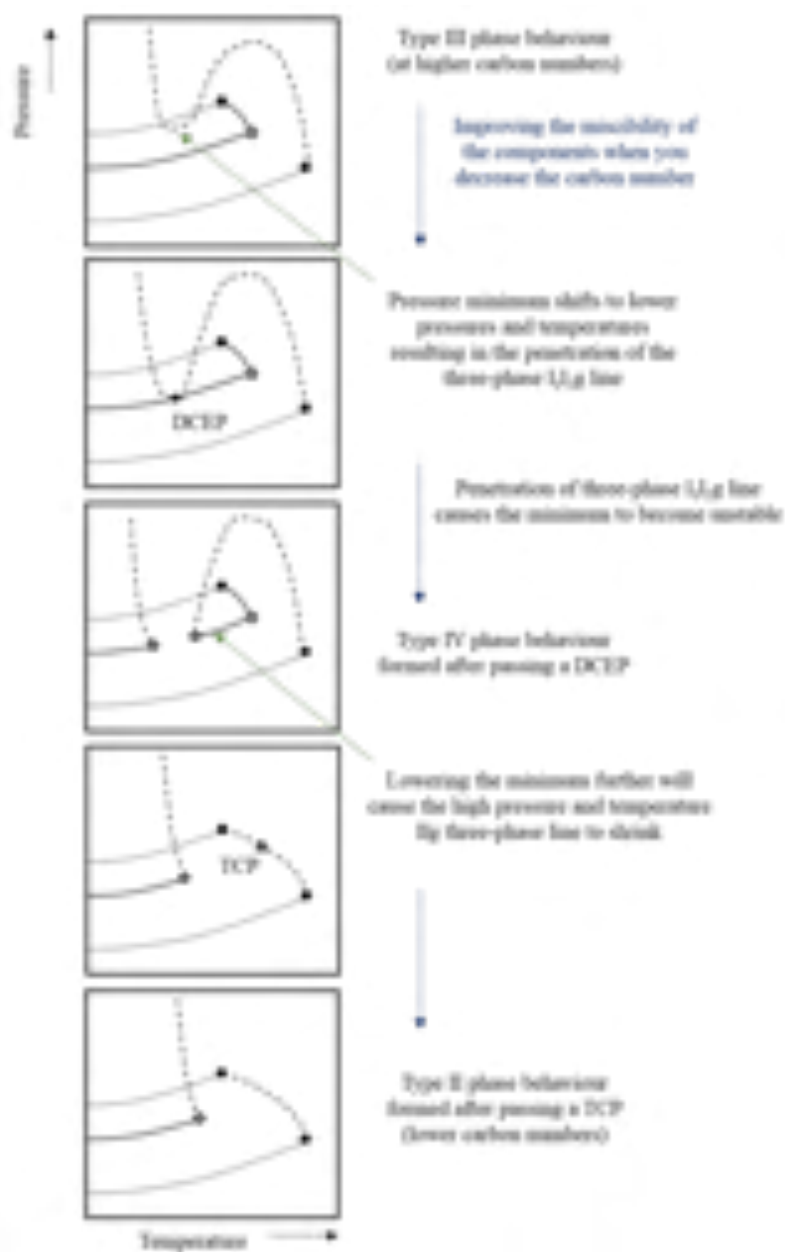


FIGURE 2- 6: SEQUENCE OF PHASE BEHAVIOUR TRANSITIONS FOR A BINARY SYSTEM FROM TYPE III TO TYPE IV TO TYPE II (COMING FROM HIGHER CARBON NUMBERS OF THE SOLUTE TO LOWER ONES) [52], [54].

2.1.4. LITERATURE DATA FOR THE CO₂ BINARY SUB-SYSTEMS

The available literature sources containing solubility data for the CO₂ binary sub-systems are listed in *Table 2-1*. To ensure the most accurate interpretation of the phase behaviour, the data measured by Zamudio et al. [15] and Bonthuys [17] will be used in this investigation as a basis for the CO₂ binary sub-systems.

This decision is based on the following:

- (i) The solubility data of several sources are limited to, at times, one set temperature [66], [67] or pressure [68].
- (ii) The data published by Lam et al. [62] and Patton & Luks [40] do not cover the necessary supercritical phase behaviour regions of interest to this study.
- (iii) The data published by Zamudio et al. [15] and Bonthuys [17] provide measurements covering a large temperature and pressure range.

To validate the use of the data published by Zamudio et al. [15] and Bonthuys [17] their results were compared to data published by the remaining research groups. In *Figure 2-7 (a)* and *Figure 2-7 (b)* the 1-decanol system is compared to work conducted by Lee & Chen [69], Weng et al. [70], and Chang et al. [71]. In *Figure 2-7 (c)* the *n*-tetradecane system is compared to the work measured by Gasem et al. [67].

TABLE 2- 1: PUBLISHED PHASE EQUILIBRIA DATA FOR THE CO₂ BINARY SUB-SYSTEMS OF IMPORTANCE TO THIS STUDY, NAMELY CO₂ + 1-DECANOL[†] AND CO₂ + N-TETRADECANE[‡].

<i>Temperature Range</i>	<i>Pressure Range</i>	<i>Type</i>	<i>Reference</i>
308.2 – 348.2 K	Up to 33.83 MPa	VLE	Zamudio et al. [15] ^{†a}
284.0 – 313.5 K	0.1 MPa partial	Solubility	Wilcock et al. [68] [†]
270.5 – 307.2 K	Up to 7.8 MPa	LLV	Lam et al. [62] [†]
348.2 – 453.2 K	Up to 5.0 MPa	VLE	Lee & Chen [69] [†]
348.2 – 453.2 K	Up to 19.0 MPa	VLE	Weng et al. [70] [†]
271.1 – 279.6 K	Up to 3.2 MPa	Liquid compositions	Patton & Luks [40] [†]
308.1 – 328.2 K	Up to 15.0 MPa	VLE densities*	Chang et al. [71] [†]
318.0 K	Up to 12.4 MPa	VLE	Gardeler & Gmehling [66] [†]
313.2 – 358.2 K	Up to 19.25 MPa	VLE	Bonthuys [17] ^{‡b}
344.3 K	Up to 16.38 MPa	VLE densities*	Gasem et al. [67] [‡]

* Measured densities converted to phase equilibrium data

^a $u(P) = 0.06$ MPa and $u(T) = 0.2$ K

^b $u(P) = 0.06$ MPa and $u(T) = 0.1$ K

The data published by Lee & Chen [69] as well as Weng et al. [70] are in good agreement with the data published by Zamudio et al. [15] (see *Figure 2-7 (b)*). However, the data published by Chang et al. [71]

and Gasem et al. [67] does not correlate very well to the measurements of Zamudio et al. [15] and Bonthuys [17], respectively. It is postulated that this occurs due to the use of dissimilar experimental methods. Both Lee & Chen [69] and Weng et al. [70] made use of a semi-flow type apparatus to measure the equilibrium compositions. Zamudio et al. [15] and Bonthuys [17] both employed the use of a visual static synthetic view cell. Therefore, these research groups made use of VLE measurement techniques. On the other hand, Chang et al. [71] and Gasem et al. [67], measured the densities of the co-existing phases with densitometers and converted the readings to phase equilibrium data. It may thus be that their data is not at complete phase equilibrium. Furthermore, there is a 1 K temperature difference between the two publications being compared in *Figure 2-7 (c)*, which may also contribute towards the discrepancies.

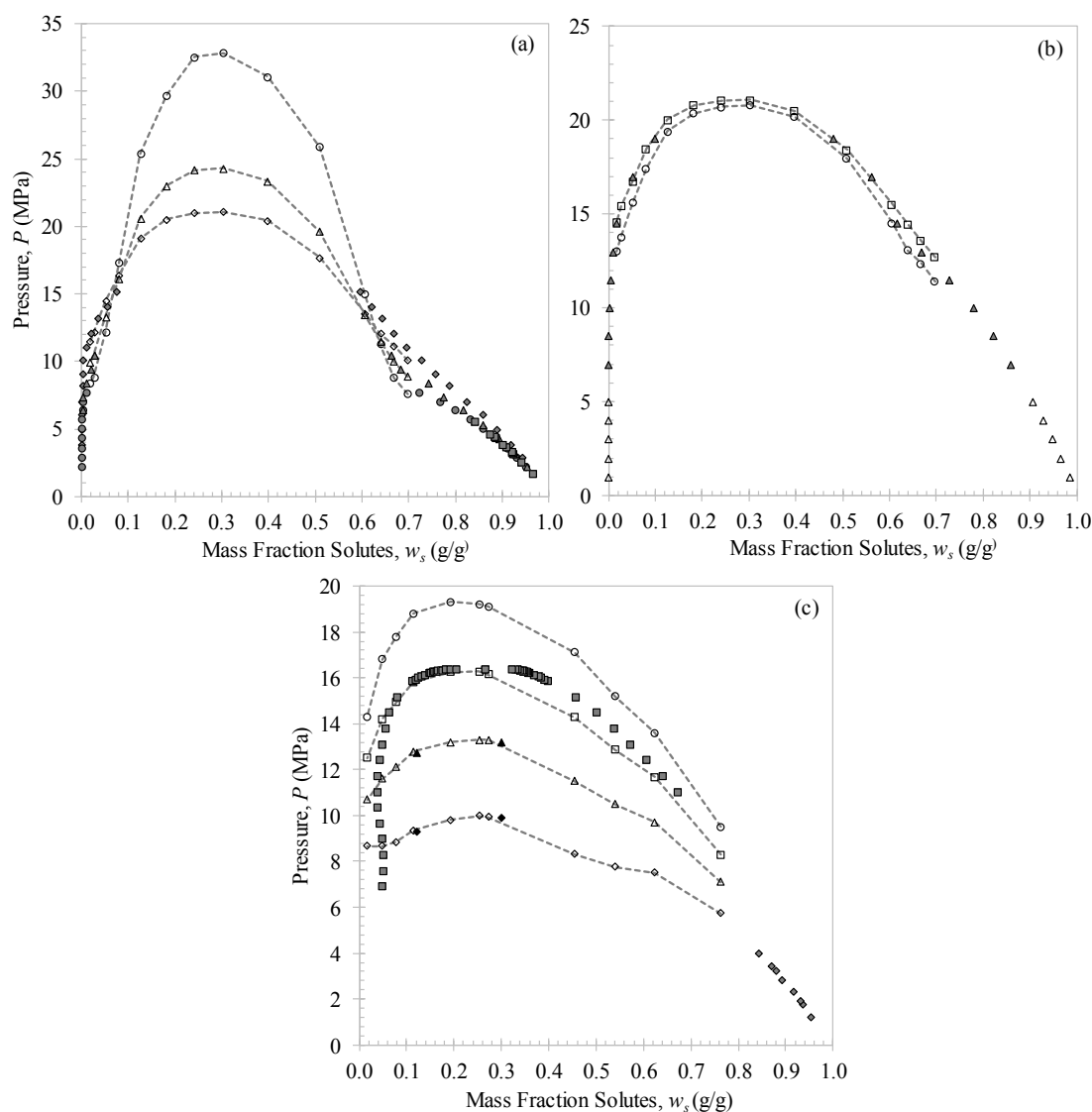
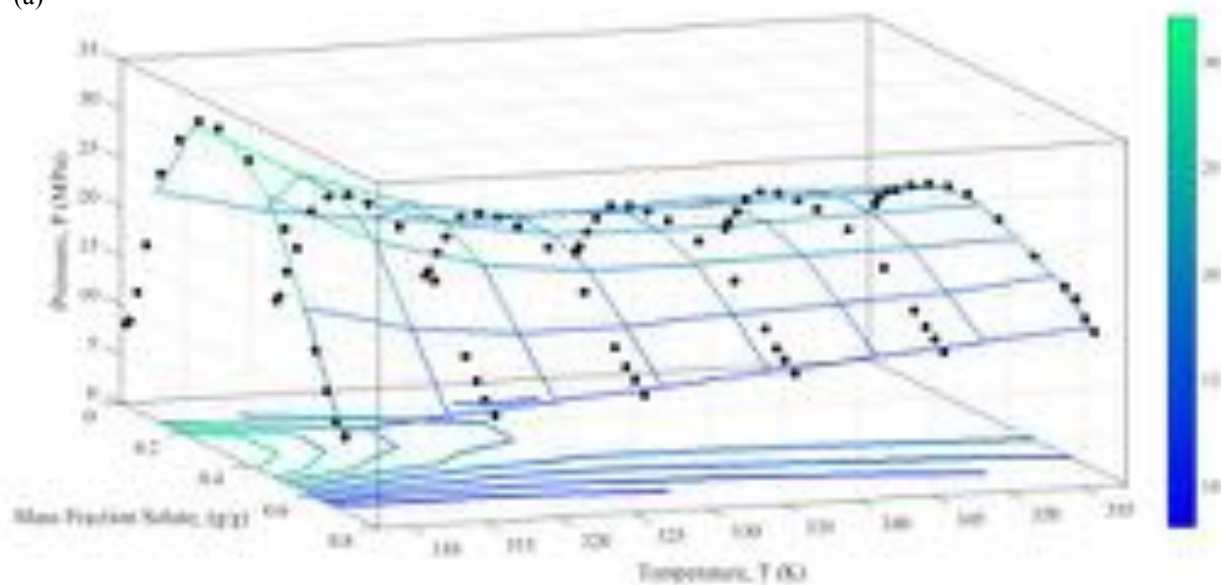


FIGURE 2- 7: LITERATURE COMPARISONS BETWEEN VARIOUS RESEARCH GROUPS FOR THE CO_2 + 1-DECANOL SYSTEM
 (A) ZAMUDIO ET AL. [15] AT $T = 308 \text{ K}$ $\cdots\circ\cdots$; $T = 318 \text{ K}$ $\cdots\Delta\cdots$; $T = 328 \text{ K}$ $\cdots\Diamond\cdots$ AND CHANG ET AL. [71] AT $T = 308 \text{ K}$ \bullet ;
 $T = 318 \text{ K}$ \blacktriangle ; $T = 328 \text{ K}$ \blacklozenge (B) AT $T = 348 \text{ K}$ FOR ZAMUDIO ET AL. [15] $\cdots\square\cdots$; LEE & CHEN Δ AND FOR WENG ET AL. [70] \blacktriangle .
 SIMILARLY, FOR THE CO_2 + *N*-TETRADECANE SYSTEM (C) BONTTHUYS [17] AT $T = 343 \text{ K}$ $\cdots\square\cdots$ AND GASEM ET AL. [67] AT
 $T = 344 \text{ K}$ \blacksquare .

For binary systems of CO₂ as the critical solvent and components of interest to this study, belonging to the homologous series of *n*-alkanes and of 1-alcohols, a general decrease in solubility is to be expected for an increase in temperature over the entire composition range. In *Figure 2-8* the *P-T-w_s* phase transition curves for the CO₂ binary sub-systems are provided using data obtained from literature [15], [17].

(a)



(b)

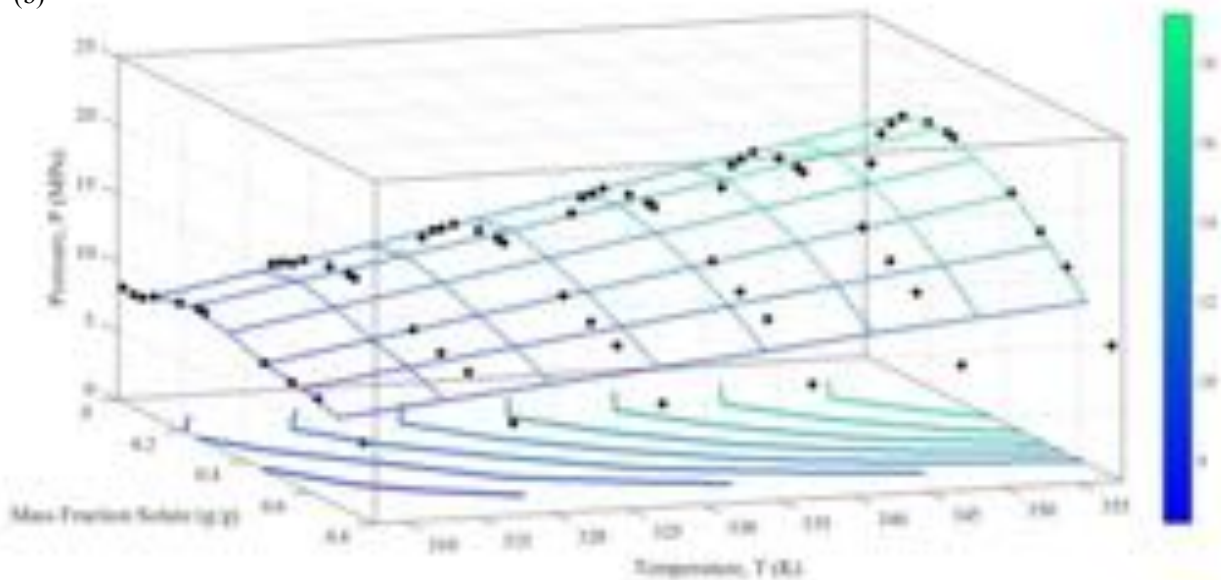


FIGURE 2- 8: PHASE BEHAVIOUR OF THE BINARY SYSTEMS (A) CO₂ + 1-DECANOL [15] AND (B) CO₂ + *N*-TETRADECANE [17] AT TEMPERATURES BETWEEN 308 AND 358 K AND SOLUTE COMPOSITIONS BETWEEN 0.01 AND 0.8 G/G.

The phase behaviour of the CO₂ + *n*-tetradecane system does indicate this trend as shown in *Figure 2-8 (b)*. However, as shown in *Figure 2-8 (a)* between approximately 0.07 g/g and 0.64 g/g solute, the CO₂ + 1-decanol system requires a higher phase transition pressure at $T = 308$ K than at $T = 358$ K. This phenomenon is defined as a temperature inversion.

Zamudio [18] further illustrates the temperature inversion by plotting the P - T relationship (isotherm) of the system at solute compositions close to 0.07 g/g and 0.64 g/g (see *Figure 5-16*, [18]). The isotherm indicates that the solubility of 1-decanol does not decrease with a temperature increase. The observed phenomenon causes the phase transition pressures to decrease between $T = 308$ K and $T = 338$ K before resuming the normal increasing pressure trend as the temperature increases to $T = 358$ K. Temperature inversions are a common occurrence over a certain range of the CO₂ + 1-alcohol homologous series [15], [16], [19]. *Figure 2-9* below provides a possible explanation for the unique phase behaviour occurring in certain CO₂ + 1-alcohol systems.

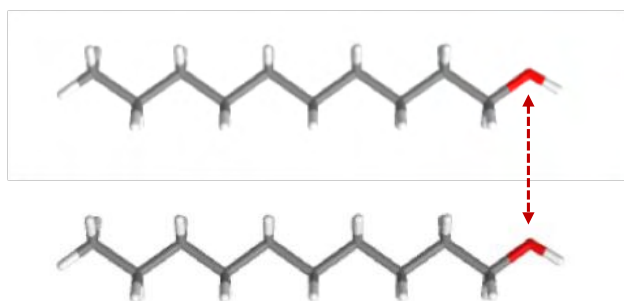


FIGURE 2- 9: MULTIMER HYDROGEN BONDS BETWEEN TWO 1-DECANOL MOLECULES.

Strong solute + solute interactions take place within the system. However, in primary linear alcohols such as 1-decanol, the exposed hydroxyl group forms multimer hydrogen bonds resulting in the formation of dense alcohol structures as illustrated in *Figure 2-9* [15], [16], [18], [19]. Here, at $T = 308$ K, the multimer bonds are too strong to be broken due to the kinetic energy of the molecules alone. Therefore, a very high pressure of 32.8 MPa is required to force a substantial amount of CO₂ molecules in between the 1-decanol molecules and break the multimer bonds, allowing the solute to dissolve into a single phase. As temperatures increase above $T = 308$ K, the CO₂ units have increasing kinetic energy available to disrupt the multimer hydrogen bonds, allowing the solute to dissolve in the solvent at lower pressures. Lastly, the temperature inversion does not take place at 1-decanol mass fractions below 0.07 g/g and above 0.64 g/g [15], [18]. This occurs due to the dilute mixtures not containing enough 1-decanol molecules to form multimer bonds and the concentrated mixtures not containing enough solvent molecules to prevent the formation of multimers irrespective of the temperature.

2.1.5. CLASSIFICATION OF THE CO₂ BINARY SUB-SYSTEMS

Having established the published literature suitable for use in this investigation, the two systems are compared to one another (see *Figure 2-10*). The dew-point region is most prominent for SFF and is used to investigate the viability of using this process to separate the two solutes. The separation task considered in this study is the removal of residual *n*-tetradecane from 1-decanol. Regardless of 1-decanol being more volatile, it remains less soluble than *n*-tetradecane in supercritical CO₂. Based on this finding, both CO₂ binary sub-systems are completely miscible in the bubble-point/liquid region. *Figure 2-10 (a)* shows that a higher phase transition pressure is required for 1-decanol (filled markers) to form a single phase despite the temperature change. However, as indicated by the broken arrows on *Figure 2-10 (a)* and *(b)*, the difference in solubility pressure decreases with an increase in temperature from $T = 308$ K to 358 K.

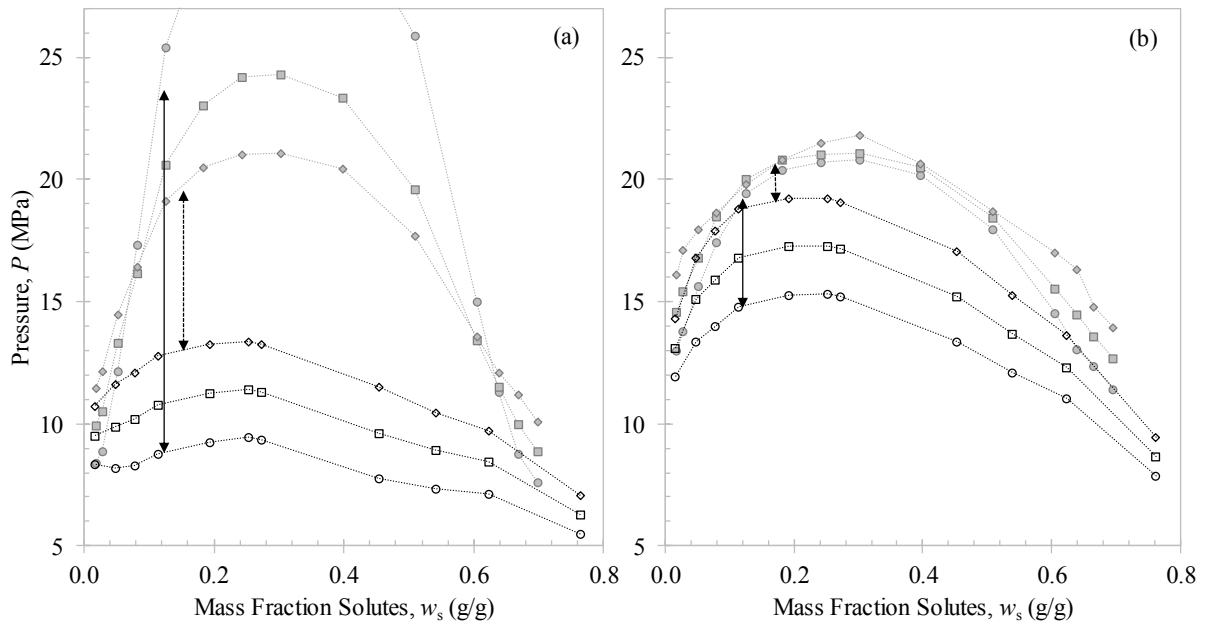


FIGURE 2- 10: PHASE BEHAVIOUR COMPARISON OF THE CO₂ + 1-DECANOL SYSTEM [15] (INDICATED WITH FILLED MARKERS) AND CO₂ + *N*-TETRADECANE SYSTEM [17] (INDICATED WITH OPEN MARKERS) AT: (A) $T = 308$ K $\cdots\circ\cdots$; $T = 318$ K $\cdots\square\cdots$; $T = 328$ K $\cdots\Diamond\cdots$ AND (B) $T = 338$ K $\cdots\circ\cdots$; $T = 348$ K $\cdots\square\cdots$; $T = 358$ K $\cdots\Diamond\cdots$.

Relative solubility can be used to determine the separation of a specific component in a solvent, relative to another at a set temperature and pressure [20]:

$$\alpha_{ij} = \frac{K_i}{K_j} = \frac{y_i/x_i}{y_j/x_j} \quad (2.5)$$

Here, y and x refer to the vapour and liquid fractions of components i and j , respectively. To ensure separation occurs the relative solubility should be greater than 1.05 or smaller than 0.95. The more soluble component, i should be divided by the less soluble component, j to ensure a relative solubility

greater than 1. Therefore, for ease of reference, i and j will represent n -tetradecane and 1-decanol, respectively.

The P - x solubility curves shown in *Figure 2-10* were used to calculate the relative solubility of n -tetradecane to 1-decanol in supercritical CO_2 . Horizontal tie lines were drawn from the vapour phase data to the liquid phase data at a set pressure. Interpolation of these points produced data from which the relative solubilities were calculated (see *Figure 2-11*). The results shown confirm that the solubility of n -tetradecane in CO_2 decreases with an increase in temperature. Furthermore, it is shown that at each set temperature, the relative solubility can be improved with an increase in pressure.

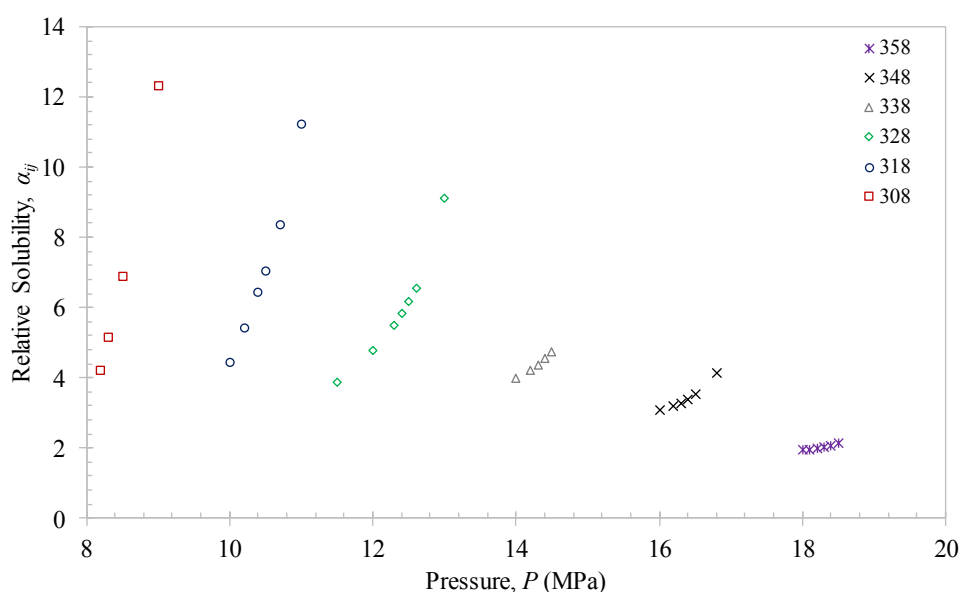


FIGURE 2- 11: RELATIVE SOLUBILITY OF $\text{CO}_2 + n$ -TETRADECANE TO $\text{CO}_2 + 1$ -DECANOL AT 6 SET TEMPERATURES AS A FUNCTION OF PRESSURE. BINARY DATA USED OBTAINED FROM ZAMUDIO ET AL.[15] AND BONTHUYS [17], RESPECTIVELY.

Comparison of the binary systems alone confirms that SFF is probably a viable process for the separation of these two components. However, the temperature inversion in the 1-decanol binary system restricts the use of the overall solute concentration range. The temperature at which optimum separation will occur with SFF is still unclear. Therefore, analysis of the ternary mixture is required to formulate the interactions between 1-decanol and n -tetradecane molecules. In addition, there are enough hydrogen bonding in 1-decanol to make the $\text{CO}_2 + 1$ -decanol binary system l_1l_2g immiscible [72], even more than that of the $\text{CO}_2 + n$ -tetradecane sub-system [73]. Additional studies of the binary l_1l_2g system, $\text{CO}_2 + n$ -tetradecane, were conducted by van der Steen et al.[74] and Laugier et al.[75]. The two CO_2 binary sub-systems exhibit the characteristic UCEPs ($l_1 = g + l_2$) which were measured by Patton et al.[40]:

- For $\text{CO}_2 + 1$ -decanol the UCEP is at $P = 7.75$ MPa and at $T = 307.15$ K
- For $\text{CO}_2 + n$ -tetradecane the UCEP is at $P = 8.25$ MPa and $T = 311.15$ K

Therefore, it can be concluded that both CO₂ binary sub-systems exhibit Type III fluid phase behaviour per the classification scheme of Van Konynenburg and Scott [52], [53]. These observations confirm the inferred Type III fluid phase behaviour when considering the three-phase behaviour depicted in Figure 2-5.

2.1.6. LITERATURE DATA FOR THE 1-ALCOHOL + N-ALKANE SUB-SYSTEMS

To the author's knowledge, no known experimental data have been published for the 1-decanol + *n*-tetradecane binary system. Furthermore, the classification of this third binary sub-system of the ternary CO₂ + 1-decanol + *n*-tetradecane has not yet been defined in literature. It is therefore imperative that the binary system be thoroughly and explicitly investigated in this work through experimental measurements. If the ternary system has been classified in literature, the type of phase behaviour to be expected for the 1-decanol + *n*-tetradecane system can be identified.

2.2. PHASE BEHAVIOUR OF TERNARY SYSTEMS

In contrast to binary systems, to investigate the phase behaviour of ternary systems, a composition-dependent surface must be generated. The properties of ternary mixtures are therefore much more intricate to characterize and less often considered due to its high demand in time, resources and general difficulty in measurement [55], [76], [77]. To date, no equivalent classification scheme for ternary fluid mixtures have been established. Ternary mixtures have shown to exhibit similar phenomena as that found in the constituting binary mixtures with Types I and II phase behaviour. However, the phenomena generated by ternary systems resulting from constituting Type III, IV, V, or VI binary sub-systems will not necessarily exhibit similar phenomena observed for the respective binary mixtures and therefore completely different effects are to be expected [34]. For the interested ternary system, the correct interpretation of phase diagrams is therefore of high importance.

2.2.1. TERNARY PHASE DIAGRAMS

The list of possible ternary phase diagram classes far exceeds that of the binary phase behaviour Types. To ensure accurate characterisation of the CO₂ + 1-decanol + *n*-tetradecane ternary phase behaviour, graphical representations are required. Thus, the ternary classes will need to be investigated using either, (i) a Gibbs phase triangle, (ii) a prismatic representation, or (iii) a pseudo-binary (P - T - w_c^{red}) diagram. Here, w_c^{red} denotes the solvent-free or reduced mass fraction of the *n*-alkane, mathematically defined by [54]:

$$w_c^{red} = \frac{w_c}{w_B + w_c} \quad (2.6)$$

The boundary conditions, $w_c^{red} = 0.00$ g/g and $w_c^{red} = 1.00$ g/g represent the phase diagrams of the CO₂ + 1-decanol and CO₂ + *n*-tetradecane binary sub-systems, respectively.

Bluma and Deiters [78] developed a classification for ternary fluid mixtures that is based on the binary classification of Van Konynenburg and Scott [52]. Various *EoS* can be used for the construction of the ternary global phase diagram including the critical states. However, each method produces a similar phase behaviour. Generally, a difference in the quantitative location of the boundary curves will be observed but not a qualitative difference (different arrangements of the phase domains). The VdW *EoS* with standard one-fluid mixing rules is the preferred *EoS* to simplify the calculations without losing generality. Bluma and Deiters [78] further assumed the Berthelot-Lorentz combining rules for the binary interaction parameters. This assumption allows one to express all the parameters of one of the binary sub-systems of a ternary mixture by those of the two others. The calculation theory is beyond the scope of this study and has been discussed in detail elsewhere [78]–[80].

The global ternary phase diagram can be constructed in terms of the pure component attraction parameter ratio, ζ , and the binary attraction parameter ratio, λ . *Figure 2-12* shows the resulting global phase diagram of a binary mixture when the molecules are of equal size (the pure component size ratio, ξ is equal to zero).

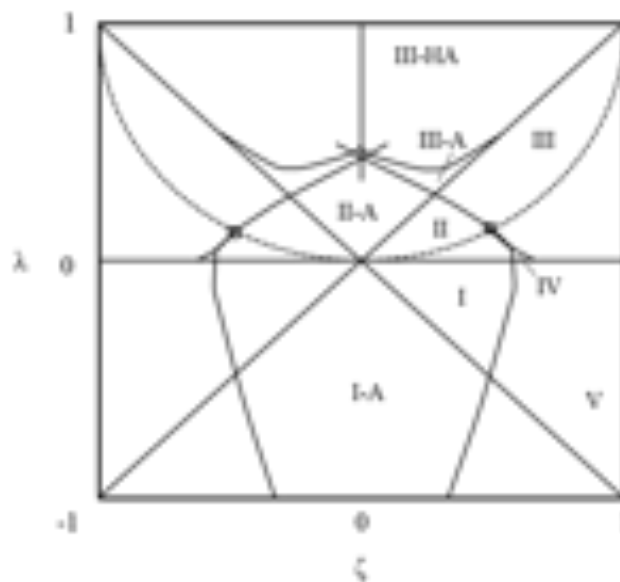


FIGURE 2- 12: GLOBAL PHASE DIAGRAM OF A BINARY MIXTURE OF EQUAL SIZED MOLECULES USING THE VdW *EoS*, REDRAWN USING BLUMA AND DEITERS [78].

Characteristics of the global phase diagram include:

- (i) TCP curves (phase transition from Type II to Type IV).
- (ii) DCEP curves (phase transition from Type III to Type IV or Type IV to Type V).
- (iii) Azeotropic boundary curves, here the azeotrope forms at composition $x = 0$ or $x = 1$ (phase transition from Type I to Type I-A).
- (iv) Critical azeotropic endpoints (phase transition from Type III-A to Type III-HA).

In this study, the components under investigation are not symmetrical and the different molecular sizes need to be considered. Previous studies have established the influence of the molecular sizes after calculating a series of ζ - λ cross sections when varying ξ . The asymmetric co-volumes of the components in the mixture caused the global phase diagram to become asymmetric [79]. Therefore, once again, only a quantitative change in the phase behaviour was observed and the phase regions remained the same. *Figure 2-13* shows a global phase diagram where the co-volume of component 2 is twice that of component 1, i.e. $\xi = 1/3$.

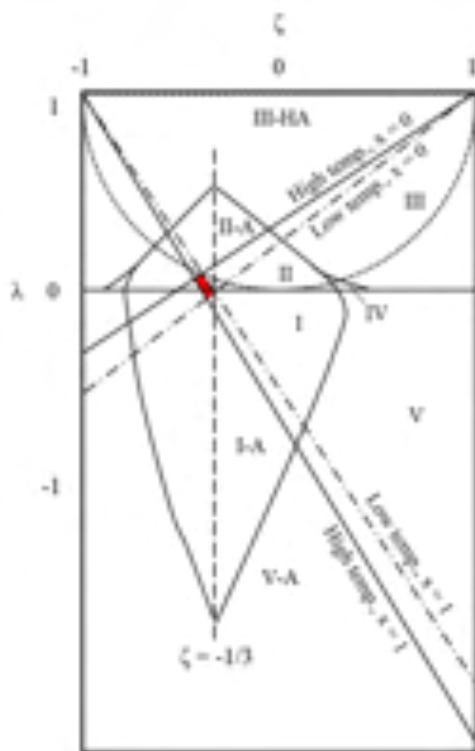


FIGURE 2- 13: GLOBAL PHASE DIAGRAM OF A BINARY MIXTURE OF NON-EQUAL SIZED MOLECULES USING THE vdW *EoS*, REDRAWN USING KIRAN AND LEVELT SENGERS [30].

One topological change is the added low-temperature and high-temperature limits due to an azeotropic composition change along the azeotropic boundary curve [52]. The highlighted rectangle on *Figure 2-13* (formed by the intersecting curves) represents a region in which double azeotropic behaviour occurs. This phenomenon is observed on P - xy phase diagrams as the formation of a pressure minimum azeotrope and a pressure maximum azeotrope [81].

For simplicity in defining the ternary classes the symmetric global phase diagram (*Figure 2-12*) will be used. Regardless of the curves being distorted in the global phase diagram of asymmetrical mixtures they still have the same general features as that of the symmetrical case. The outcomes will therefore be applicable to the system investigated in this study. *Figure 2-14* shows the global phase diagram class combinations for a ternary mixture with equal-sized molecules. The combinations allow for the ternary phase behaviour to be defined in 8 major classes [78].

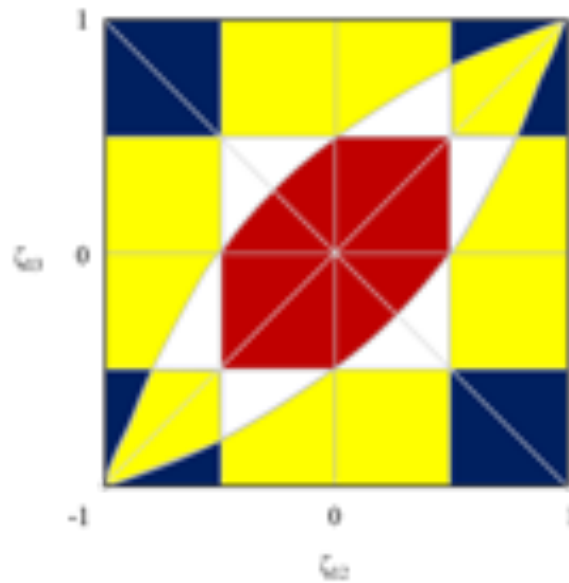


FIGURE 2- 14: GLOBAL PHASE DIAGRAM OF A TERNARY MIXTURE FOR EQUAL SIZED MOLECULES WHEN USING THE vdW *EoS*. FIELD COLOURS ARE FOR BINARY SUBSYSTEMS FORMING THE TERNARY SYSTEM; RED: II + II + II; WHITE: II + II + III; YELLOW: II + III + III; BLUE: III + III + III. REDRAWN USING BLUMA AND DEITERS [78].

Characteristics of the global phase diagram of ternary class classifications include:

- (i) Horizontal and vertical boundaries for phase transitions from Type II to Type III or vice-versa (only for binary subsystems 1-2 (ζ_{12}) and 1-3 (ζ_{13}), respectively).
- (ii) Curved boundaries for phase transitions from Type II to Type III for the binary subsystem 2-3 (ζ_{23}).
- (iii) A positive slope diagonal representing a ternary mixture when $\zeta_{12} = \zeta_{13}$ (the two subsystems are thus equal).
- (iv) A negative slope diagonal representing a ternary mixture when $a_{11} = a_{22} = a_{33}$.

The 8 ternary phase diagram classes can be defined by their constituting binary sub-systems (1-2 or A + B), (1-3 or A + C) and (1-3 or B + C) as shown in *Figure 2-15*. For example, if the three binary sub-systems are comprised of Type III + Type I + Type III fluid phase behaviour, the ternary system will display Class T-IV or T-VI phase behaviour (highlighted on *Figure 2-15* in red).

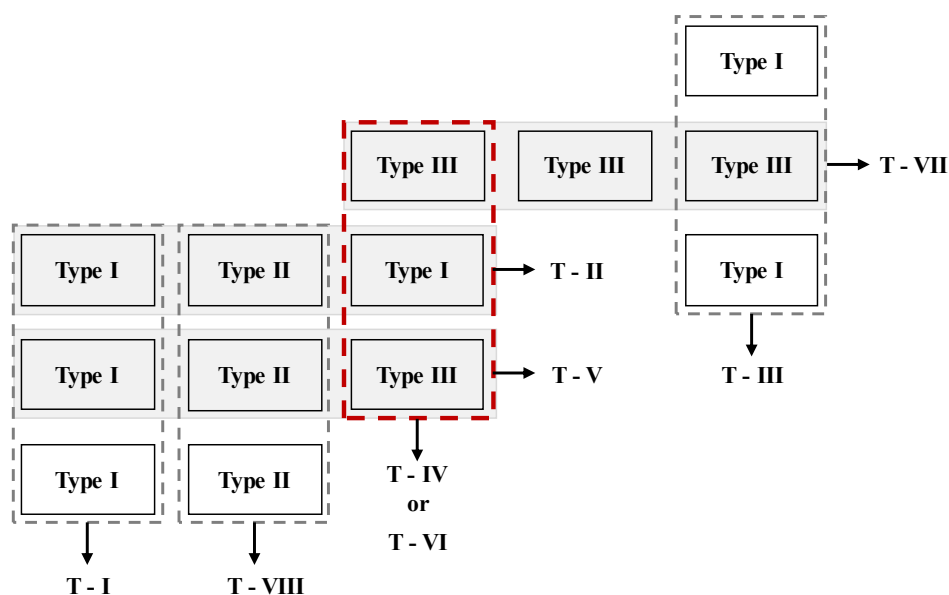


FIGURE 2- 15: TERNARY PHASE DIAGRAM CLASSES FORMED FROM DIFFERENT CONFIGURATIONS OF TYPE I, II AND III BINARY SUBSYSTEMS. ADAPTED USING BLUMA AND DIETERS [78] .

Therefore, the approach suggested by Bluma and Deiters [78] will provide a possible classification for the ternary system and for the third binary sub-system. Having classified the CO₂ binary sub-systems as Type III fluid phase behaviour, *Figure 2-15* can be used to identify the possible classification for the third binary sub-system (1-decanol + *n*-tetradecane). The only combinations that can be made are: III + III + I or III + III + III which indicate that three ternary classes (T-IV, T-VI and T-VII) are possible outcomes in this study. Consequently, the 1-decanol + *n*-tetradecane binary sub-system will exhibit either Type I or Type III fluid phase behaviour.

Ternary Class IV [78], [79]:

This class will occur if the third binary sub-system, 1-decanol + *n*-tetradecane, is of Type I phase behaviour. Typical ternary systems belonging to this class consist of two similar heavy components and one very light component. Type III behaviour will be shown by each of the binary sub-systems with the light component. The expected phase diagrams of this ternary class are shown in *Figure 2-16*. At high temperatures, the large critical surface (green) will continue upwards to infinite pressure. A second smaller critical surface (blue) will also form at low temperatures which is bounded by an upper critical endpoint (UCEP curve marking the beginning of a three-phase domain).

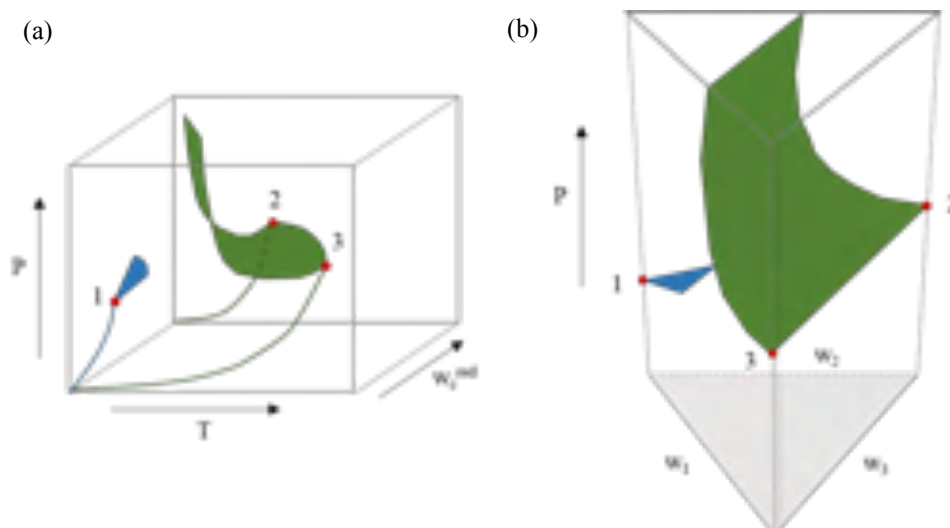


FIGURE 2- 16: CRITICAL SURFACES FOR A TERNARY CLASS IV SYSTEM (A) PSEUDO-BINARY REPRESENTATION, (B) PRISMATIC REPRESENTATION. ADAPTED AND REDRAWN USING [78].

Ternary Class VI [78], [79]:

The binary subsystems of this ternary class consist of the same phase behaviour types as that of the T-IV ternary class, i.e. Type III. However, now the components will comprise of two similar light compounds and one heavy component. In this study, two similar heavy components are to be separated, namely 1-decanol and *n*-tetradecane. A common lighter component, CO₂, will be used as the solvent to separate the two solutes in a SFF process. Therefore, ternary class T-VI is not a possible classification for the interested ternary mixture.

Ternary Class VII [78], [79]:

This class will occur if the third binary subsystem, 1-decanol + *n*-tetradecane, is of Type III phase behaviour. *Figure 2-17* shows the three critical planes formed on the phase diagrams of T-VII mixtures. The critical surfaces of the three components in the ternary mixture will show the following critical phase behaviour:

- (i) The component with the highest critical data → *l-l* critical behaviour (green surface).
- (ii) The component with the lowest critical data → *l-g* critical behaviour (orange surface).
- (iii) The third component will show *l-l* critical behaviour with component 1 (lighter) and *l-g* with component 2 (blue surface).

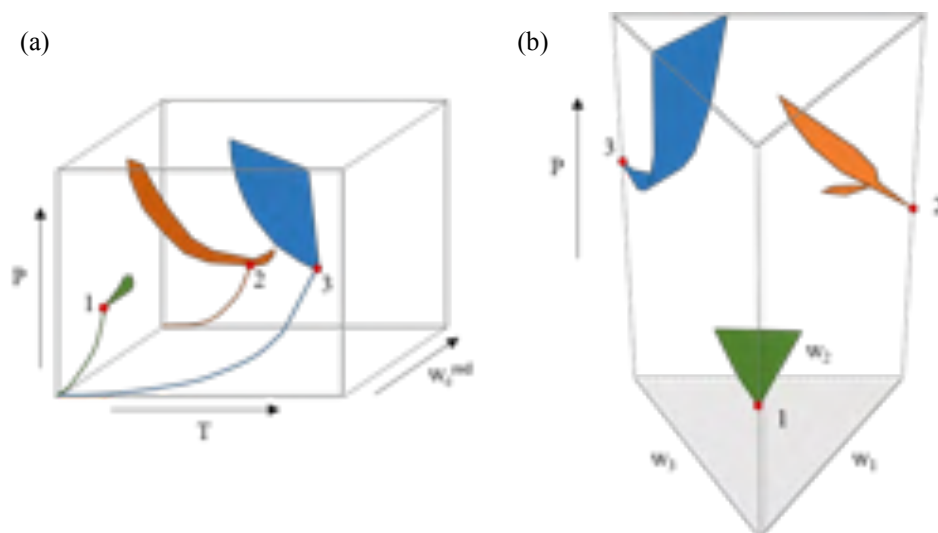


FIGURE 2- 17: CRITICAL SURFACES FOR A TERNARY CLASS VII SYSTEM (A) PSEUDO-BINARY REPRESENTATION, (B) PRISMATIC REPRESENTATION. ADAPTED AND REDRAWN USING [78].

The classes, T-IV and T-VII, are the probable classes for the CO_2 + 1-decanol + n -tetradecane mixture being investigated in this work. However, literature shows that T-IV mixtures will contain two-immiscible binary sub-systems that might form a two-phase region within the three-phase region of the ternary phase diagram [3], [32]–[35]. To identify this topological phenomenon and formulate a final classification for the ternary system an extensive and systematic study of the CO_2 + 1-decanol + n -tetradecane system is required.

2.2.2. LITERATURE DATA FOR CO_2 + 1-DECANOL + N -TETRADECANE

Interesting phenomena occur frequently in CO_2 + 1-alcohol + n -alkane systems within the temperature, pressure, and composition range of technological processes [82]. The phenomena were confirmed by extensive experimental investigations on ternary systems comprised of CO_2 as the near critical solvent and 1-alcohols + n -alkanes as the two heavier solutes [37]. Table 2-2 tabulates the most well-known phenomena found by several research groups to frequently occur in CO_2 + 1-alcohol + n -alkane systems. The phenomena can be directly linked to the vapour-liquid-liquid equilibria (VLLE) three-phase regions observed in certain types of phase behaviour when operating at conditions near the critical point of the solvent. As a result, difficulties in the control of SFF processes are encountered in these regions and must be avoided [18]. With the correct insight into the fluid phase behaviour of these systems the phenomena can now be understood, applied and controlled in the design of separation processes.

TABLE 2- 2: FLUID PHASE PHENOMENA OCCURRING IN CO_2 + 1-ALCOHOL + *N*-ALKANE TERNARY SYSTEMS EXAMINED BY KORDIKOWSKI AND SCHNEIDER [39], SCHEIDGEN AND SCHNEIDER [3] AND PÖHLER ET AL. [83].

<i>Ternary system</i> CO_2 + ...	<i>Cosolvency</i> (\blacktriangle), <i>island system</i> (\triangle)	<i>Closed miscibility</i> <i>windows, isobaric</i> (\blacklozenge), <i>isothermal</i> (\diamond)	<i>Hole in the critical</i> <i>surface, closed</i> (\bullet), <i>open</i> (\circ)	<i>Reference</i>
1-dodecanol + <i>n</i> -tetracosane	-	-	-	[39]
1-dodecanol + <i>n</i> -eicosane	\blacktriangle	\blacklozenge	-	[39]
1-dodecanol + <i>n</i> -nonadecane	\blacktriangle	\blacklozenge/\diamond	-	[39]
1-dodecanol + <i>n</i> -hexadecane	\blacktriangle	\blacklozenge	-	[39]
1-undecanol + <i>n</i> -octadecane	\blacktriangle	\blacklozenge	-	[83]
1-decanol + <i>n</i> -heptadecane	\blacktriangle	\blacklozenge	-	[83]
1-decanol + <i>n</i> -tetradecane	\blacktriangle	\blacklozenge	\bullet	[3]
1-nonanol + <i>n</i> -hexadecane	\blacktriangle	\blacklozenge	-	[83]
1-nonanol + <i>n</i> -pentadecane	\blacktriangle	\blacklozenge	-	[83]
1-octanol + <i>n</i> -hexadecane	\blacktriangle	\blacklozenge	-	[3]
1-heptanol + <i>n</i> -pentadecane	\blacktriangle	\blacklozenge/\diamond	\bullet	[3]
1-hexanol + <i>n</i> -pentadecane	\blacktriangle	\diamond	\bullet	[3]
1-hexanol + <i>n</i> -tetradecane	\blacktriangle	-	\circ	[3]

The phenomena present in the ternary system of interest to this work include: isothermal cosolvency effects, closed isobaric miscibility windows and a closed *l*-g hole (highlighted in *Table 2-2*). Each of these occurrences will be defined and discussed in the following section to obtain a fundamental understanding of the thermodynamic phenomena at near- and supercritical conditions. In addition, a systematic literature study is conducted for the ternary system to identify where there is a need for further experimental research. To the author's knowledge, all published data on the CO_2 + 1-decanol + *n*-tetradecane system are listed in *Table 2-3*.

TABLE 2- 3: PUBLISHED PHASE EQUILIBRIA DATA FOR THE CO_2 + 1-DECANOL + *N*-TETRADECANE SYSTEM.

<i>Temperature Range</i>	<i>Pressure Range</i>	<i>Type</i>	<i>Reference</i>
290.7 – 305.6 K	Up to 7.23 MPa	Cailletet VLLE apparatus	Peters et al. [38]
283.6 – 311.2 K	Up to 8.25 MPa	Visual glass VLLE cell	Patton et al. [40]
278.8 – 393.1 K	Up to 100 MPa	Analytical VLLE method	Scheidgen and Schneider [3]

2.2.3. CLOSED LIQUID-GAS HOLE IN THE THREE-PHASE SURFACE

Most of the well-defined CO_2 + hydrocarbons systems provided in *Table 2-2* displayed an unusual two-phase *l*-g area in their three-phase surface (l_1l_2g). The 'hole' is completely bounded by a closed loop critical endpoint locus where the liquid phases are critically identical ($l_1 = l_2 + g$) [40]. In *Figure 2-18* the visual description of this phenomenon is shown. Each part of the locus starts at a binary l_1l_2g

boundary and extends to a $l_1 = l_2 + g$ critical endpoint. When these two critical endpoints overlap a DCEP forms. Patton et al. [40] first observed unexpected fluid multiphase behaviour for the ternary system $\text{CO}_2 + 1\text{-decanol} + n\text{-tetradecane}$ when they found the two-phase l - g hole in the l_1l_2g three phase surface. The phenomenon was later confirmed by Peters et al.[38]. From their research, it was found that the complex phase behaviour arising in the ternary system is due to the aggregates of 1-decanol occurring from the multimer hydrogen bonds [38], [40].

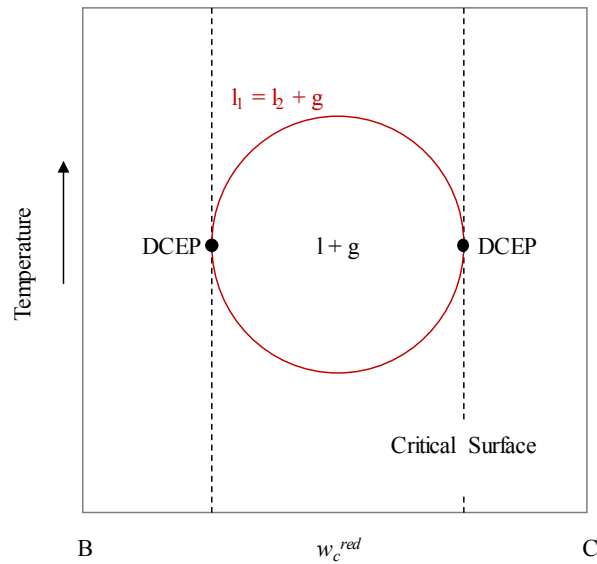


FIGURE 2- 18: SCHEMATIC REPRESENTATION OF THE CLOSED L-G HOLE PHENOMENON OCCURRING IN TERNARY SYSTEMS.

ADAPTED AND REDRAWN USING PETERS ET AL. [36].

Scheidgen and Schneider [3] later proved that the l - g hole originates from the strong influence of cosolvency on the multiphase behaviour in the ternary system [33]. Essentially, the cosolvency effects shift the critical surface to low enough pressures for it to penetrate the l_1l_2g three-phase surface below it. For ease of clarity, this penetration is shown using a pseudo-binary representation in *Figure 2-19*.

The non-critical l - g hole in the critical surface is caused by the same miscibility enhancement (cosolvency effects) that resulted in the two-phase l - g hole in the three-phase l_1l_2g surface. Therefore, the l - g holes are identical.

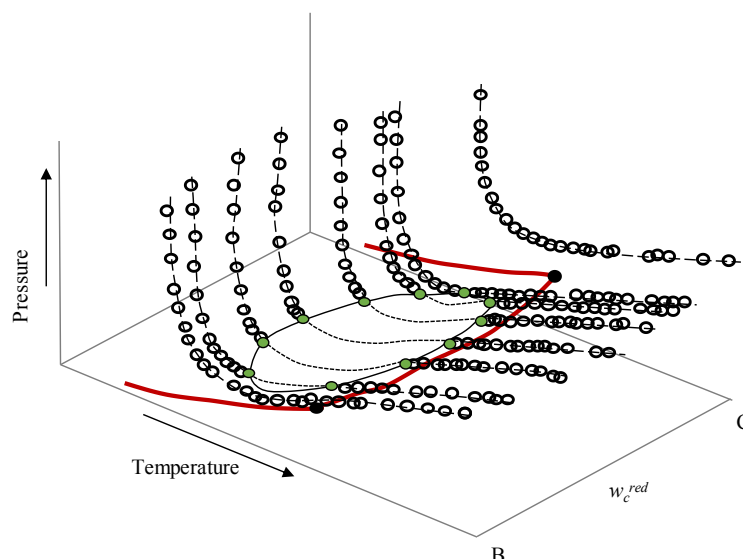


FIGURE 2- 19: QUASI-BINARY REPRESENTATION OF THE CRITICAL SURFACE PENETRATING THE THREE-PHASE L_1L_2G SURFACE TO FORM A L-G HOLE/NON-CRITICAL HOLE. ADAPTED AND REDRAWN USING GAUTER ET AL. [54]. — (RED) L_1L_2G THREE-PHASE SURFACE, ○ CRITICAL POINTS, ● (GREEN) CRITICAL ENDPOINTS, METASTABLE CRITICAL LINE.

2.2.4. COSOLVENCY EFFECTS

Cosolvency indicates that a mixture of two solute components B and C in a supercritical solvent A, ($A + B + C$), will be more soluble than when mixed individually in A, ($A + B$ or $A + C$). The phenomenon will occur for ternary mixtures if the following conditions are met [3]:

- (i) The low volatile components (solute B and C) are chemically different.
- (ii) The critical temperature and pressures of the solutes are very similar.
- (iii) There are no interactions, i.e. hydrogen bonding, between solute B and C.

Mathematically, the cosolvency effects are defined as the difference between the lower of the two binary sub-systems upper critical pressure and the pressure minimum of the isothermal ternary critical line [3]:

$$\Delta P_{min} = P_{A+C, min}^c - P_{A+B+C, min}^c \text{ with } P_{A+C}^c < P_{A+B}^c \quad (2.7)$$

The presence of cosolvency effects in the interested ternary system were confirmed by Patton et al. [40] who measured the phase compositions for two mixtures as a function of pressure over the three-phase l_1l_2g region of the ternary system at $T = 293.15$ K. The two mixture isotherms are shown in Figure 2-20 to indicate the ternary critical line at $T = 293.15$ K.

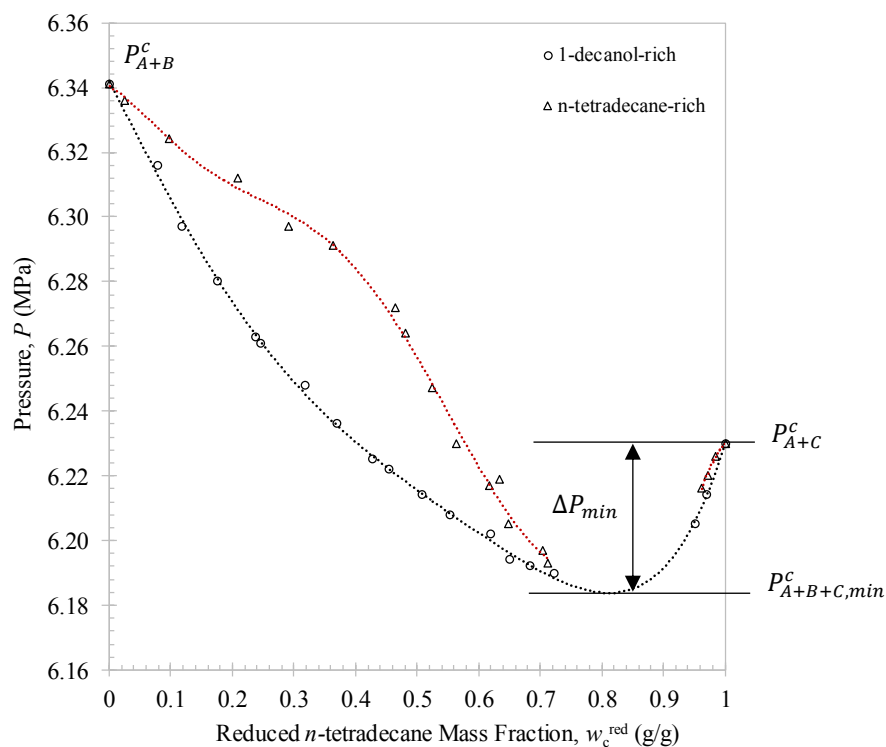


FIGURE 2- 20: ISOTHERMAL PRESSURE AGAINST REDUCED *N*-TETRADECANE OF THE TERNARY CRITICAL LINE, TO ILLUSTRATE THE SIZE AND RANGE OF COSOLVENCY EFFECTS. MEASURED BY PATTON ET AL.[40].

This extreme in the mixture pressure under isothermal conditions will result in the formation of an azeotrope. The phenomenon is defined as the formation of a point/plane where the vapour and liquid equilibrium w_c^{red} compositions are equal. Smith et al. [63], explains that in the presence of CO₂ azeotropes form when the difference in magnitude of the attractions between the like and unlike liquid phase intermolecular molecules are great enough. Therefore, as shown in *Figure 2-20*, the exact size and range of the cosolvency effects can be obtained visually by plotting a vapour-like and a liquid-like isotherm together on a P - w_c^{red} graph at isothermal conditions. The line formed between the critical surface of the ternary system ($P_{A+B+C,min}^c$) and the critical point of the lower binary system ($P_{A+C,min}^c$) of the separated two-phase areas in *Figure 2-20* indicates the ternary critical line at a constant temperature.

The ternary critical line is shown more clearly in *Figure 2-21* with the use of a three-dimensional prism of the system under isothermal conditions and varying the pressure. Due to the line running through a pressure minimum, the one-phase region in the ternary system has become much larger than the two-phase regions, indicating that the solubility of the mixture in supercritical CO₂ is higher than that of the pure components in supercritical CO₂ [40]. The critical isopleth, at constant w_c^{red} , is now at a lower pressure than its counterparts for the binary systems [78]. Subsequently this will result in the formation of miscibility windows.

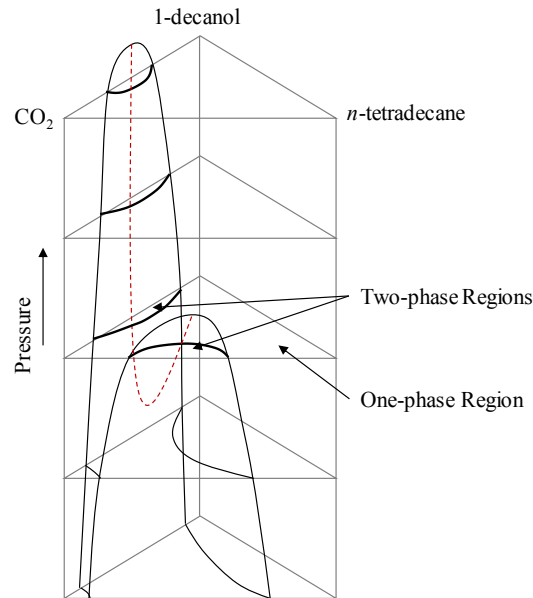


FIGURE 2- 21: ISOTHERMAL PHASE PRISM FOR A TERNARY SYSTEM WITH COSOLVENCY EFFECTS WITH THE P - w_c^{RED} PROJECTION OF THE RIGHT REAR FACE.

2.2.5. CLOSED ISOBARIC MISCIBILITY WINDOWS

The phenomenon is defined as a homogenous one-phase region that is completely surrounded by a two-phase region [3], [54]. The one-phase region will form upon adding a third component to a binary mixture that is in the two-phase state [78]. The P - T - w_c^{red} phase cube can be used to visually define the phenomenon. The critical surface is shaped in the form of a ‘chair’ as shown in *Figure 2-22*.

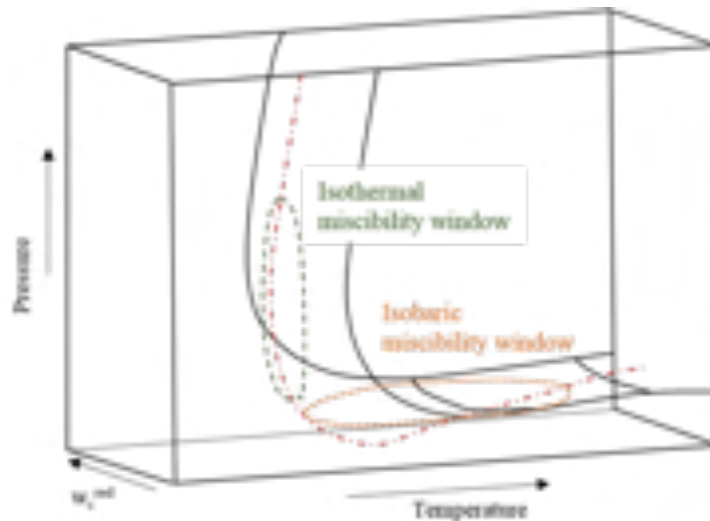


FIGURE 2- 22: QUASI-BINARY REPRESENTATION OF A TERNARY SYSTEM EXHIBITING MISCIBILITY WINDOWS. ADAPTED AND REDRAWN USING SCHEIDGEN AND SCHNEIDER [82]. - · - · - (RED) CRITICAL LINE OF ISOPLETH, - - - ISOBARIC AND - - - ISOTHERMAL CRITICAL LINES.

A decrease in pressure due to cosolvency effects (miscibility enhancement) will cause the ‘seat’ to sink and form the isobaric miscibility window [82]. Similarly, a decline in temperature will form an

isothermal miscibility window and has been described in detail elsewhere [3]. For the phenomenon to occur, the following criteria must be met [3]:

- (i) The critical lines of the binary sub-systems A + B and A + C have a similar shape.
- (ii) The critical lines display a pressure minimum.
- (iii) The A + B + C ternary system shows isothermal cosolvency effects.

Evidently, all three the criteria required for the topological phenomenon, miscibility windows, have been identified for the interested system. Published data by Scheidgen and Schneider [3] is used to construct the phase diagram shown in *Figure 2-23*. The isobaric miscibility window is only present between the pressure minimum of the CO₂ + *n*-tetradecane critical line at $P = 7.82$ MPa [17] and the highest critical end point pressure limiting the *l*-g hole at $P = 7.32$ MPa (LCEP of the ternary system). The critical end points are indicated by the larger solid circles and the hatched region represents where the closed isobaric miscibility windows appear.

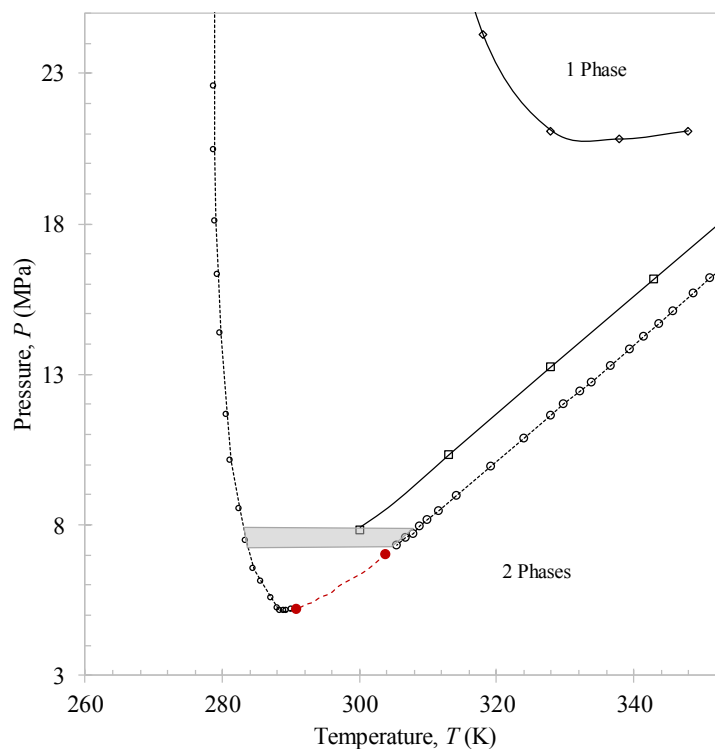


FIGURE 2-23: P - T PROJECTION OF THE TWO BINARY CRITICAL CURVES ($-\diamond-$ CO₂ + 1-DECANOL SYSTEM [15]; $-\square-$ CO₂ + *N*-TETRADECANE [17]) AND THE MINIMUM CURVE OF THE CRITICAL SURFACE AT A REDUCED *N*-TETRADECANE MASS FRACTION OF 0.84 G/G, $\cdots\circ\cdots$ MEASURED BY SCHEIDGEN AND SCHNEIDER [3].

2.2.6. CLASSIFICATION OF THE CO_2 + 1-DECANOL + *N*-TETRADECANE SYSTEM AND THIRD BINARY SUB-SYSTEM

The miscibility window measured by Scheidgen and Schneider [3] within the l_1l_2g three-phase region of the CO_2 + 1-decanol + *n*-tetradecane system infers T-IV phase behaviour. Therefore, the ternary system will have two Type III binary sub-systems (CO_2 + 1-decanol and CO_2 + *n*-tetradecane) and one Type I sub-system (1-decanol + *n*-tetradecane). Type I behaviour assumes that only one liquid phase exists throughout the phase diagram. Therefore, the two solutes, 1-decanol and *n*-tetradecane are miscible, with close boiling points, possibly resulting in a homogeneous azeotrope. These systems will be identified as displaying Type I-A fluid phase behaviour [79]. The two main variants of azeotropic behaviour, i.e. positive and negative, are well defined in literature [79], [84]–[87]:

Positive azeotropy:

Positive azeotropy is most commonly observed for non-polar or weakly polar molecules where *the interactions between the like molecules (solute + solute) are stronger than the interactions between the unlike molecules (solute + solvent)*. Thus, a positive deviation from Raoult's law occurs **due to solvation or association effects**, i.e. the vapour pressure of the azeotropic mixture is greater than the pure component vapour pressures at a constant temperature.

Negative azeotropy:

Negative azeotropy is seldomly observed for non-polar or weakly polar molecules. Therefore, they are more likely to occur in mixtures where *the interactions between the unlike molecules (solute + solvent) are stronger than those between the like molecules (solute + solute)*. Thus, a negative deviation from Raoult's law will take place due to **hydrogen bonding or proton transfers**, i.e. the vapour pressure of the azeotropic mixture is less than the pure component vapour pressures at a constant temperature.

It is postulated that a positive azeotrope (positive deviation from Raoult's law) will be observed for the 1-decanol + *n*-tetradecane binary sub-system. This assumption is based on the following:

- (i) The complex phase behaviour identified in the ternary system indicates strong solute + solute interactions.
- (ii) The binary sub-system comprises of non-polar *n*-tetradecane molecules and weakly polar 1-decanol molecules.
- (iii) Pertinent 1-alcohol + *n*-alkane literature data were gathered and are tabulated in *Table 2-4* to identify the type of phase behaviour to be anticipated for the 1-decanol + *n*-tetradecane system. For each of the 1-alcohol + *n*-alkane binary systems a general trend is identified: in 1-alcohol +

n -alkane systems with $m < n$, where m and n represent the number of carbon atoms in the *alkyl*-chains of the 1-alcohol and n -alkane, respectively, an azeotrope is identified.

Based on the non-ideal phase behaviour illustrated by these polar + non-polar systems and the complex phase behaviour phenomena in the ternary system, an extensive experimental study of binary 1-alcohol + n -alkane VLE data will be carried out in this work to verify the new 1-decanol + n -tetradecane phase equilibria data. The binary systems that will be measured for verification include: 1-pentanol + n -nonane, 1-hexanol + n -decane, 1-heptanol + n -undecane and 1-octanol + n -dodecane. Furthermore, due to the high boiling points of the interested systems, it is preferred to measure the data at sub-atmospheric conditions. This is in line with literature findings, as *Table 2-4* shows that sub-atmospheric pressures are generally used to measure 1-alcohol + n -alkane binary systems. A suitable setup that can be operated at sub-atmospheric conditions and high temperatures should therefore also be considered for the systems of interest to this work.

TABLE 2- 4: COMPILATION OF AVAILABLE BINARY VLE DATA FOR 1-ALCOHOL + *N*-ALKANE SYSTEMS TO DEFINE THE EXPECTED PHASE BEHAVIOUR; SUMMARISED USING GÖREL ET AL.[88].

<i>Alcohol</i>	<i>n-alkane</i>	<i>Azeotropic</i> ●; <i>non-azeotropic</i> ○	<i>Positive</i> +; <i>Negative</i> -	<i>Temperature and Pressure Range</i>	<i>Reference</i>
1-pentanol	<i>n</i> -pentane	○		T: 303 K; 323 K P: 0-160 kPa	Ronc & Ratcliff [89]
	<i>n</i> -hexane	●	-	T: 303 K; 323 K P: 0-55 kPa	Ronc & Ratcliff [89]
	<i>n</i> -heptane	●	-	T: 313 K; 348 K P: 0-50 kPa	Rhodes et al.[90] Máchová et al.[91]
	<i>n</i> -octane	●	+	T: 313 K; 373 K P: 0-55 kPa	Oracz [92] Treszczanowicz & Treszczanowicz [93]
	<i>n</i> -decane	●	+	T: 363 K P: 6-17 kPa	Treszczanowicz & Treszczanowicz [93]
1-hexanol	<i>n</i> -hexane	○		T: 298 K; 323 K; P: 0-105 kPa	Wieczorek & Stecki [94]
1-octanol	<i>n</i> -hexane	○		T: 313 K; 333 K P: 8-80 kPa	Heintz et al.[95] Schmelzer & Taummler [96]
	<i>n</i> -heptane	○		T: 293 K; 313 K P: 0-13 kPa	Geiseler et al.[97]
	<i>n</i> -decane	●	+	T: 393 K; 413 K P: 7-40 kPa	Schmelzer & Taummler [96]
	<i>n</i> -undecane	●	+	T: 393 K; 413 K P: 7-25 kPa	Schmelzer & Taummler [96]
	<i>n</i> -dodecane	●	+	T: 393 K; 413 K P: 4-20 kPa	Schmelzer & Taummler [96]
1-decanol	<i>n</i> -hexane	○		T: 283 K; 303 K; P: 0-53 kPa	Wieczorek [98]
1-dodecanol	<i>n</i> -hexane	○		T: 298 K; 323 K; P: 0-102 kPa	Heintz et al.[99] Wieczorek [100]
	<i>n</i> -tridecane	●	+	T: 413 K; 453 K P: 1-24 kPa	Schmelzer et al.[101]
1-tetradecanol	<i>n</i> -undecane	○		T: 393 K; 413 K P: 0-21 kPa	Schmelzer et al.[102]

2.3. CHAPTER OUTCOMES

The aim of this chapter was to investigate the phase behaviour of the ternary system and its three binary sub-systems. Each of the CO₂ binary sub-systems could be classified as Type III fluid phase behaviour using data available in open literature [40], [72], [73]. On the other hand, no experimental data could be found for the 1-decanol + *n*-tetradecane binary sub-system and consequently, no classification for its phase behaviour could be established. However, the finding of a two-phase *l*-g hole, a closed isobaric miscibility window and isothermal cosolvency suggests distinct solute + solute interactions in the CO₂ + 1-decanol + *n*-tetradecane ternary mixture. The complex phase behaviour infers Class T-IV ternary fluid phase behaviour which further hints at Type I-A fluid phase behaviour for the 1-decanol + *n*-tetradecane sub-system. Evidently, the literature study conducted on the CO₂ + 1-decanol + *n*-tetradecane ternary system proves that there remains a lack in supercritical data available. *Table 2-5* summarises each of the literature findings and where there was information needed. In addition, *Table 2-5* lists how this work contributed to solving these problem areas and which objectives were achieved in each chapter.

TABLE 2- 5: RESEARCH GAPS IN OPEN LITERATURE FOR THE TERNARY CO₂ + 1-DECANOL + *N*-TETRADECANE SYSTEM AND HOW EACH WILL BE ADDRESSED IN THIS WORK.

<i>Rational for further investigation</i>	<i>Additional work to be done in this study</i>	<i>Objective(s) achieved and in what Chapter</i>
Scheidgen and Schneider [3] measured a single CO ₂ + 1-decanol + <i>n</i> -tetradecane mixture ($w_c^{red} = 0.84$ g/g) to illustrate the miscibility window on a <i>P-T</i> projection. However, additional w_c^{red} mixtures are required to construct the 3D ternary critical surface and Gibbs phase triangles. In so doing, an adequate representation of the ternary phase behaviour surface can be obtained. Once the three-phase region has been defined the miscibility regions can be confirmed and a final classification of the ternary system can be established.	New HPBDP data were measured for the ternary system.	Objective 1.1 and 1.3 (Chapter 5)
Patton et al.[40] and Peters et al.[36] both measured the full <i>l</i> -g hole forming within the ternary system at near-critical conditions which serves as an important phenomenon to be considered in near-critical separation processes. However, the precise <i>P T-w_c^{red}</i> conditions where cosolvency will occur for the interested ternary system have not yet been measured. Knowing the size and range of this phenomenon will help improve the separation process at supercritical conditions.	New HPBDP data were measured for the ternary system.	Objective 1.1 and 1.3 (Chapter 5)

<i>Rational for further investigation</i>	<i>Additional work to be done in this study</i>	<i>Objective(s) achieved and in what Chapter</i>
Scheidgen and Schneider [3] were also successful in measuring the isobaric miscibility window in the CO ₂ + 1-decanol + <i>n</i> -tetradecane system. According to the classification of Bluma and Deiters [78], the miscibility window infers T-IV fluid phase behaviour for the interested ternary system. Ternary Class T-IV phase behaviour indicates Type I-A phase behaviour for the 1-decanol + <i>n</i> -tetradecane binary sub-system. To confirm the Type I phase behaviour, experimental VLE data are required to investigate the 1-decanol + <i>n</i> -tetradecane system.	New LPVLE data were measured for the binary sub-system 1-decanol + <i>n</i> -tetradecane as well as 4 pertinent binary systems to verify the 1-decanol + <i>n</i> -tetradecane binary data.	Objective 2 (Chapter 6)
The complex phase behaviour phenomena measured, by Scheidgen and Schneider [3], Patton et al.[40] and Peters et al.[36], at operating conditions near the solvent critical region indicate VLLE three-phase regions which will cause difficulties in the control of SFF processes. In the past, the three-phase regions would be ignored and avoided in these types of separation processes. Instead of avoiding the <i>l₁l₂g</i> three-phase regions, the solute + solute interactions can be better investigated by constructing the tie lines of the ternary phase diagrams (within the cosolvency effects region). In so doing, one can establish the relative solubility of the components using supercritical CO ₂ .	New HPVLE data were measured for the ternary system.	Objective 1.2 and 1.4 (Chapter 5)

Table 2-5 highlights the first three scientific contributions that were made in this work (see Section 1.5). The use of HPBDP, HPVLE and LPVLE phase equilibria data can help to design, operate and optimise SFF process. However, measuring phase equilibria data can be a tedious, time consuming and expensive exercise. The necessary equipment to ensure accurate and robust measurements are not always readily available. Based on this, the use of thermodynamic models which can be used to correlate the thermodynamic properties and predict the high- and low-pressure phase behaviour are becoming increasingly popular. Essentially, this is done with the use of a predictive model. However, predictive models are not always equipped to take into consideration complexities from undesired phase behaviour. Therefore, suitable thermodynamic models that can improve their phase equilibria correlations by incorporating, amongst others, solute + solute BIPs into their algorithm were considered alongside predictive models in the next chapter (**Objective 3.1**).

Chapter 3

HOLISTIC THERMODYNAMIC MODEL SELECTION

This chapter introduces the second part of this thesis, which is devoted to the thermodynamic modelling of the ternary system and its three binary sub-systems. Emphasis will be placed on the use of property methods available within Aspen Plus[®].

*The aim of this chapter is twofold: first, to assess both classical and advanced thermodynamic models; and second, to select suitable methods within Aspen Plus[®] (**Objective 3.1**), which can potentially be used not simply for modelling complex VLE behaviour, but also for industrial applications.*

First, a short-unified presentation of the phase equilibria fundamentals will be given, highlighting the direction for selecting a suitable model. The flexible and predictive property methods will be described in separate sections to define their fundamental equations. The chapter will close with a discussion of the selected association *EoS* property method and the parameters to be used for correlating the complex phase behaviour of the CO₂ + 1-decanol + *n*-tetradecane system.

3.1. INDUSTRIAL RELEVANCE OF ASPEN PLUS[®]

The purpose of evaluating, selecting and improving thermodynamic models found in Aspen Plus[®] is to ultimately end with a working process model like that designed by Zamudio et al. [12]. However, the design of a process model falls beyond the scope of this work. The focus will remain on obtaining a fundamental understanding of the impact the solute + solute interaction parameters have on the ability of thermodynamic models to correlate measured equilibrium data. Aspen Plus[®] is a popular commercial process simulator that is available to various industrial sectors. Furthermore, it was validated as a reliable thermodynamic tool in a previous research project conducted by Lombard [51]. Parameters were regressed for the Redlich-Kwong-Aspen (RK-Aspen) model [103] in Aspen Plus[®] and the resultant correlations agreed with those obtained by an in-house developed model with MATLAB software. Based on the ease of availability and accuracy of Aspen Plus[®], the strategies developed in this work with this commercial simulator can be repeated and implemented in similar separation processes elsewhere.

3.2. PHASE EQUILIBRIA FUNDAMENTALS

The first step in modelling the measured data is to determine the correct thermodynamic model to use for the close boiling point detergent range 1-alcohols and n -alkanes. There are two main approaches to phase equilibria: γ - ϕ and ϕ - ϕ . Here, γ accounts for the deviations from ideality via the activity coefficient and the deviation of the fluid from ideal **solution** behaviour. Analogously, ϕ accounts for the deviations from ideality via the fugacity coefficient and the deviation from ideal **gas** behaviour.

The fundamental property determining the equilibrium of a specific component between phases and chemical reactions is chemical potential. The chemical potential of species i , can mathematically be defined using the partial Gibbs energy equation [63]:

$$\mu_i = \left(\frac{\partial(nG)}{\partial x_i} \right)_{T,P,x_j} \quad (3.1)$$

When the chemical potential of multiple species is the same in all phases, at the same temperature and pressure, they are said to be in equilibrium with one another [63]:

$$\mu_i^\alpha = \mu_i^\beta = \mu_i^\pi \quad (3.2)$$

To define the chemical potential of real gasses and liquids the concept of fugacity needs to be utilised. Fugacity is a representation of the effective or real partial pressure of species i , in a specific phase and can mathematically be defined using [63]:

$$\mu_i = \bar{G}_i = G_i(T) + RT \ln(\hat{f}_i) \quad (3.3)$$

Therefore, fugacity will be a function of the temperature, pressure and composition of species i in a solution, at phase equilibrium:

$$\hat{f}_i^l(T, P, x) = \hat{f}_i^v(T, P, y) \quad (3.4)$$

Fugacity can be estimated with either the γ approach or the ϕ approach. For the γ approach, deviations from the ideal solution can be calculated using:

$$\hat{f}_i = x_i \gamma_i \phi_i^{sat} P_i^{sat} \exp \frac{1}{RT} \int_{P_i^{sat}}^{P_i} V_i^l dP \quad (3.5)$$

For the ϕ approach the deviations from the ideal gas can be calculated using equations (3.6) and (3.7) for the vapour and liquid phase, respectively.

$$\hat{f}_i^v = y_i P \hat{\phi}_i^v \quad (3.6)$$

$$\hat{f}_i^l = x_i P \hat{\phi}_i^l \quad (3.7)$$

Unfortunately, the γ approach requires the calculation of saturation pressures and therefore, all compounds must remain below their respective critical point. Thus, applications of this method for critical and supercritical pressures can become rather difficult and inaccurate.

For each component in equilibrium can be expressed using equation (3.8) after the substitution of equations (3.6) and (3.7) into (3.4).

$$y_i \hat{\phi}_i^v = x_i \hat{\phi}_i^l \quad (3.8)$$

To solve for the fugacity of component i in a mixture, $\hat{\phi}_i$ the residual Gibbs energy equation for a mixture (3.9) must be used:

$$\ln \hat{\phi}_i^v = \left[\frac{\partial(nG^R)}{\partial x_i} \right]_{P,T,x_j} \quad (3.9)$$

EoS s can be used to calculate nG^R . Among other techniques, the ϕ - ϕ approach is the best method to use in calculating the fluid phase equilibria of the system of interest. For further details of the ϕ - ϕ approach one is referred to Smith et al. [63].

3.3. CUBIC EoS PROPERTY METHODS

Systematic literature investigations have shown that classical cubic EoS models can, to a certain degree, accurately represent hydrocarbon + gas and hydrocarbon + hydrocarbon VLE mixtures at low- and high-pressures [43], [45], [101], [102], [104]–[107]. Thus, the SRK and PR EoS are further investigated in this work. In general, a cubic EoS can be written using equation (3.10).

$$P = \frac{RT}{V_m - b} - \frac{a}{(V_m + \lambda_1 b)(V_m + \lambda_2 b)} \quad (3.10)$$

Where, $\lambda_1 = 1$ and $\lambda_2 = 0$ (SRK); or $\lambda_1 = 1 - \sqrt{2}$ and $\lambda_2 = 1 + \sqrt{2}$ (PR).

The current study deals with mixtures and therefore, mixing rules are required. To calculate the energy parameter and co-volume parameters, the quadratic vdW one fluid mixing rules can be applied with the cross coefficient written in terms of an inclusive binary interaction parameter. The geometric mean rule is applied to represent the attractive force between two molecules (equation 3.11) and the arithmetic mean rule to relate to the volume that a species occupies (equation 3.12) [18], [107], [108]. The pure component parameters can be calculated with equations (3.13 a) and (3.13 b).

$$a = \sum_{i=1}^n \sum_{j=1}^n x_i x_j (a_i a_j)^{0.5} (1 - k_{ij}) \quad (3.11)$$

$$b = \sum_{i=1}^n \sum_{j=1}^n x_i x_j \frac{(b_i + b_j)}{2} (1 - l_{ij}) \quad (3.12)$$

$$a_i = \alpha_i(T) \cdot \Omega_a \cdot \frac{R^2 T_{c,i}^2}{P_{c,i}} \quad (3.13 \text{ a})$$

$$b_i = \Omega_b \cdot \frac{RT_{c,i}}{P_{c,i}} \quad (3.13 \text{ b})$$

Where, $\Omega_a = 0.42747$ and $\Omega_b = 0.08664$ (SRK); or $\Omega_a = 0.45724$ and $\Omega_b = 0.07780$ (PR).

The temperature dependent alpha function, $\alpha_i(T)$ shown in equation (3.13 a) can be calculated using equation (3.14) and substituting equation (3.15 a) or (3.15 b) for the SRK or PR EoS , respectively. In general, these terms were empirically established to best fit experimental data [109].

$$\alpha_i(T) = [1 + m_i(1 - \sqrt{T_{r,i}})]^2 \quad (3.14)$$

$$m_i = 0.48 + 1.574\omega_i - 0.176\omega_i^2 \quad (3.15 \text{ a})$$

$$m_i = 0.37464 + 1.54226\omega_i - 0.26992\omega_i^2 \quad (3.15 \text{ b})$$

Cubic *EoS* with the classical mixing and combining rules could, to a certain degree, represent polar mixtures when considering the BIPs. However, regardless of the added BIPs, for highly polar and hydrogen bonding mixtures, the classical quadratic mixing rules fail to represent the phase equilibria accurately and false phase splits are calculated [42], [107], [110]. This problem area can partially be addressed within the framework of cubic *EoS* with more advanced mixing rules, i.e. the *EoS-G^E* mixing rules proposed by Huron and Vidal [111].

3.4. PREDICTIVE PROPERTY METHODS IN ASPEN PLUS[®]

EoS-G^E mixing rules permit an expression for the excess Gibbs energy, *G^E* to be incorporated into the *EoS*. In so doing, a single model is established which combines the strengths of both the cubic *EoS* and the activity coefficient models [107]. The predictive models can be derived from the following equality at a reference pressure:

$$\left(\frac{G^E}{RT}\right)_P^{EoS} = \left(\frac{G^E}{RT}\right)_P^{model,*} \quad (3.16)$$

The left-hand side of equation (3.16) represents the *G^E* of the *EoS* and can be obtained using the fugacity coefficient as computed by *EoS* (see equation (3.9)). The right-hand side of equation (3.16) defines the *G^E* expression of an explicit activity coefficient model. Here, the subscript, * will give reference to, for example the Wilson [112], NRTL [113] or UNIQUAC [114] model. Any activity coefficient model with available BIPs can be used.

$$\therefore \frac{G^E}{RT} = \ln \varphi - \sum_i x_i \ln \hat{\varphi}_i = \sum_i x_i \ln \gamma_i \quad (3.17)$$

3.4.1. UNIFAC GROUP CONTRIBUTION METHOD

If low-pressure data are unavailable for the regression of BIPs, a group contribution method can be used to predict the missing phase equilibria data [115]. With group contribution methods, the mixture is described using different functional groups (group-group interaction parameters), not molecules, as shown in *Figure 3-1* for 1-decanol and *n*-tetradecane [116]. In this manner, for example, group interaction parameters derived from LPVLE experimental data of an available alcohol + alkane system can be used to predict the real behaviour of the alcohol + alkane system of interest to this work [117]–[119].

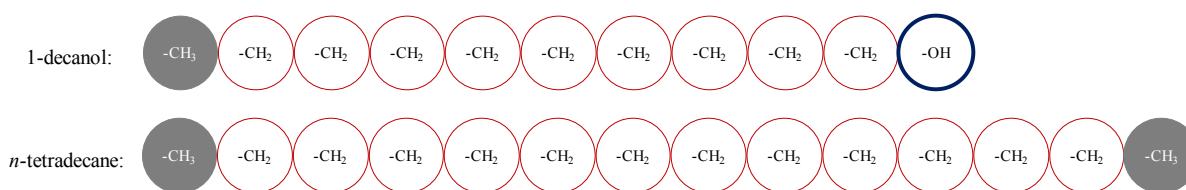


FIGURE 3- 1: GROUP CONTRIBUTION APPROACH FOR 1-DECANOL (1 X OH, 1 X CH₃, 9 X CH₂) AND *N*-TETRADECANE (2 X CH₃, 12 X CH₂).

The most common group contribution method in industry today is UNIFAC [120]–[122] due to its large collection of group interaction parameters available in a computerised data bank DDB¹ (Christensen et al.[123] for 1984 to 1991 and Gmehling et al.[124] for 1977 to 1996). The required UNIFAC activity coefficient shown in equation (3.17) is calculated by two parts:

$$\ln \gamma_i = \ln \gamma_i^c + \ln \gamma_i^r \quad (3.18)$$

- (i) A combinatorial part that accounts for the size and shape of the molecules, γ_i^c calculated with the Guggenheim-Staverman term shown in equation (3.19). The molecular volume, Φ_i (3.19 a) and surface fraction, θ_i (3.19 b) are calculated using the group volume, r_i and group area, q_i parameters shown in equation (3.19 c) and (3.19 d), respectively [2], [116], [125], [126].

$$\ln \gamma_i^c = \ln \left(\frac{\Phi_i}{x_i} \right) + 1 - \frac{\Phi_i}{x_i} - \frac{z}{2} \left[\ln \frac{\Phi_i}{\theta_i} + 1 - \frac{\Phi_i}{\theta_i} \right] \quad (3.19)$$

$$\Phi_i = \frac{x_i r_i}{\sum_j^{nc} x_j r_j} \quad (3.19 \text{ a})$$

$$\theta_i = \frac{x_i \frac{z}{2} q_i}{\sum_j^{nc} x_j \frac{z}{2} q_j} \quad (3.19 \text{ b})$$

$$r_i = \sum_k^{ng} v_{ki} R_k \quad (3.19 \text{ c})$$

$$q_i = \sum_k^{ng} v_{ki} Q_k \quad (3.19 \text{ d})$$

Where, z is the coordination number set to a default value of 10; and v_{ki} is the number of groups of type k in molecule i .

- (ii) A residual part that accounts for the interactions between each group, γ_i^r is calculated with the solution of groups concept shown in equation (3.20). The activity coefficient, Γ_k of a group, k at mixture composition shown in equation (3.20 a) is dependent on the group surface area fraction (3.20 b) rewritten in terms of the group mole fraction of group k in the liquid, X_k [2], [116], [125], [126]:

$$\ln \gamma_i^r = \sum_k^{ng} v_{ki} [\ln \Gamma_k - \ln \Gamma_k^i] \quad (3.20)$$

¹ Dortmund Data Bank

$$\ln \Gamma_k = Q_k \left[1 - \ln \sum_m^{ng} \theta_m \tau_{mk} - \sum_m^{ng} \left(\frac{\theta_m \tau_{km}}{\sum_n^{ng} \theta_n \tau_{nm}} \right) \right] \quad (3.20 \text{ a})$$

$$\theta_k = \frac{X_k \frac{Z}{2} Q_k}{\sum_j^{nc} X_m \frac{Z}{2} Q_m} \quad (3.20 \text{ b})$$

$$X_k = \frac{\sum_j^{nc} v_{kj} x_j}{\sum_j^{nc} \sum_m^{ng} v_{mj} x_j} \quad (3.20 \text{ c})$$

Using a generated function, τ_{mn} the residual term of the activity coefficient model is corrected with a temperature independent group interaction parameter, b_{mn} between group m and group n [127], [128]:

$$\tau_{mn} = \exp \left(-\frac{b_{mn}}{T} \right) \quad (3.21)$$

3.4.2. *EoS- G^E MIXING RULES*

The *EoS- G^E* mixing rules allows for the advantages of the group contribution models to be directly connected with the *EoS*. Subsequently, a strictly predictive tool is available for the prediction of VLE data at low- and high-pressures, irrespective of the presence of polar compounds [128], [129]. Various well known *EoS- G^E* models have been developed by different authors to enable VLE predictions at high and low temperatures or pressures as well as for supercritical compounds. These predictive *EoS* include, amongst others:

- (i) Huron-Vidal type mixing rules:
 - Predictive SRK (PSRK) mixing rule as suggested by Holderbaum and Gmehling [115], [116], [125], [127], [128], [130]–[136].
 - Modified Huron-Vidal second order approximation (MHV2) [115], [137]–[143].
- (ii) Linear combinations of Vidal and Michelsen mixing rules (LCVM) [115], [137], [144], [145].
- (iii) Wong-Sandler mixing rules (W-S) with an additional k_{ij} parameter [115], [119], [137], [142], [146]–[149].

Of importance to this study are *EoS- G^E* models available within Aspen Plus® and therefore, the LCVM mixing rules will not be investigated further. *Figure 3-2* summarises the predictive *EoS- G^E* property methods suggested by the Aspen Plus® software guide. For each of the property methods the distinctive *EoS* models on which they are based, the activity coefficient models implemented in their algorithm and some of their mixture characteristics are specified.

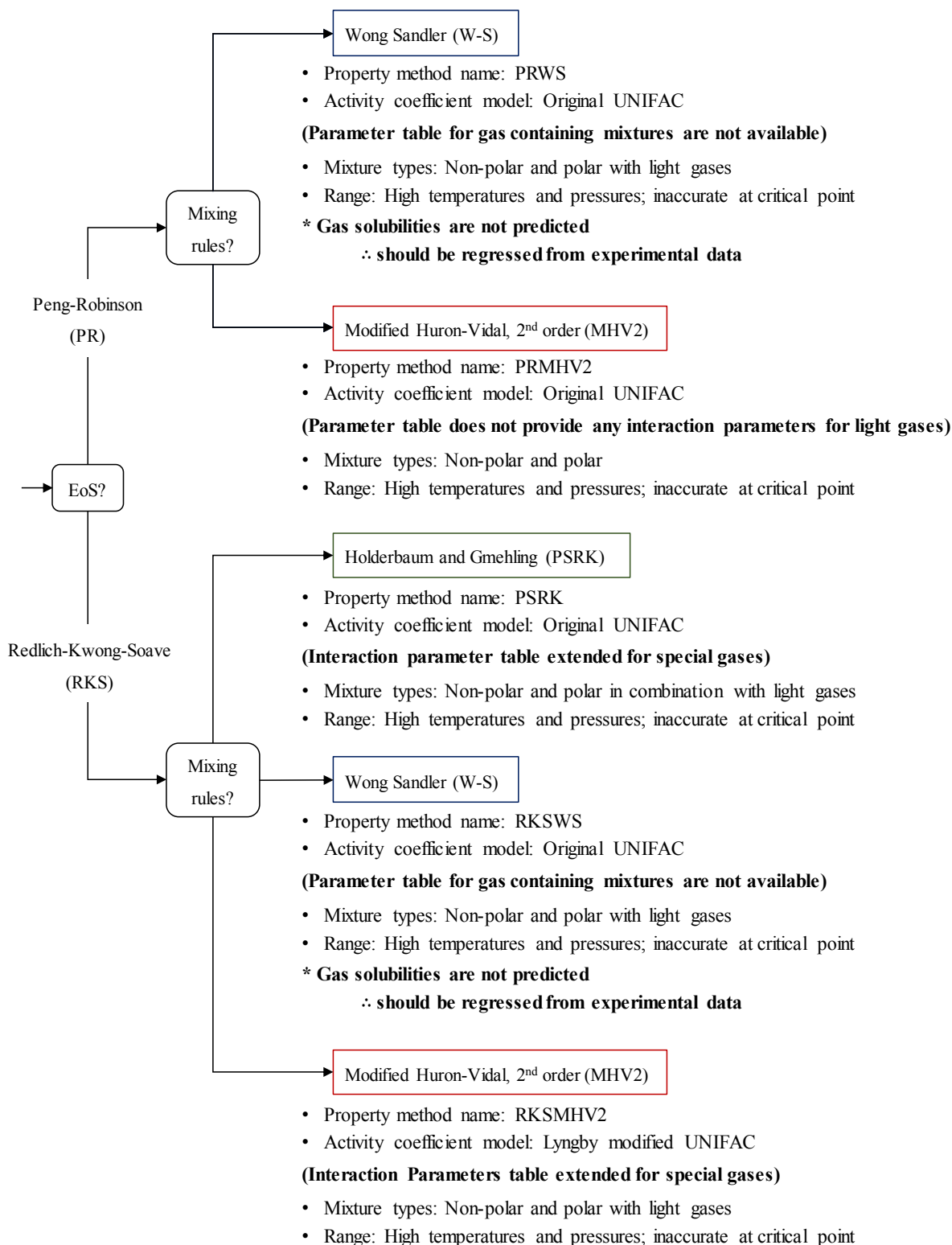


FIGURE 3- 2: BREAKDOWN OF THE PREDICTIVE $EoS-G^E$ PROPERTY METHODS SUGGESTED BY THE ASPEN PLUS[®] SOFTWARE GUIDE TO EVALUATE THEIR APPLICABILITY TO THE TERNARY SYSTEM OF INTEREST TO THIS STUDY.

Based on its predictive capabilities, the original UNIFAC model was chosen by Aspen Plus® for the PRWS and RKSWS models. Unfortunately, the W-S mixing rules have not been used extensively for mixtures with light gases. Therefore, no interaction parameter table is available for the gas containing mixtures of interest to this work when using the PRWS and RKSWS models and will thus be omitted from further investigation.

The G^E model for the PSRK property method is also the original UNIFAC model. However, unlike the W-S model, selecting the PSRK model in Aspen Plus® activates the new built-in temperature dependent group interaction parameters to the Aspen Plus® Physical Property System for the gas-containing mixtures [115]. The original UNIFAC generated function in equation (3.21) is replaced by [116]:

$$\tau_{mn} = \exp\left(-\frac{a_{mn} + b_{mn}T + c_{mn}T^2}{T}\right) \quad (3.22)$$

In the case of the RKSMHV2 method, the Lyngby modified UNIFAC model [127], [128], [132], [150] is used for optimum performance, allowing it to be applied to multiphase equilibria, i.e. VLLE of difficult mixtures. The group interaction parameters are temperature dependent and the G^E model parameters are calculated using the following generated function:

$$\psi_{mn} = \exp\left(-\frac{a_{mn,1} + a_{mn,2}(T-298.15) + a_{mn,3}\left(T \ln \frac{298.15}{T} + T - 298.15\right)}{T}\right) \quad (3.23)$$

For the full mathematical changes made to the original UNIFAC model, see literature elsewhere [150]. This extension has not yet been made for the PRMHV2 property method in Aspen Plus® as it still utilises the original UNIFAC model. Thus, the model is not suitable for predicting the VLE phase equilibria of the CO₂ binary systems nor the CO₂ + 1-decanol + *n*-tetradecane ternary system of interest to this study. It is recommended that the model only be applied to non-polar and polar mixtures. Based on these findings, the PSRK and RKSMHV2 property methods are the only two *EoS-G^E* models, within Aspen Plus®, that present suitable interaction parameters for the three binary sub-systems of interest to this work.

3.4.3. PSRK AND RKSMHV2 MODEL PREDICTIONS OF THE CO₂ BINARY SUB-SYSTEMS

A screening process of the PSRK and RKSMHV2 models was done to evaluate their applicability in predicting the VLE phase equilibria of the CO₂ + 1-decanol [15] (*Figure 3-3 a, c and e*) and CO₂ + *n*-tetradecane [17] (*Figure 3-3 b, d and f*) binary systems at $T = 308$ K, 328 K and 348 K. In so doing, the thermodynamic model providing the most accurate prediction of the experimental phase behaviour is identified.

As the temperature conditions of the binary CO₂ + 1-decanol system are increased from $T = 308$ K (*Figure 3-3 e*) to 328 K (*Figure 3-3 c*) and again to $T = 348$ K (*Figure 3-3 a*) the trend predicted by the

models move closer towards the literature phase equilibria. The RKSMHV2 model overshoots the phase split envelope at $T = 348$ K whereas the PSRK model provides an accurate prediction of the literature data at $T = 348$ K. Due to the temperature inversion taking place in the $\text{CO}_2 + 1\text{-decanol}$ system at $T = 308$ K, neither of the two group contribution models can predict the VLE phase equilibria. It is for this reason that other forms of EoS , such as those derived from Statistical thermodynamics, will also be investigated in this work [151]. The large association effects at temperatures near the critical point of the solvent are considered in statistical models and might lead to improved correlation of the complex phase behaviour [42], [107], [152], [153].

For the binary $\text{CO}_2 + n\text{-tetradecane}$ binary system at $T = 328$ K (Figure 3-3 d) and 348 K (Figure 3-3 b) the PSRK model under predicts the phase split envelope and the RKSMHV2 model overpredicts the VLE phase behaviour. Furthermore, at $T = 308$ K (Figure 3-3 f) neither of the models can provide an accurate prediction of the $\text{CO}_2 + n\text{-tetradecane}$ system. In fact, the RKSMHV2 predicts three-phase behaviour at $T = 308$ K which is not the case for the binary system.

3.4.4. LI-CORRECTION FOR SIZE-ASYMMETRIC GAS-ALKANE SYSTEMS

The PSRK and RKSMHV2 model predictions highlight the poor performance of these mixing rules when applied to size-asymmetric **gas-alkane** systems, such as the $\text{CO}_2 + n\text{-tetradecane}$ binary system. This limitation is addressed for the PSRK model with a modification proposed by Li et al. [130] (further referred to as the Li-correction). The modified PSRK model makes use of an *alkyl*-carbon number (n_c) dependent function:

$$f(n_c) = 1 - 0.36983(n_c)^{\frac{1}{2}} + 1.0287(n_c)^{\frac{3}{4}} - 1.0199(n_c) + 0.41645(n_c)^{\frac{4}{3}} - 0.05536(n_c)^{\frac{3}{2}} \quad (3.24)$$

For $n_c < 45$.

This function allows one to alter the original VdW volume (R_k) and surface area (Q_k) parameters to effective values of R_k^* and Q_k^* , respectively:

$$R_k^* = f(n_c) \cdot R_k \quad (3.24 \text{ a})$$

$$Q_k^* = f(n_c) \cdot Q_k \quad (3.24 \text{ b})$$

Here, the subscript, k refers to the different alkane subgroups C, CH, CH_2 and CH_3 . The $\text{CO}_2 + n\text{-tetradecane}$ system, amongst others, was investigated by Yang and Zhong [133] who used literature data published by Gasem et al. [67] to show how the pressure average absolute deviation ($\%AAD_P$)² decreased markedly from 25.8% to 1.4% when applying the Li -correction to the PSRK model. Based on these observations, the PSRK model with the Li-correction, is the first approach selected to model

² $\%AAD_P = \frac{100}{NDP} \sum_i \frac{|P_i^{\text{Calculated}} - P_i^{\text{Experimental}}|}{P_i^{\text{Experimental}}}$, where NDP is the number of data points.

the new CO₂ + 1-decanol + *n*-tetradecane experimental data measured in this work. The Li-correction for *n*-tetradecane will be calculated and presented in Chapter 7 with an included plot showing the improvements qualitatively. It is important to note that the correction is only applicable to size-asymmetric gas-alkane systems and not for gas-alcohol systems [130].

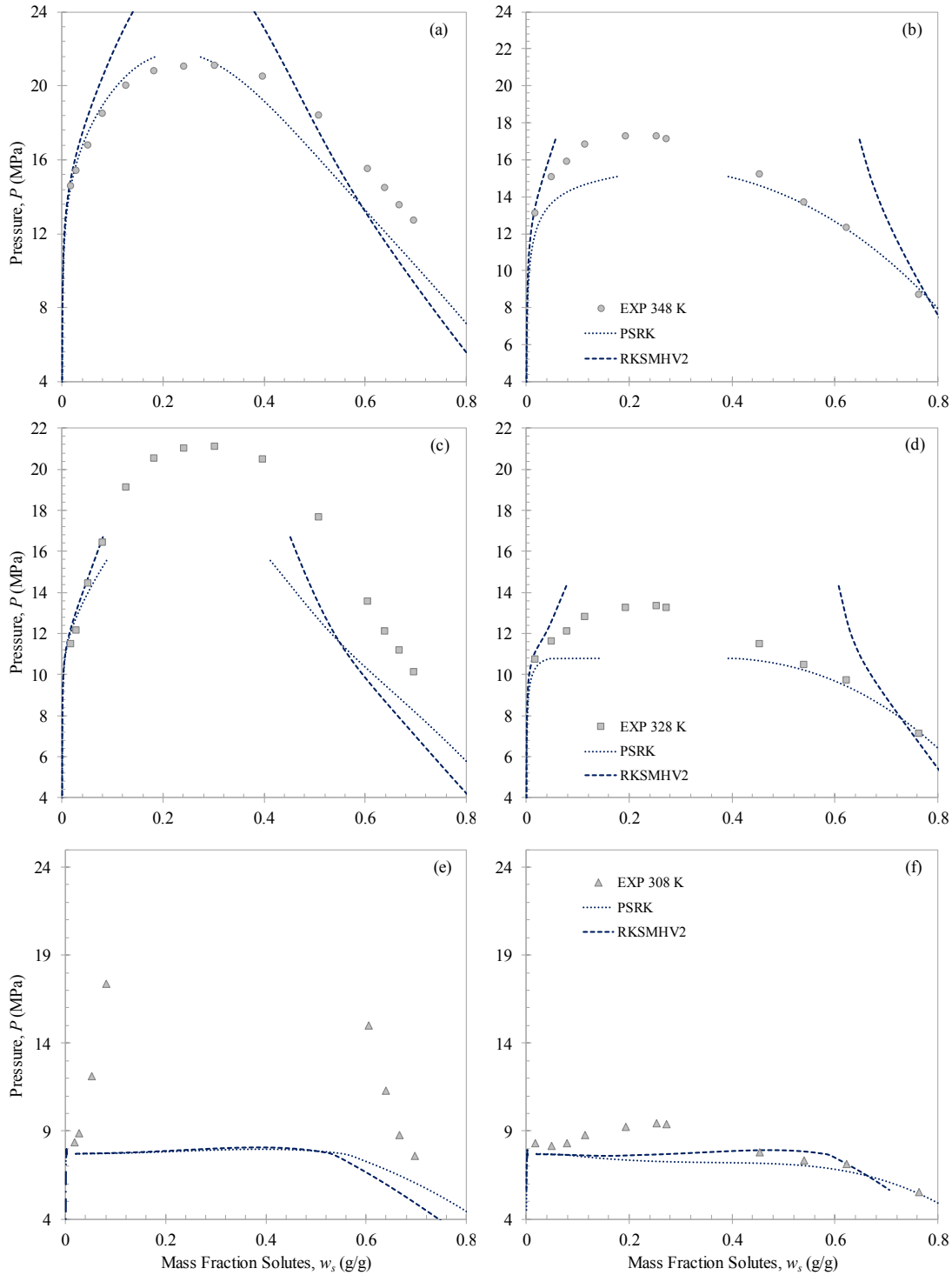


FIGURE 3-3: COMPARISON BETWEEN LITERATURE DATA AND PREDICTED DATA WITH THE PSRK AND RKSMHV2 MODELS FOR CO₂ + 1-DECANOL [15] AT (A) $T = 348$ K, (C) $T = 328$ K AND (E) $T = 308$ K; AND CO₂ + *N*-TETRADECANE [17] AT (B) $T = 348$ K, (D) $T = 328$ K AND (F) $T = 308$ K.

3.4.5. PSRK MODEL

The PSRK model within Aspen Plus® is based on the RKS *EoS* and utilises the PSRK mixing rules as developed by Holderbaum and Gmehling [127]. The PSRK method is an example of the modified Huron-Vidal mixing rules (MHV1) [111] however, makes use of a thermodynamic relationship between the excess Helmholtz energy, A^E and the SRK *EoS* [107]:

$$\frac{A^E}{RT} = \frac{A^{res}}{RT} - \sum_i x_i \frac{A_i^{res}}{RT} \quad (3.25)$$

$$A^{res} = A(T, P) - A^{ig}(T, P) = \int_{V_m=\infty}^{V_m} \left(\frac{RT}{V_m} - P \right) dV_m \quad (3.25 \text{ a})$$

$$\frac{A^{res}}{RT} = \frac{V_m}{V_m - b} - \frac{a}{bRT} \ln \frac{V_m + b}{V_m} \quad (3.25 \text{ b})$$

$$\therefore \frac{A^E}{RT} = \frac{\frac{V_m}{b}}{\frac{V_m}{b} - 1} - \frac{a}{bRT} \ln \frac{\frac{V_m}{b} + 1}{\frac{V_m}{b}} - \sum_i x_i \left(\frac{\frac{V_{m,i}}{b_i}}{\frac{V_{m,i}}{b_i} - 1} - \frac{a_i}{b_i RT} \ln \frac{\frac{V_{m,i}}{b_i} + 1}{\frac{V_{m,i}}{b_i}} \right) \quad (3.25 \text{ c})$$

The final generalization of the PSRK model, presented in equation (3.26), can be obtained based on the following assumptions [2], [115]:

- (i) A reference state pressure of approximately 1 atmosphere is assumed ($p \approx 1 \text{ atm}$).
- (ii) The packing fraction, $u = \frac{V_m}{b} = u_i = \frac{V_{m,i}}{b_i}$ is constant, i.e. $u = 1.1$.
- (iii) A linear mixing rule is used to calculate the co-volume parameter of the mixture: $b = \sum_i x_i b_i$
- (iv) The excess molar volume, v^E is neglected, i.e. $v^E = 0$.

$$\frac{A^E}{RT} = -0.64663 \left[\frac{a}{bRT} - \sum_i x_i \frac{a_i}{b_i RT} \right] = \frac{G^{E,*}}{RT} + \sum_i x_i \ln \frac{\sum_i x_i b_i}{b_i} \quad (3.26)$$

In the context of this investigation it is favourable to define the fugacity coefficient in terms of the excess Helmholtz energy. This is made possible by substituting equation (3.26) into (3.17). The species-specific energy and co-volume parameters are calculated with equation (3.13 a) and (3.13 b), respectively. For the *EoS* to predict accurate VLE data of these close boiling systems the temperature dependent alpha parameters, $\alpha_i(T)$ in equation (3.13 a) were calculated with the Mathias and Copeman expression [154]:

$$\alpha_i(T) = \left[1 + c_{1,i} \left(1 - T_{r,i}^{0.5} \right) + c_{2,i} \left(1 - T_{r,i}^{0.5} \right)^2 + c_{3,i} \left(1 - T_{r,i}^{0.5} \right)^3 \right]^2 \quad (3.27)$$

At subcritical conditions, up to three parameters $c_{1,i}$, $c_{2,i}$ and $c_{3,i}$ can be used and are regressed using pure component vapour pressure data. At supercritical conditions the constants $c_{2,i}$ and $c_{3,i}$ are set to zero and equation (3.27) reduces to the expression provided as equation (3.14).

The excess Gibbs energy, $G^{E,*}$ was obtained using the original UNIFAC model with special-gas group interaction parameters for the CO₂ binary sub-systems. The UNIFAC model was further modified with the Li-correction for the CO₂ + *n*-tetradecane combinations in the binary and ternary mixtures.

Therefore, this model has five pure component parameters for each subcritical component ($T_{c,i}$, $P_{c,i}$, $c_{i,1}$, $c_{i,2}$, $c_{i,3}$) and three for each supercritical component ($T_{c,i}$, $P_{c,i}$, ω_i). Additionally, for the CO₂ + 1-decanol and 1-decanol + *n*-tetradecane binary systems four group interaction parameters are used to improve the fit (a_{mn} , a_{nm} , Q_k , R_k); whereas for the CO₂ + *n*-tetradecane binary combination six group interaction parameters and two effective group parameters are used to improve the fit (a_{mn} , a_{nm} , b_{mn} , b_{nm} , c_{mn} , c_{nm} , Q_k^* , R_k^*).

3.5. FLEXIBLE PROPERTY METHODS IN ASPEN PLUS®

Two additional thermodynamic models suggested by the Aspen Plus® software guide for the systems considered in this investigation are:

- (i) Redlich-Kwong-Soave with Mathias mixing rules (RK-Aspen) [48], [49], [103]: The extended classical mixing rules used in this model are especially suited for systems with strong size and shape asymmetry, i.e. the CO₂ + *n*-tetradecane combinations in the ternary CO₂ + 1-decanol + *n*-tetradecane system.
- (ii) Redlich-Kwong-Soave with Schwarzenberger-Renon mixing rules (SR-Polar) [154]–[157]: The composition and temperature dependent mixing rules makes this the ideal thermodynamic model for correlating the complex phase equilibria of the CO₂ + 1-decanol + *n*-tetradecane system at the required high-temperature and high-pressure ranges.

The RK-Aspen and SR-Polar models have been investigated in multiple studies, conducted on similar high-pressure systems, which are summarised in *Table 3-1*. Both methods are selected to model the new CO₂ + 1-decanol + *n*-tetradecane and 1-decanol + *n*-tetradecane experimental data measured in this work based on the following findings:

- Lombard [51] only considered binary systems with ethane and propane as the supercritical solvents.
- Zamudio and co-workers [12], [13] did not consider the addition of solute + solute BIPs into the RK-Aspen model algorithm and saw significant deviations between the model correlations and experimental data.
- Zamudio [18] only considered binary CO₂ + *n*-alkane and CO₂ + alcohol systems with the SR-Polar model.
- Smith and Schwarz [16] continued the work of Zamudio et al.[13] by considering the effects of solute + solute BIPs and saw improved model predictions by RK-Aspen.
- In more recent studies, conducted by Fourie and co-workers [19], [158], [159], it was shown that both flexible property methods have the option to include additional BIPs and pure component polar parameters to improve the accuracy of their fit to experimental data.

TABLE 3- 1: PREVIOUS APPLICATION OF RK-ASPEN AND SR-POLAR TO SIMILAR SUPERCRITICAL SYSTEMS CONTAINING
N-ALKANES AND 1-ALCOHOLS.

<i>Reference</i>	<i>Model</i>	<i>Systems</i>
Lombard [51]	RK-Aspen and SR-Polar	Solvent [†] + <i>n</i> -alkane mixtures with: $10 \leq C_n \leq 38$ Solvent [†] + alcohol mixtures with: $10 \leq C_n \leq 18$
Zamudio et al.[13]	RK-Aspen	CO ₂ + 1-decanol CO ₂ + <i>n</i> -dodecane CO ₂ + 3,7-dimethyl-1-octanol CO ₂ + <i>n</i> -dodecane + 1-decanol CO ₂ + 1-decanol + 3,7-dimethyl-1-octanol CO ₂ + <i>n</i> -dodecane + 3,7-dimethyl-1-octanol CO ₂ + 1-decanol + <i>n</i> -dodecane + 3,7-dimethyl-1-octanol
Zamudio et al.[12]	RK-Aspen	CO ₂ + 1-decanol CO ₂ + <i>n</i> -decane CO ₂ + 3,7-dimethyl-1-octanol CO ₂ + 2,6-dimethyl-2-octanol CO ₂ + 1-decanol + <i>n</i> -decane + 3,7-dimethyl-1-octanol + 2,6-dimethyl-2-octanol
Zamudio [18]	SR-Polar	CO ₂ + 1-decanol CO ₂ + 2-decanol CO ₂ + <i>n</i> -decane CO ₂ + <i>n</i> -dodecane CO ₂ + 3,7-dimethyl-1-octanol CO ₂ + 3,7-dimethyl-2-octanol CO ₂ + 2,6-dimethyl-3-octanol
Smith and Schwarz [16]	RK-Aspen	CO ₂ + <i>n</i> -dodecane + 1-decanol
Fourie et al.[158]	RK-Aspen and SR-Polar	CO ₂ + <i>n</i> -dodecane + 3,7-dimethyl-1-octanol
Fourie et al.[159]	RK-Aspen and SR-Polar	CO ₂ + 1-decanol + 3,7-dimethyl-1-octanol
Fourie [19]	RK-Aspen and SR-Polar	CO ₂ + <i>n</i> -dodecane + 1-decanol

[†] Ethane and propane used as supercritical solvent

3.5.1. RK-ASPEN MODEL

The RK-Aspen property method is an extension of the RKS *EoS* and can be described using equation (3.10). Furthermore, quadratic Mathias mixing rules are employed in this model for calculating the energy (3.28) and co-volume (3.29) parameters, each containing a linear temperature-dependent BIP as shown in equations (3.30) and (3.31), respectively [2], [18].

$$a = \sum_{i=1}^n \sum_{j=1}^n x_i x_j (a_i a_j)^{0.5} (1 - k_{a,ij}) \quad (3.28)$$

$$b = \sum_{i=1}^n \sum_{j=1}^n x_i x_j \frac{(b_i + b_j)}{2} (1 - k_{b,ij}) \quad (3.29)$$

$$k_{a,ij} = k_{a,ji} = k_{a,ij}^0 + k_{a,ij}^1 \frac{T}{1000} \quad (3.30)$$

$$k_{b,ij} = k_{b,ji} = k_{b,ij}^0 + k_{b,ij}^1 \frac{T}{1000} \quad (3.31)$$

To ensure accurate VLE data correlations, the temperature depended $\alpha_i(T)$ parameter in equation (3.13 a) was calculated in one of two ways [103], [156]:

- (i) A Mathias alpha function, shown in equation (3.32)
- (ii) A Boston-Mathias alpha function, shown in equation (3.33)

The former method is applied for subcritical components ($T_{r,i} < 1$) and incorporates a pure component polar parameter, η_i directly into the alpha function; whereas, the latter is applied for supercritical components ($T_{r,i} > 1$) and contains a modified, d_i parameter (3.33 a) to incorporate the pure component polar parameter into the alpha function (3.33). The species-specific co-volume parameter, b_i remains temperature independent and can be calculated using equation (3.13 b).

$$\alpha_i(T) = [1 + m_i(1 - T_{r,i}^{0.5}) - \eta_i(1 - T_{r,i})(0.7 - T_{r,i})]^2 \quad (3.32)$$

$$m_i = 0.48508 + 1.55171\omega_i - 0.15613\omega_i^2 \quad (3.32 \text{ a})$$

$$\alpha_i(T) = [\exp[c_i(1 - T_{r,i}^{d_i})]]^2 \quad (3.33)$$

$$d_i = 1 + \frac{m_i}{2} + 0.3\eta_i \quad (3.33 \text{ a})$$

$$c_i = 1 - \frac{1}{d_i} \quad (3.33 \text{ b})$$

Therefore, this model has four pure component parameters for each subcritical and supercritical component ($T_{c,i}$, $P_{c,i}$, ω_i , η_i). Additionally, per binary combination up to four BIPs can be used to improve the fit ($k_{a,ij}^0$, $k_{a,ij}^1$, $k_{b,ij}^0$, $k_{b,ij}^1$).

3.5.2. SR-POLAR MODEL

The Redlich-Kwong-UNIFAC model [109], extended from the RKS *EoS* [49], [103], forms the basis of the SR-Polar property method. Once again, equation (3.10) will be applied for the model with the SRK extension. Like the RK-Aspen model the energy and co-volume BIPs remain temperature dependent when applying the Schwarzenztruber-Renon mixing rules to the *EoS*. However, a second BIP, l_{ij} is included for the SR-Polar energy parameter as shown in equation (3.34). The co-volume parameter is calculated using equation (3.29). Temperature dependency can be incorporated for the $k_{a,ij}$, $k_{b,ij}$ and l_{ij} BIPs as shown in equations (3.35), (3.36) and (3.37), respectively [2], [18].

$$a = \sum_{i=1}^n \sum_{j=1}^n x_i x_j (a_i a_j)^{0.5} [1 - k_{a,ij} - l_{ij}(x_i - x_j)] \quad (3.34)$$

$$k_{a,ij} = k_{a,ji} = k_{a,ij}^0 + k_{a,ij}^1 T + \frac{k_{a,ij}^2}{T} \quad (3.35)$$

$$k_{b,ij} = k_{b,ji} = k_{b,ij}^0 + k_{b,ij}^1 T + \frac{k_{b,ij}^2}{T} \quad (3.36)$$

$$l_{ij} = -l_{ji} = l_{ij}^0 + l_{ij}^1 T + \frac{l_{ij}^2}{T} \quad (3.37)$$

For the SR-Polar model, the Extended Mathias alpha function is used to calculate the $\alpha_i(T)$ parameter of subcritical ($T_{r,i} < 1$) components. The expression is shown in equation (3.38) which enable the incorporation of three pure component polar parameters, $p_{1,i}$, $p_{2,i}$ and $p_{3,i}$ into the *EoS* model to improve the VLE data correlations. A Boston Mathias Extrapolation with a modified d_i parameter (3.39) is used to incorporate the three polar parameters into the $\alpha_i(T)$ parameter (3.33) of the supercritical components ($T_{r,i} > 1$) [103], [156]. The m_i and c_i parameters are computed by equation (3.32 a) and equation (3.33 b), respectively.

$$\alpha_i(T) = [1 + m_i(1 - T_{r,i}^{0.5}) - p_{1,i}(1 - T_{r,i})(1 + p_{2,i}T_{r,i} + p_{3,i}T_{r,i}^2)]^2 \quad (3.38)$$

$$d_i = 1 + \frac{m_i}{2} - p_{1,i}(1 + p_{2,i} + p_{3,i}) \quad (3.39)$$

Therefore, this model has six pure component parameters for each subcritical and supercritical component ($T_{c,i}$, $P_{c,i}$, ω_i , $p_{1,i}$, $p_{2,i}$, $p_{3,i}$). Additionally, per binary combination up to nine BIPs can be used to improve the fit ($k_{a,ij}^0$, $k_{a,ij}^1$, $k_{a,ij}^2$, $k_{b,ij}^0$, $k_{b,ij}^1$, $k_{b,ij}^2$, l_{ij}^0 , l_{ij}^1 , l_{ij}^2).

3.6. ASSOCIATION *EoS* PROPERTY METHODS IN ASPEN PLUS®

The hydrogen bonding formation between the 1-decanol molecules in the CO₂ + 1-decanol mixtures indicate large self-association effects that lead to complex phase behaviour near the critical point of the solvent [15]. It is for this reason that an additional model will be considered in this study.

EoS models derived from statistical mechanics are considered as advanced models for their devotion to the development and evaluation of association theories [107]. The perturbation theory is based on the solution of integral equations using a potential function, i.e. Lennard-Jones or square-well potential, to mimic the hydrogen bonds [160]–[162]. The underlying idea is to divide the total intermolecular forces that exist between molecules into repulsive contributions (the potential of the reference system) and attractive contributions (the perturbations to the reference system) [42].

3.6.1. SAFT *EoS* FRAMEWORK

The most important theory belonging to the perturbation family is the Statistical Associating Fluid theory (SAFT) [163], [164]. The original SAFT model utilises a segment reference system to account for the repulsive interactions, represented by hard-spheres and defined using the Lennard-Jones potential function. The perturbations to this segment fluid system include chain and association contributions. These two attractive contributions result in the formation of complex chain molecules within the SAFT *EoS* [165]–[169]. In general, these contributions can mathematically be defined using a generated function, ψ :

$$\psi = (m\psi^{hs} + \psi^{disp})^{seg} + \psi^{chain} + \psi^{assoc} \quad (3.40)$$

Where, m is the mean segment number in the fluid. To better understand the SAFT *EoS* model the formation of molecules within the SAFT *EoS* is depicted in terms of ψ in *Figure 3-4*.

Each of the steps defined in *Figure 3-4* for the formation of molecules contribute to the Helmholtz energy. Therefore, the generated function is defined using the molar residual Helmholtz energy of mixtures, A^{res} [170], [171]:

$$\psi = \frac{A^{res}}{RT} = \int_0^\rho (Z_m - 1) \frac{d\rho}{\rho} \quad (3.41)$$

$$A^{res} = A(T, \rho, x_i \dots) - A^{ig}(T, \rho, x_i \dots) \quad (3.41 \text{ a})$$

Where Z_m is the compressibility factor of a mixture, A is the Helmholtz energy of a mixture and A^{ig} is the Helmholtz energy of a mixture of ideal gases at the same temperature, T , molar density, ρ , and molar composition, x_i . Based on equation (3.41), once ψ is known, all the required thermodynamic properties can be derived using an appropriate derivative of the Helmholtz energy. Therefore, the original SAFT *EoS* can be presented in terms of the Helmholtz energy using the following expression [163], [164]:

$$\frac{A^{res}}{RT} = \frac{A^{seg}}{RT} + \frac{A^{chain}}{RT} + \frac{A^{assoc}}{RT} \quad (3.42)$$

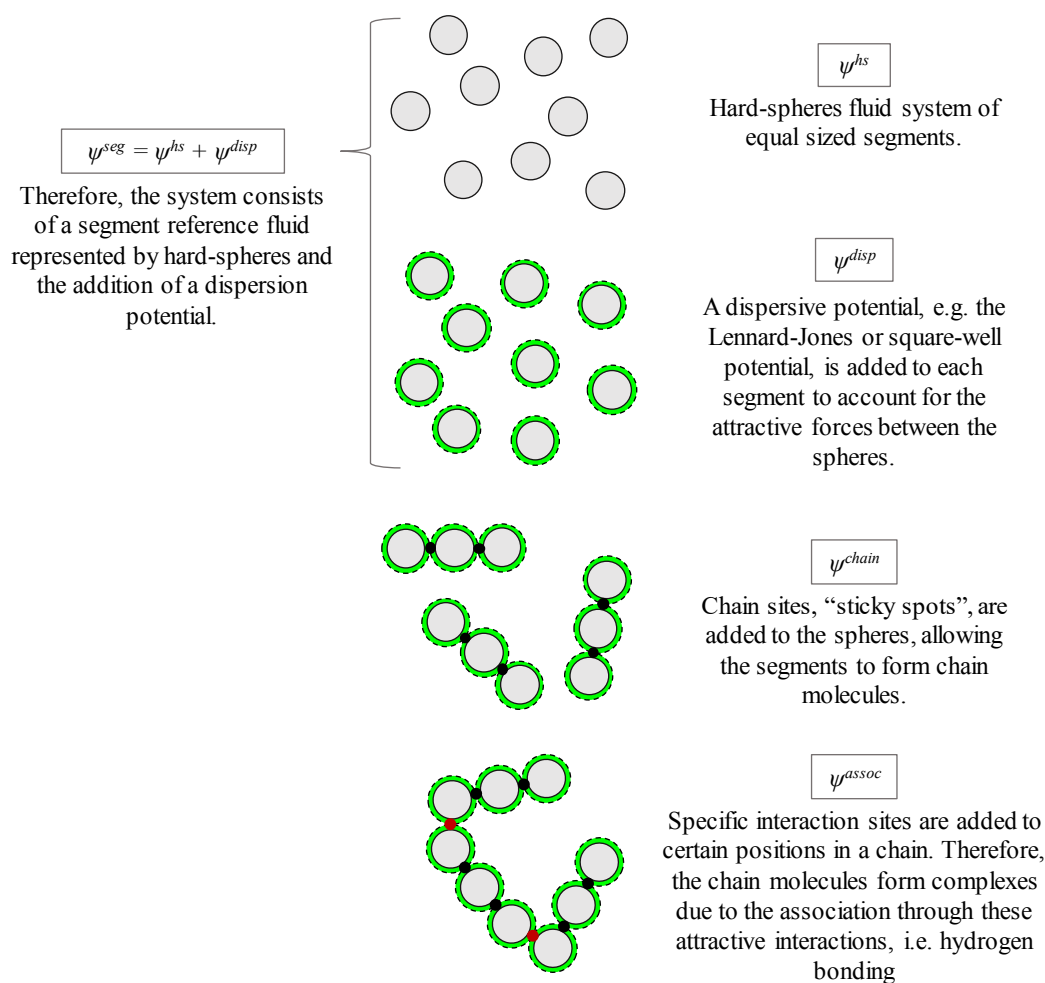


FIGURE 3- 4: PROCEDURE TO FORM A MOLECULE IN THE SAFT MODEL [163], [164].

3.6.2. SAFT FAMILY DEVELOPMENTS

Since one of the first variations made to the SAFT *EoS* by Huang and Radosz [172], [173], the development, extension and modifications of the SAFT family have been continuing rapidly. The advancements made to this state of the art thermodynamic model can be classified into one of the four directions summarised in *Figure 3-5*. For details pertaining to the theory and application of the SAFT variants, the reader is referred to the work published by, amongst others [42], [55], [151], [152], [174], [175], Kontogeorgis and Folas [107].

The Cubic-Plus-Association (CPA) *EoS* is suitable in alcohol recovery applications with high-pressure gases, making it especially suitable for the mixtures investigated in this study [176]. Furthermore, CPA is a direct approach that can be applied to hydrogen bonding components, where *EoS- G^E* models tend to fail (shown in *Figure 3-3*) [177]. Unfortunately, the addition of CPA *EoS* models to commercial process simulators can take time. As such, and to maintain generality, this work is limited by the statistical thermodynamic models currently available within the Aspen Plus® V8.6 process simulator. Two available models, from within the SAFT *EoS* framework, are the copolymer perturbed-

chain SAFT (PC-SAFT) variation developed by Sadowski and co-workers [178]–[183] and its predecessor (POLYPCSF).

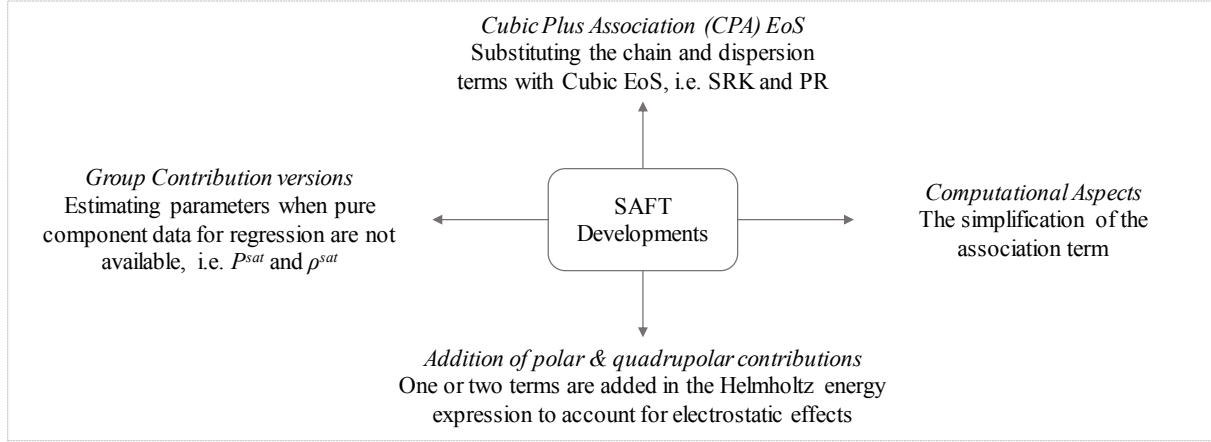


FIGURE 3- 5: EXTENSIONS OF THE SAFT APPROACH CLASSIFIED INTO THE FOUR MAIN MODIFICATIONS OF THE ORIGINAL FRAMEWORK [107].

The difference between the SAFT *EoS* and the PC-SAFT variation lies primarily in the reference fluid used and the potential function used to define the reference fluid. The PC-SAFT *EoS* is based on the perturbation theory for chain molecules where the dispersion term accounts for attractions between whole chains [184]. Therefore, in the PC-SAFT *EoS*, the hard-sphere segments form chain molecules before the addition of a dispersion potential. In general, *Figure 3-4* is rearranged to *Figure 3-6* for the formation of molecules within the PC-SAFT *EoS* and the contributions can once again be defined using a generated function, ψ :

$$\psi = (m\psi^{hs} + \psi^{chain})^{hc} + \psi^{disp} + \psi^{assoc} \quad (3.43)$$

The modified square-well potential function is used to define the hard-chain reference system, A^{hc} of the PC-SAFT model, which consist of a nonbonding contribution, A^{hs} and a bonding contribution due to chain formation, A^{chain} . The perturbations to this reference fluid include dispersion, A^{disp} and association contributions, A^{assoc} . The PC-SAFT *EoS* can be written in terms of the molar residual Helmholtz energy using the following expression:

$$\frac{A^{res}}{RT} = \frac{A^{hc}}{RT} + \frac{A^{disp}}{RT} + \frac{A^{assoc}}{RT} \quad (3.44)$$

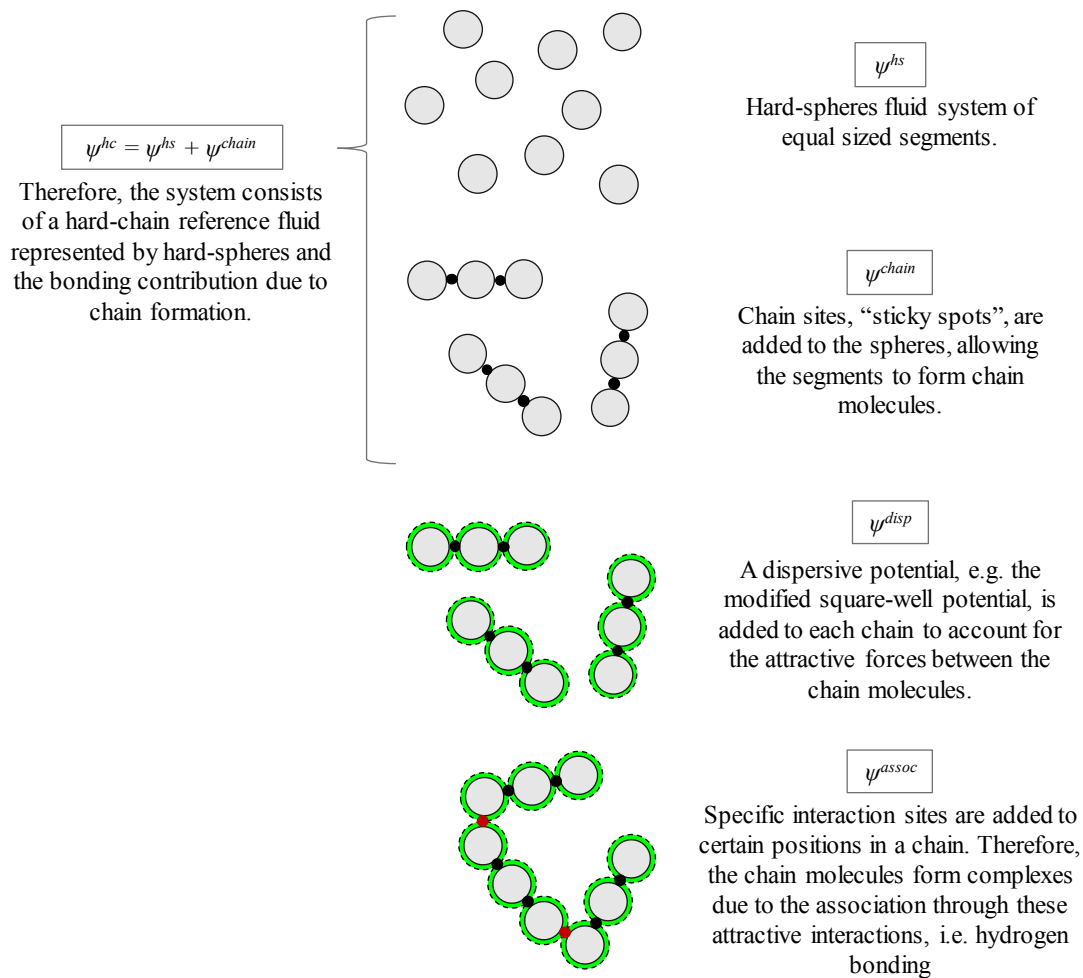


FIGURE 3- 6: PROCEDURE TO FORM A MOLECULE IN THE PC-SAFT MODEL [107].

3.6.3. PC-SAFT MODEL

The PC-SAFT *EoS* property method in Aspen Plus® was selected for use in this work based on the following 2 advances compared to the POLYPCSF model:

- (i) The addition of an association term, developed by Chapman et al. [163]
- (ii) The addition of a polar term, developed by Jog et al. [185]

With respect to literature [183], [186]–[190], the PC-SAFT property method in Aspen Plus® is more specifically known as the Perturbed-Chain-Polar-SAFT (PCP-SAFT) variant. In effect, two of the SAFT development routes (*Figure 3-5*) are being incorporated in this work: (1) the computational aspects, where the association contribution allows the PC-SAFT model correlations to be more efficient; and (2) the polar and/or quadrupolar contributions to obtain a physically more correct model. With the added polar term, the residual Helmholtz energy equation (3.44) is rewritten as:

$$\frac{A^{res}}{RT} = \frac{A^{hc}}{RT} + \frac{A^{disp}}{RT} + \frac{A^{assoc}}{RT} + \frac{A^{polar}}{RT} \quad (3.45)$$

For application of PC-SAFT to phase equilibria the residual Helmholtz energy of the mixture can be linked back to the fugacity coefficient using the following relation:

$$\ln \hat{\phi}_i = \left[\frac{\partial \left(\frac{A^{res}}{RT} \right)}{\partial x_i} \right]_{T, V_m, x_j} - \ln \frac{PV_m}{xRT} \quad (3.45 \text{ a})$$

3.6.3.1. HARD-CHAIN FLUIDS AND CHAIN CONNECTIVITY

The hard chain contribution EoS developed by Chapman et al.[163], shown in equation (3.46), requires the regression of three pure component parameters, namely:

- (i) The segment number, m_i
- (ii) The segment diameter, σ_i
- (iii) The segment energy parameter, ε_i/k

These three parameters are indicated in *Figure 3-7* for the molecule i belonging to a specific component, i.e. 1-decanol. The segment number can be used to calculate the average chain length of the molecules in the system.

$$\frac{A^{hc}}{RT} = m \frac{A^{hs}}{RT} + \frac{A^{chain}}{RT} \quad (3.46)$$

$$m = \sum_i x_i m_i \quad (3.46 \text{ a})$$

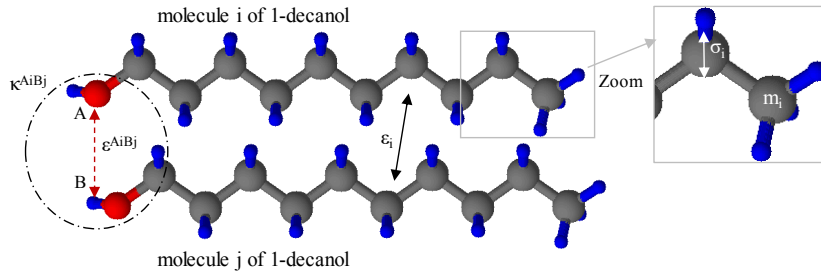


FIGURE 3- 7: TWO 1-DECANOL MOLECULES ILLUSTRATING THE ASSOCIATION EFFECTS BETWEEN TWO SITES (A AND B) AND THE FIVE PURE COMPONENT PARAMETERS TO BE REGRESSED: SEGMENT DIAMETER, SEGMENT NUMBER, DISPERSION ENERGY BETWEEN SEGMENTS, ASSOCIATION ENERGY AND ASSOCIATION VOLUME [163], [164].

The segment diameter and energy parameters are used to compute the temperature dependent segment diameter, d_i of component i . Equation (3.46 b) was proposed by Chen and Kreglewski [191] based on Barker and Henderson's [161], [162] perturbation theory for hard sphere segments. Once d_i is known, the reduced densities, ζ_n (3.46 c) of each component can be calculated and in turn the hard-sphere contribution [192], [193] in terms of the Helmholtz energy, A^{hs} .

$$d_i = \sigma_i \left[1 - 0.12 \exp \left(-3 \frac{\varepsilon_i}{kT} \right) \right] \quad (3.46 \text{ b})$$

$$\zeta_n = \frac{\pi}{6} \rho \sum_i x_i m_i d_i^n \quad n \in \{0, 1, 2, 3\} \quad (3.46 \text{ c})$$

$$\frac{A^{hs}}{RT} = \frac{1}{\zeta_0} \left[\frac{3\zeta_1\zeta_2}{1-\zeta_3} + \frac{\zeta_2^3}{\zeta_3(1-\zeta_3)^2} + \left(\frac{\zeta_2^3}{\zeta_3^2} - \zeta_0 \right) \ln(1-\zeta_3) \right] \quad (3.46 \text{ d})$$

In addition, both the d_i and ζ_n parameters are required to compute the radial pair distribution function, $g_{ii}^{hs}(d_{ii})$ which is the final requirement to calculate the contribution from the chain connectivity, A^{chain} . Equation (3.46 e) and equation (3.46 f) are derived for a mixture of hard spheres using the Carnahan-Starling *EoS* [194].

$$g_{ii}^{hs}(d_{ii}) = \frac{1}{1-\zeta_3} + \left(\frac{d_i d_j}{d_i + d_j} \right) \frac{3\zeta_2}{(1-\zeta_3)^2} + \left(\frac{d_i d_j}{d_i + d_j} \right)^2 \frac{2\zeta_2^2}{(1-\zeta_3)^3} \quad (3.46 \text{ e})$$

$$\frac{A^{chain}}{RT} = - \sum_i x_i (m_i - 1) \ln g_{ii}^{hs}(d_{ii}) \quad (3.46 \text{ f})$$

3.6.3.2. ASSOCIATION TERM – 2B MODEL

Figure 3-7 indicates how the partially negative charged oxygen on the hydroxyl group of the 1st 1-decanol molecule, i (site A) bonds with the partially positive charged hydrogen atom on the hydroxyl group of the 2nd 1-decanol molecule, j (site B). This hydrogen bonding between two like molecules indicates the self-association taking place between the 1-decanol molecules in the mixtures measured in this work [107], [110], [195], [196].

The following two pure component parameters should be regressed to account for the association taking place in the fluid system:

- (iv) The effective association volume, κ^{AiBj}
- (v) The association energy parameter, ε^{AiBj}/k

In general, the association contribution developed by Chapman et al. [163] can be written in terms of the Helmholtz energy, A^{assoc} :

$$\frac{A^{assoc}}{RT} = \sum_i x_i \left[\sum_{A_i} \left(\ln X^{A_i} - \frac{X^{A_i}}{2} \right) + \frac{1}{2} \right] \quad (3.47)$$

Here, X^{A_i} is the mole fraction of a molecule i that are not bonded at site A , and Δ^{AiBj} is the association strength between two sites A and B belonging to two different molecules i and j [197].

$$X^{A_i} = \left[1 + \sum_j \sum_{B_j} \rho_j X^{B_j} \Delta^{AiBj} \right]^{-1} \quad (3.47 \text{ a})$$

$$\Delta^{AiBj} = \sigma_{ij}^3 g_{ij}(d_{ij})^{seg} \kappa^{AiBj} \left[\exp \left(\frac{\varepsilon^{AiBj}}{kT} \right) - 1 \right] \quad (3.47 \text{ b})$$

The cross-association volume and cross-energy parameters can be calculated using mixing rules suggested by Wolbach and Sandler [195].

$$\varepsilon^{A_i B_j} = \frac{1}{2} (\varepsilon^{A_i B_i} + \varepsilon^{A_j B_j}) \quad (3.47 \text{ c})$$

$$\kappa^{A_i B_j} = \sqrt{\kappa^{A_i B_i} \kappa^{A_j B_j}} \left(\frac{\sqrt{\sigma_{ii} \sigma_{jj}}}{\frac{1}{2}(\sigma_{ii} + \sigma_{jj})} \right)^3 \quad (3.47 \text{ d})$$

In pure and binary systems, the X^{A_i} fraction can be derived explicitly if the association scheme is known. To establish the association scheme, the number and type of association sites should be identified. Fortunately, previous investigations with the use of spectroscopy data and the PC-SAFT *EoS* model have been conducted [198], [199]. Distinctions between the 2B and 3B association schemes were not always possible but, for heavier alcohols, i.e. 1-decanol, the 2B scheme will perform best [172], [179], [200], [201]. After Huang and Radosz [172] the following two approximations are made for the 2B bonding type:

$$\Delta^{A_i B_j} = \Delta^{B_i A_j} \neq 0 \quad (3.48)$$

$$X^{A_i} = X^{B_j} \quad (3.49)$$

Therefore, equation (3.47) and (3.47 a) can be simplified to equation (3.50) and (3.50 a), respectively.

$$\frac{A^{assoc}}{RT} = 2 \sum_i x_i \left(\ln X^{A_i} - \frac{X^{A_i}}{2} + \frac{1}{2} \right) \quad (3.50)$$

$$X^{A_i} = \frac{-1 + \sqrt{1 + 4\rho \Delta^{A_i B_j}}}{2\rho \Delta^{A_i B_j}} \quad (3.50 \text{ a})$$

3.6.3.3. DISPERSION TERM

The contribution term with fundamental differences to the original SAFT *EoS* is the dispersion term, A^{disp} . The Barker and Henderson [160]–[162] perturbation theory is used to compute an equation in terms of the 1st and 2nd order vdW dispersion interactions between molecules.

$$\frac{A^{disp}}{kTN} = \frac{A_1}{kTN} + \frac{A_2}{kTN} \quad (3.51)$$

$$A_1 = -2\pi\rho \sum_{i=0}^6 a_i(m) \eta^i \sum_{ij} m^2 \left(\frac{\varepsilon_{ij}}{kT} \right) \sigma_{ij}^3 \quad (3.51 \text{ a})$$

$$A_2 = -\pi\rho m C_1 \sum_{i=0}^6 b_i(m) \eta^i \sum_{ij} m^2 \left(\frac{\varepsilon_{ij}}{kT} \right)^2 \sigma_{ij}^3 \quad (3.51 \text{ b})$$

Where, η is the packing fraction and represents a reduced segment density, ζ_3 , i.e. $\eta = \zeta_3$. The compressibility of the hard chain fluid, C_1 can be calculated using equation (3.51 c) The coefficients $a_i(m)$ and $b_i(m)$ as functions of the chain length, were developed using the Lennard-Jones potential and the radial distribution function of O'Lenick et al. [202]. The model constants are derived from pure component data of alkane and can be found in literature [107], [202].

$$C_1 = \left(1 + z^{hc} + \rho \frac{\partial z^{hc}}{\partial \rho}\right)^{-1} = \left\{1 + \frac{m(8\eta - 2\eta^2)}{(1-\eta)^4} + \frac{(1-m)(20\eta - 27\eta^2 + 12\eta^3 - 2\eta^4)}{[(1-\eta)(2-\eta)]^2}\right\}^{-1} \quad (3.51 \text{ c})$$

$$a_i(m) = a_{o,i} + \frac{m-1}{m} a_{1,i} + \frac{m-1}{m} \cdot \frac{m-2}{m} a_{2,i} \quad (3.51 \text{ d})$$

$$b_i(m) = b_{o,i} + \frac{m-1}{m} b_{1,i} + \frac{m-1}{m} \cdot \frac{m-2}{m} b_{2,i} \quad (3.51 \text{ e})$$

The cross-segment diameter, σ_{ij} and cross-energy parameter, ε_{ij} are calculated with simple Berthelot-Lorentz combining rules [179]. The energy parameter contains a temperature dependent binary interaction parameter, k_{ij} to correct the segment-segment or segment-solvent interactions of unlike chains. T_{ref} is set to a default value of 298.15 K.

$$\sigma_{ij} = \frac{1}{2}(\sigma_i + \sigma_j) \quad (3.52)$$

$$\varepsilon_{ij} = (1 - k_{ij})(\varepsilon_i \cdot \varepsilon_j)^{\frac{1}{2}} \quad (3.53)$$

$$k_{ij} = k_{ij}^0 + k_{ij}^1 \frac{T}{T_{ref}} \quad (3.54)$$

3.6.3.4. POLAR/QUADRUPOLEAR TERMS

An often-overlooked issue in classical *EoS* is the large quadrupole moment of CO_2 , caused by the two electron rich oxygen molecules (negative charges) and the electron poor carbon atom (positive charges) [203], [204]. The four separate points of these partial charges are shown in *Figure 3-8*. Inspired by the recent advances made within the SAFT-family, and to obtain a physically more correct and predictive model, a quadrupolar term is used in this thesis for the CO_2 molecule.



FIGURE 3- 8: SCHEMATIC OF THE CO_2 MOLECULE HIGHLIGHTING ITS POSITIVE AND NEGATIVE CHARGES AND LINEAR SYMMETRY. MOLECULE DRAWN USING CHEMSKETCH [29].

The schematic of the CO_2 molecule highlights its linear symmetry which allows the quadrupole moment to be reduced to a scalar. Thus, two additional pure component parameters can be included for the polar/quadrupolar components without modifications [185], [205]:

- (i) The dipole or quadrupole moment, μ_i or Q_i (Debye)
- (ii) The fraction of dipolar/quadrupolar segments in the chain molecule, x_{pi}

The number of models that attempt to deal with polar interactions far exceeds the number of models that attempt to account for the quadrupolar forces between molecules [186]. Fortunately, three multipolar terms have been proposed in literature to deal with polar and quadrupolar interactions, namely (i) the quadrupolar term proposed by Gross [203], (ii) the quadrupolar term(s) proposed by

Economou and co-workers [206], [207] and (iii) the quadrupolar term proposed by de Hemptinne and co-workers [208].

The thermodynamic property method available within Aspen Plus[®] has been identified as the PCP-SAFT model that uses a two-centre Lennard-Jones pair potential as the reference fluid and no mixing rules. Therefore, the thermodynamic model used in this study is that developed by Gross [203], inspired by the perturbation theory of Stell and co-workers [209]–[212] and Gubbins & Twu [213], [214]. The new *EoS* can be employed with an experimental quadrupole moment and contrary to most other *EoS* contributions for polar and quadrupolar mixtures it can be used without any additional adjustable parameters, i.e., BIPs [215]. The quadrupolar term provided in equation (3.55) is written in the Padé approximate [210], where A_2 and A_3 represent the 2nd and 3rd order terms of the perturbation expansion developed by statistical mechanics, respectively (the so called *u*-expansion by Stell and co-workers [209]–[212] and Flytzani-Stephanopoulos et al.[216]).

$$\frac{A^{polar}}{RT} = \frac{A_2}{1 - \frac{A_3}{A_2}} \quad (3.55)$$

$$A_2 = -\frac{2\pi}{9} \frac{\rho I_2(\eta)}{(kT)^2} \sum_i \sum_j x_i x_j m_i m_j x_{pi} x_{pj} \frac{Q_i^2 Q_j^2}{d_{ij}^2} \quad (3.55 \text{ a})$$

$$A_3 = \frac{5\pi^2}{162} \frac{\rho I_3(\eta)}{(kT)^3} \sum_i \sum_j \sum_k x_i x_j x_k m_i m_j m_k x_{pi} x_{pj} x_{pk} \frac{Q_i^2 Q_j^2 Q_k^2}{d_{ij}^2 d_{jk}^2 d_{ik}^2} \quad (3.55 \text{ b})$$

$$d_{ij} = \frac{d_i + d_j}{2} \quad (3.55 \text{ c})$$

Rushbrooke et al.[210] have shown that the pure fluid integrals can be written in terms of the packing fraction, η using the following expressions that are functions of reduced density:

$$I_2(\rho^*) = \frac{1 - 0.3618\rho^* - 0.3205\rho^{*2} + 0.1078\rho^{*3}}{(1 - 0.5236\rho^*)^2} \quad (3.56)$$

$$I_3(\rho^*) = \frac{1 + 0.62378\rho^* - 0.11658\rho^{*2}}{1 - 0.59056\rho^* + 0.20059\rho^{*2}} \quad (3.57)$$

$$\rho^* = \frac{6\eta}{\pi} \quad (3.58)$$

$$I_2(\eta) = \frac{1 - 0.69099\eta - 1.16904\eta^2 + 0.75097\eta^3}{(1 - \eta)^2} \quad (3.59)$$

$$I_3(\eta) = \frac{1 + 1.19133\eta - 0.42523\eta^2}{1 - 1.12789\eta + 0.73166\eta^2} \quad (3.60)$$

Although 1-decanol is considered slightly polar, the effects of polarity may be small and, in some instances, overshadowed by the more stringent hydrogen effects (self-association). It is for this reason that 1-decanol will be considered as a non-polar, self-associating segment in this work, with five unary parameters specified (m , σ , ε/k , κ^{AB} , ε^{AB}/k). For the non-association and non-polar segment, *n*-tetradecane, three unary parameters are specified (m , σ , ε/k) and for the non-association and quadrupolar solvent, CO₂, 5 unary parameters are specified (m , σ , ε/k , Q , x_p). In addition, up to two BIPs can be used for the segment-segment pair (1-decanol + *n*-tetradecane) and for each of the segment-solvent pairs (the

CO₂ binary sub-systems) to improve the model fit. Ideally k_{ij} is temperature independent, however several researchers have used a linear temperature relationship for better model correlations [19], [181].

3.7. SIMULATION APPROACH

Aspen Plus[®] was used in this work to fit all pure component parameters as well as BIPs for each of the models summarised in *Table 3-2*.

TABLE 3- 2: SUMMARY OF PARAMETERS TO BE OBTAINED THROUGH REGRESSION OR FROM LITERATURE FOR THE 4 THERMODYNAMIC MODELS INVESTIGATED IN THIS STUDY.

<i>Parameter</i>	<i>Model</i>	<i>Molecule/Group</i>	<i>Method</i>
T_c, P_c & ω	RK-Aspen, SR-Polar & PSRK	CO ₂ , 1-C ₁₀ OH & <i>n</i> -C ₁₄	Literature/estimation techniques
$^{\ddagger} c_1, c_2$ & c_3	PSRK	CO ₂ , 1-C ₁₀ OH & <i>n</i> -C ₁₄	Mathias and Copeman $\alpha(T)$
$^{\ddagger} \eta$	RK-Aspen	CO ₂ , 1-C ₁₀ OH & <i>n</i> -C ₁₄	Mathias $\alpha(T)$ & Boston Mathias $\alpha(T)$
$^{\ddagger} p_1, p_2$ & p_3	SR-Polar	CO ₂ , 1-C ₁₀ OH & <i>n</i> -C ₁₄	Extended Boston Mathias $\alpha(T)$
$m, \varepsilon/k$ & σ	PC-SAFT	CO ₂ , 1-C ₁₀ OH & <i>n</i> -C ₁₄	Literature
ε^{AB}/k & κ^{AB}	PC-SAFT	1-C ₁₀ OH	[†] Regression
Q	PC-SAFT	CO ₂	Literature
x_p	PC-SAFT	CO ₂	[†] Regression
Q_k & R_k	PSRK	CO ₂ & 1-C ₁₀ OH	Bondi's method
Q_k^* & R_k^*	PSRK	<i>n</i> -C ₁₄	Bondi's method with *Li-correction
a_{mn} & a_{nm}	PSRK	OH/CH ₂ , OH/CO ₂ & CH ₂ /CO ₂	Literature/regression
b_{mn} & b_{nm}	PSRK	CH ₂ /CO ₂	Literature/regression
c_{mn} & c_{nm}	PSRK	CH ₂ /CO ₂	Literature/regression
$k_{a,ij}^0, k_{a,ij}^1, k_{b,ij}^0$ & $k_{b,ij}^1$	RK-Aspen & SR-Polar	CO ₂ + 1-C ₁₀ OH & CO ₂ + <i>n</i> -C ₁₄	^a Regression
$k_{a,ij}^0$ & $k_{b,ij}^0$	RK-Aspen & SR-Polar	1-C ₁₀ OH + <i>n</i> -C ₁₄	^b Regression
k_{ij}^0 & k_{ij}^1	PC-SAFT	CO ₂ + 1-C ₁₀ OH & CO ₂ + <i>n</i> -C ₁₄	^a Regression
k_{ij}^0	PC-SAFT	1-C ₁₀ OH + <i>n</i> -C ₁₄	^c Regression

[†] Regressed using pure component vapour pressure data

[†] Regressed using pure component vapour pressure data, saturated liquid density data and literature VLE data

* Calculated with equation (3.24) where $f(14) = 1.16079$

^a Regressed using literature VLE data and fixing polar parameter(s)

^b Regressed using new data measured in this work and fixing solute + solvent BIPs and polar parameter(s)

^c Regressed using new data measured in this work and fixing solute + solvent BIPs

The following conditions are set for the parameters regressed in this work:

1. Only the Aspen Plus® built-in regression function was considered for parameter fitting (see discussion in section 3.1). The regression analysis adjusts and weighs each variable (T , P , x and y) by the standard deviation, therefore it assumes the experimental data are not error free.
2. Temperature dependence was evaluated for the solute + solvent BIPs only due to the HPBDP data limiting the regression procedure (discussed in Chapter 7).
3. For the SR-Polar model, the $k_{a,ij}^2$ and $k_{b,ij}^2$ parameters were not considered for T-dependence in this study following the findings by Lombard [51] who showed an improved model performance with 3 BIPs is not due to the correlation fitting the data but rather the errors.
4. For the SR-Polar model, the l_{ij} parameters was not considered in this study due to the HPBDP data limiting the regression procedure (discussed in Chapter 7).
5. The solute + solvent BIPs are kept fixed while varying the solute + solute BIPs to avoid inter-correlation of the parameters. Inter-correlation occurs when more than two BIPs are regressed simultaneously, resulting in the formation of various parameter sets that all satisfy the regression solution.
6. For the solute + solvent BIPs only the VLE data previously measured [15], [17] at $T = 338$ K and $T = 348$ K were used for regressions. These two temperatures were selected to avoid inconsistencies caused by, e.g. temperature inversions at temperatures close to the solvent critical point. Furthermore, at lower temperatures, the HPBDP P - x curve-concavity restricts accurate interpolation at constant P to generate the binary “VLE data”, i.e. the phase transition curves are too flat.
7. Regressions near the critical region of the binary literature data [15], [17] and the HPBDP data measured in this work were excluded.

3.7.1. PURE COMPONENT PARAMETER REGRESSIONS

Most of the pure component parameters are available in literature and were thus used as is. Unfortunately, not all the required parameters are available and had to be regressed (see Table 3-2). For the Mathias and Copeman constants regressed, the polar parameter(s) regressed, the x_p parameter regressed (for CO₂) and the association parameters regressed (for 1-decanol) the following objective function (OF) was used for calculating the pure component vapour pressure data and saturated liquid density data:

$$OF = W_1 \sum_{i=1}^{NP} \left[\frac{(P_{sat,i}^{Exp} - P_{sat,i}^{Calc})^2}{(P_{sat}^{Exp})^2} \right]^{0.5} + W_2 \sum_{i=1}^{NP} \left[\frac{(\rho_{sat,i}^{Exp} - \rho_{sat,i}^{Calc})^2}{(\rho_{sat}^{Exp})^2} \right]^{0.5} \quad (3.61)$$

Where, NP is the number of data points.

The regression weights (W_n) used for each model are provided in *Table 3-3*. Therefore, for PSRK, RK-Aspen and SR-Polar the $\alpha(T)$ parameters were only fitted to saturated vapour pressure data but with PC-SAFT, the saturated liquid density data was included for the additional CO₂ parameter (x_p) and association parameters for 1-decanol (ε^{AB}/k and κ^{AB}). How each of these parameters were obtained/regressed has been further discussed in detail in Chapter 7.

TABLE 3- 3: REGRESSION WEIGHTS FOR EACH OF THE 4 MODELS TO BE USED WITH THE OF SHOWN IN EQUATION (3.61).

<i>Model</i>	W_1	W_2
PSRK	1	0
RK-Aspen	1	0
SR-Polar	1	0
PC-SAFT	0.8	0.2

3.7.2. $\alpha(T)$ PARAMETER REGRESSIONS

The accuracy of the $\alpha(T)$ -function influences not only the model correlations of supercritical VLE phase equilibria but also the derivation of supercritical thermodynamic properties, e.g. heat capacities and enthalpies [217]. Therefore, consistency tests (a list of consistent constraints) applicable to any $\alpha(T)$ -function were developed to ensure accurate correlations of systems with at least one component at supercritical conditions (here for CO₂). These include [217]:

1. A positive, and continuous $\alpha(T)$ -function for any temperature value, i.e. $\alpha(T) \geq 0$.
2. The 1st derivative of the $\alpha(T)$ -function must be continuous and monotonically decreasing for any temperature (including the critical temperature, $Tr = 1$), i.e. $d\alpha(T)/dT \leq 0$.
3. The 2nd derivative of the $\alpha(T)$ -function must be convex and continuous for any temperature (including the critical temperature, $Tr = 1$), i.e. $d^2\alpha(T)/dT^2 \geq 0$.
4. To ensure accurate predictions of state functions in the supercritical domain a negativity constraint is placed on the 3rd derivative of the $\alpha(T)$ -function, i.e. $d^3\alpha(T)/dT^3 \leq 0$.

Therefore, of relevance to this study are the first 3 constraints to ensure accurate correlations of the VLE data at supercritical conditions. *Table 3-2* lists the $\alpha(T)$ -functions applied for the three cubic *EoS* investigated in this work. Each of these were evaluated in Chapter 7 after regressing all required pure component parameters (also provided in *Table 3-2*).

3.7.3. BINARY INTERACTION PARAMETER REGRESSIONS

New BIPs were regressed in this study to improve the model correlations/calculations. Different methods can be used to fit BIPs in the model mixing rules to VLE data through regression. However, in this work the Aspen Plus[®] Data Regression System (DRS) was used to determine the binary

parameters from experimental phase equilibria data. The DRS uses the maximum likelihood principle with the algorithm derived by Britt and Luecke [218]. The estimation involves minimizing the error between the experimental and regressed data. Therefore, for the solute + solvent BIPs (using literature data) and the solute + solute BIPs (using LPVLE and HPVLE data measured in this work) the OF considers errors in all measured variables, including random experimental errors:

$$Q = \sum_{n=1}^{NDG} W_n \sum_{i=1}^{NP} \left[\left(\frac{T_{Exp} - T_{Calc}}{\sigma_{T,i}} \right)^2 + \left(\frac{P_{Exp} - P_{Calc}}{\sigma_{P,i}} \right)^2 \sum_{j=1}^{NC-1} \left(\frac{x_{Exp,ij} - x_{Calc,ij}}{\sigma_{x,ij}} \right)^2 + \left(\frac{y_{Exp,ij} - y_{Calc,ij}}{\sigma_{y,ij}} \right)^2 \right] \quad (3.62)$$

Where NDG is the number of data groups, NC is the number of components, W_n is the weight assigned to each data group (dependent on the regression errors) and σ is the standard deviation.

For the HPBDP data, a different method was used to fit BIPs in the models through regression. The method involved constructing the entire phase envelope and minimizing the errors in phase transition pressure by iterating the BIPs values to minimize the following explicit OF:

$$OF = \sum_{i=1}^{NP} \left[\frac{(P_{sat,i}^{Exp} - P_{sat,i}^{Calc})^2}{(P_{sat}^{Exp})^2} \right]^{0.5} \quad (3.63)$$

Lastly, for the PSRK model, the following OF was applied for fitting the new LPVLE data measured in this study:

$$OF = \sum_{i=1}^{NP} \left[\frac{(P_{sat,i}^{Exp} - P_{sat,i}^{Calc})^2}{(P_{sat}^{Exp})^2} \right]^{0.5} + \sum_{i=1}^{NP} \left[\frac{(y_{sat,i}^{Exp} - y_{sat,i}^{Calc})^2}{(y_{sat}^{Exp})^2} \right]^{0.5} \quad (3.64)$$

The accuracy of the regressed pure component data, literature data and experimental data were statistically evaluated by utilising the %AAD in the specific property, Z regressed defined as:

$$\%AAD_Z = \frac{100}{NP} \sum_i \frac{|Z_i^{Calculated} - Z_i^{Experimental}|}{Z_i^{Experimental}} \quad (3.65)$$

3.8. CHAPTER OUTCOMES

The aims of this chapter were, (i) to assess classical and advanced thermodynamic models and, (ii) to identify which methods within Aspen Plus® can be used to predict and/or correlate the HPBDP, HPVLE and LPVLE data (identified in chapter 2). In achieving this chapter aim, the key **Objective 3.1** was also successfully achieved. The flow diagram provided in *Figure 3-9* summarises the process of elimination in obtaining the final four thermodynamic models that will be investigated in this work, namely: PSRK, RK-Aspen, SR-Polar and PC-SAFT.

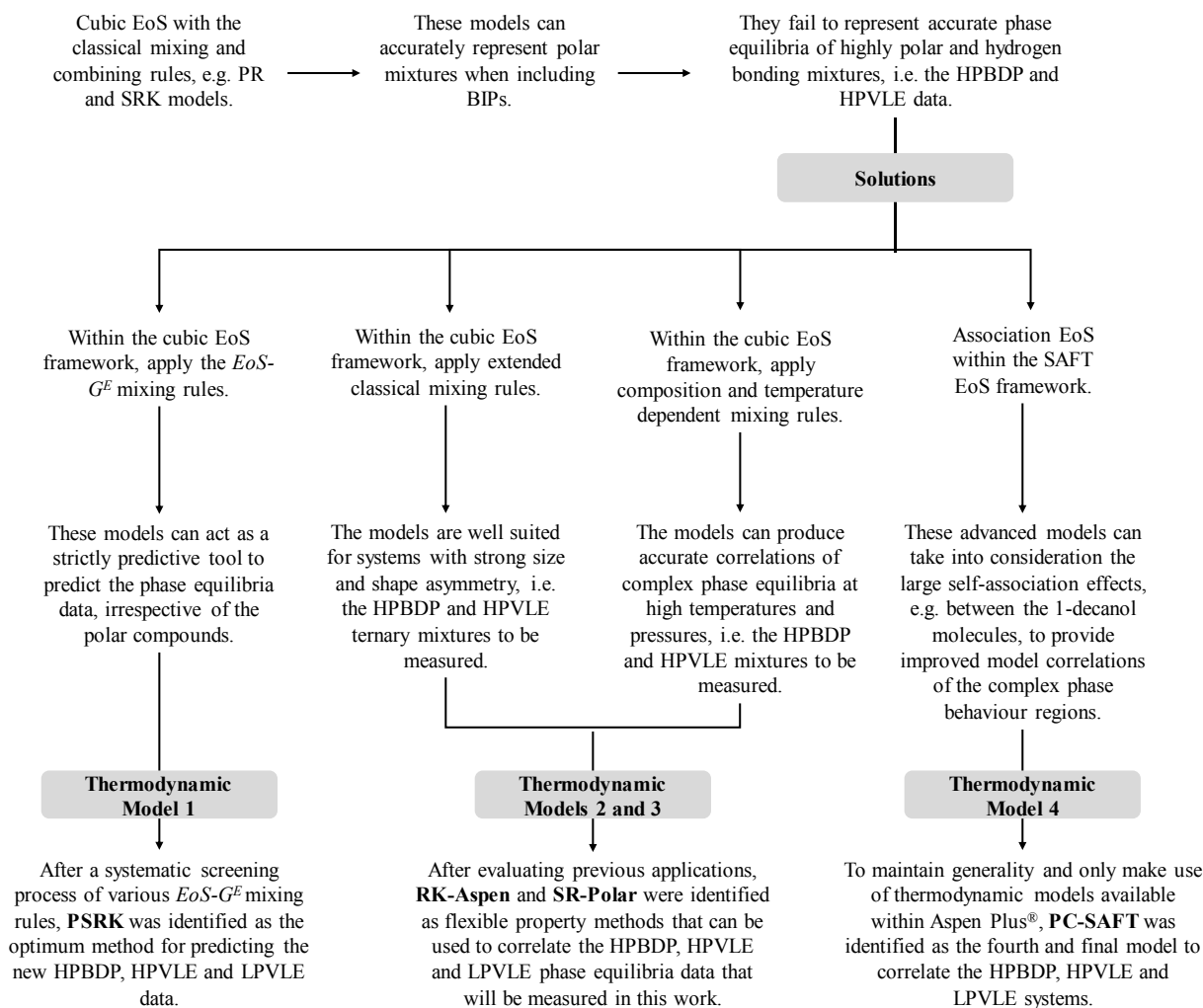


FIGURE 3- 9: CHAPTER SUMMARY OF WHY THE FOUR THERMODYNAMIC MODELS WERE SELECTED FOR CORRELATING THE INTERESTED SYSTEMS IN THIS STUDY.

The RK-Aspen, SR-Polar and PC-SAFT methods have the option to include additional BIPs and pure component parameters to improve the accuracy of their fit to experimental data (**Objective 3.2**). This key objective highlights the 4th scientific contribution that was made in this work (see Section 1.5) and was addressed in Chapter 7 after the new phase equilibria data were measured and analysed. Therefore, the experimental materials and methods used to measure the new HPBDP, HPVLE and LPVLE data are discussed in the next chapter.

Chapter 4

EXPERIMENTAL MATERIALS AND METHODS

With a premise of the work presented in this thesis covered in the previous chapters, focus now shifts to how the work was done. To achieve the first two key objectives of this work, experimental measurements were to be conducted, namely: HPBDP and HPVLE (**Objective 1**) and LPVLE (**Objective 2**). Various methods are available to measure fluid phase equilibria [219]–[221]. However, each method is limited with respect to the type of data obtained.

The aim of this chapter is to provide a systematic overview of the experimental materials and methods employed in this work to measure new high- and low-pressure phase equilibria data.

The materials and apparatus used, methods applied, calibrations conducted, and accuracy of the experimental results are presented in this chapter.

4.1. MEASUREMENT TECHNIQUES

4.1.1. HIGH-PRESSURE PHASE EQUILIBRIA

There is yet no superior method for measuring high-pressure phase equilibria. The dynamic approach is used to classify measuring equipment where the system components are continuously circulated through the equilibrium cell. The second approach, static methods, are used to classify non-flowing systems [222]. The type of equipment will also depend on whether sampling (analytic) of the phases takes place or not (synthetic). A summary of the two main techniques employed namely, dynamic and static methods, are shown in *Figure 4-1* and discussed in some detail in Appendix A1 [222], [223]. Each type has its advantages and drawbacks for the measurement of high-pressure phase equilibria data. The dynamic method will not be used as it is not suitable to measure the critical region of the mixtures and thermal degradation of the hydrocarbons could occur [18]. Furthermore, experience is required to ensure the correct quantity of components are added to the equilibrium cell.

Fast, simple and efficient measurements can be achieved using a synthetic method and will thus be used to measure the bubble- and dew-point data of the ternary system. It is also the most suitable method for measuring the super and near-critical phenomena of the system. For ternary systems and multicomponent systems, the only approach suitable to measure data points of phases that are in equilibrium and construct the tie lines on phase diagrams is the analytical method (synthetic method

only produces P - T - x data). The analytical method will thus be used to measure the high-pressure VLE data of the CO_2 + 1-decanol + n -tetradecane system. However, the number of tests are limited due to complicated and expensive equipment needed for analysing the samples.



FIGURE 4- 1: CLASSIFICATION OF EXPERIMENTAL HIGH-PRESSURE VLE METHODS. ADAPTED USING [221]–[225].

4.1.2. LOW-PRESSURE PHASE EQUILIBRIA

Over the past few decades, the different techniques to utilise in the measurement of low-pressure phase equilibria have improved immensely [226], [227]. A brief discussion of the less conventional techniques can be found in Appendix A2. The only measurement required for the binary system was the pressure, making the preferred technique isothermal. However, the phase equilibria measurement of the 1-decanol + n -tetradecane binary system will need to be conducted at a sub-atmospheric pressure and therefore an isobaric technique is required. The Gillespie dynamic still was investigated for measuring low-pressure phase equilibria due to the suitability of the technique and the isobaric requirement (see Appendix A2 for a discussion on the use of the Othmer dynamic still).

The Gillespie equilibrium still is effective in establishing phase equilibria, including azeotropic properties of liquid systems. It was initially pioneered in 1931 by Lee [228] who established a means of obtaining accurate equilibrium temperature readings using a Platinum resistance element (Pt -100). Several years later in 1946, Gillespie designed a disengagement chamber to separate the liquid from the vapour to induce mass transfer effects taking place between phases. The vapour-liquid mixture is pumped from the boiling chamber to the separation chamber by means of the Cottrell tube/pump. The

mixture is first sprayed over the thermometer before the liquid returns to the boiling chamber and the vapour is distributed through a condenser to form condensate that passes a drop counter before returning to the boiling chamber [226]. The original Gillespie dynamic VLE still is schematically presented in *Figure 4-2*. The original Gillespie design was deemed unsatisfactory due to the liquid sample not being in equilibrium with the vapour sample taken from the sample trap as condensate has mixed with the liquid. Furthermore, the separation chamber is not insulated, resulting in partial condensation of the equilibrium vapour.

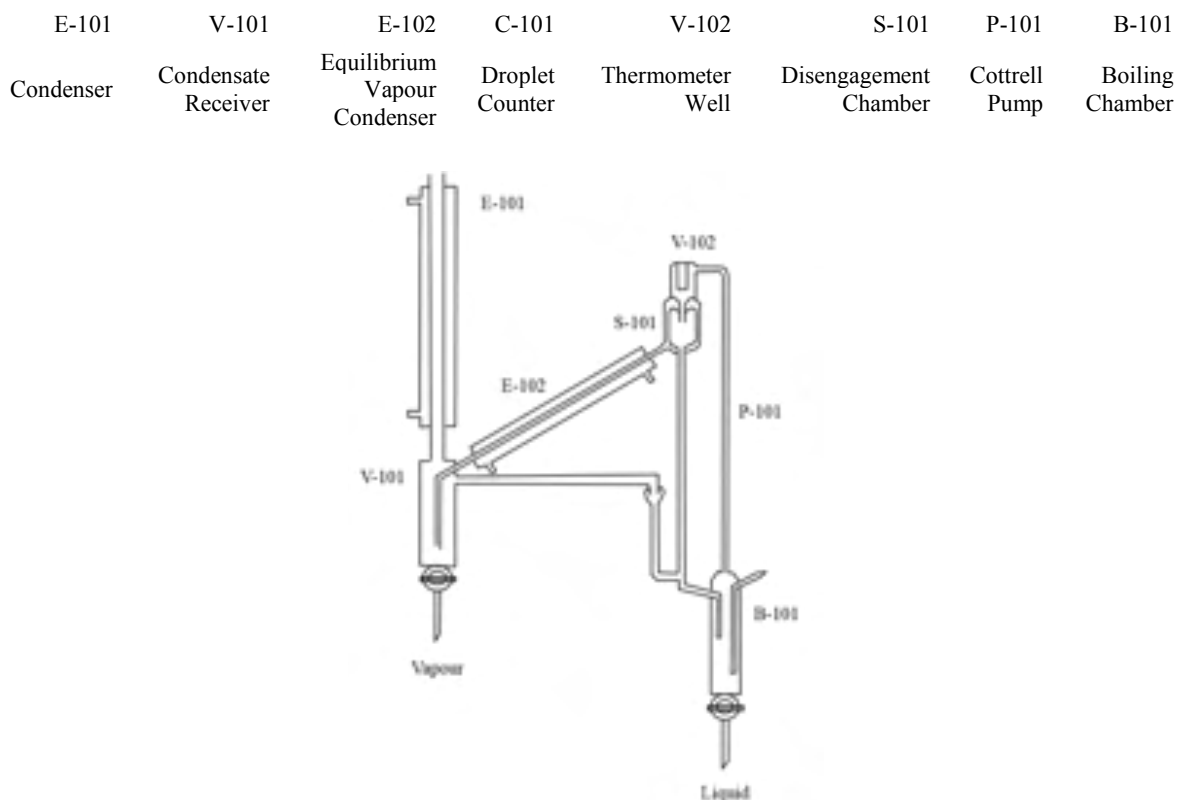


FIGURE 4- 2: ORIGINAL DYNAMIC GILLESPIE VLE STILL. REDRAWN AND ADAPTED USING RAAL AND MULBAUER [226].

The current project will make use of a modified Gillespie dynamic still for separating the interested system as it is the best available means of calculating the isobaric VLE data. The issues of the original design have been resolved with an improved design. The still contains two sampling ports for simultaneous sampling of the VLE phase composition, and an insulation jacket has been placed around the equilibrium chamber to induce proper condensation of the vapour composition.

4.2. HPBDP PHASE EQUILIBRIA MEASUREMENTS

4.2.1. EXPERIMENTAL SETUP AND APPARATUS

A static synthetic visual view cell was used to measure the bubble- and dew-point data of the ternary mixture (see *Figure 4-3*). The experimental setup consisted of a large high-pressure piston-cylinder device with two chambers separated by a piston (5) with two different areas. The larger piston area was exposed to the low-pressure chamber (7) whilst the small area was exposed to the high-pressure chamber (6). A magnet was placed inside of the high-pressure chamber (6) of the equilibrium cell. This allowed for constant and sufficient mixing throughout the experiment and speeded up the rate at which equilibrium was obtained. The use of Teflon seals and O-rings ensured the correct sealing for the high-pressure operations. Consequently, the pressures were maintained throughout an experimental run and nitrogen leaks from the low-pressure chamber were avoided.

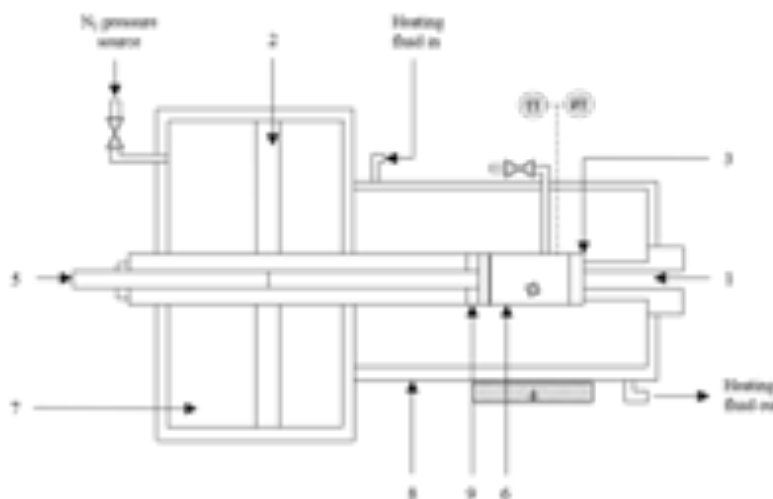


FIGURE 4- 3: SCHEMATIC OF SYNTHETIC VISUAL CELL TO MEASURE THE PHASE BEHAVIOUR OF THE TERNARY SYSTEM: (1) CAMERA, LIGHT-SOURCE AND MONITOR; (2) PRESSURE DISC; (3) SIGHT GLASS; (4) MAGNETIC STIRRER; (5) PISTON ROD; (6) HIGH-PRESSURE EQUILIBRIUM CHAMBER; (7) LOW-PRESSURE CHAMBER; (8) HEATING JACKET; (9) TEFLON SEAL. (ADAPTED AND REDRAWN FROM [18], [58]).

The equilibrium temperature of the cell was measured with a 4-wire *Pt-100* probe [58]. The front end of the temperature probe was placed inside of the sensor well of the equilibrium cell. External temperature control was induced by connecting the rear end of the probe to a Julabo water unit. From the unit, water was pumped through a 5-mm heating mantle (8) surrounding the equilibrium cell. However, the synthetic setup had no controlled environment. Therefore, insulation material was placed around the outside wall of the equilibrium cell to avoid heat loss and maintain a steady mixture temperature. Visual internal observation was enforced using a high-definition medical camera and endoscope (1) located in front of a sight glass (3). The images were magnified and projected onto a

monitor from which the separated phases were visually observed. Design details are available in literature elsewhere [14], [18], [19], [58], [77].

4.2.2. EXPERIMENTAL PROCEDURE

A brief outline of the synthetic procedure is provided here. For a detailed step-by-step procedure, the reader is referred to Appendix B1.

At ambient conditions, the magnet and a known quantity (mass) of solutes were inserted into the equilibrium cell. A vacuum pump was then used to extract all the air out of the cell, followed by flushing the unit with solvent. The solutes were then combined with a known amount of solvent (added gravimetrically with the use of a CO₂ bomb) and the cell was heated to the first set temperature (using the water bath).

A one-phase region, in which equilibrium was to be achieved, was obtained by adjusting the pressure accordingly. Therefore, compressed nitrogen was pumped into the low-pressure chamber which generated the high-pressure in the pressure cell containing the ternary mixture. After approximately 40 minutes, thermal equilibrium was reached. The equilibrium cell pressure was decreased systematically by slowly releasing the compressed nitrogen from the low-pressure chamber. The cell contents were carefully monitored, and the formation of a second phase was visually observed. The phase transition pressure, piston position, and temperature were confirmed and recorded. The next set temperature was selected on the water bath and the process repeated.

4.3. HPVLE PHASE EQUILIBRIA MEASUREMENTS

4.3.1. EXPERIMENTAL SETUP AND APPARATUS

To measure the coexisting equilibrium phases in the ternary mixture, a high-pressure analytical phase equilibria setup was used (see *Figure 4-4*). The large high-pressure piston-cylinder device has a similar construction to that shown in *Figure 4-3*. However, in addition here, the equilibrium cell was situated in a convection oven and included a sample transfer section and a sample analysis unit. The continuous bottom interior is ensured by not aligning the cylinder and the equilibrium cell at the centre point, but at the bottom. A detailed overview of the setup is provided by Fourie et al. [76].

Figure 4-4 shows the added sample transfer section and sample analysis unit of the analytical method. Two electromagnetic ROLSI™ samplers (*R*) allowed for the simultaneous sampling of the vapour and liquid phases. A movable piston attached to the top section of the sampler and a manual displacement device moved the capillary into the equilibrium cell without deviating the inside pressure. The capillary is 15-cm long and has an internal diameter of 15-mm [76]. The same *Pt-100* temperature probes described for the synthetic setup were used in the analytical setup for temperature measurements of the equilibrium cell, with added temperature probes to control the oven temperature.

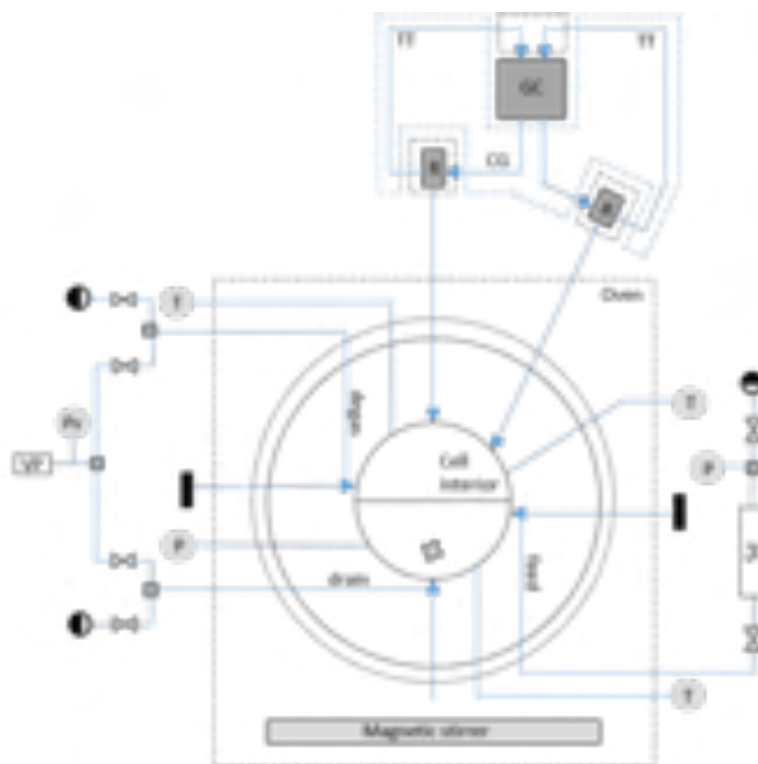


FIGURE 4- 4: CROSS-SECTIONAL SCHEMATIC OF THE HIGH-PRESSURE ANALYTIC PHASE EQUILIBRIA SETUP: [GC] GAS CHROMATOGRAPH; [P] PRESSURE TRANSMITTER; [PS] PRESSURISED SOLVENT; [PV] VACUUM GAUGE; [R] ROLSI SAMPLER; [T] PT-100; [TT] CARRIER GAS AND SAMPLE TRANSFER TUBING; [VP] VACUUM PUMP, (ADAPTED AND REDRAWN FROM FOURIE ET AL. [76]).

4.3.2. EXPERIMENTAL PROCEDURE

A brief outline of the analytical procedure is provided here. For a detailed step-by-step procedure, the reader is referred to Appendix B2.

The same loading procedure as discussed for the HPBDP experiments was repeated here. After the components were loaded, the oven was setup around the cell accordingly.

The isothermal and isobaric set point values were specified. Upon reaching these values the dense-phase sampler and displacement device were adjusted to ensure the capillary tip thereof is in the bottom phase. A one-phase region was therefore not required for reaching phase equilibrium. Approximately 1 hour of magnetic stirring was undergone to ensure equilibrium had been reached. Thereafter, another hour (resting period) was allowed for phase separation.

The final step was conducted over approximately 4-6 hours. At each specified temperature and pressure, an online GC analysis was conducted on the liquid and vapour phase samples simultaneously. A schematic representation of the Agilent 7890A gas chromatograph used is given in Fourie et al. [76]. The analysis was replicated three to four times for each vapour and liquid sample to ensure minimum systematic error of the analytical data. The mass of the vapour sample varied between 0.04 mg and 0.77 mg and the mass of the liquid sample varied between 0.07 mg and 1.1 mg.

4.4. LPVLE PHASE EQUILIBRIA MEASUREMENTS

4.4.1. EXPERIMENTAL SETUP AND APPARATUS

An all glass dynamic recirculating still was used to measure the VLE phase behaviour of the 1-pentanol + *n*-nonane, 1-hexanol + *n*-decane, 1-heptanol + *n*-undecane, 1-octanol + *n*-dodecane and 1-decanol + *n*-tetradecane binary systems at a sub-atmospheric pressure of 40 kPa. *Figure 4-5* illustrates the commercial still (VLE 100 D) manufactured by Pilodist that was utilised in this work for measuring the binary phase behaviour. The full legend of the apparatus is provided in *Table 4-2*.

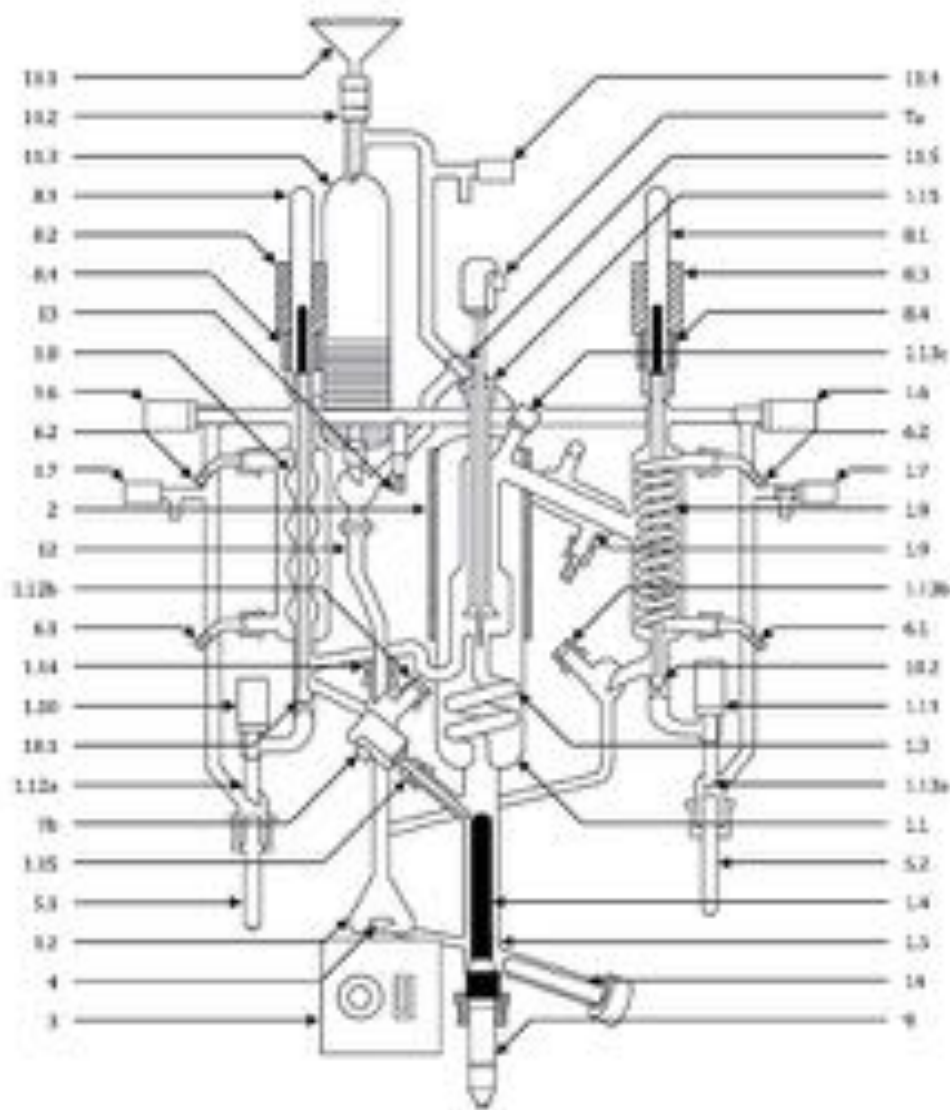


FIGURE 4- 5: SCHEMATIC REPRESENTATION OF THE PILODIST DYNAMIC RECIRCULATING STILL USED FOR VLE MEASUREMENTS.

FIGURE REPRINTED WITH PERMISSION [85], [229], [230].

The still contains an electrical immersion heater (9) that was installed concentrically into the flow heater (1.4) to supply enough heat to the liquid mixture for partial evaporation. A spiral contact line referred to as the Cottrell tube (1.3) is placed before the separation chamber to enable the phase change. The separation chamber was modified to prevent partial condensation of the vapour phase. The two-phase mixture can therefore be sent over the thermometer to measure the bubble-point (equilibrium temperature) before the two phases are separated, condensed and returned to the mixing chamber (1.2). A magnet in the mixing chamber (1.2) ensures a uniform composition and temperature for the mixture throughout the experiment. The mixture was returned to the immersion heater (9) before being recirculated. Further design details can be found in literature elsewhere [84], [230], [231].

TABLE 4- 1: DESCRIPTION OF SEGMENTS ON THE DYNAMIC RECIRCULATING STILL USED IN THIS STUDY.

<i>No.</i>	<i>Description</i>	<i>No.</i>	<i>Description</i>
1.1	Glass body of phase equilibrium apparatus	5.2	Vapour phase glass receiver vial
1.2	Mixing chamber	6.1	Hose connection olive - inlet
1.3	Cottrell pump with silvered vacuum jacket	6.2	Hose connection olive - outlet
1.4	Flow heater	7	Temperature sensor
1.5	Discharge valve	8.1	Valve cap
1.6	Stop valve	8.2	Liquid phase solenoid coil
1.7	Aeration valve	8.3	Vapour phase solenoid coil
1.8	Liquid phase cooler	8.4	Spacer
1.9	Condenser	9	Immersion heater rod
1.10	Liquid phase stop valve	10.1	Liquid phase valve rod
1.11	Vapour phase stop valve	10.2	Vapour phase valve rod
1.12	Liquid phase sampling nozzle	11.1	Funnel
1.13	Vapour phase sampling nozzle	11.2	Feed burette filler nozzle
1.14	Liquid phase filler nozzle	11.3	Feed burette
1.15	Temperature probe nozzle	11.4	Feed burette aeration valve
2	Heating jacket	11.5	Feed burette stop valve
3	Magnetic stirrer	12	Inlet line
4	Stirring magnet	13	Glass connecting olive for pressure control
5.1	Liquid phase glass receiver vial	14	Ultrasonic homogeniser

4.4.2. EXPERIMENTAL PROCEDURE

All numerical references in the procedure provided below refers to those illustrated in *Figure 4-5*. For a detailed step-by-step procedure, the reader is referred to Appendix B3.

The still was initially dried with compressed air. The nitrogen cylinder was opened, and the cooling water system switched on to pass through the cooler for the liquid phase (1.8) and two condensers on the vapour side (1.9). The still was switched on and the controlling software opened.

The still was prepared by selecting the operation to be performed, securing the ultrasonic homogenizer probe (14), closing the discharge valve (1.5) and adding approximately 110 ml of the feed mixture to the mixing chamber (1.2). Once the immersion heater rod (9) was completely submerged in mixture, the magnetic stirrer (3) was switched on. The heater power is important as it established the feed mixture temperature (inserted as a percentage). The pressure was also set accordingly and balanced using nitrogen gas.

After approximately 1-hour equilibrium was achieved and confirmed with a steady vapour temperature on the display unit. When at least 30 drops per minute was observed at the droplet point of the vapour condensation side, in combination with the constant temperature equilibrium, a large enough sample of both phases were taken. Thereafter, a vapour and liquid sample was collected through the two sampling ports and prepared for GC analysis on an Agilent 7820A gas chromatograph. Each of the samples were prepared by adding a known mass amount of the analyte to 1.5 ml of solvent in a vial. In addition, approximately 30 mg of internal standard (IS) was also added to the solvent mixture and measured accurately to 10^{-5} g.

Once enough samples had been obtained the apparatus was stopped and allowed to cool down. The components were drained from the still and discarded into the appropriate waste container. Approximately 110 ml of acetone was fed into the mixing chamber (1.2) to wash out the still by boiling the acetone. After another 40 minutes, the acetone was drained and the still dried with compressed air.

4.4.3. EXPERIMENTAL ERROR ANALYSIS

Two user-controlled, dependent variables need to be considered with respect to the outcome of the experimental runs, namely (1) the heater power (%), and (2) isobaric pressure (kPa).

The first input does not require alternation while running the still and was thus not considered as a variable factor. The influence of the heater power on the equilibrium composition is considered negligible in this study. The pressure fluctuations present during the experiment cannot be regarded in the same light. For investigating the effect of pressure fluctuations on the equilibrium composition, the PSRK model, in Aspen Plus®, will be used. It produces an excellent prediction of the 1-octanol + *n*-dodecane VLE data as will be presented later (see section 7.2.1) but has been produced in *Figure 4-6* for analysis here.

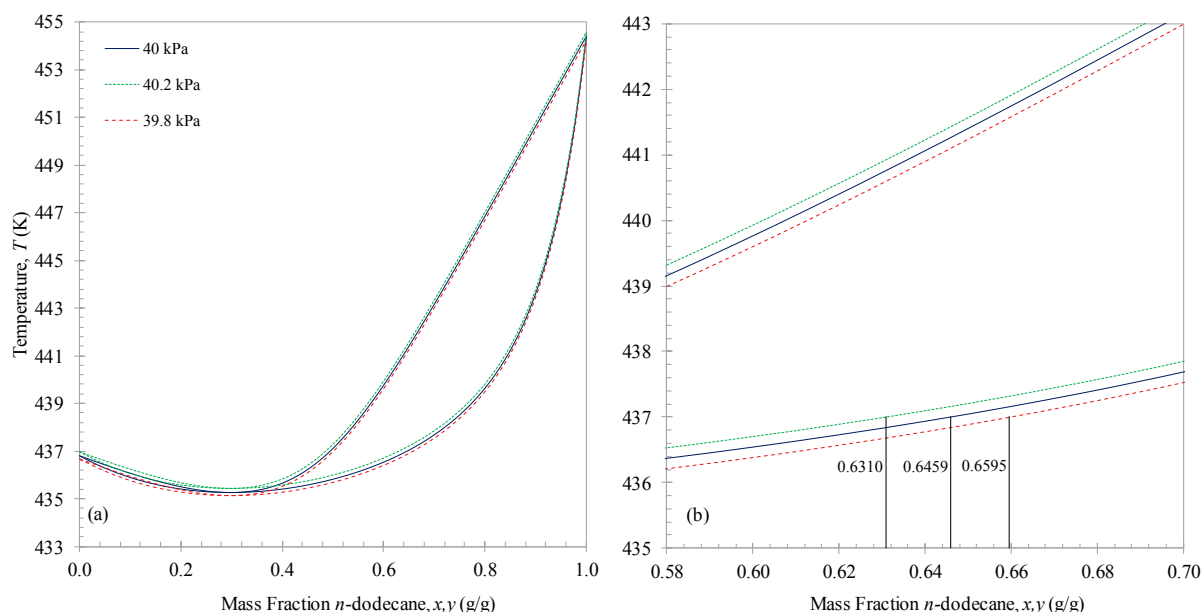


FIGURE 4- 6: (A) EFFECTS OF WORST CASE PRESSURE DEVIATIONS ON THE VLE COMPOSITION MEASUREMENTS. (B) REPRESENTATIVE SECTION OF WORST CASE DEVIATIONS HIGHLIGHTING EFFECTS OF PRESSURE DEVIATIONS ON REPORTED COMPOSITION. DATA GENERATED WITH THE PSRK MODEL IN ASPEN PLUS®.

Visually, maximum pressure fluctuations were estimated to be ± 0.2 kPa and has been indicated on *Figure 4-6 (a)*. Analysing the compositional error of this maximum pressure deviation at a set temperature will provide the worse-case scenario for each test in this study. *Figure 4-6 (b)* provides a closer look at the effect at a constant output temperature (vapour temperature) of 473 K. Equilibrium composition errors of approximately 0.014 mass fraction are observed here, which indicate the significant influence of pressure on the accuracy of each experimental run. Errors of similar magnitude will be obtained for the vapour composition.

In general, control was maintained well within this deviation and the compositional error is in fact much smaller. Previous studies, conducted on the experimental error associated with the equipment used, have verified that the temperature variations directly affect the pressure fluctuations [84], [230], [231]. Visually, temperature fluctuations of approximately 0.02 K were observed during the experiments. Using the same approach as demonstrated in *Figure 4-6* the actual, instantaneous pressure fluctuation and the compositional error can be obtained. The intersecting points of the vertical and horizontal dotted lines in *Figure 4-7* indicate the position of the phase envelopes passing through the same sample composition at $T = 436.98$ K and 470.02 K. These phase envelopes indicate that the actual pressure fluctuation is indeed much smaller than 0.2 kPa. A final value of 0.02 kPa is observed in *Figure 4-7*, effectively producing a compositional error of approximately 0.002 mass fraction.

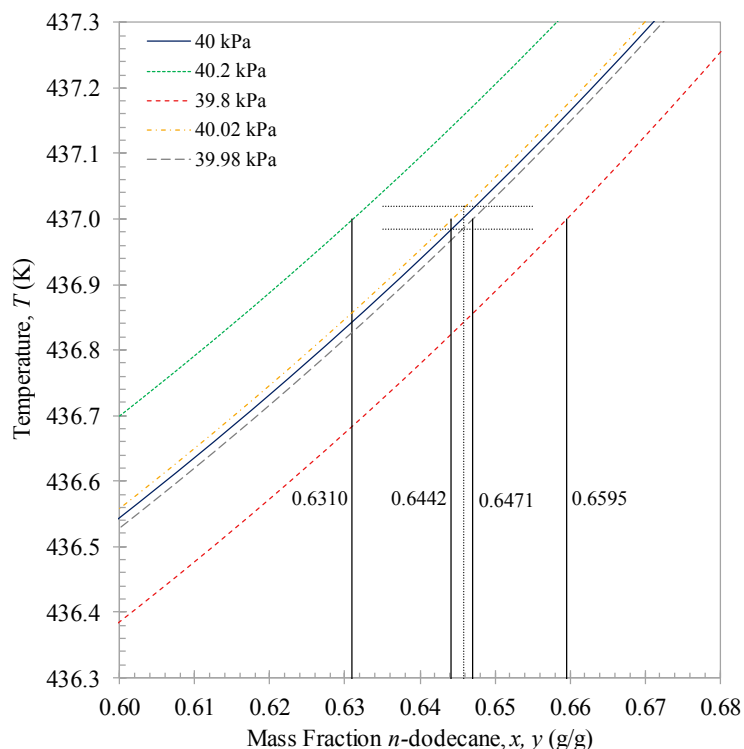


FIGURE 4- 7: EFFECTS OF ANTICIPATED PRESSURE DEVIATIONS ON THE VLE COMPOSITION MEASUREMENTS. PHASE ENVELOPES INDICATED ARE FOR THE LIQUID PHASE. AN EQUIVALENT ANALYSIS CAN BE MADE FOR THE VAPOUR PHASE. DATA GENERATED WITH THE PSRK MODEL IN ASPEN PLUS®.

4.5. ACCURACY OF DATA

4.5.1. CALIBRATION CURVES FOR GC ANALYSIS

To ensure accurate and precise qualitative determinations of any analyte it is essential to consider good calibration and the sensitivity of the instrumental analysis. The solvents and ISs used for the GC calibration are provided in *Table 4-1*. The IS used to quantify the results depend on the system being investigated and has been indicated for each chemical. GC calibration curves were constructed to enable replicate injections within a relative standard deviation of 1%. The linear curves have a regression coefficient equal to or greater than 0.9995 and can be found in Appendix G.

For HPVLE, the calibration procedure involved 3 to 8 manual injections of known mass amounts for the liquids (1-decanol + *n*-tetradecane) and the gas (CO₂). The liquid analytes were diluted with 2-ethyl-1-hexanol (solvent) prior to injections. Linear relationships between injected mass (of analyte) and detector response were obtained with a slow plunger depression rate. The rate of change of response with the amount of analyte defines the sensitivity of the analysis. However, the response factors (the slope of the curves) are dependent on the amount of analyte and is therefore a numerical representation of the sensitivity of the analysis.

For LPVLE calibrations, the procedure involved 5 injections of known mass amounts for the liquids (each analyte of interest) and an internal standard. The analyte + IS mixture were diluted with *n*-hexane (solvent) prior to injections. The linear curves were constructed using the response of each analyte relative to its respective IS response at separate points all along the composition spectrum. Therefore, the linear curves indicate constant sensitivity in each system because the slopes were constant.

4.5.2. HIGH-PRESSURE EXPERIMENTAL MEASUREMENTS

The measurement uncertainty are as follows:

For the HPBDP measurements, two calibrated analytical balances with a precision of 0.0001 g and 0.01 g were used to weigh the solutes and solvent, respectively. The maximum relative uncertainties in the mass fraction is 0.01 times the value, i.e. $u(w) = 0.01w$.

For the HPVLE measurements, the simultaneous analysis of the two phases (composition) will show an estimated relative uncertainty of 0.5 mass % for the species-specific data measured in this work and should not exceed a maximum of 0.9 mass %, i.e. $u(w_i) = \pm 0.005$ g/g with $u(w_i) \leq 0.009$ g/g.

ONEhalf20 Melt pressure transducers were used for both high-pressure experimental procedures. An in-house calibration was conducted for each transducer using a Barnet Instruments dead-weight tester. The calibration data used for HPBDP and HPVLE pressure corrections are tabulated in Appendix C1. The Barnet pressure balance was calibrated by the South African National Accreditation System (SANAS) to take into consideration the weight of each plate used. After suitable corrections for gravity, temperature and air buoyancy were made (i.e. the deviation from the nominal value) a maximum error of 0.04 % was obtained above 2 MPa (see Appendix C2 for the calibration certificates).

- (i) *HPBDP*: The absolute uncertainty of the pressure measurement is no greater than 0.06 MPa, i.e. $u(P) \leq 0.06$ MPa, and includes all contributions towards the error in pressure measurements.
- (ii) *HPVLE*: The absolute uncertainty of the pressure measurement is smaller than or equal to 0.035 MPa, i.e. $u(P) \leq 0.035$ MPa, and includes the 0.01 MPa fluctuation during the sampling process.

The temperature for both experimental methods were measured with 4-wire *Pt-100* probes. The most recent temperature calibration certificates can be found in Appendix C3.

- (i) *HPBDP*: A calibration was conducted by Wika Instruments (Pty) Ltd, South Africa, with a maximum absolute uncertainty of 0.1 K, i.e. $u(T) = 0.1$ K.
- (ii) *HPVLE*: Calibrations were conducted by a SANAS accredited institute (InterCal) for 12 *Pt-100* probes (4 x in the equilibrium cell block, 4 x in the heating fluid inlets and outlets, and 4 x inside the oven environment). The probe-, controller-, and logger-inaccuracies were taken into

consideration and a total absolute uncertainty of 0.1 K was measured, i.e. $u(T) = 0.1$ K, which includes the 0.01 K fluctuation during the sampling process.

4.5.3. LOW-PRESSURE EXPERIMENTAL MEASUREMENTS

The measurement uncertainties are as follows:

The *Pt-100* temperature probes were calibrated by Thermon South Africa (SANAS accredited). After completing a temperature calibration, the *Pt-100* temperature probe connected to a digital Hart Scientific thermometer measured the equilibrium temperature of the mixture with an accuracy of 0.1 K. Fluctuations of 0.03 K in the temperature were observed during sampling. However, the deviation never exceeded 0.1 K. The maximum absolute uncertainty of the temperature is no greater than 0.2 K, i.e. $u(T) \leq 0.2$ K. The latest calibration certificates for the vapour and evaporator temperature probes are provided in Appendix C4.


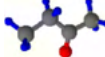
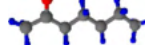
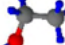

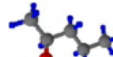
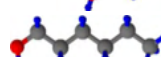
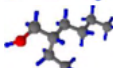
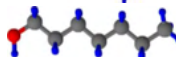
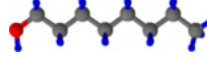
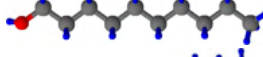
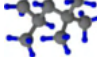
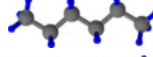
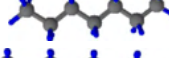
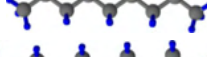
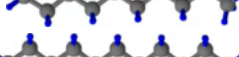
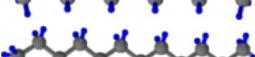
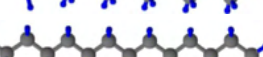

A Wika *UT-10* unit with a maximum operating pressure of 160 kPa absolute and a quoted accuracy of 0.1 % (0.16 kPa) of full scale output per the most recent calibration certificate (see Appendix C5) was utilized to measure the pressure. Furthermore, pressure fluctuations of up to 0.2 kPa were observed during sampling. Therefore, the absolute uncertainty of the pressure transducer is no greater than 0.36 kPa, i.e. $u(P) \leq 0.36$ kPa.

Manual repeatability tests were completed on the GC for samples with a known mass composition. A maximum uncertainty of 0.022 g/g for the analysis was calculated, i.e. $u(x) = u(y) = 0.022$ g/g.

4.6. MATERIALS

Table 4-1 contains the list of components with their respective suppliers, CAS numbers, purity, and chemical structures. Each of the components were used for either the low-pressure and/or the high-pressure experimental measurements. Technical grade air and high purity helium, supplied by Afrox, were used for the gas chromatography (GC) analysis. Nitrogen, also supplied by Afrox was used for overpressure control in the phase equilibrium still and high-pressure equilibrium cells. An additional GC-Mass Spectrometry (GC-MS) analysis was conducted for the two main solutes of interest to this study, namely 1-decanol and *n*-tetradecane for which purity values of 99.5% and 99.7% were obtained, respectively. For each of the components used in the LPVLE systems Karl-Fischer titrations were conducted and showed negligible amounts of water. Based on these tests, the purity of the chemicals given in *Table 4-1* were confirmed and all components were used without further purification.

TABLE 4- 2: COMPONENTS USED FOR HPBDP, HPVLE AND LPVLE EXPERIMENTAL WORK, THEIR SUPPLIERS, CAS NUMBERS, PURITY AND CHEMICAL STRUCTURES (DRAWN USING CHEMSKETCH [29]).

<i>Chemical Name</i>	<i>Formula</i>	<i>Supplier</i>	<i>CAS number</i>	<i>Purity (Mass %)</i>	<i>Chemical Structure</i>
Carbon dioxide	CO ₂	Air-products	124389	> 99.9	
2-butanone	C ₄ H ₈ O	Sigma	78933	≥ 99.7	
2-heptanone	C ₇ H ₁₄ O	Sigma	110430	99	
ethanol	C ₂ H ₅ OH	Sigma	64175	≥ 99.8	
1-pentanol [†]	C ₅ H ₁₁ OH	Sigma	71410	≥ 99	
2-pentanol	C ₅ H ₁₂ O	Fluka	6032297	≥ 98	
1-hexanol	C ₆ H ₁₃ OH	Sigma	111273	≥ 99	
2-ethyl-1-hexanol [‡]	C ₈ H ₁₈ O	Sigma	104767	> 99	
1-heptanol	C ₇ H ₁₅ OH	Sigma	111706	98	
1-octanol [†]	C ₈ H ₁₇ OH	Sigma	111875	≥ 99.5	
1-decanol	C ₁₀ H ₂₁ OH	Sigma	112301	99	
2,2,4-trimethylpentane	C ₈ H ₁₈	Sigma	540841	≥ 99	
<i>n</i> -hexane*	C ₆ H ₁₄	Merck	2867980	≥ 96	
<i>n</i> -heptane	C ₇ H ₁₆	Sigma	142825	99	
<i>n</i> -nonane	C ₉ H ₂₀	Merck	111842	≥ 99	
<i>n</i> -decane	C ₁₀ H ₂₂	Sigma	124185	≥ 99	
<i>n</i> -undecane	C ₁₁ H ₂₄	Sigma	1120214	≥ 99	
<i>n</i> -dodecane	C ₁₂ H ₂₆	Sigma	112403	≥ 99	
<i>n</i> -tetradecane	C ₁₄ H ₃₀	Sigma	629594	≥ 99	

[†] Internal standards used for LPVLE analysis[‡] Solvent used for HPVLE analysis

* Solvent used for LPVLE analysis

4.7. CHAPTER OUTCOMES

This chapter provided an overview of the materials and methods used for the three experimental studies conducted in this work, namely:

- (i) A static synthetic equilibrium cell to measure the HPBDP phase transition points of six CO_2 + 1-decanol + *n*-tetradecane mixtures at 6 set temperatures and 12 varying solute concentrations.
- (ii) A static analytical equilibrium cell to measure the HPVLE of four CO_2 + 1-decanol + *n*-tetradecane mixtures at 40 different isothermal and isobaric conditions.
- (iii) An all-glass dynamic recirculating still to measure the LPVLE of the 1-decanol + *n*-tetradecane system and 4 pertinent binary systems (1-pentanol + *n*-nonane, 1-hexanol + *n*-decane, 1-heptanol + *n*-undecane and 1-octanol + *n*-dodecane) to help verify the 1-decanol + *n*-tetradecane binary data.

The HPBDP and HPVLE results are presented and discussed in Chapter 5 after first verifying the setup of each equilibrium cell with reproducibility tests. Similarly, the LPVLE results of all 5 1-alcohol + *n*-alkane binary systems are presented and discussed in Chapter 6 after verifying the setup of the still with, amongst others, reproducibility tests.

Chapter 5

SUPER- AND NEAR-CRITICAL PHASE EQUILIBRIA OF THE TERNARY SYSTEM CO₂ + 1-DECANOL + N-TETRADECANE

The literature study conducted in Chapter 2 indicates a lack of ternary data available for the system of interest to this work (see *Table 2-5*).

The aim of this chapter is to address these shortcomings by studying the high-pressure phase equilibria of the CO₂ + 1-decanol + n-tetradecane ternary system (Objective 1).

The materials and high-pressure phase equilibria methods discussed in Chapter 4 were used to measure new HPBDP and HPVLE data for the ternary system. The phase equilibria data were used to:

- (i) Construct the necessary phase diagrams for investigating where the solute + solute interactions are most prominent (**Objective 1.1**);
- (ii) Construct the tie lines on the ternary phase diagrams (**Objective 1.2**);
- (iii) Visually identifying the topological phenomena (**Objective 1.3**);
- (iv) Establish the relative solubility and separation potential of the components when using supercritical CO₂ (**Objective 1.4**).

5.1. HPBDP RESULTS AND DISCUSSION

5.1.1. VERIFICATION OF EXPERIMENTAL SETUP

The synthetic setup has been verified several times by previous researchers through comparisons of data to literature [14], [15], [56]. *Table 5-1* provides a select few of the errors obtained by the researchers involved in the design and construction of the equipment being used in this investigation. The experimental setup has therefore been proven accurate through comparisons to literature data.

TABLE 5- 1: VALIDATION OF THE SYNTHETIC EXPERIMENTAL SETUP THROUGH COMPARISONS OF LITERATURE DATA.

<i>System Measured</i>	<i>Error</i>	<i>Reference</i>
Ethane + <i>n</i> C ₂₄	≤ 0.02 MPa	Schwarz and Nieuwoudt [56] with [232], [233]
CO ₂ + 1-octanol	≤ 0.02 MPa	Fourie et al. [14] with [71], [234], [235]

Reproducibility tests were conducted on the CO_2 + 1-decanol and CO_2 + *n*-tetradecane binary systems to further validate their use in this chapter. Two loadings of very similar composition were measured for the binary systems and compared to literature data. The reproduced data for the CO_2 + 1-decanol and CO_2 + *n*-tetradecane binary systems are shown in *Figure 5-1 (a)* and *Figure 5-1 (b)*, respectively. For the 1-decanol system, solubility pressure errors of $\leq 2\%$ were obtained and for the *n*-tetradecane binary system, errors in pressure were at times smaller than the markers used to represent the points measured. Therefore, the synthetic equipment was successfully validated as all data points are well within the accuracy of the pressure measurement.

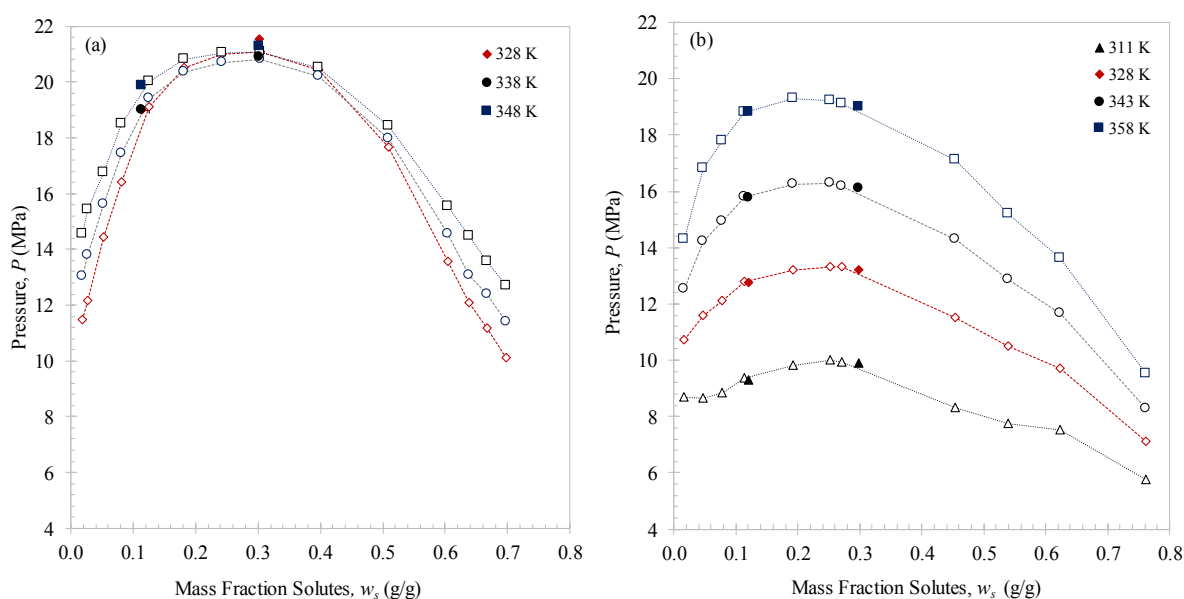


FIGURE 5- 1: (A) REPRODUCIBILITY OF THE CO_2 + 1-DECANOL [15] BINARY SYSTEM AT $T = 328\text{ K}$, $T = 338\text{ K}$ AND $T = 348\text{ K}$; (B) REPRODUCIBILITY OF THE CO_2 + *N*-TETRADECANE [17] BINARY SYSTEM AT $T = 311\text{ K}$, $T = 328\text{ K}$, $T = 343\text{ K}$ AND $T = 358\text{ K}$. SOLID MARKERS REPRESENT THE DATA MEASURED IN THIS WORK.

5.1.2. EXPERIMENTAL RESULTS

A total of 6 solute mixtures were experimentally measured, namely:

$$- w_c^{red} (\text{g/g}) \in \{0.2405; 0.5000; 0.6399; 0.7698; 0.8162; 0.9200\}$$

The order in which the ternary mixtures were measured are presented in *Figure 5-2*. Mixture 1 was selected as the starting point to establish the mixture solubility direction with respect to each of the CO_2 binary subsystems. The $w_c^{red} = 0.5000$ g/g phase transition curve was skewed towards the CO_2 + *n*-tetradecane binary system, confirming the higher solubility of *n*-tetradecane over 1-decanol in the presence of supercritical CO_2 . Mixture 2 and 3 were selected based on the findings by Scheidgen and Schneider [3] for possible cosolvency effects around $w_c^{red} = 0.84$ g/g. Thereafter, mixture 4 was measured to broaden the composition range being investigated and to observe the impact of association effects in 1-decanol-rich systems. However, the focus point of this study was the solute + solute

interactions in the ternary mixture, and thus mixture 5 and 6 were selected to further investigate the complex phase behaviour region initially identified by Patton et al.[40].

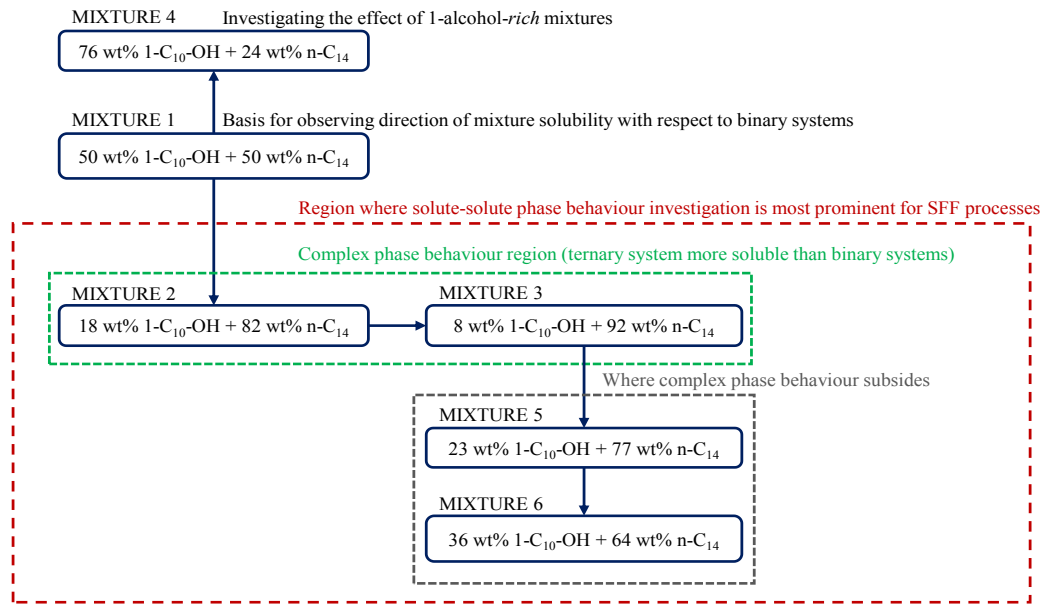


FIGURE 5- 2: HIGH-PRESSURE BUBBLE- AND DEW-POINT MIXTURES MEASURED IN THIS STUDY TO ACHIEVE OBJECTIVE 1.1.

The phase transition pressure of the ternary CO₂ + 1-decanol + *n*-tetradecane mixtures were measured at 6 different temperatures ($T_{Approx.} = 308 \text{ K}, 318 \text{ K}, 328 \text{ K}, 338 \text{ K}, 348 \text{ K}$ and 358 K). At each temperature, the phase transition pressure for 12 known (1-decanol + *n*-tetradecane) solute mass fractions ($w_{s, Approx.} = 0.015, 0.025, 0.05, 0.08, 0.12, 0.18, 0.25, 0.33, 0.40, 0.47, 0.55$ and 0.62) were measured. Thus, approximately 72 readings were measured per w_c^{red} mixture with pressures ranging from $P = 6 \text{ MPa}$ to 27 MPa .

Fluctuations in temperature during measurements resulted in the necessity to interpolate the P - T data before comparing the various mixtures with one another. The *n*-tetradecane-rich ($w_c^{red} > 0.2405 \text{ g/g}$) ternary systems produced linear P - T correlations, whereas the 1-decanol-rich ($w_c^{red} = 0.2405 \text{ g/g}$) ternary system required, at times, a second or third order polynomial correlation to ensure a regression coefficient higher than 0.98 and a pressure error of less than 2 % and 0.2 MPa. The same interpolation process has been implemented successfully in previous studies [14], [15], [56]. In Figure 5-3 the P - T relationships at a low, intermediate and high solute mass fraction for the $w_c^{red} = 0.2405 \text{ g/g}$ ternary system are given to illustrate the polynomial correlations observed in this study. To avoid large inaccuracies, it is recommended that the correlations only be used for interpolation purposes. However, when necessary, extrapolation should not exceed a maximum of 10 K. It should be made clear that the uncertainty on the experimental data will remain unchanged. However, on the smoothed data derived by the P - T correlations, 0.2 MPa should be added to the total uncertainty.

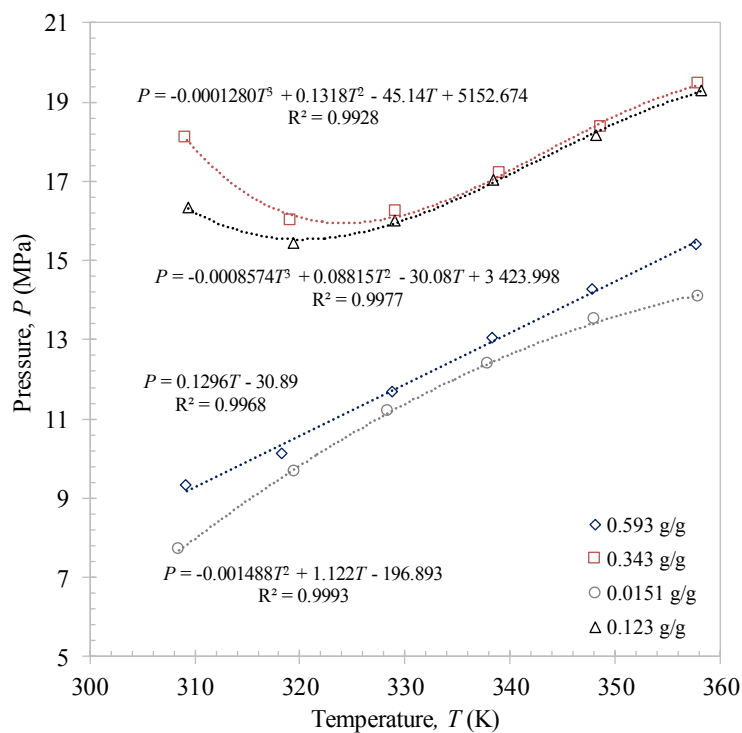


FIGURE 5- 3: P - T CORRELATIONS AT DIFFERENT SOLUTE MASS FRACTIONS FOR THE CO_2 + 1-DECANOL + n -TETRADECANE TERNARY SYSTEM WHEN $w_c^{RED} = 0.2405 \text{ G/G}$.

Figure 5-4 to Figure 5-6 contain the isothermal P - w_s data produced for the six CO_2 + (1-decanol + n -tetradecane) mixtures. The raw experimental data, and parameters to be used for the temperature corrections, are provided for each respective solute composition in Appendix E1 and can be used to interpolate pressures at any temperature between $T = 308 \text{ K}$ and 358 K .

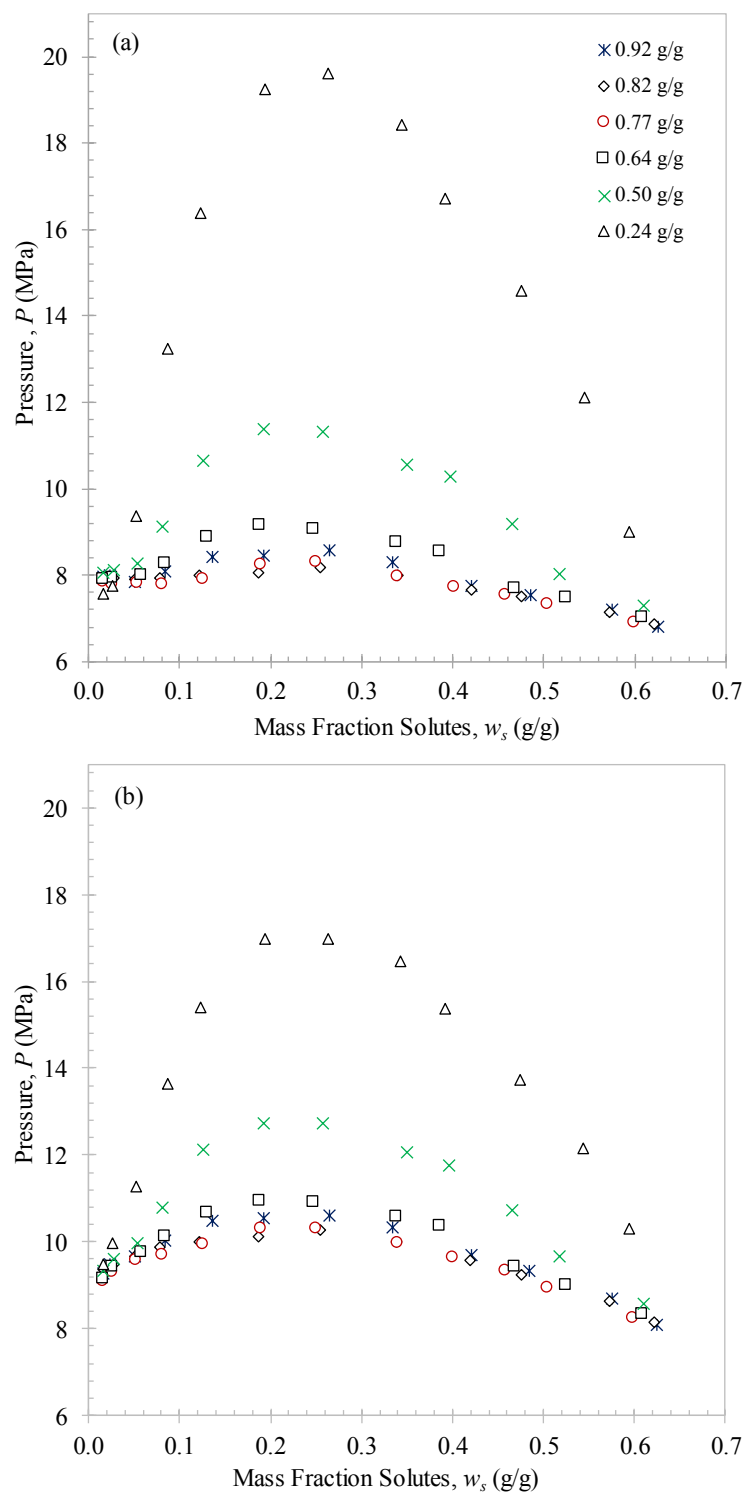


FIGURE 5- 4: P - w_s PLOT OF THE BUBBLE- AND DEW-POINT DATA MEASURED FOR SIX CO_2 + (1-DECANOL + N -TETRADECANE) MIXTURES AT (A) $T = 308$ K AND (B) $T = 318$ K.

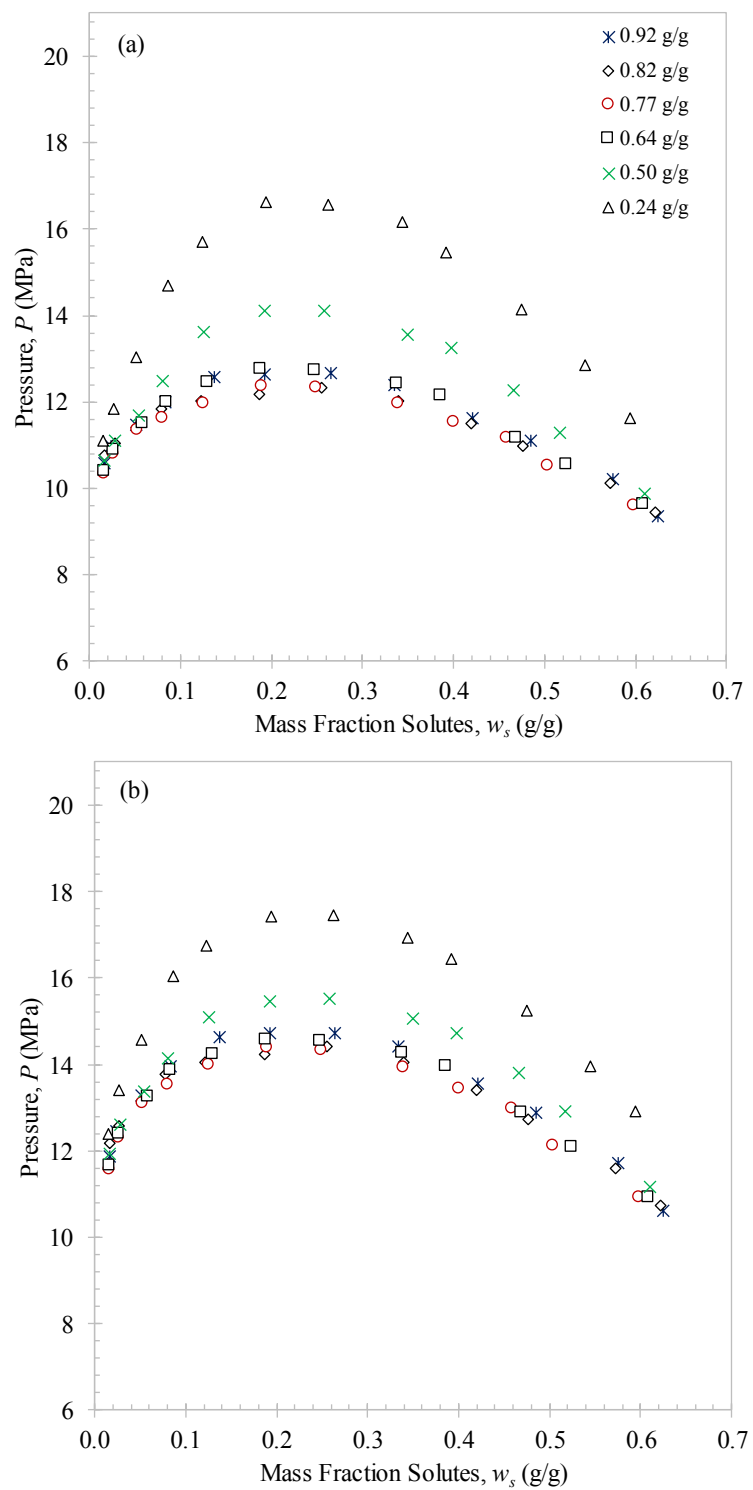


FIGURE 5- 5: P - w_s PLOT OF THE BUBBLE- AND DEW-POINT DATA MEASURED FOR SIX $\text{CO}_2 + (1\text{-DECANOL} + N\text{-TETRADECANE})$ MIXTURES AT (A) $T = 328$ K AND (B) $T = 338$ K.

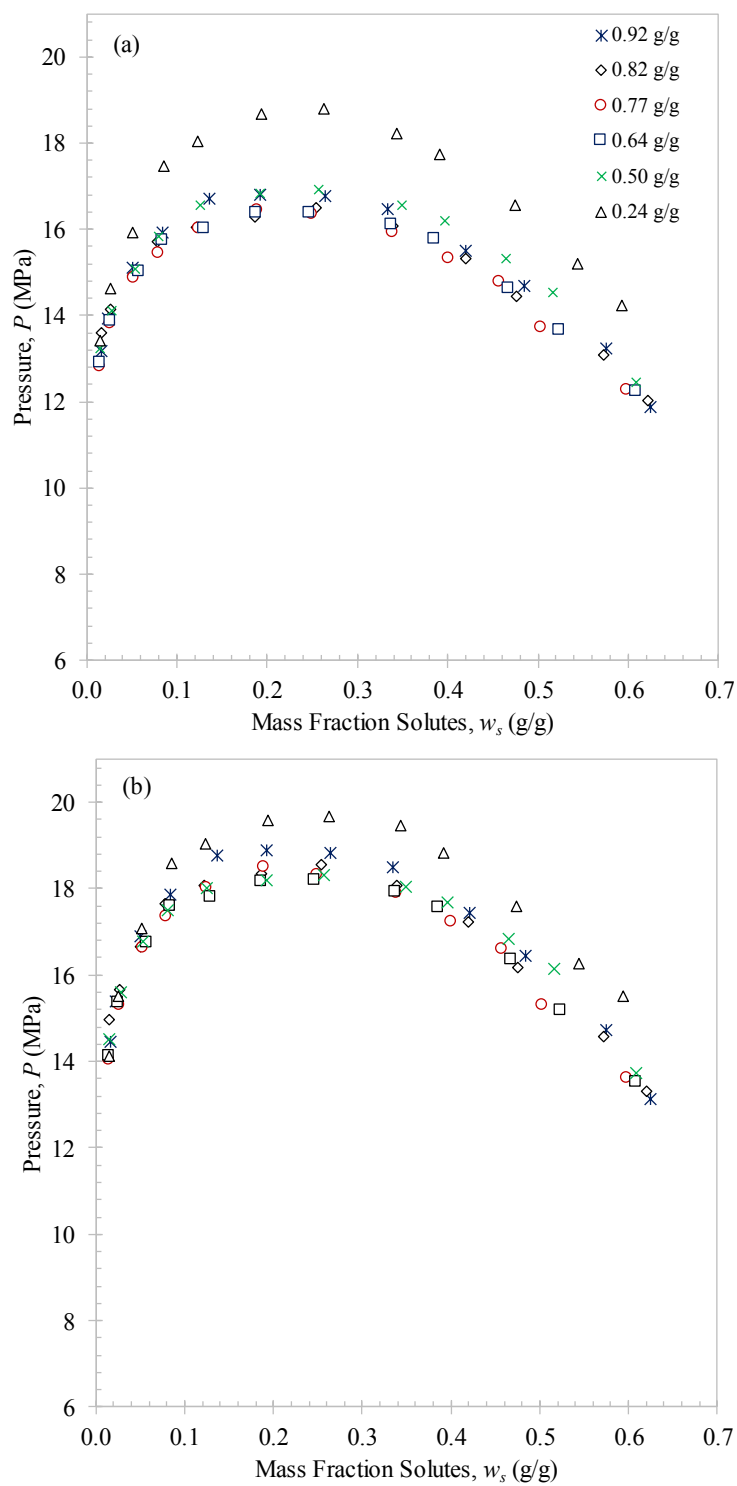


FIGURE 5- 6: P - w_s PLOT OF THE BUBBLE- AND DEW-POINT DATA MEASURED FOR SIX $\text{CO}_2 + (1\text{-DECANOL} + N\text{-TETRADECANE})$ MIXTURES AT (A) $T = 348$ K AND (B) $T = 358$ K.

5.1.3. COMPARISON TO CO₂ BINARY SUB-SYSTEMS

The six experimental CO₂ + 1-decanol + *n*-tetradecane ternary mixtures are compared to the CO₂ + 1-decanol and CO₂ + *n*-tetradecane literature data in *Figure 5-7* for $T = 308$ K.

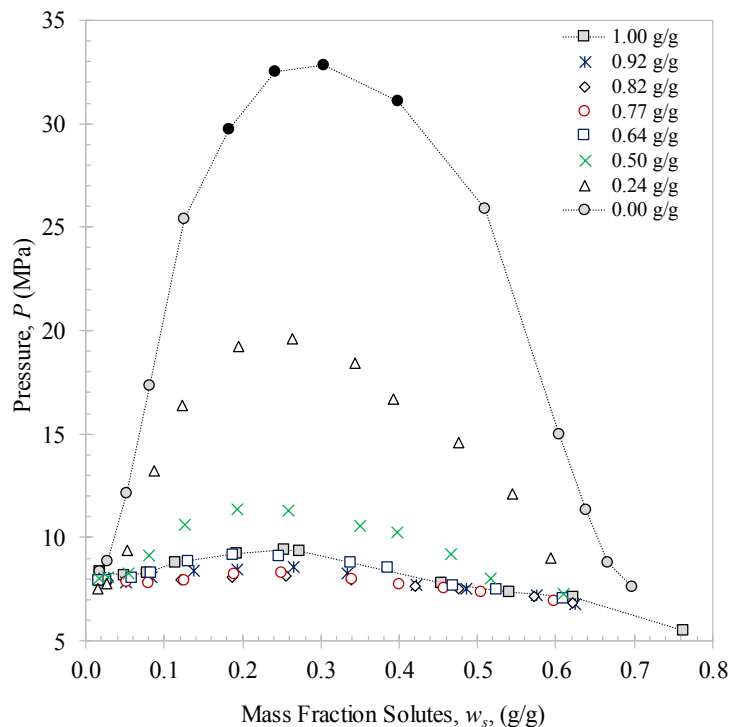


FIGURE 5- 7: P - w_s PLOT OF THE BUBBLE- AND DEW-POINT DATA MEASURED FOR SIX CO₂ + (1-DECANOL + *N*-TETRADECANE) MIXTURES AT $T = 308$ K. THE BOUNDARY CONDITIONS, $w_c^{RED} = 0.00$ G/G AND $w_c^{RED} = 1.00$ G/G, REPRESENT LITERATURE DATA OF THE CO₂ + 1-DECANOL [15] AND CO₂ + *N*-TETRADECANE [17] BINARY SYSTEMS, RESPECTIVELY. THE ● MARKERS REPRESENT EXTRAPOLATED DATA POINTS.

In this system, similar 1-alcohol and *n*-alkane interactions are observed to those previously published for the CO₂ + 1-decanol + *n*-dodecane [13], [16] and CO₂ + 1-dodecanol + *n*-tetradecane [11], [17] ternary systems. The phase transition pressures were expected to lie between the two binary systems. However, the solubility curves of the *n*-tetradecane-rich mixtures are, at times, lower than the CO₂ + *n*-tetradecane binary sub-system and the 1-decanol-rich system ($w_c^{red} = 0.2405$ g/g) lies approximately halfway between the two binary systems. To illustrate these findings more clearly a 3D plot of the experimental mixtures measured, along with binary literature data [15], [17] at $T = 308$ K, 328 K and 348 K are given in *Figure 5-8* to *Figure 5-10*, respectively.

As can be seen in *Figure 5-8*, 1-decanol-rich mixtures are less soluble than *n*-tetradecane-rich mixtures in supercritical CO₂ and requires a much higher phase transition pressure to form a single phase. According to Zamudio et al. [15], the higher phase transition pressure of 1-decanol and 1-decanol-rich mixtures could be attributed to the increased polarity of 1-decanol compared to *n*-tetradecane. The observed trend is further verified by the findings of Schwarz et al. [4], who investigated the effects of functional end groups on the phase behaviour of, amongst others, *n*-alkanes

and alcohols and concluded that the polarity of the functional end group causes the decreased solubility of the 1-alcohol compared to the corresponding *n*-alkane in a non-polar solvent. The polar hydroxyl group on 1-decanol results in the formation of hydrogen bonded multimers of 1-alcohol molecules in the 1-decanol-rich mixture [4], [15]. On the other hand, non-polar *n*-tetradecane molecules cannot form multimers and subsequently it is much easier for the supercritical CO₂ to get access to the *n*-alkane. All these factors result in the *n*-tetradecane-rich mixtures to be much more soluble than those rich in 1-decanol.

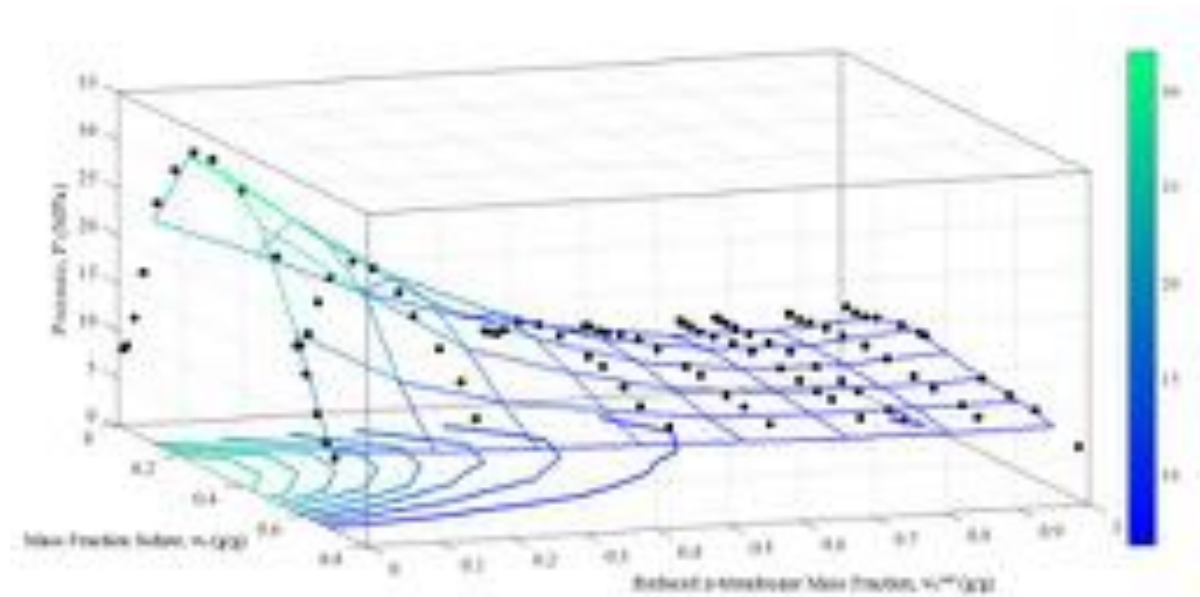


FIGURE 5- 8: P - w_s - w_c^{RED} , 3D PLOT OF THE BUBBLE-POINT, DEW-POINT AND CRITICAL ENDPOINT DATA EXPERIMENTALLY MEASURED AT $T = 308$ K. THE BOUNDARY CONDITIONS, $w_c^{RED} = 0.00$ G/G AND $w_c^{RED} = 1.00$ G/G, REPRESENT BINARY PHASE DIAGRAMS OBTAINED FROM LITERATURE [15], [17].

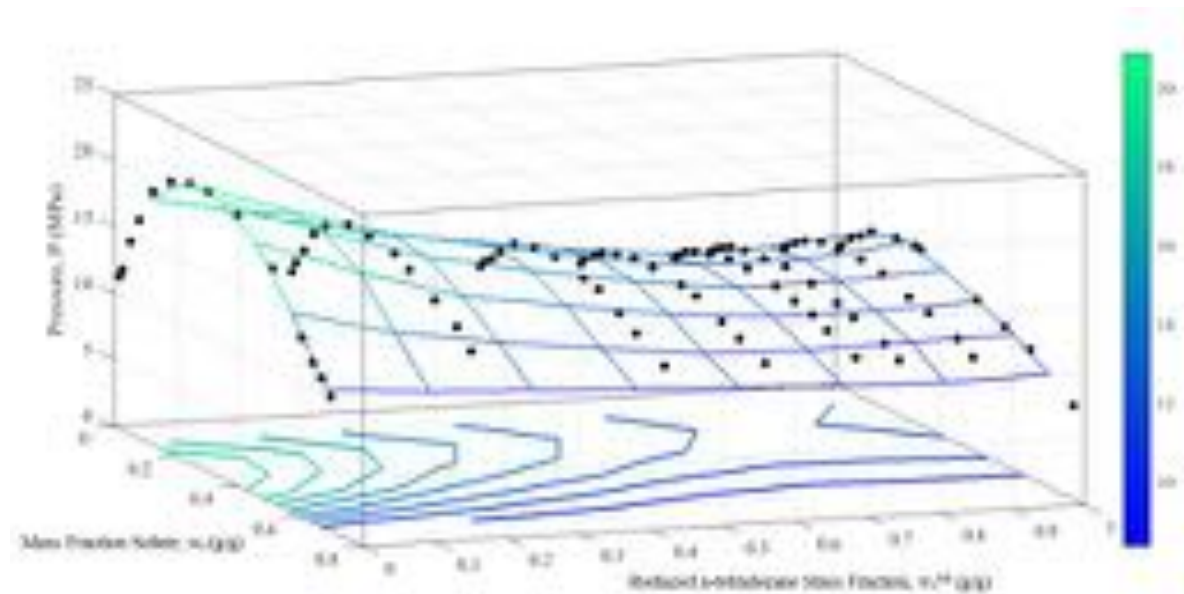


FIGURE 5- 9: P - w_s - w_c^{RED} , 3D PLOT OF THE BUBBLE-POINT, DEW-POINT AND CRITICAL ENDPOINT DATA EXPERIMENTALLY MEASURED AT $T = 328$ K. THE BOUNDARY CONDITIONS, $w_c^{RED} = 0.00$ G/G AND $w_c^{RED} = 1.00$ G/G, REPRESENT BINARY PHASE DIAGRAMS OBTAINED FROM LITERATURE [15], [17].

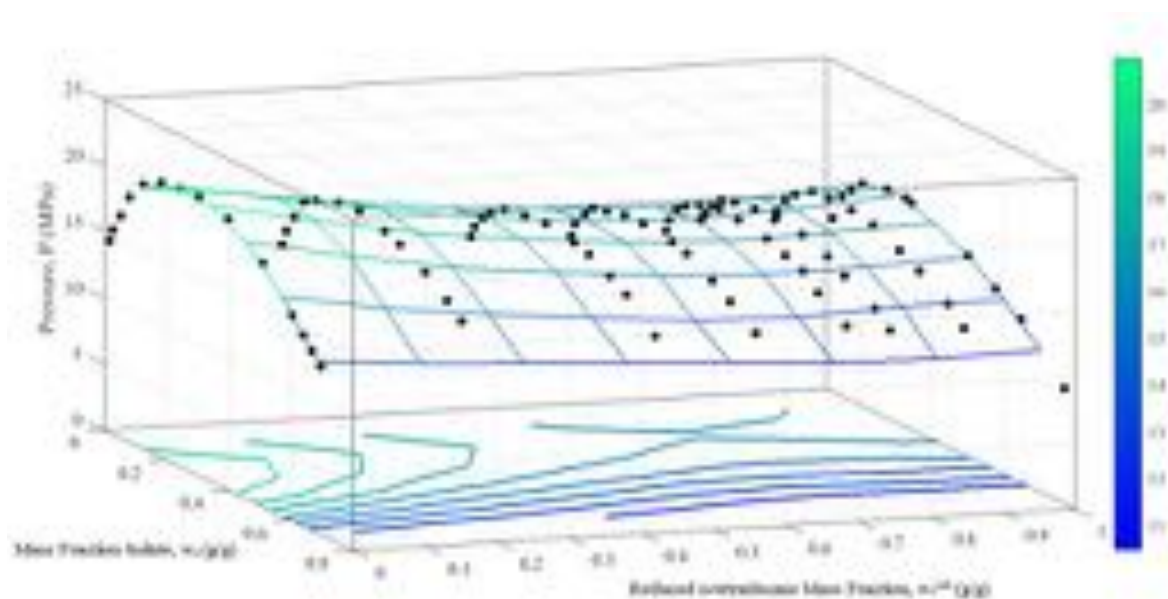


FIGURE 5- 10: P - w_1 - w_2^{red} , 3D PLOT OF THE BUBBLE-POINT, DEW-POINT AND CRITICAL ENDPOINT DATA EXPERIMENTALLY MEASURED AT $T = 348$ K. THE BOUNDARY CONDITIONS, $w_2^{red} = 0.00$ G/G AND $w_2^{red} = 1.00$ G/G, REPRESENT BINARY PHASE DIAGRAMS OBTAINED FROM LITERATURE [15], [17].

5.1.4. TEMPERATURE INVERSIONS AND EFFECTS

From *Figure 5-9* and *Figure 5-10* it is evident that with an increase in temperature the solubility of the 1-decanol-rich mixtures increase in supercritical CO_2 . A temperature inversion was observed between $T = 308$ K and 318 K for the $w_c^{red} = 0.2405$ g/g mixture (see *Figure 5-11*). As explained previously in section 2.1.4, this contradicts the common behaviour of increasing phase transition pressure with an increasing temperature.

The unique behaviour occurs at temperatures close to the solvents critical temperature. Here, similar multimer bonds are required to be broken as those discussed for the CO_2 + 1-decanol system in section 2.1.4. For the $w_c^{red} = 0.2405$ g/g system at temperatures above about $T = 318$ K, the 1-decanol units in the mixture have sufficient kinetic energy to effectively disrupt the multimer hydrogen bonds, allowing the 1-decanol to dissolve in the CO_2 at lower pressures.

For $w_c^{red} \geq 0.5000$ g/g no temperature inversions were observed. Therefore, the phase transition pressure increases with temperature over the entire composition range. It is postulated that at these conditions sufficient n -tetradecane is present to limit the macroscopic effects of the multimer bonds between the 1-alcohol molecules.

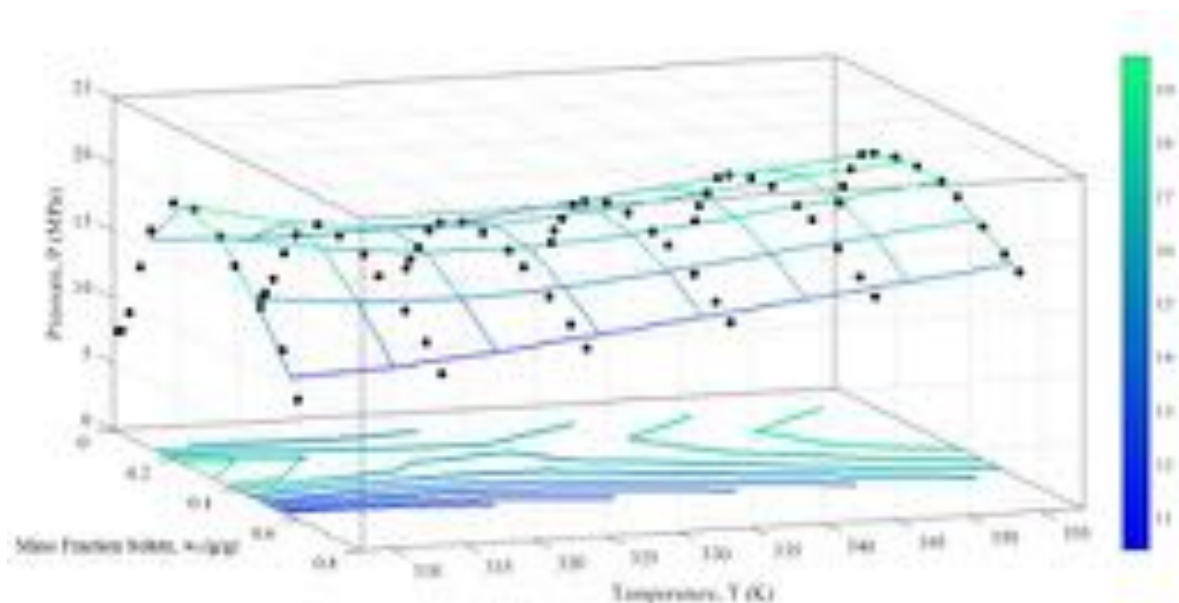


FIGURE 5- 11: P - T - w_s , 3D PLOT OF THE BUBBLE-POINT, DEW-POINT AND CRITICAL ENDPOINT DATA EXPERIMENTALLY MEASURED
AT $w_c^{RED} = 0.2405$ G/G.

The 3D plots in *Figure 5-8* to *Figure 5-10* can be ‘sliced’ perpendicular to the w_s -axis at constant w_s . In effect, this display (P - w_c^{red} projection in the P - w_s - w_c^{red} plot) allows one to observe the effect of composition more clearly. In *Figure 5-12*, constant solute mass fraction isotherms are given as a function of P and w_c^{red} . A constant linear-downward solubility pressure trend was expected. However, a slight increase in the solubility pressures is observed at approximately, $w_c^{red} = 0.8162$ g/g. This phase behaviour effect occurs due to the change in composition at each respective temperature (moving from $w_s = 0.65$ g/g to $w_s = 0.05$ g/g).

From these plots, at $T = 308$ K, a temperature inversion is observed at w_c^{red} between 0 g/g and approximately 0.4 g/g when w_s is varied between approximately 0.65 g/g and 0.05 g/g. Similarly, the temperature inversion at $T = 318$ K occurs at w_c^{red} between 0 g/g and approximately 0.28 g/g when w_s is varied between approximately 0.62 g/g and 0.08 g/g. Solute + solute interactions between the 1-decanol and n -tetradecane molecules can therefore not be ignored as they will in this manner decrease the required phase transition pressures at which the solutes will dissolve into a single phase.

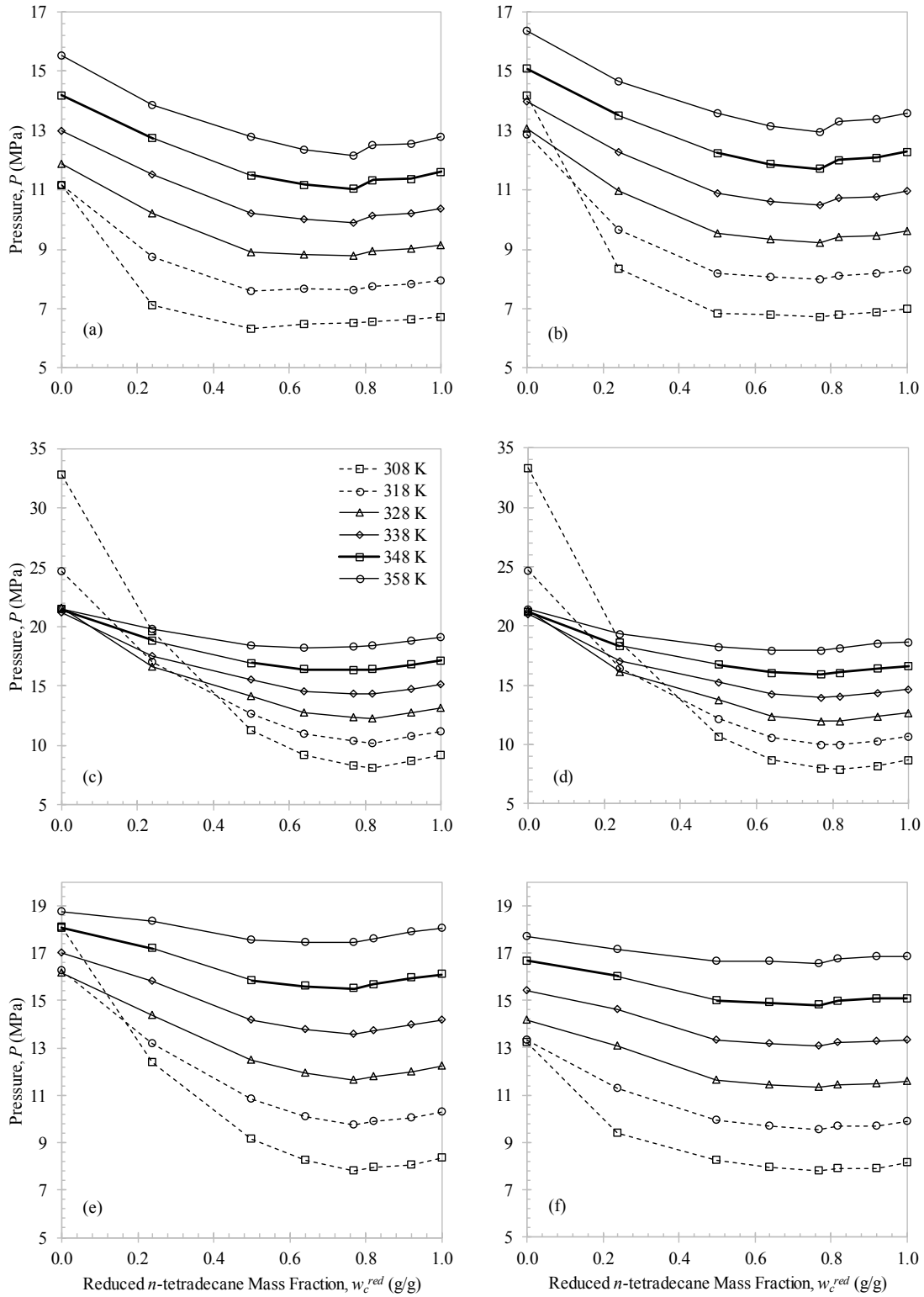


FIGURE 5- 12: ISOTHERMS ON P - w_c^{RED} PLOTS FOR IDENTIFYING THE COMPOSITION AT WHICH TEMPERATURE INVERSIONS WILL OCCUR. CONSTANT SOLUTE MASS FRACTIONS w_s ARE INVESTIGATED IN THE BUBBLE-POINT REGION: (A) 0.65 g/g; (B) 0.62 g/g; THE MIXTURE CRITICAL REGION: (C) 0.25 g/g; (D) 0.33 g/g; AND THE DEW-POINT REGION: (E) 0.08 g/g; (F) 0.05 g/g. THE BOUNDARY CONDITIONS, $w_c^{RED} = 0.00$ g/g AND $w_c^{RED} = 1.00$ g/g, REPRESENT BINARY DATA OBTAINED FROM LITERATURE [15], [17].

The aim of separation considered in this study is the removal of residual *n*-tetradecane from 1-decanol by means of SFF. The dew-point region is important for distinguishing whether the process will be feasible. Therefore, for dilute solute composition mixtures ($w_s < 0.12$ g/g) CO₂ will preferentially dissolve *n*-tetradecane from the mixtures. An enlarged view of the dew-point region is provided in Figure 5-13 on a pressure-composition diagram for (a) $T = 308$ K, (b) $T = 328$ K and (c) $T = 358$ K, to illustrate the effect of temperature on the separation of each mixture.

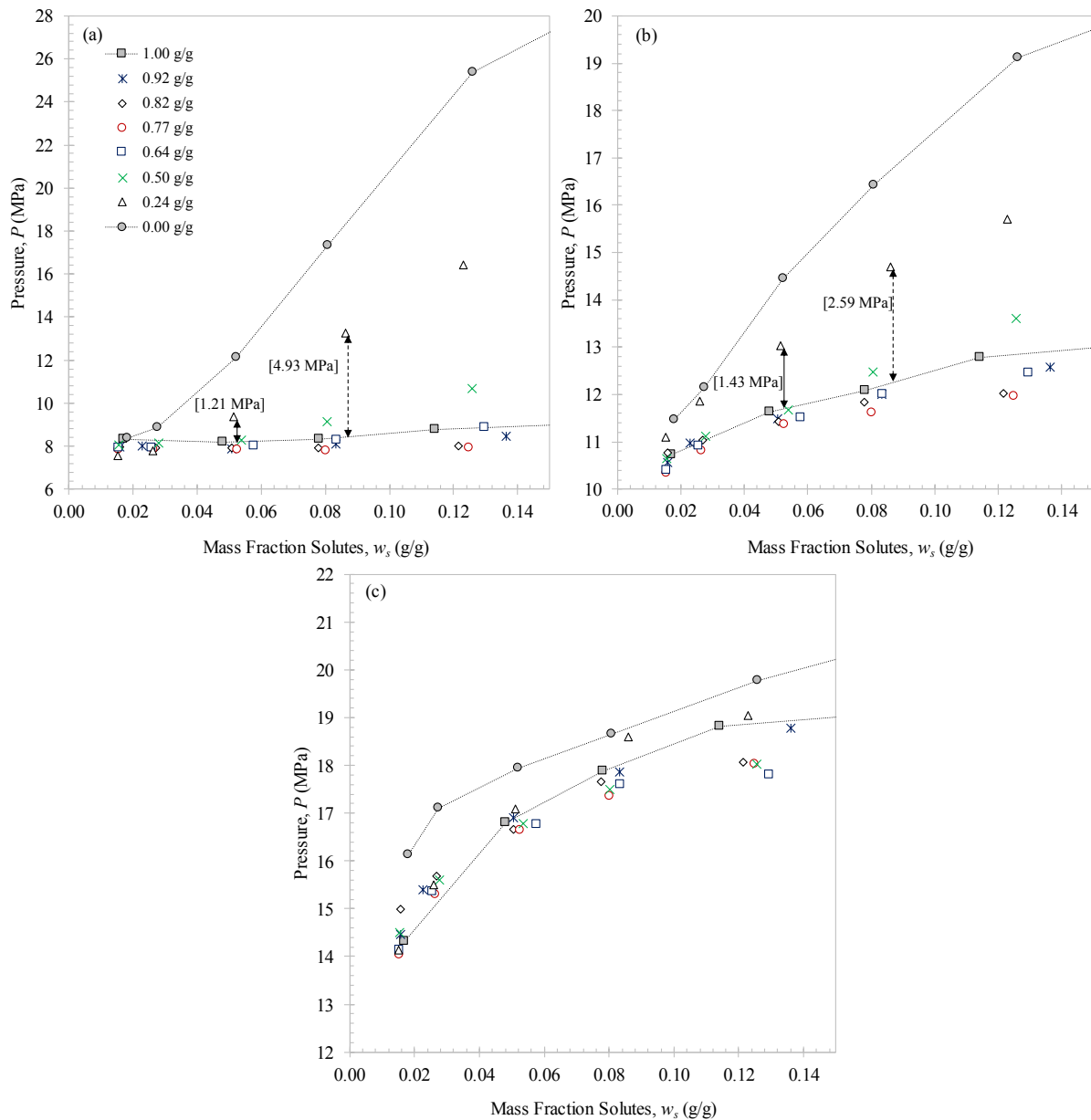


FIGURE 5- 13: DEW-POINT REGION DATA MEASURED FOR EACH MIXTURE TO SHOW THE DECREASE IN SOLUBILITY WITH AN INCREASE IN TEMPERATURE FROM: (A) $T = 308$ K; TO (B) $T = 328$ K; TO (C) $T = 358$ K. THE BOUNDARY CONDITIONS, $w_c^{RED} = 0.00$ G/G AND $w_c^{RED} = 1.00$ G/G, REPRESENT BINARY PHASE DIAGRAMS OBTAINED FROM LITERATURE [15], [17].

The phase transition pressures for the *n*-tetradecane-rich mixtures are very similar at the lower temperature of $T = 308$ K. The large difference for the $w_c^{red} = 0.2405$ g/g mixture is due to the temperature inversion at this isothermal condition. Therefore, it is postulated that the separation was enhanced at temperatures closer to the solvent's critical temperature. The broken arrows in *Figure 5-13* indicate the difference in phase transition pressures between the binary system $\text{CO}_2 + n$ -tetradecane and the $w_c^{red} = 0.2405$ g/g mixture at $\pm w_s = 0.08$ g/g. The pressure difference of each is indicated in the square brackets. The pressure difference **decreased** from $P = 4.93$ MPa to 2.59 MPa when **increasing** the temperature from $T = 308$ K to 328 K, supporting the observation. However, by diluting the solute composition to $\pm w_s = 0.05$ g/g, the separation was optimised at $T = 328$ K. Once again, the solubility pressure differences are shown by the values in the brackets, now indicated by solid arrows. The pressure difference between the 1-decanol-rich mixture and the $\text{CO}_2 + n$ -tetradecane binary system **increased** from $P = 1.21$ MPa to 1.43 MPa when **increasing** the temperature from $T = 308$ K to 328 K. The overall composition therefore controls the temperature at which optimum separation with SFF will occur. Regardless of the temperature inversion at $T = 308$ K, the phase behaviour differences at $T = 328$ K increased, indicating separation with SFF will be enhanced. Therefore, moderate temperatures such as $T = 328$ K are advised for the process to be feasible by avoiding temperature inversion discrepancies and similar phase behavioural properties.

At the highest temperature investigated, $T = 358$ K (*Figure 5-13 (c)*) all the mixtures have closer phase transition pressures and thus exhibit very similar phase behaviour properties. The use of SFF under these circumstances will prove very difficult and most likely unsuccessful.

5.1.5. SECTION OUTCOMES

New contributions:

- (i) New high-pressure bubble- and dew-point data for six $\text{CO}_2 + (1\text{-decanol} + n\text{-tetradecane})$ mixtures were measured.
- (ii) The data successfully defined the range and region in which distinct solute + solute interactions were occurring when compared to the $\text{CO}_2 + 1\text{-decanol}$ and $\text{CO}_2 + n\text{-tetradecane}$ binary systems.

Key objective(s) achieved: Objective 1.1

The HPBDP phase behaviour of the $w_c^{red} = 0.2405$ g/g mixture differs tremendously from the remaining 5 mixtures at $T = 308$ K and $T = 318$ K due to the occurrence of temperature inversions. Separation was enhanced at temperatures closer to the solvents critical temperature. However, the overall concentration of the mixture determined the temperature at which optimum separation took place. Regardless of the temperature inversion, at very dilute solute compositions ($w_s < 0.07$ g/g), where SFF is most prominent, the separations were believed to be optimised at $T = 328$ K. In terms of phase behaviour differences, $T = 328$ K is the recommended operating temperature for the ternary system.

The HPBDP data can be used to characterise the complex phase behaviour and will be done in the next section. Furthermore, to confirm the optimum separations conditions, HPVLE phase equilibria data are required and will be presented and discussed in section 5.3.

5.2. COMPLEX PHASE BEHAVIOUR

5.2.1. AZEOTROPE AND COSOLVENCY EFFECTS

Published literature shows that an azeotrope forms in the CO₂ + 1-decanol + *n*-tetradecane ternary system (see section 2.2.2) [40]. The azeotropic phase behaviour was expected for the system due to the close boiling points of the pure components (only 22 K apart) [63].

To identify in which pressure range the azeotrope will form the influence of solute composition on the ternary system was investigated. The azeotropic point is where the vapour and liquid equilibrium w_c^{red} compositions are equal. Knowing this, one can obtain the approximate location of the azeotrope graphically by plotting a dew-point and a bubble-point isotherm together on a P - w_c^{red} graph under isothermal conditions. For example, as shown in *Figure 5-14* by plotting the P - w_c^{red} curves at $w_s = 0.245$ g/g (liquid-like) and $w_s = 0.180$ g/g (vapour-like) at $T = 318$ K, 328 K and 338 K, a pressure minimum occurs within a range surrounding the $w_c^{red} \approx 0.8162$ g/g mixture. Near this point the ratio of the solutes in the liquid-like and the vapour-like phases are the same; an azeotrope therefore occurs. According to the Gibbs phase rule, the azeotrope will be a plane in the temperature and pressure domain for this ternary system. *Figure 5-14* is only illustrative and can be repeated for various temperatures and solute ratios (w_c^{red}).

Figure 5-14 (a), (c) and (e) illustrates that the addition of *n*-tetradecane to a pure CO₂ + 1-decanol binary system will cause a non-linear decrease in the solubility pressures of the system. The line running through a pressure minimum indicates that the solubility of the mixture in supercritical CO₂ is at times higher than that of the pure components in supercritical CO₂ [40].

Figure 5-14 (b), (d) and (f) show a closer view of the pressure minimum which graphically defines the cosolvency effect taking place. The line formed between the critical surface of CO₂ + 1-decanol + *n*-tetradecane ternary system ($P_{c,min}^{A+B+C}$ at $w_c^{red} \approx 0.8162$ g/g)³ and the critical point of the CO₂ + *n*-tetradecane binary system (P_c^{A+C} at $w_c^{red} \approx 1.00$ g/g) of the separated two-phase areas in *Figure 5-14 (f)* indicates the ternary critical line at $T = 338$ K. Consequently, the finding of the azeotrope revealed the exact pressure range in which cosolvency will be observed between $T = 308$ K and 358 K.

³ It is important to note that this is the lowest point measured in this work and not necessarily the minimum.

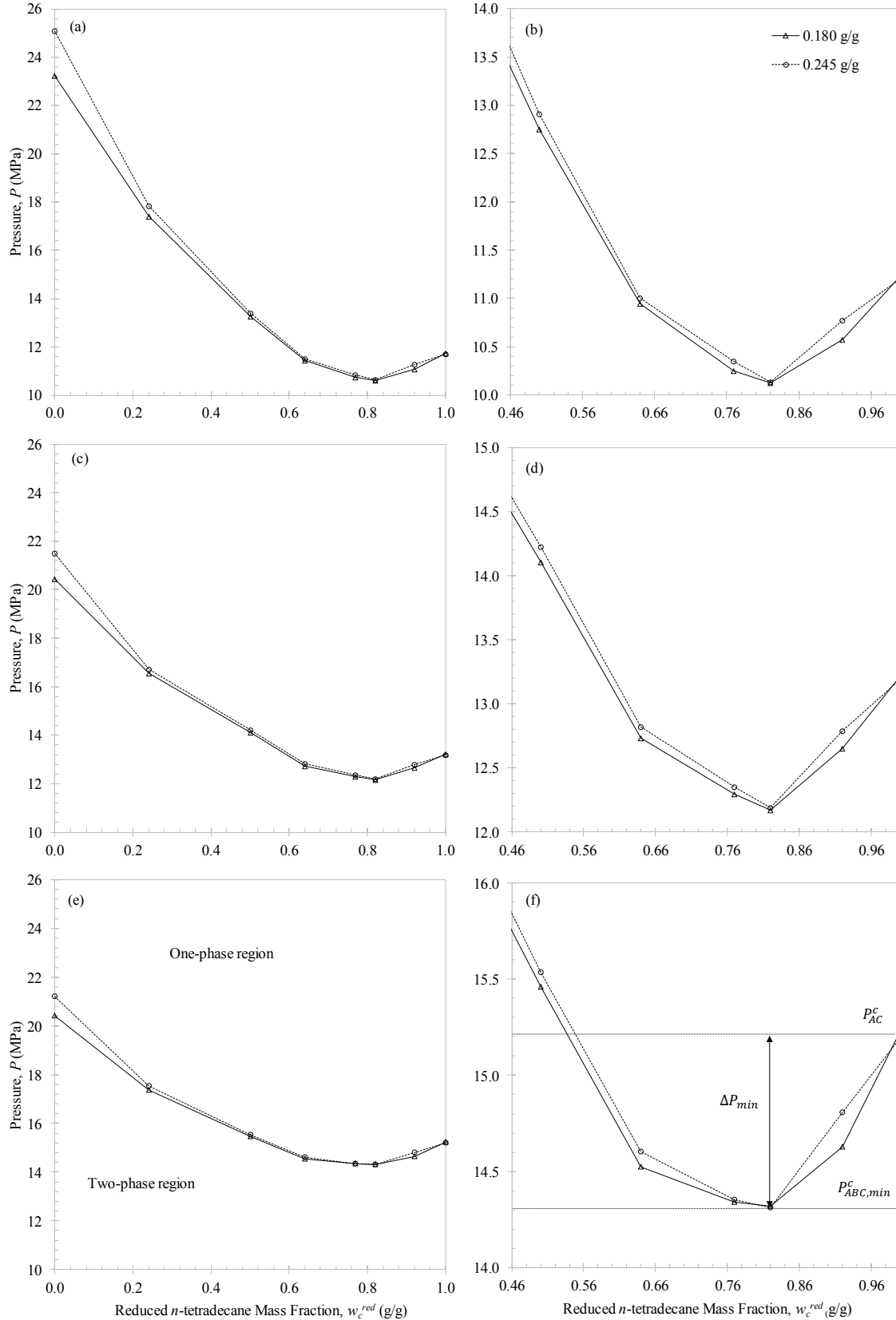


FIGURE 5- 14: NORMAL VIEW OF THE BUBBLE- AND DEW-POINT ISOTHERMS AT (A) $T=318$ K, (C) $T=328$ K AND (E) $T=338$ K TO INDICATE THE AZEOTROPE. DETAILED VIEW INDICATING THE APPROXIMATED SIZE AND RANGE OF THE COSOLVENCY EFFECTS AT (B) $T=318$ K, (D) $T=328$ K AND (F) $T=338$ K. THE BOUNDARY CONDITIONS, $w_c^{RED} = 0.00$ G/G AND $w_c^{RED} = 1.00$ G/G, REPRESENT THE BINARY DATA OBTAINED FROM LITERATURE [15], [17].

Table 5-2 lists the size and range of the cosolvency effects in CO₂ + 1-decanol + *n*-tetradecane at isothermal conditions.

TABLE 5- 2: COSOLVENCY SIZE, ΔP_{min} AND PRESSURE RANGE, P_{range} IN THE $w_c^{red} = 0.8162$ G/G TERNARY SYSTEM CO₂ + 1-DECANOL + *N*-TETRADECANE OBTAINED AT TEMPERATURES, T .

T (K)	ΔP_{min} (MPa)	P_{range} (MPa)
308	1.14	8.07 to 9.21
318	1.08	10.14 to 11.21
328	1.00	12.20 to 13.20
338	0.90	14.31 to 15.21
348	0.88	16.33 to 17.21
358	0.81	18.39 to 19.20

Having established that certain mixtures of 1-decanol and *n*-tetradecane display a higher solubility in supercritical CO₂ than each of the pure components 1-decanol or *n*-tetradecane, Gibbs phase triangles are used to illustrate the solute + solute interactions. Referring to the phase rule, the degrees of freedom necessary to fix the ternary system is 4, under the assumption that at least one phase is present in the system. The bubble- and dew-point data are therefore used to construct the two solubility curves on the ternary phase diagram. In addition, the vapour and liquid compositions measured for the ternary system are used to construct tie lines for the respective phase diagrams at $T = 308$ K, 328 K and 348 K.

The 3D plots, such as those given in Figure 5-8 to Figure 5-10, are now ‘sliced’ perpendicular to the w_c^{red} axis at constant w_c^{red} (P - w_s projection of the P - w_s - w_c^{red} plot). Pressures at fixed temperatures are then selected and the respective CO₂ (w_A), 1-decanol (w_B) and *n*-tetradecane (w_C) compositions were calculated using the P - T correlations. A fixed pressure was selected and the intercepting points of the P - T correlations for the P - w_s projections were used to obtain the composition values.

The resultant data at $T = 308$ K are shown in Figure 5-15 to Figure 5-17 at $P = 8.0$ MPa, 8.2 MPa, and 8.4 MPa, respectively. An increase in pressure causes the two-phase band to shrink until the band becomes extremely narrow as shown in Figure 5-15, after increasing the pressure another 0.2 MPa the phase bands split into two separate two-phase regions with a single contact point as shown in Figure 5-16. Another increase of 0.2 MPa results in the formation of a second miscibility gap. The two regions have therefore detached from one another giving the final separation shown in Figure 5-17. Similar observations are shown for the ternary phase diagrams constructed at $T = 318$ K, 328 K, 338 K, 348 K and 358 K (see Appendix F).

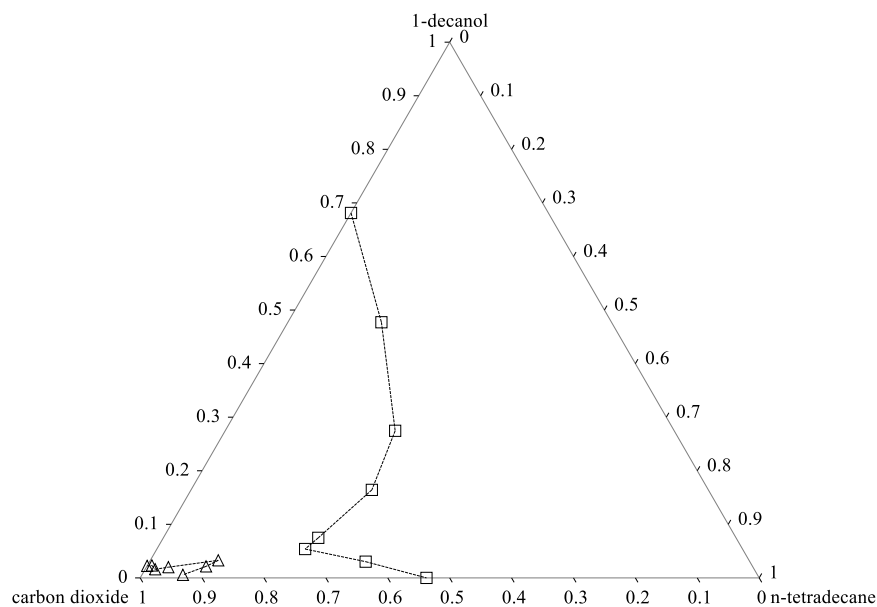


FIGURE 5- 15: TERNARY PHASE DIAGRAM WITH SOLUBILITY CURVES CONSTRUCTED WITH HPBDP DATA AT $T = 308 \text{ K}$ AND $P = 8.0 \text{ MPa}$. THE BINARY DATA WERE OBTAINED FROM LITERATURE [15], [17].

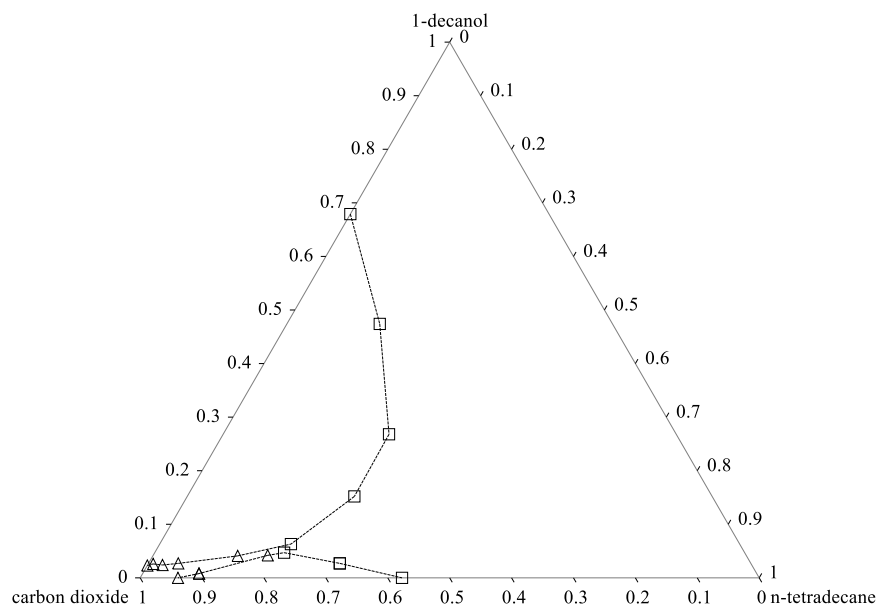


FIGURE 5- 16: TERNARY PHASE DIAGRAM WITH SOLUBILITY CURVES CONSTRUCTED WITH HPBDP DATA AT $T = 308 \text{ K}$ AND $P = 8.2 \text{ MPa}$. THE BINARY DATA WERE OBTAINED FROM LITERATURE [15], [17].

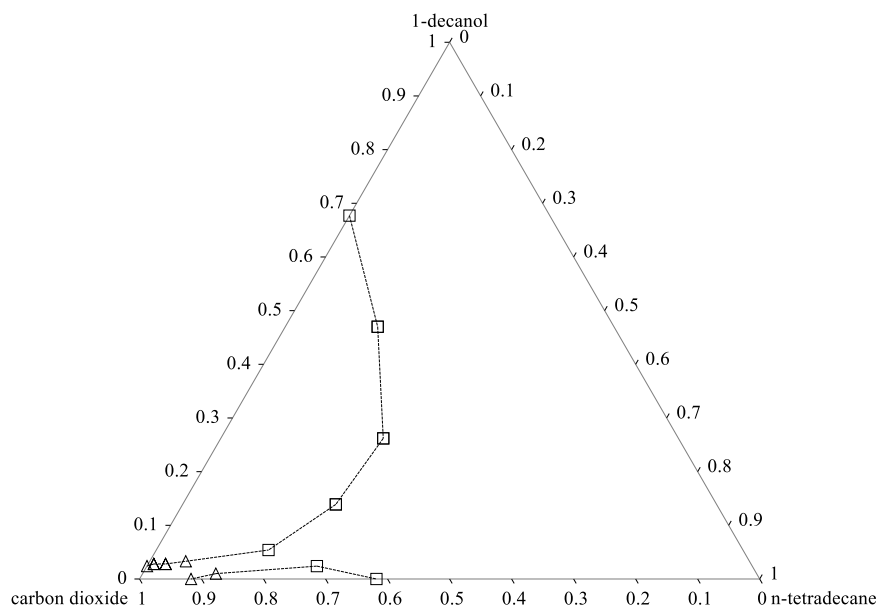


FIGURE 5- 17: TERNARY PHASE DIAGRAM WITH SOLUBILITY CURVES CONSTRUCTED WITH HPBDP DATA AT $T = 308$ K AND $P = 8.4$ MPa. THE BINARY DATA WERE OBTAINED FROM LITERATURE [15], [17].

5.2.2. NEAR-CRITICAL LIQUID-GAS HOLE

The increased solubility of 1-decanol and *n*-tetradecane in supercritical CO_2 was shown by an extension of the one-phase region due to the occurrence of isothermal cosolvency effects. The large occurrence of cosolvency inevitably shifts the critical surface of the ternary mixture to lower temperatures and pressures, which ultimately ends in the penetration of the l_1l_2g three-phase surface below it. To illustrate this effect graphically, a critical surface is constructed by stringing together each of the isothermal $P-w_c^{red}$ projections of the ternary critical lines in a $P-T-w_c^{red}$ plot, as shown in *Figure 5-18*. Above this critical surface one phase exists and below it co-exists two phases. When the surface is shifted downwards (due to the miscibility enhancement) the critical lines and the l_1l_2g three-phase lines intercept, resulting in the occurrence of CEPs. The point of intercept for the ternary system in this work is at the lowest point of the critical surface, indicated by the darker region of the mesh plot (the minimum pressure ternary critical “point”).

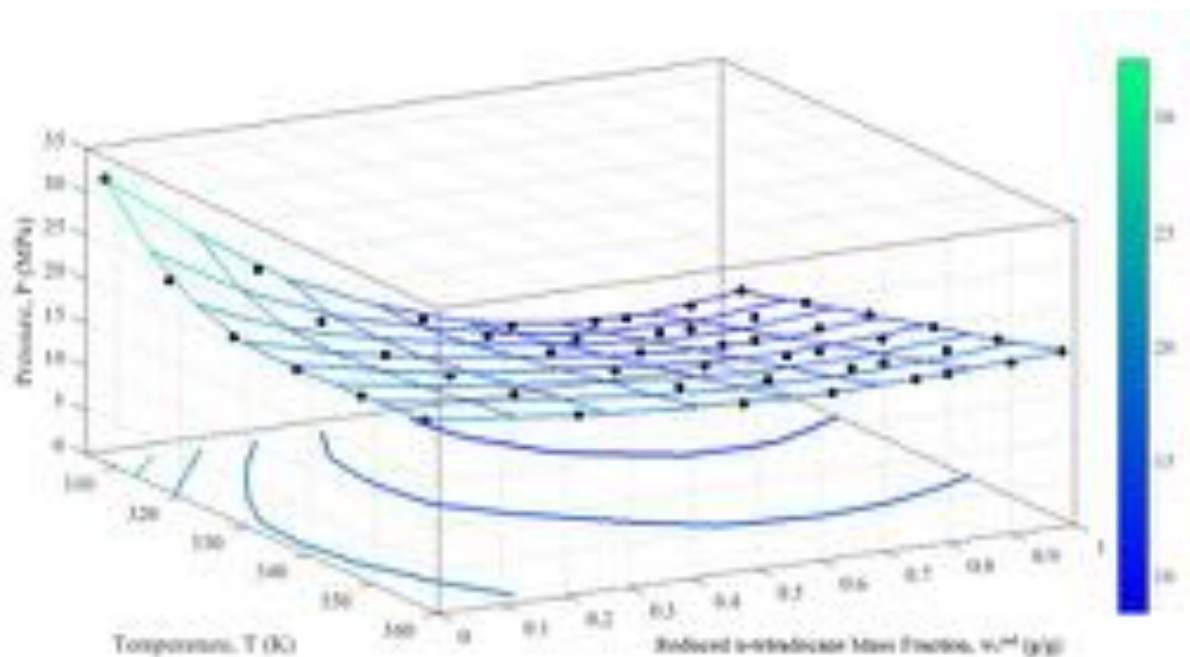


FIGURE 5- 18: PSEUDO-BINARY P - T - w_c^{RED} CRITICAL SURFACE FOR THE TERNARY SYSTEM CO_2 + 1-DECANOL + n -TETRADECANE.

THE CRITICAL POINTS OF THE MIXTURES MEASURED AT EACH TEMPERATURE: ●, WERE TAKEN FOR A CONSTANT SOLUTE MASS FRACTION $w_s = 0.25$ G/G. THE BOUNDARY CONDITIONS, $w_c^{RED} = 0.00$ G/G AND $w_c^{RED} = 1.00$ G/G, WERE OBTAINED FROM LITERATURE AND REPRESENT THE CEPs OF THE CO_2 + 1-DECANOL [15] AND CO_2 + n -TETRADECANE [17] BINARY SYSTEMS, RESPECTIVELY.

The penetration leads to the formation of a non-critical, closed l - g , two-phase hole in the CO_2 + 1-decanol + n -tetradecane critical surface [3], [38], [40]. The synthetic equilibrium cell allowed for the observation of the LCEP data at temperatures near and above the critical point of CO_2 . Three LCEPs (at $w_c^{red} = 0.7698$ g/g, 0.8162 g/g and 0.9200 g/g) are inferred from the experiments conducted at near-critical conditions and compared to published literature in *Figure 5-19*. The postulated LCEP data from this work are in agreement with the findings by Scheidgen and Schneider [3], Peters et al. [38], and Patton et al.[40] with errors bars smaller than the markers used to represent the data.

Due to both the binary solvent + solute systems having Type III phase behaviour it was initially assumed that the ternary system will display a simple CEP locus to form where the liquid phase l_1 and the gaseous phase g , are critical in the presence of the liquid phase l_2 ($l_1 = g + l_2$) as shown in *Figure 5-19* [36]. However, the ternary system displays an additional closed-loop, critical end-point locus of the nature $l_1 = l_2 + g$ that surrounds a two-phase l - g region. The two-phase l - g hole for the ternary system CO_2 + 1-decanol + n -tetradecane extends over a temperature and pressure range of approximately 17.37 K and 2.28 MPa, respectively. The temperatures and pressures of this work are given in the square brackets alongside published literature data on *Figure 5-19 (a)* and *(b)*, respectively.

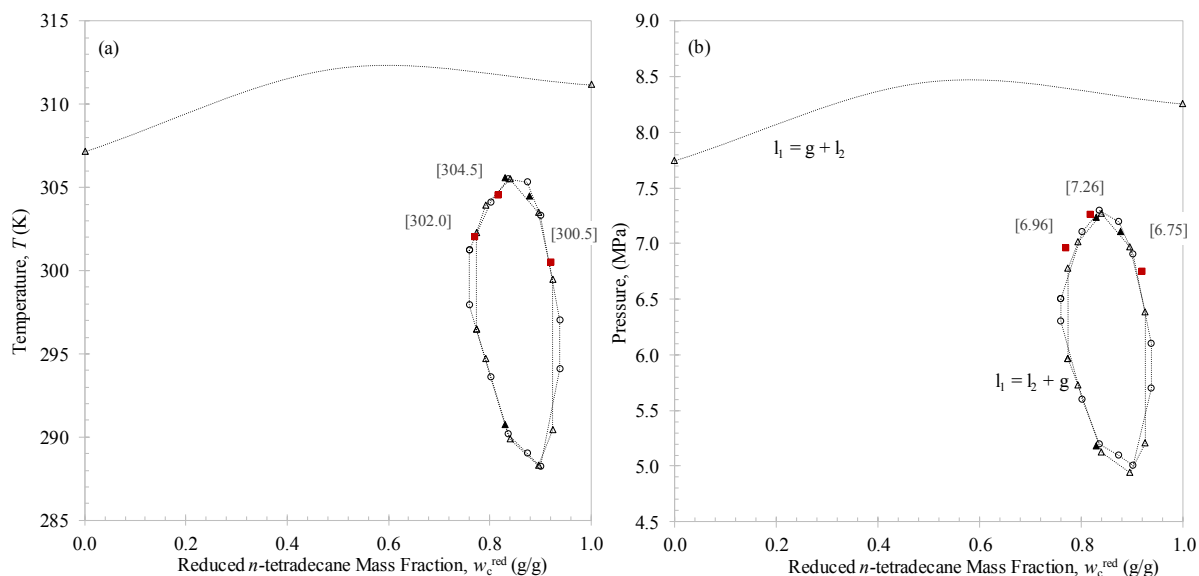


FIGURE 5- 19: (A) TEMPERATURE, T AND (B) PRESSURE, P VS. THE REDUCED n -TETRADECANE MASS FRACTION, w_c^{RED} TO INDICATE THE EXPECTED $L_1 = G + L_2$ CRITICAL END-POINT LOCUS AND THE ACTUAL $L_1 = L_2 + G$ CRITICAL END-POINTS BOUNDING THE LIQUID-GAS HOLE IN THE TERNARY LIQUID-LIQUID-GAS THREE-PHASE SURFACE FOR INFERRED DATA FROM: ■ THIS WORK AND LITERATURE DATA: Δ PATTON ET AL.[40]; ▲ PETERS ET AL.[38] AND ···· SCHEIDGEN AND SCHNEIDER [3].

5.2.3. CLOSED ISOBARIC MISCIBILITY WINDOWS

The initial discovery of the miscibility window by Scheidgen and Schneider [3] confirms the formation of the non-critical l - g two-phase hole in the $\text{CO}_2 + 1$ -decanol + n -tetradecane ternary system. The closed isobaric window was linked to the cosolvency effects in this work and found at pressures between the highest inferred LCEP of the ternary system and the lower pressure minimum of the two binary critical lines. It appears from $P = 7.26$ MPa to 7.83 MPa at $w_c^{red} = 0.8162$ g/g. This region is within close proximity (0.88% difference in pressure) to that found by Scheidgen and Schneider [3] who observed a pressure range for closed isobaric miscibility windows between $P = 7.32$ MPa and 7.82 MPa at $w_c^{red} = 0.84$ g/g. A P - T projection of the P - T - w_c^{red} plot (Figure 5-20) is used to illustrate the isobaric miscibility window in the critical surface of the ternary system. The experimental results collected in this work are plotted together with previous findings in Figure 5-20.

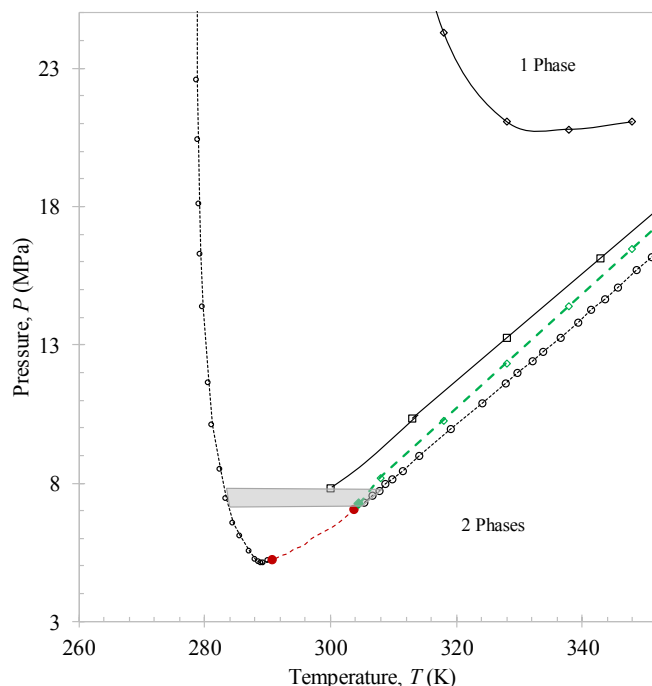


FIGURE 5- 20: P - T PROJECTION OF THE BINARY CRITICAL CURVES FOR CO_2 + 1-DECANOL: \diamond [15] AND CO_2 + n -TETRADECANE: \square [17]. THE MINIMUM CRITICAL SURFACE CURVES ARE SHOWN FOR $w_c^{\text{RED}} = 0.84$ G/G: $\cdots\circ\cdots$ [3] AND $w_c^{\text{RED}} = 0.8162$ G/G: $--\diamond--$ FOR THIS WORK. THE CRITICAL END POINTS ARE INDICATED BY \bullet , [3] AND \blacklozenge , FOR THIS WORK. THE SHADED REGION REPRESENTS WHERE THE INFERRED CLOSED ISOBARIC MISCIBILITY WINDOWS APPEAR.

5.2.4. SECTION OUTCOMES

New contributions:

- (i) The w_c^{red} mixtures were used to construct new Gibbs phase triangles and a 3D pseudo-binary critical surface to illustrate the true ternary phase behaviour of the CO_2 + 1-decanol + n -tetradecane system.
- (ii) Bubble- and dew-point isotherms were used to identify possible azeotropic phase behaviour within the miscibility region, suggesting that fractionation in this region might not be effective.
- (iii) The size and range of the cosolvency effects were identified at six set temperatures measured for the ternary CO_2 + 1-decanol + n -tetradecane system.
- (iv) The three-phase surface constructed on the Gibbs phase triangles and the pseudo-binary diagram were used to identify the miscibility regions. The addition of n -tetradecane to a 1-decanol-rich mixture will disrupt multimer bonds between the 1-decanol molecules and enhance the miscibility of the solutes in supercritical CO_2 .
- (v) Inferred data allowed for the cosolvency effects to be linked to the formation of a l - g hole and miscibility windows in the l/l_2g three-phase surface near the critical point of the solvent (initially suggested by Scheidgen and Schneider [3]).

Key objective(s) achieved: Objective 1.3

5.3. HPVLE RESULTS AND DISCUSSION

5.3.1. VERIFICATION OF EXPERIMENTAL SETUP

The analytical setup has been verified by Fourie et al. [76], the main researcher involved in the design and construction of the equipment being used in this investigation [19]. *Table 5-3* provides a select few of the errors obtained. The experimental setup has therefore been proven accurate through extensive comparisons to literature data and repeatability tests.

TABLE 5- 3: VALIDATION OF THE EXPERIMENTAL SETUP THROUGH COMPARISONS OF LITERATURE DATA BY FOURIE ET AL. [76] AND REPRODUCIBILITY ERRORS CALCULATED IN THIS WORK.

<i>System Measured</i>	<i>Species specific mass fraction error</i>	<i>Reference</i>
ethane + 1-dodecanol + <i>n</i> -hexadecane (one-phase region)	^a 0.004 - 0.007 g/g (ethane)	Fourie et al. [76]
	^a 0.002 - 0.004 g/g (1-dodecanol)	
	^a 0.002 - 0.003 g/g (<i>n</i> -hexadecane)	
CO ₂ + 1-octanol	^b 0.007 - 0.069 g/g (1-octanol)	Fourie et al. [76] with [14], [235]
CO ₂ + 1-dodecanol + <i>n</i> -hexadecane (two-phase region)	^b 0 - 0.05 g/g (CO ₂)	Fourie et al. [76] with [39], [236]
	^b 0 - 0.03 g/g (1-dodecanol)	
	^b 0 - 0.02 g/g (<i>n</i> -hexadecane)	
CO ₂ + 1-decanol + <i>n</i> -dodecane (vapor phase)	^c 0.26-0.84 % (CO ₂)	This work with Fourie [19]
	^c 0.19-0.53 % (1-decanol)	
	^c 0.07-0.31 % (<i>n</i> -dodecane)	
CO ₂ + 1-decanol + <i>n</i> -dodecane (liquid phase)	^c 0.26-0.52 % g/g (CO ₂)	This work with Fourie [19]
	^c 0.22-0.32 % (1-decanol)	
	^c 0.06-0.34 % (<i>n</i> -dodecane)	

^a Root mean square error

^b Absolute deviations

^c Absolute average deviation

To ensure the measurements are correctly conducted, two reproducibility tests (see *Figure 5-21*) were conducted in this investigation for the CO₂ + (75% 1-decanol + 25% *n*-dodecane) ternary system at three isothermal and isobaric conditions: $T = 308$ K (8.30 MPa), $T = 328$ K (12.3 MPa) and $T = 348$ K (15.7 MPa). The absolute average deviations calculated for each component in comparison to previously measured data are presented in *Table 5-3*. Based on these values, the VLE data measured on two separate occasions for this study both agreed well with literature data [19]. To further determine the repeatability of the work, a total of 5 samples for the two phases were simultaneously measured at each set point. Satisfactory standard deviations for each component were obtained that never exceeded 0.005 (CO₂), 0.003 (1-decanol) and 0.002 (*n*-dodecane). Thus, the analytical equipment was successfully validated as all data points are well within the accuracy of the pressure measurement and lie within the 2% composition error margin.

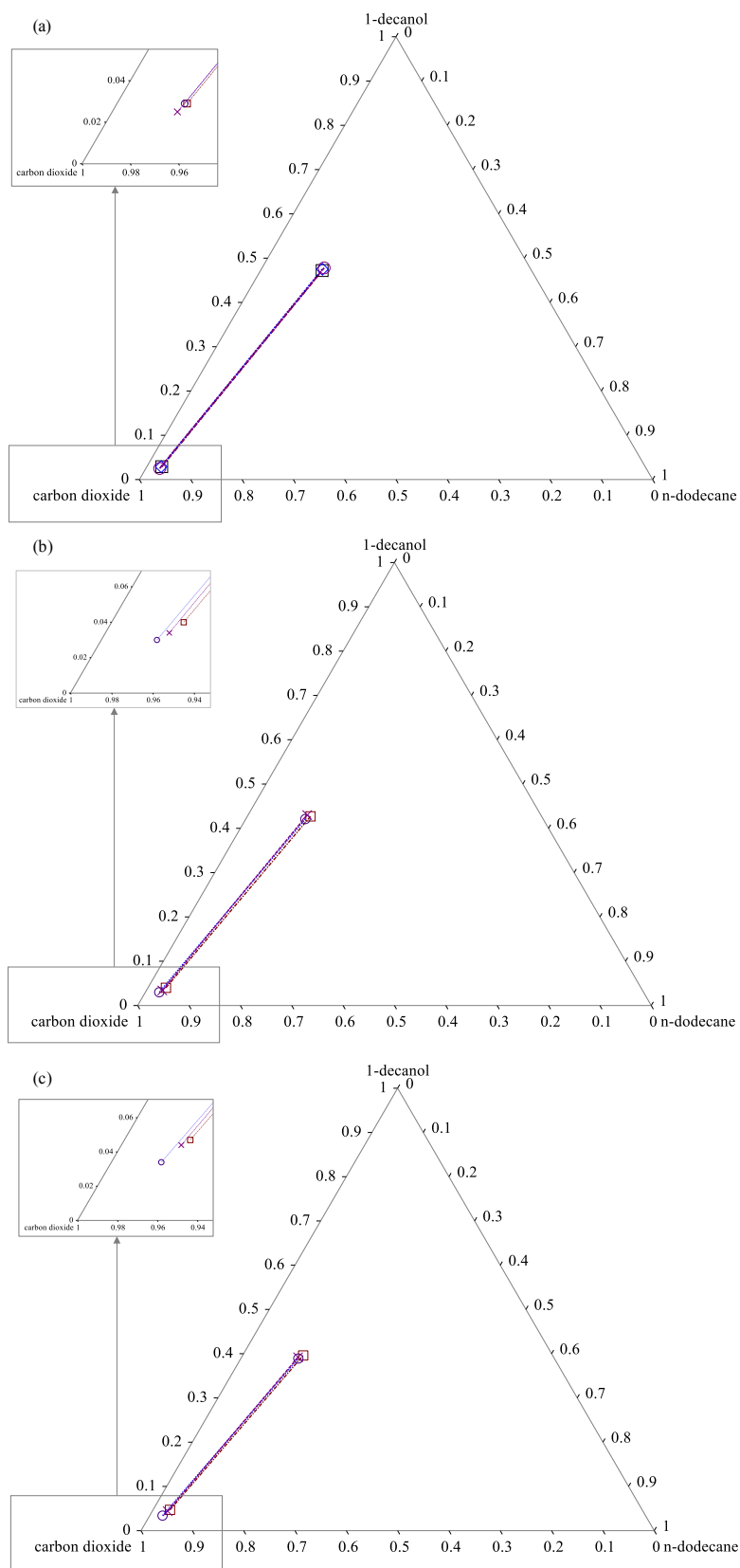


FIGURE 5-21: REPRODUCIBILITY RUN 1 (O) AND RUN 2 (X) COMPARED TO THE LITERATURE DATA (□) OF FOURIE ET AL.[19] FOR THE TERNARY SYSTEM $\text{CO}_2 + 1\text{-DECANOL} + n\text{-DODECANE}$ AT (A) $T = 308 \text{ K}$ AND $P = 8.3 \text{ MPa}$; (B) $T = 328 \text{ K}$ AND $P = 12.3 \text{ MPa}$; AND (C) $T = 348 \text{ K}$ AND $P = 15.7 \text{ MPa}$.

5.3.2. EXPERIMENTAL RESULTS

The VLE data of four CO₂ + 1-decanol + *n*-tetradecane mixtures were measured at $T = 308$ K, 328 K and 348 K and pressures ranging from $P = 8.0$ MPa to 16.4 MPa, namely:

- $w_c^{red} \text{ (g/g)} \in \{0.2403; 0.6245; 0.7979; 0.9004\}$

The size and range of the cosolvency effects at each isothermal condition (*Table 5-2*) were considered when selecting the isobaric pressures for the HPVLE measurements. Therefore, to maximise the number of tie-lines measured, pressures before, during and after the phase split were selected, whilst remaining at supercritical conditions, i.e. above $P = 7.38$ MPa. *Figure 5-22* summarises the 40 conditions at which the experimental data for the CO₂ + 1-decanol + *n*-tetradecane system were measured in this work.

	$w_c^{red} = 0.2403 \text{ g/g}$	$w_c^{red} = 0.6245 \text{ g/g}$	$w_c^{red} = 0.7979 \text{ g/g}$	$w_c^{red} = 0.9004 \text{ g/g}$
$T_1 = 308 \text{ K}$	$P \text{ (MPa)} \in \{8.0; 8.2; 8.4\}$	$P \text{ (MPa)} \in \{8.0; 8.2; 8.4\}$	$P \text{ (MPa)} \in \{8.0; 8.1\}$	$P \text{ (MPa)} \in \{8.0; 8.1; 8.2\}$
$T_2 = 328 \text{ K}$	$P \text{ (MPa)} \in \{11.1; 12.0; 12.4\}$	$P \text{ (MPa)} \in \{11.1; 12.0; 12.4\}$	$P \text{ (MPa)} \in \{11.1; 11.5; 12.0\}$	$P \text{ (MPa)} \in \{11.1; 11.5; 12.0; 12.3; 12.4\}$
$T_3 = 348 \text{ K}$	$P \text{ (MPa)} \in \{16.0; 16.2; 16.4\}$	$P \text{ (MPa)} \in \{16.0; 16.2; 16.4\}$	$P \text{ (MPa)} \in \{14.0; 16.0; 16.2\}$	$P \text{ (MPa)} \in \{14.0; 16.0; 16.2; 16.3; 16.4\}$

FIGURE 5- 22: HPVLE EXPERIMENTAL OUTLINE FOR THE CO₂ + 1-DECANOL + N-TETRADECANE TERNARY MIXTURES.

Sampling-related disturbances might occur within these 1-alcohol + *n*-alkane mixtures in supercritical CO₂. These include global mist formation, localised mist formation and no-warning droplet formation [237]. For a detail explanation of these disturbances the reader is referred to literature elsewhere [19], [237]. Fortunately, visual observations of the cell content showed no such phase behaviour disturbances for the CO₂ + 1-decanol + *n*-tetradecane mixtures measured in this work. The stability of the pressure and temperature gauges were thus sufficient in assuring accurate sampling. The simultaneous vapour and liquid samples analysed with species specific standard deviations for the mass fractions are tabulated in Appendix E2 for all four mixtures. The HPVLE experimental data are shown alongside the HPBDP solubility curves at $T = 308$ K, 328 K and 348 K in *Figure 5-23* to *Figure 5-25*, respectively.

The HPVLE results agree well with the HPBDP results as it too indicates the presence of two distinct two-phase regions forming after a co-solubility pinch. This indicates that the more time and cost effective static synthetic method will produce accurate solubility curves to describe the phase transitions. However, it does not provide information regarding the composition of the co-existing phases. The tie lines can thus be further used to calculate the relative solubility (an indicator of fractionation sharpness) of the ternary system.

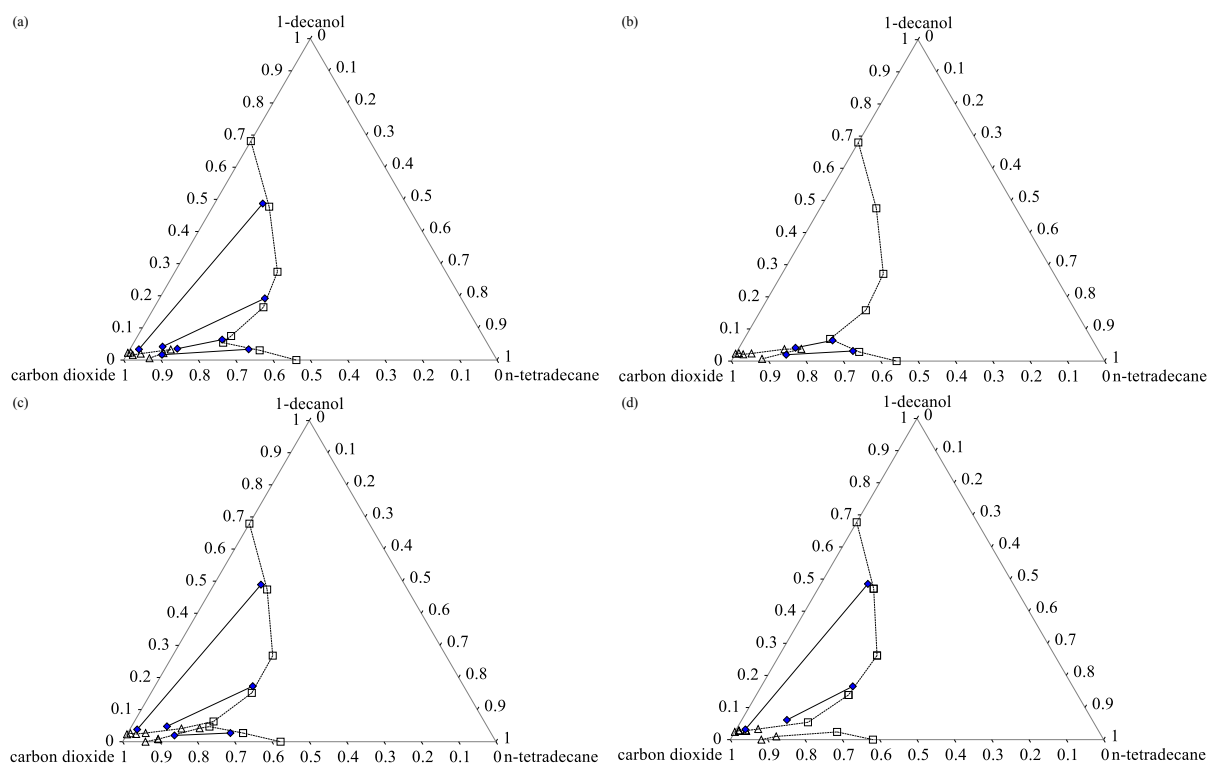


FIGURE 5- 23: TERNARY PHASE DIAGRAM WITH --□-- BUBBLE-POINT AND --Δ-- DEW-POINT SOLUBILITY CURVES (HPBDP DATA)

AND —◆— TIE-LINES (HPVLE DATA) AT $T = 308$ K AND (A) $P = 8.0$ MPa; (B) $P = 8.1$ MPa; (C) $P = 8.2$ MPa; AND (D) $P = 8.4$ MPa. BOUNDARY CONDITIONS OBTAINED FROM LITERATURE: $\text{CO}_2 + 1\text{-DECANOL}$ [15] AND $\text{CO}_2 + N\text{-TETRADECANE}$ [17].

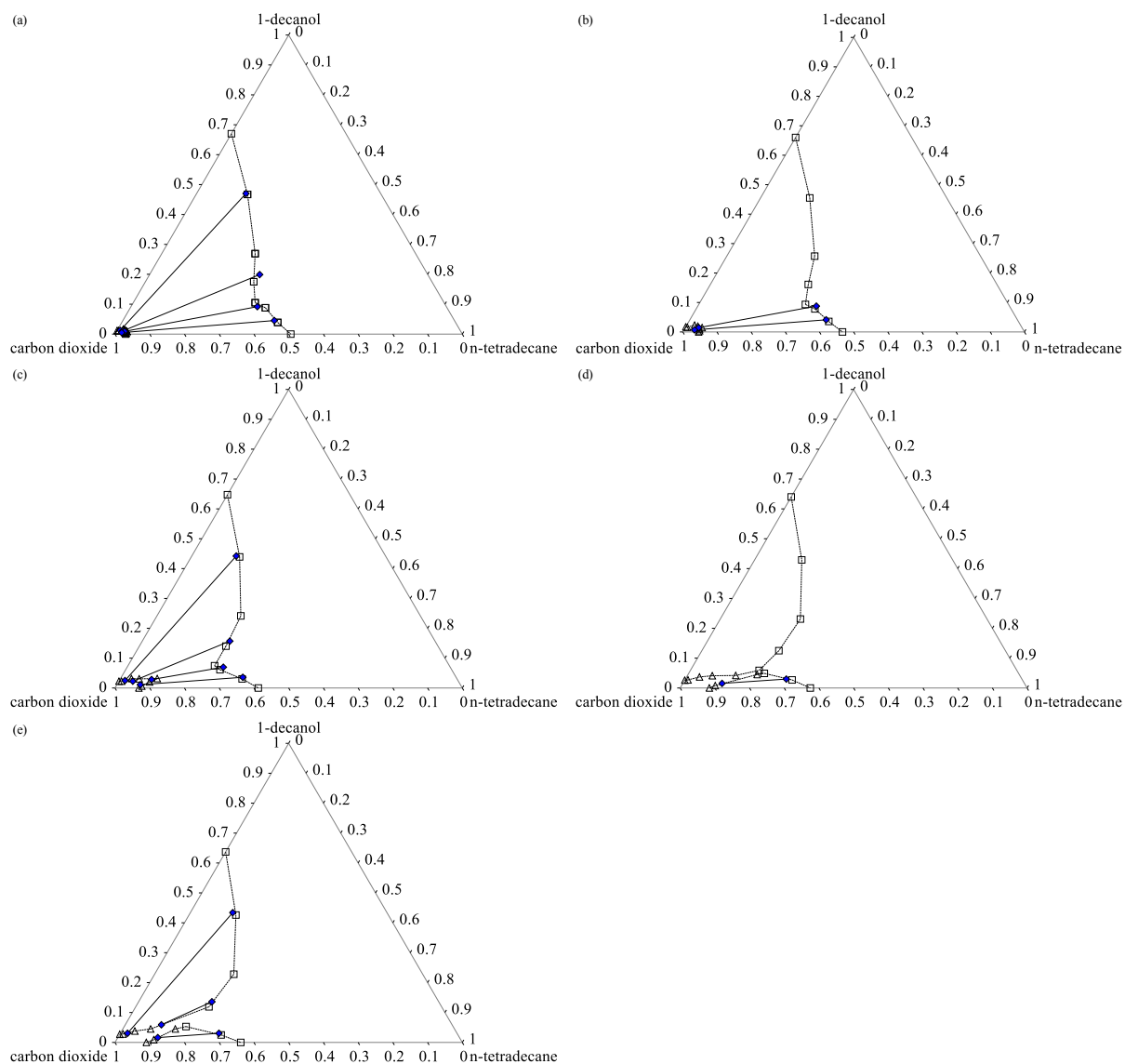


FIGURE 5- 24: TERNARY PHASE DIAGRAM WITH $--\square--$ BUBBLE-POINT AND $--\Delta--$ DEW-POINT SOLUBILITY CURVES (HPBDP DATA) AND $--\blacklozenge--$ TIE-LINES (HPVLE DATA) AT $T = 328$ K AND (A) $P = 11.1$ MPa; (B) $P = 11.5$ MPa; (C) $P = 12.0$ MPa; (D) $P = 12.3$ MPa; AND (E) $P = 12.4$ MPa. BOUNDARY CONDITIONS OBTAINED FROM LITERATURE: $\text{CO}_2 + 1\text{-DECANOL}$ [15] AND $\text{CO}_2 + N\text{-TETRADECANE}$ [17].

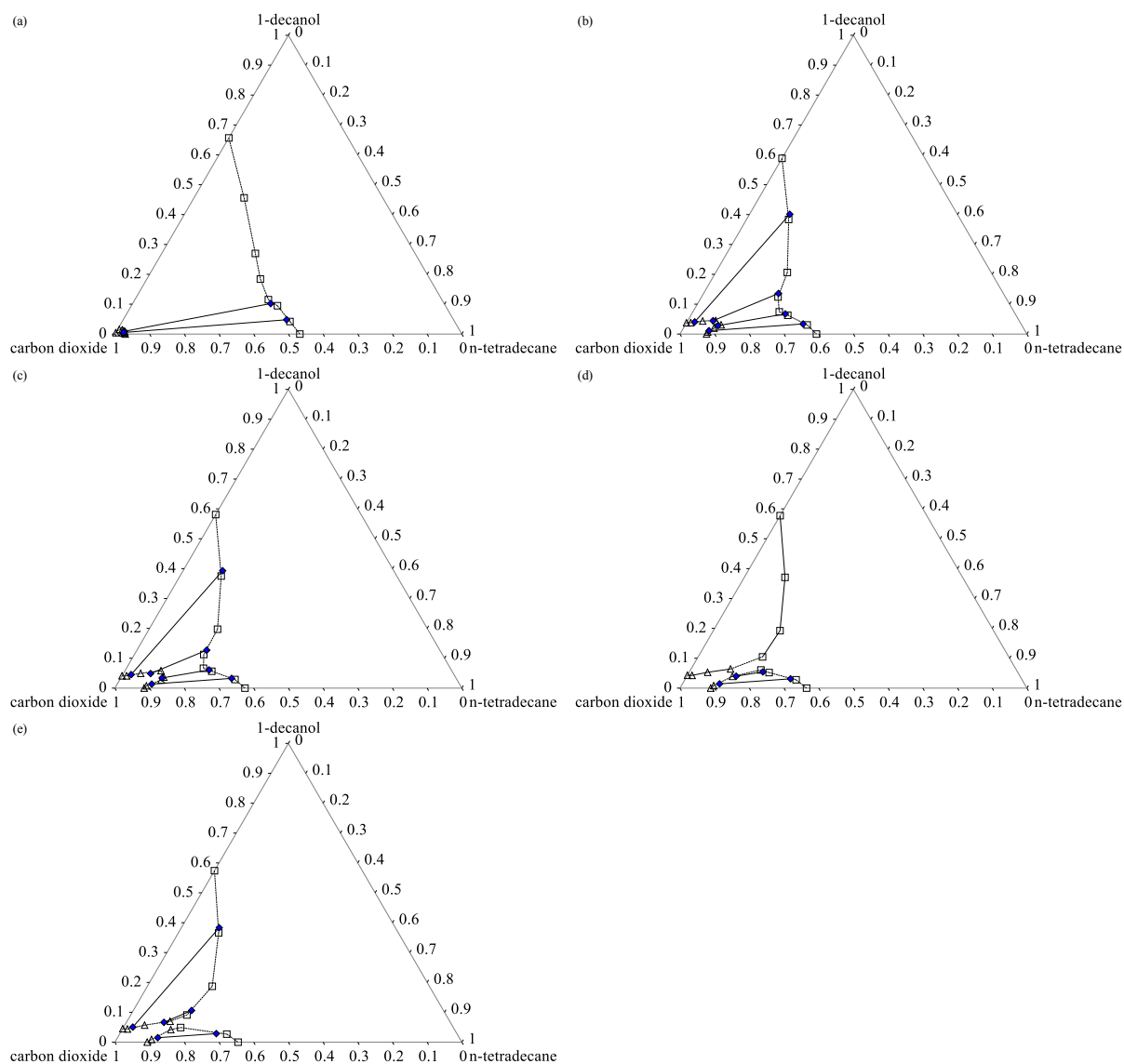


FIGURE 5- 25: TERNARY PHASE DIAGRAM WITH $--\square--$ BUBBLE-POINT AND $--\Delta--$ DEW-POINT SOLUBILITY CURVES (HPBDP DATA) AND $--\blacklozenge--$ TIE-LINES (HPVLE DATA) AT $T = 348$ K AND (A) $P = 14.0$ MPa; (B) $P = 16.0$ MPa; (C) $P = 16.2$ MPa; (D) $P = 16.3$ MPa; AND (E) $P = 16.4$ MPa. BOUNDARY CONDITIONS OBTAINED FROM LITERATURE: $\text{CO}_2 + 1\text{-DECANOL}$ [15] AND $\text{CO}_2 + N\text{-TETRADECANE}$ [17].

5.3.3. RELATIVE SOLUBILITY OF THE TERNARY SYSTEM

The solubility of a solute will establish the pressure requirements of a mixture to dissolve a certain mass fraction of a component into a solvent. The relative solubility at each isothermal and isobaric measurement were calculated (using equation 2.5) for the four VLE mixtures to establish the preferred separation conditions (see Figure 5-26).

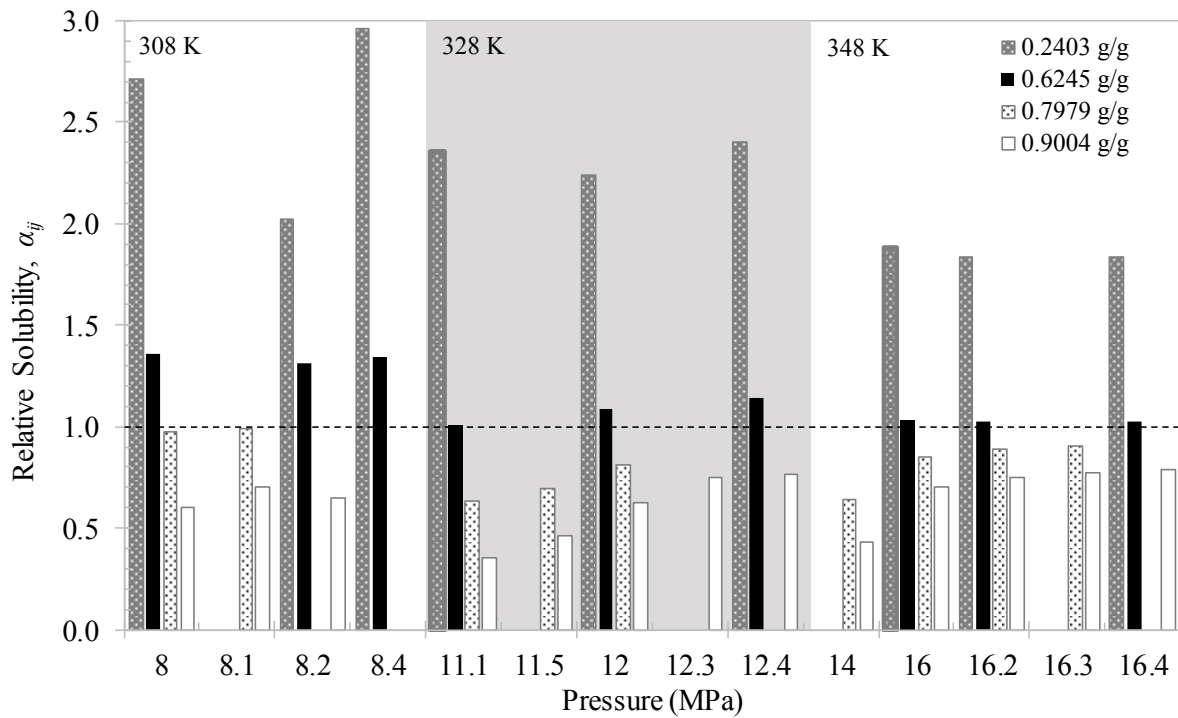


FIGURE 5- 26: EXPERIMENTAL RELATIVE SOLUBILITY FOR THE FOUR w_c^{red} MIXTURES OF CO₂ + 1-DECANOL + *N*-TETRADECANE AT $T = 308$ K, $T = 328$ K AND $T = 348$ K.

At each isobaric and isothermal condition, α_{ij} values well below 0.95 were obtained for the $w_c^{red} = 0.9004$ g/g mixture, whereas α_{ij} values well above 1.05 were obtained for the $w_c^{red} = 0.2403$ g/g mixture. This indicates that separation will be possible for these compositions when using supercritical CO₂; however, for $w_c^{red} = 0.9004$ g/g, 1-decanol will be the more soluble compound and for $w_c^{red} = 0.2403$ g/g, *n*-tetradecane will be the more soluble compound. Furthermore, it is evident that there is indeed an azeotrope in the ternary system within the complex phase behaviour region from the following observations:

- (i) At $T = 308$ K, fractionation of the $w_c^{red} = 0.7979$ g/g mixture is ineffective; however, with an increase in temperature to $T = 328$ K and $T = 348$ K, the solubility of the mixture increases (1-decanol as the more soluble compound).
- (ii) At $T = 308$ K, fractionation of the $w_c^{red} = 0.6245$ g/g mixture is possible with *n*-tetradecane as the more soluble compound; however, with an increase in temperature to $T = 328$ K and $T = 348$ K, the solubility of the mixture decreases and becomes virtually impossible.

It is postulated that this occurs due to the l_1l_2g three-phase behaviour in this composition range, caused by the miscibility enhancement. Therefore, to overcome these difficulties in fractionation, a pressure-temperature swing is required, analogous to pressure swing distillation.

Considering a constant temperature of $T = 308$ K, no clear trend in the pressure for each mixture can be established. This is not uncommon due to the relative solubility at these low pressures being severely sensitive to the vapour phase composition [158] as well as the temperature inversion. At a constant temperature of $T = 328$ K, a positive correlation between the relative solubility and pressure for each mixture is observed. However, for the $T = 348$ K isothermal condition in the low-pressure region, the α_{ij} - P correlation will change depending on w_c^{red} :

- (i) For the $w_c^{red} = 0.9004$ g/g and $w_c^{red} = 0.7979$ g/g mixtures the correlation will change from negative to positive; this indicates that an increase in pressure will favour the less soluble component, 1-decanol.
- (ii) For the $w_c^{red} = 0.2403$ g/g mixture the correlation changes from positive to negative; this indicates that an increase in pressure will increase the solubility of *n*-tetradecane

The slope of the tie lines constructed on the ternary phase diagrams are another indication of the degree of separability that is occurring in the mixtures. The steeper the slope, the higher the relative solubility and the more effective the separation in the mixture. As an example, *Figure 5-27* shows the constant solute:solute ratio lines (CSSRL) in comparison to the HPVLE results at $T = 328$ K and $P = 11.1$ MPa. The CSSRL are to aid in establishing how effective fractionation will be for the system at a constant temperature and pressure and only varying the w_c^{red} value. Similar to what was shown by the calculated α_{ij} values, the $w_c^{red} = 0.6245$ g/g mixture is either ineffective or virtually impossible to fractionate as its tie line runs parallel to the CSSRL.

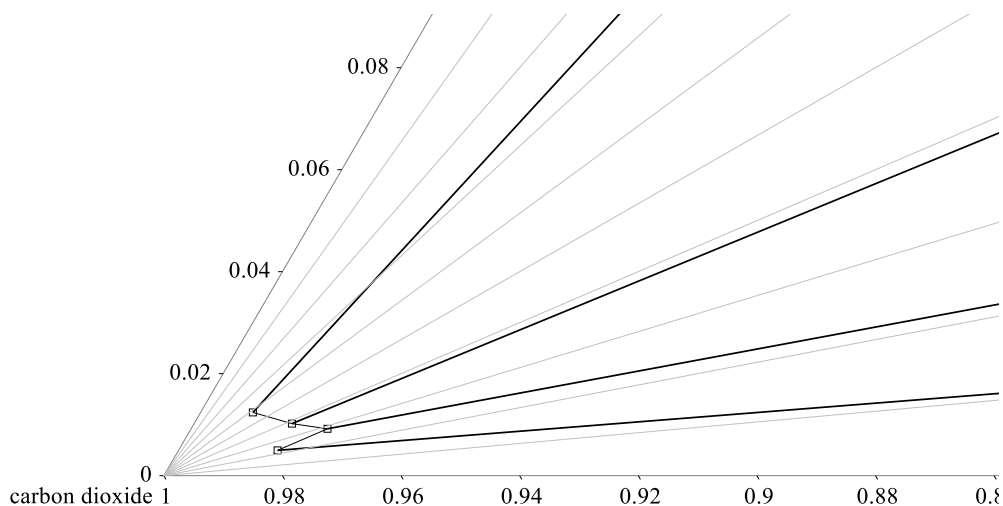


FIGURE 5- 27: VAPOUR PHASE DETAIL FOR CO₂ + 1-DECANOL + N-TETRADECANE AT T = 328 K AND P = 11.1 MPa. THE ANGULAR DIFFERENCE BETWEEN EXPERIMENTAL TIE LINES AND CSSRL ARE DIRECTLY PROPORTIONAL TO THE EFFECTIVENESS OF FRACTIONATION.

5.3.4. SECTION OUTCOMES

New contributions:

- (i) New high-pressure vapour-liquid equilibria data for four CO₂ + (1-decanol + *n*-tetradecane) mixtures were measured.
- (ii) The HPVLE results proved that fractionation will not be possible within the miscibility region (only inferred by HPBDP data). To overcome these difficulties in fractionation, a pressure-temperature swing is required.

Key objective(s) achieved: Objective 1.2 and Objective 1.4

A total of 40 isothermal and isobaric conditions were investigated for the ternary system. The data were accurate within the 0.06 MPa error region of the HPBDP data measured and successfully used to construct tie lines on the ternary phase diagrams. The slope of the tie lines as well as the relative solubilities were used to determine the degree of separation between the two solutes. Having successfully constructed and evaluated the ternary three phase surface using Gibbs phase diagrams, the ternary phase behaviour can be classified.

5.4. CLASSIFICATION OF THE TERNARY SYSTEM

5.4.1. TRANSITION SEQUENCE OF FLUID PHASE BEHAVIOUR

The three-phase fluid behaviour has been discussed previously in chapter 2 to allow for the proper characterising of the types of phase behaviour transitions taking place in the ternary system.

In a quasi-binary mixture comprised of mostly *n*-tetradecane and a small amount of 1-decanol, the multimer hydrogen bonds are negligible due to the low 1-alcohol concentration preventing the formation of aggregates. The ternary system shows the same Type III fluid phase behaviour as that of the binary CO₂ + *n*-tetradecane system. A continuation of replacing incremental amounts of *n*-tetradecane with 1-decanol results in the average carbon number of the system to decrease. The nature and fluid phase behaviour of the CO₂ + *n*-tetradecane system starts to change to that of the binary CO₂ + *n*-tridecane system [36]. When the overall carbon number of the CO₂ + (1-decanol + *n*-tetradecane) ternary system is equivalent to that of the CO₂ + *n*-tridecane binary system, the LCEP and UCEP tends towards each other with mutual deteriorating solubility of the system and forms a DCEP, as shown in *Figure 5-19*. The formation of a DCEP indicates a phase transition from Type III to Type IV (see section 2.1.3). Therefore, the ternary system now shows Type IV fluid phase behaviour. This finding has been confirmed through previous studies by Fall and Luks [59] who proved that the CO₂ + *n*-tridecane system shows Type IV fluid phase behaviour.

With increasing concentrations of 1-decanol the contribution of the 1-alcohol and the formation of multimers becomes prominent. The system returns to the Type III fluid phase behaviour depicted by both the CO₂ + *n*-tetradecane and CO₂ + 1-decanol systems. The critical endpoint locus $l_1 = l_2 + g$ closes to form another DCEP and due to the CO₂ + 1-decanol displaying Type III phase behaviour, the replacement of *n*-tetradecane with 1-decanol no longer alters the fluid phase behaviour [17]. The sequence of types of fluid phase behaviour encountered for the ternary system CO₂ + 1-decanol + *n*-tetradecane takes place through a DCEP and is thus:

$$\text{Type III} \rightarrow \text{Type IV} \rightarrow \text{Type III}$$

5.4.2. BINARY SUB-SYSTEMS AND THE TERNARY SYSTEM

According to the classification by Van Konynenburg and Scott [52], published literature shows Type III phase behaviour for each of the sub-systems with CO₂. This type of fluid phase behaviour is common in systems, like these, when the components have different sized molecules and different interactions. If *n*-tetradecane is added to the CO₂ + 1-decanol system, it will lead to a decrease in their mutual miscibility and form the pressure minimum in the critical locus as shown on the *P-T* phase diagram (*Figure 5-20*). These findings confirm the non-ideal phase behaviour when operating at high temperatures and pressures which agrees with Type III fluid phase behaviour.

The inferred data measured in this investigation confirmed the miscibility window in the ternary three-phase surface. This phenomenon is shown in *Figure 5-20* and was established to occur due to a miscibility enhancement (cosolvency effects). Therefore, according to the findings by Bluma and Deiters [78], the ternary system can be classified as Class T-IV phase behaviour. This is a viable classification of the system as it consists of two similar heavy components (1-decanol and *n*-tetradecane) and one very light component (CO₂).

The critical surface of the ternary system is like that of Class T-IV, as shown by the Gibbs phase diagrams. The three-phase l_1l_2g domain was identified in full by the HPBDP data and HPVLE data forming the solubility curves and the tie lines, respectively. Near the critical point of the solvent liquid-liquid immiscibility resulted in the formation of a two-phase l - g hole in the three-phase surface (see *Figure 5-19*). A phase transition sequence from Type III to Type IV to Type III phase behaviour occurs across the hole due to the decrease in miscibility. Therefore, several LCEPs and UCEP were identified, including the two DCEP between the phase behaviour changes. Consequently, the l_1l_2g and llg critical lines occurring were identified.

The 1-decanol + *n*-tetradecane binary subsystem can be classified by the parameters of the other two binary subsystems. Having confirmed the ternary system as Class T-IV phase behaviour (Type III + Type III + Type I) it is postulated that the final sub-system will fall under Type I fluid phase behaviour.

5.4.3. SECTION OUTCOMES

New contributions:

- (i) A phase transition across the two-phase region was confirmed from Type III \rightarrow Type IV \rightarrow Type III fluid phase behaviour.
- (ii) The miscibility enhancement (cosolvency effects) lead to the occurrence of simultaneous isobaric miscibility windows. This peculiar phenomenon was linked to ternary Class T-IV phase behaviour according to the classification by Bluma and Deiters [78].

Key objective(s) achieved: Objective 1.3

5.5. CHAPTER OUTCOMES

The aim of this chapter was to study the high-pressure phase equilibria of the CO_2 + 1-decanol + n -tetradecane ternary system and address the literature gaps identified in Chapter 2 (**Objective 1**). Several new contributions to science are made in achieving this key objective and have been listed as outcomes to each section discussed in this chapter. Because of these contributions, one article has been published in a peer reviewed journal:

M. Ferreira and C.E. Schwarz, Super- and near-critical fluid phase behaviour and phenomena of the ternary system CO_2 + 1-decanol + n -tetradecane, The Journal of Chemical Thermodynamics. 111 (2017) 88-99.

The manuscript covers the new HPBDP data (**Objective 1.1**) and complex phase behaviour (**Objective 1.3**) presented and discussed in this work. A second manuscript has been submitted for publication in a second peer reviewed journal that covers the HPVLE data (**Objective 1.2**) and the relative solubility (**Objective 1.4**) presented and discussed in this chapter:

High-pressure VLE measurements and PSRK modelling of the complex CO_2 + 1-decanol + n -tetradecane ternary system, The Journal of Supercritical Fluids, manuscript reference number: SUPFL_2018_502.

The identification of the ternary system as Class T-IV fluid phase behaviour infers that the third binary sub-system, 1-decanol + n -tetradecane, belongs to Type I-A fluid phase behaviour [52], [53]. This assumption needs to be verified by means of experimental work (**Objective 2**). Thus, the next chapter deals with the 1-decanol + n -tetradecane binary system in more detail.

Chapter 6

LOW PRESSURE PHASE EQUILIBRIA OF 1-ALCOHOL + N-ALKANE BINARY SYSTEMS

The high-pressure phase equilibria data measured in this work confirmed the significant solute + solute interactions taking place between 1-decanol and *n*-tetradecane in the presence of near- and supercritical CO₂. In fact, the solute + solute interactions are directly connected to the phenomena that lead to the complex phase behaviour regions. An additional method to obtain a fundamental understanding of the distinct solute + solute binary interactions that occur between these large, complex molecules is to study the binary 1-decanol + *n*-tetradecane VLE data (**Objective 2**). In measuring the LPVLE data the following contributions will be made in this work:

- (i) The binary sub-system comprised of non-polar *n*-tetradecane molecules and weakly polar 1-decanol molecules has not yet been published (*T-xy* data at constant *P*). New LPVLE data will help bridge this gap in open literature.
- (ii) The complex ternary phase behaviour infers Class T-IV ternary fluid phase behaviour which further hints at Type I-A fluid phase behaviour for the 1-decanol + *n*-tetradecane sub-system. If the new binary data displays non-ideal, azeotropic phase behaviour this assumption can be confirmed.
- (iii) The new LPVLE data can be used as an additional means for regressing solute + solute BIPs. These parameters can then be used to achieve key **Objective 3** of this study.

The aim of this chapter is to measure and study new LPVLE data of the 1-decanol + n-tetradecane binary system. Reproducibility tests can be used to verify the experimental setup, however, 1-decanol and *n*-tetradecane both have high, cross-over boiling points that might lead to unforeseen experimental difficulties. It is for this reason that the following four pertinent systems will also be measured in this work to serve as additional verification of the new LPVLE data: (i) 1-pentanol + *n*-nonane, (ii) 1-hexanol + *n*-decane, (iii) 1-heptanol + *n*-undecane and (iv) 1-octanol + *n*-dodecane. To maintain generality, verification systems with the same 4 carbon number difference between the 1-alcohol and *n*-alkane molecules were selected. Furthermore, lower systems were chosen to avoid too high boiling point temperatures.

6.1. VERIFICATION OF EXPERIMENTAL SETUP

6.1.1. PURE COMPONENT VAPOUR PRESSURE DATA

Pure component vapour pressures were measured for the 1-alcohol and *n*-alkane components of interest to this work and are compared in *Figure 6-1* to literature data available in DIPPR⁴ [23]. Qualitatively the measured values correlate well with the literature data of each pure component and lie relatively close to their counterparts, as seen by the small %AAD_P values tabulated in *Table 6-1*. The average absolute pressure deviations were calculated for boiling temperatures measured within the temperature range provided alongside the values in *Table 6-1*. The small deviations (< 1%), and the close qualitative capture of the literature data validated the purity of the chemicals used in the LPVLE study.

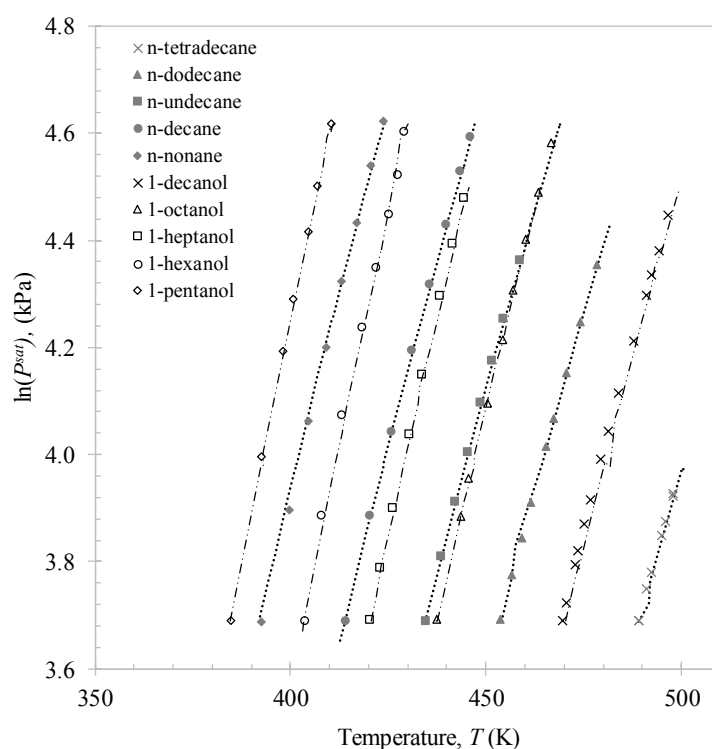


FIGURE 6- 1: COMPARISON OF EXPERIMENTALLY MEASURED VAPOUR PRESSURE DATA, INDICATED BY BULLETS, TO DIPPR CORRELATIONS, INDICATED BY LINES [23].

⁴ Design Institute for Physical Properties databank

TABLE 6- 1: CALCULATED %AAD_P BETWEEN EXPERIMENTALLY MEASURED AND LITERATURE [23] VAPOUR PRESSURES FOR THE 1-ALCOHOLS AND *N*-ALKANES OF INTEREST TO THIS WORK.

<i>Component</i>	%AAD _P	<i>T_{range}</i> (K)	<i>Component</i>	%AAD _P	<i>T_{range}</i> (K)
1-pentanol	0.338	380-410	<i>n</i> -nonane	0.341	390-430
1-hexanol	0.414	400-430	<i>n</i> -decane	0.282	410-460
1-heptanol	0.963	420-450	<i>n</i> -undecane	0.899	430-480
1-octanol	0.279	430-470	<i>n</i> -dodecane	0.504	450-500
1-decanol	0.561	460-510	<i>n</i> -tetradecane	0.754	480-530

6.1.2. THERMODYNAMIC CONSISTENCY TESTS

To test for systematic errors in the data a thermodynamic consistency test can be used to check its conformance with the Gibbs-Duhem equation. The area test, L/W consistency test (including how it is applied to the mixture with the Clausius-Clapeyron equation) and McDermott-Ellis consistency test are derived and explained in detail in Appendix A3. The L/W test will confirm the experimental data as a representation of the system dynamics by means of [84]:

- (i) A point-to-point test where, $L_k = W_k$, must be satisfied for each experimental point measured. However, due to experimental errors and the assumptions made to derive the thermodynamic test, namely: (1) the heat of vapourisation of each component is constant in the range of boiling points tested and (2) the liquid molar volumes are also negligible when compared to that of the vapour, a deviation factor must be specified.
- (ii) An area test where the deviation value D (as defined by eq. A.32) is less than 3 to 5 across the entire composition range is required to assure thermodynamic consistency.

As explained in Appendix A3, the Gibbs-Duhem equation is disregarded when using the L/W consistency test and the relationship between the excess Gibbs energy (A.13) of the binary system is compared to its boiling point temperature at equilibrium. Therefore, a second test is recommended to be used in conjunction with the L/W test. One method proven useful in literature is that of McDermott and Ellis [238] who used a two-point consistency test to evaluate each consecutive data point separately. If a deviation (D_{ev}) within the maximum deviation (D_{max}) is obtained for each data point, the data will be consistent (see Appendix A3).

The experimental results were analysed with both the L/W test and McDermott-Ellis test. Final D values of 2.104 (1-pentanol + *n*-nonane), 1.761 (1-hexanol + *n*-decane), 1.683 (1-heptanol + *n*-undecane), 1.659 (1-octanol + *n*-dodecane) and 1.261 (1-decanol + *n*-tetradecane) were obtained for the L/W consistency test, well below the higher threshold value of 5. With respect to the McDermott-Ellis consistency test for each binary system, all D_{ev} values were found to be lower than their respective

D_{max} values. Therefore, the binary VLE data measured in this work is confirmed as thermodynamically consistent.

Although both the L/W and McDermott-Ellis consistency tests are necessary, they are not sufficient on their own to prove the experimental data as accurate due to unforeseen composition, temperature and pressure inaccuracies. Therefore, reproducibility tests are required as with any new experimental procedure to validate the equipment setup.

6.1.3. REPRODUCIBILITY TESTS

The experimental setup and method were verified by measuring the binary VLE data of two systems after which they were compared to published literature. The first system, ethanol + 2,2,4-trimethylpentane, shown in *Figure 6-2*, was recently measured on the same experimental equipment by Pienaar et al. [229], and literature data measured by other research groups are also available [99], [229], [239]. A visual comparison of the results to published literature by Pienaar et al. [229], Ku and Tu [239] and Hiaki et al. [99] confirms that the equipment produces accurate results. Errors of ≤ 0.15 K, for temperature and ≤ 0.015 g/g, for composition are observed for the binary system measured in this work. The temperature and composition errors are indicated by means of error bars on *Figure 6-2*.

A second system, 2-butanone + *n*-heptane, was selected for further investigation at a sub-atmospheric pressure of 94 kPa. The results are compared, in *Figure 6-3* to the published work of Wisniak et al. [240]. A visual comparison of the two sets of data verifies the use of the experimental equipment. The qualitative analysis with respect to temperature remained constant with errors of ≤ 0.2 K calculated and indicated with error bars in *Figure 6-3*. The results compare well to literature quantitatively and qualitatively and one can conclude that the equipment is viable for use in this study.

The data of both verification systems adhere to the L/W and McDermott-Ellis tests for thermodynamic consistency. The data measured were used in combination with the PRO-VLE 2.0 software to generate the activity coefficients for each component at each data point. In turn, these values along with the maximum temperature, pressure and composition errors observed were used in conjunction with the method defined in Appendix A4 to calculate the values of D and D_{max} . Details of the pure component parameters thermodynamic consistency test results can be found in Appendix E3.

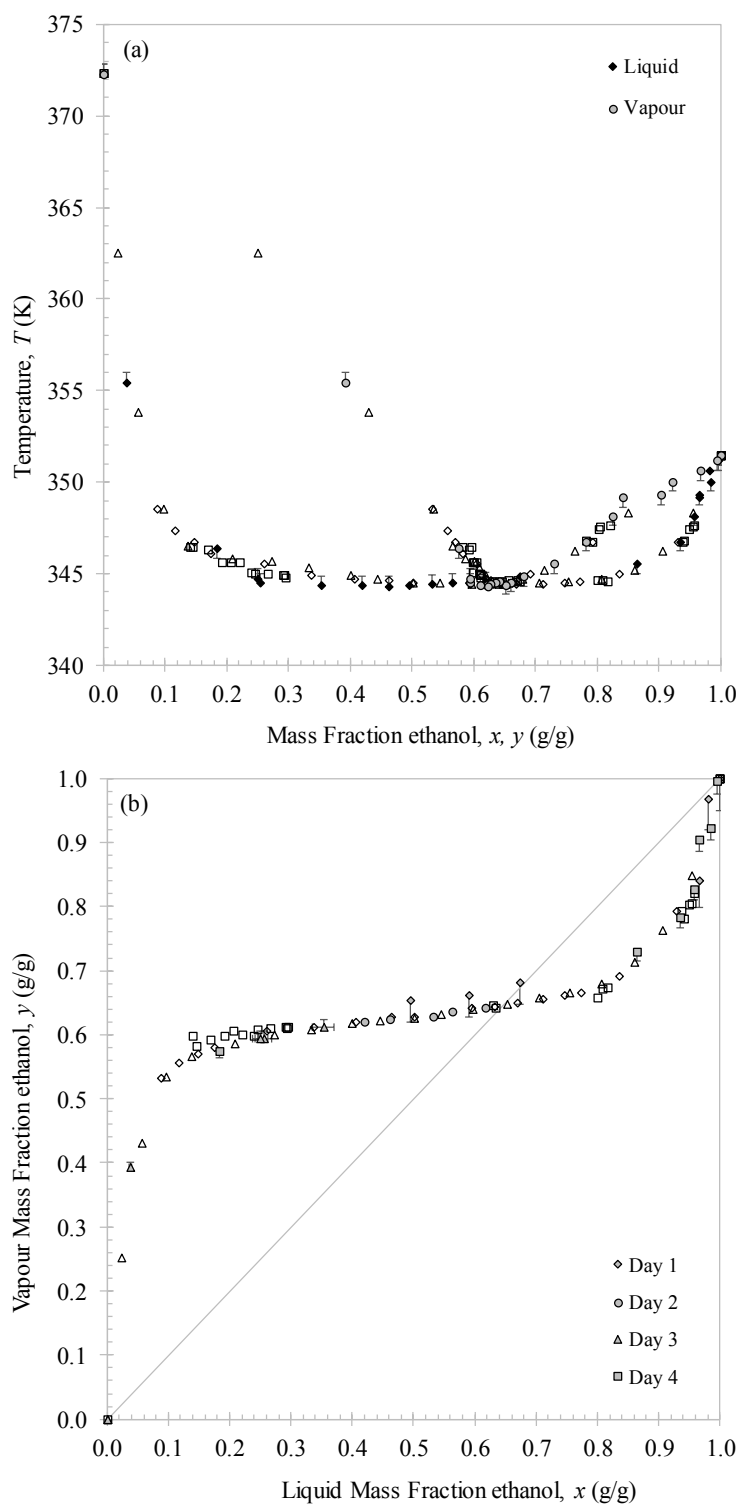


FIGURE 6- 2: (A) T - xy AND (B) x - y REPRESENTATION OF EXPERIMENTAL VLE DATA FOR THE VALIDATION SYSTEM ETHANOL + 2,2,4-TRIMETHYLPENTANE AT $P = 101.3$ kPa AGAINST LITERATURE DATA: \square PIENAAR ET AL.[229]; Δ KU AND TU [239] AND \diamond HIAKI ET AL.[99].

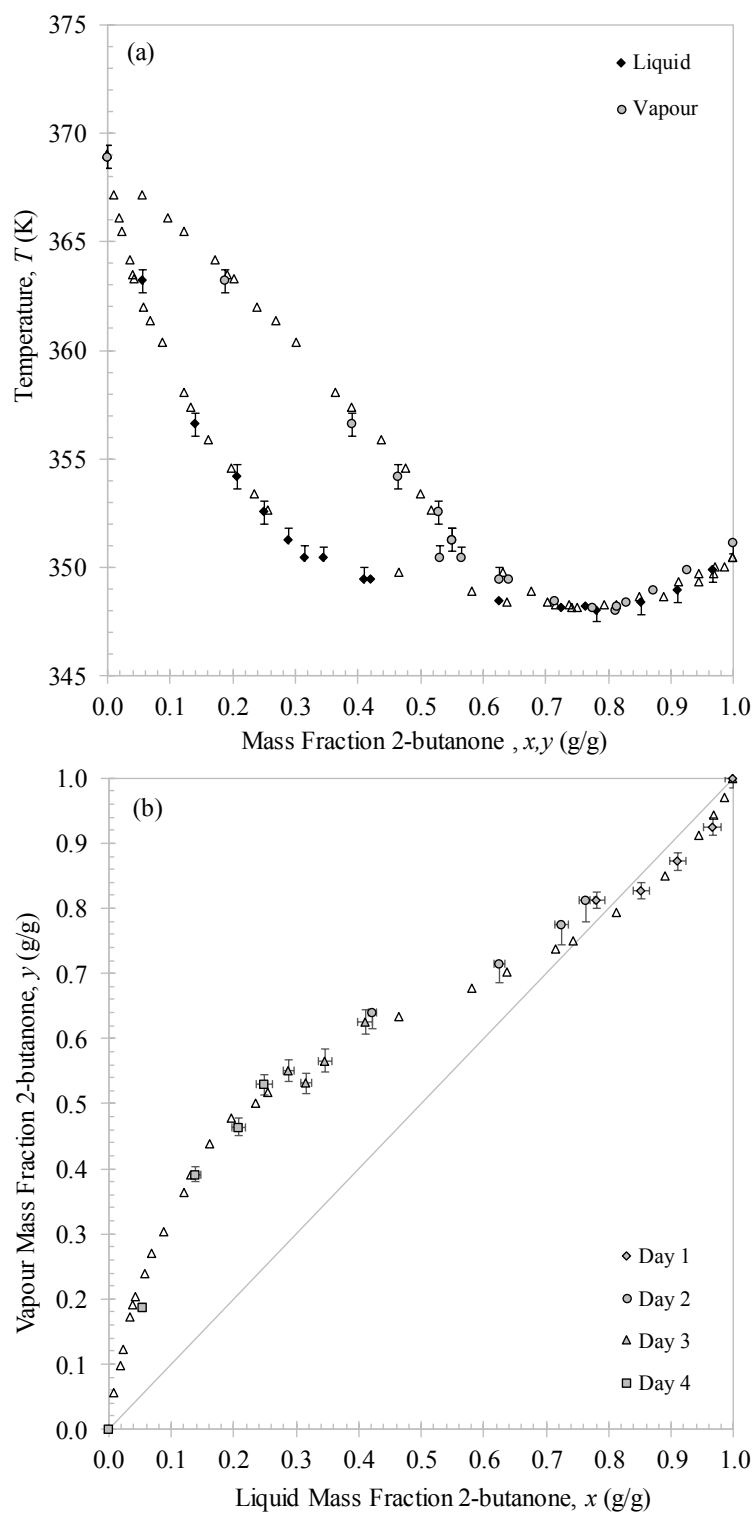


FIGURE 6- 3: (A) T - xy AND (B) x - y REPRESENTATION OF EXPERIMENTAL VLE DATA FOR THE VALIDATION SYSTEM 2-BUTANONE + n -HEPTANE AT $P = 94$ kPa AGAINST LITERATURE DATA: Δ WISNIAK ET AL. [240].

6.2. LPVLE RESULTS AND DISCUSSION

6.2.1. EXPERIMENTAL DIFFICULTIES

The normal boiling point temperatures of 1-decanol and *n*-tetradecane are 504.15 K and 526.73 K, respectively [20]. However, the maximum operating temperature of the unit is 523 K. To allow for separation of the components a vacuum had to be drawn and the tests were conducted at sub-atmospheric pressure. The allowable pressure range of the unit is 205 Pa to 200 kPa [229]. To minimize the waiting period for equilibrium to be reached, a pressure setting of 40 kPa was selected. At this pressure condition, the 1-decanol and *n*-tetradecane boiling point temperatures were lowered to 469.83 K and 489.17 K, respectively [21]. These temperatures are well within the range of operation.

The measurement of the longer, linear chain system, 1-decanol + *n*-tetradecane, was substantially more difficult than the other systems investigated in this work. This was especially noted for the 1-decanol rich-samples, where polar interactions are dominant. Initially, the system was not producing any vapour return and the following steps to solve the issue proved to be unsuccessful:

- (i) Increasing the immersion heater will only result in a faster liquid return and no vapour samples.
- (ii) Increasing the temperature of the mantle jacket around the equilibrium chamber produced vapour samples with large errors in T .

After countless experimental runs the following solution, to ensure vapour samples are obtained for the close-boiling 1-decanol + *n*-tetradecane system of interest to this work, was proposed:

To avoid having the components evaporate and condense inside of the equilibrium chamber (which will not be facilitating the necessary phase change at the vapour sampling port) the amount of mixture fed to the mixing chamber must be maintained to a volume only slightly higher than the minimum required to fully submerge the immersion heater.

To test this statement and help validate the 1-decanol + *n*-tetradecane phase behaviour data measured, four additional 1-alcohol + *n*-alkane systems were investigated in this work. The experimental T - xy and x - y data, generated at $P = 40$ kPa, for the 1-pentanol + *n*-nonane, 1-hexanol + *n*-decane, 1-heptanol + *n*-undecane, 1-octanol + *n*-dodecane and 1-decanol + *n*-tetradecane binary systems are presented in *Figure 6-4* to *Figure 6-8*, respectively. The new VLE data are tabulated in Appendix E3 alongside the liquid activity coefficients calculated and thermodynamic consistency analysis. Furthermore, reproducibility tests were conducted for each binary system and are in good agreement with the resultant data.

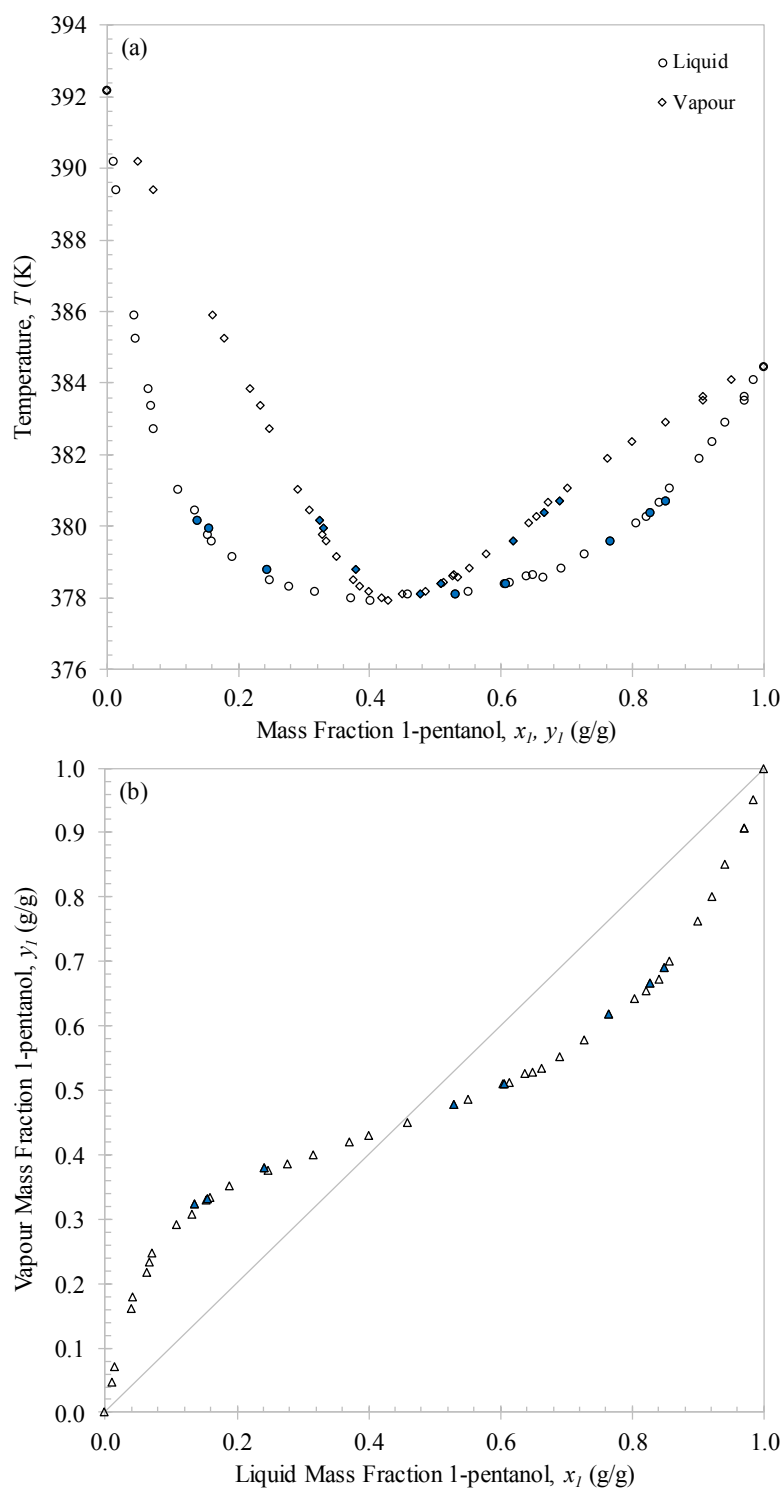


FIGURE 6- 4: (A) T - x_1 - y_1 AND (B) x_1 - y_1 REPRESENTATIONS OF THE EXPERIMENTAL VLE DATA FOR 1-PENTANOL (1) + n -NONANE (2) AT $P = 40$ kPa. SOLID BULLETS REPRESENT REPEATABILITY RUNS.

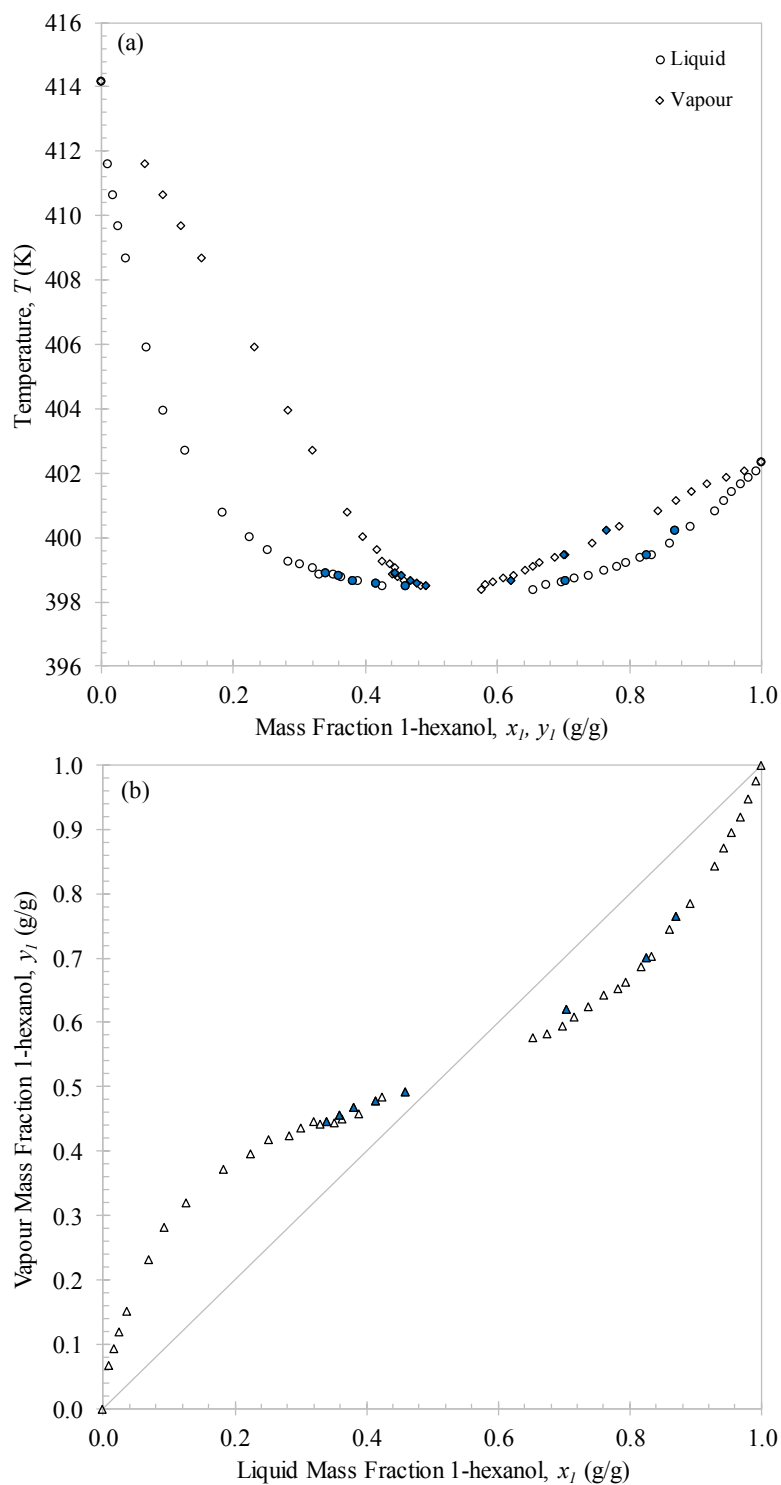


FIGURE 6- 5: (A) T - x_l - y_l AND (B) x_l - y_l REPRESENTATIONS OF THE EXPERIMENTAL VLE DATA FOR 1-HEXANOL (1) + *N*-DECANE (2) AT $P = 40$ kPa. SOLID BULLETS REPRESENT REPEATABILITY RUNS.

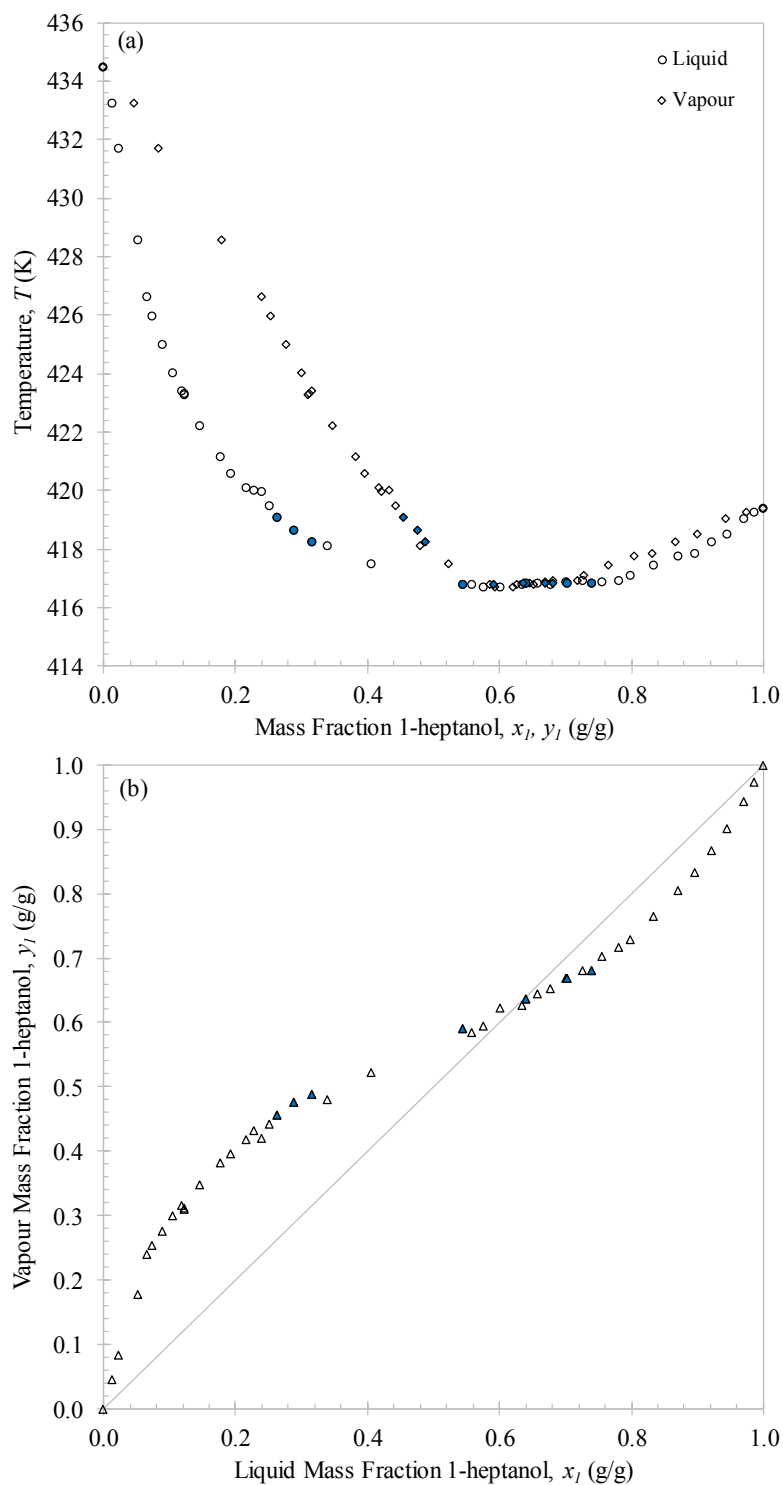


FIGURE 6- 6: (A) T - x_1 - y_1 AND (B) x_1 - y_1 REPRESENTATIONS OF THE EXPERIMENTAL VLE DATA FOR 1-HEPTANOL (1) + n -UNDECANE (2) AT $P = 40$ kPa. SOLID BULLETS REPRESENT REPEATABILITY RUNS.

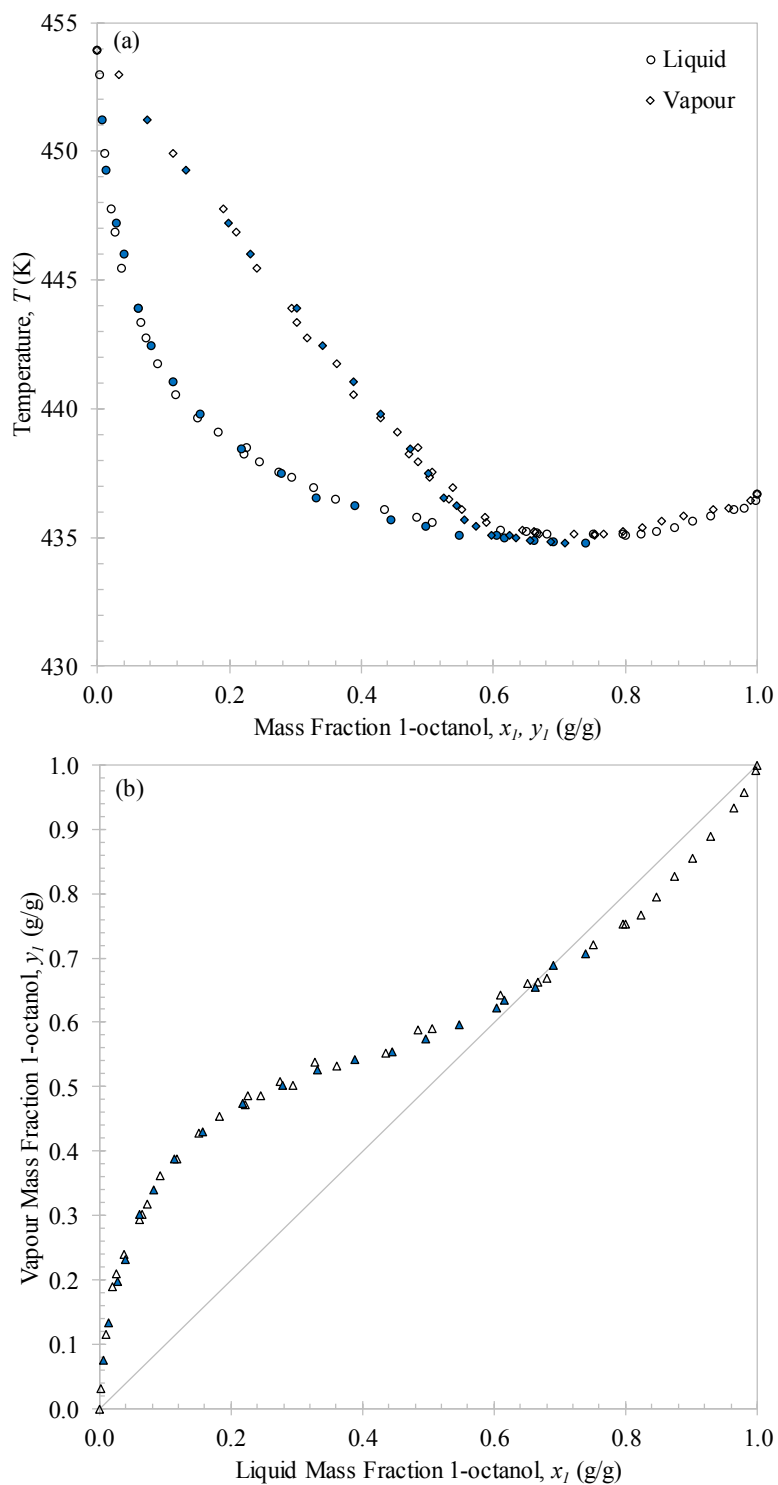


FIGURE 6- 7: (A) T - x_l - y_l AND (B) x_l - y_l REPRESENTATIONS OF THE EXPERIMENTAL VLE DATA FOR 1-OCTANOL (1) + N-DODECANE (2) AT $P = 40$ kPa. SOLID BULLETS REPRESENT REPEATABILITY RUNS.

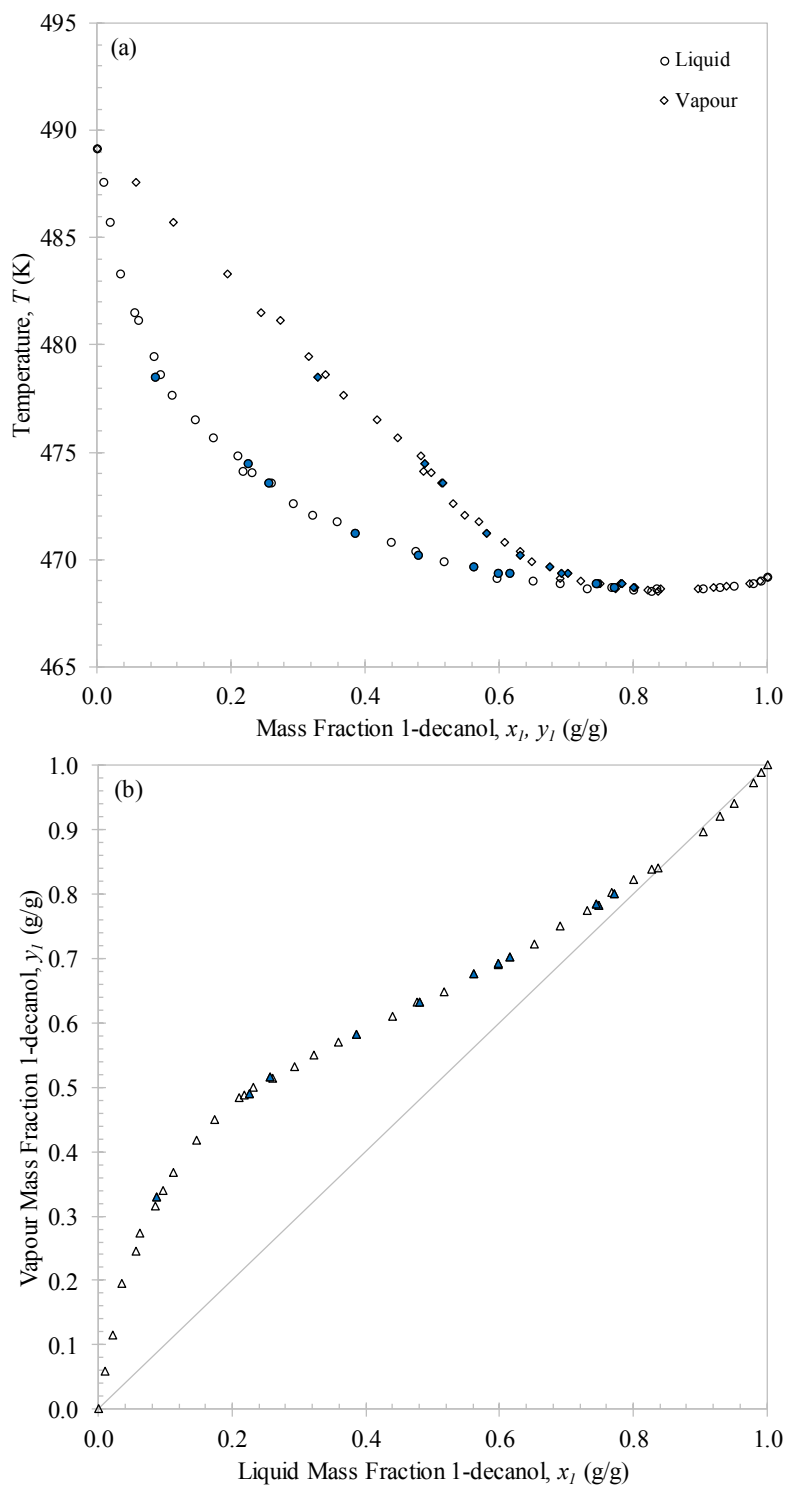


FIGURE 6- 8: (A) T - x_l - y_l AND (B) x_l - y_l REPRESENTATIONS OF THE EXPERIMENTAL VLE DATA FOR 1-DECANOL (1) + N -TETRADECANE (2) AT $P = 40$ kPa. SOLID BULLETS REPRESENT REPEATABILITY RUNS.

6.2.2. POSITIVE AZEOTROPY

A small temperature range is available for analysing each binary system because of the close boiling point temperatures between the 1-alcohol and *n*-alkane. Albeit a small temperature range, it is evident from *Figure 6-4* to *Figure 6-8*, as well as the temperature minimum observed in each data set (see Appendix E3), that there exists a minimum boiling azeotrope for each of the systems at 40 kPa. The presence of the azeotrope and the non-unity activity coefficients show that all the binary systems exhibit non-ideal phase behaviour. One can obtain the approximate location of each azeotrope graphically by plotting $(y-x)$ against x and finding the x -intercept (zero point). Applying this method, *Figure 6-9* is obtained.

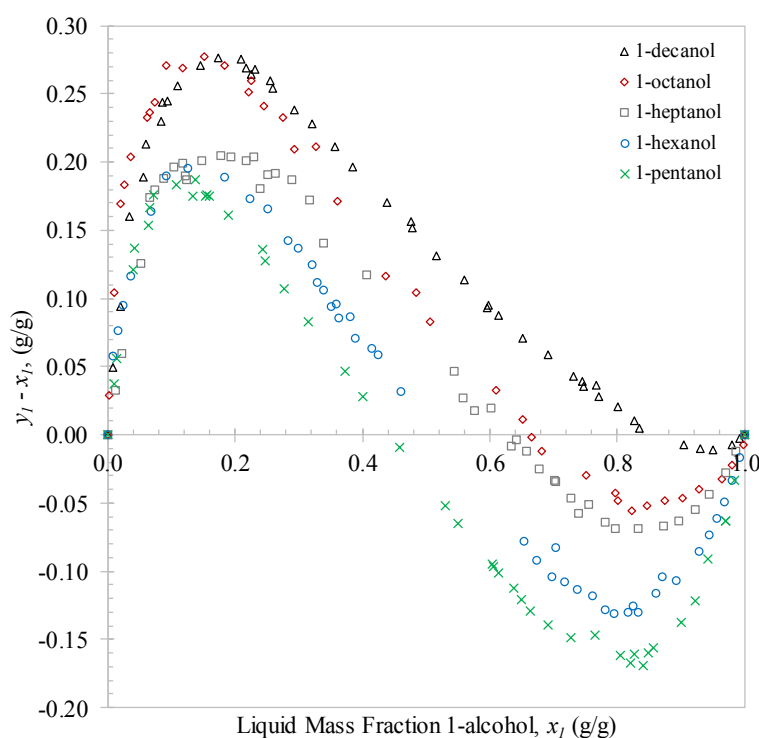


FIGURE 6- 9: PLOT OF $(y_l - x_l)$ VS. x_l YIELDING AZEOTROPIC COMPOSITION IN VLE OF THE FIVE 1-ALCOHOL (1) + *N*-ALKANE (2) BINARY SYSTEMS MEASURED IN THIS WORK (AT $P = 40$ kPa).

The estimated azeotropic temperature (through cross interpolation with the zero point) and azeotropic composition for each of the binary systems measured in this work are presented in *Table 6-2*. The azeotrope temperature increases, and the azeotrope composition shifts towards the 1-alcohol-rich region when increasing the *alkyl*- chain lengths of both molecules in the mixture. The shifting of the azeotropic point (*Table 6-2*) and change in the phase envelopes (*Figure 6-9*) highlight the effect of the increase in the *alkyl*- chain lengths on the experimental phase behaviour. The effect of the molecule sizes in the binary system is further emphasized by the liquid activity coefficients provided in Appendix E3. The infinite dilution activity coefficients have the highest values for the 1-pentanol + *n*-nonane system and decreases sequentially as the *alkyl*- chain lengths are increased towards the 1-decanol + *n*-tetradecane

binary system. These observations support the idea that the degree of association is dependent on the size of the 1-alcohol molecule: the shorter the chain length, the more polar the molecule becomes.

TABLE 6- 2: SUMMARY OF EXPERIMENTALLY ESTIMATED AZEOTROPIC TEMPERATURES AND COMPOSITIONS IN THE FIVE 1-ALCOHOL (1) + N-ALKANE (2) BINARY SYSTEMS.

	<i>Azeotropic Temperature, T (K)</i>	<i>Azeotropic Composition, x_1 (g/g)</i>
1-pentanol (1) + <i>n</i> -nonane (2)	378.05	0.445
1-hexanol (1) + <i>n</i> -decane (2)	398.47	0.516
1-heptanol (1) + <i>n</i> -undecane (2)	416.78	0.625
1-octanol (1) + <i>n</i> -dodecane (2)	435.19	0.664
1-decanol (1) + <i>n</i> -tetradecane (2)	468.66	0.864

6.2.3. PHASE BEHAVIOUR CLASSIFICATION

Each of the five binary systems infer Type I-A fluid phase behaviour due to their positive deviations from ideality and the formation of a minimum boiling homogenous azeotrope. Whether the system displays Type I fluid phase behaviour per the classification of Van Konynenburg and Scott [52] can only be established using a P - T plot to rule out possible liquid-liquid equilibria regions. Consequently, the system should be measured at several isobaric conditions to form the required phase curve and confirm the ternary system as Class T-IV (Type III + Type III + Type I-A) fluid phase behaviour.

6.3. CHAPTER OUTCOMES

The aim of this chapter was to present and discuss new LPVLE data of the 1-decanol + *n*-tetradecane binary system (**Objective 2**). Due to the low vapour pressures of the components, initial difficulties in the measurement of the LPVLE data were experienced. After overcoming the difficulties, new 1-decanol + *n*-tetradecane data were measured. Additionally, to verify the new 1-decanol + *n*-tetradecane data, additional LPVLE of 4 pertinent binary systems, all with similar relative volatility and cross-over boiling point characteristics as that of the 1-decanol + *n*-tetradecane system, were measured. Consequently, the following **new contributions** were made in this chapter:

- New LPVLE data for the 1-decanol + *n*-tetradecane system were measured at $P = 40$ kPa.
- New LPVLE data for the 1-pentanol + *n*-nonane, 1-hexanol + *n*-decane, 1-heptanol + *n*-undecane and 1-octanol + *n*-dodecane systems were measured at $P = 40$ kPa.
- Each of the binary systems displayed positive azeotropy, inferring Type I-A fluid phase behaviour per the classification of Van Konynenburg and Scott [52]. Therefore, the ternary system is postulated to consist of binary sub-systems belonging to Type III + Type III + Type I phase behaviour.

A third manuscript has been submitted for publication in a peer reviewed journal that covers the LPVLE data (**Objective 2**) presented and discussed in this chapter:

Low-pressure VLE measurements and thermodynamic modelling, with PSRK and NRTL, of binary 1-alcohol + n -alkane systems, The Journal of Chemical and Engineering Data, manuscript reference number: je-2018-006802.

Experimental data are required to obtain BIPs that can be incorporated into thermodynamic models for improved model correlations. However, as shown in this chapter, the measurement of sub-atmospheric VLE data for 1-alcohol + n -alkane systems, with crossover boiling point characteristics, becomes increasingly difficult as the chain length of these linear molecules increase. It is for this reason that predictive models have become increasingly popular, not only for modelling the phase behaviour of complex systems, but to ensure robust and industrial relevant modelling for when there is a lack in available experimental data. Based on this, the LPVLE data of all 5 binary systems measured in this work were used to investigate the predictive capability of the PSRK model in the next chapter. Furthermore, the LPVLE data of the 1-decanol + n -tetradecane system were used to regress new solute + solute BIPs for the RK-Aspen, SR-Polar and PC-SAFT thermodynamic models (Chapter 7). The LPVLE BIPs were evaluated alongside the HPBDP and HPVLE BIPs to see which set can improve the model correlations and help achieve key **Objective 3** of this study (Chapter 8).

Chapter 7

PURE COMPONENT & BINARY INTERACTION PARAMETER ESTIMATION

New high-pressure (*Objective 1*) and low-pressure (*Objective 2*) phase equilibria data have been measured and discussed in Chapter 5 and 6 of this thesis, respectively. Furthermore, four suitable thermodynamic models to correlate the experimental data (*Objective 3.1*) were identified in Chapter 3. Therefore, focus can now shift to the second step in modelling the new phase equilibria data measured in this work.

The aim of this chapter is to gather pure component parameters from literature and regress the necessary interaction parameters (Objective 3.2).

Three of the thermodynamic models, RK-Aspen, SR-Polar and PC-SAFT, have the option to include additional BIPs and pure component parameters to improve the accuracy of their fit to experimental data. The fourth model, PSRK can act as a purely predictive model through the implementation of group-group UNIFAC parameters found in literature. Thus, the chapter will include an evaluation of PSRK and its ability to correlate the 5 binary LPVLE systems measured in this work with: (i) literature interaction parameters (from DDB) and (ii) newly regressed interaction parameters. The chapter will close with a summary of the optimum parameters to be used for correlating (RK-Aspen, SR-Polar and PC-SAFT) and predicting (PSRK) the complex phase behaviour of the CO₂ + 1-decanol + *n*-tetradecane ternary system and 1-decanol + *n*-tetradecane binary system.

7.1. PURE COMPONENT PARAMETERS

7.1.1. CRITICAL PROPERTIES AND ACENTRIC FACTORS

The PSRK, RK-Aspen and SR-Polar property methods make use of the RKS *EoS* and therefore, require the estimation of pure component states parameters to calculate the species-specific energy and co-volume parameters. Accurate critical temperatures (T_c), critical pressures (P_c), and acentric factors (ω_i) are not always readily available in literature. However, several estimation techniques have been established of which more detail can be found elsewhere [241]–[246]. These estimation techniques are generally incorporated into process simulation software such as Aspen Plus®. The techniques have a

high level of accuracy and reliability to ensure that the values used in the *EoS* are as close as possible to the real values [2], [18], [43]. Several literature sources exist from which these parameters can be obtained:

- (i) The built-in National Institute of Standards and Technology (NIST) Thermodynamic Data Engine (TDE) in Aspen Plus®
- (ii) The Design Institute for Physical Properties (DIPPR) database [23]
- (iii) The Yaws' critical property database [22]
- (iv) The NIST website [21]
- (v) Perry's chemical engineers' handbook [20]
- (vi) The Properties of gases and liquids handbook [241]

For the current study, the data generated by the Aspen Plus® database will be utilised for the calculations as it correlates exactly with the DIPPR database [23]. The final pure component parameters obtained from the Aspen Plus® database are listed in *Table 7-1*.

TABLE 7- 1: PURE COMPONENT CRITICAL TEMPERATURES (T_c), CRITICAL PRESSURES (P_c), AND ACENTRIC FACTORS (ω_i) OBTAINED USING ASPEN PLUS®.

<i>Component</i>	T_c (K)	P_c (MPa)	ω
1-pentanol	588.1	3.897	0.575
1-hexanol	611.3	3.446	0.559
1-heptanol	632.3	3.085	0.562
1-octanol	652.3	2.783	0.570
1-decanol	688.0	2.308	0.607
<i>n</i> -nonane	594.6	2.290	0.443
<i>n</i> -decane	617.7	2.110	0.492
<i>n</i> -undecane	639.0	1.950	0.530
<i>n</i> -dodecane	658.0	1.820	0.576
<i>n</i> -tetradecane	693.0	1.570	0.643
CO ₂	304.2	7.383	0.224

7.1.2. SATURATED VAPOUR PRESSURE DATA

Saturated vapour pressure data were used to regress pure component parameters within the PSRK, RK-Aspen, SR-Polar and PC-SAFT model frameworks. The respective vapour pressures were calculated using the extended Antoine equation (7.1) suggested by Aspen Plus® [2].

$$\ln P_i^* = C_{1,i} + \frac{C_{2,i}}{T + C_{3,i}} + C_{4,i}T + C_{5,i}\ln T + C_{6,i}T^{C_{7,i}} \quad (7.1)$$

The constants to utilise in equation (7.1) were obtained from the Aspen Plus® database and are listed in Table 7-2. The pure component vapour pressures calculated for the 1-alcohol and *n*-alkane components (that were used for parameter regressions) are compared in Figure 7-1 to literature data available in DIPPR [23]. Qualitatively, the pure components vapour pressure data calculated using the Antoine equation correlates well to literature data and will be used for all pure component parameter regressions.

TABLE 7- 2: CONSTANTS OBTAINED FROM THE ASPEN PLUS® DATABASE FOR USE IN THE EXTENDED ANTOINE EQUATION (7.1)
WITH (P IN MPa AND T IN K).

Component	C_1	C_2	C_3	C_4	C_5	C_6	C_7	$T_{min} (K)$	$T_{max} (K)$
1-pentanol	100.93	-10643.0	0.0	0.0	-12.858	1.249E-17	6.0	195.56	588.1
1-hexanol	121.60	-12288.0	0.0	0.0	-15.732	1.270E-17	6.0	228.55	611.3
1-heptanol	133.59	-13466.0	0.0	0.0	-17.353	1.128E-17	6.0	239.15	632.3
1-octanol	130.29	-13667.0	0.0	0.0	-16.826	9.367E-18	6.0	257.65	652.3
1-decanol	142.42	-15212.0	0.0	0.0	-18.424	8.501E-18	6.0	280.05	688.0
<i>n</i> -nonane	95.53	-9030.4	0.0	0.0	-12.882	7.854E-06	2.0	219.66	594.6
<i>n</i> -decane	98.91	-9749.6	0.0	0.0	-13.245	7.127E-06	2.0	243.51	617.7
<i>n</i> -undecane	117.18	-11143.0	0.0	0.0	-15.855	8.187E-06	2.0	247.57	639.0
<i>n</i> -dodecane	123.65	-11976.0	0.0	0.0	-16.698	8.091E-06	2.0	263.57	658.0
<i>n</i> -tetradecane	126.65	-13231.0	0.0	0.0	-16.859	6.588E-06	2.0	279.01	693.0

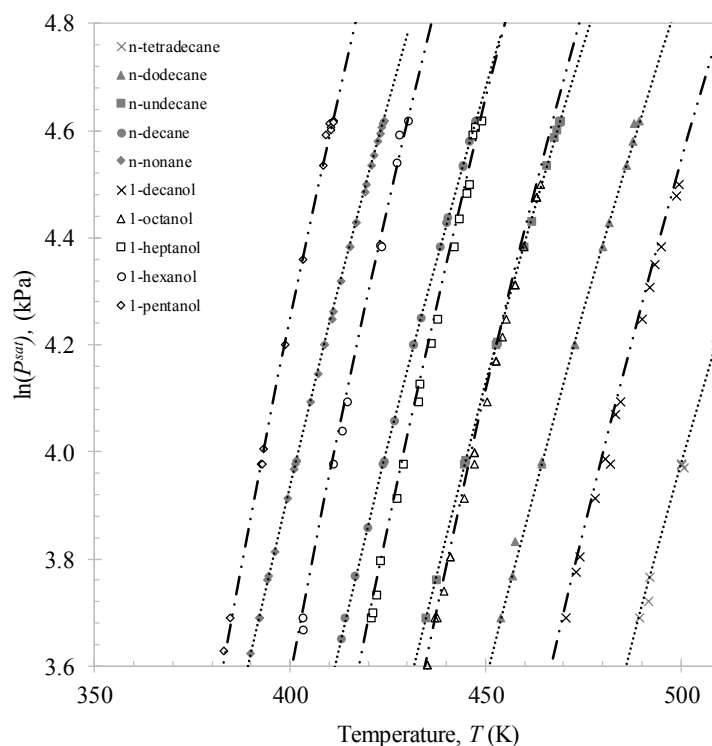


FIGURE 7- 1: PURE COMPONENT VAPOUR PRESSURE DATA CALCULATED WITH THE ANTOINE EQUATION [2], INDICATED BY LINES, COMPARED TO LITERATURE VAPOUR PRESSURE DATA, INDICATED BY BULLETS [23].

7.1.3. PSRK

The critical pure component parameters with the SRK *EoS* enables the reproduction of pure component vapour pressure data with the use of Mathias-Copeman parameters. Pure component vapour pressure data are used to fit pure component $c_{1,i}$, $c_{2,i}$ and $c_{3,i}$ constants. *Table 7-3* summarises the final Mathias-Copeman parameters for the components of interest to this investigation after regression.

TABLE 7- 3: MATHIAS-COPEMAN CONSTANTS REGRESSED WITH PURE COMPONENT VAPOUR PRESSURES USING ASPEN PLUS[®]. THE %AAD_P VALUES WERE CALCULATED USING DIPPR VAPOUR PRESSURE DATA [23] WITHIN THE SPECIFIED TEMPERATURE RANGE.

<i>Component</i>	c_1	c_2	c_3	%AAD _P	T_{range} (K)
1-pentanol	1.359	-0.414	2.297	0.859	357 - 587
1-hexanol	1.279	0.133	1.388	1.200	379 - 609
1-heptanol	1.435	-1.487	5.800	2.420	390 - 630
1-octanol	1.357	-0.627	3.704	1.593	408 - 648
1-decanol	1.639	-2.407	7.454	2.446	432 - 682
<i>n</i> -nonane	1.191	-0.413	0.806	0.195	360 - 590
<i>n</i> -decane	1.280	-0.659	1.387	0.462	384 - 614
<i>n</i> -undecane	1.335	-0.666	1.485	0.172	400 - 630
<i>n</i> -dodecane	1.413	-0.799	1.736	0.153	415 - 655
<i>n</i> -tetradecane	1.466	-0.458	1.115	0.198	450 - 680
CO ₂	0.920	-2.298	16.792	2.303	217 - 302

In addition to the Mathias-Copeman constants, the vdW surface area and volume parameters were estimated for each PSRK sub-group using Bondi's method [247]. The parameters obtained from the DDB are summarised in *Table 7-4* along with the effective surface area and volume parameters calculated for *n*-tetradecane. The CO₂ + *n*-tetradecane system is the only alkane-CO₂ binary system with strong size-asymmetry of interest to this study ($C \geq 10$). The Li-correction⁵ is a good extension to the PSRK model as it qualitatively improved the accuracy of the CO₂ + *n*-tetradecane model predictions (see *Figure 7-2*).

TABLE 7- 4: VAN DER WAALS GROUP ASSIGNMENT, VOLUME PARAMETER, Q_k , AREA PARAMETER, R_k , EFFECTIVE VOLUME PARAMETER, Q_k^* , AND EFFECTIVE SURFACE AREA PARAMETER, R_k^* , FOR ALL PSRK-UNIFAC GROUPS USED [131].

<i>Main group</i>		<i>Sub group</i>		<i>Aspen Plus[®] group number</i>	Q_k	R_k	Q_k^*	R_k^*
CH2	1	CH3	1	1015	0.8480	0.9011	0.9844	1.0460
CH2	1	CH2	2	1010	0.5400	0.6744	0.6268	0.7828
OH	5	OH	14	1200	1.2000	1.0000		
CO2		CO2		3850				

⁵ As discussed in Chapter 3, section 3.4.4, the Li-correction is only valid for size-asymmetric *gas-alkane* systems.

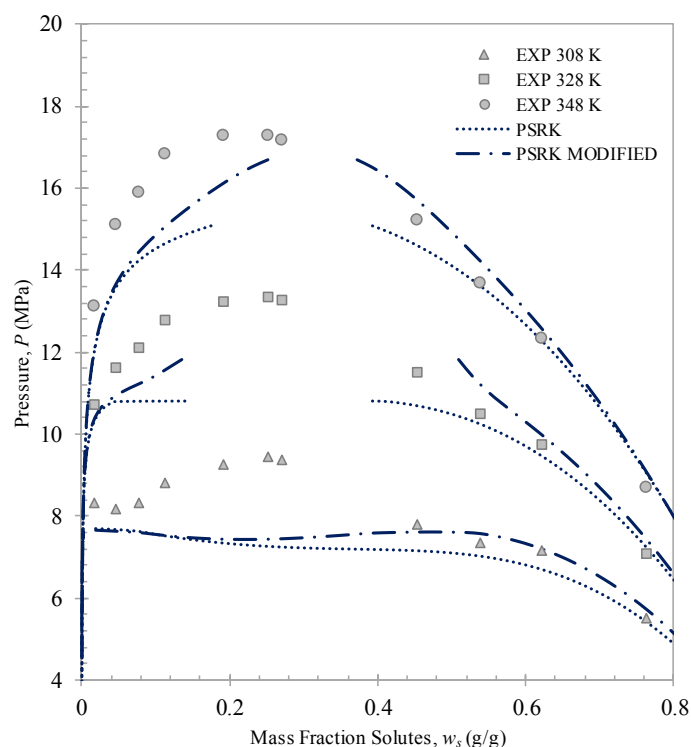


FIGURE 7- 2: LITERATURE $\text{CO}_2 + n\text{-TETRADECANE}$ DATA [17] PREDICTED WITH THE PSRK MODEL, WITH AND WITHOUT AN ADDED LI-CORRECTION: $F(14) = 1.1608$, AT $T = 308 \text{ K}$, $T = 328 \text{ K}$ AND $T = 348 \text{ K}$.

7.1.4. RK-ASPEN AND SR-POLAR

Pure component vapour pressures were used in conjunction with the T_c , P_c and ω values to fit the pure component polar parameters within the RK-Aspen and SR-Polar models using the built-in data regression function in Aspen Plus®. Polar parameters were regressed for the quadrupolar CO_2 and non-polar $n\text{-tetradecane}$ components as it is a representation of their multiple lumped effects and not necessarily a representation of their dipole moments [103], [158]. The resultant polar parameters to use with the RK-Aspen and SR-Polar models are provided in Table 7-5 with pressure deviations computed using equation (3.65) within the specified temperature range.

TABLE 7- 5: REGRESSED POLAR PARAMETERS FOR RK-ASPEN AND SR-POLAR USING VAPOUR PRESSURE DATA OBTAINED FROM THE DIPPR DATABASE [23] AND THE REGRESSION FUNCTION ON ASPEN PLUS®.

Component	RK-Aspen		SR-Polar			%AAD _P	T _{range} (K)
	η_i	%AAD _P	$p_{1,i}$	$p_{2,i}$	$p_{3,i}$		
1-decanol	-0.325	0.108	-0.607	-2.405	1.397	0.291	432 - 682
$n\text{-tetradecane}$	-0.0279	0.0353	-0.0936	-3.012	2.280	0.0614	450 - 680
CO_2	0.0454	0.0285	-0.465	-2.550	1.629	0.00345	217 - 302

7.1.5. $\alpha(T)$ PARAMETER

A recent study conducted by Le Guennec et al. [217] proved that selecting the appropriate $\alpha(T)$ parameter is just as important as selecting suitable mixing rules. Even with the most elaborated mixing rules, an inconsistent $\alpha(T)$ parameter will always lead to poor model results [217]. Having successfully regressed all the required pure component parameters for the three cubic *EoS* models, the $\alpha(T)$ -functions can be evaluated qualitatively. The $\alpha(T)$ -curves are shown in *Figure 7-3* for: (a) the RK-Aspen model (with Mathias $\alpha(T)$ and Boston Mathias $\alpha(T)$ -functions used), (b) the SR-Polar model (with Extended Boston Mathias $\alpha(T)$ -functions used) and (c) the PSRK model (with Mathias and Copeman $\alpha(T)$ -functions used).

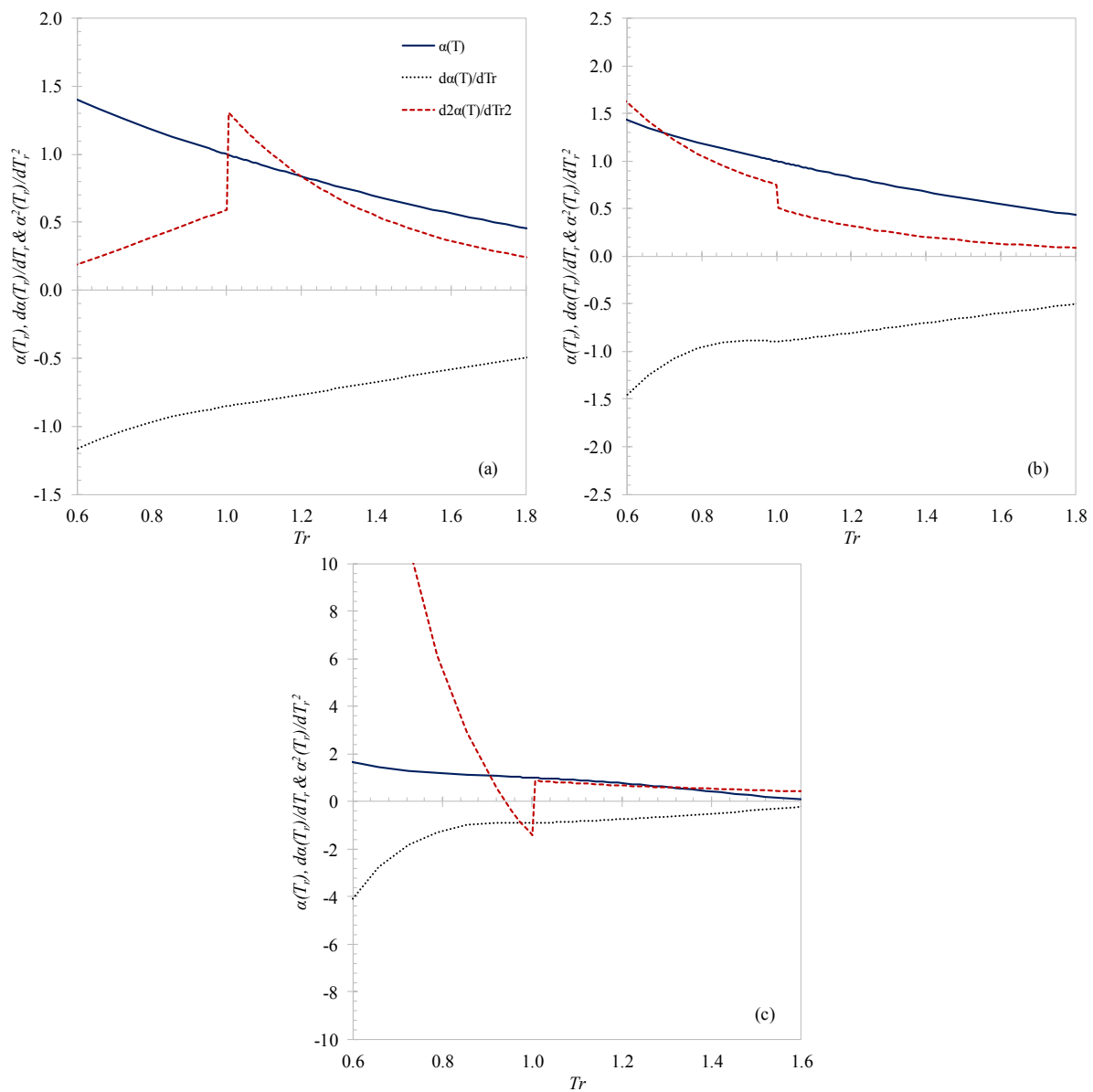


FIGURE 7- 3: THE $\alpha(T)$ -CURVE CALCULATED FOR CO_2 INCLUDING ITS 1ST AND 2ND DERIVATIVES VERSUS Tr OF CO_2 FOR: (A) THE RK-ASPEN MODEL, (B) THE SR-POLAR MODEL AND (C) THE PSRK MODEL.

For the RK-Aspen model (*Figure 7-3 (a)*) and the SR-Polar model (*Figure 7-3 (b)*) the first 3 conditions listed in section 3.7 are met. The $\alpha(T)$ -function is strictly convex over the entire temperature range with a visibly slower decrease in the supercritical domain ($Tr > 1$). Based on these findings, accurate HPBDP and HPVLE correlations are anticipated for these two models.

Although abiding by the first 2 conditions listed in section 3.7, the PSRK $\alpha(T)$ -function (shown in *Figure 7-3 (c)*) fails the $d^2\alpha(T)/dT^2 \geq 0$ constraint as negative values are seen for the 2nd derivative curve. This error can be rectified provided the c_2 parameter for CO₂ is set to 0. Therefore, the $\alpha(T)$ -function would lose one of its three adjustable parameters. In this work, the $\alpha(T)$ -function was not modified as it influenced the prediction of the experimental data at sub-critical conditions. However, it is anticipated that the PSRK model would probably struggle to predict, especially the HPVLE data, due to this constraint not being met (evaluated in Chapter 8).

7.1.6. PC-SAFT

The m , σ and ε/k pure component parameters used in this work for CO₂, 1-decanol and n -tetradecane were obtained from Gross and Sadowski [181] and are presented in *Table 7-6*. Roman-Ramirez et al. [187] used the PC-SAFT *EoS* to model CO₂ + alcohol phase equilibria data and found that when explicitly considering the CO₂ quadrupole moment, the model correlations improved. Experimental quadrupole moments of CO₂ have been well defined in literature [248]–[253]. The value obtained using direct methods resulted in Q values accurate to within 5-10% [186], [254] and will be used in this work (see *Table 7-6*). The methods employed for obtaining the quadrupole moment give both the sign (negative) and magnitude of the parameter. The pure component x_p value for CO₂ is an adjustable parameter and was correlated to saturated vapour pressure data, saturated liquid density data and the VLE data of the CO₂ + n -tetradecane binary system. This allowed for a unique x_p pure component parameter to be regressed for the quadrupolar CO₂ used in this work.

TABLE 7- 6: PC-SAFT PURE COMPONENT PARAMETERS OBTAINED THROUGH LITERATURE [181], [254] OR REGRESSION IN THIS WORK.

Component	m	σ (Å)	ε/k (K)	ε^{AB}/k (K)	κ^{AB}	Q (DÅ)	x_p^\dagger	%AAD _p	%AAD _P
CO ₂	2.0729	2.7852	169.21			-4.3	0.1235	2.73	2.78
n -tetradecane	5.9002	3.9396	254.21					1.28	4.8
1-decanol	4.8225	3.8281	267.45	2355.99	0.0032			0.33	0.31
Source	Gross and Sadowski [181]			This work		[248]–[253]	This work		

[†] %AAD_P = 2.89; %AAD_p = 1.66

CO₂ T -range: 216 – 304 K

n -tetradecane T -range: 279 – 693 K

1-decanol T -range: 344 – 619 K

The added association parameters for 1-decanol were regressed in this work using saturated vapour pressure data, saturated liquid density data and the VLE data of the CO₂ + 1-decanol [15] binary system. Regression was required for these two parameters after the literature parameters accurately correlated pure component data but failed to predict the mixture behaviour [189]. The saturated liquid density data for 1-decanol and CO₂ were estimated using the temperature dependent DIPPR 105 equation⁶ [2], [23].

7.2. BINARY INTERACTION PARAMETERS

Interaction parameters are used in the mixing rules of each property method to incorporate the interactions between two molecules (RK-Aspen and SR-Polar), groups (PSRK) or segments (PC-SAFT) and inevitably improve the phase equilibria correlations of the model. This section of the chapter will cover the interaction parameters obtain either from literature or regressed using experimental data. The influence of these interaction parameters on the model outcomes were evaluated in Chapter 8.

7.2.1. GROUP + GROUP PARAMETERS

The PSRK model is used together with the UNIFAC group contribution method. Therefore, available group + group interaction parameters existing within the DDB can be used in this work. *Table 7-7* provides the optimised PSRK parameters for the CO₂ (CO2), alcohol (OH) and alkane (CH2) groups [115].

TABLE 7- 7: GROUP INTERACTION PARAMETERS FOR THE PSRK MODEL OBTAINED FROM LITERATURE, I.E. DDB [115].

Group <i>m</i>	Group <i>n</i>	a_{mn}	b_{mn}	c_{mn}	a_{nm}	b_{nm}	c_{nm}
OH	CH2	156.4	-	-	986.5	-	-
CO2	OH	148.16	-	-	510.64	-	-
CO2	CH2	-38.672	0.86149	-0.0017906	919.8	-3.9132	0.0046309

In addition to the DDB parameters, the LPVLE data measured in this work allowed for the regression of new low-pressure activity coefficient parameters between the *n*-alkane and the 1-alcohol components (see *Table 7-8*). It is particularly interesting to note that the a_{mn} parameter regressed for each 1-alcohol + *n*-alkane systems remained the same as the a_{mn} value obtained from literature, i.e. $a_{mn} = 156.4$. This finding indicates that the regression approach is not applicable for the data measured. New interaction parameters cannot be regressed for each molecule using the UNIFAC group activity coefficient model.

⁶

$$\rho \left(\frac{\text{kg}}{\text{m}^3} \right) = \frac{A}{B \left[1 + \left(1 - \frac{T(K)}{C} \right)^D \right]}$$

However, if interaction parameters are not available, an activity coefficient model like NRTL and/or UNIQUAC can be applied for regressing new BIPs to be used with the PSRK mixing rules [115].

TABLE 7- 8: GROUP INTERACTION PARAMETERS FOR THE PSRK MODEL REGRESSED USING THE LPVLE EXPERIMENTAL DATA MEASURED IN THIS WORK.

<i>Group m</i>	<i>Group n</i>	a_{mn}	a_{nm}
1-pentanol	<i>n</i> -nonane	156.4	912.2
1-hexanol	<i>n</i> -decane	156.4	976.5
1-heptanol	<i>n</i> -undecane	156.4	888.3
1-octanol	<i>n</i> -dodecane	156.4	986.5
1-decanol	<i>n</i> -tetradecane	156.4	1096.4

The DDB and newly regressed parameters were used to predict the low-pressure phase equilibria of each of the five 1-alcohol + *n*-alkane systems measured in this work; the qualitative results are provided in *Figure 7-4*. In addition, *Table 7-9* compares the azeotropic point estimated with experimental data, predicted with PSRK + DDB parameters and correlated with newly regressed parameters from this work. Overall, the PSRK property method with the DDB parameters provided the most accurate representation of the experimental LPVLE data. Therefore, the PSRK method will be a purely predictive model in further investigations of the ternary CO₂ + 1-decanol + *n*-tetradecane system. This finding confirms that group parameters cannot be regressed for each molecule. It should be made clear that the PSRK parameters in *Table 7-7* were adopted without adjustment in the calculations shown in Chapter 3.

TABLE 7- 9: EXPERIMENTALLY ESTIMATED AZEOTROPIC POINT (VAPOUR COMPOSITION, y_1 AND TEMPERATURE, T) FOR THE FIVE 1-ALCOHOL + N-ALKANE BINARY SYSTEMS COMPARED TO PSRK MODEL PREDICTED AZEOTROPIC POINT WITH (A) DDB [115] PARAMETERS AND (B) NEWLY REGRESSED PARAMETERS IN THIS WORK.

	<i>Experimental</i>		<i>DDB</i>		<i>This work</i>	
	y_1 (g/g)	T (K)	y_1 (g/g)	T (K)	y_1 (g/g)	T (K)
1-pentanol (1) + <i>n</i> -nonane (2)	0.445	378.05	0.450	378.17	0.461	378.03
1-hexanol (1) + <i>n</i> -decane (2)	0.516	398.47	0.549	398.24	0.545	397.87
1-heptanol (1) + <i>n</i> -undecane (2)	0.625	416.78	0.630	416.81	0.642	416.87
1-octanol (1) + <i>n</i> -dodecane (2)	0.664	435.19	0.709	434.82	0.680	434.35
1-decanol (1) + <i>n</i> -tetradecane (2)	0.864	468.66	0.837	468.75	0.811	468.75

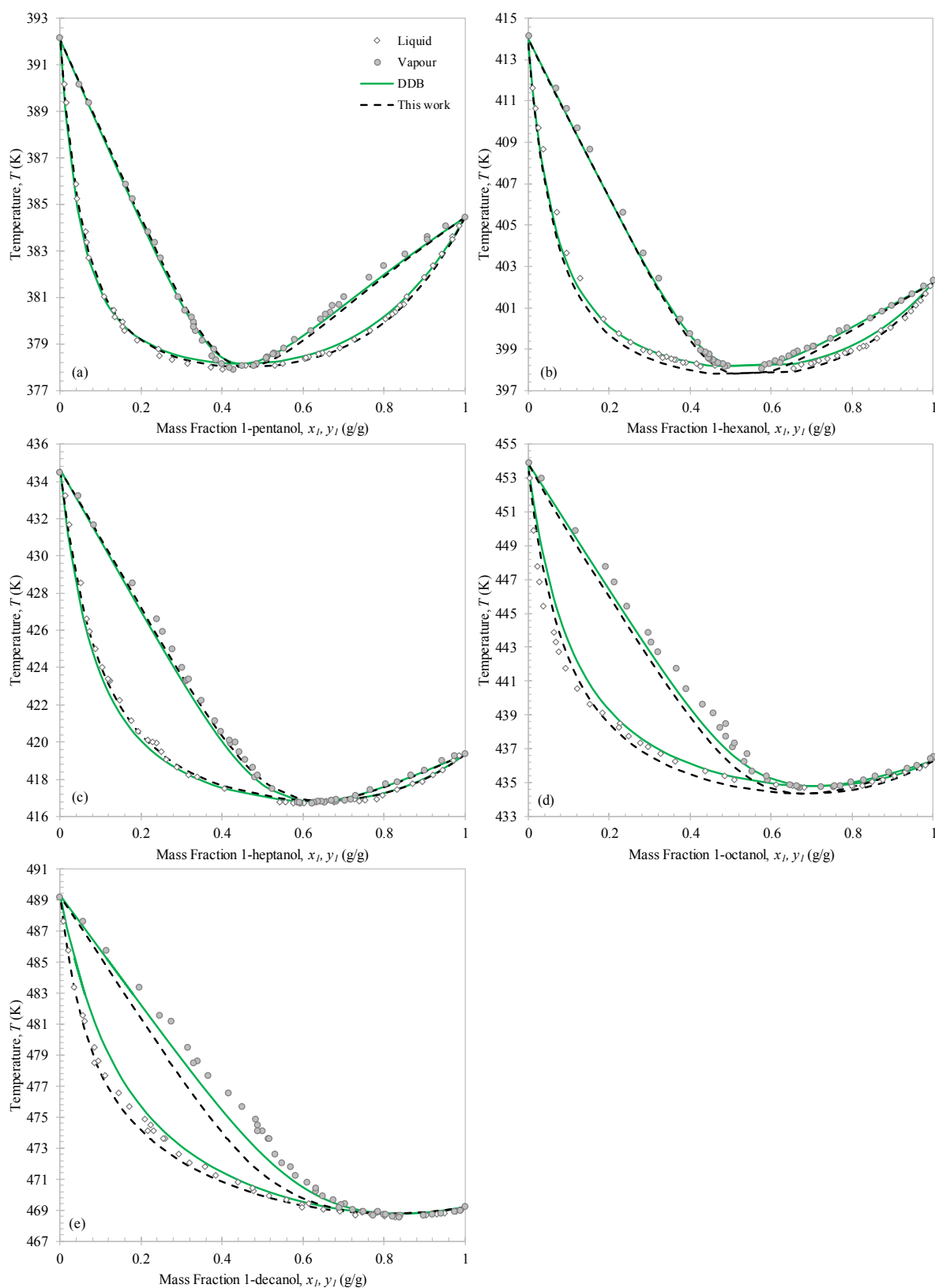


FIGURE 7- 4: EXPERIMENTAL T - $x_I y_I$ DATA FOR (A) 1-PENTANOL (1) + *N*-NONANE (2); (B) 1-HEXANOL (1) + *N*-DECANE (2); (C) 1-HEPTANOL (1) + *N*-UNDECANE (2); (D) 1-OCTANOL (1) + *N*-DODECANE (2); AND (E) 1-DECANOL (1) + *N*-TETRADECANE (2), COMPARED TO THE PSRK MODEL PREDICTIONS WITH LITERATURE GROUP INTERACTION PARAMETERS [115] AND NEWLY REGRESSED GROUP INTERACTION PARAMETERS.

Figure 7-5 shows a 10 % and 1 % parity plot that compares the experimental data and PSRK predicted data (with DDB parameters) of (a) *n*-alkane vapour composition and (b) temperature, respectively. It is clear from the figure that the PSRK model with literature parameters are very close to the LPVLE experimental data measured in this work. For the 1-octanol + *n*-dodecane and 1-decanol + *n*-tetradecane systems, the largest deviations are seen in both composition and temperature. In addition, Figure 7-3 (a) shows that the PSRK model is biased to overpredict the *n*-tetradecane vapour composition for these two systems, especially within the low 1-decanol region. This agrees with the predictions shown in Figure 7-2 (d) and (e). Therefore, it is anticipated that for the ternary CO₂ + 1-decanol + *n*-tetradecane system, at compositions rich in *n*-tetradecane, the PSRK model will struggle to predict the experimental data well.

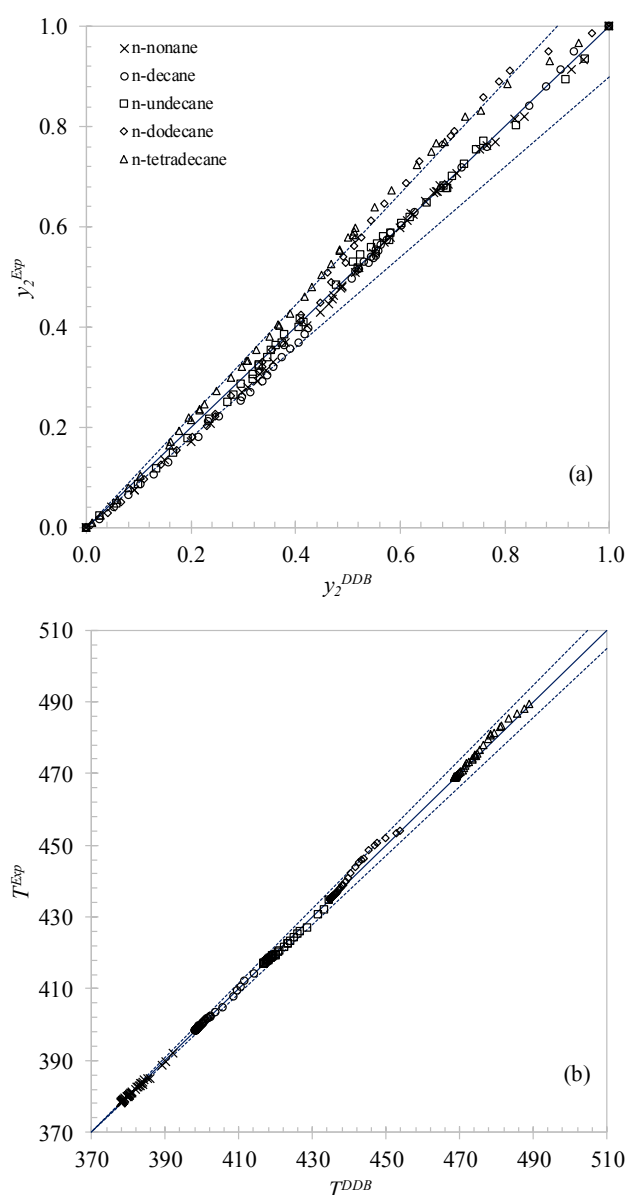


FIGURE 7- 5: PARITY PLOTS FOR THE 5 BINARY 1-ALCOHOL + *N*-ALKANE SYSTEMS (USING NEW LPVLE DATA AND THE PSRK MODEL) FOR (A) *N*-ALKANE COMPOSITION, y_2 AND (B) TEMPERATURE, T . THE DASHED LINES ARE THE +10 % AND + 1% OFF THE SOLID LINES, RESPECTIVELY.

7.2.2. SOLUTE + SOLVENT

Solute + solvent BIPs are used to quantify the interactions between the solvent (CO₂) and the solutes (1-decanol and *n*-tetradecane). The built-in data regression function within Aspen Plus® was used to regress solute + solvent BIPs for the RK-Aspen, SR-Polar and PC-SAFT models. The input data for the regression were obtained using isobars at 0.2 MPa intervals across the bubble- and dew-point *P*-*x* phase diagrams of the two CO₂ binary sub-systems [15], [17]. The final temperature dependent and temperature independent BIPs are provided in *Table 7-10*.

TABLE 7- 10: SOLUTE + SOLVENT BINARY INTERACTION PARAMETERS REGRESSED IN THIS WORK (T-INDEPENDENT VS. T-DEPENDENT).

<i>CO</i> ₂ + ...	<i>RK-Aspen</i>				<i>SR-Polar</i>				<i>PC-SAFT</i>	
	$k_{a,ij}^0$	$k_{a,ij}^I$	$k_{b,ij}^0$	$k_{b,ij}^I$	$k_{a,ij}^0$	$k_{a,ij}^I$	$k_{b,ij}^0$	$k_{b,ij}^I$	k_{ij}^0	k_{ij}^I
1-decanol	0.0876	-	-0.0319	-	0.0806	-	-0.0382	-	0.0900	-
	0.1645	-0.2286	-0.1238	0.2784	0.1730	-0.0003	-0.0661	0.0001	28.93	-24.75
<i>n</i> -tetradecane	0.0941	-	0.0031	-	0.0913	-	0.0066	-	0.1172	-
	0.0323	0.1816	-0.1983	0.6222	0.0524	0.0001	-0.2323	0.0007	28.58	-24.46

In *Figure 7-6* the %AAD for temperature, pressure and solute composition are compared for the solute + solvent BIPs regressed in this work. The %AAD values for the four variables were adjusted based on each of their standard deviations and regressed with an equal weighting ($W_n = 1$). The temperature dependence of the RK-Aspen, SR-Polar and PC-SAFT models are evaluated to ensure the most accurate representation of the experimental phase equilibria data. In all cases, clear model improvements in the form of smaller %AAD values are observed. However, the larger BIPs indicate a decrease in the model's robustness (due to the model not correlating the data but rather fitting the errors). Apart from the solute vapour phase predictions, the %AAD values of the temperature independent BIPs remained $\leq 5\%$. It is for this reason, that the temperature dependent adjustable BIPs will not be considered in this work.

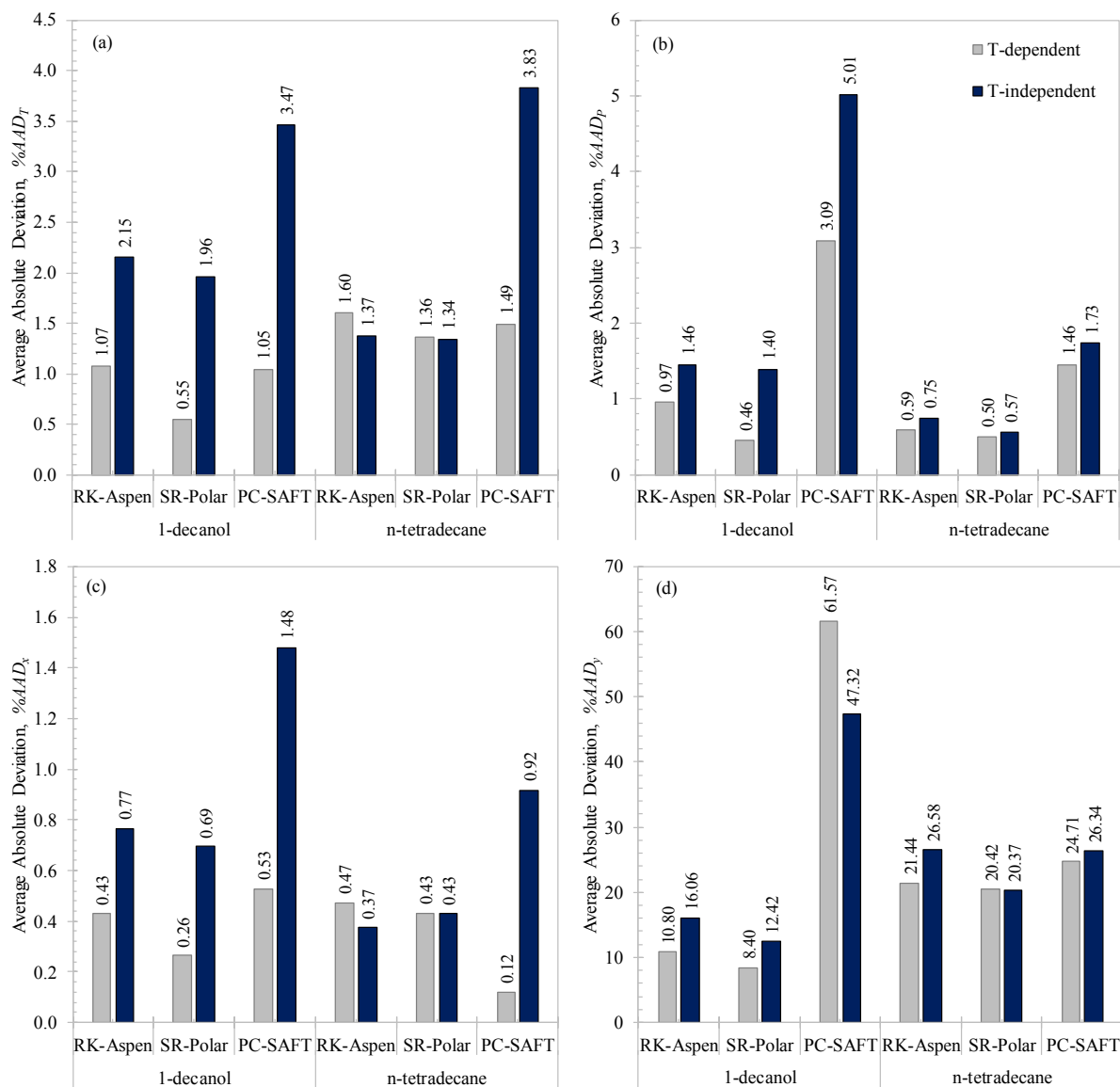


FIGURE 7- 6: %AAD VALUES FOR (A) PRESSURE, (B) TEMPERATURE, (C) SOLUTE LIQUID COMPOSITION AND (D) SOLUTE VAPOUR COMPOSITION VARIABLES FOR THE SOLUTE + SOLVENT BIP REGRESSIONS FROM THIS WORK.

7.2.3. SOLUTE + SOLUTE

Having obtained the polar parameters and regressed the solute + solvent BIPs for the interested system, focus now shifts to the fitting of solute + solute BIPs. The inclusion of the pure component polar parameters as well as the solute + solvent BIPs into the RK-Aspen and SR-Polar algorithm have previously shown improvements in the prediction of ternary data [15], [16], [19]. These parameters will therefore remain fixed in the algorithm for the investigation of solute + solute BIPs. Similarly, the solute + solvent BIPs of the PC-SAFT property method were also fixed. Three different means of obtaining the BIPs are investigated in this section, namely from HPBDP, HPVLE and LPVLE data.

7.2.3.1. REGRESSIONS WITH BUBBLE- AND DEW-POINT DATA

To use the built-in data regression function within Aspen Plus®, VLE phase equilibrium data are required. Therefore, the HPBDP solute + solute BIPs required manual regression of representative values instead of exact values. The number of possible combinations of $k_{a,ij}$ and $k_{b,ij}$ interactions between the 1-decanol and *n*-tetradecane molecules can become very large. Therefore, the BIPs are manually regressed on a temperature independent basis, i.e. the $k_{a,ij}^I$ and $k_{b,ij}^I$ interaction parameters were set to zero and only the $k_{a,ij}^0$ and $k_{b,ij}^0$ BIPs were altered. In this work, a plug-and-play method similar to that used by Zamudio [15] was applied, followed by the approach used by Smith and Schwarz [16]. A minimum value for %AAD_P was obtained at $k_{a,ij}^0 = 0.03$ for the study conducted by Zamudio [18] and $k_{a,ij}^0 = 0.03$ with $k_{b,ij}^0 = 0.03$ by Smith and Schwarz [16]. Therefore, for the RK-Aspen and SR-Polar property methods $k_{a,ij}^0 = 0.04$ and $k_{b,ij}^0 = 0.08$ BIPs were selected as a starting point and were manually varied between the following set range:

$$k_{a,ij}^0 \in \{0.00; 0.02; 0.04; 0.06; 0.08\}$$

$$k_{b,ij}^0 \in \{0.00; 0.04; 0.08; 0.12; 0.15\}$$

The experimental bubble- and dew-point data measured were used to evaluate the accuracy of each $k_{a,ij}^0$ and $k_{b,ij}^0$ BIP combination. Phase transition pressures were predicted using temperature and composition as input variables for the FLASH2 simulation unit within Aspen Plus® (see Figure 7-7). The pressure requirement of the flash drum was avoided by selecting a vapour fraction, i.e. if the data point to be predicted was within the bubble-point region, a vapour fraction of zero was specified. The combinations indicate a 5X5 matrix for each variation to the input variables.

$$\therefore k_{a,ij}^0 \text{ and } k_{b,ij}^0 = f(T, w_c^{red})$$

Input variable 1:

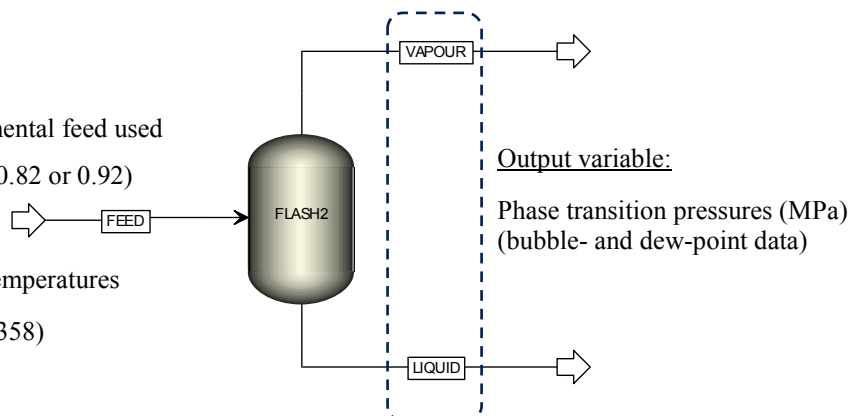
Mixture feed composition = experimental feed used

(w_c^{red} (g/g) = 0.24, 0.50, 0.64, 0.77, 0.82 or 0.92)

Input variable 2:

Temperature = fixed experimental temperatures

(T (K) = 308, 318, 328, 338, 348 or 358)



Output variable:

Phase transition pressures (MPa)
(bubble- and dew-point data)

FIGURE 7- 7: FLASH2 UNIT ON ASPEN PLUS® TO BE USED FOR THE PREDICTION OF THE SOLUBILITY DATA WITH THE THERMODYNAMIC MODELS.

The selected $k_{a,ij}^0$ and $k_{b,ij}^0$ values were evaluated by calculating the $\%AAD_P$ of each simulation run. The best fit value for $k_{a,ij}^0$ and $k_{b,ij}^0$ were established as that which resulted in the local minimum $\%AAD_P$ value. The approach is shown for the RK-Aspen (Figure 7-8) and SR-Polar (Figure 7-9) property methods with $w_c^{red} = 0.9200$ g/g and (a) $T = 338$ K or (b) $T = 348$ K as the input variables, respectively.

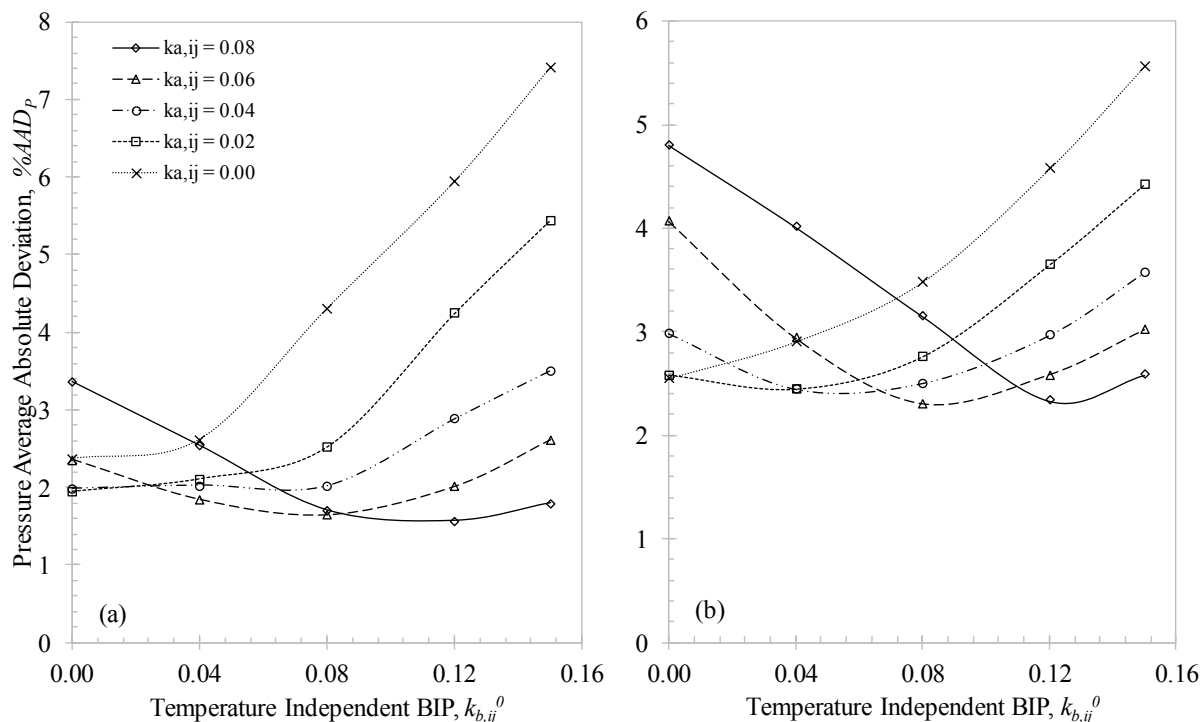


FIGURE 7- 8: LOCAL OPTIMUM $K_{A, L}^0$ AND $K_{B, L}^0$ BIPs REGRESSED FOR THE RK-ASPEN MODEL USING THE $w_c^{RED} = 0.9200$ G/G HPBDP MIXTURE AT (A) $T = 338$ K AND (B) $T = 348$ K.

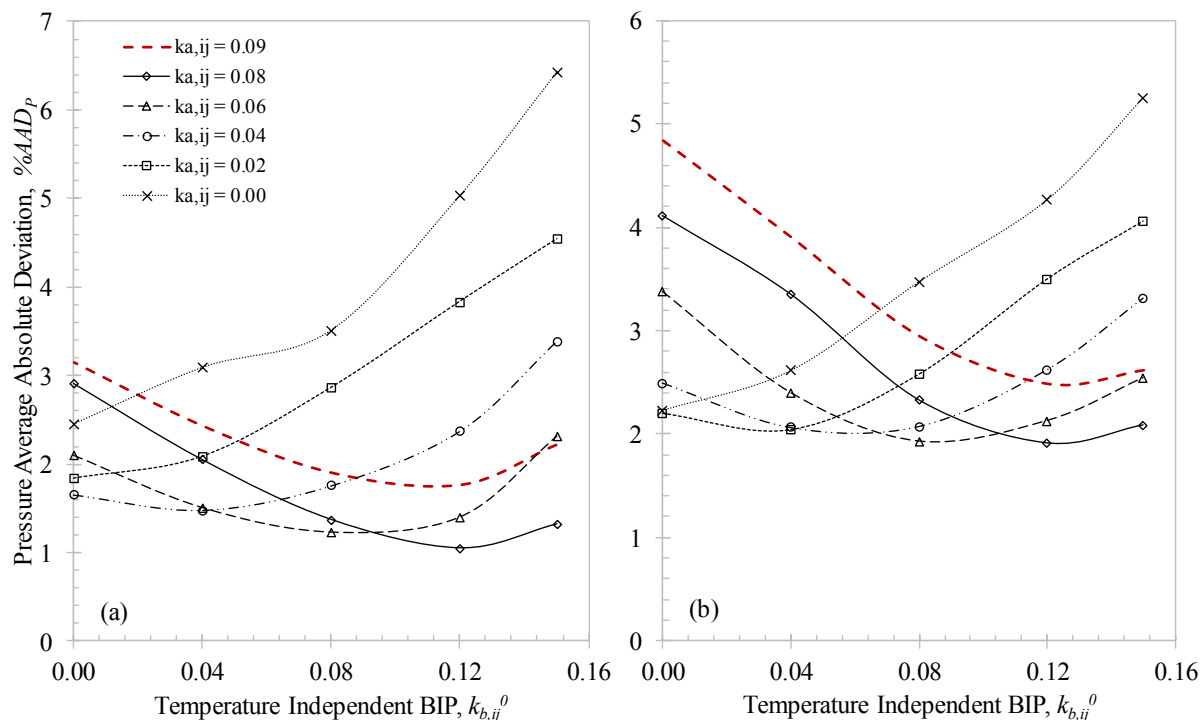


FIGURE 7- 9: LOCAL MINIMUM $K_{A, L}^0$ AND $K_{B, L}^0$ BIPs REGRESSED (OPTIMUM $\%AAD_P$ VALUE WITHIN THE RANGE CONSIDERED) FOR THE SR-POLAR MODEL USING THE $w_c^{RED} = 0.9200$ G/G HPBDP MIXTURE AT (A) $T = 338$ K AND (B) $T = 348$ K.

The findings in this work agree with that of Smith and Schwarz [16] as the inclusion of the $k_{b,ij}^0$ parameter into the two cubic *EoS* models resulted in more accurate representations of the HPBDP experimental data. For the SR-Polar model, the $k_{a,ij}^0$ BIP appears to be on the limit of the range considered. To show that this is not the case, an additional line for $k_{a,ij}^0 = 0.09$ is added to *Figure 7-9* which shows that $k_{a,ij}^0 = 0.08$ is indeed a minimum in the specified range (local minima close to $k_{a,ij}^0$ and $k_{b,ij}^0$ equal to zero).

The procedures were similar for the PC-SAFT property method. However, the local minimum k_{ij}^0 (temperature independent) BIP shown in *Figure 7-10* was established between the following set range:

$$k_{ij}^0 \in \{0.00; 0.01; 0.02; 0.03; 0.04; 0.05; 0.06; 0.07; 0.08\}$$

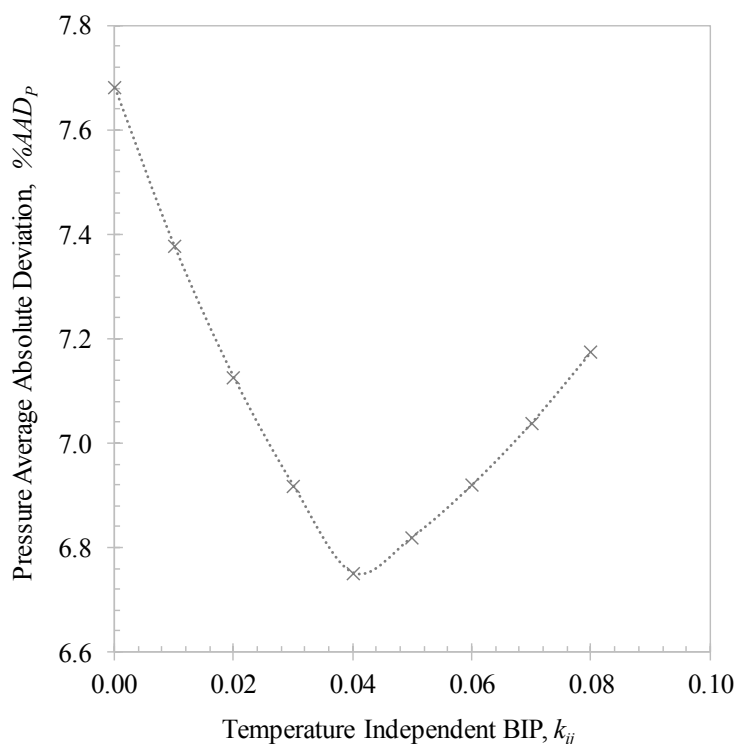


FIGURE 7- 10: LOCAL MINIMUM k_{ij}^0 BIPs REGRESSED (OPTIMUM %AAD_P VALUE WITHIN THE RANGE CONSIDERED) FOR THE PC-SAFT MODEL USING THE $w_c^{RED} = 0.9200$ G/G HPBDP MIXTURE AT $T = 338$ K.

The final local minimum (optimum %AAD_P value) $k_{ij}^0 = 0.04$ HPBDP BIP for PC-SAFT is provided in *Table 7-11* alongside the optimum BIPs for the RK-Aspen and SR-Polar models with $k_{b,ij}^0 = 0$ and $k_{b,ij}^0 \neq 0$.

TABLE 7- 11: FINAL TEMPERATURE INDEPENDENT SOLUTE + SOLUTE BIPs REGRESSED USING THE EXPERIMENTAL HPBDP DATA MEASURED IN THIS WORK WITH $K_{B,L}^0 = 0$ AND $K_{B,L}^0 \neq 0$ FOR RK-ASPEN AND SR-POLAR.

RK-Aspen		SR-Polar		PC-SAFT
$k_{a,ij}^0$	$k_{b,ij}^0$	$k_{a,ij}^0$	$k_{b,ij}^0$	k_{ij}^0
0.04	-	0.02	-	0.04
0.06	0.08	0.08	0.12	-

It is especially interesting to note, that when considering a single parameter ($k_{b,ij}^0 = 0$) the RK-Aspen and PC-SAFT models both provide the same quantitative solute + solute BIP. *To obtain a fair comparison between each model, and not have the conclusions partially clouded using temperature dependent BIPs in some methods and not in others, temperature independent solute + solute BIPs will be assumed throughout this investigation.* However, it should be made clear, that the ability to add T -dependent BIPs for these cubic EoS not only makes them more favourable for industrial use but could potentially improve the model correlations produced in this work.

For a better understanding of the $k_{a,ij}^0$ and $k_{b,ij}^0$ BIPs effects on the RK-Aspen and SR-Polar model results, Figure 7-11 was constructed.

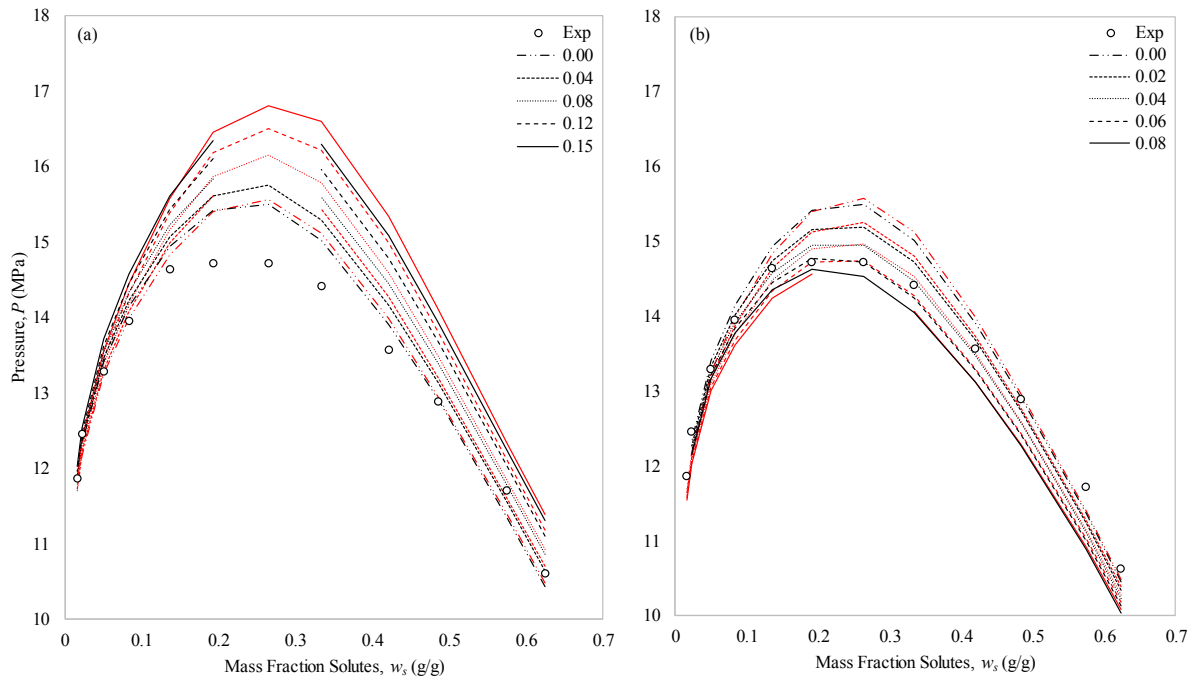


FIGURE 7- 11: EFFECT OF SOLUTE + SOLUTE BIPs ON THE PHASE TRANSITION ENVELOPE OF HPBDP DATA ($w_c^{RED} = 0.9200$ G/G AND $T = 338$ K) FOR RK-ASPEN (BLACK) AND SR-POLAR (RED) WHERE (A) $K_{A,LL} = 0$ AND VARYING $K_{B,LL}$; (B) $K_{B,LL} = 0$ AND VARYING $K_{A,LL}$.

In Figure 7-11 (a), the $k_{a,ij}^0$ parameter was held constant ($k_{a,ij}^0 = 0$) for the evaluation of the $w_c^{red} = 0.9200$ g/g mixture at $T = 338$ K and the $k_{b,ij}^0$ value was adjusted. By increasing the $k_{b,ij}^0$ parameter, both RK-Aspen and SR-Polar correlations were shifted vertically upwards and horizontally outwards. In Figure 7-11 (b), the $k_{b,ij}^0$ parameter was held constant ($k_{b,ij}^0 = 0$) and the $k_{a,ij}^0$ value adjusted to evaluate the same mixture. Again, a shift in the model correlations were observed; an increase in the $k_{a,ij}^0$ parameter caused RK-Aspen and SR-Polar to shift vertically downwards and horizontally inwards. In both cases, the largest shift occurred in the critical region, followed by the bubble-point region and only a slight shift in the dew-point region. In effect, the increase of the $k_{a,ij}^0$ parameter will cause the P - w_s curve to become more concave and an increase in the $k_{b,ij}^0$ parameter will cause the P - w_s curve to flatten.

Albeit small, the RK-Aspen model is more sensitive to the changes occurring in both the $k_{a,ij}^0$ and $k_{b,ij}^0$ parameters. It is postulated that this is the reason for the slightly higher solute + solute BIPs regressed for SR-Polar in comparison to those of RK-Aspen with $k_{b,ij}^0 \neq 0$ (see *Table 7-11*).

7.2.3.2. REGRESSIONS WITH VLE DATA

Like the solute + solvent BIPs regression, the experimental HPVLE and LPVLE data are used to regress the solute + solute interaction parameters with the built-in data regression function in Aspen Plus®. All three set temperatures, i.e. $T = 308\text{ K}$, 328 K and 348 K , were used for the HPVLE regression. Again, the influence of the second solute + solute BIP ($k_{b,ij}^0$) for the two cubic *EoS* were evaluated. The solute + solute BIPs regressed for RK-Aspen and SR-Polar using LPVLE data and HPVLE data with their associated regression errors are tabulated in *Table 7-12*.

TABLE 7- 12: RK-ASPEN AND SR-POLAR SOLUTE + SOLUTE BIPs REGRESSED IN THIS WORK USING HPVLE OR LPVLE DATA. %AAD IN PRESSURE, TEMPERATURE AND SOLUTE COMPOSITIONS FOR THE BIP REGRESSIONS ARE REPORTED FOR EACH CASE.

	RK-Aspen				SR-Polar			
	HPVLE		LPVLE		HPVLE		LPVLE	
$k_{a,ij}^0$	0.02689	0.05963	0.05812	-0.3288	0.01953	0.06207	0.05820	-0.3310
$k_{b,ij}^0$		0.05548		-0.4713		0.07589		-0.4742
%AAD [‡]								
Temperature, T	2.02	1.22	0.17	0.14	2.24	1.23	0.17	0.14
Pressure, P	0.69	0.41	0.29	0.25	1.02	0.65	0.30	0.26
Vapour composition (solutes, w_s) [†]	19.96	18.72	11.27	12.09	18.7	17.92	11.28	12.11
Liquid composition (solutes, w_s) [†]	0.40	0.31	0.078	0.075	0.45	0.35	0.079	0.075

[†] Solute absolute deviations reported as an average of 1-decanol and *n*-tetradecane deviations.

[‡] Calculated for combined BIP set.

The HPVLE BIPs regressed are very similar to the HPBDP BIPs given in *Table 7-11* and again, a decrease in the regression errors are observed with the added $k_{b,ij}^0$ parameter. The same cannot be said for the LPVLE BIPs. The regression of the $k_{b,ij}^0$ parameter caused a large shift in the magnitude of the BIPs as well as a change in sign from positive to negative. To maintain generality and avoid multiple conclusions, the LPVLE BIPs will assume $k_{b,ij}^0 = 0$ for RK-Aspen and SR-Polar. Furthermore, it is postulated that the HPVLE BIPs and HPBDP BIPs will not be successful in representing the T - xy trend of the LPVLE data if their $k_{b,ij}^0$ parameters are included in the model algorithms. An investigation into this theory will be conducted for RK-Aspen and SR-Polar in the next chapter.

For the PC-SAFT model, linear dependency in temperature resulted in an increase in regression errors. It is postulated that this occurred due to the model overestimating the phase transition pressures and as a result predicts a false liquid-liquid phase split [186]. Furthermore, the BIPs increased in magnitude when including the second, T -dependent parameter, making the model less robust (changing

its fundamental characteristics). Therefore, in this study, the use of a single temperature independent interaction parameter is preferred since it allows the thermodynamic model to retain its predictive qualities, rather than just fitting the experimental data. The temperature independent k_{ij} parameters used for the 1-decanol + n -tetradecane interactions are listed in *Table 7-13* with their associated regression errors.

TABLE 7- 13: PC-SAFT SOLUTE + SOLUTE BIPs REGRESSED IN THIS WORK USING HPVLE OR LPVLE DATA. %AAD IN PRESSURE, TEMPERATURE AND SOLUTE COMPOSITIONS FOR THE BIP REGRESSIONS ARE REPORTED FOR EACH CASE.

	HPVLE	LPVLE
k_{ij}^0	0.04454	0.02467
%AAD		
Temperature	10.78	0.37
Pressure	7.34	0.56
Vapour composition (solutes, w_s) [†]	44.32	21.86
Liquid composition (solutes, w_s) [†]	1.44	0.12

[†] Solute absolute deviations reported as an average of 1-decanol and n -tetradecane deviations.

7.3. CHAPTER OUTCOMES

The aim of this chapter was to achieve **Objective 3.2** by gathering pure component parameters from literature and regressing the necessary interaction parameters for the four thermodynamic models using (i) HPBDP, (ii) HPVLE and (iii) LPVLE data. The key conclusions drawn from this chapter are the following:

- The HPBDP data were used to manually obtain solute + solute BIPs with the use of a flash drum simulation in Aspen Plus®.
- The intercorrelation of the parameters with the two cubic *EoS* restricted the HPBDP BIPs to a maximum of 2 solute + solute interaction parameters namely, $k_{a, ij}^0$ and $k_{b, ij}^0$. Therefore, only temperature independent BIPs were investigated in this study. PC-SAFT required the regression of only one k_{ij} parameter to maintain the temperature independent trend. The accuracy of this fitting procedure is limited by the technique used for obtaining the solute + solute BIPs. The values did not represent the true interactions between the solutes, but rather enabled the most accurate fit of the thermodynamic models to the experimental data.
- HPVLE data for the ternary system and LPVLE data for the binary system were used to regress the second and third set of BIPs, respectively. Like the solute + solvent regression procedure, the built-in data regression function in Aspen Plus® was applied.
- To maintain generality and not have one method produce a biased outcome, the HPVLE and LPVLE BIPs were regressed on a temperature independent basis.

- The LPVLE BIPs were further restricted to one $k_{a,ij}^0$ parameter for the two cubic *EoS* due to the regression of the $k_{b,ij}^0$ parameter causing a large shift in the magnitude of the BIPs as well as a change in sign from positive to negative.
- Due to the limitation on the LPVLE BIPs, an additional scenario for the HPBDP and HPVLE BIPs were established: in addition to the comparisons with two BIPs ($k_{a,ij}^0$ and $k_{b,ij}^0$), correlations with one BIP ($k_{b,ij}^0 = 0$) for the HPBDP and HPVLE data were evaluated alongside the single LPVLE BIPs in representing the LPVLE data.
- The final BIPs regressed in this work that were used in the next chapter to evaluate the RK-Aspen, SR-Polar and PC-SAFT models in representing HPBDP (P - w_s plots), HPVLE (Gibbs phase triangles) and LPVLE (T - xy plots) phase behaviour data are provided in *Table 7-14*.

TABLE 7- 14: FINAL BIPs REGRESSED IN THIS WORK ON A TEMPERATURE INDEPENDENT BASIS.

	<i>RK-Aspen</i>		<i>SR-Polar</i>		<i>PC-SAFT</i>
	$k_{a,ij}^0$	$k_{b,ij}^0$	$k_{a,ij}^0$	$k_{b,ij}^0$	k_{ij}^0
CO ₂ + 1-decanol	0.0876	-0.0319	0.0806	-0.0382	0.0900
CO ₂ + <i>n</i> -tetradecane	0.0941	0.0031	0.0913	0.0066	0.1172
1-decanol + <i>n</i> -tetradecane					
HPBDP	0.06	0.08	0.08	0.12	0.04
HPVLE	0.05963	0.05548	0.06207	0.07589	0.04454
LPVLE	0.05812	-	0.05820	-	0.02467

- New low-pressure activity coefficient group-group interaction parameters were regressed for PSRK in this work. However, the literature group-group interaction parameters showed accurate qualitative predictions of the LPVLE binary systems measured in this work. This highlights the 5th and final scientific contributions that will be made in this work (see Section 1.5) as PSRK was applied in Chapter 8 as a strictly predictive model (with DDB parameters).

The thermodynamic results are presented in the next chapter to identify whether high-pressure solute + solute BIPs can be used to improve the modelling of low-pressure data and vice versa (**Objective 3.3**). Consequently, the solute + solute parameter set to be used by each of the thermodynamic models, that resulted in the overall best representation of the measured equilibrium data, are established (**Objective 3.4**). These optimum BIP sets are then used in a comparative study to identify the best suited thermodynamic model for representing the experimental HPBDP, HPVLE and LPVLE data (**Objective 3.5**).

Chapter 8

THERMODYNAMIC MODELLING USING ASPEN PLUS®

With the parameters required for the thermodynamic models of interest to this work successfully generated in the previous chapter (**Objective 3.2**), focus now shifts to their influence on representing HPBDP, HPVLE and LPVLE phase equilibria data.

The aim of this chapter is to provide a comprehensive overview of the current capabilities of thermodynamic models, within Aspen Plus®, in correlating the phase behaviour of the asymmetric $\text{CO}_2 + 1\text{-decanol} + n\text{-tetradecane}$ system and $1\text{-decanol} + n\text{-tetradecane}$ binary system. The performance of these models (RK-Aspen, SR-Polar, PC-SAFT and PSRK) will be determined over a temperature range of $T = 308 \text{ K}$ to 358 K and a pressure range of $P = 8.0 \text{ MPa}$ to 27.0 MPa for the ternary system; and at a sub-atmospheric pressure of 40 kPa for the binary system.

To identify shortcomings in the models and to provide a fair comparison between them, the solute + solute BIPs regressed from the LPVLE data are used in a consistent way for HPVLE and HPBDP calculations and vice versa (**Objective 3.3**). In so doing, better insight into the applicability of these models are gained. Furthermore, the specific strengths and weaknesses of each model family are highlighted to establish the best suited model (**Objective 3.5**) and its optimum solute + solute BIPs set (**Objective 3.4**) for the complex $\text{CO}_2 + 1\text{-decanol} + n\text{-tetradecane}$ system.

8.1. HIGH-PRESSURE PHASE BEHAVIOUR RESULTS

Model evaluation at high-pressure was conducted via two means:

- (i) Using experimental temperatures and compositions (from HPBDP results) as inputs to predict the equilibrium pressures of the bubble- and dew-point phases. These results are represented on $\%AAD_P$ plots and $P\text{-}w_s$ plots.
- (ii) Using experimental temperatures and pressures (from HPVLE results) as inputs to predict the equilibrium compositions of the liquid and vapour phases. These results are represented on a $\%AAD_{w_s}$ plot and Gibbs phase triangles.

8.1.1. RK-ASPEN

The quality of the BIPs in representing the HPBDP data were evaluated by determining the $\%AAD_P$ between the measured and calculated values for the phase transition pressures (see *Figure 8-1*). Similarly, for the evaluation of the BIPs in representing the HPVLE data the $\%AAD_{w_s}$ between measured and calculated solute compositions were determined and are shown in *Figure 8-2*. The poor correlations of the HPBDP data by all three sets of BIPs at $T = 308$ K and $T = 318$ K are not uncommon. Generally, difficulties will be experienced at temperatures that approach the complex, near-critical region of the solvent [16], [18]. The higher $\%AAD_P$ shown in *Figure 8-1* at $T = 308$ K and $T = 318$ K are attributed to the temperature inversion that is not accounted for in the RK-Aspen model. In published literature, it was shown that the RK-Aspen model is unable to predict the $\text{CO}_2 + 1\text{-decanol}$ binary system at $T = 308$ K due to a temperature inversion [16], [18]. Thus, the inaccurate predictions are a model issue, not a BIPs issue. This phenomenon was not observed for the remaining mixtures and the improved correlations at $T > 318$ K were thus expected. Based on these findings it is recommended that the near-critical solvent region be disregarded when selecting the optimum BIPs.

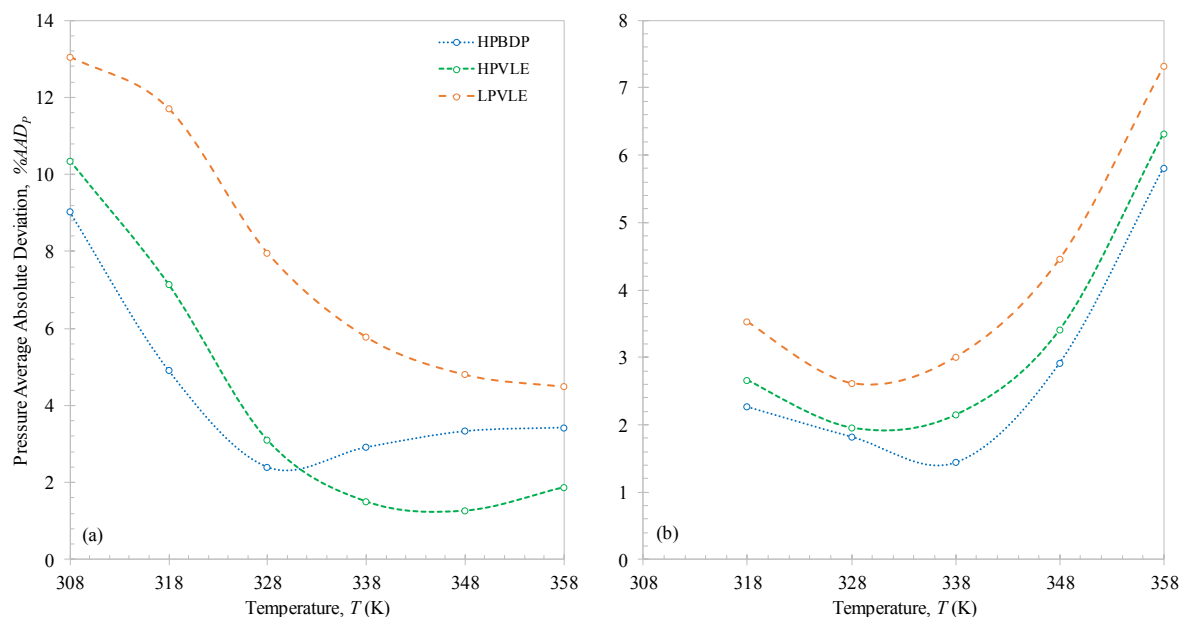


FIGURE 8- 1: RK-ASPEN $\%AAD_P$ CALCULATED FOR (A) BUBBLE-POINT CORRELATIONS AND (B) DEW-POINT CORRELATIONS, WITH ALTERNATING SOLUTE + SOLUTE BIPs. MODEL FAILED TO CORRELATE DEW-POINT PRESSURE DATA AT $T = 308$ K.

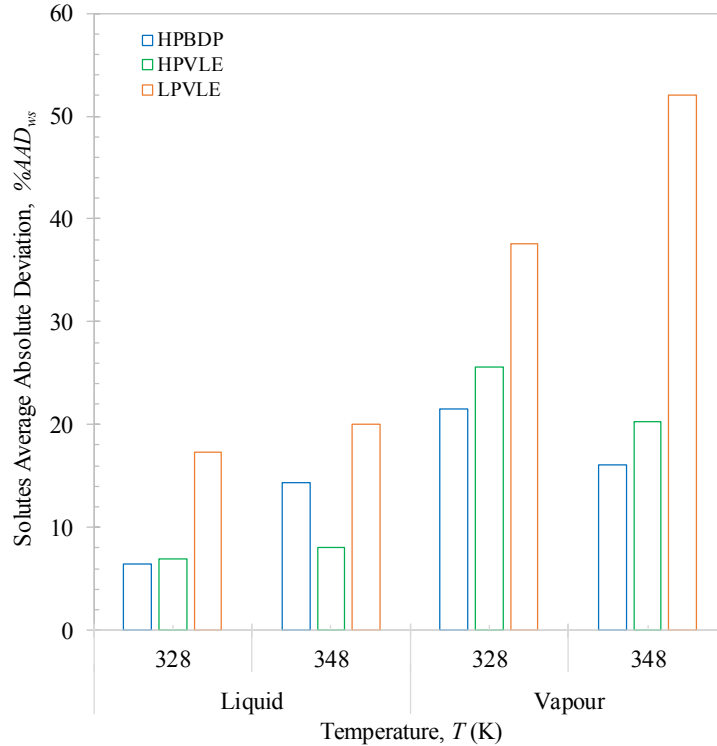


FIGURE 8- 2: RK-ASPEN %AAD_{ws} FOR SOLUTE VAPOUR AND LIQUID COMPOSITION CORRELATIONS, WITH ALTERNATING SOLUTE + SOLUTE BIPs. MODEL FAILED TO CORRELATE EXPERIMENTAL DATA AT $T=308$ K.

The RK-Aspen model was further investigated qualitatively with the three solute + solute BIPs sets to evaluate their accuracy in correlating HPBDP data (*Figure 8-3*) and HPVLE data (*Figure 8-4* and *Figure 8-5*). The HPBDP BIPs and the HPVLE BIPs for RK-Aspen are very similar in magnitude, especially the $k_{a,ij}^0$ parameters at 0.06 and 0.05963⁷, respectively. Essentially, the $k_{a,ij}^0$ parameter is the ‘constant’ and only the $k_{b,ij}^0$ parameter is being varied between the HPBDP and HPVLE sets. In agreement with *Figure 7-11 (a)*, the HPBDP BIPs curve ($k_{b,ij}^0 = 0.08$) lies above the HPVLE BIPs curve ($k_{b,ij}^0 = 0.05548$). For the LPVLE BIPs, where $k_{b,ij}^0$ is zero and $k_{a,ij}^0 = 0.05812$, the P - w_s curves have been shifted horizontally downwards, and vertically inwards, again in agreement with *Figure 7-11 (b)*. It is particularly interesting to note that the shift between the three model correlations decreased with an increase in w_c^{red} (*Figure 8-3 (d) to (f)*). It is postulated that this occurs due to insufficient 1-decanol molecules being present within the mixture to allow for significant solute + solute interactions to take place. This indicates that:

- (i) Larger solute + solute BIPs, i.e. the HPBDP BIPs, are required to ensure a more accurate P - w_s fit of 1-decanol-rich mixtures;
- (ii) The P - w_s curves of n -tetradecane-rich mixtures can be accurately predicted with simply one $k_{a,ij}$ solute + solute BIP regressed using the LPVLE data.

⁷ Decreasing the number of significant figures will provide the same $k_{a,ij}$ value as the HPBDP data (≈ 0.06).

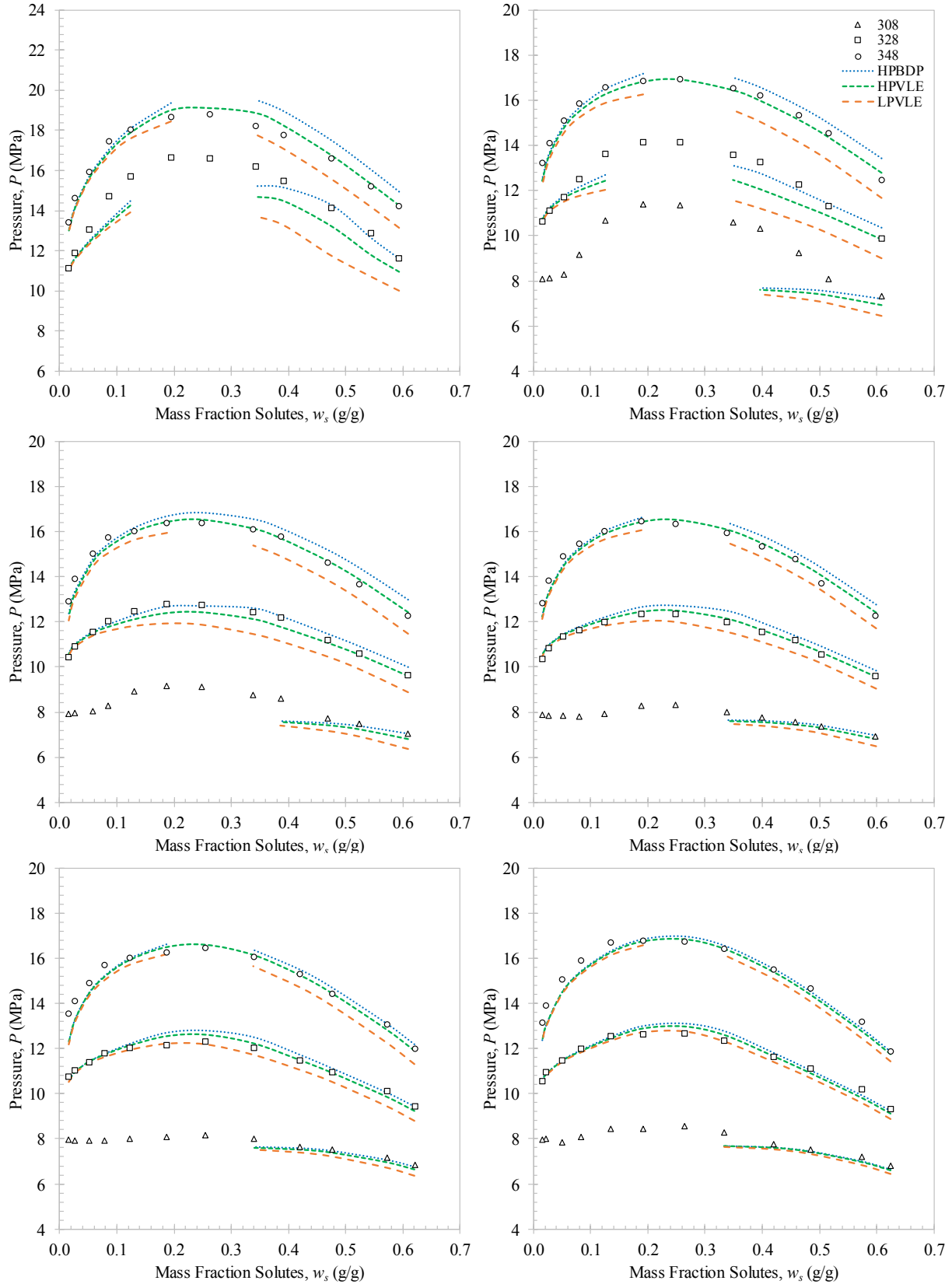


FIGURE 8- 3: RK-ASPEN MODEL CORRELATIONS OF THE HPBDP DATA (WITH VARYING SOLUTE + SOLUTE BIPs) AT $T = 308$ K, 328 K AND 348 K FOR (A) $w_c^{RED} = 0.2405$ G/G; (B) $w_c^{RED} = 0.5000$ G/G; (C) $w_c^{RED} = 0.6399$ G/G; (D) $w_c^{RED} = 0.7698$ G/G; (E) $w_c^{RED} = 0.8162$ G/G; AND (F) $w_c^{RED} = 0.9200$.

Similar model results are seen for the HPVLE data within the 1-decanol-rich region (*Figure 8-4* and *Figure 8-5*). However, the small deviations of the LPVLE P - w_s curve, especially in the bubble-point region of the n -tetradecane-rich mixtures, are amplified on the Gibbs phase triangles. The LPVLE BIPs result in overly CO_2 -rich liquid phases and CO_2 -deficient vapour phases, thereby predicting the cosolvency ‘pinch point’ and phase envelope split prematurely.

Further evidence of the temperature effects on the RK-Aspen model results are seen by the correlations of the HPBDP (bubble-point region) and HPVLE (liquid phase) experimental data. At $T = 328$ K the following relative performance is observed quantitatively and qualitatively:

$$\text{HPBDP} > \text{HPVLE} > \text{LPVLE}^8$$

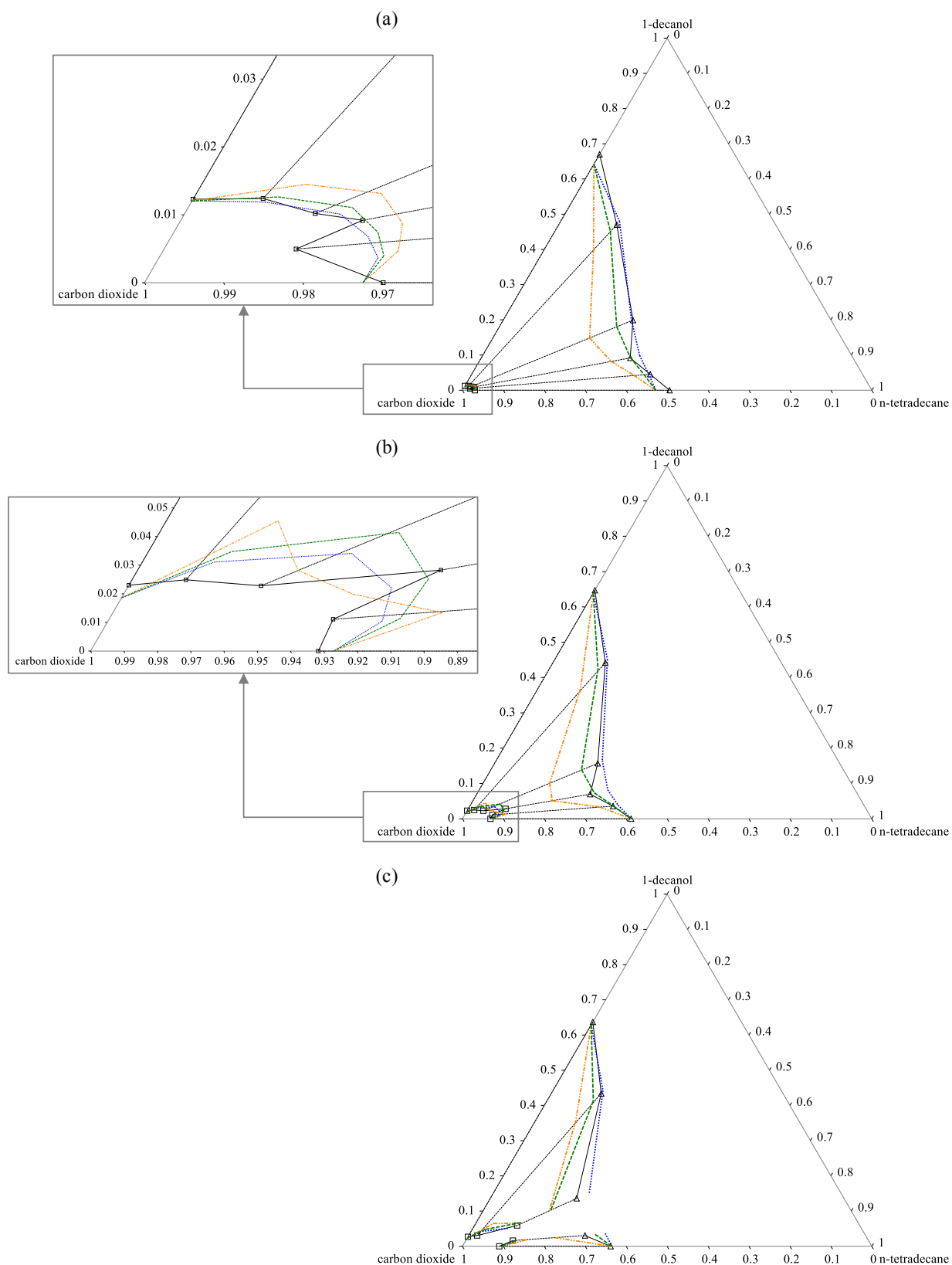
With an increase in temperature to $T = 348$ K, the order of optimum BIPs for the RK-Aspen model changes to:

$$\text{HPVLE} > \text{HPBDP} > \text{LPVLE}$$

The change in the order is attributed to the mixtures having a higher kinetic energy at $T = 348$ K than at $T = 328$ K. An increase in the kinetic energy, results in an increase in the amount of collisions taking place between molecules and in effect the volume that each species occupies is increased (b_i). The solute + solvent and solute + solute $k_{b,ij}^0$ BIPs are connected to the species-specific co-volume and with an increase in the solute + solvent interactions, less prominent solute + solute BIPs are needed for an accurate representation of the experimental phase behaviour.

It is interesting to note that the cosolvency effect outweighs the temperature effect as a shift in the optimum BIPs at $T = 328$ K is seen to occur for the bubble-point region between $w_c^{red} = 0.6399$ g/g (*Figure 8-3 (c)*) and $w_c^{red} = 0.7698$ g/g (*Figure 8-3 (d)*). As discussed in Chapter 5, the 3 mixtures within and approaching the cosolvency effect start to level out, brought on by the solubility enhancement. It is due to this decrease in phase transition pressures that the smaller (HPVLE) solute + solute BIPs can correlate the cosolvency effect more accurately and hence, the shift in the order of the optimum BIPs. The results are reflected on the Gibbs diagrams of *Figure 8-4* and *Figure 8-5* where the HPVLE BIPs can capture the s-shaped behaviour of the experimental data more closely than the HPBDP BIPs.

⁸ The ‘>’ symbol is indicative of a superior fit, i.e. HPBDP provided the most accurate fit.



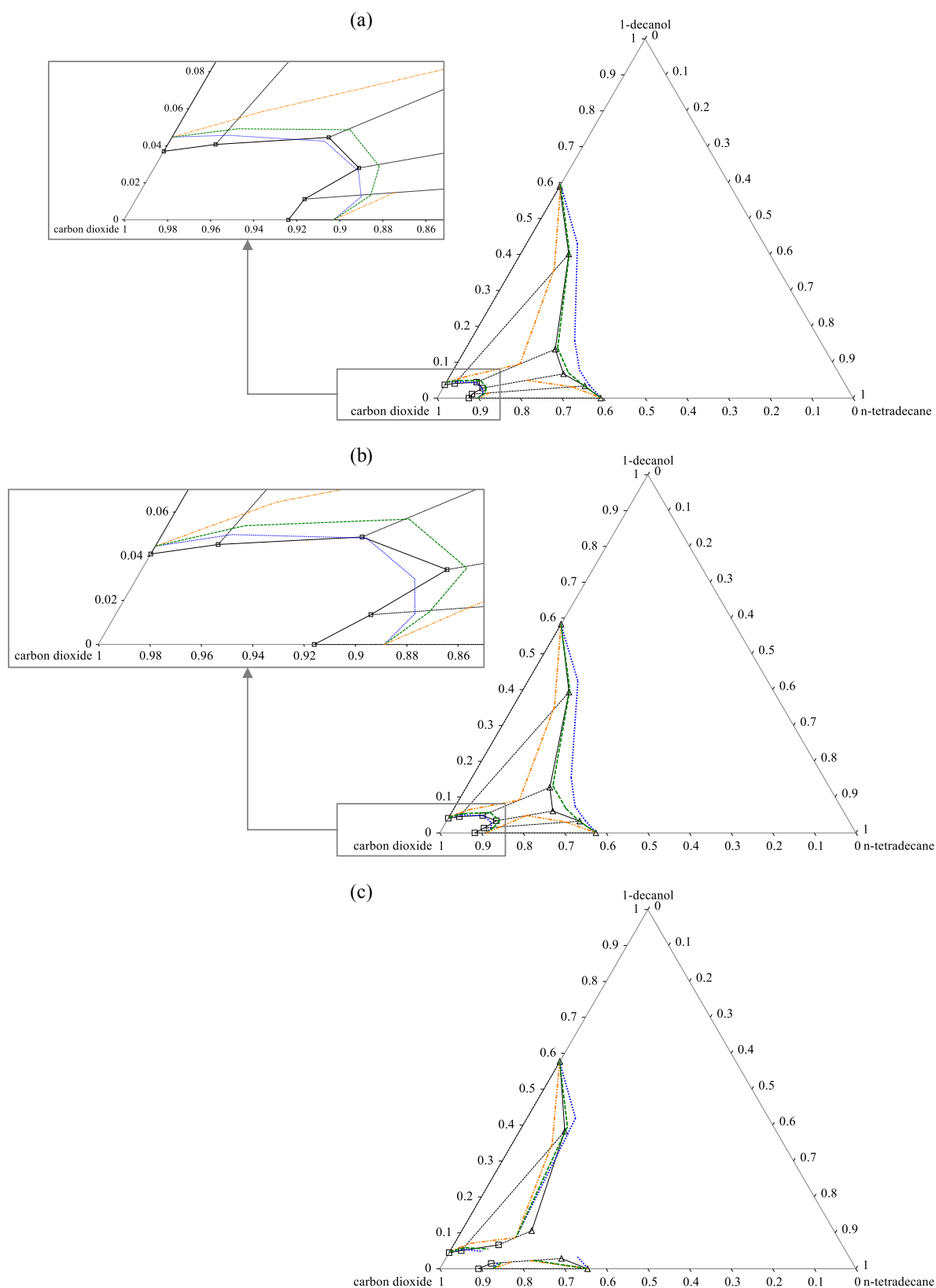


FIGURE 8- 5: RK-ASPEN MODEL CORRELATIONS OF THE HPVLE DATA WITH: HPBDP BIPs; --- HPVLE BIPs; AND, --- LPVLE SOLUTE + SOLUTE BIPs AT $T = 348$ K AND (A) $P = 16.0$ MPa; (B) $P = 16.2$ MPa; AND (C) $P = 16.4$ MPa.

The dew-point region of P - w_s curves and the vapour phase of Gibbs phase triangles are the most prominent for distinguishing whether SFF processes will be feasible. Therefore, the dew-point and vapour phase modelling results will outweigh those presented by the bubble-point and liquid phase results. The qualitative analysis proved to be more difficult after the three sets of BIPs produced trends that are all similar in accuracy for the HPBDP dew-point regions (*Figure 8-3*) and the HPVLE vapour phase envelopes (*Figure 8-4*). However, no temperature effects on the RK-Aspen model results are seen by the correlations of the HPBDP (*Figure 8-1 (b)*) and HPVLE (*Figure 8-2*) experimental data; at each set temperature, the following relative performance are observed quantitatively and qualitatively:

$$\text{HPBDP} > \text{HPVLE} > \text{LPVLE}$$

Three methods are used to evaluate how well the model can describe the split between the two phases (enhanced miscibility region):

- (i) The predicted α_{ij} values at constant T and w_c^{red} , shown in *Figure 8-6*.
- (ii) The predicted α_{ij} values at constant T and P , shown in *Figure 8-7*.
- (iii) The predicted tie lines of the HPVLE data at constant T and P , shown in *Figure 8-8*.

For the first two methods, the predicted α_{ij} values were calculated using the model predicted HPVLE data. An average predicted α_{ij} value of 1.20 was calculated for the RK-Aspen model, regardless of the solute + solute BIPs applied. Furthermore, from the results, the qualitative dependence of α_{ij} on pressure and w_c^{red} could be established for the RK-Aspen model. The following qualitative outcomes were shown, regardless of the solute + solute BIPs used:

- (i) The models can match the experimental trend of the $w_c^{red} = 0.2403$ g/g and $w_c^{red} = 0.6245$ g/g mixtures at constant $T = 348$ K; however, α_{ij} remains constant, regardless of a change in P (see *Figure 8-6 (a) and (b)*).
- (ii) Reasonable agreement between the model and experimental data is seen for the $w_c^{red} = 0.2403$ g/g and $w_c^{red} = 0.6245$ g/g mixtures at constant $T = 328$ K; however, this excludes $P = 11.1$ MPa due to the negative α_{ij} - P correlation (see *Figure 8-6 to Figure 8-8*).
- (iii) Predicted α_{ij} values showed a negative correlation with increasing w_c^{red} at constant T and P (see *Figure 8-7* as an example at $T = 328$ K and $P = 11.1$ MPa).
- (iv) For the $w_c^{red} = 0.7979$ g/g and $w_c^{red} = 0.9004$ g/g mixtures, at constant T and P , the model not only overestimates α_{ij} (*Figure 8-7*) but its compositional dependence is not captured (*Figure 8-8*). It should however be noted, that the LPVLE BIPs allow the RK-Aspen model to produce the same positive α_{ij} - P correlation as the experimental results (*Figure 8-6 (c) and (d)*).

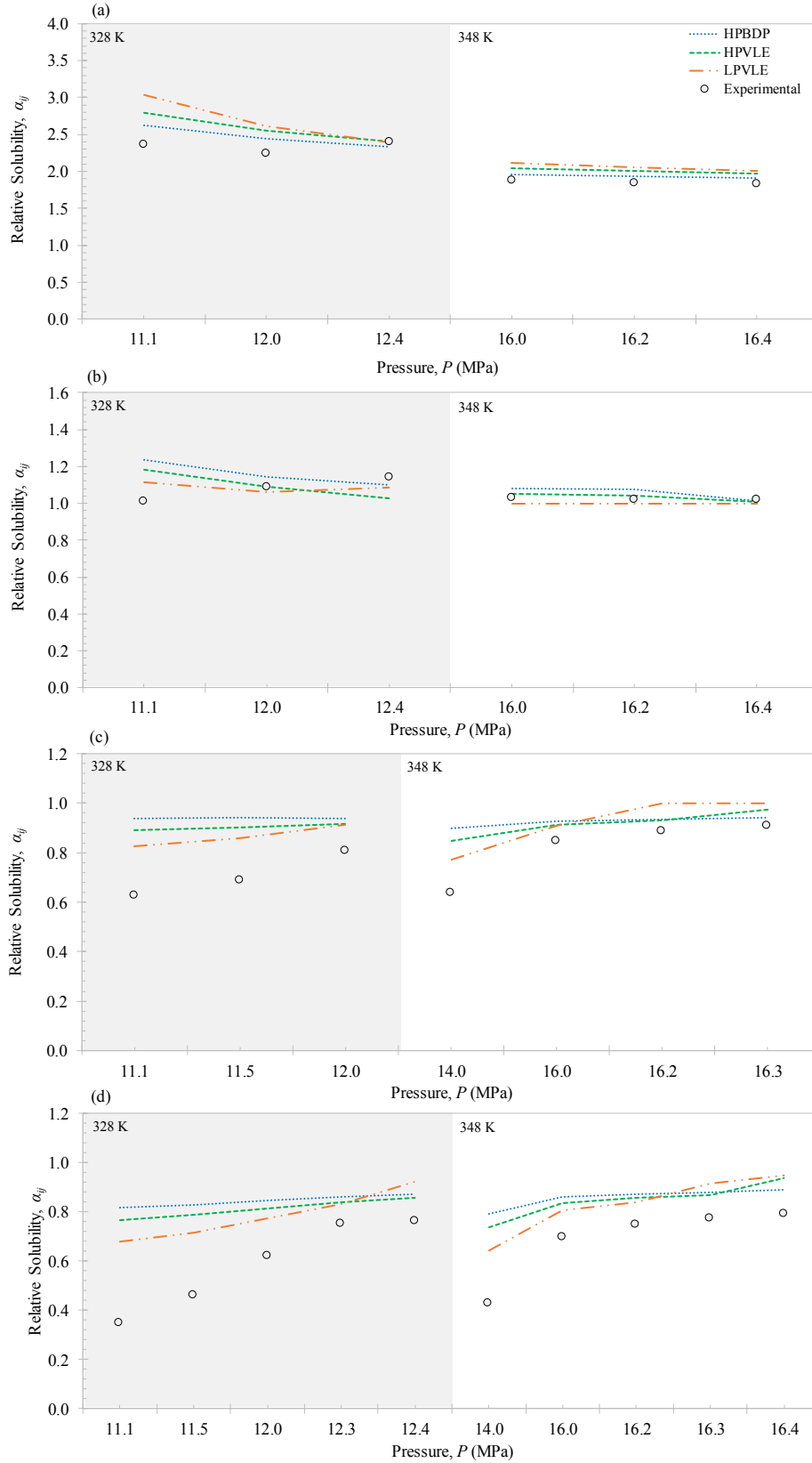


FIGURE 8- 6: PREDICTED $P-A_M$ TRENDS FOR THE RK-ASPEN MODEL WITH HPBDP, HPVLE AND LPVLE BIPs COMPARED TO EXPERIMENTAL $P-A_M$ VALUES AT CONSTANT $T = 328\text{ K}$ OR $T = 348\text{ K}$ AND (A) $w_c^{RED} = 0.2403\text{ G/G}$; (B) $w_c^{RED} = 0.6245\text{ G/G}$; (C) $w_c^{RED} = 0.7979\text{ G/G}$; AND (D) $w_c^{RED} = 0.9004\text{ G/G}$.

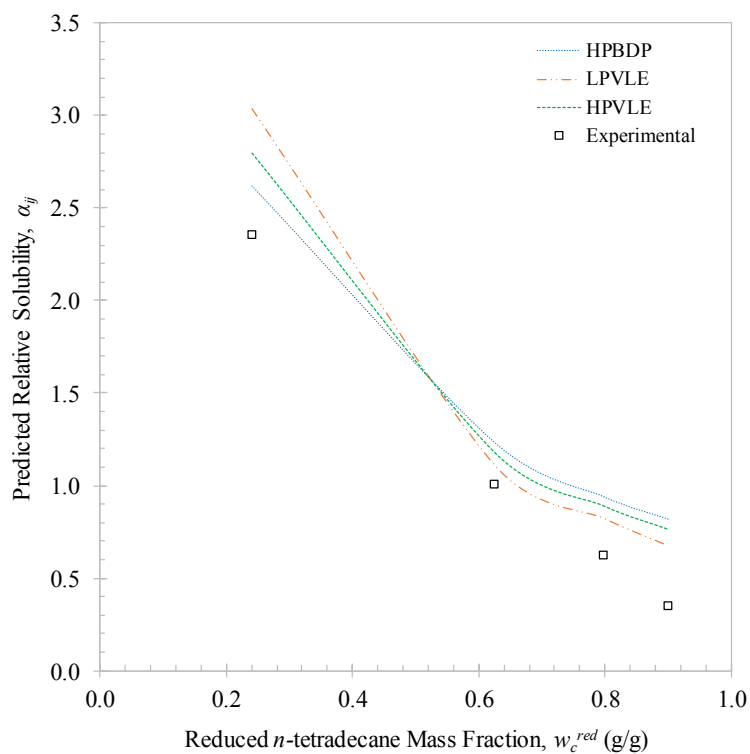


FIGURE 8- 7: PREDICTED $w_c^{RED}-A_{IJ}$ TRENDS FOR THE RK-ASPEN MODEL WITH HPBDP, HPVLE AND LPVLE BIPs COMPARED TO EXPERIMENTAL A_{IJ} VALUES AT CONSTANT $T = 328\text{ K}$ AND $P = 11.1\text{ MPa}$.

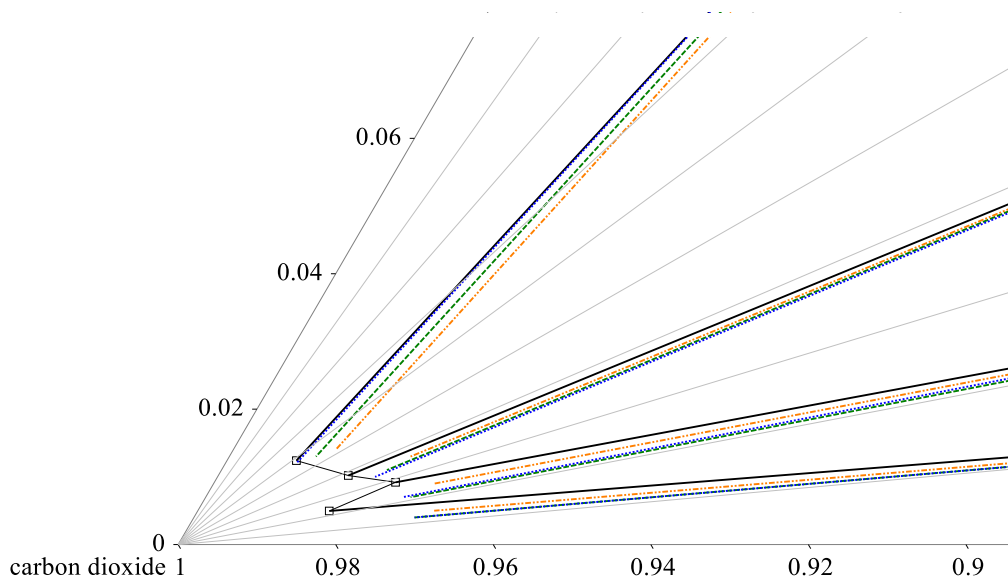


FIGURE 8- 8: VAPOUR PHASE DETAIL FOR $\text{CO}_2 + 1\text{-DECANOL} + N\text{-TETRADECANE}$ PREDICTED TIE LINES WITH THE RK-ASPEN MODEL USING HPBDP BIPs; HPVLE BIPs; AND, LPVLE SOLUTE + SOLUTE BIPs COMPARED TO EXPERIMENTAL TIE LINES AT CONSTANT $T = 328\text{ K}$ AND $P = 11.1\text{ MPa}$.

8.1.2. SR-POLAR

The SR-Polar model was investigated with the three solute + solute BIPs sets to evaluate their accuracy in correlating HPBDP data (*Figure 8-9*). The HPBDP and the HPVLE BIPs for SR-Polar are not as similar in magnitude as that seen for RK-Aspen, especially the $k_{b,ij}^0$ parameters at 0.12 and 0.07589, respectively. As expected, the HPBDP BIPs curves lie above the HPVLE BIPs curves (*Figure 8-9*) which agrees with *Figure 7-11 (a)*. However, the shift between the two curves within the bubble-point region were much smaller than anticipated and were almost non-existent within the dew-point region. It is postulated that this occurred because the effects of the three, pure component, polar parameters within the SR-Polar algorithm overpowered those of the BIPs.

For the LPVLE BIPs, where $k_{b,ij}^0$ is zero and $k_{a,ij}^0 = 0.05820$, the $P-w_s$ curves have been shifted horizontally downwards, and vertically inwards, again in agreement with *Figure 7-11 (b)*. It is particularly interesting to note that the shift of the LPVLE curves were much more prominent than the HPVLE and HPBDP curves. This finding indicates that, by only considering the attractive forces in the system ($k_{a,ij}^0$) the polar parameters are not sufficient to still allow for an accurate overall model fit.

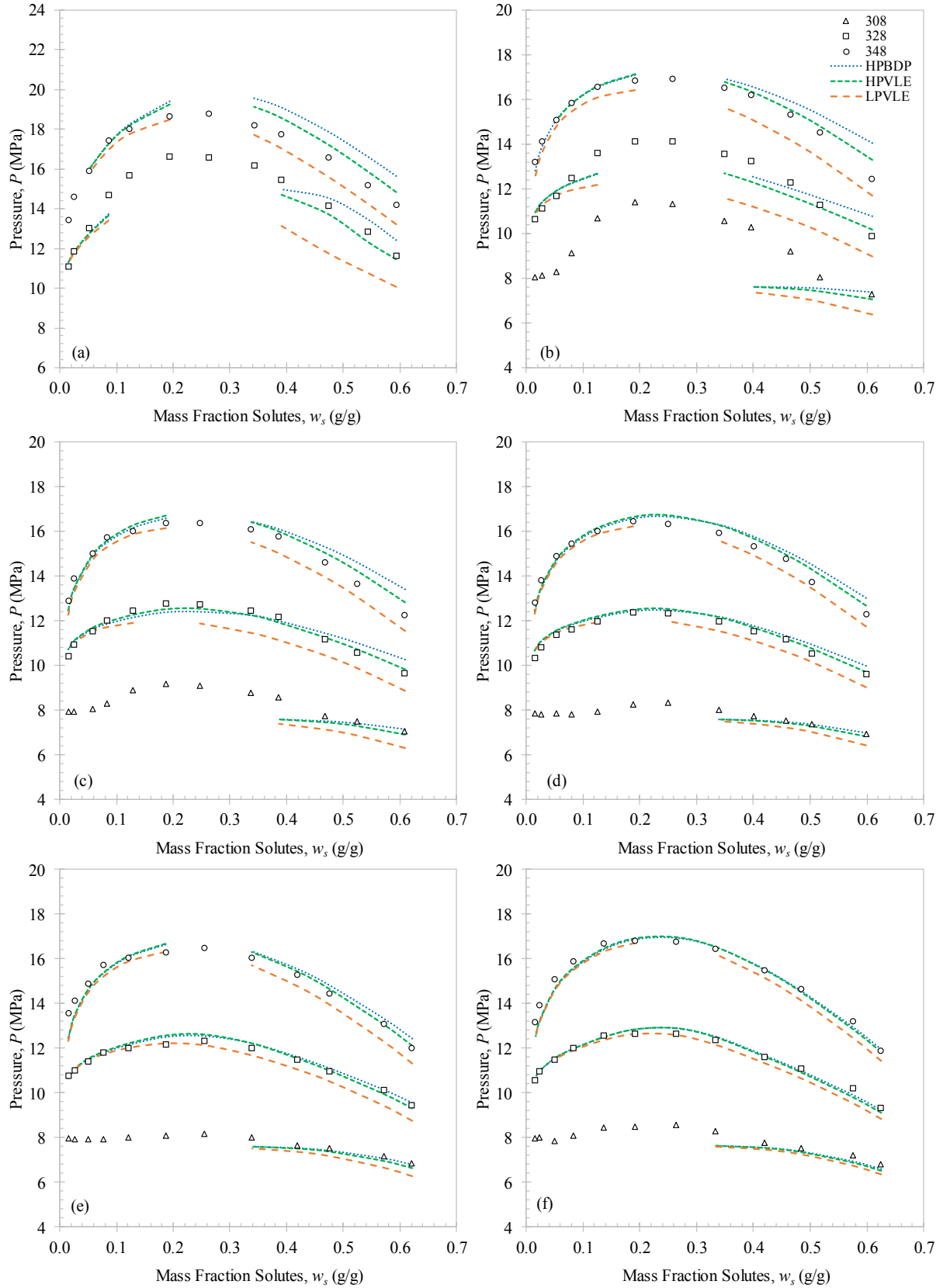


FIGURE 8- 9: SR-POLAR MODEL CORRELATIONS OF THE HPBDP DATA (WITH VARYING SOLUTE + SOLUTE BIPs) AT $T = 308$ K, 328 K AND 348 K FOR (A) $w_c^{RED} = 0.2405$ G/G; (B) $w_c^{RED} = 0.5000$ G/G; (C) $w_c^{RED} = 0.6399$ G/G; (D) $w_c^{RED} = 0.7698$ G/G; (E) $w_c^{RED} = 0.8162$ G/G; AND (F) $w_c^{RED} = 0.9200$.

The qualitative findings were confirmed by determining the $\%AAD$ between the measured and calculated values for the phase transition pressures (see *Figure 8-10*). Two solute + solute BIPs are thus required to ensure the correlations remain within 3% of the actual experimental data (*Figure 8-10 (a)*). However, this was only the case for the bubble-point region of the HPBDP data; for the dew-point region, the HPBDP, HPVLE and LPVLE BIPs ensured accurate representations within 1.81%, 1.83% and 1.92%, respectively (*Figure 8-10 (b)*). It is postulated that this occurred due to not enough solute molecules being present within the mixture to allow for significant solute + solute interactions to take place, making the model purely dependent on the quality of the polar parameters.

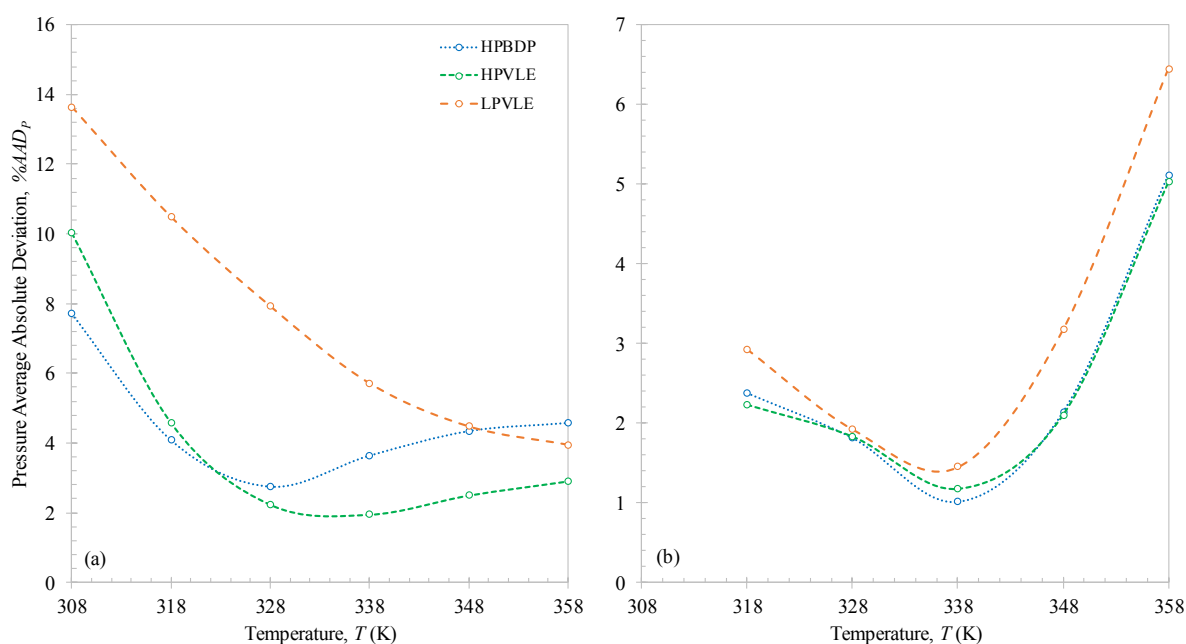


FIGURE 8- 10: SR-POLAR $\%AAD_P$ CALCULATED FOR (A) BUBBLE-POINT CORRELATIONS AND (B) DEW-POINT CORRELATIONS, WITH ALTERNATING SOLUTE + SOLUTE BIPs. MODEL FAILED TO CORRELATE DEW-POINT PRESSURE DATA AT $T=308$ K.

Like RK-Aspen, the shift between the three model correlations decreased with an increase in w_c^{red} (*Figure 8-9 (d) to (f)*). However, unlike RK-Aspen the HPVLE BIPs represent the bubble-point trends of the 1-decanol-rich mixtures more accurately than the HPBDP BIPs (*Figure 8-9 (a)*). Similar qualitative model results are seen for the HPVLE data within the 1-decanol-rich region (*Figure 8-11* and *Figure 8-12*). For the quantitative evaluation of the BIPs in representing the HPVLE data the $\%AAD_{w_s}$ between measured and calculated solute compositions were determined and are shown in *Figure 8-13*.

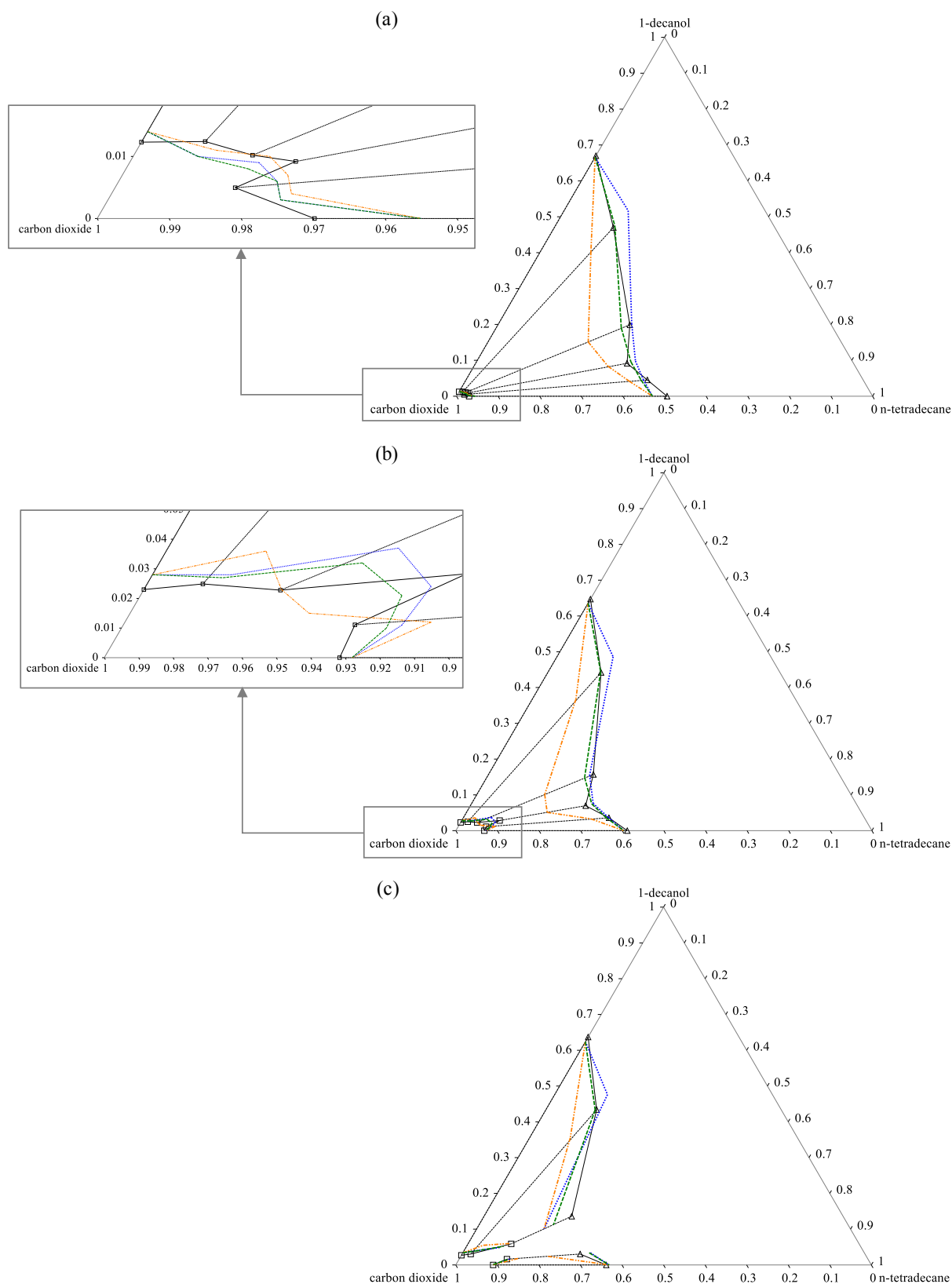


FIGURE 8- 11: SR-POLAR MODEL CORRELATIONS OF THE HPVLE DATA WITH: HPBDP BIPs; --- HPVLE BIPs; AND, -.- LPVLE SOLUTE + SOLUTE BIPs AT $T = 328$ K AND (A) $P = 11.1$ MPa; (B) $P = 12.0$ MPa; AND (C) $P = 12.4$ MPa.

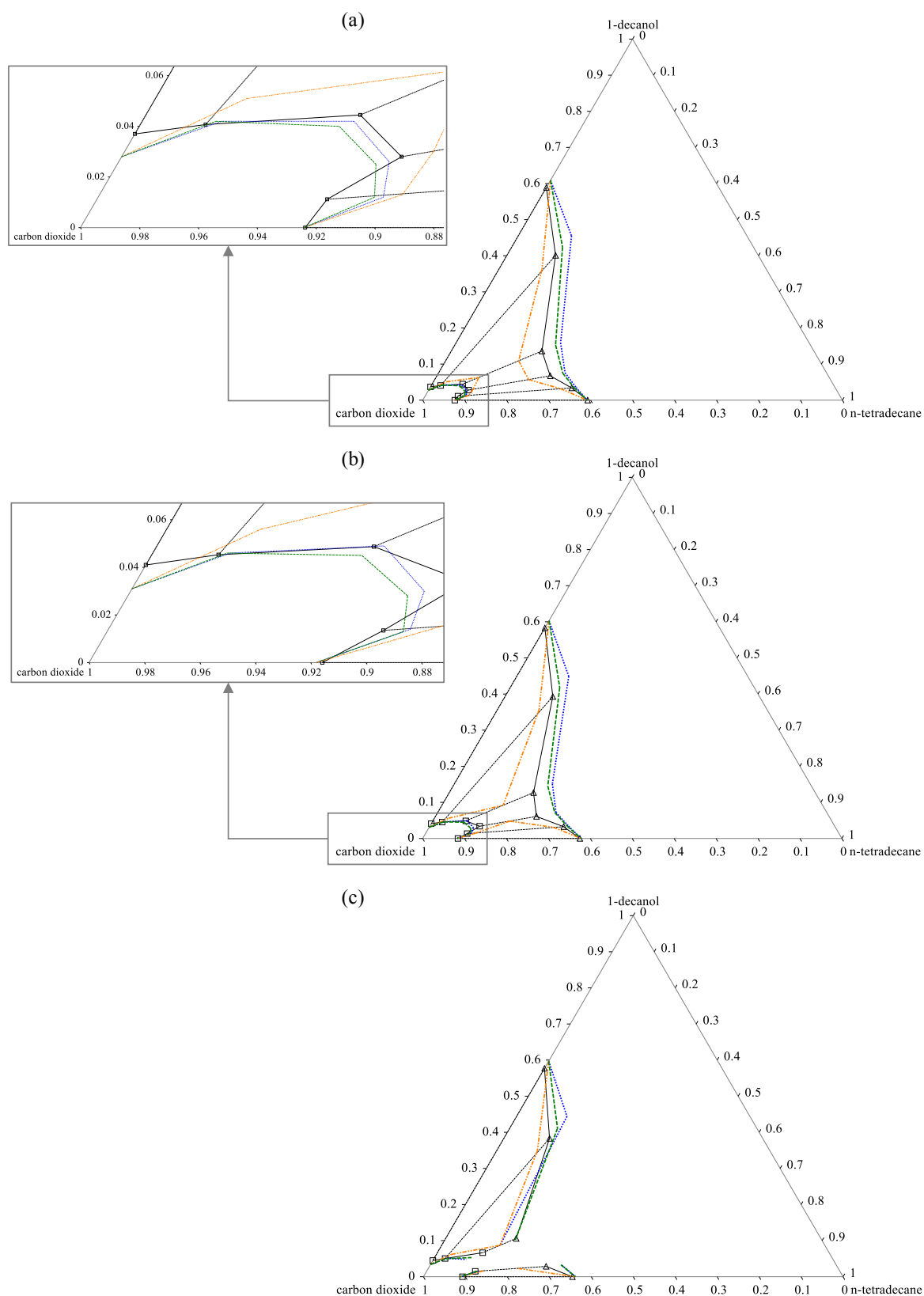


FIGURE 8- 12: SR-POLAR MODEL CORRELATIONS OF THE HPVLE DATA WITH: HPBDP BIPs; - - - HPVLE BIPs; AND, LPVLE SOLUTE + SOLUTE BIPs AT $T = 348$ K AND (A) $P = 16.0$ MPa; (B) $P = 16.2$ MPa; AND (C) $P = 16.4$ MPa.

Once again, the use of one BIP ($k_{a,ij}^0$) is not sufficient to capture the true solute + solute interactions occurring within the complex phase behaviour region. At $T = 328$ K (*Figure 8-11*), the LPVLE BIPs resulted in overly CO₂-rich liquid phases ($\%AAD_{ws} = 17.62\%$) and CO₂-deficient vapour phases ($\%AAD_{ws} = 25.28\%$), thereby overestimating the solubility enhancement. Lastly, the effects of temperature on the optimum BIPs agree for both the HPBDP (*Figure 8-10 (b)*) and HPVLE data (*Figure 8-11*). At $T = 328$ K, where SFF processes are of most significance, and only considering the dew-point region (HPBDP) or the vapour phase envelope (HPVLE) correlations the following relative performances are observed qualitatively and quantitatively:

HPBDP \approx HPVLE $>$ LPVLE

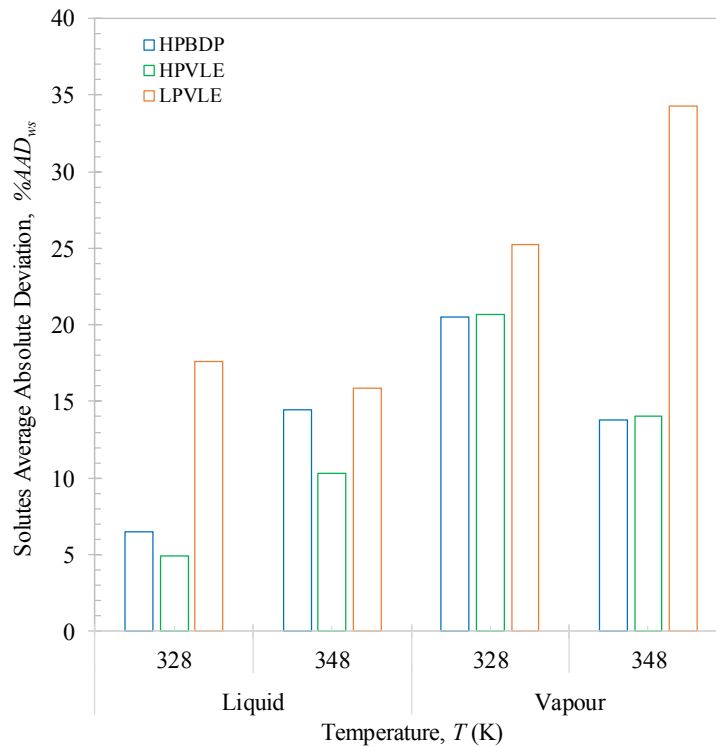


FIGURE 8- 13: SR-POLAR $\%AAD_{ws}$ FOR SOLUTE VAPOUR AND LIQUID COMPOSITION CORRELATIONS, WITH ALTERNATING SOLUTE + SOLUTE BIPs. MODEL FAILED TO CORRELATE EXPERIMENTAL DATA AT $T = 308$ K.

The predicted HPVLE data for each SR-Polar solute + solute BIPs set were used to evaluate how well the model captures the experimental co-existing phases. Average predicted α_{ij} values of 1.2 were calculated for SR-Polar with HPVLE and LPVLE BIPs (same as that of RK-Aspen); however, an average predicted α_{ij} value of 1.3 was obtained for SR-Polar with the HPBDP BIPs. The effects of this slight increase in α_{ij} could be evaluated using qualitative comparisons:

- (i) The predicted α_{ij} values at constant T and w_c^{red} , shown in *Figure 8-14*.
- (ii) The predicted α_{ij} values at constant T and P , shown in *Figure 8-15*.
- (iii) The predicted tie lines of the HPVLE data at constant T and P , shown in *Figure 8-16*.

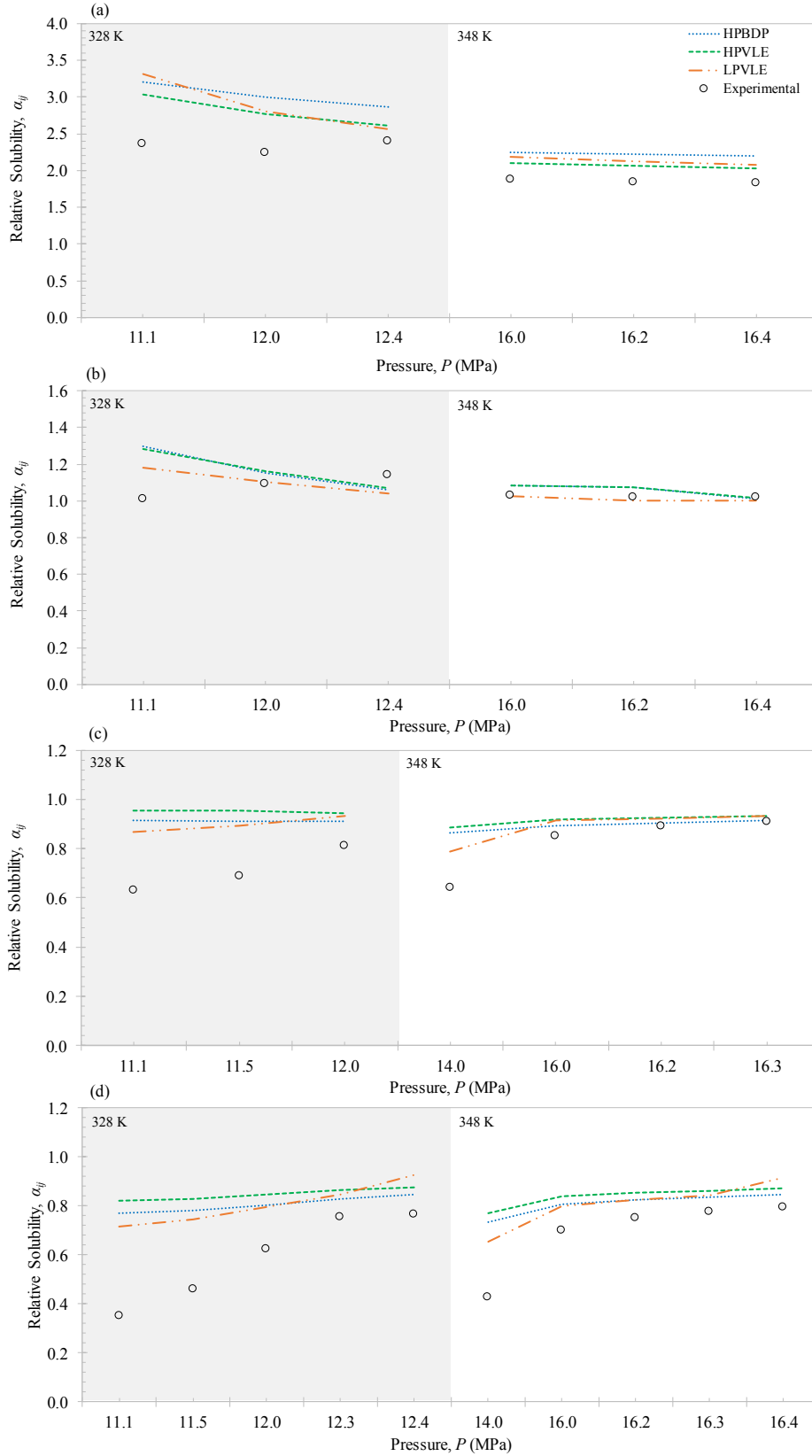


FIGURE 8- 14: PREDICTED P - A_{IJ} TRENDS FOR THE SR-POLAR MODEL WITH HPBDP, HPVLE AND LPVLE BIPs COMPARED TO EXPERIMENTAL P - A_{IJ} VALUES AT CONSTANT $T = 328$ K OR $T = 348$ K AND (A) $w_c^{RED} = 0.2403$ G/G; (B) $w_c^{RED} = 0.6245$ G/G; (C) $w_c^{RED} = 0.7979$ G/G; AND (D) $w_c^{RED} = 0.9004$ G/G.

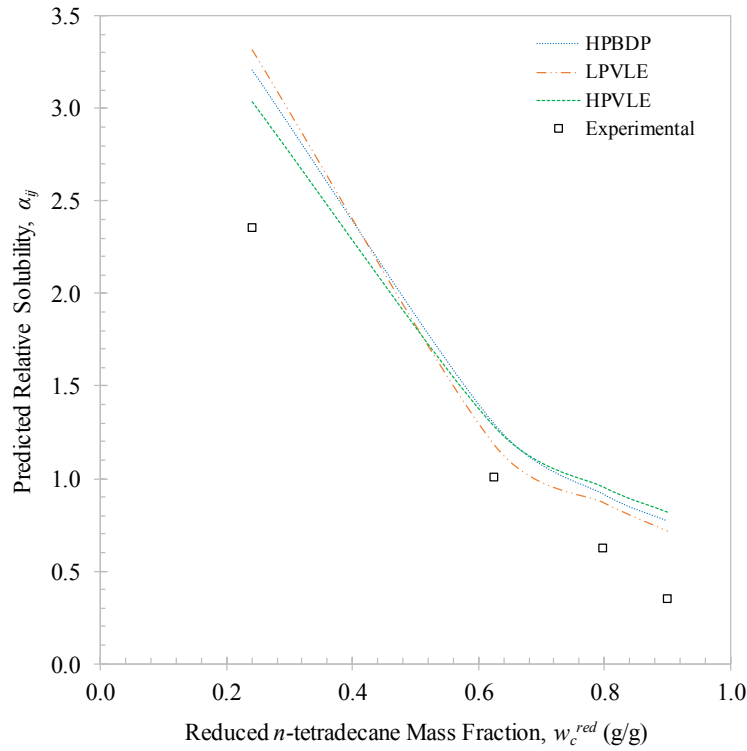


FIGURE 8- 15: PREDICTED $w_c^{RED} - A_{IJ}$ TRENDS FOR THE SR-POLAR MODEL WITH HPBDP, HPVLE AND LPVLE BIPs COMPARED TO EXPERIMENTAL A_{IJ} VALUES AT CONSTANT $T = 328\text{ K}$ AND $P = 11.1\text{ MPa}$.

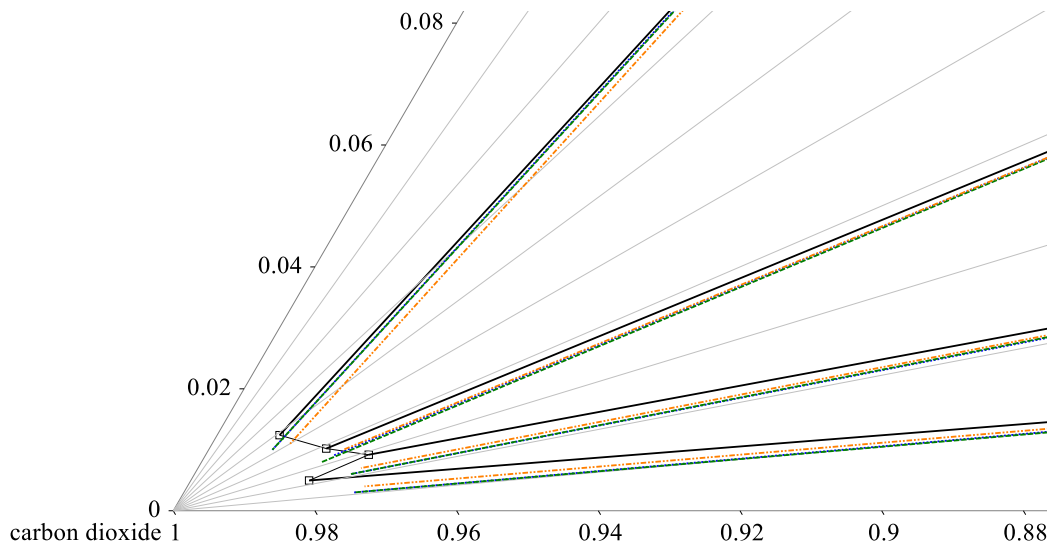


FIGURE 8- 16: VAPOUR PHASE DETAIL FOR $\text{CO}_2 + 1\text{-DECANOL} + \text{N-TETRADECANE}$ PREDICTED TIE LINES WITH THE SR-POLAR MODEL USING: HPBDP BIPs; --- HPVLE BIPs; AND, --- LPVLE SOLUTE + SOLUTE BIPs COMPARED TO EXPERIMENTAL TIE LINES AT CONSTANT $T = 328\text{ K}$ AND $P = 11.1\text{ MPa}$.

For HPVLE and LPVLE, the same qualitative conclusions as those derived for the RK-Aspen model are shown. However, for HPBDP, it is particularly interesting to note that the degree to which the compositional dependence is captured deteriorated for the $w_c^{red} = 0.2403\text{ g/g}$ and $w_c^{red} = 0.6245\text{ g/g}$ mixtures; and improved for the $w_c^{red} = 0.7979\text{ g/g}$ and $w_c^{red} = 0.9004\text{ g/g}$ mixtures.

8.1.3. PC-SAFT

The quality of the BIPs in representing the HPBDP data were evaluated by determining the $\%AAD_P$ between the measured and calculated values for the phase transition pressures (see *Figure 8-17*). The bubble- and dew-point $\%AAD_P$ values for PC-SAFT are both negatively correlated with temperature, decreasing significantly from 19.52% ($T = 308$ K) and 7.35% ($T = 328$ K) to 8.01% ($T = 358$ K) and 4.61% ($T = 358$ K), respectively. This may be because of the temperature dependent forces diminishing, i.e. polar and association, and the molecules behaving more non-polar.

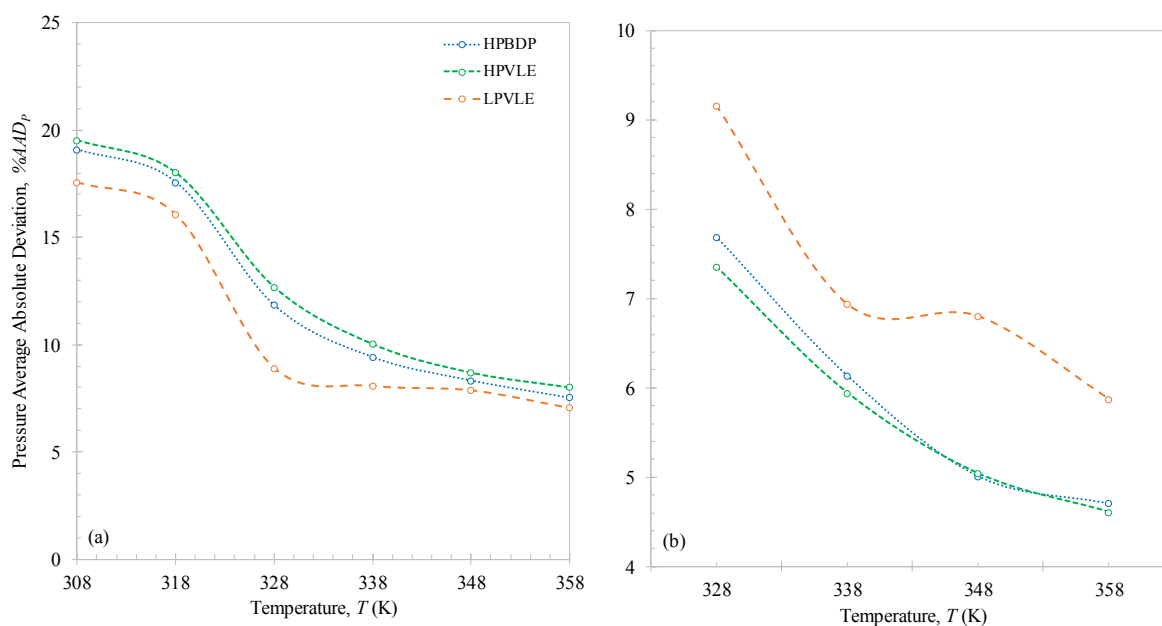


FIGURE 8- 17: PC-SAFT $\%AAD_P$ CALCULATED FOR (A) BUBBLE-POINT CORRELATIONS AND (B) DEW-POINT CORRELATIONS, WITH ALTERNATING SOLUTE + SOLUTE BIPs. MODEL FAILED TO CORRELATE DEW-POINT PRESSURE DATA AT $T = 308$ K AND $T = 318$ K.

The PC-SAFT model was further investigated qualitatively with the three solute + solute BIPs to evaluate their accuracy in correlating HPBDP data (*Figure 8-18*). The HPBDP (0.04) and the HPVLE (0.04454⁹) BIPs for PC-SAFT are very similar in magnitude. As a result, the correlations with HPBDP and HPVLE BIPs are almost identical and the model can be assumed to be independent of the type of high-pressure data used. The slightly smaller LPVLE BIP (0.02467) improves the bubble-point fit of the model, however, no visible effect on the dew-point data is seen. Lastly, it is well known that PC-SAFT deteriorates near the critical region and predicts too-high concentrations of CO₂ [57]. This was again the case here with the model overpredicting the phase transition pressures (*Figure 8-18*).

⁹ Decreasing the number of significant figures will provide the same k_{ij}^0 value as the HPBDP data (≈ 0.04).

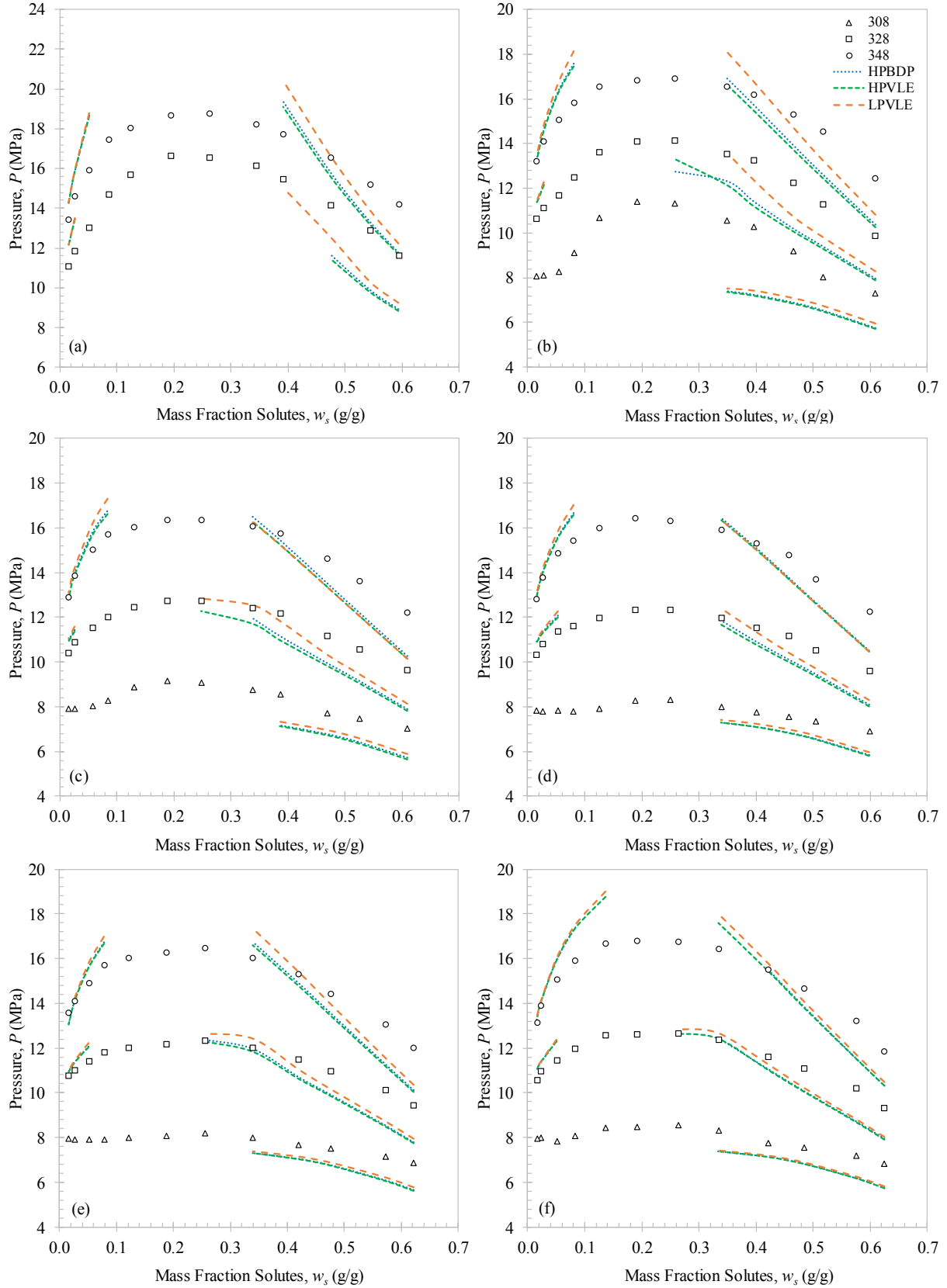


FIGURE 8- 18: PC-SAFT MODEL CORRELATIONS OF THE HPBDP DATA (WITH VARYING SOLUTE + SOLUTE BIPs) AT $T = 308$ K, 328 K AND 348 K FOR (A) $w_c^{RED} = 0.2405$ G/G; (B) $w_c^{RED} = 0.5000$ G/G; (C) $w_c^{RED} = 0.6399$ G/G; (D) $w_c^{RED} = 0.7698$ G/G; (E) $w_c^{RED} = 0.8162$ G/G; AND (F) $w_c^{RED} = 0.9200$.

With respect to the HPVLE data correlations shown in *Figure 8-19* and *Figure 8-20*, PC-SAFT can capture the liquid phase trend to some extent at $T = 348$ K (*Figure 8-20*). This is somewhat expected, since the system is influenced greatly by molecular association and this model explicitly accounts for them, i.e. the Wertheim's association term [110], [181], [255] (Chapter 3, section 3.6). However, problems with the model are still encountered in representing the vapour phase composition data (*Figure 8-19* and *Figure 8-20*). The qualitative results are confirmed with the $\%AADw_s$ values calculated for PC-SAFT (see *Figure 8-21*). The $\%AADw_s$ values calculated for the liquid phase at $T = 328$ K and $T = 348$ K are approximately one-half of those obtained from the vapour phase.

The shortcomings in the model could originate from the polar forces that are not explicitly accounted for in the ternary system. The concentration of hydrogen bonding segments in each mixture are high and lead to hydrogen bond co-operativity forming [174], [256]–[258]. Wertheim's association term cannot account for these effects which have led to the poor CO₂-rich model correlations.

The following factors are postulated to be cause for the poor representations at $T = 328$ K (*Figure 8-19*):

- (i) Cross-association [197].
- (ii) Steric hindrances in hydrogen bonding.
- (iii) The influence of mixture composition with respect to the number of bonding sites on molecules [201].

It is particularly interesting to note that all three sets of BIPs can produce the s-shaped curve within the complex phase behaviour region of the system. This finding is contradicting to the model correlations of a similar ternary system, CO₂ + 1-decanol + *n*-dodecane [19], [158]. Whether the improved correlations are attributed to the inclusion of the quadrupole moment of the CO₂ molecule can only be established if all the model factors remained the same, i.e. the temperature dependence and the components in the system. Quantitatively the HPBDP (*Figure 8-17*) and HPVLE (*Figure 8-21*) correlations agree. For the dew-point region/vapour phase compositions, at $T = 328$ K the following relative performances are observed qualitatively and quantitatively:

$$\text{HPBDP} \approx \text{HPVLE} > \text{LPVLE}$$

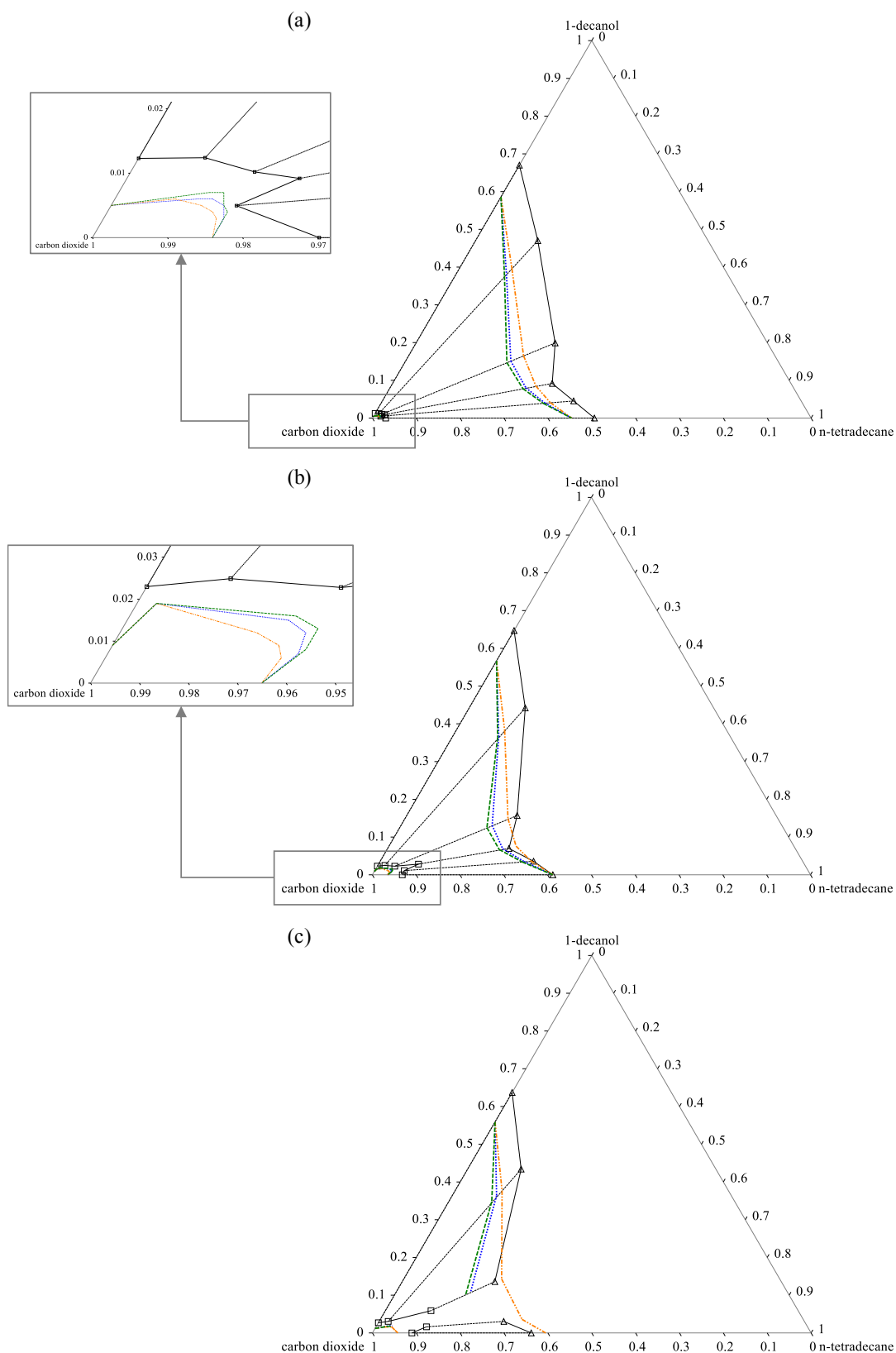


FIGURE 8- 19: PC-SAFT MODEL CORRELATIONS OF THE HPVLE DATA WITH: HPBDP BIPs; --- HPVLE BIPs; AND, -.-.- LPVLE SOLUTE + SOLUTE BIPs AT $T = 328$ K AND (A) $P = 11.1$ MPa; (B) $P = 12.0$ MPa; AND (C) $P = 12.4$ MPa.

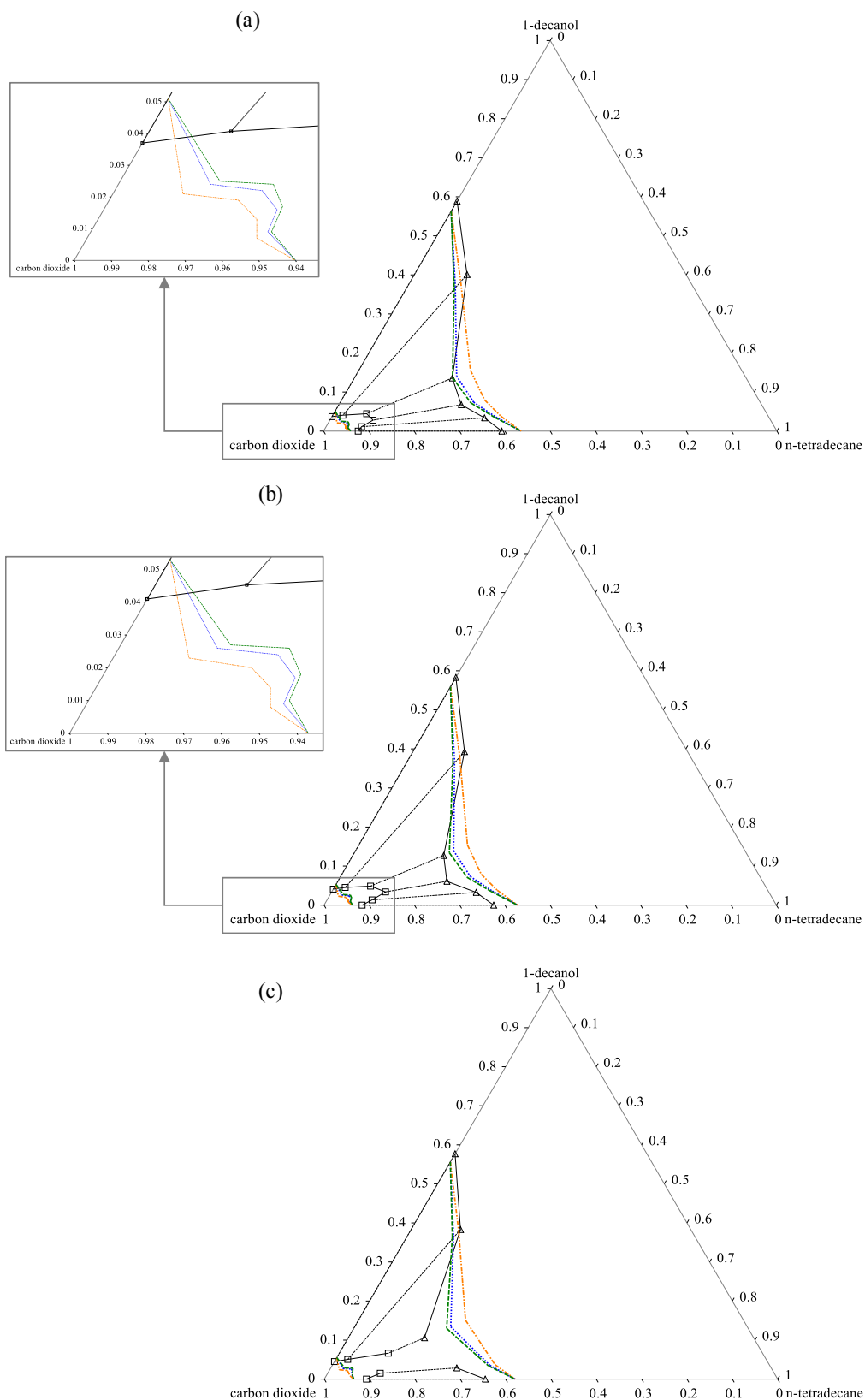


FIGURE 8-20: PC-SAFT MODEL CORRELATIONS OF THE HPVLE DATA WITH: HPBDP BIPs; --- HPVLE BIPs; AND, -.- LPVLE SOLUTE + SOLUTE BIPs AT $T = 348$ K AND (A) $P = 16.0$ MPa; (B) $P = 16.2$ MPa; AND (C) $P = 16.4$ MPa.

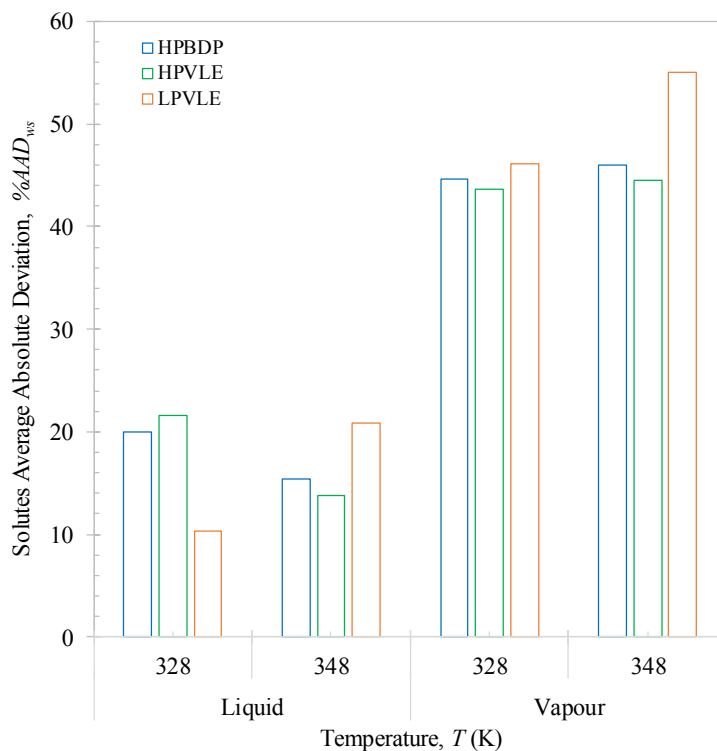


FIGURE 8- 21: PC-SAFT %AAD_{ws} FOR SOLUTE VAPOUR AND LIQUID COMPOSITION CORRELATIONS, WITH ALTERNATING SOLUTE + SOLUTE BIPs. MODEL FAILED TO CORRELATE EXPERIMENTAL DATA AT $T = 308$ K.

The average predicted α_{ij} values of HPBDP (1.6), HPVLE (1.6) and LPVLE (1.5) are slightly higher than those shown for RK-Aspen and SR-Polar. The higher values infer that the model will best capture mixtures where the solubility of *n*-tetradecane is favoured, more specifically for this study, the $w_c^{red} = 0.7979$ g/g and $w_c^{red} = 0.9004$ g/g mixtures. This assumption can be confirmed to some extent with a qualitative analysis of the predicted α_{ij} values at constant T and w_c^{red} , shown in *Figure 8-22*. For the $w_c^{red} = 0.2403$ g/g mixture (*Figure 8-22 (a)*) the model overestimates the experimental α_{ij} values completely. However, with an increase in *n*-tetradecane concentration to $w_c^{red} = 0.6245$ g/g or $w_c^{red} = 0.7979$ g/g reasonable agreement between the model and experimental α_{ij} values are seen (*Figure 8-22 (b)* and (*c*)). It is particularly interesting to note that with a further increase in the *n*-tetradecane concentration, to $w_c^{red} = 0.9004$ g/g, the model underestimates the experimental α_{ij} values (*Figure 8-22 (d)*).

How well the model can describe the split between the two phases was further evaluated using the predicted α_{ij} values (*Figure 8-23*) and predicted tie lines of the HPVLE data (*Figure 8-24*) at constant T and P . Like RK-Aspen and SR-Polar, the predicted α_{ij} values showed a negative correlation with increasing w_c^{red} at constant T and P (see *Figure 8-23* as an example at $T = 328$ K and $P = 11.1$ MPa). Furthermore, the inability of PC-SAFT to capture the HPVLE vapour phase composition of the $w_c^{red} = 0.2403$ g/g mixture is amplified in the predicted compositions of the co-existing phases at constant T and P (see *Figure 8-24*).

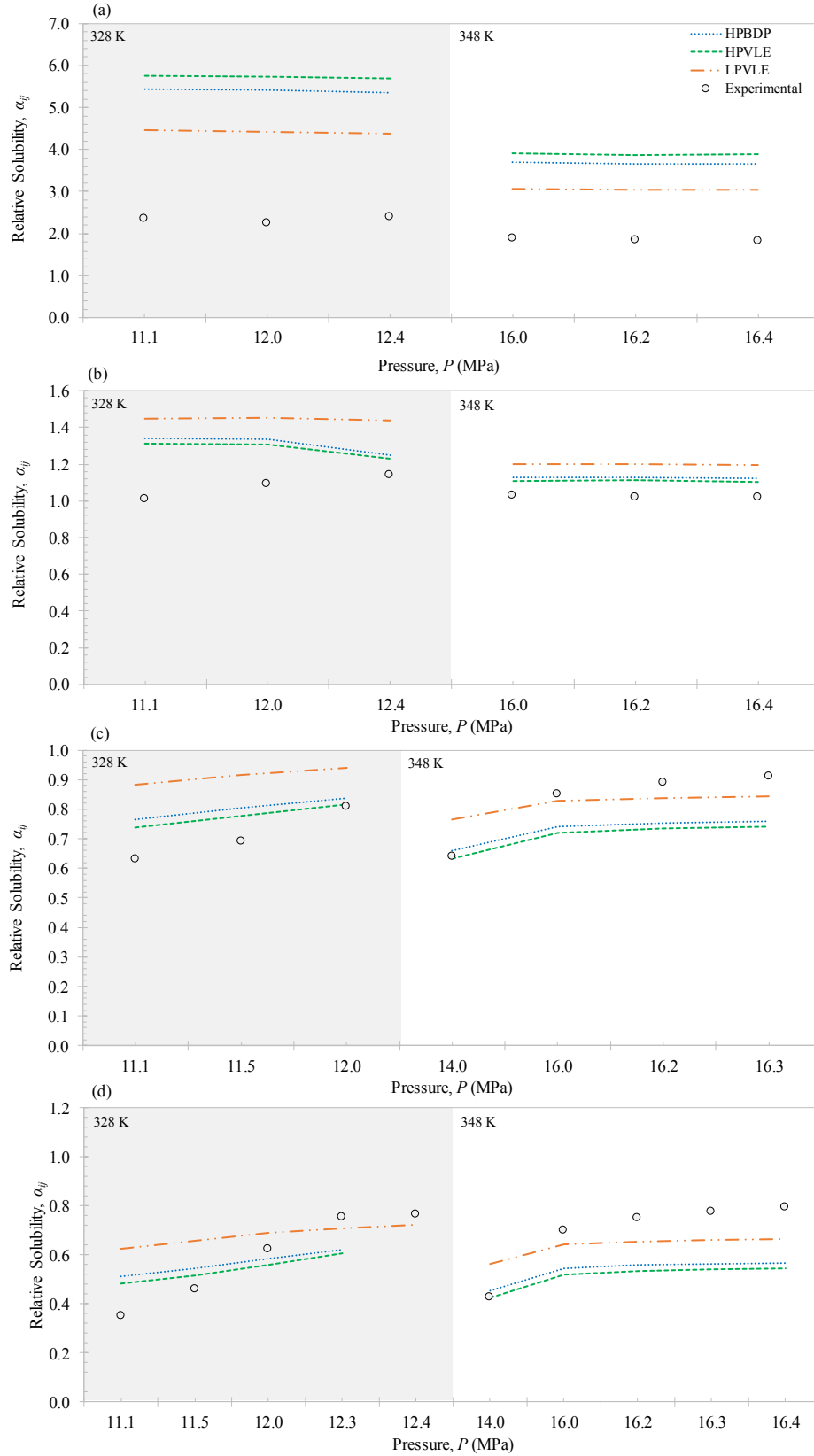


FIGURE 8- 22: PREDICTED $P-A_{IJ}$ TRENDS FOR THE PC-SAFT MODEL WITH HPBDP, HPVLE AND LPVLE BIPs COMPARED TO EXPERIMENTAL $P-A_{IJ}$ VALUES AT CONSTANT $T = 328\text{ K}$ OR $T = 348\text{ K}$ AND (A) $w_c^{RED} = 0.2403\text{ G/G}$; (B) $w_c^{RED} = 0.6245\text{ G/G}$; (C) $w_c^{RED} = 0.7979\text{ G/G}$; AND (D) $w_c^{RED} = 0.9004\text{ G/G}$.

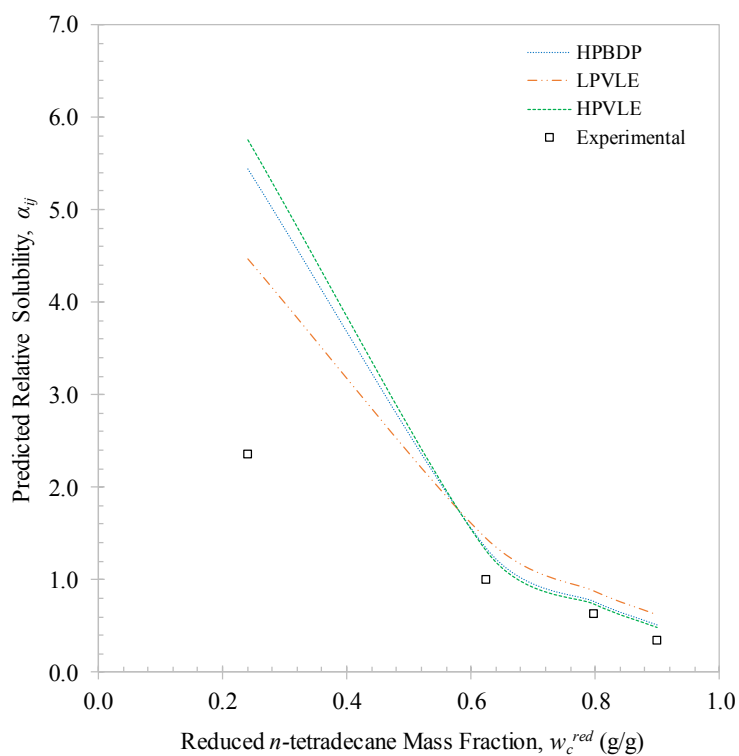


FIGURE 8- 23: PREDICTED $w_c^{RED}-A_{IJ}$ TRENDS FOR THE PC-SAFT MODEL WITH HPBDP, HPVLE AND LPVLE BIPs COMPARED TO EXPERIMENTAL A_{IJ} VALUES AT CONSTANT $T = 328\text{ K}$ AND $P = 11.1\text{ MPa}$.

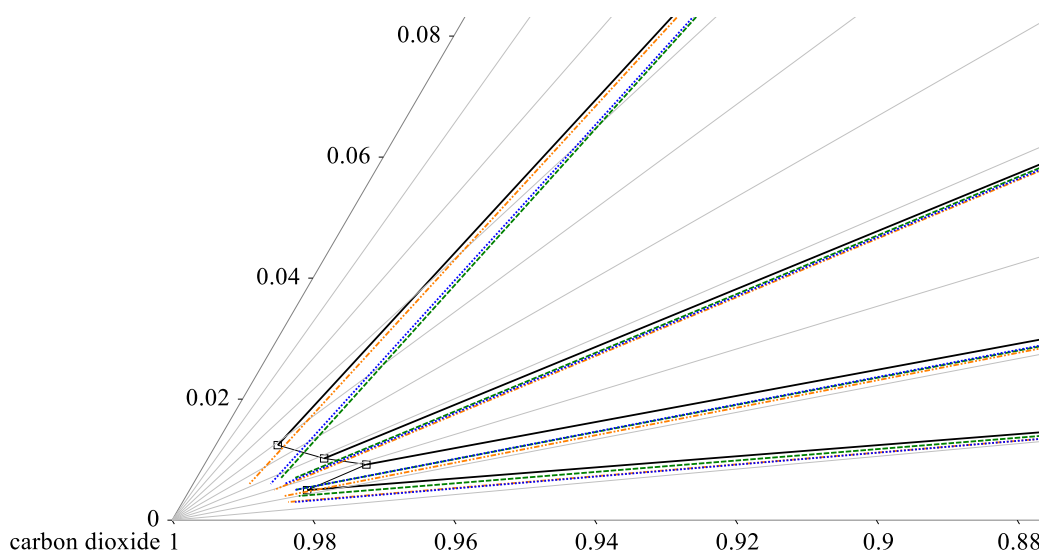


FIGURE 8- 24: VAPOUR PHASE DETAIL FOR $\text{CO}_2 + 1\text{-DECANOL} + \text{N-TETRADECANE}$ PREDICTED TIE LINES WITH THE SR-POLAR MODEL USING: HPBDP BIPs; --- HPVLE BIPs; AND, -.- LPVLE SOLUTE + SOLUTE BIPs COMPARED TO EXPERIMENTAL TIE LINES AT CONSTANT $T = 328\text{ K}$ AND $P = 11.1\text{ MPa}$.

8.1.4. PSRK

The PSRK model was investigated to evaluate its ability to *predict*:

- (i) HPBDP data (*Figure 8-25*).
- (ii) HPVLE data (*Figure 8-26*).
- (iii) The tie lines (compositional dependence) at constant T and P (*Figure 8-27*).
- (iv) The relative solubility at constant T and P (*Figure 8-28*).
- (v) The relative solubility at constant T and w_c^{red} (*Figure 8-29*).

With respect to *Figure 8-25*, PSRK strictly enforces the use of the linear mixing rule for the co-volume parameter, which limited the accuracy of the predictions, especially in the bubble-point region of the HPBDP data. Further exclusions occurred in the critical region of each mixture (*Figure 8-25*). However, of more importance to the success of SFF processes are the model's capabilities in predicting the dew-point region/vapour phase composition of the mixtures. PSRK showed remarkable results in predicting the dew-point HPBDP experimental data, especially for the mixtures within the complex phase behaviour region (*Figure 8-25 (d), (e) and (f)*).

Quantitatively, the PSRK results at $T = 328$ K are reasonably accurate in predicting the HPBDP data with bubble- and dew-point pressure deviations within 5.70% and 3.38%, respectively. Unfortunately, the same cannot be said for the HPVLE %AAD w_s values which were calculated at 19.4% and 34.1% for the liquid and vapour phase envelopes, respectively.

PSRK predictions of the HPVLE data (*Figure 8-26*) are too rich in solutes, i.e., lower CO₂ solubility, regardless of a change in temperature or pressure. Thus, the model is unable to capture the vapour or liquid phase transition curves nor predict the co-solubility pinch.

The model can to a certain degree predict the vapour phase composition of the $w_c^{red} = 0.2403$ g/g mixture (see *Figure 8-26*); which is also evident from the great predictability of the coexisting concentrations (tie line) of the $w_c^{red} = 0.2403$ g/g mixture shown in *Figure 8-27*. However, the compositional dependence of the complex phase behaviour region and the n -tetradecane-rich region could not be captured.

An average relative solubility of 1.6 was calculated from the PSRK predicted VLE data, much higher than the average experimental α_{ij} value of 1.1. The overestimation of the experimentally derived α_{ij} values are further evident from the w_c^{red} - α_{ij} correlations (*Figure 8-28*) and P - α_{ij} correlations (*Figure 8-29*). Apart from the $w_c^{red} = 0.2403$ g/g mixture, it is particularly interesting to note that the predicted α_{ij} values are negatively correlated with pressure, contradicting the positive P - α_{ij} correlations shown by the experimental results (*Figure 8-29*). Therefore, PSRK is unable to capture the trend of the data and the advantage of using regressed parameters with real data is prominent.

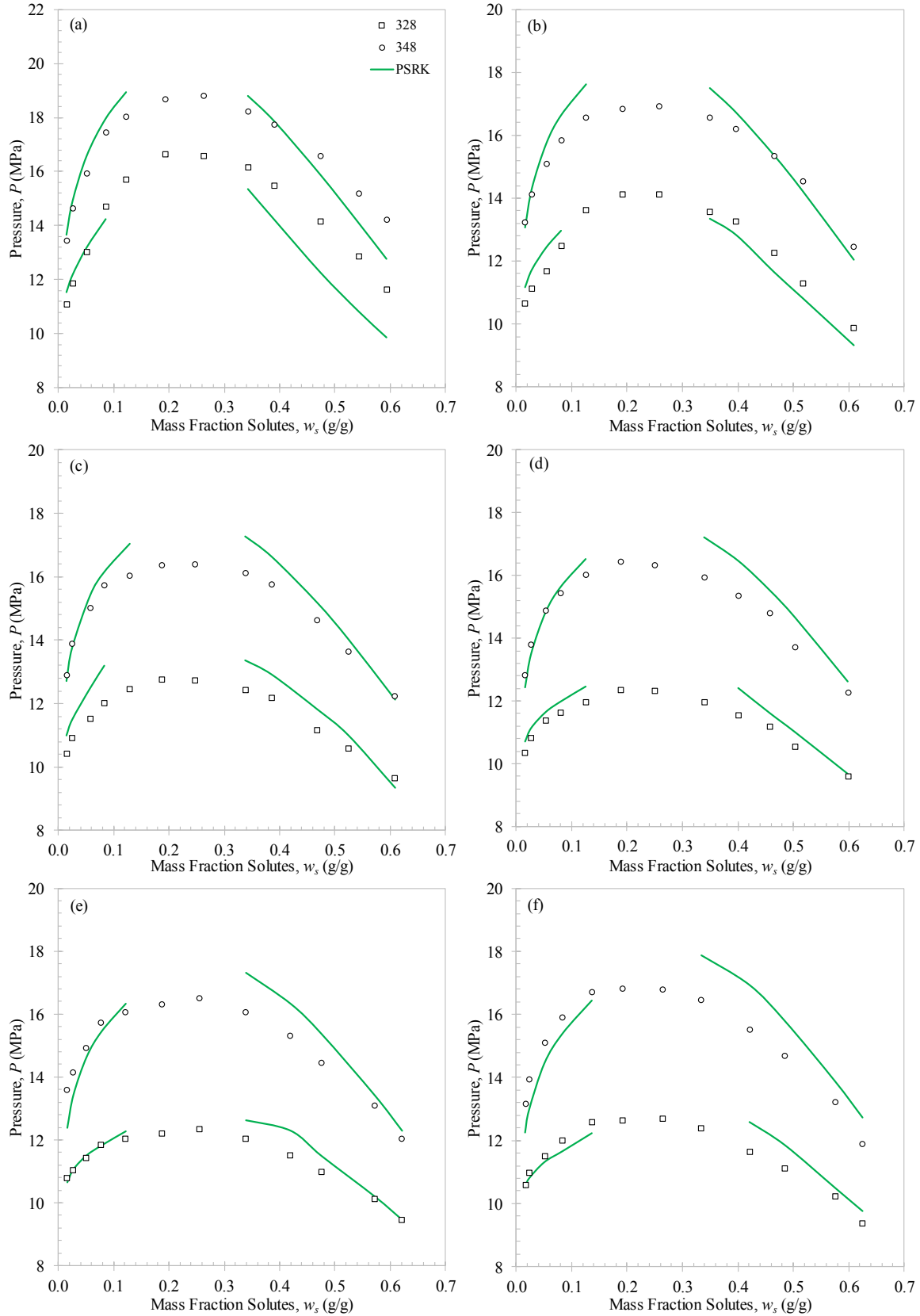


FIGURE 8- 25: PSRK MODEL CORRELATIONS OF THE HPBDP DATA AT $T = 328$ K AND $T = 348$ K FOR (A) $w_c^{RED} = 0.2405$ G/G; (B) $w_c^{RED} = 0.5000$ G/G; (C) $w_c^{RED} = 0.6399$ G/G; (D) $w_c^{RED} = 0.7698$ G/G; (E) $w_c^{RED} = 0.8162$ G/G; AND (F) $w_c^{RED} = 0.9200$.

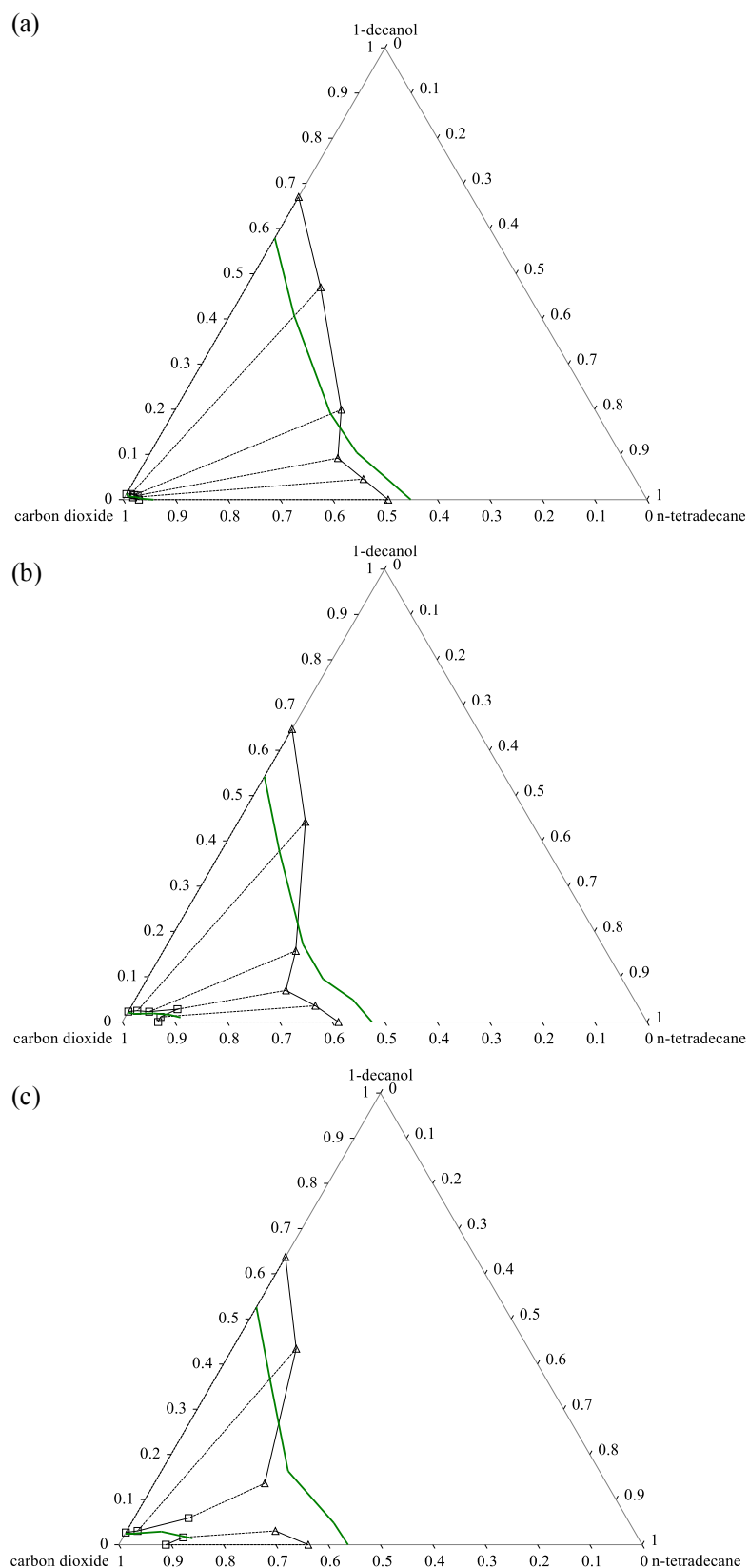


FIGURE 8- 26: PSRK MODEL CORRELATIONS OF THE HPVLE DATA AT $T = 328$ K AND (A) $P = 11.1$ MPa; (B) $P = 12.0$ MPa; AND (C) $P = 12.4$ MPa.

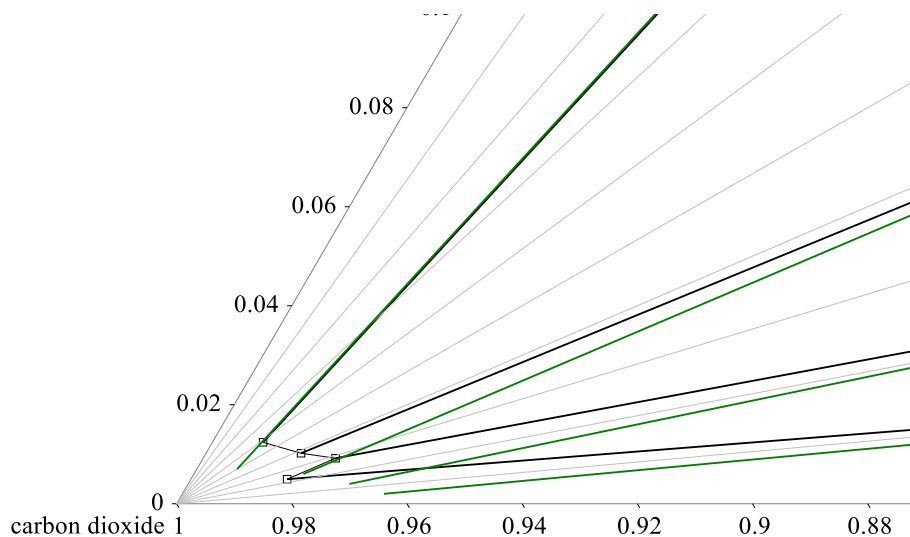


FIGURE 8- 27: VAPOUR PHASE DETAIL FOR $\text{CO}_2 + 1\text{-DECANOL} + n\text{-TETRADECANE}$ PREDICTED TIE LINES WITH THE PSRK MODEL COMPARED TO EXPERIMENTAL TIE LINES AT CONSTANT $T = 328 \text{ K}$ AND $P = 11.1 \text{ MPa}$.

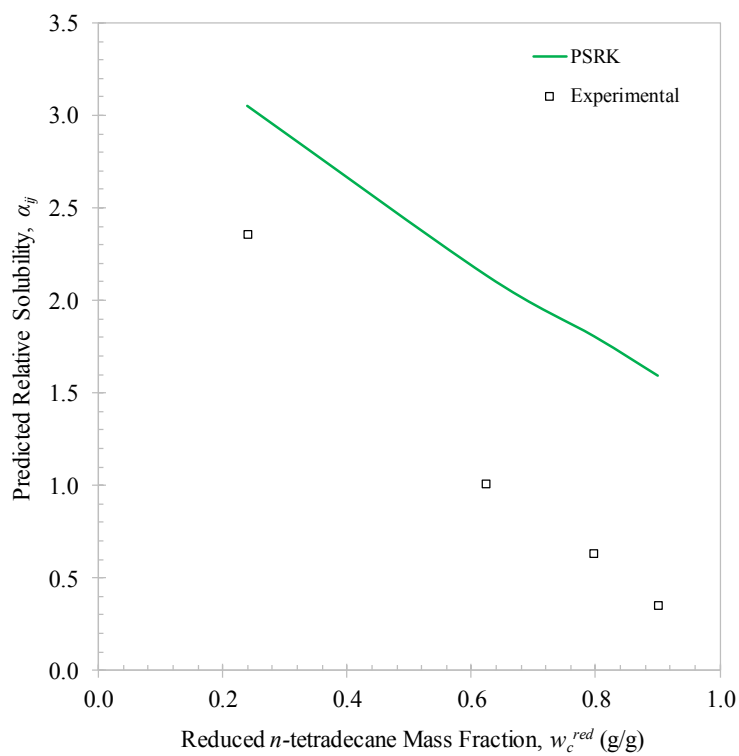


FIGURE 8- 28: PREDICTED $w_c^{\text{RED}} - A_M$ TRENDS FOR THE PSRK MODEL COMPARED TO EXPERIMENTAL A_M VALUES AT CONSTANT $T = 328 \text{ K}$ AND $P = 11.1 \text{ MPa}$.

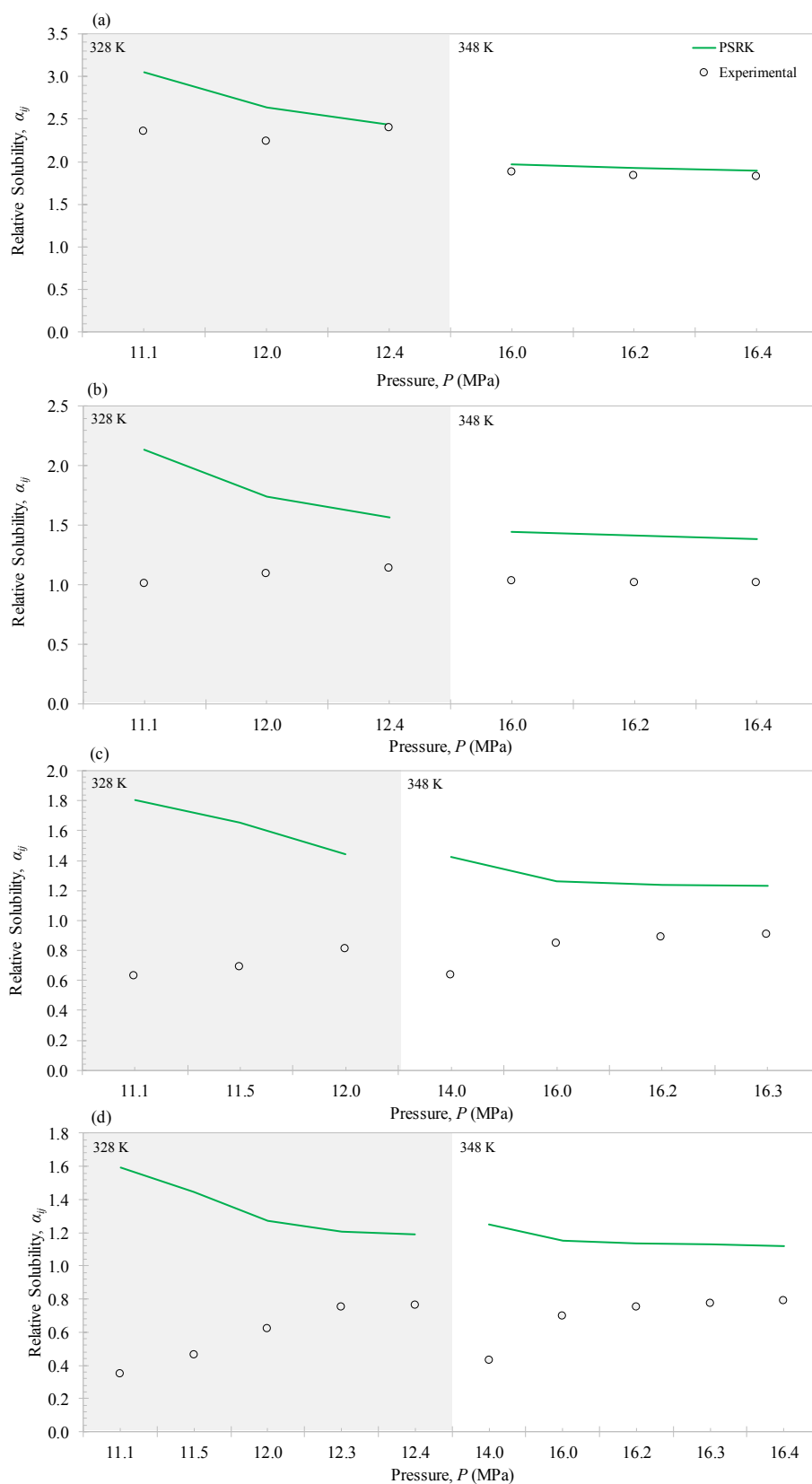


FIGURE 8- 29: PREDICTED P - a_{ij} TRENDS FOR THE PSRK MODEL COMPARED TO EXPERIMENTAL P - a_{ij} VALUES AT CONSTANT $T = 328$ K OR $T = 348$ K AND (A) $w_c^{RED} = 0.2403$ G/G; (B) $w_c^{RED} = 0.6245$ G/G; (C) $w_c^{RED} = 0.7979$ G/G; AND (D) $w_c^{RED} = 0.9004$ G/G.

8.2. LOW-PRESSURE PHASE BEHAVIOUR RESULTS

Model evaluation at low-pressure was conducted using experimental temperatures (from LPVLE data) as inputs to predict the equilibrium compositions of the binary 1-decanol + *n*-tetradecane liquid and vapour phases. These results are represented on T - x - y and x - y plots; and with the $\%AAD_{y_l}$ and $\%AAD_T$ values tabulated.

8.2.1. RK-ASPEN

The RK-Aspen model was further investigated with the three solute + solute BIPs to evaluate their accuracy in correlating LPVLE data (*Figure 8-30* and *Figure 8-31*). From the findings in section 7.2.3.2 the $k_{a,ij}^0$ solute + solute BIPs regressed for HPBDP and HPVLE with $k_{b,ij}^0 = 0$ might result in more accurate representations of the LPVLE data. It is for this reason that the following two scenarios were evaluated alongside the LPVLE BIP ($k_{a,ij}^0 = 0.05812$) in *Figure 8-30*:

- (i) (*Figure 8-17 (a)*) with HPVLE BIPs $\in \{k_{a,ij}^0 = 0.05963; k_{b,ij}^0 = 0.05548\}$ &
HPBDP BIPs $\in \{k_{a,ij}^0 = 0.06; k_{b,ij}^0 = 0.08\}$
- (ii) (*Figure 8-17 (b)*) with HPVLE BIPs $\in \{k_{a,ij}^0 = 0.02689; k_{b,ij}^0 = 0\}$ &
HPBDP BIPs $\in \{k_{a,ij}^0 = 0.04; k_{b,ij}^0 = 0\}$

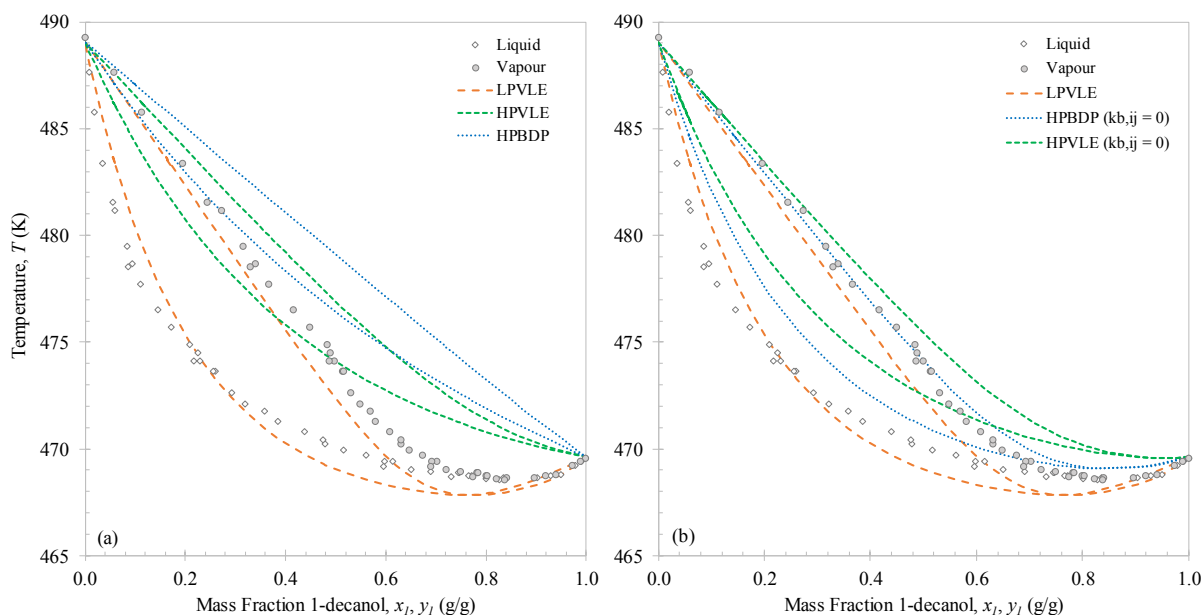


FIGURE 8- 30: RK-ASPEN MODEL CORRELATIONS OF THE T - x_1 - y_1 LPVLE DATA (WITH ALTERNATING SOLUTE + SOLUTE BIPs) AT $P = 40$ kPa. ADDITIONAL ALTERNATIONS MADE FOR HPVLE AND HPBDP BIPs: (A) SCENARIO I AND (B) SCENARIO II.

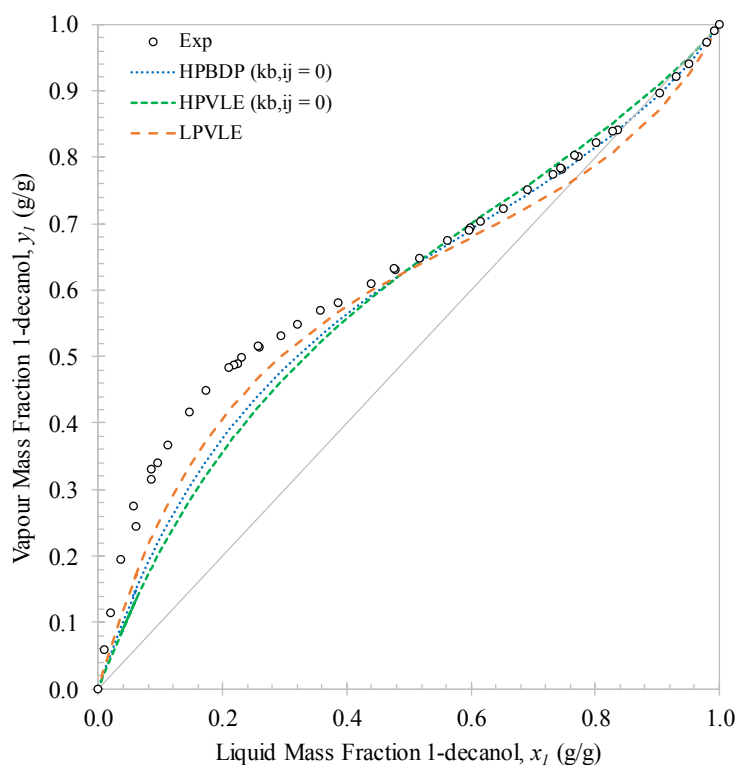


FIGURE 8- 31: RK-ASPEN MODEL CORRELATIONS OF THE x_1 - y_1 LPVLE DATA (WITH ALTERNATING SOLUTE + SOLUTE BIPs) AT $P = 40$ kPa. FOR HPVLE AND HPBDP, THE BIPs OF SCENARIO II ARE APPLIED TO INDICATE ACCURACY OF AZEOTROPIC POINT.

The azeotrope provides the most stringent test of the solute + solute BIPs influence in representing the LPVLE data accurately and will be used to identify the optimum scenario. The predicted azeotropic point for each set of BIPs is presented in *Table 8-1* along with the average deviations in 1-decanol vapour composition, y_1 and temperature, T .

TABLE 8- 1: RK-ASPEN AZEOTROPIC POINT, REPRESENTING THE EXPERIMENTAL DATA AND %AAD CALCULATED IN VAPOUR COMPOSITION, y_1 AND T OF THE 1-DECANOL (1) + *N*-TETRADECANE (2) BINARY SYSTEM.

<i>Solute + solute BIPs</i>	<i>Azeotropic Temperature (K)</i>	<i>Azeotropic composition (g/g)</i>	<i>%AAD_{y1}</i>	<i>%AAD_T</i>
Experimental	468.66	0.864	-	-
LPVLE	467.83	0.765	11.19	0.19
HPVLE Scenario (i)	NP*	NP*	18.19	0.77
Scenario (ii)	469.59	0.957	14.03	0.54
HPBDP Scenario (i)	NP*	NP*	21.88	1.08
Scenario (ii)	469.09	0.855	13.07	0.32

NP* - No azeotrope predicted

The HPVLE and HPBDP BIPs when including the $k_{b,ij}^0$ parameter (scenario (i)) are unable to predict the azeotrope and the overall representation of the phase behaviour is poor; this is reflected in the large deviations in y_1 and T in *Table 8-1*. It appears that the CO₂ molecules in the system might have an impact on the model outcome (due to their influence on the regressed $k_{b,ij}^0$ parameter) as the HPVLE

BIPs and HPBDP BIPs with $k_{b,ij}^0 = 0$ (scenario (ii)) can provide improved representations of the LPVLE data. The deviations of the high-pressure BIPs are predominantly in T as *Figure 8-31* shows the x - y data are still correlated well, especially within the 1-decanol-rich region. It is particularly interesting to note that an almost perfect representation of the azeotropic point, with respect to composition, is provided by the HPBDP BIPs (*Figure 8-31*). The large deviations in y_1 provided in *Table 8-1* are thus reflected in the poor correlations of the n -tetradecane-rich region. With reference to the BIPs used in scenario (ii) the following relative performance is observed in terms of the quality of the model fit to LPVLE data:

$$\text{HPBDP} > \text{LPVLE} > \text{HPVLE}$$

8.2.2. SR-POLAR

As with RK-Aspen, the following two scenarios were evaluated alongside the LPVLE BIP ($k_{a,ij}^0 = 0.05820$) in *Figure 8-32*:

- (i) (*Figure 8-19 (a)*) with HPVLE BIPs $\in \{k_{a,ij}^0 = 0.06207; k_{b,ij}^0 = 0.07589\}$ &
HPBDP BIPs $\in \{k_{a,ij}^0 = 0.08; k_{b,ij}^0 = 0.12\}$
- (ii) (*Figure 8-19 (b)*) with HPVLE BIPs $\in \{k_{a,ij}^0 = 0.01953; k_{b,ij}^0 = 0\}$ &
HPBDP BIPs $\in \{k_{a,ij}^0 = 0.02; k_{b,ij}^0 = 0\}$

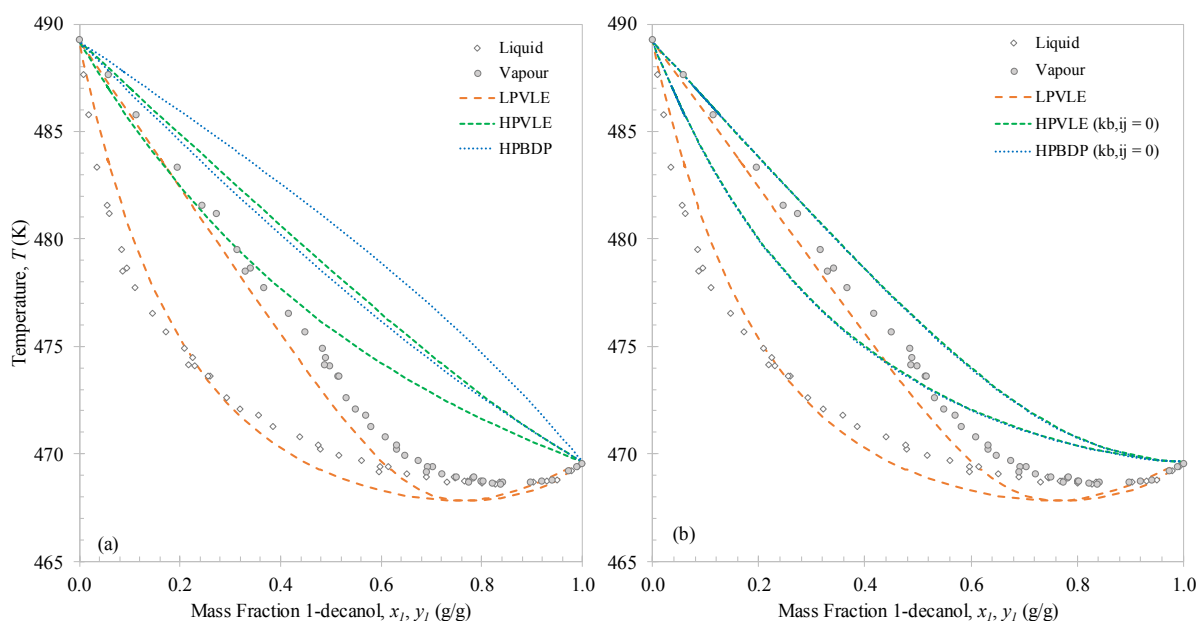


FIGURE 8- 32: SR-POLAR MODEL CORRELATIONS OF THE T - x_1 - y_1 LPVLE DATA (WITH ALTERNATING SOLUTE + SOLUTE BIPs) AT $P = 40$ kPa. ADDITIONAL ALTERNATIONS MADE FOR HPVLE AND HPBDP BIPs: (A) SCENARIO I AND (B) SCENARIO II.

Although the model correlations improved with the exclusion of the $k_{b,ij}^0$ BIP, SR-Polar (with HPBDP and HPVLE BIPs) failed to predict the azeotropic phase behaviour of the binary 1-decanol + n -tetradecane system (*Figure 8-32 (b)*). Furthermore, the HPBDP and HPVLE BIPs are very similar in magnitude which makes a qualitative analysis of the correlations difficult. The %AAD values calculated

for each BIP set and scenario are provided in *Table 8-2*. With reference to the BIPs used in scenario (ii) the following relative performance is observed in terms of the quality of the model fit to LPVLE data:

$$\text{LPVLE} > \text{HPBDP} > \text{HPVLE}$$

TABLE 8- 2: SR-POLAR %AAD CALCULATED IN VAPOUR COMPOSITION, y_1 AND T OF THE 1-DECANOL (1) + *N*-TETRADECANE (2) BINARY SYSTEM.

<i>Solute + solute BIPs</i>	$\%AAD_{y_1}$	$\%AAD_T$
LPVLE	11.35	0.19
HPVLE Scenario (i)	21.28	1.01
Scenario (ii)	15.25	0.66
HPBDP Scenario (i)	25.97	1.31
Scenario (ii)	15.13	0.65

8.2.3. PC-SAFT

The predicted azeotropic point for each of the PC-SAFT temperature independent k_{ij} parameters are presented in *Table 8-3* along with the average deviations in 1-decanol vapour composition, y_1 and temperature, T . The large deviations in y_1 and T are due to the inability of PC-SAFT to accurately account for the azeotropic behaviour in the 1-decanol + *n*-tetradecane system when using BIPs regressed from high-pressure phase equilibria data. It is interesting to note that the nature of the deviations is very similar, especially within the 1-decanol-rich region. As seen in *Figure 8-33* and *Figure 8-34*, the strength of the positive deviations in the binary mixture are overestimated, causing the azeotropic temperature to be underpredicted. The following relative performance is observed in terms of the quality of the model fit to LPVLE data:

$$\text{LPVLE} > \text{HPBDP} > \text{HPVLE}$$

TABLE 8- 3: PC-SAFT AZEOTROPIC POINT, REPRESENTING THE EXPERIMENTAL DATA AND %AAD CALCULATED IN VAPOUR COMPOSITION, y_1 AND T OF THE 1-DECANOL (1) + *N*-TETRADECANE (2) BINARY SYSTEM.

<i>Solute + solute BIPs</i>	<i>Azeotropic Temperature (K)</i>	<i>Azeotropic composition (g/g)</i>	$\%AAD_{y_1}$	$\%AAD_T$
Experimental	468.66	0.864	-	-
LPVLE	467.73	0.776	10.16	0.20
HPVLE	464.01	0.676	15.44	0.84
HPBDP	464.91	0.694	13.08	0.66

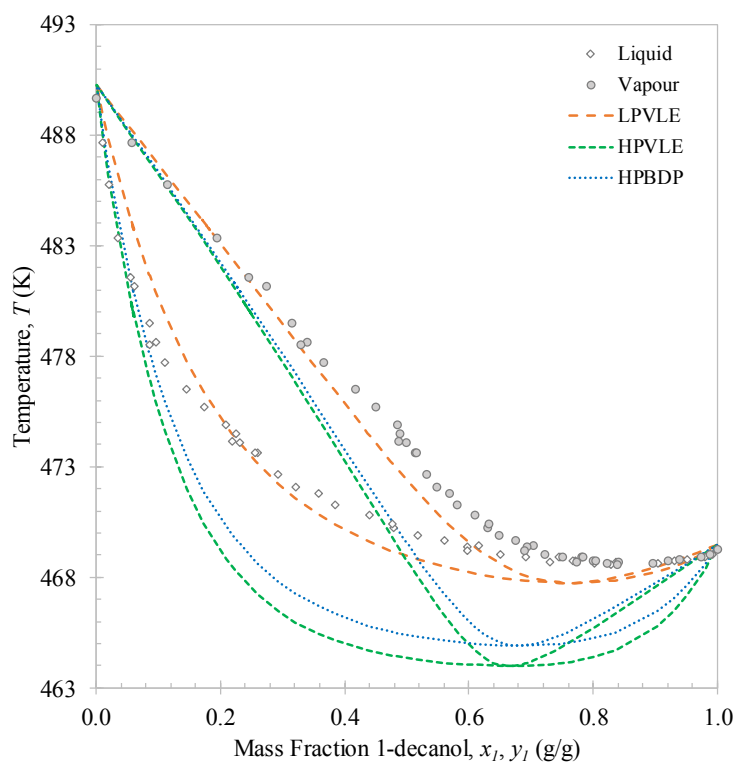


FIGURE 8- 33: PC-SAFT MODEL CORRELATIONS OF THE T - x_l - y_l LPVLE DATA (WITH ALTERNATING SOLUTE + SOLUTE BIPs) AT $P = 40$ kPa.

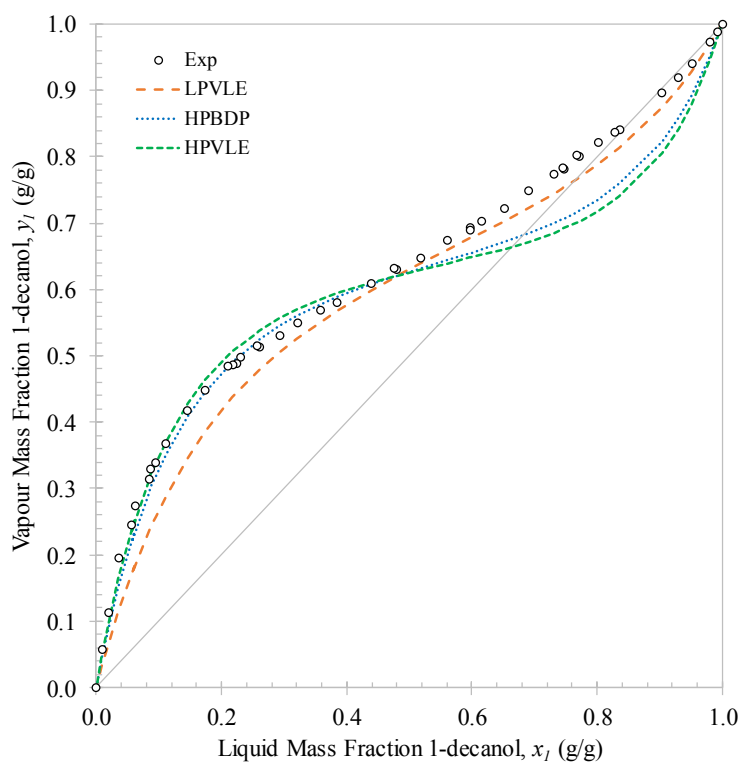


FIGURE 8- 34: PC-SAFT MODEL CORRELATIONS OF THE x_l - y_l LPVLE DATA (WITH ALTERNATING SOLUTE + SOLUTE BIPs) AT $P = 40$ kPa.

8.2.4. PSRK

Out of the four thermodynamic models evaluated in this study, PSRK resulted in the optimum representation of the LPVLE data (compared to optimum RK-Aspen, SR-Polar and PC-SAFT model correlations in the next section). The qualitative results in *Figure 8-35* show how PSRK can predict the azeotropic phase behaviour at $T = 468.75$ and $y_I = 0.837$ g/g. The overall prediction of the phase behaviour was accurate to $\%AAD_{y_I} = 6.98\%$ and $\%AAD_T = 0.14\%$; these quantitative results are seen by the small deviations in *Figure 8-35 (a)* and *Figure 8-35 (b)*, respectively.

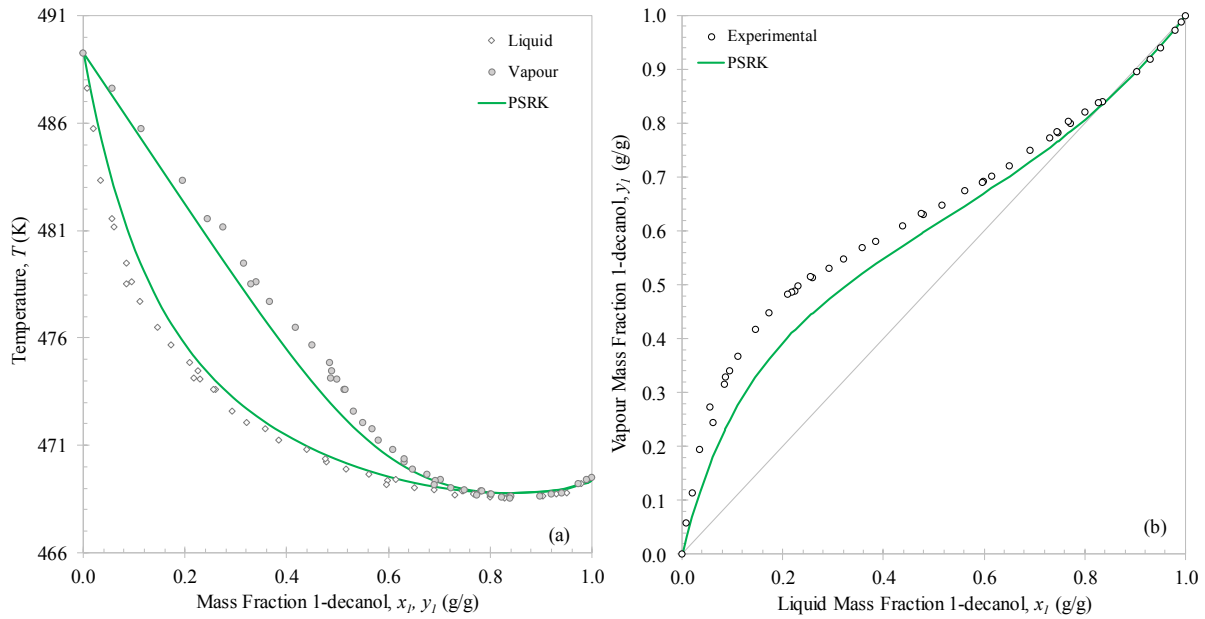


FIGURE 8- 35: PSRK MODEL PREDICTION OF THE (A) T - x_I - y_I AND (B) x_I - y_I LPVLE DATA AT $P = 40$ kPa.

8.3. OPTIMUM THERMODYNAMIC MODEL & SOLUTE + SOLUTE BIPs

Having successfully identified whether high-pressure solute + solute BIPs can be used to improve the modelling of low-pressure data and vice versa (**Objective 3.3**); the optimum BIPs for RK-Aspen, SR-Polar and PC-SAFT could be identified and are summarised in *Table 8-4* (**Objective 3.4**). Thus, in this section, these optimum BIPs were used to establish which of the four thermodynamic models will result in the most accurate representation of the measured equilibrium data (**Objective 3.5**).

TABLE 8- 4: FINAL SOLUTE + SOLUTE BIPs TO BE USED BY RK-ASPEN, SR-POLAR AND PC-SAFT FOR OPTIMUM REPRESENTATIONS OF THE HIGH-PRESSURE OR LOW-PRESSURE DATA.

Model	Representing high-pressure data	Representing low-pressure data
RK-Aspen	HPBDP: $k_{a,ij}^0 = 0.06$ & $k_{b,ij}^0 = 0.08$	HPBDP: $k_{a,ij}^0 = 0.04$
SR-Polar	HPVLE: $k_{a,ij}^0 = 0.06207$ & $k_{b,ij}^0 = 0.07589$	LPVLE: $k_{a,ij}^0 = 0.0582$
PC-SAFT	HPVLE: $k_{ij}^0 = 0.04454$	LPVLE: $k_{ij}^0 = 0.02467$

The %AAD_P (HPBDP) and %AAD_{w_s} (HPVLE) values for the four models are presented in *Figure 8-36* to allow for a direct quantitative comparison of their predictive (PSRK) and correlative (RK-Aspen, SR-Polar and PC-SAFT) accuracy. The %AAD_{w_s} values calculated for the cubic *EoS* at $T = 328$ K are approximately one-half of those obtained from the PC-SAFT results. Furthermore, for the dew-point region of the HPBDP data, PC-SAFT is the only model to produce a negative %AAD_P correlation with T (see *Figure 8-36 (b)*). Except for the HPVLE liquid phase data at $T = 348$ K, PSRK bested the phase behaviour correlations of PC-SAFT. SR-Polar and RK-Aspen are both suitable for SFF after representing the dew-point ternary data at $T = 328$ K with an equal accuracy of 1.83%. Based on these high-pressure quantitative results the thermodynamic models can be ranked as follow:

$$\text{SR-Polar} \approx \text{RK-Aspen} > \text{PSRK} > \text{PC-SAFT}$$

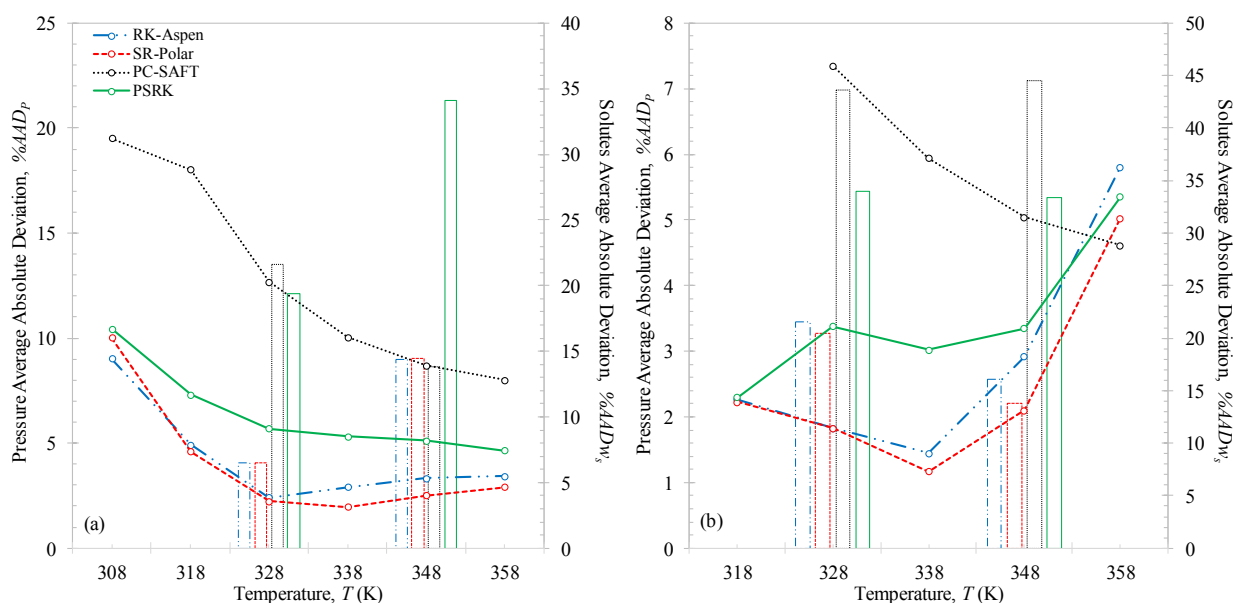


FIGURE 8- 36: COMPARISON OF THE $\%AAD$ VALUES CALCULATED FOR EACH OF THE FOUR THERMODYNAMIC MODELS WITH THEIR OPTIMUM SOLUTE + SOLUTE BIPs. THE HPVLE $\%AAD_{w_s}$ VALUES ARE REPRESENTED ON THE SECONDARY AXIS WITH BARS, AND THE HPBDP $\%AAD_P$ VALUES ARE REPRESENTED ON THE PRIMARY AXIS WITH LINES FOR (A) THE LIQUID PHASE/ BUBBLE-POINT REGION CORRELATIONS AND (B) THE VAPOUR PHASE/ DEW-POINT REGION CORRELATIONS.

Qualitative comparisons at $T = 308$ K were excluded as none of the models could capture the trends of the HPBDP and HPVLE experimental data points accurately. This occurrence is not uncommon and has been observed in literature [16], [18], [19]. The limitation is attributed to the temperature inversion that is not accounted for in the models.

The model results in representing the HPBDP data are shown in *Figure 8-37* on P - w_s plots and the model results in representing the HPVLE data are shown in *Figure 8-38* to *Figure 8-43* on Gibbs phase triangles. RK-Aspen and SR-Polar are almost identical at $T = 328$ K and $T = 348$ K, with minor differences observed in the bubble-point region of the P - w_s curves and liquid phase envelope of the ternary plots. However, as the 1-decanol concentration in the ternary system decreases the two correlations become identical. A decrease in 1-decanol molecules in the mixture will cause the number of polar interactions to decline, allowing the models to be less dependent on the polar parameters, and more so on the BIPs. In both models where attractive and co-volume forces are considered, the parameters are approximated via the vdW approach. Therefore, it is expected that the behaviour of these models will be similar since the basis of these two cubic *EoS* property methods are very similar.

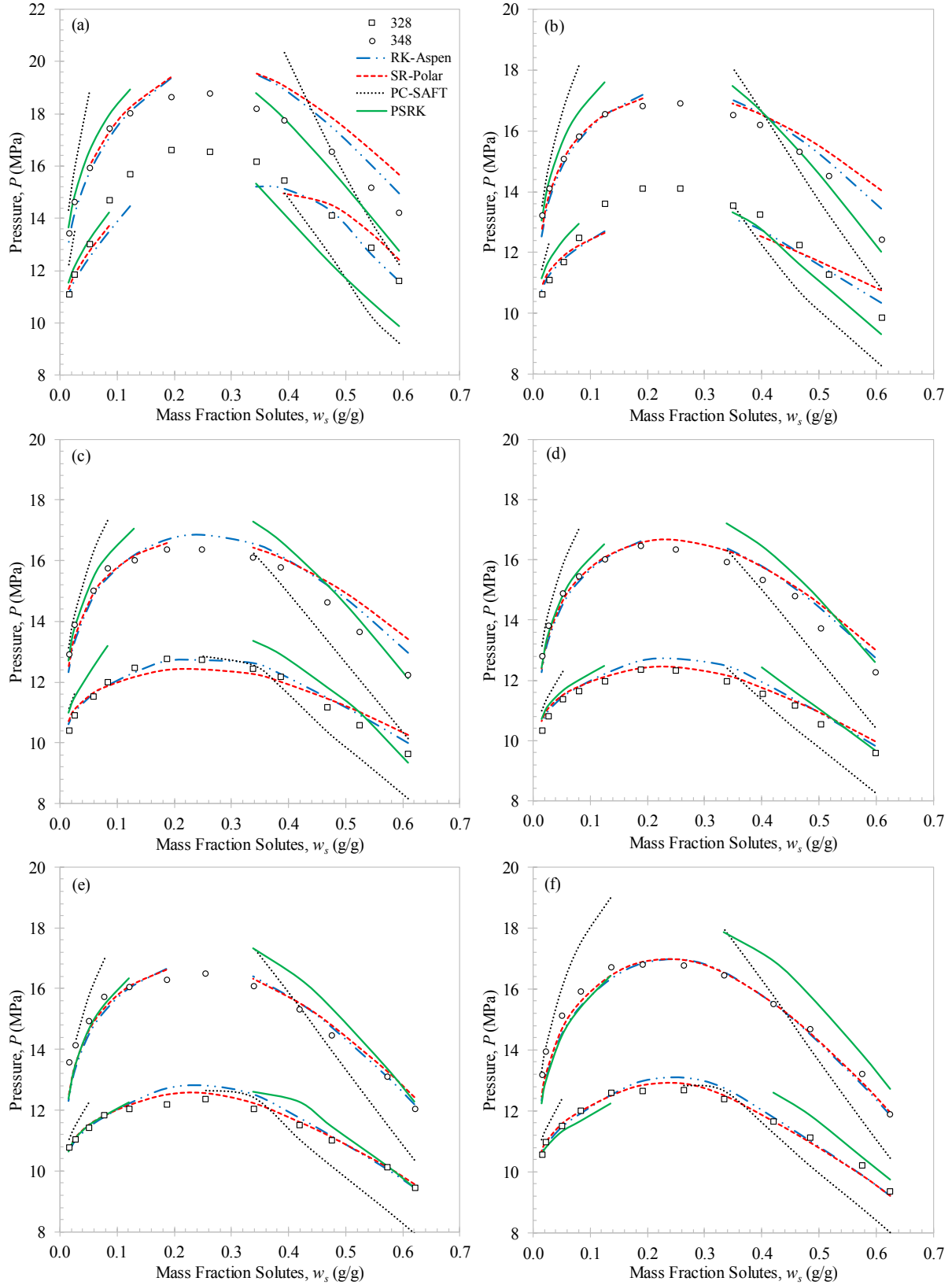


FIGURE 8- 37: RK-ASPEN (HPBDP BIPs), SR-POLAR (HPVLE BIPs), PC-SAFT (HPVLE BIPs) AND PSRK (DDB) MODEL CORRELATIONS OF THE HPBDP DATA AT $T = 328$ K AND 348 K FOR (A) $w_c^{RED} = 0.2405$ G/G; (B) $w_c^{RED} = 0.5000$ G/G; (C) $w_c^{RED} = 0.6399$ G/G; (D) $w_c^{RED} = 0.7698$ G/G; (E) $w_c^{RED} = 0.8162$ G/G; AND (F) $w_c^{RED} = 0.9200$.

The SR-Polar model has been investigated alongside the RK-Aspen model in two previous studies; the first made use of only one regressed polar parameter (p_1) [18] and the second study made use of two polar parameters (p_1 and p_2) [19]. In both cases, the RK-Aspen model remained dominant over the SR-Polar method regardless of a composition change. However, in this work, where all three regressed polar parameters (p_1 , p_2 and p_3) were used, SR-Polar produced equal in accuracy results, and at times improved results in comparison to RK-Aspen for the HPBDP and HPVLE data. Therefore, it seems that there is a trade-off in the framework of the cubic *EoS* models to give improved correlations. It is also noteworthy that the solute + solute BIPs of RK-Aspen are lower in magnitude than the parameters of SR-Polar, which might indicate better predictive capabilities of the RK-Aspen *EoS*.

EoSs derived from statistical mechanics tend to be more successful in representing systems of association such as the ternary system of interest to this study. Nevertheless, both cubic *EoS* and PSRK have proven to be much more accurate than PC-SAFT in representing the HPBDP data. With an increase in temperature from $T = 328$ K to $T = 348$ K the ability of the cubic *EoS* to accurately represent the HPVLE data slightly decreased, whereas the PC-SAFT correlations improved (Figure 8-41 and Figure 8-42). This shows that PC-SAFT can describe the liquid phase equilibria of the ternary system over a wider temperature range, however, within the limitation that the operating pressure does not exceed the pressure at which the phase envelope split occurs (Figure 8-43).

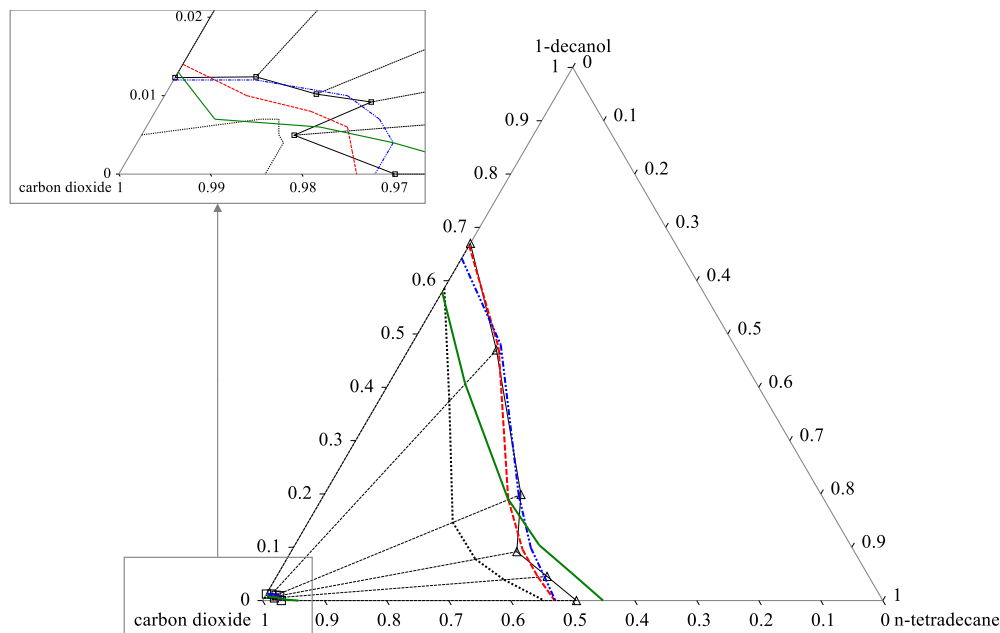


FIGURE 8- 38: THERMODYNAMIC MODEL CORRELATIONS OF THE HPVLE DATA WITH: --- RK-ASPEN (HPBDP BIPs); --- SR-POLAR (HPVLE BIPs); PC-SAFT (HPVLE BIPs); AND — PSRK (DDB) AT $T = 328$ K AND $P = 11.1$ MPa.

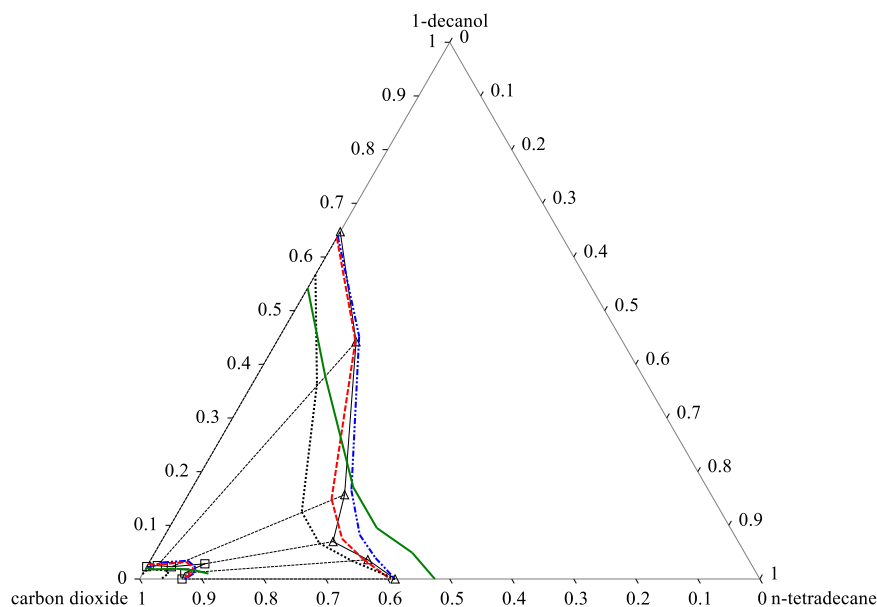


FIGURE 8- 39: THERMODYNAMIC MODEL CORRELATIONS OF THE HPVLE DATA WITH: \cdots RK-ASPEN (HPBDP BIPs); $---$ SR-POLAR (HPVLE BIPs); \cdots PC-SAFT (HPVLE BIPs); AND $---$ PSRK (DDB) AT $T = 328$ K AND $P = 12.0$ MPa.

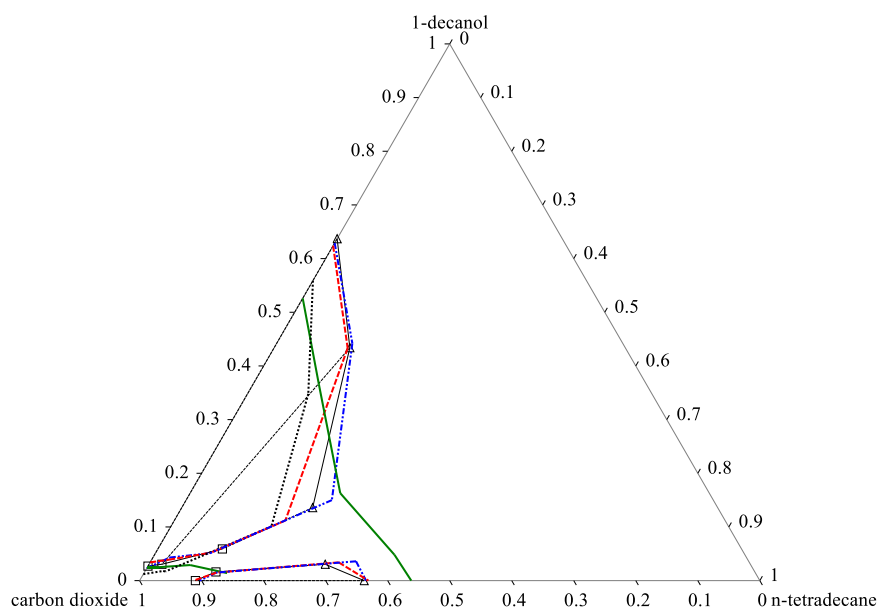


FIGURE 8- 40: THERMODYNAMIC MODEL CORRELATIONS OF THE HPVLE DATA WITH: \cdots RK-ASPEN (HPBDP BIPs); $---$ SR-POLAR (HPVLE BIPs); \cdots PC-SAFT (HPVLE BIPs); AND $---$ PSRK (DDB) AT $T = 328$ K AND $P = 12.4$ MPa.

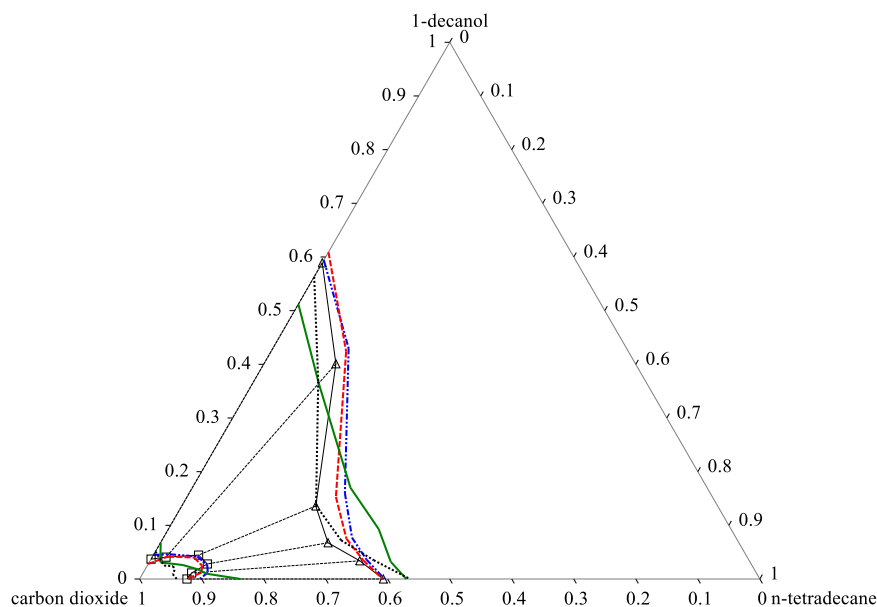


FIGURE 8- 41: THERMODYNAMIC MODEL CORRELATIONS OF THE HPVLE DATA WITH: \cdots RK-ASPEN (HPBDP BIPs); $---$ SR-POLAR (HPVLE BIPs); \cdots PC-SAFT (HPVLE BIPs); AND $---$ PSRK (DDB) AT $T = 348$ K AND $P = 16.0$ MPa.

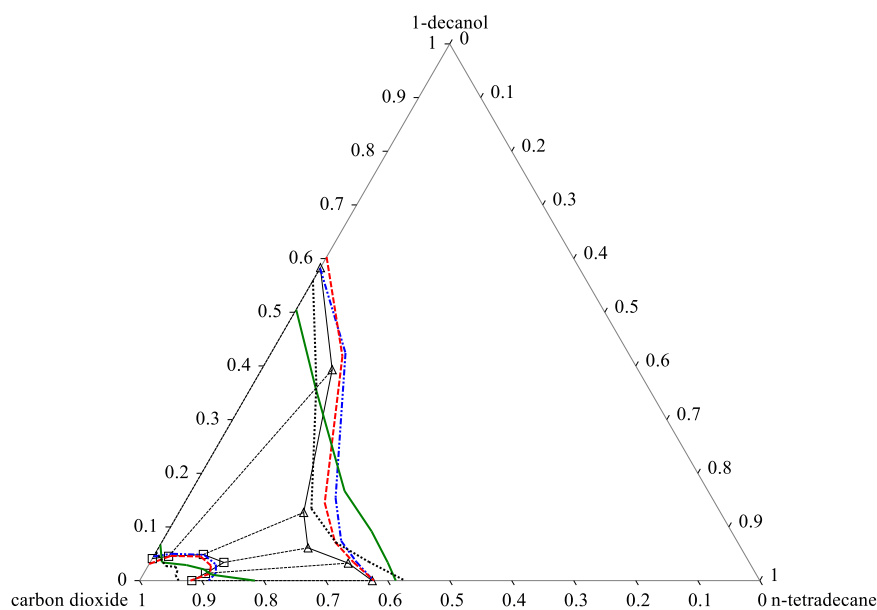


FIGURE 8- 42: THERMODYNAMIC MODEL CORRELATIONS OF THE HPVLE DATA WITH: \cdots RK-ASPEN (HPBDP BIPs); $---$ SR-POLAR (HPVLE BIPs); \cdots PC-SAFT (HPVLE BIPs); AND $---$ PSRK (DDB) AT $T = 348$ K AND $P = 16.2$ MPa.

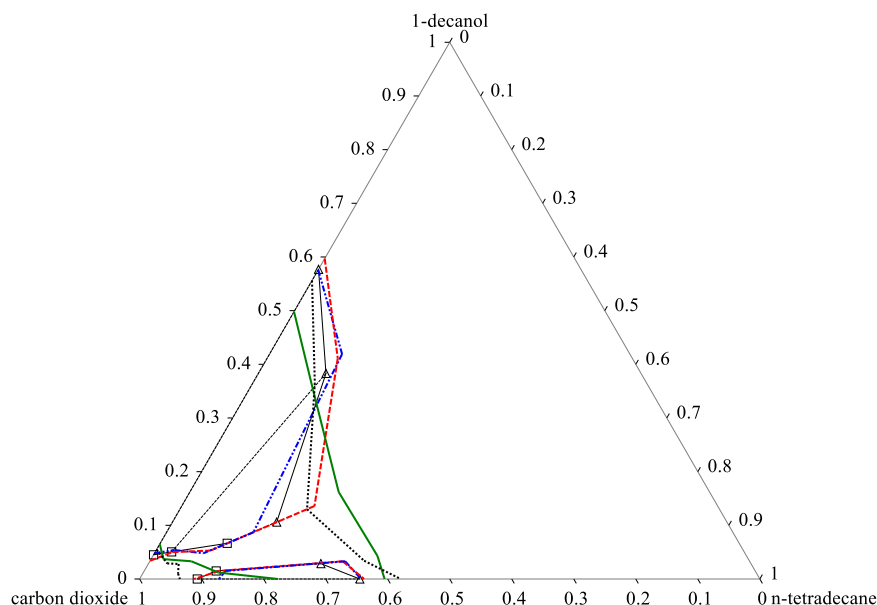


FIGURE 8- 43: THERMODYNAMIC MODEL CORRELATIONS OF THE HPVLE DATA WITH: \cdots RK-ASPEN (HPBDP BIPs); $---$ SR-POLAR (HPVLE BIPs); \cdots PC-SAFT (HPVLE BIPs); AND $---$ PSRK (DDB) AT $T = 348$ K AND $P = 16.4$ MPa.

Table 8-5 summarises the average α_{ij} calculated for the experimental HPVLE data and each of the four models evaluated in this work. The flexible property methods, RK-Aspen and SR-Polar, are equal in magnitude and only slightly overestimate the experimental α_{ij} value. Similarly, the association model, PC-SAFT, and the purely predictive model, PSRK, are also similar in magnitude and show even further deviation from the experimental α_{ij} value.

TABLE 8- 5: RELATIVE SOLUBILITY (A_{ij}) FOR THE EXPERIMENTAL AND MODEL PREDICTED SYSTEMS AVERAGED ACROSS ALL T AND P STUDIED IN THIS WORK.

	Average α_{ij}
Experimental	1.1
RK-Aspen (HPBDP BIPs)	1.2
SR-Polar (HPVLE BIPs)	1.2
PC-SAFT (HPVLE BIPs)	1.6
PSRK (DDB)	1.6

Quantitatively, RK-Aspen and SR-Polar appear to agree with one another and similarly PC-SAFT with PSRK. To prove this assumption, further evaluation of the predicted co-existing phases was done qualitatively on a constant T and P basis (see Figure 8-44 as an example at $T = 328$ K and $P = 11.1$ MPa). The predicted tie lines show that although the statement is true for RK-Aspen and SR-Polar, it is not the case for PC-SAFT and PSRK. For the predictive model (PSRK) the α_{ij} values do not appear to have any visible link to the modelling outcome of the co-existing phases. The model accuracy is purely

dependent on the *n*-tetradecane concentration within the system (w_c^{red}), i.e. the lower the w_c^{red} value, the more closely the predictive model captures the compositional dependence.

For RK-Aspen, SR-Polar and PC-SAFT, the predicted α_{ij} values can be linked to the modelling outcome of each mixture:

- (i) For the $w_c^{red} = 0.2403$ g/g mixture, the thermodynamic models with the lower predicted α_{ij} values resulted in a better representation of the compositional dependence (shown in *Figure 8-44*).
- (ii) For the $w_c^{red} = 0.6245$ g/g mixture, it is evident that the predicted α_{ij} values cannot be used to establish which thermodynamic model will accurately correlate the composition of the co-existing phases. The degree to which compositional dependence is captured is dependent on the model and its capabilities to correlate experimental data within the complex phase behaviour region.
- (iii) For the $w_c^{red} = 0.7979$ g/g mixture, the optimum model correlation is still largely governed by the type of thermodynamic model used; however, the larger α_{ij} value does indicate a slightly improved fit (by PC-SAFT) in comparison to the models with the lower α_{ij} values (RK-Aspen and PC-SAFT).
- (iv) For the $w_c^{red} = 0.9004$ g/g mixture, the thermodynamic models with the higher predicted α_{ij} values resulted in a better representation of the compositional dependence (shown in *Figure 8-44*).

Qualitatively, the α_{ij} values appear to be directly proportional to the w_c^{red} values, e.g. the higher the w_c^{red} of the mixture, the higher the experimental α_{ij} value will need to be to ensure effective separation in the mixture and consequently, the higher the predicted α_{ij} value, the more accurate the model fit will be.

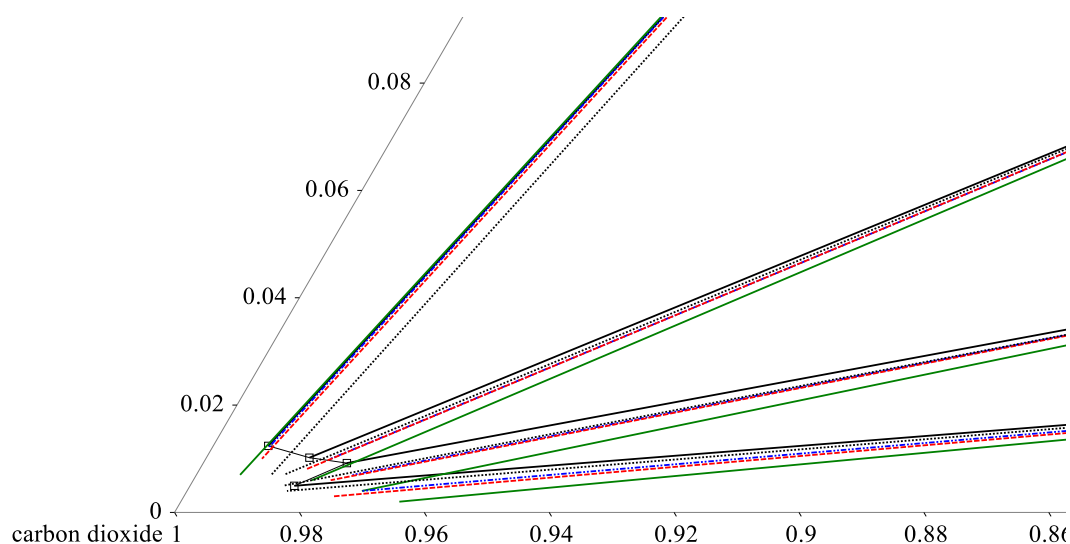


FIGURE 8- 44: VAPOUR PHASE DETAIL FOR CO₂ + 1-DECANOL + *N*-TETRADECANE PREDICTED TIE LINES WITH: ····· RK-ASPEN (HPBDP BIPs); - - - SR-POLAR (HPVLE BIPs); ····· PC-SAFT (HPVLE BIPs); AND — PSRK (DDB) MODELS COMPARED TO EXPERIMENTAL TIE LINES AT CONSTANT $T = 328\text{ K}$ AND $P = 11.1\text{ MPa}$.

The improved predictive capabilities of RK-Aspen are confirmed with the LPVLE model comparisons presented in *Figure 8-45*. Here, RK-Aspen and SR-Polar both only make use of one solute + solute BIP ($k_{a,ij}^0$), which tests the robustness of the *EoS*. The RK-Aspen correlations outperform those of SR-Polar by predicting the azeotropic point more closely and PC-SAFT proved to be in good agreement with the LPVLE experimental data. PSRK makes use of previously determined low-pressure activity coefficient parameters, allowing it to have the most accurate prediction of the LPVLE binary system. Based on these low-pressure qualitative results the thermodynamic models can be ranked as follow:

PSRK > RK-Aspen > SR-Polar > PC-SAFT

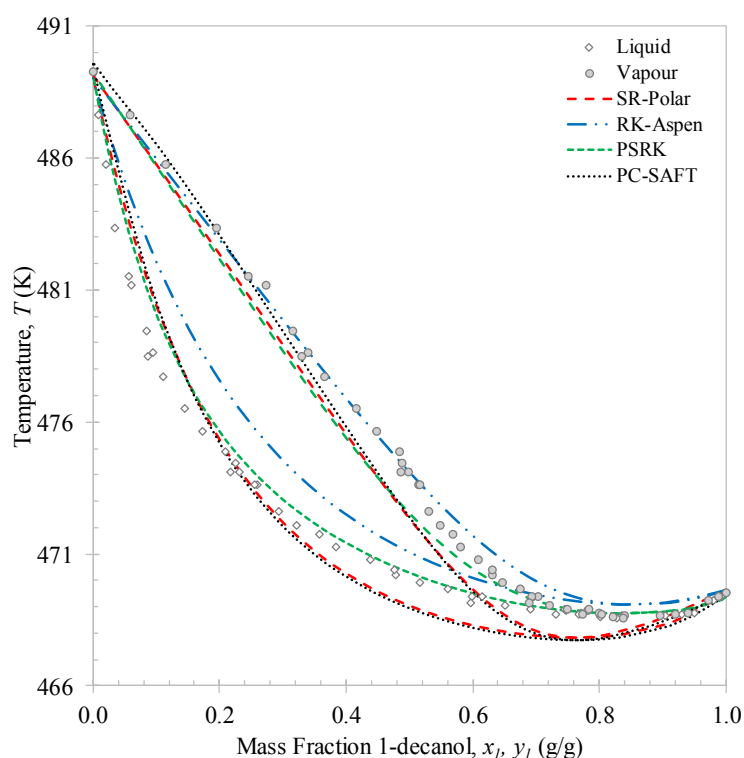


FIGURE 8- 45: RK-ASPEN (HPBDP BIPs), SR-POLAR (LPVLE BIPs), PC-SAFT (LPVLE BIPs) AND PSRK (DDB) MODEL CORRELATIONS OF THE LPVLE DATA AT $P = 40$ kPa.

Overall, if an optimum thermodynamic model should be defined based on this study, RK-Aspen was the only model to produce an accurate representation of each set of experimental data. SR-Polar was a close second, lagging in the representation of the LPVLE data. From a purely predictive perspective, PSRK can be used to represent accurate HPBDP and LPVLE data but should not be used to predict HPVLE data. Lastly, PC-SAFT can produce reasonable LPVLE and HPVLE data but failed to correlate the HPBDP data accurately.

8.4. CHAPTER OUTCOMES

The aim of this chapter was to evaluate the capabilities of the RK-Aspen, SR-Polar, PC-SAFT and PSRK thermodynamic models within Aspen Plus® to correlate the phase behaviour of the CO₂ + 1-decanol + *n*-tetradecane ternary system and the 1-decanol + *n*-tetradecane binary system. In achieving this aim, key **Objective 3.3**, **Objective 3.4** and **Objective 3.5** were successfully achieved.

On the off chance that no experimental data for parameter regression is available, the PSRK model can be used to predict semi-accurate HPBDP data and good LPVLE data but should not be used to predict HPVLE data. Thus, the PSRK model is not equipped to take into consideration the complexities from the undesired phase behaviour. The specific strengths and weaknesses of each suitable model that could incorporate, amongst others, solute + solute BIPs to improve their correlations are summarised through answering the following questions (**Objective 3.3**):

- (i) *Can solute + solute BIPs regressed from LPVLE 1-decanol + n-tetradecane data be used to correlate HPBDP CO₂ + 1-decanol + n-tetradecane data?*

Cubic EoS: Although being outperformed by the HPBDP and HPVLE BIPs, the LPVLE BIPs can represent the dew-point region of the mixtures at $T = 328$ K within 2.62% (RK-Aspen) and 1.92% (SR-Polar) of the actual data. Furthermore, qualitative trends of the dew-point region are equal in accuracy to those obtained by both HPBDP and HPVLE BIPs. For the bubble-point region, the effects of a single BIP ($k_{b,ij}^0 = 0$) are more prominent as the P - w_s curves have been shifted horizontally downwards, and vertically inwards. Quantitatively, the LPVLE BIPs represent the bubble-point region of the mixtures at $T = 328$ K within 7.97% (RK-Aspen) and 7.92% (SR-Polar) of the actual data. However, the values calculated are simply a representation of the data **points** predicted, and not the actual fit of the models. For *n*-tetradecane-rich mixtures somewhat accurate correlations of the bubble-point region were maintained.

PC-SAFT: Quantitatively the LPVLE BIPs can represent the bubble- and dew-point regions of the mixtures at $T = 328$ K within 8.90% and 9.16% of the actual data, respectively. However, the model fit to the experimental data remained poor. It is noteworthy that this finding for the LPVLE BIPs was not the exception, but the norm, as similar correlations of the HPBDP data were obtained with HPBDP and HPVLE BIPs too.

- (ii) *Can solute + solute BIPs regressed from LPVLE 1-decanol + n-tetradecane data be used to correlate HPVLE CO₂ + 1-decanol + n-tetradecane data?*

Cubic EoS: Within the complex phase behaviour region of the ternary system, where solute + solute interactions are prominent, the cosolvency ‘pinch point’ and phase envelope split were predicted prematurely. The poor fit of the models with the LPVLE BIPs were mirrored in the %AAD values calculated for the solute compositions. At $T = 328$ K, overly CO₂-rich liquid phases ($AAD_{w_s} = 17.35\%$

for RK-Aspen; 17.62% for SR-Polar) and CO₂-deficient vapour phases ($AAD_{w_s} = 37.64\%$ for RK-Aspen; 25.28% for SR-Polar) were obtained. Therefore, the use of LPVLE BIPs are not recommended for representing the HPVLE data.

PC-SAFT: The LPVLE BIPs can produce the s-shaped curve within the complex phase behaviour region of the system. However, problems with the model are still encountered in representing the vapour phase composition data. At $T = 328$ K, slightly CO₂-deficient liquid phases ($AAD_{w_s} = 10.37\%$) and overly CO₂-rich vapour phases ($AAD_{w_s} = 46.14\%$) were obtained. Therefore, like the cubic *EoS*, the use of LPVLE BIPs are not recommended for representing the HPVLE data.

(iii) Can solute + solute BIPs regressed from HPBDP and HPVLE CO₂ + 1-decanol + n-tetradecane data be used to correlate LPVLE 1-decanol + n-tetradecane data?

Cubic EoS: The assessment of high-pressure BIPs in representing low-pressure VLE data raises a further important point in the context of this study namely, the problem with parameter degeneracy. The addition of the $k_{b,ij}^0$ parameter did not only affect the predictability of the system, but the ability of the models to correlate the system as well. Therefore, HPBDP and HPVLE BIPs can be used to represent the LPVLE data if the condition of $k_{b,ij}^0 = 0$ is maintained. Overall, for RK-Aspen, the HPBDP BIP ($k_{a,ij}^0 = 0.04$) resulted in the most accurate representation of the azeotropic point. For SR-Polar, the azeotropic phase behaviour could still not be predicted, regardless of setting $k_{b,ij}^0 = 0$. Therefore, for SR-Polar, HPBDP and HPVLE BIPs are not recommended for correlating LPVLE data.

PC-SAFT: With HPBDP and HPVLE BIPs the strength of the positive deviations in the binary mixture are overestimated, causing the azeotropic temperature to be underpredicted. Therefore, HPBDP and HPVLE BIPs are not recommended for correlating LPVLE data.

(iv) Can solute + solute BIPs regressed from HPVLE CO₂ + 1-decanol + n-tetradecane data be used to correlate HPBDP CO₂ + 1-decanol + n-tetradecane data and vice versa?

Cubic EoS: Quantitatively and qualitatively both sets of high-pressure BIPs resulted in accurate representations of the true thermodynamic properties of the CO₂ + 1-decanol + n-tetradecane system. This conclusion is not unexpected, as the $k_{a,ij}^0$ and $k_{b,ij}^0$ parameters of the two are very similar. However, with respect to the optimum set of BIPs to be used in SFF processes, the HPBDP BIPs are recommended for RK-Aspen and the HPVLE BIPs are recommended for SR-Polar.

PC-SAFT: It is well known that PC-SAFT deteriorates near the critical region of HPBDP data and predicts too-high concentrations of CO₂ (decreased solubility). In this work, neither the HPBDP nor the HPVLE BIPs can improve the model fit to the HPBDP data. With respect to the HPVLE data, both sets of BIPs can capture the liquid phase trend accurately at $T = 348$ K. However, the vapour composition correlation remained poor (like the results of the LPVLE BIPs).

New contributions:

- (i) The RK-Aspen, SR-Polar, PC-SAFT and PSRK parameters were identified in this chapter and are incorporated into their model algorithms in Aspen Plus® to provide improved correlations of the CO₂ + 1-decanol + *n*-tetradecane ternary system and 1-decanol + *n*-tetradecane binary system (**Objective 3.2**).
- (ii) In comparison to SR-Polar, PC-SAFT and PSRK, RK-Aspen is the best suited thermodynamic model to capture the complex phase behaviour of the CO₂ + 1-decanol + *n*-tetradecane ternary system at high-pressures and the 1-decanol + *n*-tetradecane binary system at low-pressure (**Objective 3.5**). A summary of the RK-Aspen model requirements, in terms of solute + solute BIPs that allowed for its optimum outcome in this work, is provided in *Table 8-6* (**Objective 3.4**).

TABLE 8- 6: SUMMARY OF THE RK-ASPEN MODEL REQUIREMENTS, IN TERMS OF SOLUTE + SOLUTE BIPs THAT ALLOWED FOR ITS OPTIMUM CORRELATION OF THE HPBDP, HPVLE AND LPVLE DATA MEASURED IN THIS WORK.

<i>Data set to be modelled</i>	<i>HPBDP</i>	<i>HPVLE</i>	<i>LPVLE</i>
Suitable solute + solute BIPs that can be used	HPBDP HPVLE LPVLE	HPBDP HPVLE	HPBDP LPVLE
Optimum solute + solute BIPs set	HPBDP	HPBDP	HPBDP
$k_{a,ij}^0$ parameter	0.06	0.06	0.04
$k_{b,ij}^0$ parameter	0.08	0.08	-

A fourth manuscript is being prepared for publication in a peer reviewed journal that covers the thermodynamic modelling (**Objective 3**) presented and discussed in this chapter:

Thermodynamic modelling of the CO₂ + 1-decanol + n-tetradecane system with RK-Aspen, SR-Polar and PC-SAFT in Aspen Plus®, Fluid Phase Equilibria.

Chapter 9

CONCLUSIONS AND RECOMMENDATIONS

The aim of this thesis was to obtain a fundamental understanding of the solute + solute interactions in the CO₂ + 1-decanol + *n*-tetradecane ternary system. The aim was achieved in two main parts, namely:

- (i) Experimental measurement of new high-pressure and low-pressure phase equilibria data (key **Objective 1** and **Objective 2**).
- (ii) Thermodynamic modelling of the new experimental phase equilibria data (key **Objective 3**).

Complex phase behavior regions within the CO₂ + 1-decanol + *n*-tetradecane system, i.e. cosolvency effects, were identified with both the HPBDP and HPVLE data measured in this work. The complex phase behaviour was found to occur due to distinct solute + solute interactions taking place with the ternary system. The interactions further lead to a fractionation gap within the complex phase behaviour region, i.e. $w_c^{red} = \pm 0.6245$ g/g, that can only be overcome through a pressure-temperature swing distillation. The complexities between the two larger solutes were confirmed with LPVLE measurements of the 1-decanol + *n*-tetradecane binary system. Thermodynamic modelling in this study showed that knowledge of the co-existing phases (HPVLE and LPVLE data) are not necessary to ensure their compositions are correlated well. The HPBDP data is not only less expensive and easier to measure, but when combined with the RK-Aspen property method in Aspen Plus[®], it will allow for excellent correlations of the CO₂ + 1-decanol + *n*-tetradecane system, especially within the complex phase behaviour region where solute + solute interactions were most prominent. Therefore, it is recommended that separation experiments be conducted on a pilot plant setup to confirm the fractionation gap occurring due to the solute + solute interactions. Once the final feed ratio and reflux settings are obtained, the RK-Aspen model with HPBDP solute + solute BIPs should be used to improve the accuracy of a working process model setup within Aspen Plus[®].

The conclusions of each part are discussed separately in this chapter, followed by recommendations for possible future work. Each chapter in this study contains a separate conclusions section, the content of which are to be treated as supplemental to chapter 9.

9.1. PART 1: ACHIEVEMENT OF KEY OBJECTIVES 1 AND 2

Table 9-1 summarises the main experimental shortcomings in open literature that were identified in Chapter 2 and how each were addressed through new contributions made in Chapter 5 (HPBDP and HPVLE data) and Chapter 6 (LPVLE data) of this work. Studying the ternary system at high-pressures helped to identify:

- (i) The type of complex phase behaviour occurring within the ternary system, e.g. cosolvency, *l-g* hole and miscibility windows.
- (ii) How each phenomenon is connected to the next, e.g. cosolvency lead to *l-g* hole and the simultaneous formation of miscibility windows.
- (iii) The influence of solute + solute interactions on the fractionation of the systems.
- (iv) The relative solubility of the components to identify the fractionation gap.
- (v) The types of phase transitions occurring within the complex phase behaviour region.

Given the scarcity of HPVLE ternary data, the experimental data measured in this work represents a valuable academic contribution. However, the measurement of new HPVLE ternary data is a timely and tedious process. It is for this reason that a synthetic setup was an alternative method used to measure HPBDP data. The measurement of new HPBDP solubility pressures were far less complex and time consuming. The third and final method entailed the use of an all-glass dynamic still to measure new LPVLE data of the binary 1-decanol + *n*-tetradecane system. Measuring the binary system served to:

- (i) Confirm that non-ideal phase behaviour does arise between the two solutes.
- (ii) Help gain further insight into the distinct solute + solute interactions.
- (iii) Classify the binary 1-decanol + *n*-tetradecane system.
- (iv) Confirm Class T-IV phase behaviour for the CO₂ + 1-decanol + *n*-tetradecane system.

TABLE 9- 1: SUMMARY ON HOW EACH OF THE LITERATURE GAPS IDENTIFIED IN CHAPTER 2 WERE FILLED THROUGH THE MEASUREMENT OF NEW HIGH-PRESSURE PHASE EQUILIBRIA DATA IN CHAPTER 5 AND NEW LOW-PRESSURE PHASE EQUILIBRIA DATA IN CHAPTER 6.

<i>Research gaps in open literature for the ternary CO₂ + 1-decanol + n-tetradecane system</i>	<i>New contributions made in this work to address the shortcomings in open literature</i>
Scheidgen and Schneider [3] measured a single CO ₂ + 1-decanol + n-tetradecane mixture ($w_c^{red} = 0.84$ g/g) to illustrate the miscibility window on a P - T projection. However, additional w_c^{red} mixtures are required to construct the 3D ternary critical surface and Gibbs phase triangles. In so doing, an adequate representation of the ternary phase behaviour surface can be obtained. Once the three-phase region has been defined the miscibility regions can be confirmed and a final classification of the ternary system can be established.	<ul style="list-style-type: none"> (i) New HPBDP data for six CO₂ + (1-decanol + n-tetradecane) mixtures were measured. (ii) The w_c^{red} mixtures were used to construct new Gibbs phase triangles and a 3D pseudo-binary critical surface to illustrate the true ternary phase behaviour of the CO₂ + 1-decanol + n-tetradecane system. (iii) The three-phase surface constructed on the Gibbs phase triangles and the pseudo-binary diagram were used to identify the miscibility regions. The addition of n-tetradecane to a 1-decanol-rich mixture will disrupt multimer bonds between the 1-decanol molecules and enhance the miscibility of the solutes in supercritical CO₂. (iv) A phase transition across the two-phase region was confirmed from Type III → Type IV → Type III fluid phase behaviour. (v) The miscibility enhancement (cosolvency effects) lead to the occurrence of simultaneous isobaric miscibility windows. This peculiar phenomenon was linked to ternary Class T-IV phase behaviour according to the classification by Bluma and Deiters [78].
Patton et al.[40] and Peters et al.[36] both measured the full l - g hole forming within the ternary system at near-critical conditions which serves as an important phenomenon to be considered in near-critical separation processes. However, the precise P - T - w_c^{red} conditions where cosolvency will occur for the interested ternary system have not yet been measured. Knowing the size and range of this phenomenon will help improve the separation process at supercritical conditions.	<ul style="list-style-type: none"> (vi) The size and range of the cosolvency effects were identified at six set temperatures measured for the ternary CO₂ + 1-decanol + n-tetradecane system. (vii) Inferred data allowed for the cosolvency effects to be linked to the formation of a l-g hole and miscibility windows in the l_1l_2g three-phase surface near the critical point of the solvent (initially suggested by Scheidgen and Schneider [3]).

<i>Research gaps in open literature for the ternary CO₂ + 1-decanol + n-tetradecane system</i>	<i>New contributions made in this work to address the shortcomings in open literature</i>
<p>The complex phase behaviour phenomena measured, by Scheidgen and Schneider [3], Patton et al.[40] and Peters et al.[36], at operating conditions near the solvent critical region indicate VLLE three-phase regions which will cause difficulties in the control of SFF processes. In the past, the three-phase regions would be ignored and avoided in these types of separation processes. Instead of avoiding the <i>l₁l₂g</i> three-phase regions, the solute + solute interactions can be better investigated by constructing the tie lines of the ternary phase diagrams (within the cosolvency effects region). In so doing, one can establish the relative solubility of the components using supercritical CO₂.</p>	<p>(viii) The HPBDP data successfully defined the range and region in which distinct solute + solute interactions were occurring when compared to the CO₂ + 1-decanol and CO₂ + <i>n</i>-tetradecane binary systems.</p> <p>(ix) Bubble- and dew-point isotherms were used to identify possible azeotropic phase behaviour within the miscibility region, suggesting that fractionation in this region might not be effective.</p> <p>(x) New high-pressure vapour-liquid equilibria data for four CO₂ + (1-decanol + <i>n</i>-tetradecane) mixtures were measured.</p> <p>(xi) The HPVLE results proved that fractionation will not be possible within the miscibility region (only inferred by HPBDP data). To overcome these difficulties in fractionation, a pressure-temperature swing is required.</p>
<p>Scheidgen and Schneider [3] were also successful in measuring the isobaric miscibility window in the CO₂ + 1-decanol + <i>n</i>-tetradecane system. According to the classification of Bluma and Deiters [78], the miscibility window infers T-IV fluid phase behaviour for the interested ternary system. Ternary Class T-IV phase behaviour indicates Type I-A phase behaviour for the 1-decanol + <i>n</i>-tetradecane binary sub-system. To confirm the Type I phase behaviour, experimental VLE data are required to investigate the 1-decanol + <i>n</i>-tetradecane system.</p>	<p>(xii) New LPVLE data for the 1-decanol + <i>n</i>-tetradecane system were measured at <i>P</i> = 40 kPa.</p> <p>(xiii) New LPVLE data for the 1-pentanol + <i>n</i>-nonane, 1-hexanol + <i>n</i>-decane, 1-heptanol + <i>n</i>-undecane and 1-octanol + <i>n</i>-dodecane systems were measured at <i>P</i> = 40 kPa.</p> <p>(xiv) Each of the binary systems displayed positive azeotropy, inferring Type I-A fluid phase behaviour per the classification of Van Konynenburg and Scott [51]. Therefore, the ternary system is postulated to consist of binary sub-systems belonging to Type III + Type III + Type I phase behaviour.</p>

9.2. PART 2: ACHIEVEMENT OF KEY OBJECTIVE 3

Chapter 3 provided a systematic investigation on available thermodynamic models in Aspen Plus® and their applicability to correlate/predict the complex ternary and binary data. To improve the correlative capabilities of 3 suitable thermodynamic models, new solute + solute BIPs were regressed in Chapter 7. In addition to the RK-Aspen, SR-Polar and PC-SAFT models, 1 purely predictive model, PSRK, was also assessed in Chapter 8 to fit the new HPBDP, HPVLE and LPVLE data.

A key question that arose was if it would be possible to improve/maintain the performance of the models by using different solute + solute BIPs in their specific model algorithm, i.e. can BIPs regressed using low-pressure data be used to represent high-pressure data accurately and vice versa. Although the RK-Aspen model (with HPBDP BIPs) and SR-Polar model (with HPVLE BIPs) resulted in the most accurate representations of the ternary system, the following alternatives were also found in this study:

- (i) The use of binary VLE data to regress LPVLE BIPs did improve the RK-Aspen and SR-Polar thermodynamic model correlations for HPBDP data where distinct solute + solute interactions were prominent, i.e. $w_c^{red} \geq 0.6399$ g/g.
- (ii) LPVLE BIPs can be used for the two cubic *EoS* to identify the cosolvency effect in HPVLE data (s-shaped phase behaviour). However, the LPVLE BIPs should not be used to identify the ‘pinch point’ where the phase split takes place.
- (iii) LPVLE BIPs can be used for PC-SAFT (T-independent basis) to produce model correlations of the HPVLE data. However, the PC-SAFT model, regardless of the BIPs applied, did not provide accurate correlations of the HPBDP data.
- (iv) The PSRK model can be used without the need for experimental data as the group-group (UNIFAC) interactions allowed for accurate predictions of the HPBDP data (dew-point region). However, the PSRK model failed to provide accurate predictions of the HPVLE data.

With regards to correlating the LPVLE data the following alternatives were found in this study:

- (i) The PSRK model can be used without the need for experimental data as the group-group interactions allowed for accurate predictions of the LPVLE data.
- (ii) HPBDP BIPs ($k_{b,ij}^0 = 0$) can be used with the RK-Aspen model to produce accurate correlations of the LPVLE data.

In general, the performance of the thermodynamic models can be ranked as follow:

RK-Aspen > SR-Polar > PSRK > PC-SAFT

However, after the evaluation of all three techniques for obtaining solute + solute BIPs the incorporation of the HPBDP BIPs into the RK-Aspen model resulted in the most accurate representation of ternary

HPBDP and HPVLE data and binary LPVLE data. Therefore, RK-Aspen was the preferred model to produce an accurate representation of each set of experimental data, namely:

- (i) The dew-point and bubble-point regions of HPBDP mixtures were accurately correlated regardless of a change in w_c^{red} and T .
- (ii) The trend of the vapour phase envelope for HPVLE data on Gibbs phase triangles were exceptionally well correlated at $T = 328$ K and $T = 348$ K.
- (iii) The HPVLE s-shape behaviour seen by the liquid phase envelopes on Gibbs phase triangles as well as the two-phase split after the cosolvency ‘pinch point’ were represented well.
- (iv) The use of $k_{a,ij}^0$ and $k_{b,ij}^0$ HPBDP BIPs to correlate the LPVLE data failed to predict the azeotropic phase behaviour. However, with $k_{b,ij}^0 = 0$, the HPBDP $k_{a,ij}^0$ BIP allowed for an accurate prediction of the azeotropic point.

From this research it follows that RK-Aspen with HPBDP solute + solute BIPs should be used for the most accurate model fit within the complex phase behaviour region of the HPBDP, HPVLE and LPVLE data. However, PSRK will be more suitable for use if a purely predictive trend of the HPBDP ternary data and LPVLE binary data is required.

9.3. RECOMMENDATIONS FOR FUTURE WORK

- (i) Many data points have been measured for most of the systems listed in *Table 2-2*. These include near-critical and super-critical conditions. Therefore, it would be interesting to see whether a group contribution *EoS* can be developed to predict these CO₂ + hydrocarbon systems.
- (ii) The CPA *EoS* has shown success in representing alcohol recovery applications with high-pressure gases, making it especially suitable for the mixtures investigated in this study. Furthermore, CPA is a direct approach that can be applied to hydrogen bonding components, where *EoS-G^E* models tend to fail. The thermodynamic model was recently added to Aspen Plus® V8.8 and should be evaluated in correlating the experimental data measured in this work.
- (iii) By improving the design and analysis through controlled experiments, the modelling of the system could be enhanced. Factors based on qualitative assumptions can thus be ruled out, i.e. design of experiments on STATISTICA®.
- (iv) Experimental pilot plant testing of the ternary system should be conducted (like that done by Bonthuys [17]). The data can be used to verify the separation of residual *n*-tetradecane from 1-decanol using supercritical CO₂.
- (v) The experimental pilot plant data can be used in collaboration with the process model developed in Aspen Plus® by Zamudio [18]. The process model is ideal for the system of interest here as it was specifically designed for detergent range alkanes and alcohols with cross-over boiling points.

The models and solute + solute BIPs regressed in this work should be used to evaluate the performance of a SFF process for the separation of the ternary mixtures.

- (vi) For RK-Aspen and SR-Polar, the use of high-pressure BIPs to predict LPVLE data showed the use of only the $k_{a,ij}^0$ parameter produces an accurate fit (including $k_{b,ij}^0$ decreases the model accuracy). Based on this finding, it is recommended that a third scenario be investigated in future studies, where: $k_{a,ij}^0$ and $k_{a,ij}^1$ high-pressure BIPs are used to fit the model to LPVLE data. Due to the LPVLE data measured in this work being at much higher temperatures than the HPVLE data and HPBDP data measured, it is anticipated that taking T -dependence into consideration in this manner might improve the model fit.
- (vii) The HPBDP BIP regression approach limited the number of parameters that could be used to improve the SR-Polar model fit. It is recommended that the influence of the l_{ij} parameter be investigated using the HPVLE data and LPVLE data, e.g. see if HPVLE BIPs with 3 BIPs can improve the model fit to LPVLE data and vice versa.
- (viii) In addition to the objective functions used in this study to fit the solute + solute BIPs, it could be interesting to assess if including the relative solubility (using the K-Value) in the OF would improve the results, e.g. $OF = \sum_{i=1}^{NP} \left[\frac{(p_{sat,i}^{Exp} - p_{sat,i}^{Calc})^2}{(p_{sat}^{Exp})^2} \right]^{0.5} + \sum_{i=1}^{NP} \sum_{i=1}^{NC} \left[\frac{(K_i^{Exp} - K_i^{Calc})^2}{(K_i^{Exp})^2} \right]^{0.5}$.
- (ix) Having identified which models can correlate the interested systems accurately with no T -dependent BIPs in this work, it is recommended that the influence of T -dependent BIPs be evaluated in future studies.

Chapter 10

REFERENCES

- [1] E. Kiran and J. F. Brennecke, "Supercritical Fluid Engineering Science: Fundamentals and Applications," in *ACS Symposium Series No. 514*, 1993.
- [2] Aspen Technology, "Aspen Physical Property System," *Softw. Guid. - Phys. Prop. Model.*, vol. 7.3.2, pp. 69–70, 2012.
- [3] A. L. Scheidgen and G. M. Schneider, "Fluid phase equilibria of (carbon dioxide + a 1-alkanol+ an alkane) up to 100 MPa and T = 393 K: cosolvency effect, miscibility windows, and holes in the critical surface," *J. Chem. Thermodyn.*, vol. 32, no. 9, pp. 1183–1201, 2000.
- [4] C. E. Schwarz, G. J. K. Bonthuys, J. H. Knoetze, and A. J. Burger, "The influence of functional end groups on the high-pressure phase equilibria of long chain molecules in supercritical propane," *J. Supercrit. Fluids*, vol. 46, no. 3, pp. 233–237, 2008.
- [5] H. A. Mills, "Alcohols, Fatty (via Hydrogenation)," *Chemical and Process Technology*. 1974.
- [6] J. Falbe, W. Lipps, and D. Mayer, *Alcohols, Aliphatic, Ullmann's Encyclopaedia of Industrial Chemistry*. 2012.
- [7] J. C. Crause, "Supercritical Fluid Extraction of Paraffin Wax," P.h.D Thesis, Stellenbosch University, 2001.
- [8] A. J. Lundeen, "Alcohols," *Chemical and Process Technology*. 1974.
- [9] D. A. McKensie, "Nonionic Surfactants in: Chemical Society," *J. Am. Oil*, vol. 55, pp. 93–97, 1978.
- [10] G. J. K. Bonthuys, C. E. Schwarz, A. J. Burger, and J. H. Knoetze, "Separation of alkanes and alcohols with supercritical fluids. Part I: Phase equilibria and viability study," *J. Supercrit. Fluids*, vol. 57, no. 2, pp. 101–111, 2011.
- [11] C. E. Schwarz, G. J. K. Bonthuys, R. F. Van Schalkwyk, D. L. Laubscher, A. J. Burger, and J. H. Knoetze, "Separation of alkanes and alcohols with supercritical fluids. Part II. Influence of process parameters and size of operating range," *J. Supercrit. Fluids*, vol. 58, no. 3, pp. 352–359, 2011.
- [12] M. Zamudio, C. E. Schwarz, and J. H. Knoetze, "Methodology for process modelling of supercritical fluid fractionation processes illustrated for the separation of alkane/alcohol isomer mixtures using CO₂," *J. Supercrit. Fluids*, vol. 104, pp. 272–280, 2015.

- [13] M. Zamudio, C. E. Schwarz, and J. H. Knoetze, "Experimental measurement and modelling with Aspen Plus® of the phase behaviour of supercritical CO₂+(n-dodecane+1-decanol+3,7-dimethyl-1-octanol)," *J. Supercrit. Fluids*, vol. 84, pp. 132–145, 2013.
- [14] F. C. v N. Fourie, C. E. Schwarz, and J. H. Knoetze, "Phase equilibria of alcohols in supercritical fluids. Part I. The effect of the position of the hydroxyl group for linear C₈ alcohols in supercritical carbon dioxide," *J. Supercrit. Fluids*, vol. 47, no. 2, pp. 161–167, 2008.
- [15] M. Zamudio, C. E. Schwarz, and J. H. Knoetze, "Phase equilibria of branched isomers of C₁₀-alcohols and C₁₀-alkanes in supercritical carbon dioxide," *J. Supercrit. Fluids*, vol. 59, no. 3, pp. 14–26, 2011.
- [16] S. A. M. Smith and C. E. Schwarz, "High pressure phase behaviour of the CO₂+1-decanol+n-dodecane system," *Fluid Phase Equilib.*, vol. 406, pp. 1–9, 2015.
- [17] G. J. K. Bonthuys, "Separation of 1-dodecanol and n-tetradecane through supercritical extraction," Masters Thesis, Stellenbosch University, 2008.
- [18] M. Zamudio, "The Separation of Detergent Range Alkanes and Alcohol Isomers with Supercritical Carbon Dioxide," P.h.D Thesis, Stellenbosch University, 2014.
- [19] F. C. v N. Fourie, "The high pressure phase behaviour of detergent range alcohols and alkanes," P.h.D Thesis, Stellenbosch University, 2018.
- [20] R. H. Perry and D. W. Green, *Perry's chemical engineers' handbook*, 7th ed. New York: McGraw-Hill, 1997.
- [21] NIST Chemistry WebBook, "National Institute of Standards and Technology: Available from: <http://webbook.nist.gov/chemistry/>." .
- [22] C. L. Yaws, "Yaws' Thermophysical Properties of Chemicals and Hydrocarbons." Knovel, 2010.
- [23] DIPPR 801 Database, "Design Institute for Physical Properties. Sponsored by AIChE: Available from: <http://www.aiche.org/dippr>." .
- [24] G. Brunner, *Gas Extraction: An Introduction to Fundamentals of Supercritical Fluids and the Application to Separation Processes*, Vol. 4. Darmstadt: Steinkopf; New York: Springer, 1994.
- [25] G. Brunner, "Decaffeination of raw coffee by means of compressed nitrous oxide," in *International Symposium on Supercritical Fluids*, Vol. 2, 1987, pp. 691–698.
- [26] M. McHugh and V. Krukonsis, *Supercritical Fluid Extraction*. London: Butterworths, 1986.
- [27] L. T. Taylor, *Supercritical Fluid Extraction: Techniques in Analytical Chemistry*. John Wiley & Sons, Inc., 1996.
- [28] F. V Bright and M. E. P. McNally, "Supercritical Fluid Technology: Theoretical and Applied Approaches in Analytical Chemistry," in *ACS Symposium Series No. 488*, 1992.
- [29] V. 15. 0. ACD/ChemSketch (Freeware), "Advanced Chemistry Development, Inc." Toronto, ON, Canada, Available from: www.acdlabs.com, 2016.

- [30] T. J. Bruno and J. F. Ely, *Supercritical Fluid Technology: Reviews in Modern Theory and Applications*. CRC Press, 1991.
- [31] E. Kiran and J. M. H. Levelt Sengers, *Supercritical Fluids: Fundamentals for Application*. Dordrecht, The Netherlands: Kluwer Academic Publishers, 1994.
- [32] K. Gauter, "Fluid multiphase behavior in ternary systems of near-critical CO₂: Measurements, modeling and computation," P.h.D thesis, Delft University, 1999.
- [33] C. J. Gauter, K.; Peters, "Phase equilibria in near-critical solutions: Binary and ternary mixtures of carbon dioxide and certain solutes and the occurrence of two-phase holes," in *Supercritical Fluids: Fundamentals for Applications*, Series E., C. J. Kiran, E; Debenedetti, P. G; Peters, Ed. Turkey: Kluwer Academic, 2000, pp. 69–89.
- [34] C. J. Peters and K. Gauter, "Occurrence of Holes in Ternary Fluid Multiphase Systems of Near-Critical Carbon Dioxide and Certain Solutes.," *Chem. Rev.*, vol. 99, no. 2, pp. 419–432, 1999.
- [35] G. M. Schneider, A. L. Scheidgen, and D. Klante, "Complex phase equilibrium phenomena in fluid mixtures up to 2 GPa - Cosolvency, holes, windows, closed loops, high-pressure immiscibility, barotropy, and related effects," *Ind. Eng. Chem. Res.*, vol. 39, no. 12, pp. 4476–4480, 2000.
- [36] C. J. Peters, L. . Florusse, S. Hähre, and J. de Swaan Arons, "Fluid multiphase equilibria and critical phenomena in binary and ternary mixtures of carbon dioxide, certain n-alkanols and n-tetradecane," *Fluid Phase Equilib.*, vol. 110, pp. 157–173, 1995.
- [37] C. J. Peters, "Multiphase equilibria in near-critical solvents," in *Supercritical Fluids: Fundamentals for Applications*, E. Kiran and J. M. H. Levelt Sengers, Eds. Netherlands: Kluwer Academic, 1994, pp. 117–145.
- [38] C. J. Peters, L. J. Florusse, and S. Hähre, "Measurements on Fluid Multiphase Equilibria in Ternary Mixtures of Carbon Dioxide , Tetradecane , and Certain N -Alkanols," *J. Supercrit. Fluids*, vol. 9, no. 3, pp. 135–140, 1996.
- [39] A. Kordikowski and G. M. Schneider, "Fluid phase equilibria of binary and ternary mixtures of supercritical carbon dioxide with low-volatility organic substances up to 100 MPa and 393 K: cosolvency effects and miscibility windows," *Fluid Phase Equilib.*, vol. 90, pp. 149–162, 1993.
- [40] C. L. Patton, S. H. Kisler, and K. D. Luks, "Multiphase equilibrium behaviour of a mixture of carbon dioxide, 1-decanol, and n-tetradecane," in *Supercritical Fluid Engineering: Science-Fundamentals and Applications*, E. Kiran and J. F. Brennecke, Eds. Washington D. C: American Chemical Society, 1993, pp. 55–65.
- [41] E. H. Benmekki and G. A. Mansoori, "Phase equilibrium calculations of highly polar systems," *Fluid Phase Equilib.*, vol. 32, pp. 139–149, 1987.
- [42] G. M. Kontogeorgis and I. G. Economou, "Equations of state: From the ideas of van der Waals to association theories," *J. Supercrit. Fluids*, vol. 55, no. 2, pp. 421–437, 2010.

- [43] S. Stamatakis and D. Tassios, "Performance of cubic EoS at high pressures," *Oil Gas Sci. Technol.*, vol. 53, pp. 367–377, 1998.
- [44] J. O. Valderrama, "The State of the Cubic Equations of State," *Ind. Eng. Chem. Res.*, vol. 42, no. 8, pp. 1603–1618, 2003.
- [45] C. Tsonopoulos and J. L. Heidman, "High-pressure vapor-liquid equilibria with cubic equations of state," *Fluid Phase Equilib.*, vol. 29, no. C, pp. 391–414, 1986.
- [46] J. D. van der Waals, "Over de constinuiteit van den gas- en vloeistoestand (On the continuity of the gaseous and liquid states)," P.h.D Thesis, University of Leiden, 1873.
- [47] D. Y. Peng and D. B. Robinson, "A new two-constant equation of state," *Ind. Eng. Chem. Fundam.*, vol. 15, pp. 59–64, 1976.
- [48] O. Redlich and J. N. S. Kwong, "On the Thermodynamics of Solutions V. An Equation-of-state. Fugacities of Gaseous Solutions," *Chem. Rev.*, vol. 44, pp. 223–244, 1979.
- [49] G. Soave, "Equilibrium constants from a modified Redlich-Kwong equation of state," *Chem. Eng. Sci.*, vol. 27, pp. 1197–1203, 1972.
- [50] K. E. Gubbins, "Perturbation theories of the thermodynamics of polar and associating liquids: A historical perspective," *Fluid Phase Equilib.*, vol. 416, pp. 3–17, 2016.
- [51] J. E. Lombard, "Thermodynamic modelling of hydrocarbon-chains and light-weight supercritical solvents by," Masters Thesis, Stellenbosch University, 2015.
- [52] P. H. Van Konynenburg and R. L. Scott, "Critical Lines and Phase Equilibria in Binary Van Der Waals Mixtures," in *Mathematical and Physical Sciences*, vol. 298, no. 1442, J. S. Rowlinson, Ed. London: Royal Society, 1980, pp. 495–540.
- [53] R. L. Scott and P. H. Van Konynenburg, "Van der Waals and related models for hydrocarbon mixtures," *Discuss. Faraday Soc.*, vol. 49, pp. 87–97, 1970.
- [54] K. Gauter, C. J. Peters, A. L. Scheidgen, and G. M. Schneider, "Cosolvency effects, miscibility windows and two-phase lg holes in three-phase llg surfaces in ternary systems: A status report," *Fluid Phase Equilib.*, vol. 171, no. 1–2, pp. 127–149, 2000.
- [55] Y. S. Wei and R. J. Sadus, "Phase behaviour of ternary mixtures: a theoretical investigation of the critical properties of mixtures with equal size components," *Phys. Chem. Chem. Phys.*, vol. 1, no. 18, pp. 4329–4336, 1999.
- [56] C. E. Schwarz and I. Nieuwoudt, "Phase equilibrium of propane and alkanes. Part I: Experimental procedures, dotriacontane equilibrium and EOS modelling," *J. Supercrit. Fluids*, vol. 27, no. 3, pp. 133–144, 2003.
- [57] C. E. Schwarz, "The processing of wax and wax additives with supercritical fluids," P.h.D Thesis, Stellenbosch University, 2005.
- [58] C. E. Schwarz, "The phase equilibrium of alkanes and supercritical fluids," Masters Thesis, Stellenbosch University, 2001.

- [59] D. J. Fall and K. D. Luks, "Liquid-liquid-vapor phase equilibria of the binary system carbon dioxide + n-tridecane.," *J. Chem. Eng. Data*, vol. 30, no. 3, pp. 276–279, 1985.
- [60] D. J. Fall, J. L. Fall, and K. D. Luks, "Liquid-Liquid-Vapor Immiscibility Limits in Carbon Dioxide + n-Paraffin Mixtures," *J. Chem. Eng. Data*, vol. 30, pp. 82–88, 1985.
- [61] M. M. Miller and K. D. Luks, "Observations on the multiphase equilibria behavior of CO₂-rich and ethane-rich mixtures," *Fluid Phase Equilib.*, vol. 44, no. 3, pp. 295–304, 1989.
- [62] D. H. Lam, A. Jangkamolkulchai, and K. D. Luks, "Liquid-liquid-vapor phase equilibrium behavior of certain binary nitrous oxide + n-alkanol mixtures," *Fluid Phase Equilib.*, vol. 60, no. 1–2, pp. 131–141, 1990.
- [63] J. M. Smith, H. C. Van Ness, and M. M. Abbott, *Introduction to chemical engineering thermodynamics*, 7th ed. New York: McGraw-Hill, 2005.
- [64] A. van Pelt, "Critical phenomena in binary fluid mixtures, Classification of phase equilibria with the simplified-perturbed-hard-chain theory," Delft University of Technology, 1992.
- [65] D. Stamoulis, "Patterns of fluid phase behavior in binary and quasi-binary mixtures," Ph.D Thesis, Delft University of Technology, 1994.
- [66] H. Gardeler and J. Gmehling, "Experimental determination of phase equilibria and comprehensive examination of the predictive capabilities of group contribution equations of state with a view to the synthesis of supercritical extraction processes," in *Supercritical Fluids as Solvents and Reaction Media*, G. Brunner, Ed. Amsterdam: Elsevier B.V., 2004, pp. 3–38.
- [67] K. A. M. Gasem, K. B. Dickson, P. B. Dulcamara, N. Nagarajan, and R. L. J. Robinson, "Equilibrium Phase Compositions, Phase Densities, and Interfacial Tensions for CO₂ + Hydrocarbon Systems. 5. CO₂ + n-Tetradecane," *J. Chem. Eng. Data*, vol. 34, no. 2, pp. 191–195, 1989.
- [68] R. J. Wilcock, R. Battino, W. F. Danforth, and E. Wilhelm, "Solubilities of gases in liquids II. The solubilities of He, Ne, Ar, Kr, O₂, N₂, CO, CO₂, CH₄, CF₄, and SF₆ in n-octane 1-octanol, n-decane, and 1-decanol," *J. Chem. Thermodyn.*, vol. 10, no. 9, pp. 817–822, 1978.
- [69] M.-J. Lee and J.-T. Chen, "Vapor-liquid equilibrium for carbon dioxide/alcohol systems," *Fluid Phase Equilib.*, vol. 92, pp. 215–231, 1994.
- [70] W.-L. Weng, J.-T. Chen, and M.-J. Lee, "High-pressure vapor-liquid equilibria for mixtures containing a supercritical fluid," *Ind. Eng. Chem. Res.*, vol. 33, no. 8, pp. 1955–1961, 1994.
- [71] C. J. Chang, K.-L. Chiu, and C.-Y. Day, "A new apparatus for the determination of P–x–y diagrams and Henry's constants in high pressure alcohols with critical carbon dioxide," *J. Supercrit. Fluids*, vol. 12, pp. 223–237, 1998.
- [72] D. H. Lam, A. Jangkamolkulchai, and K. D. Luks, "Liquid—liquid—vapor phase equilibrium behavior of certain binary nitrous oxide + n-alkanol mixtures," *Fluid Phase Equilib.*, vol. 60, pp. 119–130, 1990.

- [73] J. D. Hottovy, K. D. Luks, and J. P. Kohn, "Three-phase liquid–liquid–vapor equilibria behavior of certain binary carbon dioxide–n-paraffin systems," *J. Chem. Eng. Data*, vol. 26, pp. 256–258, 1981.
- [74] J. van der steen, T. W. de Loos, and J. de Swaan Arons, "The Volumetric analysis and Prediction of Liquid-Liquid-Vapour Equilibria in Certain Carbon Dioxide + n-Alkane Systems," *Fluid Phase Equilib.*, vol. 51, pp. 353–367, 1989.
- [75] S. Laugier, D. Richon, and H. Renon, "Simultaneous determination of vapor—liquid equilibria and volumetric properties of ternary systems with a new experimental apparatus," *Fluid Phase Equilib.*, vol. 54, pp. 19–34, 1990.
- [76] F. C. v. N. Fourie, C. E. Schwarz, and J. H. Knoetze, "Analytic Setup for Multicomponent High-Pressure Phase Equilibria via Dual Online Gas Chromatography," *Chem. Eng. Technol.*, vol. 38, no. 7, pp. 1165–1172, 2015.
- [77] F. C. v. N. Fourie, C. E. Schwarz, and J. H. Knoetze, "Considerations for the design of high-pressure phase equilibrium and solubility measurements equipment," in *Supercritical Fluids*, M. R. Belinsky, Ed. Stellenbosch: Nova Science, 2009, pp. 1–42.
- [78] M. Bluma and U. K. Deiters, "A classification of phase diagrams of ternary fluid systems," *Phys. Chem. Chem. Phys.*, vol. 1, no. 18, pp. 4307–4313, 1999.
- [79] U. K. Deiters and T. Kraska, *High-pressure fluid-phase equilibria: Phenomenology and computation*, 1st ed. Amsterdam: Elsevier, 2012.
- [80] T. Kraska and U. K. Deiters, "Systematic investigation of the phase behaviour in binary fluid mixtures. II. Calculations based on the Canahan-Starling-Redlich-Kwong equation of state," *J. Chem. Phys.*, vol. 96, no. 1, pp. 539–547, 1992.
- [81] F. J. Gaw and F. L. Swinton, "Occurrence of a double azeotrope in the binary system hexafluorobenzene + benzene," *Nature*, vol. 212, pp. 283–284, 1966.
- [82] A. L. Scheidgen and G. M. Schneider, "New phase phenomena in ternary systems at high pressures - Cosolvency and miscibility windows up to 100 MPa," *Phys. Chem. Chem. Phys.*, vol. 4, no. 6, pp. 963–967, 2002.
- [83] H. Pöhler, A. L. Scheidgen, and G. M. Schneider, "Fluid phase equilibria of binary and ternary mixtures of supercritical carbon dioxide with a 1-alkanol and an n-alkane up to 100 MPa and 393 K--cosolvency effect and miscibility windows (Part II)," *Fluid Phase Equilib.*, vol. 115, pp. 165–177, 1996.
- [84] J. T. Cripwell, "Assessment of the Capabilities of Two Polar sPC-SAFT Terms Through Application To Measured Ketone-alkane Phase Equilibria Data," Masters Thesis, Stellenbosch University, 2014.
- [85] S. A. M. Smith, "Measurement and modelling of the vapour-liquid equilibria of binary mixtures of water and alkanols," Masters Thesis, Stellenbosch University, 2017.

- [86] K. Tochigi, H. Inoue, and K. Kojima, "Determination of azeotropes in binary systems at reduced pressures," *Fluid Phase Equilib.*, vol. 22, no. 3, pp. 343–352, 1985.
- [87] W. Malesinski, *Azeotropy and Other Theoretical Problems*. Canada: John Wiley & Sons, 1965.
- [88] M. Góral, P. Oracz, A. Skrzecz, A. Bok, and A. Maczyński, "Recommended vapor-liquid equilibrium data. Part 1: Binary n-alkanol-n-alkane systems," *J. Phys. Chem. Ref. Data*, vol. 31, no. 3, pp. 701–748, 2002.
- [89] M. Ronc and G. R. Ratcliff, "Measurement of vapor-liquid equilibria using a semi-continuous total pressure static equilibrium still," *Can. J. Chem. Eng.*, vol. 54, no. 4, pp. 326–332, 1976.
- [90] J. M. Rhodes, T. A. Griffin, M. J. Lazzaroni, V. R. Bhethanabotla, and S. W. Campbell, "Total pressure measurements for benzene with 1-propanol, 2-propanol, 1-pentanol, 3-pentanol, and 2-methyl-2-butanol at 313.15 K," *Fluid Phase Equilib.*, vol. 179, pp. 217–229, 2001.
- [91] I. Máchová, J. Linek, and I. Wichterle, "Vapour—liquid equilibria in the heptane - 1-pentanol and heptane - 3-methyl-1-butanol systems at 75, 85 and 95 °C," *Fluid Phase Equilib.*, vol. 41, no. 3, pp. 257–267, 1988.
- [92] P. Oracz, "Recommendations for VLE data on binary 1-alkanol+ n-alkane systems," Warsaw University, 1976.
- [93] T. Treszczanowicz and A. . Treszczanowicz, "Vapor-liquid-equilibria of non-electrolyte mixtures. 3. Vapor-liquid phase equilibria of binary-systems formed by pentane -1-ol and alkanes.," *Bull. Acad. Pol. Sci., Ser. Sci. Chim.*, vol. 27, pp. 689–695, 1979.
- [94] S. A. Wieczorek and J. A. N. Stecki, "Vapour pressures and thermodynamic properties of hexan-1-ol + n-hexane between 298 . 230 and 342 . 824 K," *J. Chem. Thermodyn.*, vol. 10, pp. 177–186, 1978.
- [95] A. Heintz, E. Dolch, and R. N. Lichtenthaler, "New experimental VLE-data for alkanol/alkane mixtures and their description by an extended real association (ERAS) model," *Fluid Phase Equilib.*, vol. 27, pp. 61–79, 1986.
- [96] J. Schmelzer and H. Taummler, "Binary VLE data of 1-alcohol + alkane systems," Leipzig, 1984.
- [97] G. Geiseler, K. Quitzsch, H. G. Vogel, D. Pilz, and H. Sachse, "Thermodynamische Untersuchungen an Mischsystemen aus stellungsisomeren hydroxygruppenhaltigen n-Alkanderivaten und n-Heptan," *Z. Phys. Chem.*, vol. 56, pp. 288–302, 1967.
- [98] S. A. Wieczorek, "Vapour pressures and thermodynamic properties of decan-1-ol + n-hexane between 283.160 and 333.151 K," *J. Chem. Thermodyn.*, vol. 11, no. 3, pp. 239–245, 1979.
- [99] T. Hiaki, K. Takahashi, T. Tsuji, M. Hongo, and K. Kojima, "Vapor-liquid equilibria of ethanol with 2,2,4-trimethylpentane or octane at 101.3 kPa," *J. Chem. Eng. Data*, vol. 39, pp. 720–722, 1994.
- [100] S. A. Wieczorek, "Vapour pressure and thermodynamic properties of dodecan-1-ol + n-hexane

- between 298.230 and 342.824 K,” *J. Chem. Thermodyn.*, vol. 10, no. 2, pp. 187–194, 1978.
- [101] J. Schmelzer, V. Creutziger, I. Lieberwirth, and R. Pfestorf, “Vapour-liquid equilibria and heats of mixing in n-alkane-1-alcohol systems. III. Vapour-liquid equilibria in n-alkane-1-dodecanol systems,” *Fluid Phase Equilib.*, vol. 15, pp. 107–119, 1983.
- [102] J. Schmelzer, I. Lieberwirth, M. Krug, and R. Pfestorf, “Vapor-Liquid Equilibria and Heats of Mixing in Alkane-Alcohol(1) Systems. I. Vapour-Liquid Equilibria in 1-Alcohol-Undecane Systems,” *Fluid Phase Equilib.*, vol. 11, no. 2, pp. 187–200, 1983.
- [103] P. M. Mathias, “A Versatile Phase Equilibrium Equation-of-state,” *Ind. Eng. Chem. Process Des. Dev.*, vol. 22, pp. 385–391, 1983.
- [104] A. R. Heidemann, “Combined excess free energy models and equations of state,” *Fluid Phase Equilib.*, vol. 56, pp. 17–37, 1990.
- [105] M. Solorzano-Zavala, F. Barragan-Aroche, and E. R. Bazua, “Comparative study of mixing rules for cubic equations of state in the prediction of multicomponent vapor-liquid equilibria,” *Fluid Phase Equilib.*, vol. 122, pp. 99–116, 1996.
- [106] S. Ionita, V. Feroiu, and D. Geana, “Phase Equilibria of the Carbon Dioxide + 1-Decanol System at High Pressures,” *J. Chem. Eng. Data*, vol. 58, pp. 3069–3077, 2013.
- [107] G. M. Kontogeorgis and G. K. Folas, *Thermodynamic Models for Industrial Applications: from classical and advanced mixing rules to association theories*. United Kingdom: John Wiley & Sons, 2010.
- [108] M. D. Koretsky, *Engineering and Chemical Thermodynamics*, 2nd ed. New Jersey: Wiley, 2004.
- [109] J. Schwartzentruber and H. Renon, “Extension of UNIFAC to High Pressures and Temperatures by the Use of a Cubic-Equation-of-State,” *Ind. Eng. Chem. Res.*, vol. 28, pp. 1049–1955, 1989.
- [110] C. Panayiotou and I. C. Sanchez, “Hydrogen bonding in fluids: An equation-of-state approach,” *J. Phys. Chem.*, vol. 95, no. 24, pp. 10090–10097, 1991.
- [111] M.-J. Huron and J. Vidal, “New mixing rules in simple equations of state for representing vapour-liquid equilibria of strongly non-ideal mixtures,” *Fluid Phase Equilib.*, vol. 3, pp. 255–271, 1979.
- [112] G. M. Wilson, “A New Expression for the Excess Free Energy of Mixing,” *J. Am. Chem. Soc.*, vol. 86, no. 2, pp. 127–130, 1964.
- [113] H. Renon and J. M. Prausnitz, “Local Compositions in Thermodynamic Excess Functions for Liquid Mixtures,” *AIChE J.*, vol. 14, no. 1, pp. 135–144, 1968.
- [114] D. S. Abrams and J. M. Prausnitz, “Statistical Thermodynamics of liquid mixtures: A new expression for the Excess Gibbs Energy of Partly or Completely Miscible Systems,” *AIChE J.*, vol. 21, p. 116, 1975.
- [115] K. Fischer and J. Gmehling, “Further development , status and results of the PSRK method for the prediction of vapor-liquid equilibria and gas solubilities,” *Fluid Phase Equilib.*, vol. 121, pp.

- 185–206, 1996.
- [116] J. Gmehling, “From UNIFAC to modified UNIFAC to PSRK with the help of DDB,” *Fluid Phase Equilib.*, vol. 107, pp. 1–29, 1995.
 - [117] P. A. Gupte and T. E. Daubert, “Extension of UNIFAC to high pressure VLE using Vidal mixing rules,” *Fluid Phase Equilib.*, vol. 28, pp. 155–170, 1986.
 - [118] S. Hirohama, D. Bluck, and M. Sasaki, “Direct prediction of the binary parameters of a cubic equation of state from those of a low-pressure gE model,” *Fluid Phase Equilib.*, vol. 302, no. 1–2, pp. 305–309, 2011.
 - [119] H. Orbey, S. I. Sandler, D. Shan, and H. Wong, “Accurate equation of state predictions at high temperatures and pressures using the existing UNIFAC model,” *Fluid Phase Equilib.*, vol. 85, pp. 41–54, 1993.
 - [120] A. Fredenslund, J. Gmehling, and P. Rasmussen, *Vapor-Liquid Equilibria using UNIFAC*. Amsterdam: Elsevier, 1977.
 - [121] A. Fredenslund, R. L. Jones, and J. M. Prausnitz, “Group-contribution estimation of activity coefficients in nonideal liquid mixtures,” *AIChE J.*, vol. 21, no. 6, pp. 1086–1099, 1975.
 - [122] H. K. Hansen, P. Rasmussen, A. Fredenslund, M. Schiller, and J. Gmehling, “Vapor-Liquid Equilibria by UNIFAC Group Contribution. 5 Revision and Extension,” *Ind. Eng. Chem. Res.*, vol. 30, pp. 2352–2355, 1991.
 - [123] C. Christensen, J. Gmehling, P. Rasmussen, U. Weidlich, and T. Holderbaum, “Heats of Mixing Data Collection,” in *DECHEMA Chemistry Data Series*, Frankfurt.
 - [124] J. Gmehling, U. Onken, W. Arlt, P. Grenzheuser, B. Kolbe, J. Rarey, and U. Weidlich, “Vapor-Liquid equilibrium Data Collection,” in *DECHEMA Chemistry Data Series*, Frankfurt.
 - [125] P. Kolar and K. Kojima, “Prediction of critical points in multicomponent systems using the PSRK group contribution equation of state,” *Fluid Phase Equilib.*, vol. 118, pp. 175–200, 1996.
 - [126] G. M. Kontogeorgis and G. K. Folas, *Thermodynamic Models for Industrial Applications: From Classical and Advanced Mixing Rules to Association Theories*. 2009.
 - [127] T. Holderbaum and J. Gmehling, “PSRK: A Group Contribution Equation of State Based on UNIFAC,” *Fluid Phase Equilib.*, vol. 70, pp. 251–265, 1991.
 - [128] S. Horstmann, K. A. I. Fischer, and J. Gmehling, “Application of PSRK for Process Design,” *Chem. Eng. Commun.*, no. 192, pp. 336–350, 2005.
 - [129] J. Gmehling, “Potential of group contribution methods for the prediction of phase equilibria and excess properties of complex mixtures *,” *Pure Appl. Chem.*, vol. 75, no. 7, pp. 875–888, 2003.
 - [130] J. Li, K. Fischer, and J. Gmehling, “Prediction of vapor – liquid equilibria for asymmetric systems at low and high pressures with the PSRK model,” *Fluid Phase Equilib.*, vol. 143, pp. 71–82, 1998.
 - [131] S. Horstmann, A. Jabłoniec, J. Krafczyk, K. Fischer, and J. Gmehling, “PSRK group

- contribution equation of state: comprehensive revision and extension IV , including critical constants and alpha-function parameters for 1000 components,” *Fluid Phase Equilib.*, vol. 227, pp. 157–164, 2005.
- [132] J. Gmehling, J. Li, and K. Fischer, “Further development of the PSRK model for the prediction of gas solubilities and vapor-liquid -equilibria at low and high pressures II,” *Fluid Phase Equilib.*, vol. 141, pp. 113–127, 1997.
- [133] Q. Yang and C. Zhong, “A modified PSRK model for the prediction of the vapor-liquid equilibria of asymmetric systems,” *Fluid Phase Equilib.*, vol. 192, no. 1–2, pp. 103–120, 2001.
- [134] L. Min, W. Lisheng, and J. Gmehling, “A modified mixing rule for PSRK model and application for the predicton of vapor-liquid equilibria of polymer solutions,” *Chinese J. Chem. Eng.*, vol. 12, no. 3, pp. 454–457, 2004.
- [135] J. Chen, K. Fischer, and J. Gmehling, “Modification of PSRK mixing rules and results for vapor – liquid equilibria, enthalpy of mixing and activity coefficients at infinite dilution,” *Fluid Phase Equilib.*, vol. 200, pp. 411–429, 2002.
- [136] J. Kiepe, S. Horstmann, H. Gardeler, K. Fischer, J. Ahlers, J. Gmehling, M. Topphoff, and J. Gmehling, “Predictive Soave-Redlich-Kwong Equation of State (PSRK),” p. 27.
- [137] E. C. Voutsas, C. J. Boukouvalas, N. S. Kalospiros, and D. P. Tassios, “The performance of EoS/GE models in the prediction of vapor-liquid equilibria in asymmetric systems,” *Fluid Phase Equilib.*, vol. 116, pp. 480–487, 1996.
- [138] A. U. Burman and K. H. U. Strom, “Excess Enthalpy and Vapor-Liquid Equilibria with the MHV2 and Soave Mixing Rules,” *Chem. Eng. Commun.*, vol. 198, pp. 1435–1452, 2011.
- [139] M. L. Michelsen, “A modified Huron-Vidal mixing rule for cubic equations of state,” *Fluid Phase Equilib.*, vol. 60, pp. 213–219, 1990.
- [140] S. Dahl, A. Dunalewicz, A. Fredenslund, and P. Rasmussen, “The MHV2 Model: Prediction of Phase Equilibria at Sub- and Supercritical Conditions,” *J. Supercrit. Fluids*, no. 5, pp. 42–47, 1992.
- [141] S. Dahl and M. L. Michelsen, “High-Pressure Vapor-Liquid Equilibrium with a UNIFAC-based Equation-of-state,” *AIChE J.*, vol. 36, pp. 1829–1836, 1990.
- [142] W. Wang, Y. Qu, C. H. Twu, and J. E. Coon, “Comprehensive comparison and evaluation of the mixing rules of WS, MHV2 and Twu et al.,” *Fluid Phase Equilib.*, vol. 116, pp. 488–494, 1996.
- [143] M. L. Michelsen, “A method for incorporating excess Gibbs energy models in equations of state,” *Fluid Phase Equilib.*, vol. 60, pp. 47–58, 1990.
- [144] C. Lermite and J. Vidal, “A group contribution equation of state for polar and non-polar compounds,” *Fluid Phase Equilib.*, vol. 72, pp. 111–130, 1992.
- [145] C. Boukouvalas, N. Spiliotis, P. Coutisikos, N. Tzouvaras, and D. Tassios, “Prediction of vapor-

- liquid equilibrium with the LCVm model: a linear combination of the Vidal and Michelsen mixing rules coupled with the original UNIFAC and the t-mPR equation of state,” *Fluid Phase Equilib.*, vol. 92, pp. 75–106, 1994.
- [146] P. Kolar and K. Kojima, “Determination of the binary cross virial coefficient in the Wong-Sandler mixing rule for cubic equations of state,” *J. Chem. Eng. Japan*, vol. 27, no. 4, pp. 460–465, 1994.
- [147] A. Naderifar, B. Khodakarami, and I. Zanganeh, “New approach for the prediction of vapor – liquid equilibria in asymmetric systems using GE – EOS mixing rules,” *Fluid Phase Equilib.*, vol. 271, pp. 38–42, 2008.
- [148] D. S. Wong, H. Orbey, and S. I. Sandler, “Equation-of-state Mixing Rule for Non-ideal Mixtures Using Available Activity Coefficient Model Parameters and That Allows Extrapolation over Large Ranges of Temperature and Pressure,” *Ind. Eng. Chem. Res.*, vol. 31, pp. 2033–2039, 1992.
- [149] D. S. Wong and S. I. Sandler, “A Theoretically Correct New Mixing Rule for Cubic Equations of State for Both Highly and Slightly Non-ideal Mixtures,” *AIChE J.*, vol. 38, pp. 671–680, 1992.
- [150] B. Larsen, P. Rasmussen, and A. Fredenslund, “A Modified UNIFAC Group-Contribution Model for Prediction of Phase Equilibria and Heats of Mixing,” *Ind. Eng. Chem. Res.*, vol. 26, pp. 2274–2286, 1987.
- [151] E. A. Muller and K. E. Gubbins, “Molecular-based equations of state for associating fluids: A review of SAFT and related approaches,” *Ind. Eng. Chem. Res.*, vol. 40, no. 10, pp. 2193–2211, 2001.
- [152] G. M. Kontogeorgis, “Association theories for complex thermodynamics,” *Chem. Eng. Res. Des.*, vol. 91, no. 10, pp. 1840–1858, 2013.
- [153] G. M. Kontogeorgis, E. C. Voutsas, I. V. Yakoumis, and D. P. Tassios, “An equation of state for associating fluids,” *Ind. Eng. Chem. Res.*, vol. 35, no. 11, pp. 4310–4318, 1996.
- [154] P. M. Mathias and T. W. Copeman, “Extension of the Peng-Robinson equation of state to complex mixtures: Evaluation of the various forms of the local composition concept,” *Fluid Phase Equilib.*, vol. 13, pp. 91–108, 1983.
- [155] A. Peneloux, E. Rauzy, and R. Freze, “A Consistent Correction For Redlich-Kwong-Soave Volumes,” *Fluid Phase Equilib.*, vol. 8, pp. 7–23, 1982.
- [156] J. F. Boston and P. M. Mathias, “Phase Equilibria in a Third- Generation Process Simulator,” in *2nd International Conference on Phase Equilibria and Fluid Properties in the Chemical Process Industries*, 1980, pp. 823–849.
- [157] J. Schwartzentruber, H. Renon, and S. Watanasiri, “K-values for Non-Ideal Systems: An Easier Way,” *Chem. Eng.*, no. March, pp. 118–124, 1990.
- [158] F. C. v. N. Fourie, C. E. Schwarz, and J. H. Knoetze, “CO₂ + n-dodecane + 3,7-dimethyl-1-

- octanol: high-pressure experimental phase equilibria data and thermodynamic modelling,” *J. Supercrit. Fluids*, vol. 130, pp. 105–117, 2017.
- [159] F. C. v. N. Fourie, C. E. Schwarz, and J. H. Knoetze, “CO₂ + 3,7-dimethyl-1-octanol + 1-decanol: High pressure experimental phase equilibria data and thermodynamic modelling,” *J. Supercrit. Fluids*, vol. 136, pp. 82–94, 2018.
- [160] J. A. Barker and D. Henderson, “What is ‘liquid’? Understanding the states of matter,” *Rev. Mod. Phys.*, vol. 48, no. 4, pp. 587–671, 1976.
- [161] J. A. Barker and D. Henderson, “Perturbation theory and equation of state for fluids: the square-well potential,” *J. Chem. Phys.*, vol. 47, no. 8, pp. 2856–2861, 1967.
- [162] J. A. Barker and D. Henderson, “Perturbation theory and equation of state for fluids. II. A successful theory of liquids,” *J. Chem. Phys.*, vol. 47, no. 11, pp. 4714–4721, 1967.
- [163] W. G. Chapman, K. E. Gubbins, G. Jackson, and M. Radosz, “New reference equation of state for associating liquids,” *Ind. Eng. Chem. Res.*, vol. 29, no. 8, pp. 1709–1721, 1990.
- [164] W. G. Chapman, K. E. Gubbins, G. Jackson, and M. Radosz, “SAFT: Equation-of-state solution model for associating fluids. Fluid Phase Equilibria,” *Fluid Phase Equilib.*, vol. 52, pp. 31–38, 1989.
- [165] M. S. Wertheim, “Thermodynamic perturbation theory of polymerization,” *J. Chem. Phys.*, vol. 87, no. 12, pp. 7323–7331, 1987.
- [166] M. S. Wertheim, “Fluids with highly directional attractive forces. I. Statistical thermodynamics,” *J. Stat. Phys.*, vol. 35, no. 1, pp. 19–34, 1984.
- [167] M. S. Wertheim, “Fluids with highly directional attractive forces. II. Thermodynamic perturbation theory and integral equations,” *J. Stat. Phys.*, vol. 35, no. 1, pp. 35–47, 1984.
- [168] M. S. Wertheim, “Fluids with highly directional attractive forces. III. Multiple attraction sites,” *J. Stat. Phys.*, vol. 42, no. 3, pp. 459–476, 1986.
- [169] M. S. Wertheim, “Fluids with highly directional attractive forces. IV. Equilibrium polymerization,” *J. Stat. Phys.*, vol. 42, no. 3, pp. 477–492, 1986.
- [170] M. L. Michelsen and J. M. Møllerup, *Thermodynamic models: Fundamentals and computational aspects*, 2nd ed. Copenhagen: Tie line publications, 2007.
- [171] N. von Solms, M. L. Michelsen, and G. M. Kontogeorgis, “Computational and physical performance of a modified PC-SAFT equation of state for highly asymmetric and associating mixtures,” *Ind. Eng. Chem. Res.*, vol. 42, no. 5, pp. 1098–1105, 2003.
- [172] S. H. Huang and M. Radosz, “Equation of state for small, large, polydisperse, and associating molecules,” *Ind. Eng. Chem. Res.*, vol. 29, no. 11, pp. 2284–2294, 1990.
- [173] S. H. Huang and M. Radosz, “Equation of State for Small, Large, Polydisperse, and Associating Molecules: Extension to Fluid Mixtures,” *Ind. Eng. Chem. Res.*, vol. 30, no. 8, pp. 1994–2005, 1991.

- [174] I. G. Economou and M. D. Donohue, "Equations of state for hydrogen bonding systems," *Fluid Phase Equilib.*, vol. 116, pp. 518–529, 1996.
- [175] S. P. Tan, H. Adidharma, and M. Radosz, "Recent advances and applications of Statistical Associating Fluid Theory," *Ind. Eng. Chem. Res.*, vol. 47, no. 21, pp. 8063–8082, 2008.
- [176] E. C. Voutsas, G. M. Kontogeorgis, and I. V. Yakoumis, "Correlation of liquid-liquid equilibria for alcohol/hydrocarbon mixtures using the CPA equation of state," *Fluid Phase Equilib.*, vol. 132, no. 1, pp. 61–75, 1997.
- [177] E. Voutsas, C. Perakis, G. Pappa, and D. Tassios, "An evaluation of the performance of the Cubic-Plus-Association equation of state in mixtures of non-polar, polar and associating compounds: Towards a single model for non-polymeric systems," *Fluid Phase Equilib.*, vol. 261, no. 1, pp. 343–350, 2007.
- [178] J. Gross and G. Sadowski, "Modeling polymer systems using the perturbed-chain statistical associating fluid theory equation of state," *Ind. Eng. Chem. Res.*, vol. 41, pp. 1084–1093, 2002.
- [179] J. Gross and G. Sadowski, "Application of the Perturbed-Chain SAFT Equation of State to Associating Systems," *Ind. Eng. Chem. Res.*, vol. 41, no. 22, pp. 5510–5515, 2002.
- [180] J. Gross, O. Spuhl, F. Tumakaka, and G. Sadowski, "Modeling Copolymer Systems Using the Perturbed-Chain SAFT Equation of State," *Ind. Eng. Chem. Res.*, vol. 42, pp. 1266–1274, 2003.
- [181] J. Gross and G. Sadowski, "Perturbed-chain SAFT: An equation of state based on a perturbation theory for chain molecules," *Ind. Eng. Chem. Res.*, vol. 40, no. 4, pp. 1244–1260, 2001.
- [182] F. Becker, M. Buback, H. Latz, G. Sadowski, and F. Tumakaka, "Cloud-Point Curves of Ethylene-(Meth)acrylate Copolymers in Fluid Ethene up to High Pressures and Temperatures – Experimental Study and PC-SAFT Modeling," *Fluid Phase Equilib.*, vol. 215, pp. 263–282, 2004.
- [183] M. Kleiner, F. Tumakaka, G. Sadowski, H. Latz, and M. Buback, "Phase Equilibria in Polydisperse and Associating Copolymer Solutions: Poly(ethaneco-(meth)acrylic acid) – Monomer Mixtures," *Fluid Phase Equilib.*, vol. 241, pp. 113–123, 2006.
- [184] J. Gross and G. Sadowski, "Application of perturbation theory to a hard-chain reference fluid: An equation of state for square-well chains," *Fluid Phase Equilib.*, vol. 168, no. 2, pp. 183–199, 2000.
- [185] P. K. Jog, S. G. Sauer, J. Blaesing, and W. G. Chapman, "Application of dipolar chain theory to the phase behavior of polar fluids and mixtures," *Ind. Eng. Chem. Res.*, vol. 40, no. 21, pp. 4641–4648, 2001.
- [186] M. G. Bjørner, "Thermodynamic modeling of CO₂ mixtures," Technical University of Denmark, 2016.
- [187] L. A. Roman-Ramirez, F. Garcia-Sanchez, C. H. Ortiz-Estrada, and D. N. Justo-Garcia, "Modeling of Vapor–Liquid Equilibria for CO₂ + 1-Alkanol Binary Systems with the PC-SAFT

- Equation of State Using Polar Contributions,” *Ind. Eng. Chem. Res.*, vol. 49, no. 23, pp. 12276–12283, 2010.
- [188] X. Tang and J. Gross, “Modeling the phase equilibria of hydrogen sulfide and carbon dioxide in mixture with hydrocarbons and water using the PCP-SAFT equation of state,” *Fluid Phase Equilib.*, vol. 293, no. 1, pp. 11–21, 2010.
- [189] A. Dominik, W. G. Chapman, M. Kleiner, and G. Sadowski, “Modeling of polar systems with the Perturbed-Chain SAFT equation of state. Investigation of the performance of two polar terms,” *Ind. Eng. Chem. Res.*, vol. 44, no. 17, pp. 6928–6938, 2005.
- [190] S. G. Sauer and W. G. Chapman, “A Parametric Study of Dipolar Chain Theory with Applications to Ketone Mixtures,” *Ind. Eng. Chem. Res.*, vol. 42, p. 5687, 2003.
- [191] S. S. Chen and A. Kreglewski, “Applications of the augmented van der Waals Theory of fluids.: I. Pure fluids,” *Berichte der Bunsengesellschaft fur Phys. Chemie*, vol. 81, no. 10, pp. 1048–1052, 1977.
- [192] T. Boublik, “Hard-sphere equation of state,” *J. Chem. Phys.*, vol. 53, no. 1, pp. 471–472, 1970.
- [193] G. A. Mansoori, N. F. Carnahan, K. E. Starling, and T. W. J. Leland, “Equilibrium thermodynamic properties of the mixture of hard spheres,” *J. Chem. Phys.*, vol. 54, no. 4, pp. 1523–1525, 1971.
- [194] N. F. Carnahan and K. E. Starling, “Equation of state for nonattracting rigid spheres,” *J. Chem. Phys.*, vol. 51, no. 2, pp. 635–636, 1969.
- [195] J. P. Wolbach and S. I. Sandler, “Using Molecular Orbital Calculations To Describe the Phase Behavior of Hydrogen-Bonding Fluids,” *Ind. Eng. Chem. Res.*, vol. 36, no. 10, pp. 4041–4051, 1997.
- [196] W. A. Fouad, L. Wang, A. Haghmoradi, S. K. Gupta, and W. G. Chapman, “Understanding the Thermodynamics of Hydrogen Bonding in Alcohol-Containing Mixtures: Self-Association,” *J. Phys. Chem. B*, vol. 119, no. 13, pp. 14086–14101, 2015.
- [197] W. A. Fouad, L. Wang, A. Haghmoradi, D. Asthagiri, and W. G. Chapman, “Understanding the Thermodynamics of Hydrogen Bonding in Alcohol-Containing Mixtures: Cross-Association,” *J. Phys. Chem. B*, vol. 120, no. 13, pp. 3388–3402, 2016.
- [198] N. von Solms, M. L. Michelsen, C. P. Passos, S. O. Derawi, and G. M. Kontogeorgis, “Investigating models for associating fluids using spectroscopy,” *Ind. Eng. Chem. Res.*, vol. 45, no. 15, pp. 5368–5374, 2006.
- [199] N. Asprien, H. Hasse, and G. Maurer, “FT-IR spectroscopic investigations of hydrogen bonding in alcohol-hydrocarbon solutions,” *Fluid Phase Equilib.*, vol. 186, no. 1, pp. 1–25, 2001.
- [200] N. M. Al-Saifi, E. Z. Hamad, and P. Englezos, “Prediction of vapor-liquid equilibrium in water-alcohol-hydrocarbon systems with the dipolar Perturbed-Chain SAFT equation of state,” *Fluid Phase Equilib.*, vol. 271, no. 1, pp. 82–93, 2008.

- [201] A. J. De Villiers, “Evaluation and improvement of the sPC-SAFT equation of state for complex mixtures,” P.h.D Thesis, Stellenbosch University, 2011.
- [202] R. O’Lenick, X. J. Li, and Y. C. Chiew, “Correlation functions of hard-sphere chain mixtures: integral equation theory and simulation results,” *Mol. Phys.*, vol. 86, p. 1123, 1995.
- [203] J. Gross, “An equation-of-state contribution for polar components: Quadrupolar molecules.,” *AIChE J.*, vol. 51, no. 9, pp. 2556–2568, 2005.
- [204] F. Tumakaka and G. Sadowski, “Application of the Perturbed-Chain SAFT equation of state to polar systems,” *Fluid Phase Equilib.*, vol. 217, no. 2, pp. 233–239, 2004.
- [205] P. K. Jog and W. G. Chapman, “Application of Wertheim’s thermodynamic perturbation theory to dipolar hard sphere chains,” *Mol. Phys.*, vol. 97, no. 3, pp. 307–319, 1999.
- [206] E. K. Karakatsani and I. G. Economou, “Perturbed chain-statistical associating fluid theory extended to dipolar and quadrupolar molecular fluids,” *J. Phys. Chem. B*, vol. 110, no. 18, pp. 9252–9261, 2006.
- [207] E. K. Karakatsani, G. M. Kontogeorgis, and I. G. Economou, “Evaluation of the Truncated Perturbed Chain-Polar Statistical Associating Fluid Theory for Complex Mixture Fluid Phase Equilibria,” *Ind. Eng. Chem. Res.*, vol. 45, no. 17, pp. 6063–6074, 2006.
- [208] D. NguyenHuynh, J.-P. Passarello, P. Tobaly, and J.-C. de Hemptinne, “Application of GC-SAFT EOS to polar systems using a segment approach,” *Fluid Phase Equilib.*, vol. 264, no. 1–2, pp. 62–75, 2008.
- [209] B. Larsen, J. C. Rasaiah, and G. Stell, “Thermodynamic perturbation theory for multipolar and ionic liquids,” *Mol. Phys.*, vol. 33, no. 4, pp. 987–1027, 1977.
- [210] G. S. Rushbrooke, G. Stell, and J. S. Hove, “Theory of polar liquids. I. Dipolar hard spheres,” *Mol. Phys.*, vol. 26, no. 5, pp. 1199–1215, 1973.
- [211] G. Stell, J. C. Rasaiah, and H. Narang, “Thermodynamic perturbation theory for simple polar fluids, I,” *Mol. Phys.*, vol. 23, no. 2, pp. 393–406, 1972.
- [212] G. Stell, J. C. Rasaiah, and H. Narang, “Thermodynamic perturbation theory for simple polar fluids. II,” *Mol. Phys.*, vol. 27, no. 5, pp. 1393–1414, 1974.
- [213] C. H. Twu and K. E. Gubbins, “Thermodynamics of polyatomic fluid mixtures—II: Polar, quadrupolar and octopolar molecules,” *Chem. Eng. Sci.*, vol. 33, no. 7, pp. 879–887, 1978.
- [214] K. E. Gubbins and C. H. Twu, “Thermodynamics of polyatomic fluid mixtures—I theory.,” *Chem. Eng. Sci.*, vol. 33, no. 7, pp. 863–878, 1978.
- [215] J. Stoll, J. Vrabec, H. Hasse, and J. Fischer, “Comprehensive study of the vapour–liquid equilibria of the pure two-centre Lennard–Jones plus pointquadrupole fluid,” *Fluid Phase Equilib.*, vol. 179, no. 1–2, pp. 339–362, 2001.
- [216] M. Flytzani-Stephanopoulos, K. E. Gubbins, and C. G. Gray, “Thermodynamics of mixtures of nonspherical molecules II. Strong polar, quadrupolar, and overlap forces,” *Mol. Phys.*, vol. 30,

- no. 6, pp. 1649–1676, 1975.
- [217] Y. Le Guennec, S. Lasala, R. Privat, and J.-N. Jaubert, “A consistency test for α -functions of cubic equations of state,” *Fluid Phase Equilib.*, vol. 427, pp. 513–538, 2016.
 - [218] H. I. Britt and R. H. Luecke, “The Estimation of Parameters in Nonlinear, Implicit Models,” *Technometrics*, vol. 15, pp. 233–247, 1973.
 - [219] R. E. Fornari, P. Alessi, and I. Kikic, “High-pressure fluid-phase equilibria: Experimental methods and systems investigated (1978-1987),” *Fluid Phase Equilib.*, vol. 57, pp. 1–33, 1990.
 - [220] J. M. S. Fonseca, R. Dohrn, and S. Peper, “High-pressure fluid-phase equilibria : Experimental methods and systems investigated (2005 – 2008),” *Fluid Phase Equilib.*, vol. 300, pp. 1–69, 2011.
 - [221] M. Christov and R. Dohrn, “High-pressure fluid phase equilibria Experimental methods and systems investigated (1994 – 1999),” *Fluid Phase Equilib.*, vol. 202, pp. 153–218, 2002.
 - [222] J. Raal and A. Mühlbauer, “The Measurement of High Pressure Vapour-Liquid Equilibria: Part II: Static Methods,” *Dev. Chem. Eng. Miner. Process.*, vol. 2, no. 2–3, pp. 88–104, 1994.
 - [223] J. Raal and A. Mühlbauer, “The Measurement of High Pressure Vapour-Liquid Equilibria: Part I: Dynamic Methods,” *Dev. Chem. Eng. Miner. Process.*, vol. 2, no. 2–3, pp. 69–87, 1994.
 - [224] R. Dohrn, S. Peper, and J. M. S. Fonseca, “High-pressure fluid-phase equilibria: Experimental methods and systems investigated (2000-2004),” *Fluid Phase Equilib.*, vol. 288, pp. 1–54, 2010.
 - [225] R. Dohrn and G. Brunner, “High-pressure fluid-phase equilibria: experimental methods and systems investigated (1988-1993),” *Fluid Phase Equilib.*, vol. 106, pp. 213–282, 1995.
 - [226] J. D. Raal and A. L. Mulbauer, *Phase Equilibria: Measurement and Computation*. Washington D. C: Taylor & Francis, 1998.
 - [227] M. M. Abbott, “Low-pressure phase equilibria: Measurement of VLE,” *Fluid Phase Equilib.*, vol. 29, no. C, pp. 193–207, 1986.
 - [228] S. C. Lee, “Partial pressure isotherms. II,” *J. Phys. Chem.*, vol. 1452, pp. 3558–3582, 1931.
 - [229] C. Pienaar, C. E. Schwarz, J. H. Knoetze, and A. J. Burger, “Vapor-liquid-liquid equilibria measurements for the dehydration of ethanol, isopropanol, and n-propanol via azeotropic distillation using DIPE and isooctane as entrainers,” *J. Chem. Eng. Data*, vol. 58, no. 3, pp. 537–550, 2013.
 - [230] C. Pienaar, “Evaluation of entrainers for the dehydration of C2 and C3 alcohols via azeotropic distillation,” Masters Thesis, Stellenbosch University, 2012.
 - [231] L. Brits, “Vapour-liquid-liquid equilibria measurements for the dehydration of low molecular weight alcohols via heterogeneous azeotropic distillation,” *Masters Thesis*, 2015.
 - [232] M. du Rand and I. Nieuwoudt, “Measurement of phase equilibria of supercritical carbon dioxide and paraffins,” *J. Supercrit. Fluids*, vol. 21, no. 3, pp. 181–193, 2001.
 - [233] C. J. Peters, H. J. Van Der Kooi, and J. De Swaan Arons, “Measurements and calculations of

- phase equilibria for (ethane + tetracosane) and (p, V_m^* , T) of liquid tetracosane,” *J. Chem. Thermodyn.*, vol. 19, no. 4, pp. 395–405, 1987.
- [234] W. L. Weng and M. J. Lee, “Phase equilibrium measurements for the binary mixtures of 1-octanol plus CO₂, C₂H₆ and C₂H₄,” *Fluid Phase Equilib.*, vol. 73, no. 1–2, pp. 117–127, 1992.
- [235] H.-S. Byun and C. Kwak, “High pressure phase behavior for carbon dioxide-1-butanol and carbon dioxide-1-octanol systems,” *Korean J. Chem. Eng.*, vol. 19, no. 6, pp. 1007–1013, 2002.
- [236] I. F. Hölscher, M. Spee, and G. M. Schneider, “Fluid-phase equilibria of binary and ternary mixtures of CO₂ with hexadecane, 1-dodecanol, 1-hexadecanol and 2-ethoxy-ethanol at 333.2 and 393.2 K and at pressures up to 33 MPa,” *Fluid Phase Equilib.*, vol. 49, no. C, pp. 103–113, 1989.
- [237] F. C. v N. Fourie, C. E. Schwarz, and J. H. Knoetze, “Analytic High-pressure phase equilibria part II: gas chromatography and sampling method development,” *Chem. Eng. Technol.*, vol. 39, pp. 1475–1482, 2016.
- [238] C. McDermott and S. R. M. Ellis, “A multicomponent consistency test,” *Chem. Eng. Sci.*, vol. 20, no. September 1964, pp. 293–296, 1965.
- [239] H. C. Ku and C. H. Tu, “Isobaric vapor-liquid equilibria for mixtures of acetone, ethanol, and 2,2,4-trimethylpentane at 101.3 kPa,” *Fluid Phase Equilib.*, vol. 231, no. 1, pp. 99–108, 2005.
- [240] J. Wisniak, E. Fishman, and R. Shaulitch, “Isobaric Vapor–Liquid Equilibria in the Systems 2-Butanone + Heptane and 2-Butanone + Oxolane,” *J. Chem. Eng. Data*, vol. 43, no. 4, pp. 537–540, 1998.
- [241] B. E. Poling, J. M. Prausnitz, and J. P. O’Connell, *The Properties of Gases and Liquids*, 5th ed. United States of America: McGraw-Hill Companies Inc., 2001.
- [242] K. G. Joback, “A unified approach to physical property estimation using multivariate statistical techniques,” Massachusetts Institute of Technology, 1984.
- [243] K. G. Joback and R. C. Reid, “Estimation of pure-component properties from group-contributions,” *Chem. Eng. Commun.*, vol. 57, pp. 233–243, 1987.
- [244] L. Constantinou and R. Gani, “New group contribution method for estimating properties of pure compounds,” *AIChE*, vol. 40, pp. 1697 – 1710, 1994.
- [245] G. M. Wilson and L. V. Jaspersion, *Critical constants T_c , P_c , estimation based on zero first and second order methods*. New Orleans, LA, 1996.
- [246] J. Marerro-Morejón and E. Radillo-Fontdevila, “Estimation of pure compound properties using group-interaction contributions,” *AIChE*, vol. 45, pp. 615–621, 1999.
- [247] A. Bondi, *Physical properties of molecular liquids, crystals, and glasses*. New York: Wiley, 1968.
- [248] A. D. Buckingham, “Molecular quadrupole moments,” *Q. Rev. Chem. Soc.*, vol. 13, pp. 183–214, 1959.

- [249] A. D. Buckingham and R. L. Disch, "The quadrupole moment of the carbon dioxide molecule," *Proc. R. Soc. London*, vol. 273, no. 1353, pp. 275–289, 1963.
- [250] A. D. Buckingham, R. L. Disch, and D. A. Dunmur, "The quadrupole moments of some simple molecules," *J. Am. Chem. Soc.*, vol. 90, no. 12, pp. 3104–3107, 1968.
- [251] D. E. Stogryn and A. P. Stogryn, "Molecular multipole moments," *Mol. Phys.*, vol. 11, no. 4, pp. 371–393, 1966.
- [252] J. E. Harries, "The quadrupole moment of CO₂, measured from the far infrared spectrum," *J. Phys. B At. Mol. Phys.*, vol. 3, no. 12, p. L150, 1970.
- [253] C. Graham, J. Pierrus, and R. E. Raab, "Measurement of the electric quadrupole moments of CO₂, CO and N₂," *Mol. Phys.*, vol. 67, no. 4, pp. 939–955, 1989.
- [254] C. G. Gray and K. E. Gubbins, *Theory of Molecular Fluids: I: Fundamentals*, Internatio. New York: Oxford University Press, 1984.
- [255] K. Mejbri, A. Tsieb, and A. Bellagi, "Phase equilibria calculation of binary and ternary mixtures of associating fluids applying PC-SAFT equation of state," *J. Supercrit. Fluids*, vol. 104, pp. 132–144, 2015.
- [256] G. V. Yukhnovich, "Hydrogen-bond cooperativity," *J. Mol. Liq.*, vol. 46, pp. 211–219, 1990.
- [257] R. B. Gupta and R. L. Brinkley, "Hydrogen-bond cooperativity in 1-alkanol plus n-alkane binary mixtures," *AIChE J.*, vol. 44, no. 1, pp. 207–213, 1998.
- [258] R. P. Sear and G. Jackson, "Thermodynamic perturbation theory for association with bond cooperativity," *J. Chem. Phys.*, vol. 105, no. 3, pp. 1113–1120, 1996.
- [259] J. Wisniak, "A new test for the thermodynamic consistency of vapor-liquid equilibrium," *Ind. Eng. Chem. Res.*, vol. 32, pp. 1531–1533, 1993.
- [260] J. T. Cripwell, C. E. Schwarz, and A. J. Burger, "Vapor–Liquid Equilibria Measurements for the Nine *n* -Alkane/Ketone Pairs Comprising 2-, 3-, and 4-Heptanone with *n* -Octane, *n* -Nonane, and *n* -Decane," *J. Chem. Eng. Data*, vol. 60, no. 3, pp. 602–611, 2015.
- [261] S. I. Sandler, *Chemical, biochemical, and engineering thermodynamics*. John Wiley and Sons, Inc., 2006.
- [262] J. Wisniak and A. Tamir, "Vapor-liquid equilibria in the ternary systems water-formic acidacetic Acid., acid and water-acetic acid-propionic," *J. Chem. Eng. Data*, vol. 22, no. 3, pp. 253–260, 1977.

Chapter 11

APPENDICES

A. SUPPLEMENTARY LITERATURE DATA	II
<i>A1. High-pressure Measurement Techniques</i>	<i>II</i>
<i>A2. Low-pressure Measurement Techniques</i>	<i>V</i>
<i>A3. Thermodynamic Consistency Tests</i>	<i>VII</i>
B. DETAILED EXPERIMENTAL PROCEDURES	XII
<i>B1. HPBDP Experimental Procedure.....</i>	<i>XII</i>
<i>B2. HPVLE Experimental Procedure</i>	<i>XVII</i>
<i>B3. LPVLE Experimental Procedure</i>	<i>XL</i>
C. CALIBRATION DATA AND CERTIFICATES	XLII
<i>C1. High-pressure Calibrations.....</i>	<i>XLIII</i>
<i>C2. Barnett Pressure Calibration.....</i>	<i>XLVII</i>
<i>C3. HPBDP Large Cell Pt-100 Calibration</i>	<i>XLIX</i>
<i>C4. LPVLE Pt-100 Calibrations</i>	<i>L</i>
<i>C5. Low-Pressure Calibration</i>	<i>LIII</i>
D. PRECAUTIONARY MEASURES	LIV
E. RAW EXPERIMENTAL RESULTS	LVI
<i>E1. HPBDP experimental data.....</i>	<i>LVI</i>
<i>E2. HPVLE experimental data.....</i>	<i>LIX</i>
<i>E3. LPVLE experimental data</i>	<i>LXI</i>
F. TERNARY PHASE DIAGRAMS (HPBDP)	LXX
G. GAS CHROMATOGRAPHY CALIBRATION CURVES.....	LXXVI
H. SUPPLEMENTARY MODELLING RESULTS	LXXXII

A. SUPPLEMENTARY LITERATURE DATA

This appendix attempts to serve as a source for additional information to several topics discussed in this work.

A1. HIGH-PRESSURE MEASUREMENT TECHNIQUES

Dynamic Methods

Three sets of experimental equipment can be used in this approach and are shown in *Figure A-1* (a) the single vapour pass method, (b) the recirculation method, and (c) the single vapour-liquid pass method [223]. Accurate measurement of the high-pressure phase equilibria is required. Therefore, the procedure and common difficulties of each method are discussed.

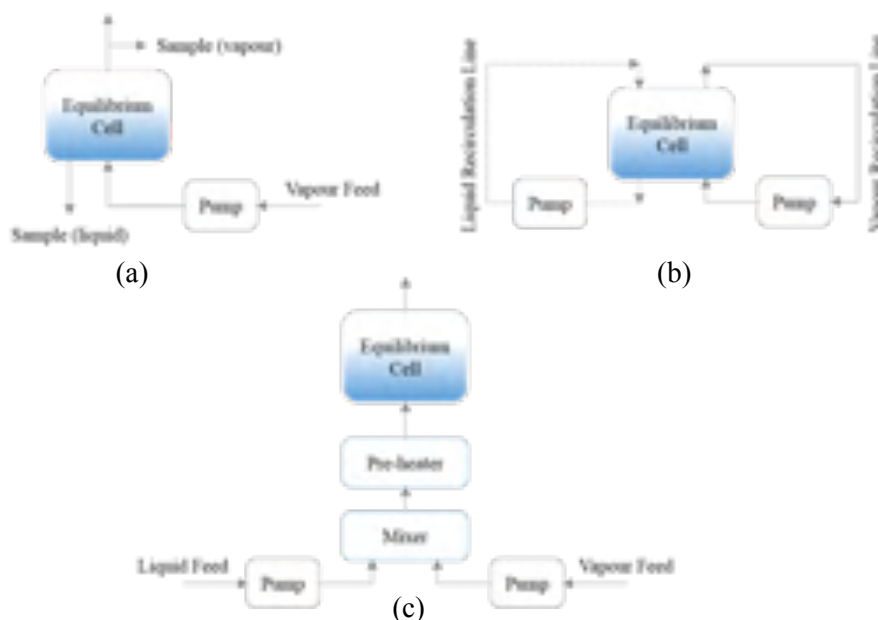


FIGURE A- 1: DYNAMIC EXPERIMENTAL METHODS (A) SINGLE VAPOUR PASS METHOD, (B) RECIRCULATION METHOD, AND (C) SINGLE VAPOUR-LIQUID PASS METHOD (ADAPTED AND REDRAWN FROM [58]).

Single Vapour Pass Method [223]:

<u>Experimental Step</u>	<u>Possible Problem Area</u>
i. Pure solvent with a known pressure is pumped through a stationary liquid phase inside of the equilibrium cell.	A large quantity of solvent is required.
ii. Solvent (gas) dissolves in the solutes (liquid) until equilibrium is reached.	Solutes restricted to those with low partial pressures. Therefore, the method is not suitable for critical regions.
iii. Vapour samples obtained after diverting an amount of the effluent stream; and liquid samples can be withdrawn from the equilibrium cell.	Droplet entrainment in the vapour effluent stream.

- iv. Isobaric and isothermal VLE data generated by controlling the vapour pressure and the liquid temperature.

The solvent flowrate must be regulated to ensure the correct amount of contact time and avoid gas bubbles.

Phase Recirculation Method [223]:

<u>Experimental Step</u>	<u>Possible Problem Area</u>
i. All the components are charged into the equilibrium cell.	Maintaining a constant liquid level inside of the cell is difficult.
ii. The pressure and temperature of the system is controlled while either one or both phases are continuously withdrawn from the equilibrium cell and recirculated.	Droplet entrainment in the vapour effluent stream; Pumps may result in the contamination of the equilibrium mixture.
iii. Sampling done by isolating a quantity of the circulating phases.	Partial condensation of the vapour stream being recirculated; Vapourisation of the recirculating liquid stream.
iv. Circulation of the phases will ensure enough mixing inside of the cell for equilibrium to be reached. No added stirring of the liquid phase is required.	The circulating pumps may cause undesired pressure gradients to form across the equilibrium cell.

Single Vapour-liquid Pass Method [223]:

<u>Experimental Step</u>	<u>Possible Problem Area</u>
i. The separate liquid and vapour streams are contacted co-currently before entering the preheater.	Pumps might result in contaminations of the equilibrium mixture.
ii. Temperature and pressure controlled in the mixing unit.	Undesirable pressure gradient still observed across the equilibrium cell.
iii. The combined mixture will pass into the equilibrium cell after being heated. The vapour and liquid phases will separate inside of the cell.	Difficult to achieve complete phase separation. Equilibrium must be achieved after 1 pass.
iv. After being separated, the vapour and liquid phases will exit the cell separately.	Difficult to ensure a steady liquid level inside of the equilibrium cell.
v. Sampling can be done once the effluent streams have been separated.	Droplet entrainment in the vapour effluent stream.

Static Methods

The experimental equipment used for a typical analytical approach is shown in *Figure A-2*. For the synthetic approach, a similar set of equipment is used. The only difference is the added equipment needed for analysing the samples [222]. The experimental procedure and common difficulties of each static method are discussed below.

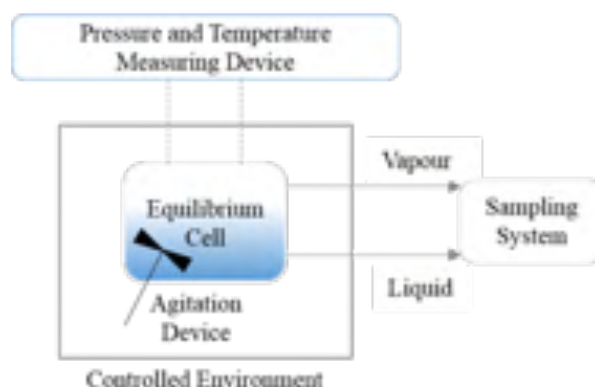


FIGURE A- 2: FEATURES OF A TYPICAL STATIC APPARATUS (ADAPTED AND REDRAWN USING [59]).

Analytical Method [222]:

<u>Experimental Step</u>	<u>Possible Problem Area</u>
i. Solutes and solvent are inserted into the equilibrium cell (the composition is not known).	Liquid components (solutes) must be thoroughly degassed before adding the solvent to the cell (dissolved gasses might compete with the low volatile component).
ii. A stirrer is used to mix the components in the cell and promote contact between the two phases (equilibrium will be achieved sooner).	True isothermal equilibrium difficult to achieve.
iii. The pressure and temperature at phase equilibrium is recorded.	Knowing when equilibrium has been achieved (require several temperature sensors). Must be measured accurately. Vertical temperature gradients might still be observed.
iv. The vapour and liquid samples are extracted from the equilibrium cell.	When taking samples, the volume of the cell is changed which might disrupt the phase equilibrium.
v. Samples extracted from the cell are analysed by, i.e. gas chromatography (GC).	Accuracy of analysis is very important. GC calibration curves must have a constant response factor ratio.

Synthetic Method [222]:

<u>Experimental Step</u>	<u>Possible Problem Area</u>
i. Solutes and solvent are inserted into the equilibrium cell (composition known).	No sampling is required and therefore, the samples must be prepared for each compositional load (the procedure might become tedious depending on the number of points being measured).
ii. A stirrer is used to mix the components in the cell and promote contact between the two phases (equilibrium will be achieved sooner).	True isothermal equilibrium difficult to achieve. A temperature gradient, regardless of thorough stirring, might occur when heating or cooling the system.

- | | |
|--|--|
| <p>iii. Pressure and temperature are manually controlled to achieve phase separation of the homogenous phase.
The pressure and temperature at the phase transition point is recorded.</p> | <p>Information obtained for mixtures with more than two components is limited (usually bubble, dew and critical point data).</p> |
| <p>iv. Once the second phase has been noted, the pressure and temperature are manually controlled again to achieve a homogenous phase.</p> | <p>De-mixing and layering of the phases can occur if the mixture is not adjusted back to a homogenous phase.</p> |
| <p>v. A $T(P)$ isopleth (the pressure is varied while the temperature is kept constant) is formed when continuously adjusting the temperature and noting the phase transition pressures (while keeping a constant composition).</p> | <p>It is easy to overlook the dew point phase transitions (liquid phase might condense as this film on the cell wall).</p> |

A2. LOW-PRESSURE MEASUREMENT TECHNIQUES

Special techniques include:

i. Dew point/ bubble point (DPBP) methods:

A calibrated piston/ cylinder assembly that is submerged in a bath that is kept under isothermal conditions. The composition is known beforehand, and the pressures are measured in turn as a function of volume. This technique can be hindered by small amounts of dissolved gasses that complicate the accuracy at which bubble point pressures are measured.

ii. An Isopiestic method:

This method is more suitable for mixtures that are comprised of a single volatile component which is not the case for the system being investigated in this study [227].

iii. Semi-micro techniques:

In instances when the chemicals being measured are expensive and therefore limited the Semi-micro technique is useful as high volumes for phase equilibria measurement is not required [84].

iv. Measurement of infinitely dilute activity coefficients

The measurement of infinitely dilute activity coefficients provides an indication of the non-ideality of the system in the highly dilute composition area. This method is extremely expensive and does not cover the entire composition range. It is for this reason that one of the most comprehensive low-pressure measurement techniques should be utilised for this project. These techniques include [227]:

- Dynamic circulation stills; and
- Static cells

The only measurement required was the pressure, making the technique isothermal. However, the phase equilibria measurement of the 1-decanol + *n*-tetradecane binary system will need to be conducted at a sub-atmospheric pressure and therefore an isobaric technique is required. A more thorough discussion of the less conventional techniques can be found in literature elsewhere [226]. In the next section, a more in-depth study of an additional dynamic method for measuring low pressure phase equilibria will be covered due to the availability of a dynamic still and the isobaric requirement.

Othmer Dynamic Still

In the early stages of low pressure VLE measurements with dynamic stills, the older Othmer type of apparatus was the most successful. Essentially, a vapour will form above a boiling liquid, condense and be recirculated to the boiling flask. *Figure A-3* schematically shows the simple setup of the still and the sampling ports for gathering the vapour and liquid phase data.

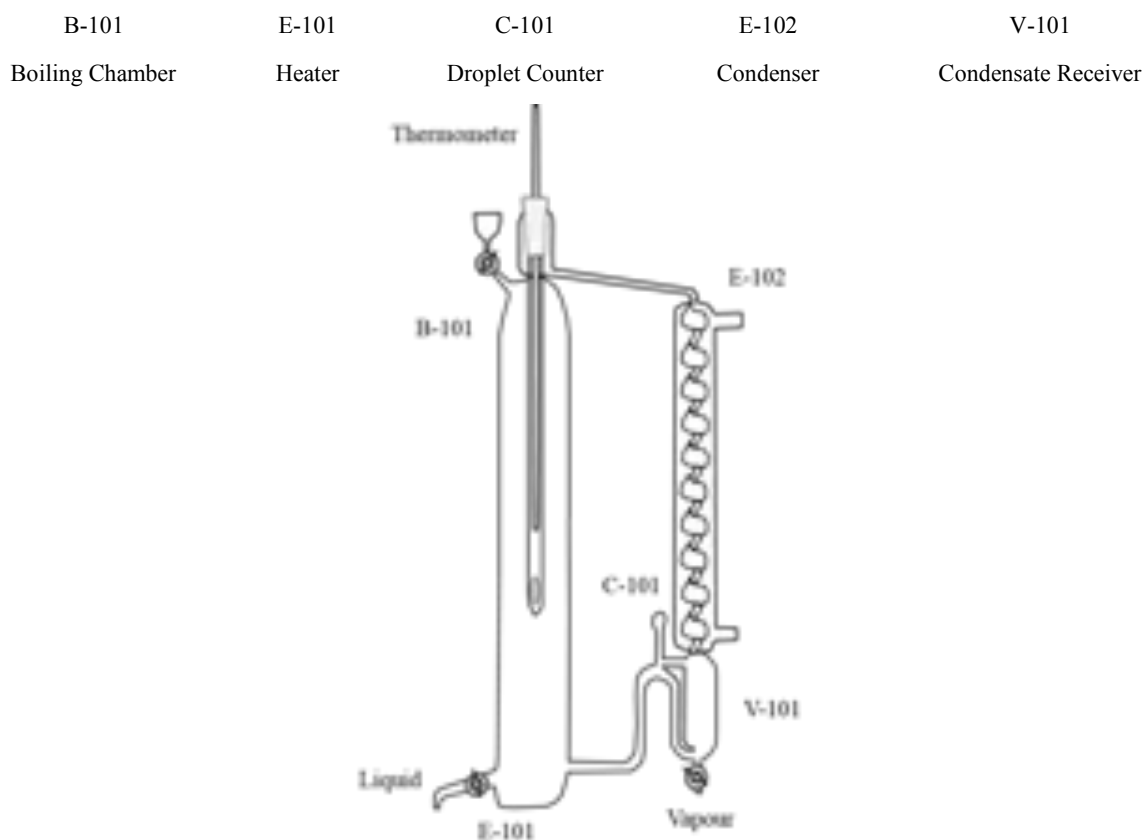


FIGURE A- 3: DYNAMIC VLE STILL BASED ON THE OTHMER PRINCIPLE. FIGURE REDRAWN AND ADAPTED FROM [44].

Although the approach was useful in measuring VLE phase behaviour at low pressures, it was not deemed accurate enough for highly non-ideal systems. A number of serious problems were found, among others are the following [84], [226]:

- The vapour condensate receiver is too large, preventing true equilibrium from being attained as well as errors in the composition measurements.
- Due to the boiling chamber walls being too large, partial condensation of the equilibrium vapour will occur.
- A lack of stirring will result in uneven boiling and minimum fluctuations in temperature.
- Poor contact between the temperature probe and both equilibrium phases will cause inaccuracies in measurements. The Othmer still only takes the vapour phase measurement and therefore the temperature readings are unsatisfactory.

Based on these complications the Othmer still was deemed unusable for the generation of accurate VLE data. The Gillespie still [226] that utilises a Cottrell vapour lift pump to circulate not only the vapour phase but also the liquid phase is a good alternative for generating accurate VLE data.

A3. THERMODYNAMIC CONSISTENCY TESTS

The experimental data will need to be validated by checking its conformance with the Gibbs/Duhem equation. The variable M will be used as the molar value to represent any extensive thermodynamic property throughout the derivation. Therefore, knowing that [63]:

$$nM = f(T, P, n_i) \quad (\text{A.1})$$

We can formulate the differential:

$$d(nM) = \left[\frac{\partial(nM)}{\partial P} \right]_{T, n_i} dP + \left[\frac{\partial(nM)}{\partial T} \right]_{P, n_i} dT + \sum_i \left[\frac{\partial(nM)}{\partial n_i} \right]_{T, P, n_i} dn_i \quad (\text{A.2})$$

Where a simplification can be made for the partial property of species i in (A.2):

$$\left[\frac{\partial(nM)}{\partial n_i} \right]_{T, P, n_i} = \overline{M}_i \quad (\text{A.3})$$

Furthermore, with constant total moles, (A.2) can be simplified to:

$$d(nM) = n \left[\frac{\partial M}{\partial P} \right]_{T, x_i} dP + n \left[\frac{\partial M}{\partial T} \right]_{P, x_i} dT + \sum_i \overline{M}_i dn_i \quad (\text{A.4})$$

Applying the product rule the following simplifications can be made to (A.4):

$$dn_i = x_i dn + n dx_i \quad (\text{A.5})$$

$$d(nM) = n dM + M dn \quad (\text{A.6})$$

Once (A.5) and (A.6) have been substituted into (A.4), simplifying will result in:

$$0 = n \left[\left(\frac{\partial M}{\partial P} \right)_{T, x_i} dP + \left(\frac{\partial M}{\partial T} \right)_{P, x_i} dT + \sum_i \overline{M}_i dx_i - dM \right] + [\sum_i \overline{M}_i x_i - M] dn \quad (\text{A.7})$$

By equating both sections bringing together (A.7) to zero and applying summability relations to the second part, the mixture properties can be calculated from the partial properties and differentiated to form:

$$dM = \left(\frac{\partial M}{\partial P}\right)_{T, x_i} dP + \left(\frac{\partial M}{\partial T}\right)_{P, x_i} dT + \sum_i \bar{M}_i dx_i \quad (\text{A.8})$$

$$dM = \sum_i x_i d\bar{M}_i + \sum_i \bar{M}_i dx_i \quad (\text{A.9})$$

Finally, the Gibbs/Duhem equation can be constructed by substituting (A.9) into (A.8) and simplifying:

$$0 = \left(\frac{\partial M}{\partial P}\right)_{T, x_i} dP + \left(\frac{\partial M}{\partial T}\right)_{P, x_i} dT - \sum_i x_i d\bar{M}_i \quad (\text{A.10})$$

To formulate the two king-pin equations for the performance of thermodynamic consistency tests, at an assumed constant temperature and pressure, the Excess Gibbs Energy equation can be used. Knowing from fundamentals the first relationship to be satisfied can be defined:

$$\bar{G}_i^E = RT \ln \gamma_i \quad (\text{A.11})$$

The definition of partial molar properties can now be used to define:

$$G^E = \sum_i x_i \bar{G}_i^E \quad (\text{A.12})$$

By incorporating (A.11) into (A.12), the excess Gibbs equation for a multicomponent system can be constructed based on summability:

$$G^E = RT \sum_i x_i \ln \gamma_i \quad (\text{A.13})$$

Replacing the thermodynamic variable M in (A.10) with the Gibbs Energy thermodynamic property, G and taking into consideration the assumed constant temperature and pressure, the Gibbs/Duhem equation can be simplified to:

$$\sum_i x_i d\bar{G}_i^E = 0 \quad (\text{A.14})$$

Lastly, by incorporating (A.11) into (A.14) the second relationship to be satisfied by the measured data can be defined:

$$\sum_i x_i d \ln \gamma_i = 0 \quad (\text{A.15})$$

If the measured data for γ_i are not satisfying both (A.11) and (A.15) it will be considered as inconsistent and therefore not useful for modelling the system.

Area Test

During the experimental procedure for testing the phase behaviour of the 1-decanol + n -tetradecane binary system, samples of both the vapour and liquid phase will be taken for analyses at a set temperature and pressure. Therefore, the activity coefficient for each component in the mixture can be determined. Equation (A.15) therefore reduces to:

$$0 = x_1 \frac{d \ln \gamma_1}{dx_1} + x_2 \frac{d \ln \gamma_2}{dx_1} \quad (\text{A.16})$$

Unfortunately, (A.16) is not linked to the Gibbs/Duhem equation and cannot be used to verify consistency. The two-component system can therefore be substituted into (A.11) to give:

$$G^E = RT[x_1 \ln \gamma_1 + (1 - x_1) \ln \gamma_2] \quad (\text{A.17})$$

$$\therefore \frac{dG^E}{dx_1} = RT \left(\ln \gamma_1 - \ln \gamma_2 + \frac{x_1 d \ln \gamma_1 + x_2 d \ln \gamma_2}{dx_1} \right) \quad (\text{A.18})$$

Now substituting (A.15) into (A.18) and simplifying:

$$dG^E = RT \ln \left(\frac{\gamma_1}{\gamma_2} \right) dx_1 \quad (\text{A.19})$$

Integrating (A.19) from pure 1-decanol to pure *n*-tetradecane:

$$\int_{\text{pure 1-C10OH}}^{\text{pure } n\text{-C14}} dG^E = RT \int_{x_1=0}^{x_1=1} \ln \left(\frac{\gamma_1}{\gamma_2} \right) dx_1 \quad (\text{A.20})$$

Furthermore, due to G^E being a state property, the pure Gibbs energy of each component will tend to zero as that component tends to unity resulting in the activity coefficient of that component similarly tending to unity:

$$\therefore G_i^E \rightarrow 0 \text{ when } x_i \rightarrow 0, \text{ since } \gamma_i \rightarrow 1 \quad (\text{A.21})$$

The left-hand side of (A.20) is zero and at constant temperature and pressure simplifies to:

$$\int_{x_1=0}^{x_1=1} \ln \left(\frac{\gamma_1}{\gamma_2} \right) dx_1 = 0 \quad (\text{A.22})$$

This equation is therefore used to formulate the thermodynamic consistency test, as a plot of $\ln \left(\frac{\gamma_1}{\gamma_2} \right)$ versus x_1 will produce a curve crossing the x-axis at an arbitrary point. The total area under the curve should be close to zero for the data to be considered as thermodynamically consistent with (A.11) and (A.15). In the generation of true vapour-liquid data sets (A.22) will unfortunately not be viable as either the temperature or pressure must be altered to effect a change in the equilibrium composition.

The activity coefficients are strongly dependent on temperature and only slightly dependent on pressure. Therefore, under isothermal conditions the activity coefficient will remain constant and (A.22) will be valid for testing the thermodynamic consistency. However, in the isobaric case as is with the present study (A.22) should be modified to compensate for the temperature effects. It is for this reason that a different approach needs to be considered where the experimental data can be tested under isobaric conditions. One such approach was developed in 1993 by Wisniak [259], namely the *L/W* consistency test.

L/W Consistency Test

Wisniak [259] proposed an approach where the relationship between the excess Gibbs energy (A.13) of the binary system is compared to its boiling point temperature at equilibrium and the Gibbs/Duhem equation is disregarded in this case. Assuming all the non-ideality of the pure components are

concentrated in the liquid phase the vapour phase will behave like an ideal gas. An approximation of the activity coefficients can be calculated at low pressures using [259]:

$$\gamma_i \approx \frac{y_i P}{x_i P_i^{sat}} \quad (\text{A.23})$$

To calculate the $\frac{P}{P_i^{sat}}$ ratio in (A.23) the Clausius-Clapeyron equation can be used:

$$\ln \frac{P}{P_i^{sat}} = \frac{\Delta H_i^{sat}(T_i^{sat} - T)}{RT_i^{sat}T} \quad (\text{A.24})$$

However, in order to use (A.24), the heat of vaporization of each component is assumed to be constant in the range of boiling points tested and the liquid molar volumes are also assumed negligible when compared to that of the vapour [259]. Therefore, (A.24) can be further simplified to:

$$\ln \frac{P}{P_i^{sat}} = \frac{\Delta S_i^{sat}(T_i^{sat} - T)}{RT} \quad (\text{A.25})$$

Combining (A.25) with (A.23) and then substituting the result into (A.13) will yield:

$$G^E = \sum_i x_i \Delta S_i^{sat}(T_i^{sat} - T) + RT \sum_i x_i \ln \left(\frac{y_i}{x_i} \right) \quad (\text{A.26})$$

Furthermore, Wisniak [259] defined two equations that can be utilised with (A.26) to construct the expression for determining the bubble-point temperature of the binary mixture. The two equations along with the final bubble-point temperature expression are:

$$\Delta S = \sum_i x_i \Delta S_i^{sat} \quad (\text{A.27})$$

$$w = \sum_i x_i \ln \left(\frac{y_i}{x_i} \right) \quad (\text{A.28})$$

$$T^{Bub} = \sum_i \frac{T_i^{sat} x_i \Delta S_i^{sat}}{\Delta S} - \frac{G^E}{\Delta S} + \frac{RTw}{\Delta S} \quad (\text{A.29})$$

The bubble-point temperature expression of the mixture (A.29) is rearranged to construct a thermodynamic consistency test:

$$L_k = \sum_k \frac{T_i^{sat} x_i \Delta S_i^{sat}}{\Delta S} - T^{Bub} = \frac{G^E}{\Delta S} - \frac{RTw}{\Delta S} = W_k \quad (\text{A.30})$$

L_k will always be positive except in the case where there is an azeotrope formed, as is expected for this study, in which case the left hand side of (A.30) will be negative [259]. The right-hand side of (A.30), W_k , will be consistent with the L_k value. Lastly, G^E can be calculated using (A.13) and will be positive or negative based on the deviations from ideality. The test is applied to each of the vapour-liquid equilibrium data pairs, k , experimentally measured and integration over this entire range will therefore provide the final values of L and W :

$$L = \int_0^1 L_k dx_1 = \int_0^1 W_k dx_1 = W \quad (\text{A.31})$$

If equal values for both L and W , are obtained using (A.31), the data will be verified as thermodynamically consistent. Unfortunately, due to experimental errors and the assumptions made to derive the thermodynamic test, a deviation factor must be defined. Wisniak [259] proposed the following:

$$D = \frac{100|L-W|}{L+W} \quad (\text{A.32})$$

To assure thermodynamic consistency, the value calculated using (A.32) should be less than 3 to 5. The lower limit is specified in order to abide by the Herrington test for consistency and the upper limit for cases when the heat of vaporization is unknown and requires estimating [259], [260].

The L/W test will confirm the experimental data as a representation of the system dynamics by means of [84]:

- i. An area test where the D value (A.32) is within reason across the entire composition range.
- ii. A point-to-point test where (A.30) must be satisfied for each experimental point measured.

As mentioned previously, the Gibbs-Duhem equation is disregarded when using this consistency test. Therefore, a second test is recommended to be used in conjunction with the L/W test. One consistency test proven useful in literature is the McDermott-Ellis test.

McDermott-Ellis Consistency Test

With reference to (A.16) and applying the trapezoidal rule, the two-point consistency test can be derived through integration for, i.e. points c and d [238]:

$$0 = \sum_{i=1}^N (x_{ic} + x_{id}) (\ln \gamma_{id} - \ln \gamma_{ic}) \quad (\text{A.33})$$

Consistency of each consecutive data point is thus evaluated separately. McDermott and Ellis [238] judged the data as consistent or inconsistent depending on a constant deviation of 0.01 for (A.33). therefore, the vapour and liquid fractions had to lie within a maximum composition deviation of ± 0.001 [261].

Several years later it was argued that the inaccuracies of the parameters should be considered within the criteria of the consistency test. Therefore, the maximum deviation would no longer be a constant, but rather a function of the measured composition (Δx), temperature (ΔT) and pressure (ΔP) accuracies. Wisniak and Tamir [262] redefined (A.33) to:

$$0 = \sum_{i=1}^N (x_{ic} + x_{id}) \left(\frac{1}{x_{ic}} + \frac{1}{x_{id}} + \frac{1}{y_{ic}} + \frac{1}{y_{id}} \right) \Delta x + 2 \sum_{i=1}^N |\ln \gamma_{id} - \ln \gamma_{ic}| \Delta x + \sum_{i=1}^N (x_{ic} + x_{id}) \frac{\Delta P}{P} + \sum_{i=1}^N (x_{ic} + x_{id}) \beta_i \left(\frac{1}{|T_c + \delta_i|^2} + \frac{1}{|T_d + \delta_i|^2} \right) \Delta T \quad (\text{A.34})$$

Where, $\beta_i = B_i$ and $\delta_i = C_i$ constants for the components being evaluated.

B. DETAILED EXPERIMENTAL PROCEDURES

The following section will cover the details regarding the experimental work conducted in this work. Schematic diagrams are provided for each of the experimental setups followed by a step-by-step description of the procedure to follow.

B1. HPBDP EXPERIMENTAL PROCEDURE

Loading procedure

<i>No.</i>	<i>Step</i>
1	The cell should be carefully turned vertically
2	The magnetic stirrer can be inserted into the cell
3	The equilibrium cell valve is closed
4	Measure the correct amount of solute mixture as per the mass fraction specified can now be insert it into the cell using a pipette
5	The piston head piece should then be screwed onto the cell
6	The piston should be tightened to avoid variations in volume
7	The cell should then be turned horizontally
8	The four-way section is to be connected onto the equilibrium cell outlet/ inlet
9	All valves should be closed
10	The vacuum pump is switched on
11	One can collect the carbon dioxide using the gas cylinder provided
12	The carbon dioxide gas cylinder can then be connected to the four-way valve
13	Once secured correctly onto the cell, the vacuum valve can be opened slightly
14	The equilibrium cell valve can now also be opened fractionally to evacuate as much air as possible from the cell (careful not to remove any solute)
15	The valves should again be closed
16	The television monitor is switched on and the medical camera with the endoscope is inserted in front of the sapphire window
17	The cell is now flushed 6 times with carbon dioxide (solvent) to remove any residual air in the equilibrium cell
18	The carbon dioxide cylinder is opened and closed to flush solvent into the four-way section
19	The equilibrium valve is then opened a quarter of a way slowly to allow the solvent into the cell
20	The valve to atmosphere on the four-way connection is opened to flush the solvent out of the cell
21	After the final flush, the cell can remain open and all the other valves should be closed.

- 22 The magnetic stirrer and hot plate can now be placed under the cell and switched on to remove air bubbles from pressure build-up in the cell
 - 23 Release the last bit of built up pressure to atmosphere
 - 24 Close the equilibrium cell valve and all the valves on the four-way connector
 - 25 The carbon dioxide gas cylinder should now be removed from the four-way connector and weighed
 - 26 If enough solvent is left in the cylinder to load into the cell no more should be collected
 - 27 The solvent should be gravimetrically measured to the specified amount
 - 28 If too little solvent remained in the cylinder more should be collected
 - 29 The cylinder is placed back onto the four-way connector
 - 30 The vacuum is opened once more to air out the four-way connection
 - 31 The solvent in the cylinder should be heated with the hair-dryer
 - 32 The vacuum valve can be closed
 - 33 Once hot enough the equilibrium cell inlet/ outlet valve can be opened 100 %
 - 34 The cylinder is then opened, and the solvent released into the cell
 - 35 The four-way connector should also be heated with the hair-dryer to remove solvent from the piping network
 - 36 Once all the solvent has been loaded the cell can be closed
 - 37 The four-way connector valve to the atmosphere is opened to relief the pressure in the piping network
 - 38 The solvent cylinder can now be removed from the four-way connector and weighed
 - 39 The total mass of the components in the cell can now be measured
 - 40 If the mass fraction is incorrect the solvent loading should be repeated
 - 41 If correct, the vacuum can be switched off and the four-way connector can be removed from the equilibrium cell
 - 42 The Julabo circulating liquid bath can now be switched on and the first temperature set point entered
 - 43 A metal container containing the insulation material is placed around the equilibrium cell to conserve heat
 - 44 The magnetic plate is positioned below the equilibrium cell and secures the container around the cell
 - 45 The magnetic stirrer can be switched on
 - 46 The temperature Pt-100 probe can be inserted inside the cell wall
 - 47 The piston ruler is attached to the cell and zeroed
 - 48 The nitrogen gas line is connected to the piston head (low pressure region) and the pressure systematically increased in the high-pressure chamber
 - 49 A cap is placed on the equilibrium cell inlet/outlet port
 - 50 The cell can now be left to achieve thermal equilibrium (approximately 30min)
-

Testing Procedure

<i>No.</i>	<i>Step</i>
1	Once thermal equilibrium has been reached and the pressure is high enough to ensure a single phase the measurements can be taken
2	The components are observed on the TV monitor
3	If a single phase has not been attained, additional nitrogen gas should be added to the cell
4	Nitrogen gas is then to be slowly released from the chamber to decrease the pressure until the first sign of vapour bubbles
5	An extrapolation method can then be applied to iteratively take readings until the exact phase transition point is obtained with an accuracy of 0.2 bar
6	The phase transition will occur at the highest possible pressure before the single phase is converted into two phases
7	The pressure, temperature, piston position and phase criteria must be recorded
8	The next set temperature should now be selected
9	The nitrogen gas can be increased to create a pressure increase and allow for equilibrium to be attained once more in a single phase

Unloading Procedure

<i>No.</i>	<i>Step</i>
1	The nitrogen cylinder can be closed once all the tests have been completed
2	The nitrogen from the cell can be drained
3	The heating bath can be switched off
4	The medical camera and endoscope can be removed and switched off
5	The Pt-100 probe and the piston ruler can be removed from the cylinder
6	The magnetic plate can be switched off and removed
7	The insulation material and the container can be removed
8	The cell can now be left to cool down (cooling water system switched on)
9	All the correct protection clothing should now be worn
10	The cap on the equilibrium cell inlet/ outlet port can now be removed
11	The cell should be turned at an angle and the nozzle pointing downwards
12	An Erlenmeyer flask can be used to capture the exiting components when opening the equilibrium cell valve
13	The cell can be turned vertically, and the piston loosened
14	A three-point test needs to be conducted to make sure it is safe before removing the head of the cylinder. <ul style="list-style-type: none"> - The piston rod should be loosened to move down when force is applied onto it. This gives an indication that there is not a lot of pressure inside the cell. - The equilibrium cell valve should be open - The reading of the pressure transmitter should be close to the initial zero point.

Cleaning Procedure

<i>No.</i>	<i>Step</i>
1	The cell can now be angled with the open end slanted downwards at a 45°
2	The magnetic stirrer can be removed
3	The cell is first thoroughly washed out with xylene
4	The chemicals are captured in a waste bucket
5	The nozzle should also be cleaned with xylene
6	The cell can now be rinsed using methanol to remove the xylene
7	Pressurised air can then be used to dry the cell
8	Paper towel is also used to ensure the cell is completely dry and clean
9	The cooling system can now be switched off
10	The heating batch can be switched off
11	The magnetic stirrer should also be cleaned with xylene, followed by methanol
12	Ensure everything is returned to the correct place
13	The chemicals should be disposed in the correct waste bin

B2. HPVLE EXPERIMENTAL PROCEDURE

Loading & setup

<i>No.</i>	<i>Step</i>	<i>Notes</i>
<i>i</i>	<i>Loading</i>	
	- <i>Place the CO₂ gas bomb in the freezer</i>	<i>± 3 hours required</i>
1	Remove plastic cover from monitor	Place in top drawer
2	Switch on electrical plugs	
3	Switch on water bath	
4	Switch on vacuum pump	Warm-up
5	Switch on monitor and place camera probe in front of the cell	Recording device?
6	Check weight-scale reading against the calibration data	Use weights 7 and 8
7	Flush the equilibrium cell with compressed air	Use tubes in drawer
8	Close feed line microvalve	With 11 spanner
9	Clean magnetic stirrer and place inside cell	Acetone & compressed air
10	Clean piston	Acetone & compressed air
11	Attach low-pressure chamber	To check if correctly aligned, move piston in and out of cell.
12	Tighten piston (first screw)	4mm rod & 17 spanner
13	Set water bath to 27 °C (27.57 °C)	Remember the temperature correction from calibration data
14	Tighten ROLSI screws and close drain line microvalve	Top & bottom of the cell
15	Tighten the sight glass	With?
	- <i>Every time back at atmospheric pressure, tighten the sight glass again to avoid the seal from deforming 'expanding' too much and then having to be replaced</i>	
16	Attach the nitrogen line	
17	Tighten piston (second screw)	4mm rod and 17 spanner
18	Open degas line microvalve to apply vacuum to equilibrium cell	With 11 spanner
	- <i>Make sure top blue microvalves are closed to the atmosphere and open to the vacuum</i>	
19	Take room temperature	Record in °C
20	Monitor the pressure	
	- <i>When drawing vacuum, the pressure should drop by approximately 1 bar, i.e. -2.3 bar to -3.3 bar</i>	
21	Close top blue and degas line microvalves to vacuum	

22	Remove feed line microvalve ‘screw’	Cell will now be open to atm.
23	Clean the pin	Acetone and compressed air
24	Remove gas bomb from the freezer and fill with CO₂	
A	Unwrap paper from the loading side	
B	Open valve to slowly release CO ₂	Don’t close all the way
C	Place CO ₂ bomb onto CO ₂ cylinder	Finger tighten
D	Close CO ₂ bomb valve	
E	Flush CO ₂ into connecting lines 6 times, i.e. - <i>Open and close CO₂ cylinder; open connecting point and release CO₂ to the atm.; close the connecting point again before all CO₂ has been released</i>	
F	Open the CO ₂ cylinder	
G	Open the CO ₂ bomb and fill with CO ₂	Monitor pressure on the gauge
H	Close CO ₂ bomb when at approximately 90 bar	
I	Open CO ₂ bomb again for 10 seconds and then close properly	
J	Close the CO ₂ cylinder	
K	Remove CO ₂ bomb from the cylinder	
25	Dry gas bomb and valves from moisture in the lab - <i>When pressure increases to 300 bar, release CO₂ to get it down to 250 bar</i>	Use hairdryer (compressed air added for the valves)
26	Weigh solute mixture	With the lid, on
27	Weigh solute mixture	Without the lid
28	Release all air from the syringe to be used for loading the solutes	
29	Weigh the syringe	With needle attached
30	Extract components into the syringe	Approximately 23 ml
31	Clean tip with tissue paper and weigh the syringe	With loaded components
32	Carefully insert solutes into the equilibrium cell through opening at the feed line valve (where the microvalve screw has been removed)	Watch last drop
33	Weigh syringe after loading	Empty
34	Weigh solute mixture	Without the lid
35	Weigh solute mixture	With the lid
36	Close equilibrium cell feed line with microvalve screw	With 11 spanner
37	Record temperature and pressure of the cell	

38	Place stirrer plate under the high-pressure chamber and connect it to the blue control box	± 2 cm below the screws
40	Open degas line to vacuum	Open the blue microvalve too
41	Vacuum cell for approximately 5 minutes	Stirrer on
42	Make sure the condensate on the gas bomb is gone	Use hairdryer and tissue paper
43	Weigh gas bomb	Should be ± 3325 g (ref only)
44	Close degas line microvalve	
45	Take away stirrer plate and place 'sponge' in place on lifting plate for gas bomb to be attached to the cell	Check cupboard near window for the sponges
46	Place CO ₂ bomb onto the sponge and elevate it to be in-line with the connection point to the feed line	Be careful of the Pt-100 probe
47	Finger tighten the gas bomb	Ensure cell is closed properly
48	Open gas bomb to pipelines and close again	
49	Release CO ₂ slowly (don't release all of it)	With 11 spanner
50	Repeat 48 and 49 another 3 times (flushing pipelines)	
51	Open gas bomb again and close	
52	Open feed line microvalve to flush the cell and close again	Press increase to ± 2 bar
53	Release CO ₂ slowly by opening the degas line (pressure will drop back to approximately -2.3 bar)	Can release to atmosphere or to vacuum (blue microvalves)
54	Repeat 51 to 53 another 3 times (flushing cell)	
55	Leave cell open to vacuum and remove gas bomb	
56	Weigh gas bomb	If less than 3300 g might have to fetch CO ₂ again
57	Place magnetic stirrer plate back under cell	Switch on stirrer (while cell is open to vacuum)
58	Heat up gas bomb properly (on stand)	Monitor pressure at 250 bar
59	Release CO ₂ until at the correct weight for loading	± 3303 g (ref only)
60	Plug in hairdryer at a point closer to the cell	
61	Repeat steps 44 to 50	
62	While heating the gas bomb with the hairdryer open the bomb valve completely	
63	Slowly open feed line microvalve to start loading the CO ₂	
64	Gradually start opening the microvalve more	Monitor the liquid level inside of the equilibrium cell
65	When inlet flow starts to decrease (close to empty), close the gas bomb and start heating the piping network	Cell pressure ± 63 bar (ref only)

- 66 Close the feed line microvalve securely
- 67 Remove gas bomb and weigh it ± 3260 g (loading 40 g)
- *Whether too much CO₂ has been added will depend on the minimum required pressure at T_{set1} . If the pressure is already higher, then must degas at a later stage to be able to reach lower pressures*

68 Place gas bomb back on stand

69 Record pressure and temperature of cell

70 Make sure all microvalves are closed properly With 11 spanner

ii Setup

- | | | |
|----|---|--|
| 1 | Place insulation material below the oven 'base' | Outside of the oven |
| 2 | Take the camera probe away | |
| 3 | Attach the back of the oven (place 2 sections over the correct screws) | Tighten with wingnuts M4/M6 |
| 4 | Place black rubber sponge over pressure transducer wire | |
| 5 | Place insulation material on top of the oven 'base' | Inside of the oven |
| 6 | Place heat control stands inside of the oven (with holes) | Follow according to picture |
| 7 | Attach the left-hand side of the oven (towards water bath) | Holes in it |
| 8 | Secure heating fluid inlets and outlets onto the oven | Be careful of electrical wires |
| 9 | Neatly tie pipes in place with zip-lock ties and ribbons | Pink and orange |
| 10 | Place and secure Pt-100 probe into the top of the oven (properly in front of the inlet flow pipe) | To monitor oven temperature |
| 11 | Make sure piston is tighten properly | 4mm rod and 17 spanner |
| 12 | Attach right hand side of the oven | |
| 13 | Place camera probe in front of cell | Secure cables out of the way with zip-lock ties |
| 14 | Attach the oven Pt-100 probes <ul style="list-style-type: none"> - #9 left front (yellow label) - #10 right front (yellow label) - #11 left back (reddish label) - #12 right back (reddish label) | Secure cables with zip-lock ties |
| 15 | Attach front of oven | |
| 16 | Check the water level of the heating bath (RO water) | |
| 17 | Set temperature to first set point (taking into consideration the temperature correction from calibration data) | i.e. 55 °C set to 52.37 °C first and when the oven has been heated set to 54.37 °C |

	- <i>Set oven temperature & overtemp (monitor the steady temperature to avoid any influence of density change inside the cell due to the temperature differences)</i>	
18	Switch on the oven temperature control unit	Black box
19	Place insulation material at the back of the oven	
20	Increase the pressure of the cell to see if the one-phase region can be reached at set temperature	N ₂ cylinder 'back left'
	- <i>If not able to reach the one-phase region, then the temperature must be increased to i.e. 75 °C (74.34 °C) and checked again if the one-phase region can be obtained</i>	Change overtemp of oven to 105 °C and of water bath to 85 °C
	- <i>Usually wait for approximately 3 hours each time a new temperature has been set rather than having issues with varying temperature during the sampling procedure</i>	*Only when doing sampling – not necessary to wait this long for the one-phase region
21	Switch off monitor	
22	Switch off vacuum pump	

Measurements

Terminology:

- i. Purge series = pre-pre-purge (to clean capillary)
- ii. Slow purge = pre-purge (until peaks level out → liquid peaks are larger due to more solutes)
- iii. Fast purge = purge (before each sample series, i.e. alternating)
- iv. Sample series = analysis A1, A2, A3 and A4

Important to know:

- i. Front ROLSI (#2) inlet at the back of GC; therefore, on computer = SSL Back
- ii. Back ROLSI (#1) inlet at the front of GC; therefore, on computer = SSL Front
- iii. When sampling at a pressure close to the one phase region:
 - Do the purge series 1st.
 - Then set the cell pressure higher to reach the one-phase region before taking the system back down to the required isobaric condition.
 - Once all droplets in the capillary cone are gone (high solute vapour phase it will disappear; and low solute vapour phase it will drop down).
 - Start the slow purge series
 - Alternate between the fast purge and the sample series (total of 4 samples)
- iv. The slow purge series will require different timer settings for the vapour and the liquid phases to clear the capillaries properly:
 - Vapour: Multiple, smaller purge extractions (less disruptive)
 - Liquid: Can be much more vigorous due to no dew interferences; therefore, use small number of large extractions at 30 secs apart
- v. The pressure sensitivity increases as the total solubility pressure is approached (the pressure at which the mixture enters a one-phase region).
- vi. For measurements close to the phase transition point increase the pressure to the one-phase region first and then decrease to the set pressure;
For measurements, further away from the transition point, start at lower pressures in the two-phase region and increase to the set pressure.
- vii. It is helpful to sync up both computers with a watch; therefore, when observing something odd in the equilibrium cell, the videos and recorded temperatures/pressures can be referred to per the logged time of the occurrence (data is logged on each day).
- viii. Make sure to always monitor the pressure and keep it as constant as possible throughout each measurement.
- ix. At higher temperature measurements, the viscosity of the vapour phase is more vapour intensive than liquid intensive which creates small drops with lower surface areas (global mist formation)

- x. Global mist formation should be avoided and can occur due to:
 - a. Vigorous stirring; therefore, the mist particles will shoot up into the vapour phase
 - b. Pressure drops
- xi. Possible issues with the position of the capillary:
 - a. At the top: during the lowering procedure for liquid sampling could cause global mist formation and it is more straining on the O-rings
 - b. Slightly above the liquid phase: Less hindrance when moving it into the liquid phase; however, surface area of the capillary is bigger and droplets might form that will run down to the sampling point
- xii. Localised mist formation does not influence the sampling (a small mist drop from the sampler during an extraction)
- xiii. Transitional phase of intermediate density occurs more prominently at higher pressures; therefore, much larger to help remove a bubble from the ROLSI cone
- xiv. Measurement of the one phase region does not include the purge series step

<i>No.</i>	<i>Step</i>	<i>Notes</i>
1	<i>Temperature settings (reference only):</i> - <i>Water bath = 54.37 °C</i> - <i>Oven = 54.6 °C</i> - <i>Overtemp = 75 °C</i>	<i>Require approximately 3 hours to reach thermal equilibrium; therefore, usually set it the day before</i>
2	Pressure is not yet important (let out all pressure in cell)	
3	Switch on GC to warm up	
4	Instruments - <i>Parameters</i> - <i>Detectors (magnifying glass)</i> - <i>Tick all boxes for both FIDs and TCD</i>	DON'T PRESS APPLY YET
5	Open air, helium and then the hydrogen	All regulators to 400
6	Select apply straight after opening hydrogen	
7	Set oven temperature to 250 °C - <i>Set time to 90 min</i>	Although hardly ever this long
8	ROLSI transfer tubing to GC to be increased on temperature control box systematically to 280 °C - <i>The other 4 temperature controls (in red) should be set to 220 °C; 280 °C; 220 °C; 280 °C</i>	Black box
9	Push back ROLSI inwards (clockwise rotation)	#1
10	Pull front ROLSI outwards (counter-clockwise rotation)	#2

i	Purge series (pre-pre-purge)	
A	Methods <ul style="list-style-type: none"> - <i>Select pre-pre-purge</i> Run setup <ul style="list-style-type: none"> - <i>Sample info</i> - <i>Manually change folder name & number</i> 	Where to log data (folder) i.e. pre_pre_purge_0001
B	Instruments → parameters <ul style="list-style-type: none"> - <i>Switch on the septum purge flow of both SSL Back and Front</i> 	For analysis
C	Switch gas saver off <ul style="list-style-type: none"> - <i>Check that valves are ticked</i> 	
E	Set split ratio of SSL Front (6:1) <ul style="list-style-type: none"> - <i>23 ml/min</i> 	Not using the sampler
F	Set split ratio of SSL Back (80:1) <ul style="list-style-type: none"> - <i>245 ml/min</i> 	Using this sampler
G	Switch on ROLSI timers <ul style="list-style-type: none"> - <i>Set1 = time off (when the sampler will open)</i> - <i>Set2 = time on (how long the sampler will be open)</i> 	0.30 secs (NEVER = 0) 0.18 secs
H	Wet bubble flow meter tubing	
I	Start timer <ul style="list-style-type: none"> - <i>GC will start the method automatically</i> - <i>Check the computer if the GC registers the solutes</i> 	Monitor screen for each purge 'click' and record temperature and pressure values
J	Continue with purge series until peak heights level out	15-20 minutes
K	Turn off timer	
L	Wait for the final peaks to appear on graphs and then press stop on the GC	Stop the method run
M	Instruments → parameters <ul style="list-style-type: none"> - <i>Detectors (magnifying glass)</i> - <i>Untick everything except the heater</i> 	Press apply
N	Close hydrogen immediately after switching off detectors	Cylinder and regulator
O	Close the air and helium regulators	
P	After 10 minutes tick the gas saver box for both SSL front and back (to ensure capillaries clean first at a faster rate)	Flow rate will then decrease to 23 ml/min
Q	After another 5 minutes set oven temperature to 100 °C	
11	Increase cell pressure with the nitrogen gas <ul style="list-style-type: none"> - <i>Open release valve 180 ° turn only</i> - <i>Open nitrogen gas cylinder</i> 	

	<ul style="list-style-type: none"> - <i>Open regulator slowly until pressure starts increasing</i> - <i>Start closing the release valve while still increasing the cell pressure</i> 	
12	Increase pressure till a one-phase region is obtained	Slowly to spare the seals
13	While forming the one-phase region set the stirrer to 1400rev	
14	Wait approximately 25 minutes	
15	Open data control program (Aglient Benchlink...) on the computer	For temp and press control
	<ul style="list-style-type: none"> - <i>Press start button to start MUX</i> 	
16	Begin to decrease pressure to get to set point pressure	Stirrer on but lower (300 rev)
17	Switch on detectors on computer (tick boxes)	BUT DON'T PRESS APPLY YET
	<ul style="list-style-type: none"> - <i>Both FIDs and TCD</i> 	
18	Open air, helium and then hydrogen cylinders	400
19	Select apply straight after opening the hydrogen	Oven can remain at 100 ⁰ C
20	On the data control program check what was the 1 st pressure was detected as in mA and specify it for the pressure curve	Baseline Purple block, i.e. 8.4 mADC
	<ul style="list-style-type: none"> - <i>After approximately 10 minutes of regulating the pressure the value can be increased slightly to get it away from the temperature curves, i.e. 8.8 mADC</i> 	To be more visible
21	Take ambient temperature	
22	After ±45 minutes of regulating the temperature to get rid of the transitional phase of intermediate density, tick the septum purge flow box of each	
23	Regulate the pressure with the stirrer on and off	To get rid of droplets in ROLSI cone
	<ul style="list-style-type: none"> - <i>For solute rich vapour phases the droplet won't drop but rather starts to disappear</i> - <i>Droplet formation is promoted by stirring therefore avoid if possible (however, still needed to help get rid of the intermediate density phase)</i> 	
ii	Slow purge series (pre-purge)	
A	Methods	Where to log data (folder)
	<ul style="list-style-type: none"> - <i>Select slow purge</i> 	
	Run setup	
	<ul style="list-style-type: none"> - <i>Sample info</i> - <i>Manually change folder name & number</i> 	i.e. pre_purge_0001
B	Instruments → parameters	Make sure oven temp at 250 °C
	<ul style="list-style-type: none"> - <i>Set method time to 90 mins</i> 	Make sure detectors are on

	<ul style="list-style-type: none"> - <i>Switch off gas saver</i> - <i>Switch on septum purge flow</i> - <i>Set split ratio of front inlet to 6:1</i> 	Check GC regulators Then press apply - 23 ml/min
C	Monitor the pressure	
D	Wet bubble flow meter tubing	Back port
E	Start the timer when still at 30 sec and after first tick, change set time to 2 minutes and 30 sec	2.30 secs and 0.18 secs
F	Continue with slow purge until peaks level out <ul style="list-style-type: none"> - <i>Solute rich vapour phases tend to be shorter but system is much more sensitive when this close to the one-phase region</i> 	Can set method time higher if needed, i.e. 120 min If time is not increased and it has run out, the next purge will create a new folder in which the data will be logged, i.e. pre_purge_0002
G	Monitor the screen and pressure	
H	Once the peaks have levelled out <ul style="list-style-type: none"> - <i>Stop the timer</i> - <i>Wait for the last peaks to form and then press stop on the GC</i> - <i>Screenshot the outcomes</i> 	

iii Fast purge series (purge)

A	Methods <ul style="list-style-type: none"> - <i>Select fast purge</i> Run setup <ul style="list-style-type: none"> - <i>Sample info</i> - <i>Manually change folder name & number</i> 	Where to log data (folder) i.e. purge_0001
B	Instruments → parameters <ul style="list-style-type: none"> - <i>Method time to start with already set</i> - <i>Switch off gas saver</i> - <i>Switch on septum purge flow</i> - <i>Leave split ratio of both inlets at 80:1</i> 	Make sure oven temp at 250 °C Make sure detectors are on Check GC regulators Then press apply - 245 ml/min for both
C	Monitor the pressure	
D	Wet bubble flow meter tubing	Back port
E	Set timers for fast purge	0.24 sec and 0.4 secs
F	Start timer for two fast purges 4secs apart and then stop the timer <ul style="list-style-type: none"> - <i>Monitor the screen during purges</i> - <i>Record temperature and pressure</i> 	

- G** Switch on gas saver & press apply
- H** Set timers for sample while waiting for peaks to appear 0.29 secs and 0.4 secs
- I** Fast purge run time = 1.8 mins
- *Press stop on the GC as soon as at 1.8 min*
 - *The GC should be set to display the oven temperature which will now start to decrease to 100 °C*
- Limited time to get the sample ready before at set temp

iv Sample series (analysis)

- A** Methods
- *Select sample name*
- Run setup
- *Sample info*
 - *Manually change folder name & number* i.e. Sample_A_0001
- B** Instruments → parameters
- *Check if the split ratios are both at 20:1* 63 ml/min
 - *Switch off septum purge flow*
 - *Switch off gas saver*
 - *Press apply*
- C** Switch the valves (untick the boxes) and wait for temperature of GC to get to 100.5 °C before pressing apply
- D** Take sample straight away by starting the timer for ONE extraction and then stop the timer
- *Monitor the screen during sample*
 - *Record the temperature and pressure*
- E** Switch on the gas saver and press apply
- F** Do bubble flow meter test 3 or 4 flow rates Write down on paper
- G** Take screenshots while waiting for the analysis
- *Fast purge peaks*
 - *Fast purge baseline*
 - *Pressure control curves when the peaks appeared*
 - *Sample peak*
 - *Sample peak baseline*
 - *Pressure control curves when the peak appears*
- H** Set timers back again for the next fast purge 0.24 secs and 0.4 secs
- I** Monitor the pressure throughout both series
- J** Log recorded data to an excel spreadsheet
- *Bubble test split vent times*
 - *GC analysis of sample (areas of the components)* Identified by retention times

K	After 7 mins the oven temperature should be back to 250 °C	
	<ul style="list-style-type: none"> - <i>Set the temperature of the oven to 250 °C under parameters</i> - <i>Change the method time to 10 minutes</i> - <i>Press tab to observe change</i> - <i>Switch back valves (tick the boxes again)</i> - <i>Press apply and ok</i> 	Replace 5 min with 7 min
L	After 10 minutes the run is completed; close the PDF document that will pop up	
24	Repeat the <ul style="list-style-type: none"> - <i>iii. Fast purge series and</i> - <i>iv. Sample series</i> Another 3 times to have a total of 4 fast purges and 4 samples of the vapour phase	
25	End off as if a 5 fast purge would need to be done <ul style="list-style-type: none"> - <i>set method to fast purge after sample A4</i> - <i>Rename, i.e. purge_0005</i> - <i>Switch on septum purge flow</i> - <i>Switch off gas saver</i> 	Depends on the outcome of the data
26	ROLSI now has to be moved into the liquid phase <ul style="list-style-type: none"> - <i>For large space gaps between vapour and liquid it will be better to first switch off the detectors</i> - <i>For high pressure tests close to the one phase region this the distance is small enough to leave them on</i> 	
27	The back ROLSI will be rotated out of the cell (counter clockwise) while the front ROLSI is being rotated into the cell (clockwise)	To keep the pressure constant
28	Use the data control curves to know which ROLSIs to adjust <ul style="list-style-type: none"> - <i>When the pressure curve is below the centre line the pressure has decreased; therefore, the volume can be decreased to counter for it</i> - <i>i.e. two rotations at the back & one rotation at the front or one rotation of each</i> 	Vice versa
29	Once the ROLSI is in the liquid phase, switch on the stirrer for a few minutes to check for miscibility waves/ vapour bubbles in the sampler cone	At low revs
30	Repeat the slow purge, fast purge and sample series steps again but now for the liquid phase <ul style="list-style-type: none"> - <i>Slow purge timer setting is now 30 secs and 0.2 secs</i> 	

- *With a front inlet split ratio of 7:1*
 - *Fast purge timer setting is now 0.4 secs and 0.28 secs*
 - *Sample series timer settings are also 0.4 secs and 0.28 secs*
- 31 End the last sample as if a 5 fast purge should be done
- 32 After the last scan of the control program stop the MUX by selecting the top stop button Turn off MUX power button
- *Screenshot final curve outcomes*
- 33 Take note of anything strange inside of the equilibrium cell
- 34 Switch off timers (properly)
- 35 Switch off detectors under parameters Leave the heaters on
- 36 Close hydrogen cylinder followed by the air and helium cylinders The cylinders and regulators
- 37 Switch on the stirrer to 700 revs and push the pressure up to the one phase region
- 38 Set the temperature of the transfer tubes to the GC to 300 °C To help clean out the GC tubes properly
- *And the other 4 thermal regulators to 240 °C; 300 °C; 240 °C and 300 °C, respectively*
- 39 Leave the gas saver off to have a faster flow rate through the tubes for cleaning
- 40 After approximately 10 minutes switch off the thermal regulators (all 5)
- 41 Measure the phase transition point of the ternary mixture at the set temperature Same as synthetic method
- 42 Copy work logged for the day to a flash drive
- 43 Methods
- *Select the sleep method*
- 44 Release the cell pressure and set the water bath to the next isothermal condition
-

Adding CO₂ & Venting vapour phase

Important to know:

- i. Venting CO₂ = for measuring the lower pressures
- ii. Adding CO₂ = for measuring the higher pressures
- iii. The liquid level in the cell is increased when adding more CO₂. Therefore, to avoid the loss of solutes (due to the level being too close to the degas line) it is better to always vent first and load more CO₂ last.
- iv. Adding of CO₂ is like the loading procedure of CO₂; however, here it might seem as though a lot more is being added than what should be. This is simply due to having vented CO₂ previously for the lower pressures.

<i>No.</i>	<i>Step</i>	<i>Notes</i>
i	Venting vapour	
1	Have ice ready to cool down the water bath the night before	
2	Release the pressure in the cell (piston at max out)	The day/night before
3	Set the temperature of the water bath to 35 °C	
4	On the day of venting, set the temperature down to 12 °C	
5	Drain some of the water from the water bath and add colder RO water (twice)	Careful not too low (the pump is still on)
6	Add ice to the water bath <ul style="list-style-type: none"> - <i>Ice is likely to be tap water; however, if making own ice, rather use RO water to save the effort of having to drain the water bath again and refill it with RO water later</i> 	
7	Adjust the water bath set point to a low value, i.e. 0.5 °C to avoid an overshoot	
8	Once the cell is at approximately 12 °C, start the vent	
9	Release CO ₂ until the pressure has dropped by approximately 10 bar	Use the degas line; open the microvalve with 11 spanner
10	Record temperature and pressure after each vent, i.e. <ul style="list-style-type: none"> - <i>40 bar → 34 bar; T = 11.5 °C</i> - <i>34 bar → 37 bar; T = 11 °C</i> - <i>37 bar → 29 bar; T = 10.3 °C</i> - <i>29 bar → 36.4 °C; T = 10.2 °C</i> - <i>36.4 bar → 33 bar; T = 10.1 °C</i> - <i>33 bar → 37 bar; T = 10.1 °C</i> 	Venting Pressure stabilizing Venting Pressure stabilizing Venting Pressure stabilizing
11	Once satisfied with the pressure drop, gradually start increasing the temperature of the water bath to 35 °C	

12	Make sure all valves are securely closed	
13	Once at the set temperature check if the required set pressure is in the two-phase region	If not, vent more CO ₂
<hr/>		
ii	Adding CO₂	
<hr/>		
1	Place the CO ₂ gas bomb in the freezer	± 3 hours required
2	Remove the front of the oven	
<hr/>		
3	Remove gas bomb from the freezer and fill with CO₂	
<hr/>		
A	Unwrap paper from the loading side	
B	Open valve to slowly release CO ₂	Don't close all the way
C	Place CO ₂ bomb onto CO ₂ cylinder	Finger tighten
D	Close CO ₂ bomb valve	
E	Flush CO ₂ into connecting lines 6 times, i.e. - <i>Open and close CO₂ cylinder; open connecting point and release CO₂ to the atm.; close the connecting point again before all CO₂ has been released</i>	
F	Open the CO ₂ cylinder	
G	Open the CO ₂ bomb and fill with CO ₂	Monitor pressure on the gauge
H	Close CO ₂ bomb when at approximately 90 bar	
I	Open CO ₂ bomb again for 10 seconds and then close properly	
J	Close the CO ₂ cylinder	
K	Remove CO ₂ bomb from the cylinder	
<hr/>		
4	Dry gas bomb and valves from moisture in the lab - <i>When pressure increases to 300 bar, release CO₂ to get it down to 250 bar</i>	Use hairdryer (compressed air added for the valves)
5	Make sure the condensate on the gas bomb is gone	Use hairdryer and tissue paper
6	Weigh gas bomb	Should be ± 3325 g (ref only)
7	Heat up gas bomb properly (on stand)	Monitor pressure at 250 bar
8	Release CO ₂ until at the correct weight for loading	± 3303 g (ref only)
9	Plug in hairdryer at a point closer to the cell	
10	Take away stirrer plate and place 'sponge' in place on lifting plate for gas bomb to be attached to the cell	Check cupboard near window for the sponges
11	Place CO ₂ bomb onto the sponge and elevate it to be in-line with the connection point to the feed line	Be careful of the Pt-100 probe
12	Finger tighten the gas bomb	Ensure cell is closed properly
13	Open gas bomb to pipelines and close again	

- | | | |
|----|---|---|
| 14 | Release CO ₂ slowly (don't release all of it) | With 11 spanner |
| 15 | Repeat 13 and 14 another 3 times (flushing pipelines) | |
| 16 | Tighten the cylinder to the inlet valve properly | |
| 17 | While heating the gas bomb with the hairdryer open the bomb valve completely | |
| 18 | Slowly open feed line microvalve to start loading the CO ₂ | |
| 19 | Gradually start opening the microvalve more | Monitor the liquid level inside of the equilibrium cell |
| 20 | When inlet flow starts to decrease (close to empty), close the gas bomb and start heating the piping network | |
| 21 | Close the feed line microvalve securely | |
| 22 | Remove gas bomb and weigh it | ± 3260 g (loading 40 g) |
| | - <i>Whether enough CO₂ has been added will depend on the minimum required pressure at T_{set1}. If the pressure is higher than the value required then it is enough.</i> | |
| 23 | Place gas bomb back on stand | |
| 24 | Record pressure and temperature of cell | |
| 25 | Make sure all microvalves are closed properly | With 11 spanner |
-

Unloading & Cleaning

Important to know:

- i. When working at lower temperatures of 35 °C it is difficult to get the oven temperature and cell down to 35 °C; therefore, add extra rings to the outlet pipe of the oven (top RHS and front side) to make a 5-mm gap.
- ii. If returned to atmospheric pressure the sight glass should be tightened again to prevent the seal from expanding.

No.	Step	Notes
	<i>Place the CO₂ gas bomb in the freezer</i>	<i>Need ± 3 hours</i>
1	Take out the oven temperature probes	Place into sponges
2	Remove front of oven	Wingnuts to be placed in their respective containers
3	Take the camera and endoscope away	
4	Remove heating and venting tubes of the oven and secure them away with the strings (orange and pink)	
5	Remove the insulation material at the back of the oven	Including the paper towel
6	Remove the back of the oven	
7	Clean the oven doors with acetone	
8	Unplug the stirrer and clean the plate	Remove the stand as well
9	Place the camera and endoscope back in place	
10	Switch on the monitor and camera	
11	Switch on the water bath	Record ambient and cell temps
12	Vent CO ₂ from the degas line - <i>Open blue microvalve to atmosphere</i>	With 11 spanner
13	Set the water bath temperature to approximately 57 °C to allow for a faster release of the components from the cell	Decreases the viscosity
14	Allow the cell to vent for approximately 20 mins	
15	Place a plastic container at the bottom of the cell and drain the components through the bottom drain line	With 11 spanner
16	Open feed line valve completely (remove the screw)	
17	Use a syringe to insert acetone into the cell	
18	Flush out the cell with compressed air	Components will drain through drain line at the bottom

19	Repeat 17 and 18 another three times	Use 90° angle tube
20	Loosen the piston	4 mm rod and 17 spanner
21	Unscrew the low pressure chamber of the cell	
22	Clean the piston with acetone and paper towels	Remove piston and clean each part separately
23	Place blue waste container underneath the cell in front of the opening (upright)	
24	Place paper towel around the bottom and sides of the outlet to avoid splashing the components everywhere	
25	Cover the GC with the black cloth	
26	Close the drain line - <i>To avoid excess solutes in that line</i>	
27	Remove the stirrer from the cell with the magnet	
28	Clean the stirrer with acetone and paper towel	
29	Wash the cell with acetone and flush with compressed air - <i>Until satisfied</i> - <i>Leave bottom drain line open</i>	Use curved tube to place inside of opening
30	Flush through the bottom drain line with compressed air	Short, curvy tube
31	Add acetone to the cell through the feed line	With syringe
32	Flush out the cell with compressed air through the bottom drain line	
33	Repeat 31 and 32 another three times and then close the bottom drain line	
34	Open degas line and top blue microvalve to the atmosphere	
35	Wash the degas line by spraying acetone into the top 'vent line' and flushing it out with compressed air	Repeat three times
36	Once satisfied close the degas line microvalve at the top to atmosphere and at the back	
37	Use syringe to add acetone to the cell through the feed line	
38	Flush out with compressed air through the port where CO ₂ is added	Use 90° tube
39	Repeat 37 and 38 another three times	
40	Place back the T screw for the feed line once satisfied	
41	Take out syringe with metal line (extract acetone)	In the cupboard below the cell
42	Attach to the feed line used for adding solvents to the cell	
43	Spray the acetone into the cell and then remove the syringe	
44	Flush out with compressed air until well dry	Use small curvy tube
45	Close the feed line microvalve properly	

	- <i>All microvalves have been washed out and closed</i>	
46	Wash out the cell once more through the opening on the RHS	Acetone and compressed air
47	Switch off the water bath	
48	Continue washing the cell until visibly clean	
	- <i>Look for viscous drops on the sight glass</i>	
49	Lower the ROLSI samplers all the way into the cell in order to wash the shaft of each	At lower pressures there will be less strain on the O-rings
50	Fold paper towel \pm 9 times (arm length), wet the tip and then wipe out the high pressure chamber	Careful of the temperature and pressure probes on the inside
	- <i>Don't push the paper towel in all the way</i>	
51	Discard the waste into the respective containers	
i	Load cell with 'dirty' CO₂	
1.1	Place stirrer inside of the cell	
1.2	Place low pressure chamber back onto cell	
1.3	Tighten the piston	4 mm rod and 17 spanner
1.4	Repeat the adding CO ₂ procedure (described in section 3)	
	- <i>No need to flush the connecting pipelines/cell this time as the air inside the cell is irrelevant 'dirty CO₂'</i>	
1.5	Once the CO ₂ has been loaded switch on the water bath and set it to 57 °C	
	<i>Place the CO₂ gas bomb in the freezer</i>	<i>Need \pm 3 hours</i>
	- <i>Will need to use it for a second loading</i>	
1.6	Place magnetic stirrer plate back underneath the cell and switch it on	
1.7	Push up the pressure to the one-phase region	
	- <i>Allow a waiting period of approximately 20 min</i>	
1.8	Switch off the water bath and stirrer	
1.9	Remove the stirring plate	
1.10	Slowly vent the CO ₂ to the atmosphere with a collecting bottle at the outlet of the vent line to capture any solutes	
52	Remove the feed line T microvalve screw	
53	Loosen the piston	4 mm rod and 17 spanner
54	Remove the low pressure chamber	
55	Remove stirrer with the magnet	
56	Flush out the vent line used with compressed air	Small, curvy tube
57	Close the degas line microvalve	

58	Flush out the degas line once more with compressed air	
	- <i>A check to see if the O-rings of the microvalve are still working properly or need to be replaced</i>	
59	Repeat steps 56 to 58 for the feed line used to load the CO ₂	
60	Repeat steps 23 to 25	
61	Wash out the cell through the piston opening on the RHS	Acetone and compressed air
62	Open the blue microvalve to the vacuum (the degas line microvalve should remain closed)	
63	Switch on the vacuum pump	To warm-up
64	Clean the piston and magnetic stirrer	Acetone, compressed air and paper towel if needed
65	Place the magnetic stirrer back into the cell	
66	Place the low-pressure chamber back onto the cell	
	- <i>Tighten the piston</i>	4mm rod and 17 spanner
<hr/>		
ii	Cleaning the GC lines/ROLSI samplers	
<hr/>		
2.1	Remove gas bomb from the freezer and fill it with CO ₂ as explained in the loading procedure (section 1)	
2.2	Open degas line microvalve to apply vacuum to equilibrium cell	With 11 spanner
	- <i>Make sure top blue microvalves are closed to the atmosphere and open to the vacuum</i>	
2.3	Monitor the pressure	
	- <i>When drawing vacuum the pressure should drop by approximately 1 bar, i.e. -2.3 bar to -3.3 bar</i>	
2.4	Close top blue and degas line microvalves to vacuum	
2.5	Dry gas bomb and valves from moisture in the lab	Use hairdryer (compressed air added for the valves)
	- <i>When pressure increases to 300 bar, release CO₂ to get it down to 250 bar</i>	
2.6	Make sure the condensate on the gas bomb is gone	Use hairdryer and tissue paper
2.7	Weigh gas bomb	Should be ± 3325 g (ref only)
2.8	Heat up gas bomb properly (on stand)	Monitor pressure at 250 bar
2.9	Release CO ₂ until at the correct weight for loading	± 3303 g (ref only)
2.10	Plug in hairdryer at a point closer to the cell	
2.11	Take away stirrer plate and place 'sponge' in place on lifting plate for gas bomb to be attached to the cell	Check cupboard near window for the sponges
2.12	Place CO ₂ bomb onto the sponge and elevate it to be in-line with the connection point to the feed line	Be careful of the Pt-100 probe

- 2.13 Finger tighten the gas bomb Ensure cell is closed properly
- 2.14 Open gas bomb to pipelines and close again
- 2.15 Release CO₂ slowly (don't release all of it) With 11 spanner
- 2.16 Repeat 14 and 15 another 3 times (flushing pipelines)
- 2.17 Tighten the cylinder to the inlet valve properly
- 2.18 While heating the gas bomb with the hairdryer open the bomb valve completely
- 2.19 Slowly open feed line microvalve to start loading the CO₂
- 2.20 Gradually start opening the microvalve more Monitor the liquid level inside of the equilibrium cell
- 2.21 When inlet flow starts to decrease (close to empty), close the gas bomb and start heating the piping network
- 2.22 Close the feed line microvalve securely
- 2.23 Remove gas bomb and weigh it ± 3260 g (loading 40 g)
- 2.24 Place gas bomb back on stand
- 2.25 Record pressure and temperature of cell
- 2.26 Make sure all microvalves are closed properly With 11 spanner
- 2.27 *Temperature settings (reference only):* Not need to wait for thermal equilibrium
- *Water bath = 34.37 °C*
 - *Oven = 34.6 °C*
 - *Overtemp = 55 °C*
- 2.28 Pressure is not important (so let out all pressure in cell)
- 2.29 Switch on GC to warm up
- 2.30 Instruments
- *Parameters*
 - *Detectors (magnifying glass)*
 - *Tick all boxes for both FIDs and TCD*
- 2.31 Open air, helium and then the hydrogen DON'T PRESS APPLY YET
- 2.32 Select apply straight after opening hydrogen All regulators to 400
- 2.33 Set oven temperature to 250 °C
- *Set time to 90 min*
- 2.34 ROLSI transfer tubing to GC to be increased on temperature control box systematically to 280 °C
- *The other 4 temperature controls (in red) should be set to 220 °C; 280 °C; 220 °C; 280 °C*
- Although hardly ever this long
- Black box

2.35	Push back ROLSI inwards (clockwise rotation)	#1
2.36	Pull front ROLSI outwards (counter-clockwise rotation)	#2
i	Purge series (pre-pre-purge)	
A	Methods	Where to log data (folder)
	- <i>Select pre-pre-purge</i>	
	Run setup	
	- <i>Sample info</i>	
	- <i>Manually change folder name & number</i>	i.e. pre_pre_purge_0001
B	Instruments → parameters	For analysis
	- <i>Switch on the septum purge flow</i>	
	- <i>Switch of the gas saver</i>	
	- <i>Check that the valves are ticked</i>	
	- <i>Set front inlet split ratio to 6:1</i>	
	- <i>Set back inlet split ratio to 80:1</i>	
C	Switch on ROLSI timers	
	- <i>Set1 = time off (when the sampler will open)</i>	0.30 secs (NEVER = 0)
	- <i>Set2 = time on (how long the sampler will be open)</i>	0.18 secs
D	Wet bubble flow meter tubing/ check flow rates	
E	Start timer	Monitor screen for each purge
	- <i>GC will start the method automatically</i>	‘click’ and record temperature
	- <i>Check the computer if the GC registers the solutes</i>	and pressure values
F	Continue with purge series until peak heights level out	15-20 minutes
G	Turn off timer	
H	Wait for the final peaks to appear on graphs and then press stop on the GC	Stop the method run
I	Instruments → parameters	
	- <i>Detectors (magnifying glass)</i>	
	- <i>Untick everything except the heater</i>	Press apply
J	Close hydrogen immediately after switching off detectors	Cylinder and regulator
K	Close the air and helium regulators	
L	After 10 minutes tick the gas saver box for both SSL front and back (to ensure capillaries clean first at a faster rate)	Flow rate will then decrease to 23 ml/min
M	After another 5 minutes set oven temperature to 100 °C	
N	Methods	
	- <i>Select the sleep method</i>	
2.37	Switch off the vacuum pump	
2.38	Switch off the water bath and stirrer	

2.39 Remove the stirring plate

2.40 Slowly vent the CO₂ to the atmosphere with a collecting bottle at the outlet of the vent line to capture any solutes

67	Remove the feed line T microvalve screw	
68	Loosen the piston	4 mm rod and 17 spanner
69	Remove the low-pressure chamber	
70	Remove stirrer with the magnet	
71	Flush out the vent line used with compressed air	Small, curvy tube
72	Close the degas line microvalve	
73	Flush out the degas line once more with compressed air	
	- <i>A check to see if the O-rings of the microvalve are still working properly or need to be replaced</i>	
74	Repeat steps 71 to 73 for the feed line used to load the CO ₂	
75	Repeat steps 23 to 25	
76	Wash out the cell through the piston opening on the RHS	Acetone and compressed air
77	Discard the waste in the correct containers	
78	Clean the piston and the stirrer	Acetone and compressed air
79	Disassemble the oven and pack away everything in their respective places	Switch off all plugs

B3. LPVLE EXPERIMENTAL PROCEDURE

Step-by-Step of Procedure

No.	Step
1	Switch on apparatus and ensure the oil level in the pump is midrange in the oil sight glass (with the correct clarity)
2	Make sure (14) has been fitted and secured with (1.5) and (11.1) closed. It is important that (1.10, 1.11 and 1.7) are also closed.
3	Make sure the still is dry and fill (11.3) via (11.1) fitted with the screw cap. The substances should be filled to measure approximately 110 ml. For more volatile components use 120 ml and for heavier mixtures 100 ml.
4	Open (11.4) on (11.3), closing the valve as soon as the liquid covers (1.4). Make sure (9) is also submerged in feed mixture.
5	Close (11.3) and switch on the control device.
6	To ensure constant mixing of the substances, adjust the speed of (3) accordingly.
7	Open cooling water valve to allow flow through (1.8 and 1.9).
8	If operations are to take place at temperatures exceeding 100 °C, (2) must be applied to the column to prevent partial condensation of the rising vapour. The temperature of (2) is set to approximately 3-5 °C below the mixture boiling point by adjusting the set point controller on the control device.
9	If substances display solidification points within a region of room temperature, the strip heater should be wrapped around the return lines from the coolers to (1.2).
10	Ensure that (1.12 b, 1.13 b, 5.1 and 5.2) are securely fitted with (1.7 and 11.4). Furthermore, (11.5) must be closed and (1.16) opened to maintain equal pressure.
11	The heating capacity should be adjusted using the power controller on the control device.
12	The operating pressure conditions should also be selected on the control device/ switching the three-way valve on the hydraulic box (atmospheric, vacuum or over-pressure). For the current study, over-pressure will be selected to allow for operations at standard atmospheric pressure (1 atm).
13	Set the pressure switch to 'pressure' on the apparatus after specifying the pressure at which the set-up should be controlled on the control device.
14	Open the valve to the pressure compensation cylinder.
15	Set the heating capacity of (1.4) via the power controller on the control device. A continuous flow of condensate will exit on the liquid side once the heating capacity is correctly set.
16	The number of droplets at the droplet point on the vapour condensation side can be observed. The optimum load will be at a rate of approximately 30 drops per minute.
17	Select 'start' on the control device.
18	For VLLE measurements, the ultrasonic homogenizer should be switched on as soon as the mixture starts boiling.

- 19 Start taking actual equilibrium measurements as soon as the boiling point of the pure substance is reached.
 - 20 If the vapour temperature remains constant, equilibrium has been reached (occurs after approximately 1 hour of operation). The vapour temperature is shown on the digital display of the control device.
 - 21 Once the boiling temperature has been recorded, take the respective vapour and liquid samples.
 - 22 To perform more than one test select 'stop' on the control device.
 - 23 Switch off (14) and (3).
 - 24 Add more feed to (1.2) via (11.3) to make up the volume lost through sampling (roughly 10 ml).
 - 25 Repeat steps 17 to 21.
 - 26 The experimental procedure can be repeated until the required number of samples have been obtained.
 - 27 Once done, select 'stop' on the control device.
 - 28 Switch off (14) and (3).
 - 29 Allow the mixture and (9) to cool down.
 - 30 Drain all liquid from (1.2), the equilibrium chamber and the boiling chamber through (1.5).
 - 31 Remove (14) to drain all remaining liquid. Once done reattach (14) and close (1.5).
 - 32 Rinse the system with acetone through (1.2), approximately 110 ml.
 - 33 Dry the apparatus with compressed air or allow it to dry by itself.
-

C. CALIBRATION DATA AND CERTIFICATES

The following appendix contains the certificates issued by companies that performed the necessary calibration tests on the experimental equipment used in this study. The in-house HPBDP and HPVLE pressure calibrations performed by the author are also included in this chapter.

C1. High-pressure experimental equipment

- (i) Pressure calibration
- (ii) Deadweight tester calibration
- (iii) Temperature calibration

C2. Low-pressure experimental equipment

- (i) Temperature calibration (vapour and evaporator)
- (ii) Pressure calibration

C1. HIGH-PRESSURE CALIBRATIONS

TABLE C- 1: STATIC SYNTHETIC PRESSURE SENSOR CALIBRATIONS DONE FOR THE LARGE EQUILIBRIUM CELL USED FOR ALL HPBDP EXPERIMENTAL WORK.

P_{dw}	$T = 34\text{ }^{\circ}\text{C}$			$T = 45\text{ }^{\circ}\text{C}$			$T = 53\text{ }^{\circ}\text{C}$			$T = 62\text{ }^{\circ}\text{C}$			$T = 71\text{ }^{\circ}\text{C}$			$T = 80\text{ }^{\circ}\text{C}$			$T = 88\text{ }^{\circ}\text{C}$		
	P_{cell} (bar)	T_{cell} ($^{\circ}\text{C}$)	P_{Dev} (bar)	P_{cell} (bar)	T_{cell} ($^{\circ}\text{C}$)	P_{Dev} (bar)	P_{cell} (bar)	T_{cell} ($^{\circ}\text{C}$)	P_{Dev} (bar)	P_{cell} (bar)	T_{cell} ($^{\circ}\text{C}$)	P_{Dev} (bar)	P_{cell} (bar)	T_{cell} ($^{\circ}\text{C}$)	P_{Dev} (bar)	P_{cell} (bar)	T_{cell} ($^{\circ}\text{C}$)	P_{Dev} (bar)	P_{cell} (bar)	T_{cell} ($^{\circ}\text{C}$)	P_{Dev} (bar)
35.0	34.4	34.0	0.6	32.5	43.4	2.5	33.2	51.6	1.8	33.9	60.7	1.1	34.6	69.2	0.4	35.5	78.4	-0.5	36.1	85.7	-1.1
50.0	49.0	34.0	1.0	47.9	43.6	2.1	48.5	51.6	1.5	49.2	60.7	0.8	50.0	69.4	0.0	50.7	78.5	-0.7	51.4	85.7	-1.4
65.0	63.7	34.0	1.3	63.1	43.9	1.9	63.7	51.8	1.3	64.4	60.8	0.6	65.2	69.5	-0.2	65.9	78.5	-0.9	66.6	85.7	-1.6
80.0	78.5	34.0	1.5	78.3	44.2	1.7	78.9	51.8	1.1	79.6	60.9	0.4	80.4	69.6	-0.4	81.1	78.6	-1.1	81.8	85.7	-1.8
95.0	93.2	34.0	1.8	93.4	44.5	1.6	94.0	51.8	1.0	94.7	60.9	0.3	95.4	69.7	-0.4	96.2	78.6	-1.2	96.8	85.7	-1.8
110.0	108.0	34.0	2.0	108.5	44.6	1.5	109.1	51.8	0.9	109.8	60.9	0.2	110.6	69.7	-0.6	111.3	78.7	-1.3	112.0	85.7	-2.0
125.0	122.9	34.0	2.1	123.6	44.7	1.4	124.2	51.9	0.8	125.0	61.0	0.0	125.7	69.8	-0.7	126.3	78.7	-1.3	127.0	85.7	-2.0
140.0	138.0	33.9	2.0	138.7	44.8	1.3	139.3	51.9	0.7	140.0	61.1	0.0	140.7	69.9	-0.7	141.4	78.7	-1.4	142.1	85.8	-2.1
155.0	152.9	33.9	2.1	153.7	44.9	1.3	154.4	51.9	0.6	155.1	61.1	-0.1	155.8	70.0	-0.8	156.5	78.8	-1.5	157.2	85.8	-2.2
170.0	167.9	33.9	2.1	168.9	44.9	1.1	169.5	51.9	0.5	170.2	61.1	-0.2	170.9	70.1	-0.9	171.6	78.8	-1.6	172.2	85.8	-2.2
185.0	182.9	33.9	2.1	183.9	45.0	1.1	184.6	52.0	0.4	185.3	61.1	-0.3	186.0	70.1	-1.0	186.7	78.8	-1.7	187.3	85.8	-2.3
200.0	197.9	33.9	2.1	199.1	45.0	0.9	199.8	52.0	0.2	200.5	61.1	-0.5	201.1	70.2	-1.1	201.8	78.8	-1.8	202.5	85.8	-2.5
215.0	213.0	33.9	2.0	214.2	45.0	0.8	214.9	52.1	0.1	215.6	61.2	-0.6	216.2	70.2	-1.2	217.0	78.8	-2.0	217.6	85.8	-2.6
230.0	228.0	33.9	2.0	229.2	45.0	0.8	230.0	52.1	0.0	230.8	61.2	-0.8	231.4	70.3	-1.4	232.2	78.8	-2.2	232.7	85.8	-2.7
245.0	243.0	33.9	2.0	244.3	45.0	0.7	245.2	52.1	-0.2	245.9	61.2	-0.9	246.5	70.3	-1.5	247.3	78.8	-2.3	247.9	85.8	-2.9
260.0	258.0	33.8	2.0	259.4	45.0	0.6	260.2	52.2	-0.2	261.0	61.3	-1.0	261.8	70.4	-1.8	262.5	78.8	-2.5	263.0	85.8	-3.0
275.0	272.7	33.8	2.3	274.3	45.0	0.7	275.2	52.2	-0.2	276.1	61.3	-1.1	276.9	70.4	-1.9	277.7	78.8	-2.7	278.3	85.8	-3.3
290.0	287.4	33.8	2.6	289.3	45.0	0.7	290.2	52.2	-0.2	291.2	61.3	-1.2	292.1	70.4	-2.1	292.8	78.8	-2.8	293.5	85.8	-3.5

TABLE C- 2: STATIC ANALYTICAL PRESSURE SENSOR CALIBRATIONS DONE OVER THE COURSE OF HPVLE EXPERIMENTAL WORK
AT $T = 308$ K.

<i>March 2016</i>		<i>September 2016</i>		<i>April 2017</i>	
$T_{\text{setpoint-GP}} (^{\circ}\text{C})$	34.7	$T_{\text{setpoint-GP}} (^{\circ}\text{C})$	34.6	$T_{\text{setpoint-GP}} (^{\circ}\text{C})$	34.6
$T_{\text{display-GP}} (^{\circ}\text{C})$	34.8/9/35.0/34.9	$T_{\text{display-GP}} (^{\circ}\text{C})$	34.6	$T_{\text{display-GP}} (^{\circ}\text{C})$	34.6/7
P_{applied} (bar)	P_{display} (bar)	P_{applied} (bar)	P_{display} (bar)	P_{applied} (bar)	P_{display} (bar)
0.0	-1.4	5.0	-4.1	5.0	-2.1
5.0	3.2	20.0	9.3	20.0	9.7
20.0	17.4	34.9	23.8	35.0	23.8
35.0	32.1	49.9	38.6	50.0	38.5
50.0	46.9	64.9	53.6	64.9	53.4
64.9	62.0	79.8	68.7	79.9	68.5
79.9	76.9	94.8	83.8	94.9	83.7
94.9	92.1	109.7	99.0	109.9	98.9
109.9	107.2	124.7	114.2	124.9	114.2
124.9	122.4	139.7	129.3	139.9	129.5
139.9	137.6	154.6	144.6	154.9	144.8
154.9	152.6	169.6	159.8	169.8	160.0
169.8	167.8	184.6	175.0	184.8	175.2
184.8	183.0	199.5	190.1	199.8	190.4
199.8	198.1	214.5	205.3	214.8	205.6
214.8	213.3	229.4	220.5	229.8	220.8
229.8	228.4	244.4	235.6	244.8	236.0
244.8	243.4	259.4	250.8	259.7	251.0
259.7	258.5	274.3	265.8	274.7	266.1
274.7	273.6	289.3	280.9	289.7	281.2
289.7	288.6	294.3	286.0		
294.7	293.7	299.3	290.9		
299.7	298.6	303.3	294.9		
303.7	302.5				

TABLE C- 3: STATIC ANALYTICAL PRESSURE SENSOR CALIBRATIONS DONE OVER THE COURSE OF HPVLE EXPERIMENTAL WORK
AT $T = 328$ K.

<i>March 2016</i>		<i>September 2016</i>		<i>April 2017</i>	
$T_{\text{setpoint-GP}} (^{\circ}\text{C})$	54.6	$T_{\text{setpoint-GP}} (^{\circ}\text{C})$	54.6	$T_{\text{setpoint-GP}} (^{\circ}\text{C})$	54.6
$T_{\text{display-GP}} (^{\circ}\text{C})$	54.6/7	$T_{\text{display-GP}} (^{\circ}\text{C})$	54.7	$T_{\text{display-GP}} (^{\circ}\text{C})$	54.7
P_{applied}	P_{display}	P_{applied}	P_{display}	P_{applied}	P_{display}
(bar)	(bar)	(bar)	(bar)	(bar)	(bar)
0.0	1.0	5.0	-2.4	5.0	-0.3
5.0	6.0	20.0	11.0	20.0	11.8
20.0	20.1	34.9	25.7	35.0	25.8
35.0	34.8	49.9	40.5	50.0	40.5
50.0	49.7	64.9	55.6	64.9	55.5
64.9	64.6	79.8	70.5	79.9	70.5
79.9	79.7	94.8	85.7	94.9	85.7
94.9	94.8	109.7	100.9	109.9	100.9
109.9	109.8	124.7	116.1	124.9	116.1
124.9	124.9	139.7	131.3	139.9	131.4
139.9	140.1	154.6	146.5	154.9	146.6
154.8	155.2	169.6	161.7	169.8	161.8
169.8	170.2	184.6	176.9	184.8	177.0
184.8	185.4	199.5	192.0	199.8	192.2
199.8	200.5	214.5	207.2	214.8	207.3
214.8	215.6	229.4	222.2	229.8	222.5
229.8	230.7	244.4	237.4	244.8	237.7
244.7	245.7	259.4	252.5	259.7	252.8
259.7	260.8	274.3	267.6	274.7	268.0
274.7	275.8	289.3	282.6	289.7	283.0
289.7	290.9	294.3	287.7	294.7	288.0
294.7	295.8	299.3	292.6	299.7	293.0
299.7	300.9	303.3	296.6	303.7	297.0
303.7	304.9				

TABLE C- 4: STATIC ANALYTICAL PRESSURE SENSOR CALIBRATIONS DONE OVER THE COURSE OF HPVLE EXPERIMENTAL WORK
AT $T = 348$ K.

<i>March 2016</i>		<i>September 2016</i>		<i>April 2017</i>	
$T_{\text{setpoint-GP}} (^{\circ}\text{C})$	74.5	$T_{\text{setpoint-GP}} (^{\circ}\text{C})$	74.6	$T_{\text{setpoint-GP}} (^{\circ}\text{C})$	74.6
$T_{\text{display-GP}} (^{\circ}\text{C})$	74.7/6	$T_{\text{display-GP}} (^{\circ}\text{C})$	74.7	$T_{\text{display-GP}} (^{\circ}\text{C})$	74.7
P_{applied}	P_{display}	P_{applied}	P_{display}	P_{applied}	P_{display}
(bar)	(bar)	(bar)	(bar)	(bar)	(bar)
0.0	2.9	5.0	-0.1	5.0	1.2
5.0	7.8	20.0	13.3	20.0	14.1
20.0	22.1	34.9	28.0	35.0	28.1
35.0	36.8	49.9	42.8	50.0	42.8
50.0	51.6	64.9	57.6	64.9	57.7
64.9	66.5	79.8	72.8	79.9	72.8
79.9	81.6	94.8	87.8	94.9	88.0
94.9	96.5	109.7	103.0	109.9	103.0
109.9	111.7	124.7	118.1	124.9	118.4
124.9	126.9	139.7	133.3	139.9	133.5
139.9	142.0	154.6	148.5	154.9	148.7
154.8	157.0	169.6	163.6	169.8	164.0
169.8	172.1	184.6	178.8	184.8	179.0
184.8	187.3	199.5	194.0	199.8	194.2
199.8	202.5	214.5	209.2	214.8	209.4
214.8	217.5	229.4	224.2	229.8	224.6
229.8	232.5	244.4	239.4	244.8	239.7
244.7	247.7	259.4	254.4	259.7	254.8
259.7	262.6	274.3	269.6	274.7	270.0
274.7	277.7	289.3	284.6	289.7	285.0
289.7	292.6	294.3	289.6	294.7	290.0
294.7	297.7	299.3	294.5	299.7	295.0
299.7	302.6	303.3	298.6	303.7	299.0
303.7	306.6				

C2. BARNETT PRESSURE CALIBRATION




UNIQUE ACCREDITED CALIBRATION LABORATORY No. 003

PRESSURE METROLOGY

CERTIFICATE OF CALIBRATION

Date of issue : 2022/07/18

Certificate No. : 00029622-1

Technical Signature:

[Signature]

W. B. Boshman

Page 1 of 4 pages

The results of all measurements are traceable to the relevant measuring standards.

The values on this certificate are correct at the time of calibration. Subsequently the accuracy will deteriorate and therefore the only solution is handling and use within the given validity time period of use. Recalibration should be performed after the validity period in order to ensure that the instrument's accuracy remains within the acceptable limits.

This certificate is issued in accordance with the conditions of the accreditation granted by the South African Accreditation Board (SAB) - SANAS. It is a record of the measurements made. This certificate may not be repeated after the validity period without prior written approval from Unique Metrology. Legal liability and/or claims to the user of calibration data or certificate, and the applicator of calibration data, shall remain the responsibility of the user of the data.

The South African National Accreditation System (SANAS) is a member of the International Laboratory Accreditation Cooperation (ILAC) and the European Cooperation for Accreditation (EA). The organization adheres to the mutual recognition of national accreditation data in the context of calibration under the guidelines of the International Laboratory Accreditation Cooperation (ILAC) and the European Cooperation for Accreditation (EA).

The South African National Accreditation System (SANAS) is a member of the International Laboratory Accreditation Cooperation (ILAC) and the European Cooperation for Accreditation (EA). The organization adheres to the mutual recognition of national accreditation data in the context of calibration under the guidelines of the International Laboratory Accreditation Cooperation (ILAC) and the European Cooperation for Accreditation (EA).




CERTIFICATE OF CALIBRATION

Page 2 of 4 pages

Certificate Number	00029622-1		
Customer's Name	Pressure Balance		
Device Model	Barnett		
Device Serial	B0000000		
Customer's Name	Stellenbosch University, Stellenbosch		
Procedure Number	00-100		
Date of Calibration	2022/07/18		
Date of Issue	2022/07/18		
Calibration Environment	20 ± 1 °C		
Reference Standards	20V-0.05	Subsiding Weight	W0000000
	20V-0.07	Subsiding Weight Set	Set 200.0-0.07
	20V-0.10	Mass Set	Set 1000-01
	20V-0.11	Mass Set	Set 1000-02

1. Procedure

The values of the pressure balance and weight and of the weight of the system assembly were determined by comparison against calibration requirements.

The pressure balance assembly was calibrated against a calibrated standard piston-cylinder assembly at various pressures within the stated working range. The effective area was determined and corrected to 20 °C assuming an increase in area of 0.0001 mm² per °C.

2. Results

2.1 Weights

Uncertainty (kg) for weight values

Calibrating : W. B. Boshman

Technical Signature



Unique Metrology

Unique Metrology (Pty) Ltd
10000 10000 10000 10000 10000 10000 10000 10000 10000 10000
10000 10000 10000 10000 10000 10000 10000 10000 10000 10000
10000 10000 10000 10000 10000 10000 10000 10000 10000 10000



CERTIFICATE OF CALIBRATION

Certificate Number
Calibration of the
Resolution of Type

Resolution of
Pressure Resistor
Series

Page 1 of 4 pages

1.1 Measuring point

Component measured	Serial No.	Value measured kPa	Uncertainty of measurement kPa	Value kPa
Pressure	1	1.0000	0.01	1.0000
Pressure	2	1.0000	0.01	1.0000
Pressure	3	1.0000	0.01	1.0000
Pressure	4	1.0000	0.01	1.0000
Pressure	5	1.0000	0.01	1.0000
Pressure	6	1.0000	0.01	1.0000
Pressure	7	1.0000	0.01	1.0000
Pressure	8	1.0000	0.01	1.0000
Pressure	9	1.0000	0.01	1.0000
Pressure	10	1.0000	0.01	1.0000
Pressure	11	1.0000	0.01	1.0000
Pressure	12	1.0000	0.01	1.0000
Pressure	13	1.0000	0.01	1.0000
Pressure	14	1.0000	0.01	1.0000
Pressure	15	1.0000	0.01	1.0000
Pressure	16	1.0000	0.01	1.0000
Pressure	17	1.0000	0.01	1.0000
Pressure	18	1.0000	0.01	1.0000
Pressure	19	1.0000	0.01	1.0000
Pressure	20	1.0000	0.01	1.0000
Pressure	21	1.0000	0.01	1.0000
Pressure	22	1.0000	0.01	1.0000
Pressure	23	1.0000	0.01	1.0000
Pressure	24	1.0000	0.01	1.0000
Pressure	25	1.0000	0.01	1.0000
Pressure	26	1.0000	0.01	1.0000
Pressure	27	1.0000	0.01	1.0000
Pressure	28	1.0000	0.01	1.0000
Pressure	29	1.0000	0.01	1.0000
Pressure	30	1.0000	0.01	1.0000
Pressure	31	1.0000	0.01	1.0000
Pressure	32	1.0000	0.01	1.0000
Pressure	33	1.0000	0.01	1.0000
Pressure	34	1.0000	0.01	1.0000
Pressure	35	1.0000	0.01	1.0000
Pressure	36	1.0000	0.01	1.0000
Pressure	37	1.0000	0.01	1.0000
Pressure	38	1.0000	0.01	1.0000
Pressure	39	1.0000	0.01	1.0000
Pressure	40	1.0000	0.01	1.0000
Pressure	41	1.0000	0.01	1.0000
Pressure	42	1.0000	0.01	1.0000
Pressure	43	1.0000	0.01	1.0000
Pressure	44	1.0000	0.01	1.0000
Pressure	45	1.0000	0.01	1.0000
Pressure	46	1.0000	0.01	1.0000
Pressure	47	1.0000	0.01	1.0000
Pressure	48	1.0000	0.01	1.0000
Pressure	49	1.0000	0.01	1.0000
Pressure	50	1.0000	0.01	1.0000
Pressure	51	1.0000	0.01	1.0000
Pressure	52	1.0000	0.01	1.0000
Pressure	53	1.0000	0.01	1.0000
Pressure	54	1.0000	0.01	1.0000
Pressure	55	1.0000	0.01	1.0000
Pressure	56	1.0000	0.01	1.0000
Pressure	57	1.0000	0.01	1.0000
Pressure	58	1.0000	0.01	1.0000
Pressure	59	1.0000	0.01	1.0000
Pressure	60	1.0000	0.01	1.0000
Pressure	61	1.0000	0.01	1.0000
Pressure	62	1.0000	0.01	1.0000
Pressure	63	1.0000	0.01	1.0000
Pressure	64	1.0000	0.01	1.0000
Pressure	65	1.0000	0.01	1.0000
Pressure	66	1.0000	0.01	1.0000
Pressure	67	1.0000	0.01	1.0000
Pressure	68	1.0000	0.01	1.0000
Pressure	69	1.0000	0.01	1.0000
Pressure	70	1.0000	0.01	1.0000
Pressure	71	1.0000	0.01	1.0000
Pressure	72	1.0000	0.01	1.0000
Pressure	73	1.0000	0.01	1.0000
Pressure	74	1.0000	0.01	1.0000
Pressure	75	1.0000	0.01	1.0000
Pressure	76	1.0000	0.01	1.0000
Pressure	77	1.0000	0.01	1.0000
Pressure	78	1.0000	0.01	1.0000
Pressure	79	1.0000	0.01	1.0000
Pressure	80	1.0000	0.01	1.0000
Pressure	81	1.0000	0.01	1.0000
Pressure	82	1.0000	0.01	1.0000
Pressure	83	1.0000	0.01	1.0000
Pressure	84	1.0000	0.01	1.0000
Pressure	85	1.0000	0.01	1.0000
Pressure	86	1.0000	0.01	1.0000
Pressure	87	1.0000	0.01	1.0000
Pressure	88	1.0000	0.01	1.0000
Pressure	89	1.0000	0.01	1.0000
Pressure	90	1.0000	0.01	1.0000
Pressure	91	1.0000	0.01	1.0000
Pressure	92	1.0000	0.01	1.0000
Pressure	93	1.0000	0.01	1.0000
Pressure	94	1.0000	0.01	1.0000
Pressure	95	1.0000	0.01	1.0000
Pressure	96	1.0000	0.01	1.0000
Pressure	97	1.0000	0.01	1.0000
Pressure	98	1.0000	0.01	1.0000
Pressure	99	1.0000	0.01	1.0000
Pressure	100	1.0000	0.01	1.0000

Calibration by: A. M. M. M.

Technical Signature



Unique Metrology

Unique Metrology (Pty) Ltd
10000 10000 10000 10000 10000 10000 10000 10000 10000 10000
10000 10000 10000 10000 10000 10000 10000 10000 10000 10000
10000 10000 10000 10000 10000 10000 10000 10000 10000 10000



CERTIFICATE OF CALIBRATION

Certificate Number
Calibration of the
Resolution of Type

Resolution of
Pressure Resistor
Series

Page 1 of 4 pages

1.1 Measuring point

The effective value of the high-pressure pressure resistor assembly was found to be

Value: 1.0000 ± 0.01
 1.0000 ± 0.01 and
 1.0000 ± 0.01 in MPa
 at the pressure of 0.01 MPa
 The nominal value is 1.0000 MPa

2. Accuracy of pressure measurement

When the pressure resistor is used with the highest rated value and the loading voltage

3. Notes

The tolerance level for the pressure measurements was determined on the basis of

4. Uncertainty of calibration

The measured uncertainty is based on a standard uncertainty multiplied by a

5. Comments

The weight of the resistor is 1.0000 MPa

Calibration by: A. M. M. M.

Technical Signature

C3. HPBDP LARGE CELL *PT-100* CALIBRATION

medRxiv preprint doi: <https://doi.org/10.1101/2020.04.20.20075002>; this version posted May 1, 2020. The copyright holder for this preprint (which was not certified by peer review) is the author/funder, who has granted medRxiv a license to display the preprint in perpetuity. It is made available under a CC-BY 4.0 International license.

Abstract

10. **Answer: D**
 The passage states that the author is a member of the "New York City Police Department" and that he is "a member of the New York City Police Department" (line 1). The author is a member of the New York City Police Department.

They're not alone in the world.
We should all grow that beautiful skin.

4	1	1	1
1	1	1	1

1. The first step is to identify the problem or question that needs to be answered. This involves understanding the context and the specific requirements of the task.

Received 15 November 2005; accepted 12 January 2006
Published online 12 April 2006 in Wiley InterScience (www.interscience.wiley.com). DOI: 10.1002/anie.200526200

$$P = \frac{\left(\frac{1}{\lambda_1} + \frac{1}{\lambda_2} \right) \left(\frac{1}{\lambda_1} + \frac{1}{\lambda_2} \right) + \left(\frac{1}{\lambda_1} - \frac{1}{\lambda_2} \right) \left(\frac{1}{\lambda_1} - \frac{1}{\lambda_2} \right)}{4} = \frac{1}{2} \left(\frac{1}{\lambda_1} + \frac{1}{\lambda_2} \right)$$

© 2006 The Authors
Journal compilation © 2006 Blackwell Publishing Ltd

1. **Introduction**
2. **Background**
3. **Methodology**
4. **Results**
5. **Discussion**
6. **Conclusion**
7. **References**
8. **Appendix**
9. **Index**
10. **Summary**

1999



WIKA Instruments (Pty) Ltd
 Cape Town Branch
 115/117 Van St. Street & Arcadia St
 Milnerton 7945
 Tel: 021 551 5555
 Fax: 021 551 5555
 E-Mail: instruments@wika.co.za
 Web: www.wika.co.za

Temperature Calibration Certificate

Compliance: Full Compliance 2.1 according to EN 10358

Certificate Number: 017000175 - 0170002

Customer: University of Stellenbosch Medical Wing

Customer Ref Number: 00000000

Which are Number: 00000000

Serial Number: 1

Tag Number: 00000000

Temperature: 20.00 °C

Calibration at: 20.00 °C

Uncertainty: 0.05 °C (k=2) according to EN 10358

Serial Number: 000000000000

Range: 10 °C to 30 °C

Resolution: 0.01 °C

Calibration Instrument:

Type: 017000175

Serial No.: 000000000000

Scale:

Scale Range:

Resolution: 0.01 °C

Notes:

EN 10358 2.1 Full Compliance

Point	Setpoint	Measured	Uncertainty
1	20.00	20.00	0.05
2	20.00	20.00	0.05
3	20.00	20.00	0.05
4	20.00	20.00	0.05
5	20.00	20.00	0.05
6	20.00	20.00	0.05
7	20.00	20.00	0.05
8	20.00	20.00	0.05
9	20.00	20.00	0.05
10	20.00	20.00	0.05

EN 10358 2.1 Full Compliance

1. The accuracy of the calibration is in accordance with the requirements of EN 10358 2.1 and is in accordance with the requirements of EN 10358 2.1.

2. The values in this certificate are based on the use of calibration instruments, which are in accordance with the requirements of EN 10358 2.1 and are in accordance with the requirements of EN 10358 2.1.

3. The values in this certificate are based on the use of calibration instruments, which are in accordance with the requirements of EN 10358 2.1 and are in accordance with the requirements of EN 10358 2.1.

4. The values in this certificate are based on the use of calibration instruments, which are in accordance with the requirements of EN 10358 2.1 and are in accordance with the requirements of EN 10358 2.1.

Signature: 

Date: 01/01/2017

Signature: 

Date: 01/01/2017

C4. LPVLE $PT-100$ CALIBRATIONS



WIKA Instruments (Pty) Ltd
 Cape Town Branch
 Westgate Park, 12, Seacom's Island Road
 Fouriesburg
 Tel: +27 (0) 21 935 9000
 Fax: +27 (0) 21 935 9001
 Email: SouthAfrica@wika.com
 Web: www.wika.com

Temperature Calibration Certificate

Compliance Test Certificate (in accordance with ISO 9001)

Certificate Number: CTR-0020-101000

Customer: University of Cape Town

Customer's Reference: 101000

WIKA Job Number: 101000

Serial Number: 1

Tag Number: 101000

Instrument under Test	Reference Instrument
Calibration of: 101000	Tag: 101000
Description: Digital read out thermometer 0-100°C	Model: 101000
Serial Number: 101000	Model: 101000
Range: 0 to 100 °C	Model: 101000
Manufacturer: 101000	Calibration Method: 101000

Notes:

1. The instrument is calibrated in accordance with the requirements of the relevant standards and is suitable for use as a reference instrument.

2. The instrument is calibrated in accordance with the requirements of the relevant standards and is suitable for use as a reference instrument.

3. The instrument is calibrated in accordance with the requirements of the relevant standards and is suitable for use as a reference instrument.

4. The instrument is calibrated in accordance with the requirements of the relevant standards and is suitable for use as a reference instrument.

For: 101000

By: 101000

For: 101000

By: 101000



Thermom
South Africa (Pty) Ltd



Certification certificate

UNIQUE NUMBER
00000000000000000000

REQUIREMENT

Item	Requirement	Result
Temperature	±0.1°C	±0.1°C
Pressure	±0.1 bar	±0.1 bar
Humidity	±0.1%	±0.1%

NOTE

Calibrated at 20°C ambient. Uncertainty: ±0.1°C, ±0.1 bar, ±0.1%.

Location: 123 Main Street
Department of Science & Technology



Customer Address: University of Johannesburg
Pretoria, 2000
Western Cape

Order No: 123456789

Date of calibration: 15 Nov 2019

Valid until: 15 Nov 2020

What adjustment of the instrument does?

☒ Yes
 ☐ No

Readings at 20°C were stable using an in-house 1000g force cell and scale with 0.01g accuracy.

Readings are stable on the scale.

Calibration was performed in accordance with ISO 9001:2015, ISO 17025:2017 and ISO 15189:2013.

For further information, please contact us at 011 555 5555 or 0800 123 456.

Website: www.thermom.co.za

From: 123 Main Street, Pretoria, 2000

To: 123 Main Street, Pretoria, 2000



Signature



Certification & Calibration & Training

Email: sales@thermom.co.za **Web:** www.thermom.co.za



[illegible]



Thermo
Scientific (Pty) Ltd.



Calibration certificate

UNIVERSITY OF THE WESTERN CAPE



Lab instrument calibrated with certified accuracy to international standards

Instrument	Lab No.	Customer Name
Sanas Calibration	UNIVERSITY	UNIVERSITY

Article description

Temperature

20 °C ± 0.1 °C

Measuring procedure details

The measurements were performed in a temperature-stable, noise-reduced and vibration-free environment.

The result is calculated from an average of 3 readings ± 30 second intervals

Measurement results for 3 readings, determined with 10 min. zero

Reading no. 1-3	Reading no. 4-6	Reading no. 7-9	Measured value 1-3	Measured value 4-6	Measured value 7-9	10 min. zero	Result
20.00	20.00	20.00	20.00	20.00	20.00	20.00	20.00
20.00	20.00	20.00	20.00	20.00	20.00	20.00	20.00
20.00	20.00	20.00	20.00	20.00	20.00	20.00	20.00
20.00	20.00	20.00	20.00	20.00	20.00	20.00	20.00
20.00	20.00	20.00	20.00	20.00	20.00	20.00	20.00
20.00	20.00	20.00	20.00	20.00	20.00	20.00	20.00

Uncertainty of calibration

The measurement results recorded in this certificate apply only to the instrument & measurement system, and apply solely at the time this data was generated. The measurement system is subject to change. Subsequent changes will depend on factors such as: date, facility and frequency of use. It is recommended that institutions for calibration of an instrument should ensure that the instrument complies with the latest rules.

UNIVERSITY OF THE WESTERN CAPE

Calibration • Validation • Training

Email: info@thermo.co.za Web: www.thermo.co.za





C5. LOW-PRESSURE CALIBRATION

[illegible]

D. PRECAUTIONARY MEASURES

Take note of several aspects during each of the experimental procedures to ensure the operator is always safe when working with the equipment. The first is the different chemicals used during testing. It is advised that latex gloves, safety glasses and a lab coat be worn at all times when working with the chemicals. Closed shoes should also be worn to avoid spills on open skin.



It is required to study the potential harm that can be inflicted on the operator by not only the alcohols and *n*-alkanes used in this work but also the chemicals used for cleaning. The operator should study the material Safety Data Sheets (MSDS) for the respective components that will be utilized in this project before starting. CO₂ and nitrogen were also utilised in the experimental procedures of this work. If the operator is exposed to large amounts of these gases he/ she might experience weakness, dizziness and in some instances a loss of consciousness. These symptoms develop due to a decline in oxygen in the body. It is advised that the room be evacuated immediately in such instances.

The all glass dynamic recirculating still has been installed inside and extraction cabinet for safety with respect to the flammable nature of the chemicals being tested. Maximum operating levels have also been enforced for protection:

- The pressure should remain within a 2.5 mbar to 3 bar range
- The temperature should not exceed 250 °C

The high pressure analytical phase equilibria setup contains the following upper operating limits:

- The pressure should not exceed 300 bar
- The temperature should not be increased over 150 °C

The high-pressure visual synthetic method has the following constraints specified:

- Low pressure chamber maximum pressure of 15 bar
- High pressure chamber maximum pressure of 500 bar
- Working pressure inside cell at a maximum of 275 bar
- Sight glass operating temperature limit of 200 °C

E. RAW EXPERIMENTAL RESULTS

E1. HPBDP EXPERIMENTAL DATA

Table E-1 to Table E-6 contain the isothermal P - w_s data produced for the six CO_2 + (1-decanol + n -tetradecane) mixtures. The parameters used for the temperature corrections are provided for each respective solute composition and can be used to interpolate pressures at any temperature between $T = 308$ K and $T = 358$ K.

TABLE E- 1: ISOTHERMAL DATA FOR THE TERNARY SYSTEM CO_2 + (0.7595 G/G 1-DECANOL + 0.2405 G/G N -TETRADECANE).

Mass Fraction Solute, w_s (g/g)	Parameters for temperature correction					Isothermal P - w_s Data (MPa)					
	$P = A x T^3 + B x T^2 + C x T + D$					Temperature, T (K)					
	A	B	C	D	R^2	308	318	328	338	348	358
0,593	-	-	0,1296	-30,892	0.997	9.02	10.32	11.62	12.91	14.21	15.50
0,544	-0,00004487	0,04612	-15,68	1776,973	0.996	12.12	12.16	12.86	13.96	15.18	16.25
0,474	-0,00008586	0,08812	-30,01	3408,015	0.998	14.61	13.75	14.13	15.24	16.56	17.58
0,391	-0,00009181	0,09476	-32,47	3709,845	0.997	16.72	15.38	15.46	16.43	17.74	18.82
0,343	-0,0001280	0,1318	-45,14	5152,674	0.993	18.44	16.48	16.16	16.92	18.21	19.47
0,262	-0,0001467	0,1509	-51,61	5887,019	0.990	19.61	16.99	16.56	17.45	18.78	19.66
0,194	-0,0001230	0,1269	-43,52	4976,771	0.994	19.27	16.99	16.62	17.42	18.66	19.59
0,123	-0,00008574	0,08815	-30,08	3423,998	0.998	16.40	15.41	15.70	16.74	18.02	19.04
0,0860	-0,00004843	0,04930	-16,58	1859,626	0.999	13.24	13.65	14.69	16.05	17.45	18.60
0,0513	-	0,0009454	0,7833	-142,270	1.000	9.38	11.30	13.03	14.57	15.92	17.09
0,0259	-	0,001641	1,248	-220,818	1.000	7.78	9.98	11.85	13.40	14.61	15.50
0,0151	-	0,001488	1,122	-196,893	0.999	7.57	9.48	11.09	12.40	13.42	14.13

$u(w_s) = 0.01w_s$, $u(P) = 0.06$ MPa and $u(T) = -0.1$ K

TABLE E- 2: ISOTHERMAL DATA FOR THE TERNARY SYSTEM CO_2 + (0.5000 G/G 1-DECANOL + 0.5000 G/G N -TETRADECANE).

Mass Fraction Solute, w_s (g/g)	Parameters for temperature correction					Isothermal P - w_s Data (MPa)					
	$P = A x T^3 + B x T^2 + C x T + D$					Temperature, T (K)					
	A	B	C	D	R^2	308	318	328	338	348	358
0,609	-	-	0,1286	-32,302	0.997	7.29	8.58	9.86	11.15	12.44	13.72
0,517	-	-	0,1618	-41,797	0.996	8.05	9.67	11.28	12.90	14.52	16.14
0,465	-	-	0,1530	-37,918	0.998	9.20	10.73	12.26	13.79	15.32	16.85
0,397	-	-	0,1476	-35,183	0.997	10.29	11.77	13.24	14.72	16.20	17.67
0,349	-	-	0,1493	-35,413	0.995	10.57	12.06	13.55	15.05	16.54	18.03
0,257	-	-	0,1397	-31,686	0.989	11.33	12.73	14.12	15.52	16.92	18.31
0,192	-	-	0,1361	-30,531	0.987	11.39	12.75	14.11	15.47	16.83	18.19
0,126	-	-	0,1472	-34,669	0.998	10.66	12.13	13.61	15.08	16.55	18.02
0,0803	-	-	0,1674	-42,430	0.994	9.13	10.80	12.48	14.15	15.82	17.50
0,0536	-	-	0,1702	-44,139	0.990	8.27	9.97	11.68	13.38	15.08	16.78
0,0278	-	-	0,1496	-37,965	0.986	8.12	9.62	11.11	12.61	14.11	15.60
0,0154	-	-	0,1290	-31,684	0.974	8.05	9.34	10.63	11.92	13.21	14.50

$u(w_s) = 0.01w_s$, $u(P) = 0.06$ MPa and $u(T) = -0.1$ K

TABLE E- 3: ISOTHERMAL DATA FOR THE TERNARY SYSTEM CO₂ + (0.3601 G/G 1-DECANOL + 0.6399 G/G *N*-TETRADECANE).

Mass Fraction Solute, w_s (g/g)	Parameters for temperature correction					Isothermal P - w_s Data (MPa)					
	$P = A \times T^3 + B \times T^2 + C \times T + D$					Temperature, T (K)					
	A	B	C	D	R^2	308	318	328	338	348	358
0,608	-	-	0,1302	-33,06882	0.998	7.02	8.33	9.63	10.93	12.23	13.53
0,524	-	-	0,1539	-39,91933	0.998	7.48	9.02	10.56	12.10	13.63	15.17
0,468	-	-	0,1729	-45,53976	0.997	7.70	9.43	11.16	12.89	14.62	16.34
0,386	-	-	0,1799	-46,85658	0.998	8.56	10.36	12.16	13.96	15.76	17.56
0,338	-	-	0,1833	-47,69218	0.998	8.76	10.59	12.42	14.26	16.09	17.92
0,247	-	-	0,1820	-46,96478	0.998	9.09	10.91	12.73	14.55	16.37	18.19
0,187	-	-	0,1801	-46,30563	0.999	9.15	10.95	12.75	14.55	16.36	18.16
0,130	-	-	0,1785	-46,09320	0.998	8.88	10.66	12.45	14.23	16.02	17.80
0,0836	-	-	0,1862	-49,07070	0.997	8.28	10.14	12.00	13.86	15.72	17.59
0,0577	-	-	0,1747	-45,79426	0.992	8.02	9.77	11.52	13.26	15.01	16.76
0,0256	-	-	0,1484	-37,76628	0.988	7.93	9.42	10.90	12.38	13.87	15.35
0,0153	-	-	0,1242	-30,33952	0.984	7.92	9.16	10.40	11.65	12.89	14.13

 $u(w_s) = 0.01w_s$, $u(P) = 0.06$ MPa and $u(T) = -0.1$ KTABLE E- 4: ISOTHERMAL DATA FOR THE TERNARY SYSTEM CO₂ + (0.2302 G/G 1-DECANOL + 0.7698 G/G *N*-TETRADECANE).

Mass Fraction Solute, w_s (g/g)	Parameters for temperature correction					Isothermal P - w_s Data (MPa)					
	$P = A \times T^3 + B \times T^2 + C \times T + D$					Temperature, T (K)					
	A	B	C	D	R^2	308	318	328	338	348	358
0,598	-	-	0,1339	-34,319	0.997	6.91	8.24	9.58	10.92	12.26	13.60
0,504	-	-	0,1588	-41,551	0.999	7.35	8.94	10.53	12.11	13.70	15.29
0,458	-	-	0,1809	-48,167	0.999	7.54	9.35	11.16	12.97	14.77	16.58
0,401	-	-	0,1897	-50,689	0.999	7.74	9.63	11.53	13.43	15.33	17.22
0,339	-	-	0,1982	-53,040	0.999	7.99	9.97	11.95	13.93	15.92	17.90
0,249	-	-	0,2004	-53,414	0.999	8.31	10.31	12.32	14.32	16.32	18.33
0,189	-	-	0,2045	-54,734	0.998	8.26	10.30	12.35	14.39	16.44	18.48
0,125	-	-	0,2019	-54,256	0.998	7.92	9.94	11.96	13.98	16.00	18.01
0,0801	-	-	0,1909	-51,004	0.998	7.80	9.70	11.61	13.52	15.43	17.34
0,0525	-	-	0,1759	-46,350	0.997	7.83	9.59	11.35	13.11	14.87	16.63
0,0264	-	-	0,1496	-38,266	0.996	7.81	9.30	10.80	12.30	13.79	15.29
0,0154	-	-	0,1238	-30,277	0.995	7.85	9.09	10.32	11.56	12.80	14.04

 $u(w_s) = 0.01w_s$, $u(P) = 0.06$ MPa and $u(T) = -0.1$ K

TABLE E- 5: ISOTHERMAL DATA FOR THE TERNARY SYSTEM CO₂ + (0.1838 G/G 1-DECANOL + 0.8162 G/G *N*-TETRADECANE).

Mass Fraction Solute, w_s (g/g)	Parameters for temperature correction					Isothermal P- w_s Data (MPa)					
	$P = A \times T^3 + B \times T^2 + C \times T + D$					Temperature, T (K)					
	A	B	C	D	R ²	308	318	328	338	348	358
0,621	-	-	0,1289	-32,820	0.999	6.87	8.15	9.44	10.73	12.02	13.31
0,572	-	-	0,1480	-38,433	0.999	7.16	8.64	10.12	11.60	13.08	14.56
0,476	-	-	0,1731	-45,787	1.000	7.52	9.25	10.98	12.71	14.45	16.18
0,419	-	-	0,1911	-51,203	0.999	7.67	9.58	11.49	13.40	15.31	17.22
0,339	-	-	0,2014	-54,026	0.998	8.00	10.02	12.03	14.04	16.06	18.07
0,255	-	-	0,2074	-55,673	0.999	8.19	10.27	12.34	14.42	16.49	18.56
0,187	-	-	0,2052	-55,119	0.996	8.08	10.13	12.18	14.24	16.29	18.34
0,121	-	-	0,2010	-53,889	0.997	8.01	10.02	12.03	14.04	16.05	18.06
0,0777	-	-	0,1947	-52,027	0.998	7.93	9.88	11.82	13.77	15.72	17.66
0,0506	-	-	0,1747	-45,867	0.997	7.92	9.67	11.42	13.16	14.91	16.66
0,0268	-	-	0,1546	-39,689	0.995	7.94	9.49	11.03	12.58	14.12	15.67
0,0157	-	-	0,1402	-35,219	0.992	7.97	9.37	10.77	12.17	13.58	14.98

 $u(w_s) = 0.01w_s$, $u(P) = 0.06$ MPa and $u(T) = -0.1$ KTABLE E- 6: ISOTHERMAL DATA FOR THE TERNARY SYSTEM CO₂ + (0.0800 G/G 1-DECANOL + 0.9200 G/G *N*-TETRADECANE).

Mass Fraction Solute, w_s (g/g)	Parameters for temperature correction					Isothermal P- w_s Data (MPa)					
	$P = A \times T^3 + B \times T^2 + C \times T + D$					Temperature, T (K)					
	A	B	C	D	R ²	308	318	328	338	348	358
0,624	-	-	0,1263	-32,069	1.000	6.82	8.09	9.35	10.61	11.88	13.14
0,575	-	-	0,1501	-39,020	1.000	7.21	8.71	10.21	11.71	13.21	14.71
0,485	-	-	0,1779	-47,247	0.999	7.55	9.33	11.11	12.89	14.67	16.45
0,420	-	-	0,1936	-51,859	0.999	7.76	9.70	11.63	13.57	15.51	17.44
0,334	-	-	0,2034	-54,332	0.997	8.31	10.35	12.38	14.41	16.45	18.48
0,264	-	-	0,2048	-54,504	0.998	8.58	10.63	12.67	14.72	16.77	18.82
0,192	-	-	0,2080	-55,608	0.996	8.48	10.56	12.64	14.72	16.80	18.88
0,136	-	-	0,2066	-55,197	0.995	8.44	10.50	12.57	14.64	16.70	18.77
0,0833	-	-	0,1953	-52,082	0.996	8.09	10.04	12.00	13.95	15.90	17.86
0,0505	-	-	0,1809	-47,846	0.998	7.86	9.67	11.48	13.29	15.10	16.91
0,0228	-	-	0,1478	-37,496	0.996	8.01	9.49	10.97	12.45	13.93	15.40
0,0158	-	-	0,1297	-31,963	0.994	7.97	9.27	10.57	11.86	13.16	14.46

 $u(w_s) = 0.01w_s$, $u(P) = 0.06$ MPa and $u(T) = -0.1$ K

E2. HPVLE EXPERIMENTAL DATA

TABLE E- 7: HIGH-PRESSURE VLE DATA MEASURED FOR THE CO₂ + 1-DECANOL + *N*-TETRADECANE TERNARY MIXTURES AT $T = 308$ K. LIQUID AND VAPOUR COMPOSITIONS GIVEN AS AVERAGE MASS FRACTIONS AFTER 4 SAMPLES.

<i>Pressure, P (MPa)</i>	<i>CO₂</i>	<i>n-tetradecane liquid</i>	<i>l-decanol</i>	<i>CO₂</i>	<i>n-tetradecane vapour</i>	<i>l-decanol</i>
8.0	0.384	0.129	0.487	0.942	0.0240	0.0335
	0.526	0.282	0.192	0.875	0.0832	0.0417
	0.704	0.232	0.0635	0.838	0.126	0.0353
	0.648	0.318	0.0335	0.889	0.0944	0.0166
	0.320	0.000	0.680	0.977	0.000	0.023
8.1	0.697	0.239	0.0643	0.807	0.151	0.0414
	0.658	0.310	0.0314	0.843	0.137	0.0198
8.2	0.385	0.126	0.489	0.942	0.0198	0.0381
	0.566	0.262	0.173	0.857	0.0948	0.0478
	0.697	0.275	0.0271	0.852	0.129	0.0196
8.4	0.389	0.126	0.485	0.944	0.0244	0.0317
	0.589	0.245	0.166	0.817	0.121	0.0613

$u(w_i) = \pm 0.005$ g/g with $u(w_i) \leq 0.009$ g/g, $u(P) \leq 0.035$ MPa and $u(T) = 0.1$ K

TABLE E- 8: HIGH-PRESSURE VLE DATA MEASURED FOR THE CO₂ + 1-DECANOL + *N*-TETRADECANE TERNARY MIXTURES AT $T = 328$ K. LIQUID AND VAPOUR COMPOSITIONS GIVEN AS AVERAGE MASS FRACTIONS AFTER 4 SAMPLES.

<i>Pressure, P (MPa)</i>	<i>CO₂</i>	<i>n-tetradecane liquid</i>	<i>l-decanol</i>	<i>CO₂</i>	<i>n-tetradecane vapour</i>	<i>l-decanol</i>
11.1	0.389	0.142	0.470	0.979	0.00881	0.0124
	0.484	0.317	0.199	0.973	0.0165	0.0102
	0.544	0.364	0.0917	0.968	0.0230	0.00919
	0.519	0.436	0.0453	0.978	0.0167	0.00496
11.5	0.566	0.347	0.0877	0.946	0.0394	0.0144
	0.559	0.399	0.0412	0.962	0.0308	0.00689
12.0	0.430	0.128	0.442	0.959	0.0162	0.0249
	0.591	0.252	0.157	0.937	0.0398	0.0228
	0.653	0.277	0.0697	0.881	0.0911	0.0283
	0.614	0.350	0.0359	0.922	0.0673	0.0111
12.3	0.679	0.291	0.0299	0.872	0.113	0.0154
12.4	0.444	0.122	0.434	0.949	0.0207	0.0305
	0.653	0.211	0.136	0.837	0.104	0.0590
	0.685	0.284	0.0305	0.869	0.115	0.0162

$u(w_i) = \pm 0.005$ g/g with $u(w_i) \leq 0.009$ g/g, $u(P) \leq 0.035$ MPa and $u(T) = 0.1$ K

TABLE E- 9: HIGH-PRESSURE VLE DATA MEASURED FOR THE CO₂ + 1-DECANOL + *N*-TETRADECANE TERNARY MIXTURES AT $T = 348$ K. LIQUID AND VAPOUR COMPOSITIONS GIVEN AS AVERAGE MASS FRACTIONS AFTER 4 SAMPLES.

<i>Pressure, P (MPa)</i>	<i>CO₂</i>	<i>n-tetradecane liquid</i>	<i>1-decanol</i>	<i>CO₂</i>	<i>n-tetradecane vapour</i>	<i>1-decanol</i>
14.0	0.499	0.398	0.102	0.968	0.0231	0.00933
	0.481	0.471	0.0479	0.973	0.0220	0.00523
16.0	0.483	0.116	0.401	0.937	0.0222	0.0407
	0.649	0.216	0.136	0.883	0.0729	0.0445
	0.663	0.270	0.0675	0.877	0.0952	0.0280
	0.628	0.338	0.0339	0.911	0.0783	0.0112
16.2	0.493	0.114	0.393	0.931	0.0241	0.0453
	0.671	0.201	0.127	0.873	0.0785	0.0487
	0.698	0.241	0.0610	0.847	0.119	0.0339
	0.647	0.320	0.0326	0.887	0.0995	0.0135
16.3	0.734	0.212	0.0543	0.818	0.142	0.0399
	0.666	0.303	0.0311	0.879	0.107	0.0142
16.4	0.508	0.109	0.383	0.923	0.0264	0.0505
	0.726	0.168	0.106	0.825	0.108	0.0665
	0.693	0.278	0.0286	0.869	0.116	0.0150

$u(w_i) = \pm 0.005$ g/g with $u(w_i) \leq 0.009$ g/g, $u(P) \leq 0.035$ MPa and $u(T) = 0.1$ K

E3. LPVLE EXPERIMENTAL DATA

The L/W thermodynamic consistency tests were performed with the use of a PRO-VLE software that required the use of component specific parameters. All values were obtained from the DIPPR database [23] unless otherwise stated.

TABLE E- 10: REPRODUCIBILITY COMPONENT PARAMETERS USED FOR THE L/W THERMODYNAMIC CONSISTENCY TESTS [23].

<i>Parameters</i>	<i>Symbol</i>	<i>Units</i>	<i>Components</i>			
			<i>Ethanol</i>	<i>Iso-octane</i>	<i>2-butanone</i>	<i>n-heptane</i>
A			8.112	6.888	6.613	6.509
B		mmHg and $^{\circ}\text{C}$	1592.864	1319.529	1010.546	1041.244
C			226.184	211.625	191.244	188.569
Critical Temperature	T_c	K	514.0	559.7	536.8	540.3
Critical Pressure	P_c	atm	60.567	24.673	41.549	27.042
Critical Volume	V_c	cm^3/mol	168	488	267	432
Normal Boiling Point	T_b	K	351.44	390.80	350.35	371.60
Liquid Molar Volume	V_L	cm^3/mol	58.620	164.401	98.230	158.855
Acentric Factor	w		0.644	0.380	0.320	0.349
Dipole Moment		D (Debye)	1.691	0.000	2.780	0.000
Heat of Vapourisation	H_v	cal/mol	9359	8030	7589	9096

Antoine equation as $\log_{10}(\text{mmHg}) = A - (B/(T(^{\circ}\text{C}) + C))$

TABLE E- 11: 1-ALCOHOL COMPONENT PARAMETERS USED FOR THE L/W THERMODYNAMIC CONSISTENCY TESTS [23].

<i>Parameters</i>	<i>Symbol</i>	<i>Units</i>	<i>Components</i>				
			<i>1-pentanol</i>	<i>1-hexanol</i>	<i>1-heptanol</i>	<i>1-octanol</i>	<i>1-decanol</i>
A			7.771	7.462	7.350	7.274	8.153
B		mmHg and $^{\circ}\text{C}$	1695.022	1572.478	1573.510	1601.290	2658.552
C			204.976	183.114	172.836	167.617	255.725
Critical Temperature	T_c	K	588.1	611.3	632.3	652.3	688
Critical Pressure	P_c	atm	38.490	34.049	30.496	27.466	22.778
Critical Volume	V_c	cm^3/mol	326	382	444	509	645
Normal Boiling Point	T_b	K	410.90	429.90	448.60	467.10	503.00
Liquid Molar Volume	V_L	cm^3/mol	108.500	125.200	141.500	157.700	192.800
Acentric Factor	w		0.575	0.559	0.562	0.570	0.607
Dipole Moment		D (Debye)	1.700	1.649	1.739	1.649	1.619
Heat of Vapourisation	H_v	cal/mol	10485	10865	11183	11447	11915

Antoine equation as $\log_{10}(\text{mmHg}) = A - (B/(T(^{\circ}\text{C}) + C))$

TABLE E- 12: N-ALKANE COMPONENT PARAMETERS USED FOR THE L/W THERMODYNAMIC CONSISTENCY TESTS [23].

<i>Parameters</i>	<i>Symbol</i>	<i>Units</i>	<i>Components</i>				
			<i>n-nonane</i>	<i>n-decane</i>	<i>n-undecane</i>	<i>n-dodecane</i>	<i>n-tetradecane</i>
A			7.141	7.143	7.152	7.184	6.257
B		mmHg and °C	1559.556	1631.047	1694.395	1772.573	1929.961
C			215.025	207.968	200.346	195.283	186.791
Critical Temperature	T_c	K	594.6	617.7	639	658	693
Critical Pressure	P_c	atm	22.601	20.824	19.245	17.962	15.495
Critical Volume	V_c	cm ³ /mol	551	617	685	755	894
Normal Boiling Point	T_b	K	423.97	447.31	469.08	489.47	526.00
Liquid Molar Volume	V_L	cm ³ /mol	178.890	195.827	212.243	228.605	260.166
Acentric Factor	w		0.443	0.492	0.530	0.576	0.643
Dipole Moment		D (Debye)	0.000	0.000	0.000	0.000	0.000
Heat of Vapourisation	H_v	cal/mol	8904	9424	10013	10546	11509

Antoine equation as $\log_{10}(\text{mmHg}) = A - (B/(T(^{\circ}\text{C}) + C))$

TABLE E- 13: LPVLE REPEATABILITY AND THERMODYNAMIC CONSISTENCY TEST RESULTS FOR THE ETHANOL (1) +
2,2,4-TRIMETHYLPENTANE (2) BINARY SYSTEM AT $P = 101.3$ kPa.

$T(K)$	x_1	y_1	γ_1	γ_2	L	W
351.44	1.000	1.000				
351.17	0.996	0.995	1.007	4.584	0.191	0.163
349.29	0.966	0.903	1.013	10.228	1.538	1.534
350.03	0.984	0.922	0.987	17.013	0.934	0.917
350.63	0.982	0.967	1.014	6.128	0.670	0.652
349.17	0.966	0.841	0.949	16.742	1.599	1.597
348.16	0.957	0.826	0.978	15.037	2.200	2.208
346.77	0.935	0.782	1.001	13.086	3.120	3.150
345.54	0.864	0.730	1.062	8.097	4.387	4.466
344.84	0.674	0.682	1.308	4.075	5.829	5.988
344.53	0.591	0.661	1.465	3.497	6.088	6.267
344.40	0.494	0.653	1.738	2.911	6.026	6.215
344.37	0.419	0.620	1.951	2.773	5.741	5.927
344.58	0.618	0.641	1.355	3.962	6.042	6.216
344.48	0.564	0.635	1.477	3.538	6.105	6.289
344.42	0.532	0.627	1.552	3.372	6.102	6.289
344.33	0.462	0.624	1.785	2.967	5.947	6.136
344.35	0.353	0.612	2.284	2.549	5.318	5.494
344.49	0.255	0.594	3.056	2.302	4.362	4.510
344.73	0.251	0.594	3.082	2.266	4.288	4.433
346.37	0.184	0.575	3.807	2.054	3.269	3.377
355.43	0.038	0.393	8.890	1.811	0.635	0.651
372.26	0.000	0.000				

$u(T) \leq 0.2$ K, $u(x_1) = u(y_1) = 0.022$ g/g and $u(P) \leq 0.36$ kPa

TABLE E- 14: LPVLE REPEATABILITY AND THERMODYNAMIC CONSISTENCY TEST RESULTS FOR THE 2-BUTANONE (1) +
N-HEPTANE (2) BINARY SYSTEM AT $P = 101.3$ kPa.

$T(K)$	x_1	y_1	γ_1	γ_2	L	W
351.13	1.000	1.000				
349.86	0.966	0.925	0.973	3.929	0.633	0.540
348.93	0.910	0.872	1.001	2.647	1.616	1.380
348.36	0.852	0.828	1.033	2.210	2.329	1.964
348.04	0.781	0.812	1.117	1.646	2.896	2.401
348.17	0.764	0.813	1.138	1.515	2.929	2.411
348.12	0.725	0.775	1.146	1.558	3.117	2.545
348.42	0.625	0.715	1.215	1.435	3.285	2.624
349.47	0.421	0.641	1.567	1.128	2.907	2.248
349.47	0.410	0.625	1.568	1.156	2.877	2.224
350.44	0.346	0.566	1.635	1.167	2.488	1.893
350.46	0.316	0.531	1.681	1.204	2.366	1.798
351.28	0.289	0.550	1.856	1.083	2.124	1.597
352.53	0.249	0.529	1.994	1.030	1.773	1.310
354.18	0.208	0.464	1.993	1.055	1.395	1.005
356.58	0.140	0.391	2.335	1.022	0.865	0.599
363.19	0.056	0.187	2.329	1.018	0.206	0.114
368.90	0.000	0.000				

$u(T) \leq 0.2$ K, $u(x_1) = u(y_1) = 0.022$ g/g and $u(P) \leq 0.36$ kPa

TABLE E- 15: LPVLE EXPERIMENTAL AND THERMODYNAMIC CONSISTENCY TEST RESULTS FOR THE 1-PENTANOL (1) +
N-NONANE (2) BINARY SYSTEM AT $P = 40$ kPa.

$T(K)$	x_1	y_1	γ_1	γ_2	L	W	$T(K)$	x_1	y_1	γ_1	γ_2	L	W
469.23	1.000	1.000					470.80	0.439	0.609	2.116	11.611	9.800	9.381
469.01	0.992	0.989	1.602	24.724	16.938	18.540	471.26	0.385	0.581	2.271	11.191	8.747	9.219
468.92	0.980	0.973	1.600	23.770	16.909	17.486	471.77	0.358	0.569	2.360	10.857	8.159	7.389
468.77	0.951	0.940	1.600	21.541	16.773	15.989	472.08	0.321	0.549	2.515	10.648	7.405	7.040
468.72	0.930	0.920	1.604	20.185	16.640	16.625	472.62	0.293	0.531	2.619	10.479	6.775	6.774
468.65	0.904	0.897	1.611	19.119	16.451	17.296	473.61	0.260	0.514	2.783	10.061	5.987	6.343
468.66	0.836	0.841	1.633	17.249	15.826	14.583	473.61	0.256	0.516	2.830	9.981	5.906	6.295
468.56	0.828	0.838	1.648	16.779	15.793	14.834	474.09	0.231	0.499	2.991	9.858	5.342	5.819
468.60	0.801	0.822	1.668	15.966	15.494	15.373	474.47	0.225	0.489	2.982	9.860	5.178	5.701
468.74	0.772	0.800	1.679	15.536	15.130	15.890	474.12	0.218	0.487	3.099	9.905	5.074	4.666
468.73	0.767	0.803	1.695	15.019	15.072	15.951	474.88	0.209	0.484	3.137	9.639	4.806	4.489
468.88	0.747	0.782	1.689	15.206	14.794	16.245	475.67	0.173	0.449	3.447	9.614	3.986	3.990
468.90	0.745	0.784	1.697	14.931	14.757	16.239	476.52	0.146	0.417	3.702	9.612	3.350	3.519
468.69	0.731	0.774	1.717	14.931	14.674	14.716	477.70	0.111	0.367	4.155	9.695	2.529	2.548
468.92	0.691	0.750	1.750	14.241	14.101	13.834	478.64	0.0950	0.340	4.359	9.673	2.138	2.217
469.03	0.651	0.722	1.782	13.981	13.536	13.959	478.50	0.0860	0.330	4.727	9.754	1.952	2.059
469.40	0.615	0.703	1.816	13.397	12.923	14.185	479.47	0.0850	0.315	4.429	9.697	1.889	1.998
469.39	0.598	0.693	1.842	13.259	12.683	13.711	481.54	0.0560	0.245	4.960	9.770	1.206	1.321
469.17	0.597	0.690	1.850	13.439	12.733	13.488	483.34	0.0350	0.195	5.898	9.694	0.731	0.764
469.68	0.561	0.675	1.895	12.769	12.053	11.596	481.17	0.0610	0.274	5.116	9.540	1.321	1.310
469.91	0.517	0.648	1.962	12.461	11.306	11.780	485.76	0.0200	0.114	5.840	9.821	0.398	0.430
470.22	0.479	0.631	2.040	12.028	10.609	9.858	487.63	0.0090	0.0580	5.953	9.815	0.172	0.186
470.40	0.476	0.632	2.049	11.830	10.517	10.781	489.17	0.000	0.000				

$u(T) \leq 0.2$ K, $u(x_1) = u(y_1) = 0.022$ g/g and $u(P) \leq 0.36$ kPa

TABLE E- 16: LPVLE EXPERIMENTAL AND THERMODYNAMIC CONSISTENCY TEST RESULTS FOR THE 1-HEXANOL (1) +
N-DECANE (2) BINARY SYSTEM AT $P = 40$ kPa.

$T(K)$	x_1	y_1	γ_1	γ_2	L	W	$T(K)$	x_1	y_1	γ_1	γ_2	L	W
436.67	1.000	1.000					436.94	0.327	0.538	2.780	11.198	7.285	6.718
436.42	0.998	0.991	1.706	76.106	15.328	14.631	437.32	0.294	0.503	2.860	11.352	6.610	6.177
436.13	0.980	0.958	1.696	34.379	15.372	15.268	437.54	0.275	0.508	3.069	10.859	6.214	6.005
436.07	0.965	0.933	1.679	32.521	15.303	15.643	437.94	0.246	0.487	3.248	10.756	5.595	5.679
435.82	0.929	0.889	1.675	26.506	15.182	14.264	438.49	0.226	0.486	3.454	10.336	5.129	5.370
435.62	0.902	0.856	1.673	24.954	15.079	14.985	438.25	0.222	0.473	3.458	10.607	5.077	5.352
435.38	0.875	0.827	1.677	23.866	14.966	15.629	439.11	0.183	0.454	3.909	10.198	4.191	3.866
435.26	0.848	0.796	1.673	23.129	14.790	14.069	439.64	0.152	0.429	4.384	10.107	3.499	3.339
435.14	0.824	0.768	1.669	22.724	14.626	14.584	440.57	0.119	0.388	4.928	10.127	2.733	2.762
435.08	0.801	0.753	1.683	21.571	14.426	14.975	441.75	0.0920	0.363	5.728	9.863	2.088	2.207
435.13	0.797	0.754	1.692	21.018	14.368	15.020	442.73	0.0740	0.318	6.093	10.048	1.661	1.811
435.16	0.752	0.722	1.717	19.361	13.901	13.773	443.33	0.0660	0.302	6.369	10.011	1.468	1.359
435.13	0.681	0.669	1.761	17.879	13.111	13.951	443.90	0.0620	0.295	6.479	9.900	1.364	1.240
435.18	0.666	0.664	1.782	17.342	12.910	13.067	445.45	0.0370	0.241	8.539	9.915	0.797	0.743
435.22	0.651	0.662	1.814	16.708	12.708	13.183	446.86	0.0270	0.210	9.707	9.794	0.566	0.537
435.29	0.611	0.644	1.876	15.752	12.168	13.147	447.76	0.0210	0.190	10.755	9.718	0.432	0.415
435.59	0.507	0.590	2.052	14.168	10.601	10.983	449.91	0.0110	0.115	12.096	9.869	0.216	0.212
435.79	0.484	0.588	2.130	13.504	10.194	10.946	452.99	0.00300	0.0320	10.015	9.798	0.055	0.054
436.07	0.436	0.552	2.199	13.320	9.358	8.610	453.92	0.000	0.000				
436.47	0.361	0.532	2.531	12.113	7.987	8.358							

$u(T) \leq 0.2$ K, $u(x_1) = u(y_1) = 0.022$ g/g and $u(P) \leq 0.36$ kPa

TABLE E- 17: LPVLE EXPERIMENTAL AND THERMODYNAMIC CONSISTENCY TEST RESULTS FOR THE 1-HEPTANOL (1) +
N-UNDECANE (2) BINARY SYSTEM AT $P = 40$ kPa.

$T(K)$	x_1	y_1	γ_1	γ_2	L	W	$T(K)$	x_1	y_1	γ_1	γ_2	L	W
419.40	1.000	1.000					417.52	0.406	0.523	3.092	26.982	8.527	8.690
419.26	0.986	0.974	2.208	60.169	14.573	14.272	418.12	0.339	0.480	3.314	25.867	7.261	6.605
419.03	0.971	0.943	2.194	61.262	14.586	14.642	418.26	0.317	0.489	3.593	24.471	6.846	6.311
418.52	0.945	0.901	2.198	57.821	14.638	15.256	418.66	0.289	0.476	3.772	23.759	6.273	6.058
418.24	0.922	0.867	2.193	55.675	14.582	13.370	419.09	0.264	0.456	3.888	23.461	5.748	5.784
417.86	0.896	0.833	2.201	53.337	14.533	13.899	419.47	0.252	0.443	3.900	23.296	5.474	5.618
417.75	0.872	0.805	2.195	50.830	14.367	14.261	419.98	0.240	0.421	3.811	23.398	5.184	5.429
417.47	0.834	0.765	2.204	47.856	14.128	12.725	420.00	0.229	0.433	4.101	22.582	4.973	5.293
417.12	0.798	0.729	2.227	45.926	13.907	13.283	420.10	0.217	0.418	4.165	22.740	4.733	5.130
416.95	0.782	0.718	2.254	44.536	13.805	13.509	420.59	0.193	0.397	4.356	22.461	4.216	3.867
416.87	0.755	0.704	2.301	41.467	13.545	13.805	421.15	0.177	0.382	4.480	22.112	3.851	3.555
416.84	0.740	0.682	2.276	42.127	13.383	13.918	422.23	0.147	0.348	4.691	21.668	3.171	3.093
416.92	0.727	0.681	2.306	40.100	13.205	13.992	423.30	0.123	0.310	4.798	21.455	2.624	2.678
416.86	0.704	0.670	2.347	38.378	12.957	14.155	423.33	0.122	0.312	4.853	21.359	2.602	2.660
416.90	0.702	0.669	2.346	38.220	12.918	14.150	423.42	0.118	0.317	5.111	21.011	2.518	2.595
416.79	0.678	0.653	2.385	37.126	12.666	13.961	424.02	0.105	0.301	5.286	20.776	2.225	2.347
416.84	0.658	0.646	2.425	35.630	12.399	13.362	424.99	0.0890	0.277	5.558	20.388	1.861	2.027
416.85	0.641	0.637	2.455	34.746	12.177	11.174	425.97	0.0740	0.254	5.868	20.009	1.524	1.673
416.80	0.634	0.626	2.443	35.226	12.101	11.226	426.63	0.0660	0.240	6.116	19.740	1.345	1.239
416.72	0.602	0.622	2.561	32.910	11.695	11.395	428.56	0.0530	0.179	5.263	19.680	1.038	0.962
416.73	0.576	0.594	2.559	33.093	11.334	11.482	431.70	0.0230	0.0830	4.994	19.159	0.423	0.424
416.78	0.558	0.585	2.593	32.446	11.061	11.486	433.25	0.0130	0.0460	4.559	18.739	0.231	0.238
416.78	0.544	0.591	2.691	30.926	10.860	11.501	434.50	0.000	0.000				

$u(T) \leq 0.2$ K, $u(x_1) = u(y_1) = 0.022$ g/g and $u(P) \leq 0.36$ kPa

TABLE E- 18: LPVLE EXPERIMENTAL AND THERMODYNAMIC CONSISTENCY TEST RESULTS FOR THE 1-OCTANOL (1) +
N-DODECANE (2) BINARY SYSTEM AT $P = 40$ kPa.

$T(K)$	x_l	y_l	γ_l	γ_2	L	W	$T(K)$	x_l	y_l	γ_l	γ_2	L	W
402.36	1.000	1.000					398.49	0.425	0.484	2.313	14.619	8.636	7.868
402.07	0.992	0.975	1.763	45.310	13.861	14.394	398.59	0.415	0.478	2.332	14.487	8.449	7.837
401.87	0.980	0.947	1.745	38.670	13.877	14.730	398.65	0.388	0.459	2.390	14.323	7.981	7.566
401.66	0.968	0.919	1.727	37.188	13.894	15.060	398.67	0.381	0.468	2.480	13.916	7.857	7.540
401.43	0.956	0.895	1.716	35.321	13.916	12.999	398.79	0.364	0.450	2.485	13.946	7.541	7.447
401.16	0.944	0.871	1.707	34.395	13.952	13.366	398.81	0.360	0.456	2.545	13.699	7.467	7.424
400.83	0.929	0.844	1.701	33.161	13.987	13.804	398.86	0.351	0.445	2.543	13.759	7.301	7.366
400.34	0.893	0.786	1.676	30.670	13.904	12.853	398.92	0.340	0.446	2.625	13.478	7.096	7.287
400.21	0.870	0.766	1.684	27.719	13.754	12.865	398.87	0.330	0.442	2.685	13.395	6.926	7.225
399.84	0.861	0.745	1.676	28.597	13.830	13.176	399.07	0.321	0.446	2.766	13.036	6.731	7.122
399.47	0.834	0.704	1.657	28.134	13.723	13.740	399.19	0.300	0.437	2.888	12.799	6.331	6.915
399.45	0.826	0.701	1.667	27.131	13.650	13.858	399.25	0.283	0.425	2.971	12.736	6.009	5.454
399.38	0.817	0.687	1.655	27.066	13.586	14.006	399.64	0.252	0.418	3.238	12.198	5.375	5.031
399.23	0.795	0.664	1.653	26.064	13.416	14.335	400.04	0.224	0.397	3.412	12.021	4.793	4.710
399.12	0.782	0.654	1.661	25.331	13.319	14.521	400.78	0.184	0.373	3.804	11.600	3.940	4.138
399.00	0.761	0.643	1.686	23.934	13.132	14.394	402.73	0.126	0.321	4.472	11.002	2.647	2.423
398.84	0.738	0.625	1.699	23.055	12.928	12.812	403.95	0.0930	0.283	5.152	10.755	1.928	1.880
398.75	0.717	0.609	1.709	22.321	12.712	11.616	405.92	0.0690	0.233	5.313	10.527	1.379	1.406
398.67	0.704	0.621	1.780	20.741	12.583	11.782	408.68	0.0360	0.152	6.085	10.297	0.682	0.743
398.63	0.698	0.594	1.720	21.805	12.524	11.856	409.70	0.0250	0.120	6.779	10.229	0.464	0.505
398.54	0.674	0.582	1.751	20.858	12.254	12.101	410.66	0.0170	0.0930	7.390	10.150	0.309	0.333
398.38	0.654	0.576	1.796	20.041	12.049	12.301	411.62	0.00900	0.0670	9.475	10.060	0.160	0.149
398.50	0.460	0.492	2.172	15.320	9.203	9.909	414.18	0.000	0.000				

$u(T) \leq 0.2$ K, $u(x_l) = u(y_l) = 0.022$ g/g and $u(P) \leq 0.36$ kPa

TABLE E- 19: LPVLE EXPERIMENTAL AND THERMODYNAMIC CONSISTENCY TEST RESULTS FOR THE 1-DECANOL (1) +
N-TETRADECANE (2) BINARY SYSTEM AT $P = 40$ kPa.

$T(K)$	x_1	y_1	γ_1	γ_2	L	W	$T(K)$	x_1	y_1	γ_1	γ_2	L	W
384.45	1.000	1.000					378.09	0.530	0.478	221.911	1.746	6.702	6.115
384.09	0.985	0.952	162.944	4.247	13.103	13.172	378.09	0.459	0.450	241.719	1.595	5.496	5.345
383.61	0.970	0.907	162.352	4.109	13.032	12.632	377.93	0.401	0.429	266.797	1.503	4.608	4.998
383.50	0.970	0.907	163.555	4.094	13.085	12.688	377.98	0.372	0.419	279.981	1.456	4.157	4.370
382.89	0.942	0.851	164.082	3.460	12.807	12.030	378.18	0.316	0.399	309.609	1.374	3.319	3.576
382.36	0.922	0.800	162.929	3.503	12.645	13.115	378.32	0.278	0.385	335.681	1.328	2.789	3.037
381.87	0.901	0.763	164.035	3.310	12.437	11.346	378.78	0.243	0.379	368.560	1.256	4.718	4.481
381.04	0.857	0.701	166.892	2.975	11.904	12.563	378.49	0.247	0.375	364.739	1.285	4.844	4.662
380.69	0.850	0.690	169.392	2.972	11.910	12.362	379.16	0.190	0.351	425.418	1.212	3.540	3.763
380.66	0.841	0.672	166.917	2.978	11.740	11.922	379.59	0.159	0.334	470.990	1.180	2.872	2.784
380.37	0.828	0.667	171.537	2.814	11.595	11.383	379.95	0.155	0.331	465.778	1.167	2.765	2.649
380.27	0.822	0.655	170.763	2.828	11.515	11.130	379.76	0.154	0.329	473.574	1.175	2.760	2.632
380.09	0.805	0.643	173.212	2.681	11.239	10.347	380.17	0.137	0.324	510.519	1.144	2.331	2.156
379.57	0.766	0.619	181.040	2.433	10.662	9.875	380.46	0.133	0.308	490.275	1.155	2.304	2.103
379.20	0.727	0.578	182.562	2.333	10.022	10.722	381.03	0.109	0.292	547.996	1.127	1.335	1.455
378.81	0.691	0.552	187.973	2.222	9.460	9.180	382.71	0.0720	0.248	634.840	1.087	1.113	1.069
378.57	0.664	0.535	192.468	2.137	9.016	8.348	383.36	0.0670	0.234	618.288	1.077	1.010	0.949
378.64	0.649	0.528	193.518	2.071	8.708	7.984	383.85	0.0640	0.218	583.702	1.079	0.946	0.877
378.59	0.638	0.526	196.784	2.020	8.517	7.843	385.23	0.0430	0.180	665.210	1.057	0.810	0.750
378.44	0.614	0.513	201.369	1.956	8.114	8.694	385.89	0.0410	0.162	604.106	1.055	0.593	0.655
378.39	0.605	0.510	203.840	1.927	7.965	8.621	389.38	0.0150	0.0710	582.959	1.017	0.246	0.260
378.40	0.607	0.510	202.825	1.939	7.999	8.713	390.17	0.0110	0.0480	504.532	1.013	0.176	0.183
378.17	0.551	0.486	215.923	1.795	7.051	6.392	392.17	0.000	0.000				

$u(T) \leq 0.2$ K, $u(x_1) = u(y_1) = 0.022$ g/g and $u(P) \leq 0.36$ kPa

F. TERNARY PHASE DIAGRAMS (HPBDP)

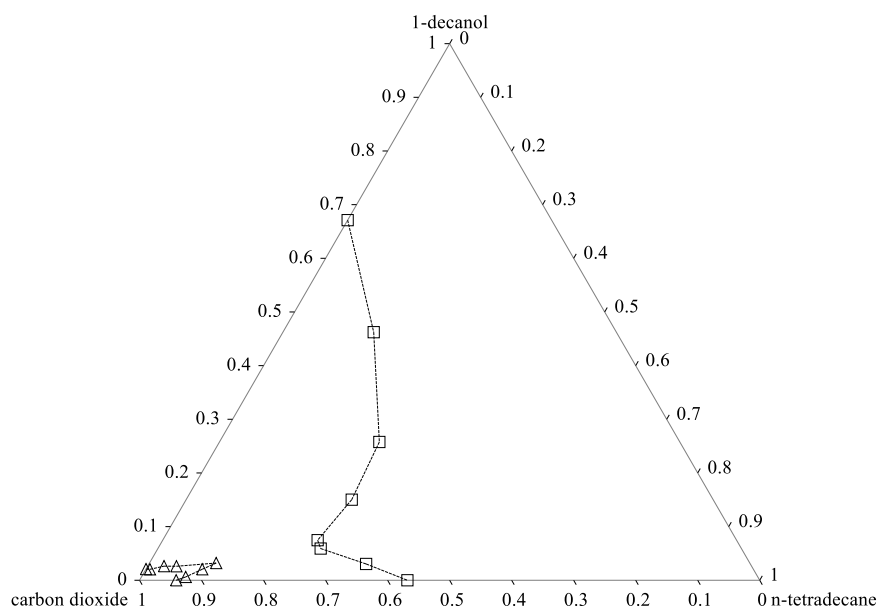


FIGURE F- 1: TERNARY PHASE DIAGRAM WITH SOLUBILITY CURVES CONSTRUCTED BY -- \triangle -- DEW-POINT AND -- \square -- BUBBLE-POINT EXPERIMENTAL DATA AT 318 K AND 10.0 MPa.

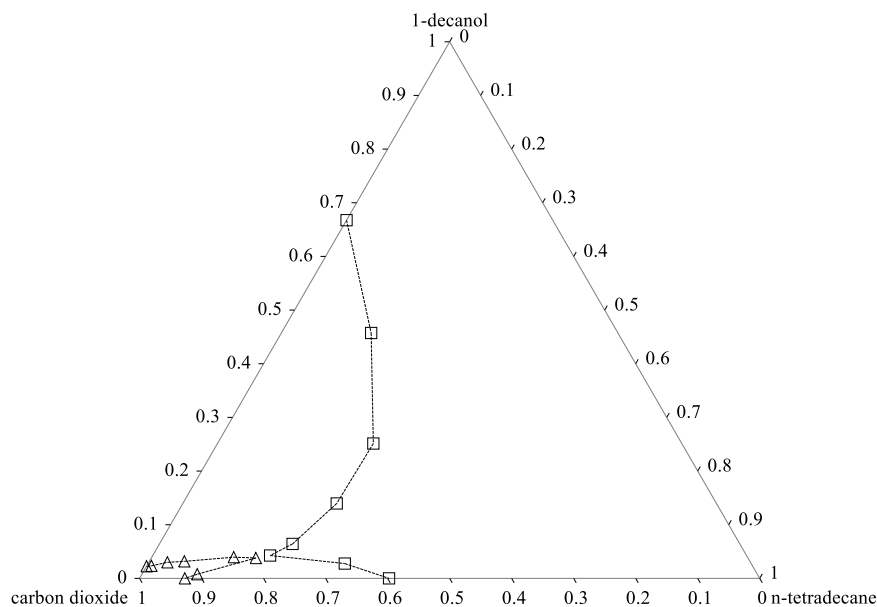


FIGURE F- 2: TERNARY PHASE DIAGRAM WITH SOLUBILITY CURVES CONSTRUCTED BY -- \triangle -- DEW-POINT AND -- \square -- BUBBLE-POINT EXPERIMENTAL DATA AT 318 K AND 10.2 MPa.

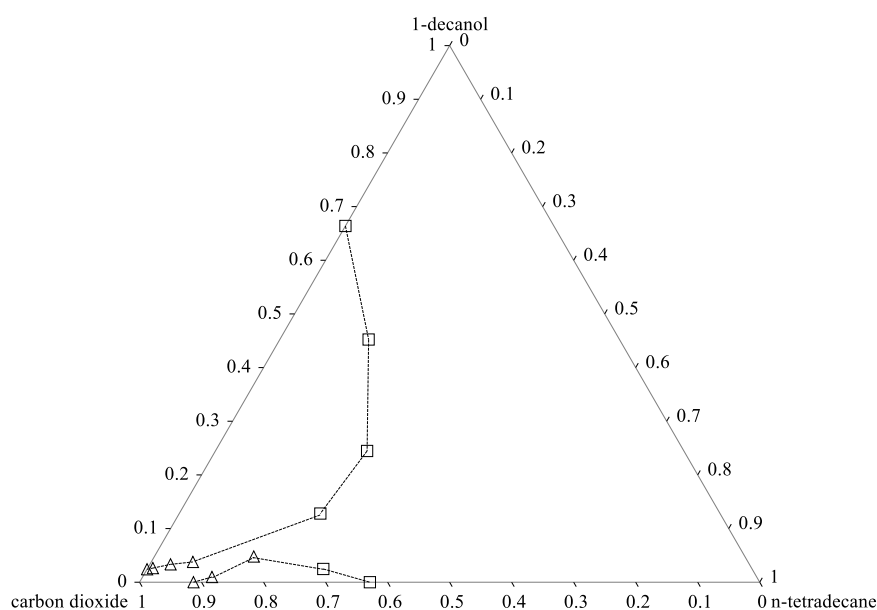


FIGURE F- 3: TERNARY PHASE DIAGRAM WITH SOLUBILITY CURVES CONSTRUCTED BY -- \triangle -- DEW-POINT AND -- \square -- BUBBLE-POINT EXPERIMENTAL DATA AT 318 K AND 10.4 MPa.

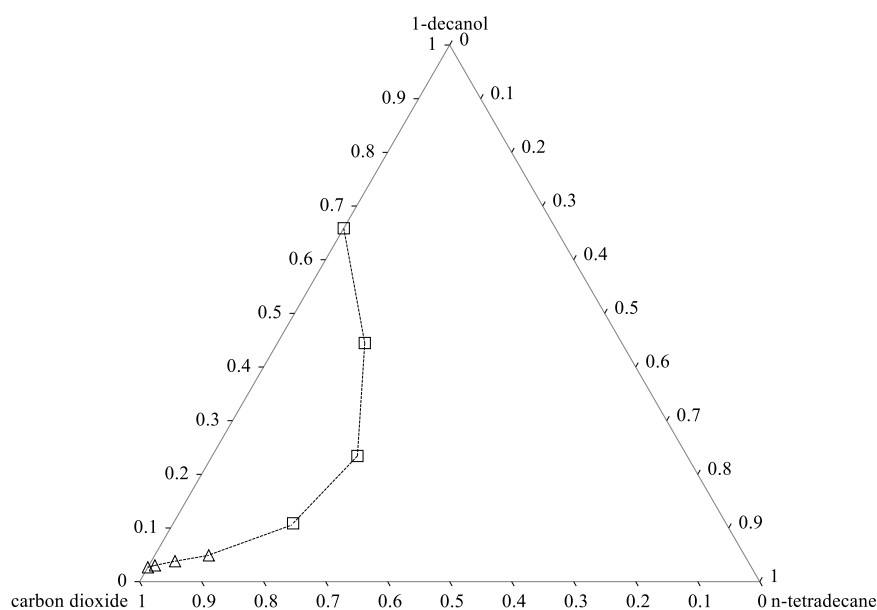


FIGURE F- 4: TERNARY PHASE DIAGRAM WITH SOLUBILITY CURVES CONSTRUCTED BY -- \triangle -- DEW-POINT AND -- \square -- BUBBLE-POINT EXPERIMENTAL DATA AT 318 K AND 10.7 MPa.

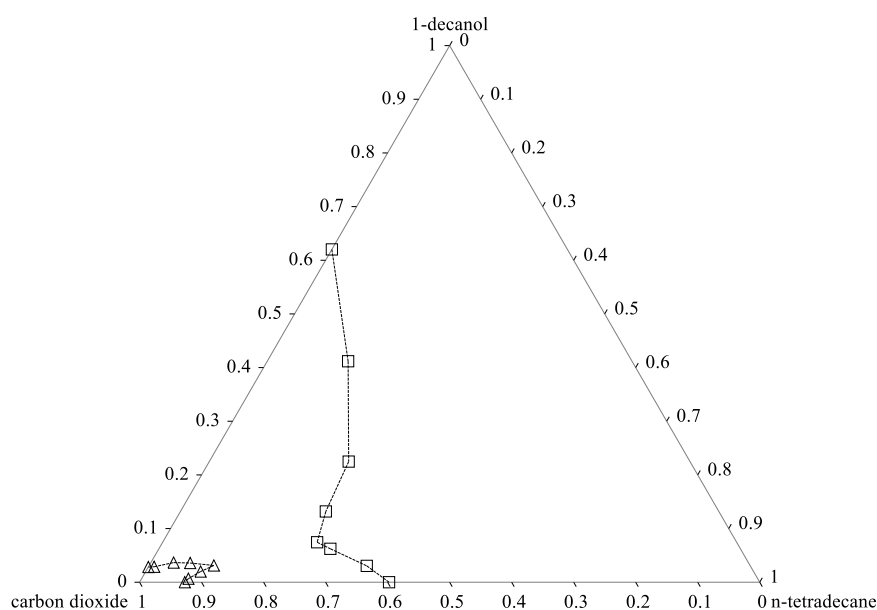


FIGURE F- 5: TERNARY PHASE DIAGRAM WITH SOLUBILITY CURVES CONSTRUCTED BY -- \triangle -- DEW-POINT AND -- \square -- BUBBLE-POINT EXPERIMENTAL DATA AT 338 K AND 14.0 MPa.

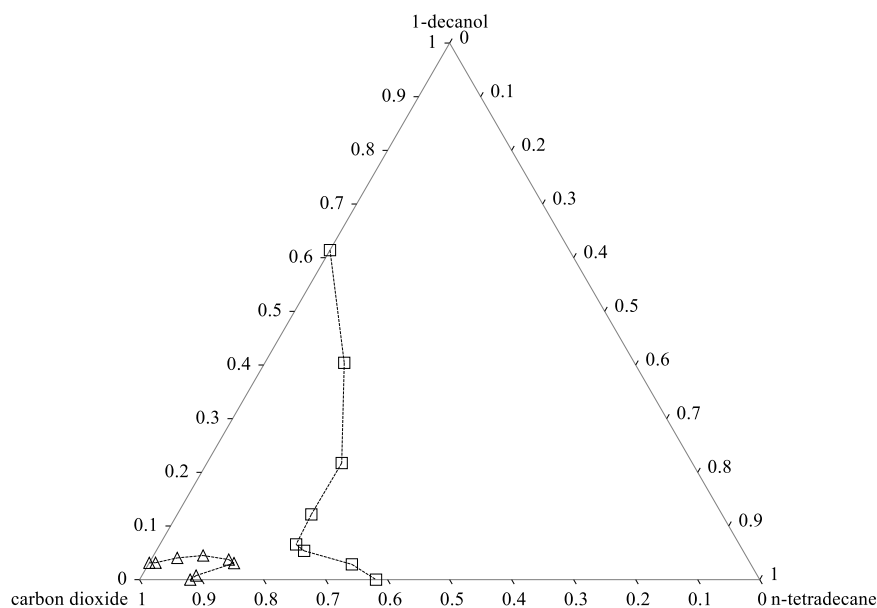


FIGURE F- 6: TERNARY PHASE DIAGRAM WITH SOLUBILITY CURVES CONSTRUCTED BY -- \triangle -- DEW-POINT AND -- \square -- BUBBLE-POINT EXPERIMENTAL DATA AT 338 K AND 14.2 MPa.

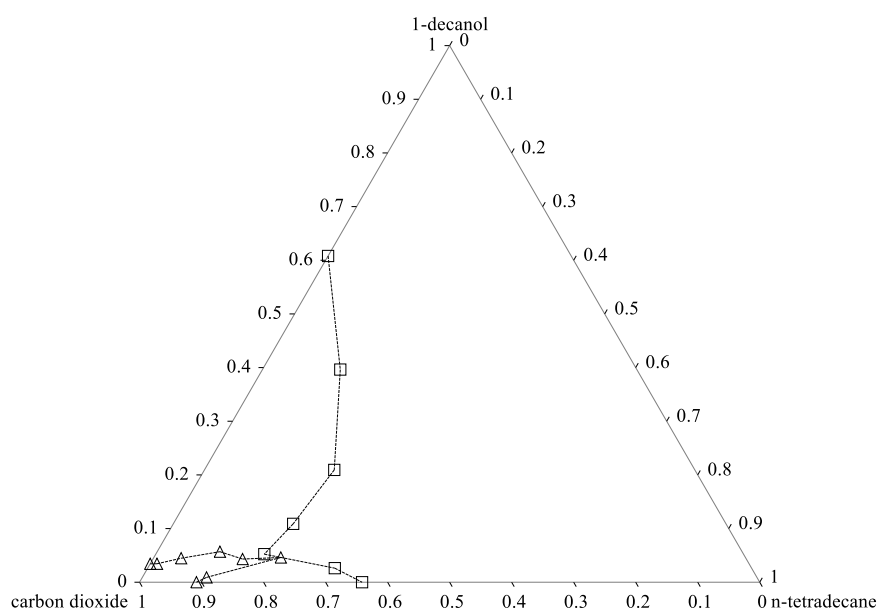


FIGURE F- 7: TERNARY PHASE DIAGRAM WITH SOLUBILITY CURVES CONSTRUCTED BY -- \triangle -- DEW-POINT AND -- \square -- BUBBLE-POINT EXPERIMENTAL DATA AT 338 K AND 14.4 MPa.

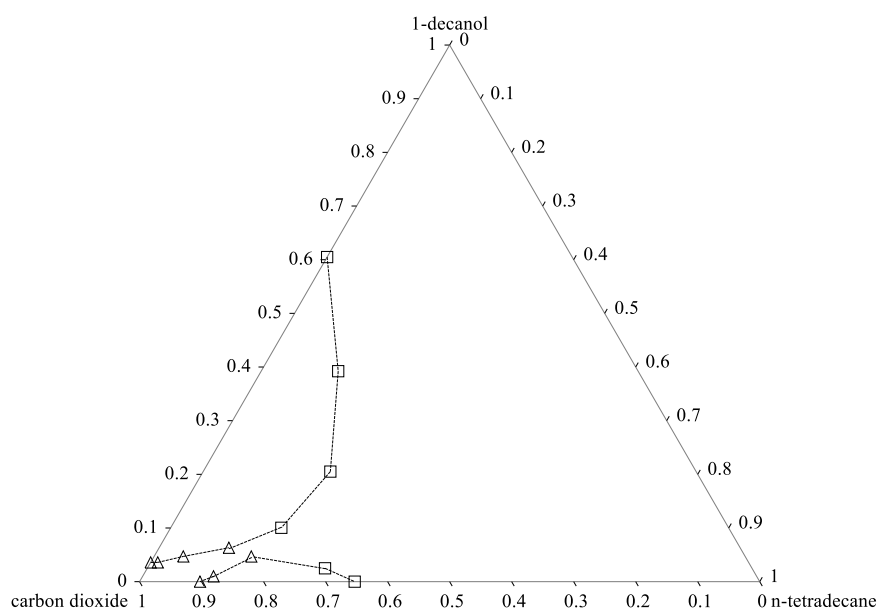


FIGURE F- 8: TERNARY PHASE DIAGRAM WITH SOLUBILITY CURVES CONSTRUCTED BY -- \triangle -- DEW-POINT AND -- \square -- BUBBLE-POINT EXPERIMENTAL DATA AT 338 K AND 14.5 MPa.

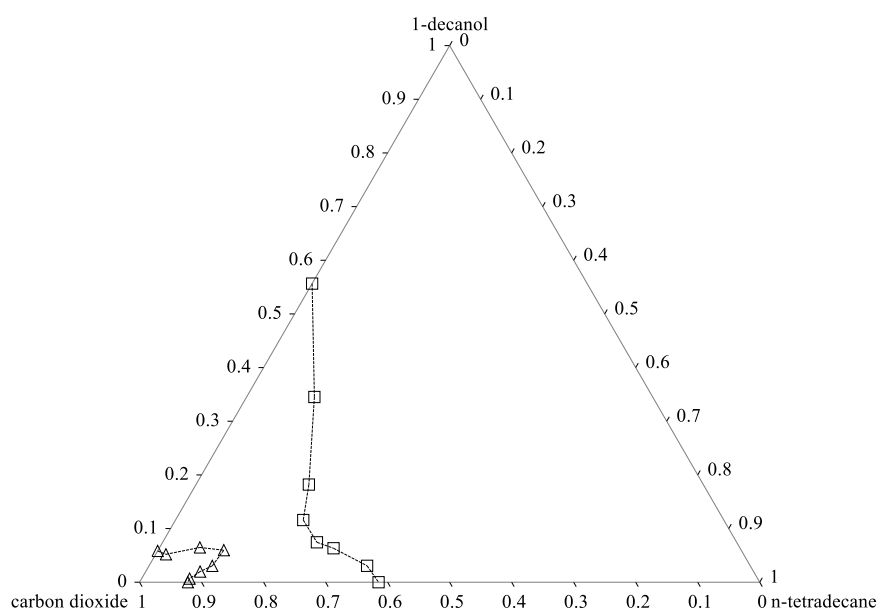


FIGURE F- 9: TERNARY PHASE DIAGRAM WITH SOLUBILITY CURVES CONSTRUCTED BY -- \triangle -- DEW-POINT AND -- \square -- BUBBLE-POINT EXPERIMENTAL DATA AT 358 K AND 18.0 MPa.

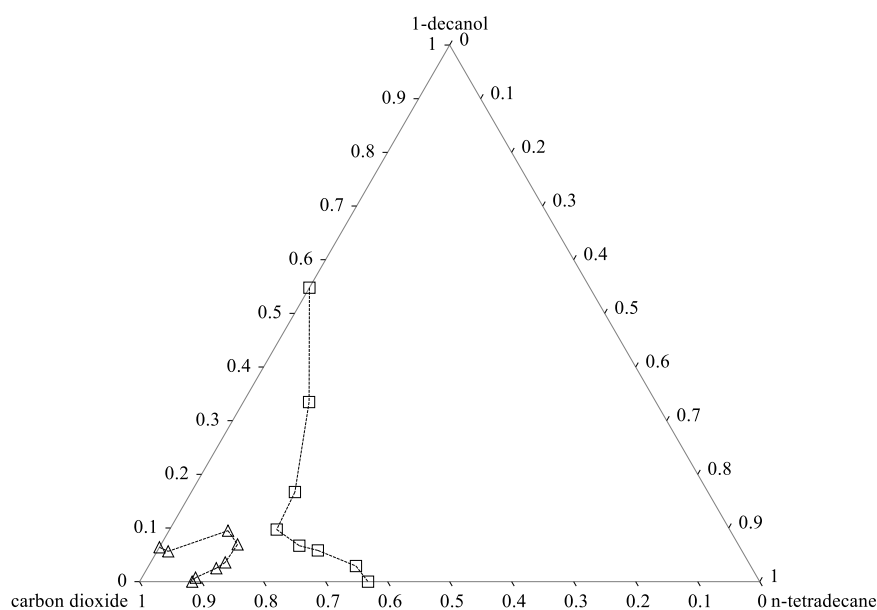


FIGURE F- 10: TERNARY PHASE DIAGRAM WITH SOLUBILITY CURVES CONSTRUCTED BY -- \triangle -- DEW-POINT AND -- \square -- BUBBLE-POINT EXPERIMENTAL DATA AT 358 K AND 18.2 MPa.

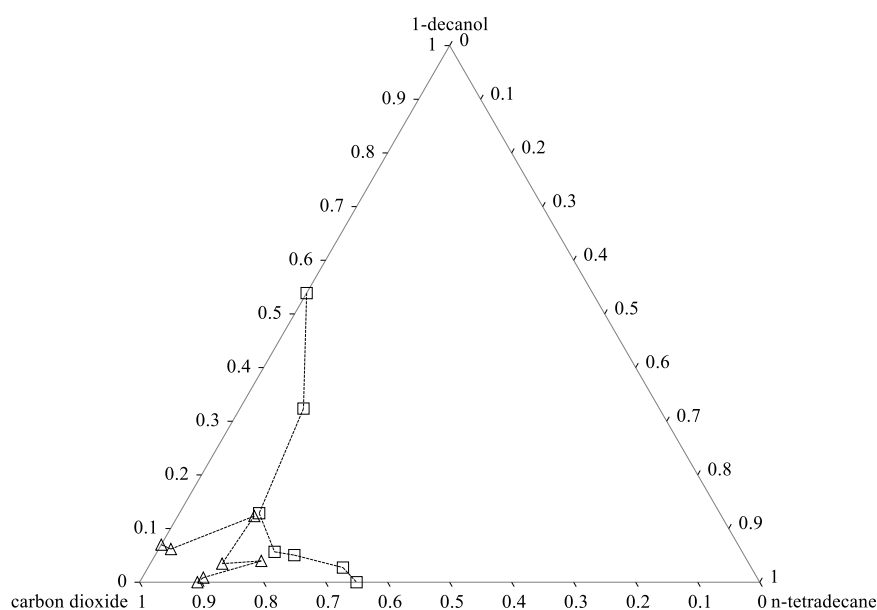


FIGURE F- 11: TERNARY PHASE DIAGRAM WITH SOLUBILITY CURVES CONSTRUCTED BY -- \triangle -- DEW-POINT AND -- \square -- BUBBLE-POINT EXPERIMENTAL DATA AT 358 K AND 18.4 MPa.

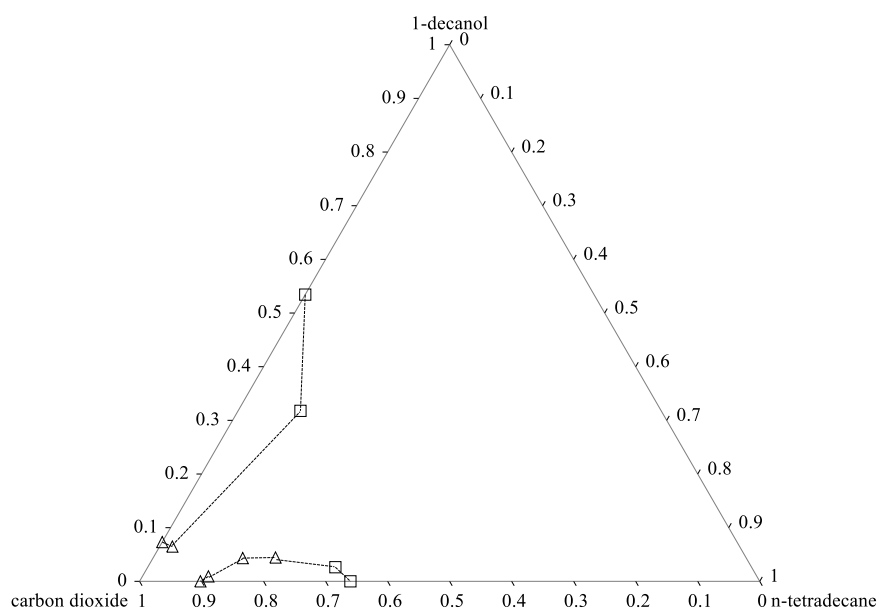


FIGURE F- 12: TERNARY PHASE DIAGRAM WITH SOLUBILITY CURVES CONSTRUCTED BY -- \triangle -- DEW-POINT AND -- \square -- BUBBLE-POINT EXPERIMENTAL DATA AT 358 K AND 18.5 MPa.

G. GAS CHROMATOGRAPHY CALIBRATION CURVES

TABLE G- 1: GAS CHROMATOGRAPHY METHOD PARAMETERS FOR ONLINE ANALYSIS, REDRAWN FROM [64].

<i>Gas chromatography unit</i>	<i>Operating factor</i>
Carrier gas	Helium
Columns	Flow = $3 \frac{mL}{min}$
FIDs	$T = 300\text{ }^{\circ}\text{C}$
Inlets	$T = 300\text{ }^{\circ}\text{C}$
Split ratio	5:1, 20:1 or 80:1
Thermal conductivity detector	$T = 250\text{ }^{\circ}\text{C}$
Oven	$T_1 = 100\text{ }^{\circ}\text{C}$ (2 min) $T_2 = 250\text{ }^{\circ}\text{C}$ (3 min)
Ramp	$30 \frac{^{\circ}\text{C}}{min}$ (5 min)
Valves	Switching at 4.5 min
Valve box	$T = 195\text{ }^{\circ}\text{C}$

G1. HPVLE

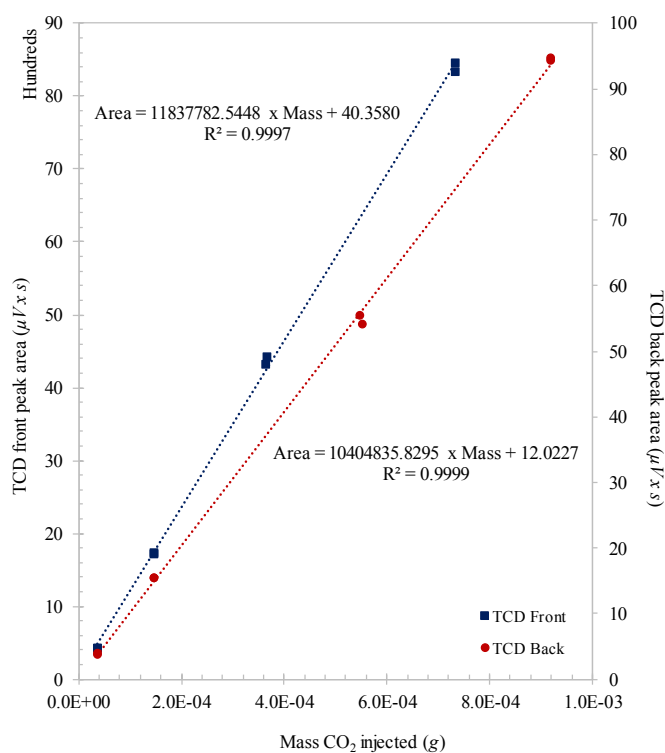


FIGURE G- 1: GAS CHROMATOGRAPHY CALIBRATION CURVE OF PURE CO₂ FOR THE HPVLE SAMPLE ANALYSIS.

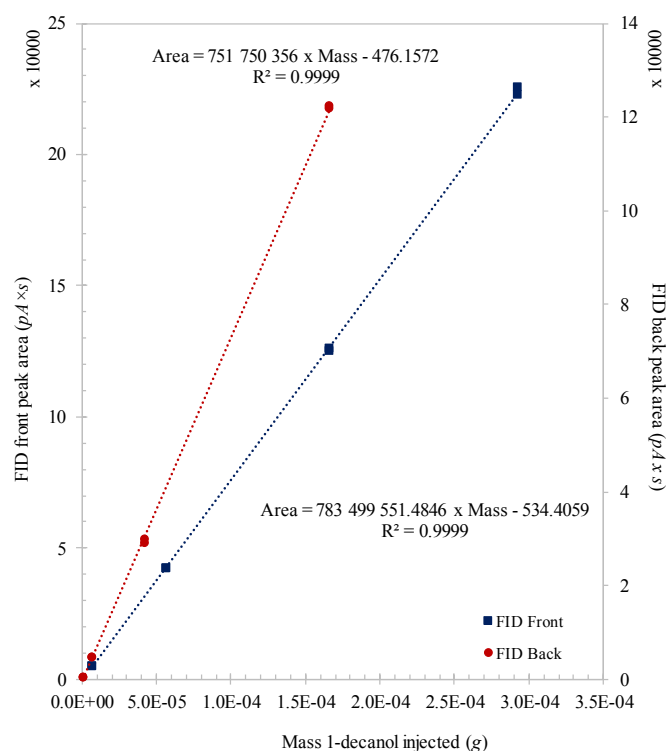


FIGURE G- 2: GAS CHROMATOGRAPHY CALIBRATION CURVE OF PURE 1-DECANOL FOR THE HPVLE SAMPLE ANALYSIS.

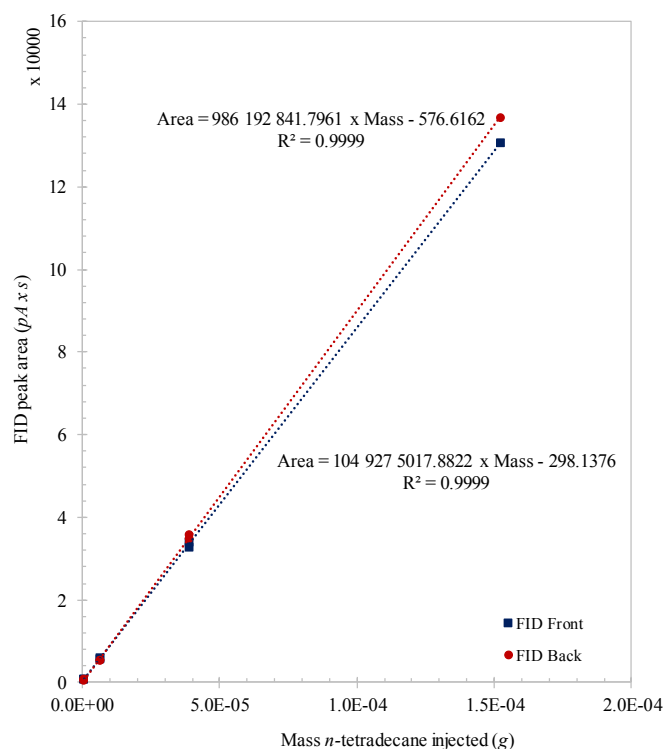


FIGURE G- 3: GAS CHROMATOGRAPHY CALIBRATION CURVE OF PURE *N*-TETRADECANE FOR THE HPVLE SAMPLE ANALYSIS.

G2. LPVLE

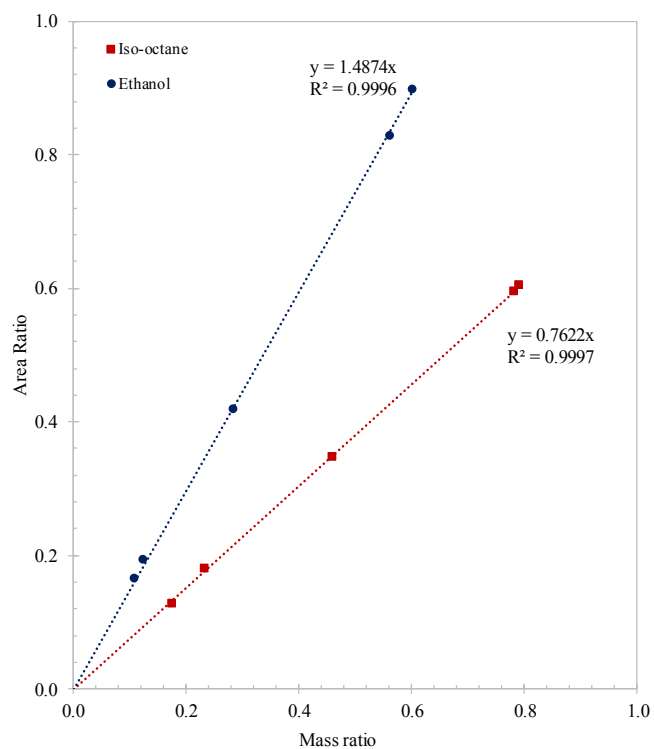


FIGURE G- 4: GAS CHROMATOGRAPHY CALIBRATION CURVES OF PURE 2,2,4-TRIMETHYLPENTANE (ISO-OCTANE) AND ETHANOL FOR THE LPVLE SAMPLE ANALYSIS.

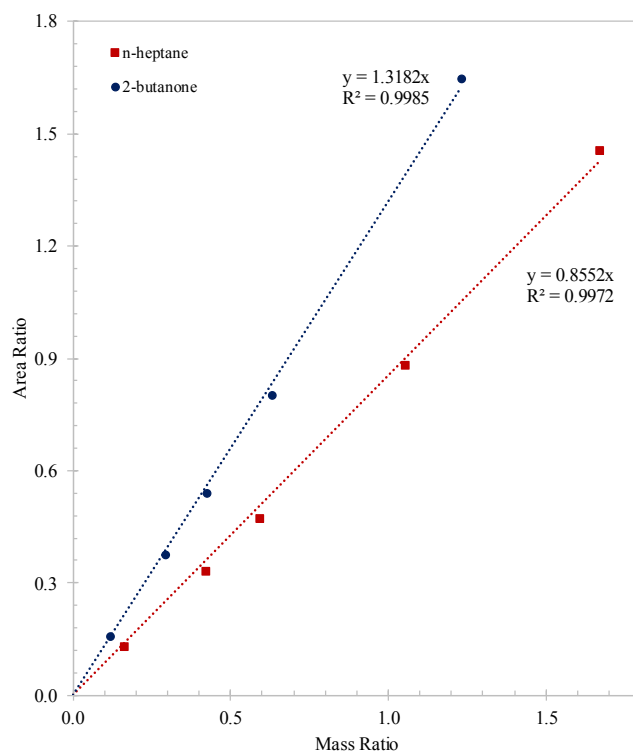


FIGURE G- 5: GAS CHROMATOGRAPHY CALIBRATION CURVES OF PURE *N*-HEPTANE AND 2-BUTANONE FOR THE LPVLE SAMPLE ANALYSIS.

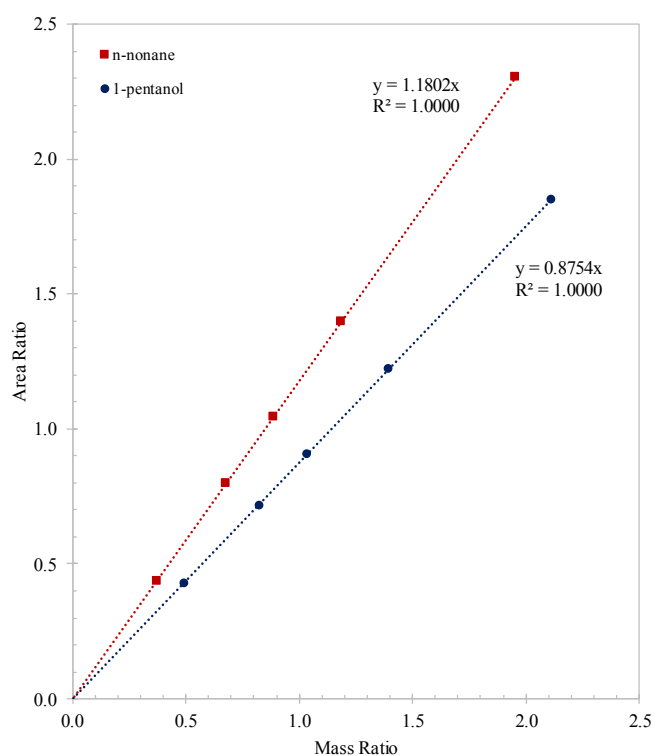


FIGURE G- 6: GAS CHROMATOGRAPHY CALIBRATION CURVES OF PURE *N*-NONANE AND 1-PENTANOL FOR THE LPVLE SAMPLE ANALYSIS.

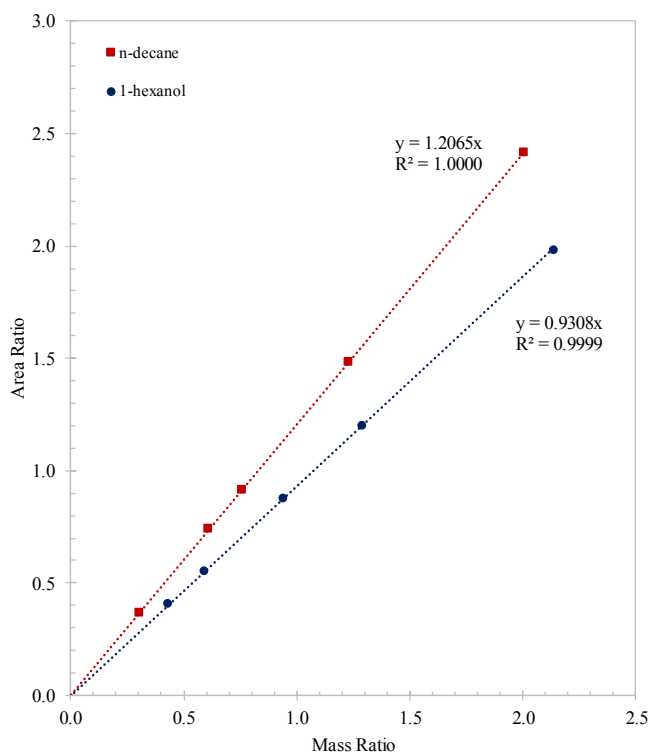


FIGURE G- 7: GAS CHROMATOGRAPHY CALIBRATION CURVES OF PURE *N*-DECANE AND 1-HEXANOL FOR THE LPVLE SAMPLE ANALYSIS.

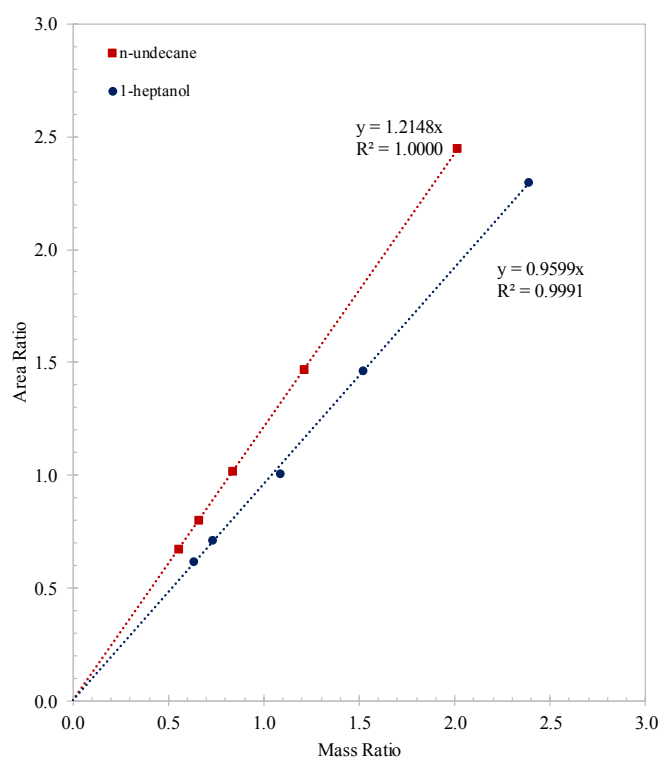


FIGURE G- 8: GAS CHROMATOGRAPHY CALIBRATION CURVES OF PURE *N*-UNDECANE AND 1-HEPTANOL FOR THE LPVLE SAMPLE ANALYSIS.

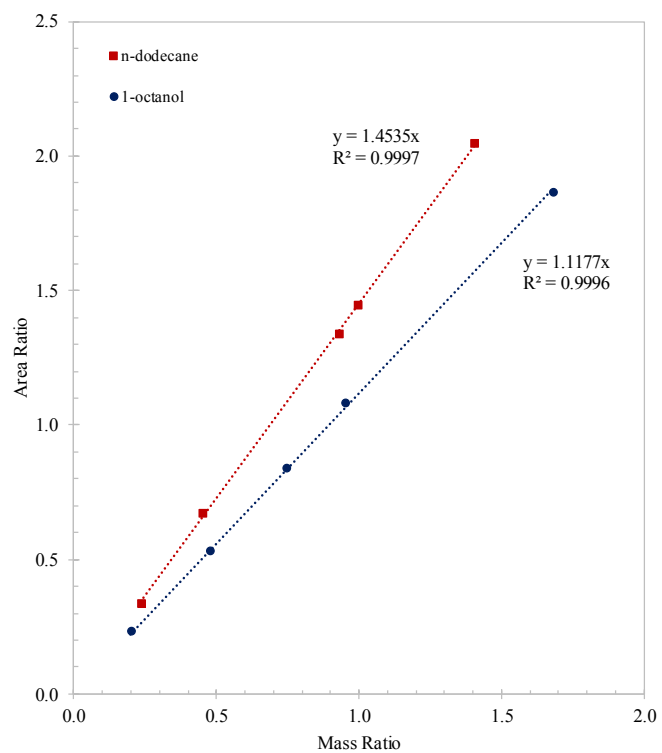


FIGURE G- 9: GAS CHROMATOGRAPHY CALIBRATION CURVES OF PURE *N*-DODECANE AND 1-OCTANOL FOR THE LPVLE SAMPLE ANALYSIS.

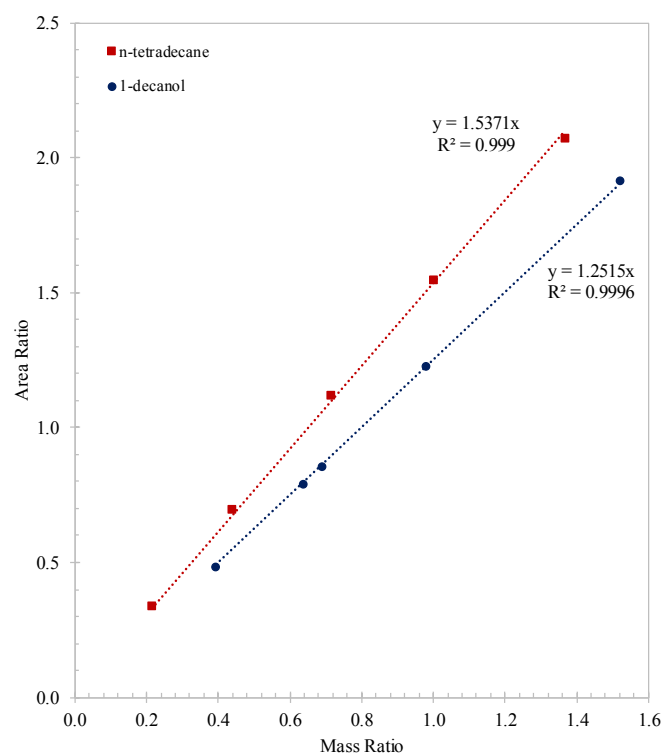


FIGURE G- 10: GAS CHROMATOGRAPHY CALIBRATION CURVES OF PURE *N*-TETRADECANE AND 1-DECANOL FOR THE LPVLE SAMPLE ANALYSIS.

H. SUPPLEMENTARY MODELLING RESULTS

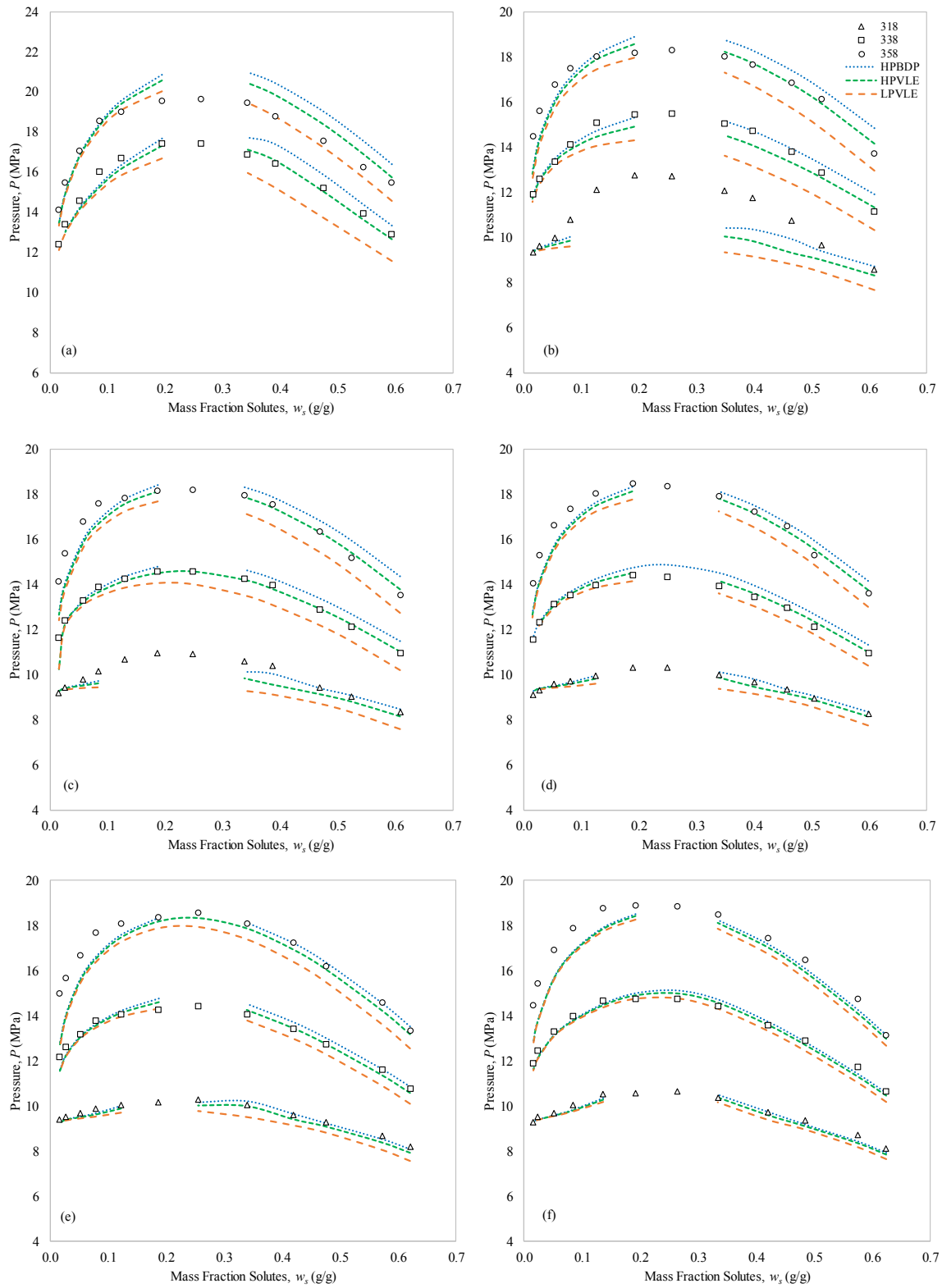


FIGURE H- 1: RK-ASPEN MODEL CORRELATIONS OF THE HPBDP DATA (WITH ALTERNATING SOLUTE + SOLUTE BIPs) AT

$T = 318 \text{ K}, 338 \text{ K}$ AND 358 K FOR (A) $w_c^{RED} = 0.2405 \text{ G/G}$; (B) $w_c^{RED} = 0.5000 \text{ G/G}$; (C) $w_c^{RED} = 0.6399 \text{ G/G}$;

(D) $w_c^{RED} = 0.7698 \text{ G/G}$; (E) $w_c^{RED} = 0.8162 \text{ G/G}$; AND (F) $w_c^{RED} = 0.9200$.

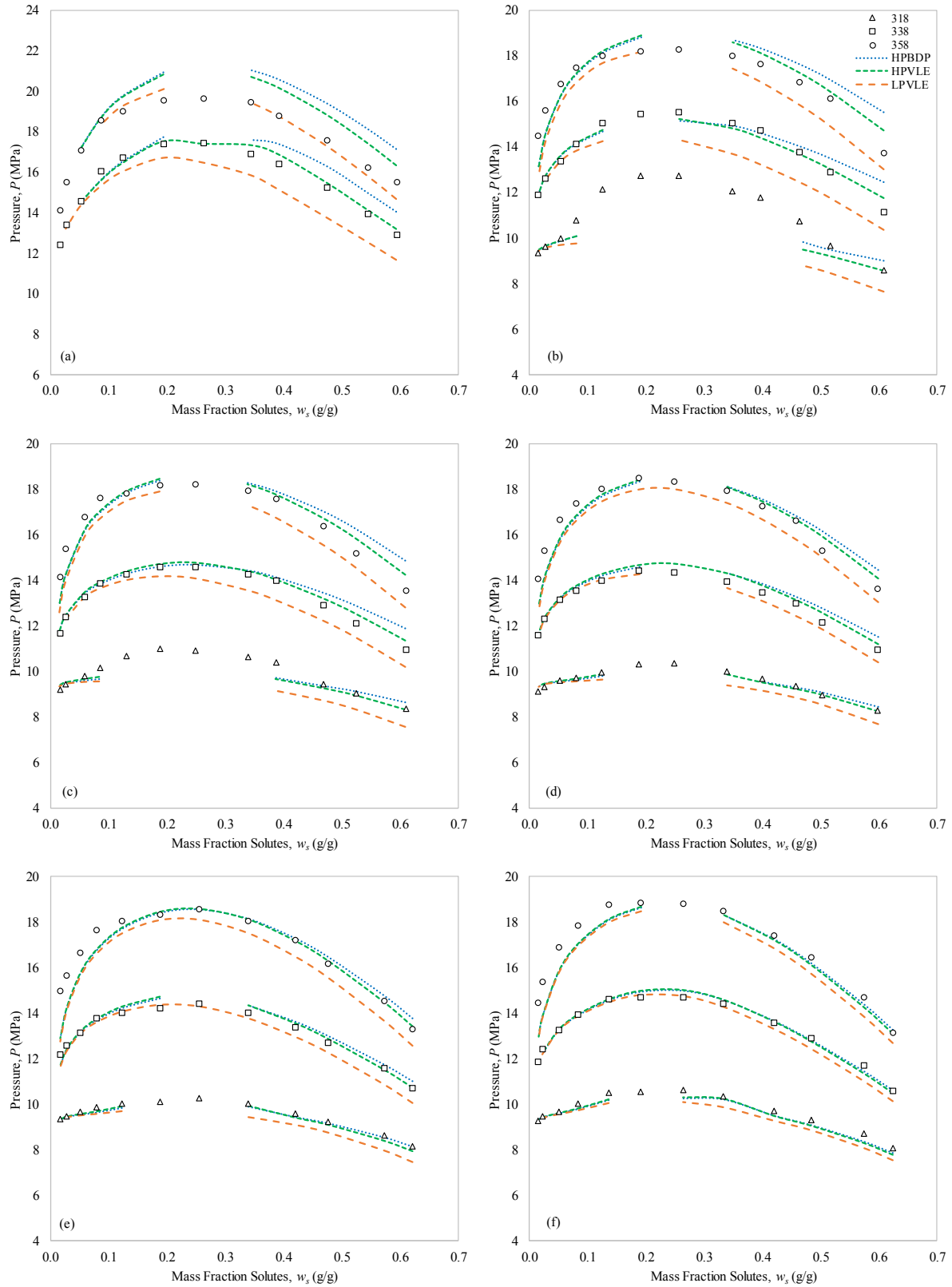


FIGURE H- 2: SR-POLAR MODEL CORRELATIONS OF THE HPBDP DATA (WITH ALTERNATING SOLUTE + SOLUTE BIPs) AT $T = 318$ K, 338 K AND 358 K FOR (A) $w_c^{RED} = 0.2405$ G/G; (B) $w_c^{RED} = 0.5000$ G/G; (C) $w_c^{RED} = 0.6399$ G/G; (D) $w_c^{RED} = 0.7698$ G/G; (E) $w_c^{RED} = 0.8162$ G/G; AND (F) $w_c^{RED} = 0.9200$.

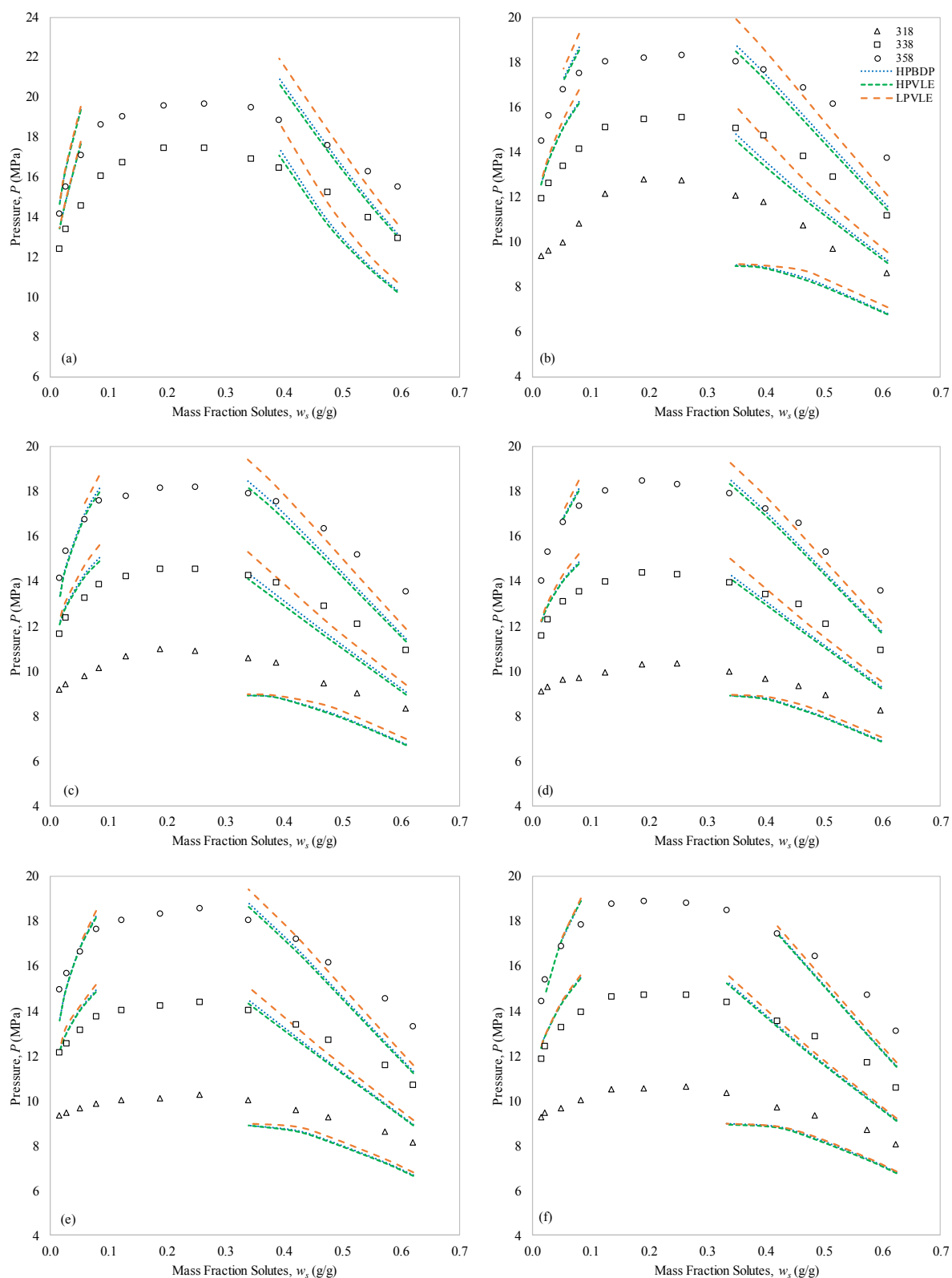


FIGURE H- 3: PC-SAFT MODEL CORRELATIONS OF THE HPBDP DATA (WITH ALTERNATING SOLUTE + SOLUTE BIPs) AT $T = 318$ K, 338 K AND 358 K FOR (A) $w_c^{RED} = 0.2405$ G/G; (B) $w_c^{RED} = 0.5000$ G/G; (C) $w_c^{RED} = 0.6399$ G/G; (D) $w_c^{RED} = 0.7698$ G/G; (E) $w_c^{RED} = 0.8162$ G/G; AND (F) $w_c^{RED} = 0.9200$.

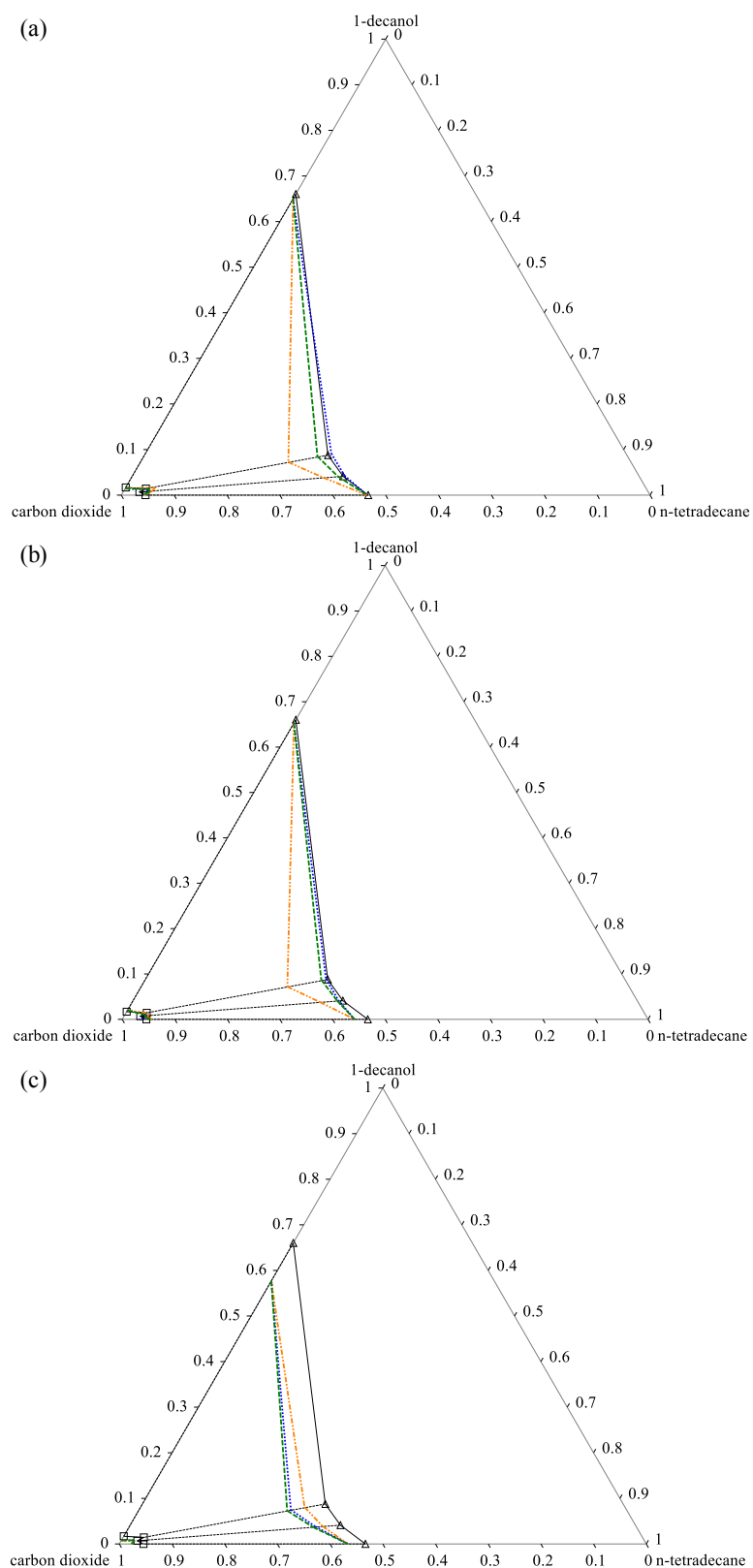


FIGURE H- 4: THERMODYNAMIC MODEL CORRELATIONS OF THE HPVLE DATA WITH: HPBDB BIPs; --- HPVLE BIPs; AND, -.- LPVLE SOLUTE + SOLUTE BIPs AT $T = 328$ K AND $P = 11.5$ MPa FOR (A) RK-ASPEN (B) SR-POLAR; AND (C) PC-SAFT.

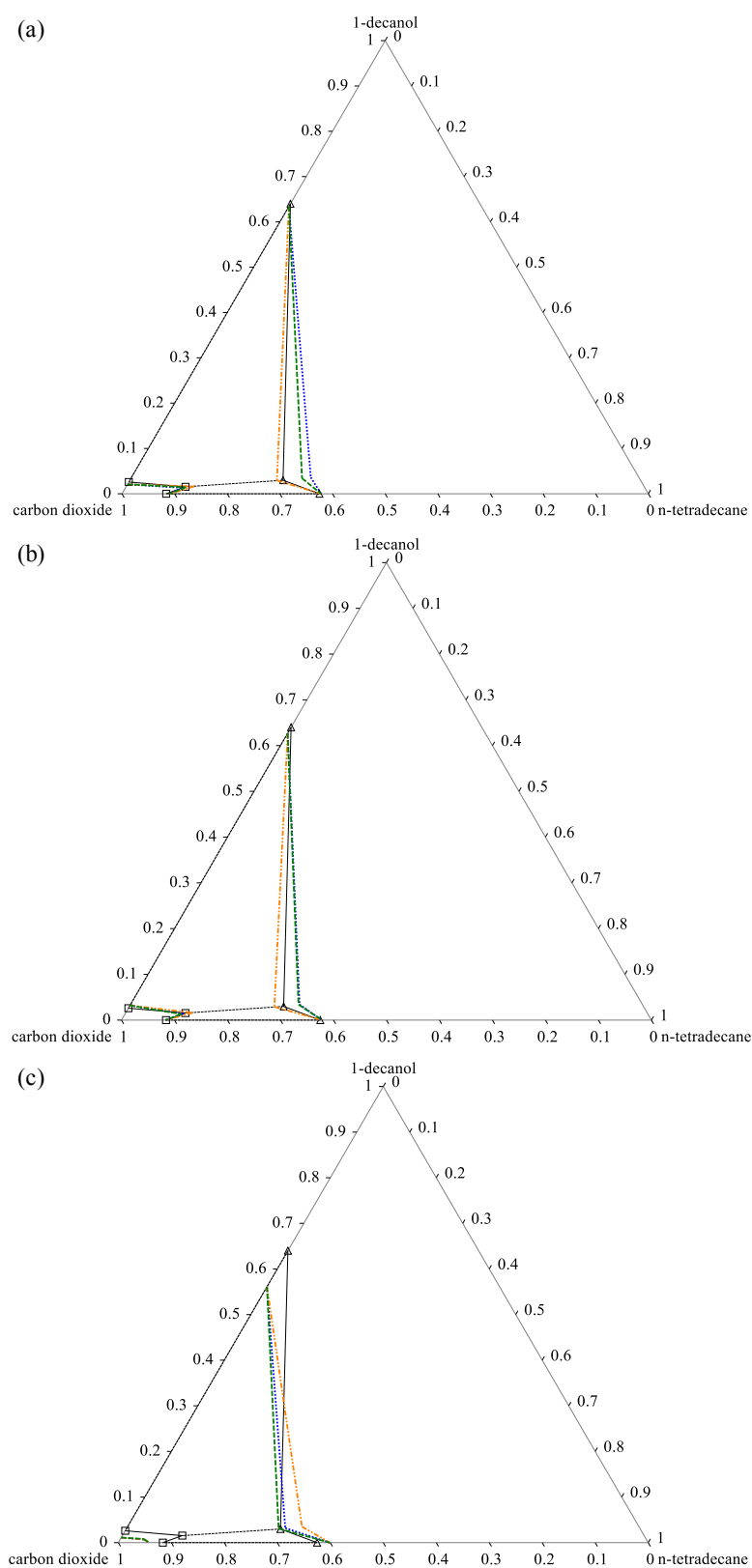


FIGURE H- 5: THERMODYNAMIC MODEL CORRELATIONS OF THE HPVLE DATA WITH: HPBDP BIPs; --- HPVLE BIPs; AND, -.- LPVLE SOLUTE + SOLUTE BIPs AT $T = 328$ K AND $P = 12.3$ MPa FOR (A) RK-ASPEN (B) SR-POLAR; AND (C) PC-SAFT.

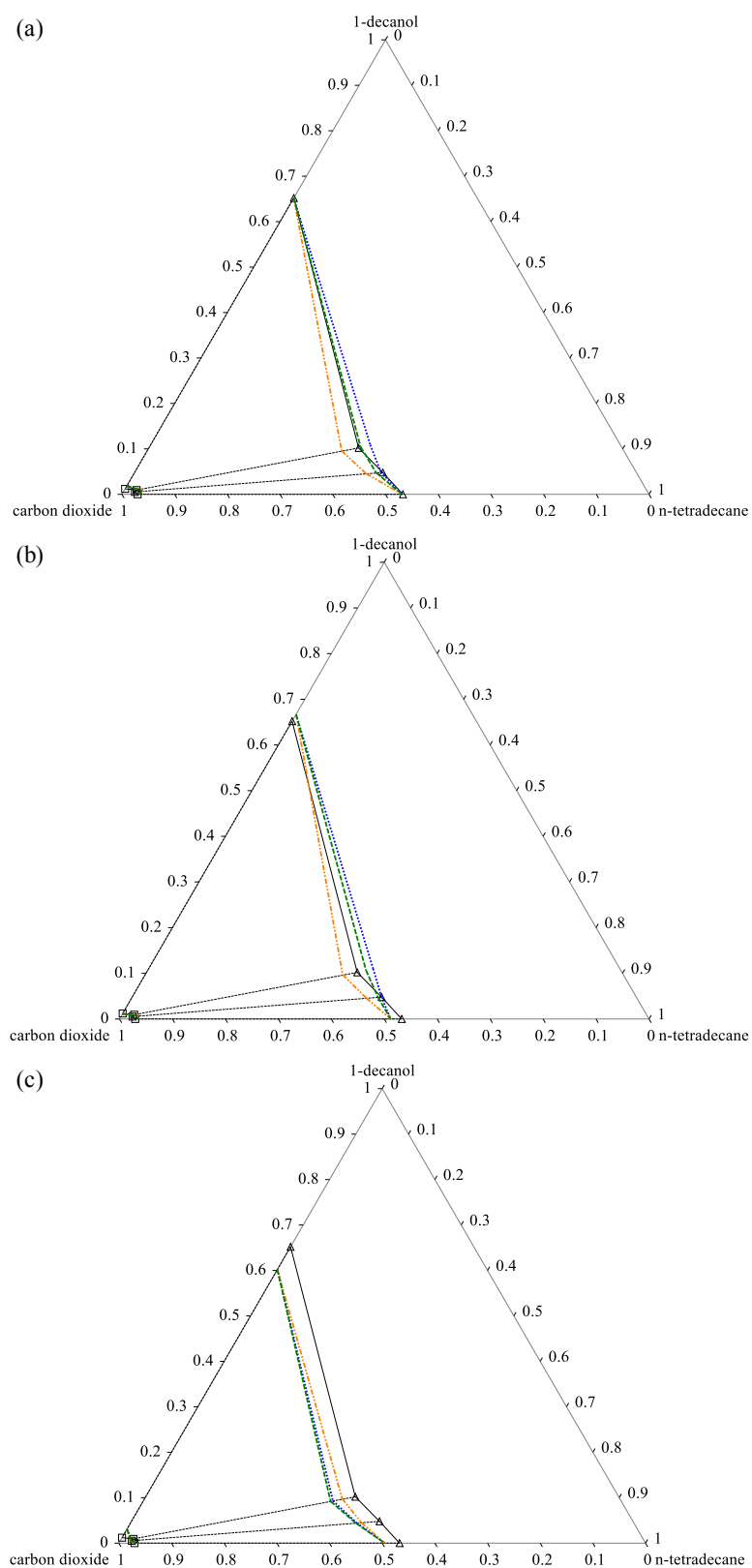


FIGURE H- 6: THERMODYNAMIC MODEL CORRELATIONS OF THE HPVLE DATA WITH: HPBDP BIPs; --- HPVLE BIPs; AND, -.- LPVLE SOLUTE + SOLUTE BIPs AT $T = 348$ K AND $P = 14.0$ MPa FOR (A) RK-ASPEN (B) SR-POLAR; AND (C) PC-SAFT.

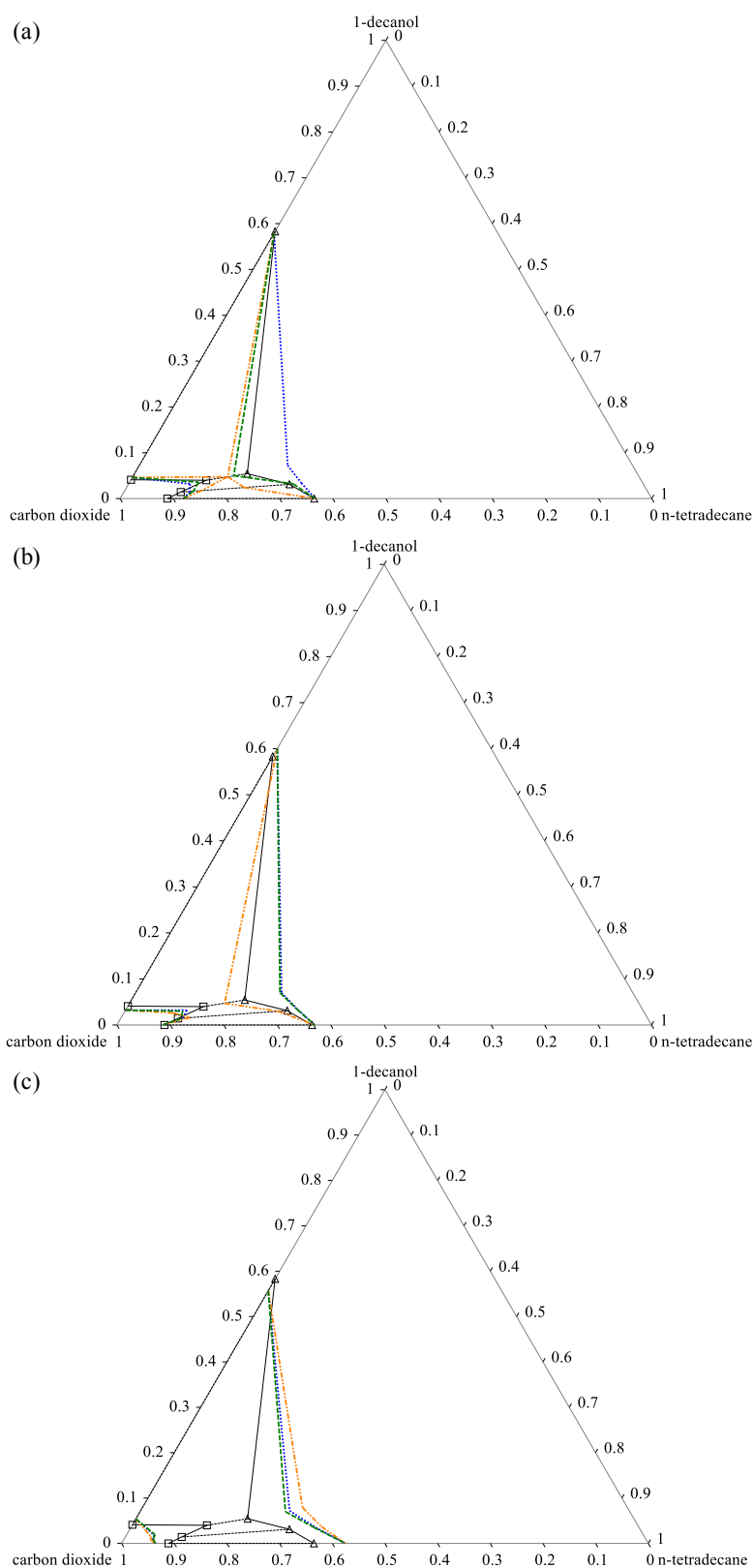


FIGURE H- 7: THERMODYNAMIC MODEL CORRELATIONS OF THE HPVLE DATA WITH: HPBDP BIPs; --- HPVLE BIPs; AND, LPVLE SOLUTE + SOLUTE BIPs AT $T = 348$ K AND $P = 16.3$ MPa FOR (A) RK-ASPEN (B) SR-POLAR; AND (C) PC-SAFT.